Advanced Structured Materials

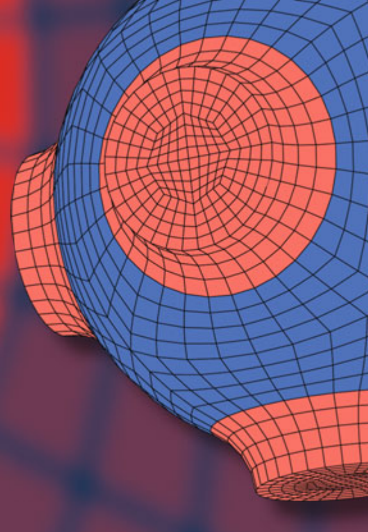

Gennadi I. Mikhasev
Holm Altenbach

Thin-walled Laminated Structures

Buckling, Vibrations and Their Suppression

Springer

Advanced Structured Materials

Volume 106

Common engineering materials reach in many applications their limits and new developments are required to fulfil increasing demands on engineering materials. The performance of materials can be increased by combining different materials to achieve better properties than a single constituent or by shaping the material or constituents in a specific structure. The interaction between material and structure may arise on different length scales, such as micro-, meso- or macroscale, and offers possible applications in quite diverse fields.

This book series addresses the fundamental relationship between materials and their structure on the overall properties (e.g. mechanical, thermal, chemical or magnetic etc) and applications.

The topics of *Advanced Structured Materials* include but are not limited to

- classical fibre-reinforced composites (e.g. glass, carbon or Aramid reinforced plastics)
- metal matrix composites (MMCs)
- micro porous composites
- micro channel materials
- multilayered materials
- cellular materials (e.g., metallic or polymer foams, sponges, hollow sphere structures)
- porous materials
- truss structures
- nanocomposite materials
- biomaterials
- nanoporous metals
- concrete
- coated materials
- smart materials

Advanced Structured Materials is indexed in Google Scholar and Scopus.

More information about this series at http://www.springer.com/series/8611

Gennadi I. Mikhasev · Holm Altenbach

Thin-walled Laminated Structures

Buckling, Vibrations and Their Suppression

Springer

Gennadi I. Mikhasev
Department of Bio- and Nanomechanics
Belarusian State University
Minsk, Belarus

Holm Altenbach
Lehrstuhl für Technische Mechanik
Otto-von-Guericke-Universität Magdeburg
Magdeburg, Sachsen-Anhalt, Germany

ISSN 1869-8433 ISSN 1869-8441 (electronic)
Advanced Structured Materials
ISBN 978-3-030-12759-6 ISBN 978-3-030-12761-9 (eBook)
https://doi.org/10.1007/978-3-030-12761-9

This Springer imprint is published by the registered company Springer Nature Switzerland AG
The registered company address is: Gewerbestrasse 11, 6330 Cham, Switzerland

Preface

Among the modern structural materials laminates and sandwiches have a lot of applications as materials for lightweight structures. The history of layered materials is approximately 100 years old. However, in this short period of time, there has been an uncountable advancements in science and technology of this new class of materials. The low density, high strength, high stiffness to weight ratio, excellent durability, and design flexibility of these materials are the primary reasons for their use in many structural components in the aircraft, automotive, marine, building, and other industries. Laminates are now used in applications ranging from rail cars to oxygen tanks, from aircraft wings to automobile doors, from race cars to tennis rackets. Their use is increasing at such a rapid rate that they are no longer considered advanced materials. The main representatives of layered materials are laminates (in modern structures in some cases up to 50-60 layers and more) and sandwiches (three-layered materials with two skin sheets and a core).

There are several variants of thin-walled laminated structures: beams, rods, plates, shells, folded structures, etc. The common property of these structural elements is that one or two spatial dimension are much smaller than the remaining dimension(s). In this book the focus is on beams, plates and shells. Extensions to other classes of thin-walled structures can be realized without any difficulties.

There are a lot of monographs and textbooks devoted to classical laminates and sandwich structures. An overview and actual state of the art report is given in

- H. Altenbach, J. Altenbach, W. Kissing (2018): Mechanics of Composite Structural Elements (2^{nd} ed.), Springer, Singapore

During the last decades there are new applications with the progress, for example, in adaptive structures. Instead of layers characterized by mechanical properties only now we have layers showing in addition magnetorehological and electrorheological behavior. They consist of electrorheological composites or magnetorheological elastomers and fluids. If they are affected by electrical or magnetic fields the mechanical properties (among them stiffness or damping) of such structures can be changed or controlled. As result one gets an adaptive structure, buckling can be avoided or vibrations can be suppressed. In this sense such a material is named functional material. The novelty of this monograph is given by presenting a theoretical approach allowing the analysis of structures with magnetorehological and electrorheological layers and showing with the help of examples how the mechanical behaviour of thin-walled laminated structures can be influenced.

The book contains six chapters. Chapter 1 (Introduction) presents a brief overview on derivation approaches for theories of thin-walled structures, modeling of composites and modeling of laminated and sandwich structures. The presented theory is based on the application of the generalized Timoshenko hypotheses, the equivalent single layer model in the theory of layered structures and asymptotic methods in the shell theory. The generalized Timoshenko hypotheses was firstly presented in

- E.I. Grigolyuk, G.M. Kulikov (1988): Multilayered Reinforced Shells. Calculation of Pneumatic Tires (in Russ.), Mashinostroenie, Moscow

and the asymptotic approach used in this book is discussed, for example, in

- P.E. Tovstik, A.L. Smirnov (2001): Asymptotic Methods in the Buckling Theory of Elastic Shells, World Scientific, Singapore
- G.I. Mikhasev, P.E. Tovstik (2009): Localized Vibrations and Waves in Thin Shells. Asymptotic Methods (in Russ.), FIZMATLIT, Moscow

Chapter 2 is devoted to the equivalent single layer model for thin laminated cylindrical shells containing also the special cases of plates and beams. In addition to the classical mechanical properties, electrorheological and magnetorheological properties are taken into account.

Chapter 3 presents the elastic buckling of laminated beams, plates, and cylindrical shells. Among other problems, the influence of the boundary conditions, the external loading and the magnetic fields is discussed. For the asymptotic approach different approximations are suggested.

Chapter 4 is focussed on the free vibrations of elastic laminated beams, plates, and cylindrical shells. Again, the influence of the boundary conditions and other items are investigated.

Chapter 5 presents new results concerning vibrations of laminated structures composed of smart materials. The influence of electric and magnetic fields on smart structures is discussed in detail. From these results one can get recommendations for optimal design of these structures.

Chapter 6 is a short appendix presenting asymptotic estimates and series.

Finally, we have to acknowledge to Dr. E.V. Korobko (A.V. Lykov Heat and Mass Transfer Institute of National Academy of Sciences of Belarus) acting as a coauthor of one section, Mr. I.R. Mlechka (Belorussian State University) performing several computations and Dr. M.G. Botogova (Belorussian State University) and Mrs. S.S. Maevskaya (Vitebsk State University) supporting us with numerical computations and graphical design.

Minsk, Magdeburg
December 2018

Gennadi I. Mikhasev
Holm Altenbach

Contents

Chapter 1
Introduction

Abstract Laminates and sandwiches belong to lightweight structures of rather thin cross sections in comparison with the other structural dimensions. Both have a layered structure. The first one are composed of many layers (in modern structures up to 40 - 60) each of them have as usual the same thickness and properties. The second one are composed of three layers and in classical applications the outer layers are made of uniform (homogeneous) materials, while the inner layer consists either of a soft, relatively continuous material (different foams) or of a structurally complicated, inhomogeneous material (cellular fillers, corrugations). However, in multilayered structures each layer is a composite material itself. A short introduction into the modelling of composite structures is given in Chapt. 1. In Sect. 1.1 some general formulation approaches of plate and shell theories are presented. In Sect. 1.2 an introduction to composite modelling is given. Section 1.3 is devoted to modeling of laminated and sandwich plates and shells.

1.1 Derivation Approaches for Theories of Plates and Shells

Modeling and calculation of three- and multilayered structures is a complicated problem of the mechanics of deformable solid bodies. Since they are as usual thin in on direction (thickness) they belong to the so-called surface structures. In the classical sense two families of structures can be distinguished: plates and shells. Both families are characterized by the assumption that the thickness is smaller in comparison with other spatial dimensions and this allows to approximate the three-dimensional solid mechanics problem by a two-dimensional. Within the geometrical linear theory for isotropic plates the in-plane and the out-of-plane behavior can be decoupled. With respect to the shell curvature such decoupling for shells is not possible without additional assumptions.

Let us present at first the derivation approaches for the governing equations of the theories of plates and shells. In Sects. 1.2 and 1.3 the special cases of laminate and sandwich structures will be discussed starting with the description of composite ma-

G. I. Mikhasev and H. Altenbach, *Thin-walled Laminated Structures*,
Advanced Structured Materials 106, https://doi.org/10.1007/978-3-030-12761-9_1

terials and a brief introduction of averaging methods resulting in effective properties of composites.

One of the basic problems in engineering mechanics is the analysis of the strength, the vibration behavior and the stability of structural elements with the help of a structural model (Altenbach and Meenen, 2008). In this context, structural models are approximations of a general continuum theory. The following classification of structural models can be given

- by certain geometrical (spatial) dimensions,
- by certain applied loads and
- by the use of kinematical and/or statical hypotheses approximating their mechanical behavior.

Structural elements and models for their analysis can be categorized into three main classes, depending on the ratio of their characteristic dimensions. The first class is the class of three-dimensional structural elements, which can be defined as follows:

Definition 1.1 (Three-dimensional structural element).
A three-dimensional structural element has three spatial dimensions of the same order, no predominant dimension exists.

Typical examples of geometrically simple, compact structural elements in the theory of elasticity are cube, prism, cylinder, sphere, etc. The second basic class is the class of two-dimensional structural elements which can be defined as follows:

Definition 1.2 (Two-dimensional structural element).
Two-dimensional structural elements are bodies, which have two spatial dimensions of comparable size, and a third spatial dimension, the so-called thickness, which is at least one order of magnitude smaller.

Typical examples of two-dimensional structural elements in civil engineering and structural mechanics are membrane, disc, plate, shell, folded structure, etc. It should be noted that the applied loading results in various sub-classes: for plane structures one should distinguish the in-plane and the out-of-plane loading cases; for curved structures only in some special cases such split makes sense. The last class is related to the one-dimensional structural elements which can be defined as follows:

Definition 1.3 (One-dimensional structural element).
Two spatial dimensions, which can be related to the cross-section, have a comparable size. The third dimension, which is related to the length of the structural element, is at least one order of magnitude larger than the size of the cross-section dimensions.

Typical examples in engineering mechanics are rod, truss, beam, torsion bar, etc. Like in the case of two-dimensional structural elements the applied loading allows to distinguish special cases (tension/compression, bending, torsion).

In general, it is possible to introduce other classes. For example, in shipbuilding, thin-walled structural elements are often used. These are thin-walled light-weight structures with a special profile and they require an extension of the classical one-dimensional structural models:

Definition 1.4 (Quasi-onedimensional structural elements).
If the spatial dimensions are of significantly different order and the thickness of the profile is small in comparison to the other cross-section dimensions, and the cross-section dimensions are much smaller in comparison to the length of the structure one can introduce quasi-onedimensional structural elements.

Suitable theories for the analysis of quasi-onedimensional structural elements are the thin-walled beam theory (Vlasov-Theory) and the semi-membrane theory or generalized beam theory (Altenbach et al, 1994, 2018). Typical thin-walled cross-section profiles are closed cross-section profiles, open cross-section profiles, open-closed cross-section profiles, etc.

Here the focus is on the second and third class of structural elements. Since the characteristic length in thickness direction is much smaller than the characteristic length in the surface direction, for a two-dimensional structures it is tempting to look for procedures that eliminate the thickness dimension (reduction of the coordinates). From the mathematical point of view it is obvious that instead of a three-dimensional coupled partial differential equations, one can analyze a two-dimensional problem, which is described by two spatial coordinates only. These coordinates represent a surface in three-dimensional space, and a procedure has to be developed that maps the real behavior in thickness direction onto the mechanical behavior of the surface. The transition from the three-dimensional to the two-dimensional problem is non-trivial, but once a two-dimensional theory has been obtained, the solution effort decreases significantly and the possibilities to solve problems analytically are increased (Altenbach and Meenen, 2008). One-dimensional theories are here presented as special cases of the two-dimensional one.

During the last 50 years various scientific papers, textbooks, monographs and proceedings on the state of the art and recent developments in the plate and shell theories were published, for example, in Altenbach et al (2016, 2010); Grigolyuk and Seleznev (1973); Libai and Simmonds (1998); Naghdi (1972); Reissner (1985); Rothert (1973). In addition, new developments were discussed on conferences and courses, s. Altenbach and Eremeyev (2011); Altenbach and Mikhasev (2014); Jaiani and Podio-Guidugli (2008); Kienzler et al (2004), among others. From these publications one can conclude that for the formulation of any plate or shell theory there are two starting points:

- the reduction technique, which starts from the equations of three-dimensional (3D) continuum and develops approximate two-dimensional (2D) continuum theories; and
- the direct approach, which starts from a rigorous 2D continuum theory (deformable surface)

If one starts from the 3D continuum theory, the following approaches can be distinguished:

- the use of hypotheses to approximate the three-dimensional equations (e.g. by introducing these hypotheses into the principle of virtual displacements),
- the use of mathematical approaches, such as series expansions, special functions or asymptotic integration, or

- the formulation of consistent theories

All these approaches have their own advantages and disadvantages, and it is difficult to argue what is the best method for deriving a plate or shell theory. Additionally, in many cases different derivation methods result in identical or similar sets of governing equations.

Theories which are based on hypotheses are preferred by engineers because of their simplicity. For example, there is a huge number of theories which are based on displacement assumptions. Note that the three displacements in the classical three-dimensional continuum are split into in-plane displacements and transverse displacement (deflection). Probably the first theory of plates based on displacement assumptions was presented by Kirchhoff (1850). Kirchhoff used similar hypotheses for the kinematics as in the Euler-Bernoulli beam theory. He ignored the in-plane displacements and with the deflection w which was assumed to be independent from the thickness coordinate he got the following kinematical constraints: no transverse shear and no thickness changes. The final version of his theory he presented, for example, in Kirchhoff (1883)

$$D\triangle\triangle w = q,$$

where the bending stiffness[1] which is assumed to be constant

$$D = \frac{Eh^3}{12(1-\nu^2)}$$

is a combination of material parameters (E is the Young's modulus and ν is the Poisson's ratio) and a property of the geometry (h is the plate thickness). $\triangle$ denotes the Laplace operator ($\triangle = \boldsymbol{\nabla} \cdot \boldsymbol{\nabla}$ with $\boldsymbol{\nabla}$ as the Hamilton (nabla) operator) and q the transverse load. It is interesting that Kirchhoff's approach has shown immediately that any approximation results in difficulties. Kirchhoff' final equation was a partial differential equation of fourth order for the deflection. But it was well-known that one has satisfy three boundary conditions in the general case. Kirchhoff solved this problem introducing a combination of the transverse shear force and the torsion moment (Kirchhoff's Ersatzkraft) and special edge forces. Kirchhoff's theory failed if we have thick plates or sandwiches since the constraints of the kinematics are no more valid. The theory was seriously improved about 100 years later (s., for example, Reissner, 1944, 1945; Hencky, 1947; Mindlin, 1951). In the various improved theories, similar to Timoshenko's beam theory additional degrees of freedom (cross-section rotations) were introduced, so that transverse shear was considered in an approximate sense. Such type of theory is named first order shear deformation theory. The introduction of independent rotations is in some cases not enough, since it is assumed that any cross-section will be plane before and after deformation. To solve this problem, Ambartsumyan (1970) introduced an additional distribution function in the thickness direction. A less restrictive approximation was proposed by Levinson (1980) and Reddy (1984b), among others. These refined theories which named third order shear

[1] Note that the term stiffness always means a combination of material parameters and geometrical characteristics.

deformation theories can be understood as theories that introduce additional degrees of freedom, or as some part of a power series expansion. The first suggestion of this type was done by Lo et al (1977). A generalization of the power series approach was given in Meenen and Altenbach (2001).

An alternative approach considering assumptions for the stress state was suggested by Reissner (1944, 1945). It can be shown that Mindlin's and Reissner's plate theories contain partly identical equations, but the coefficients take slightly different values and their physical interpretation is not the same. The similarities are so great that in the Finite Element references as usual the name *Reissner-Mindlin element* is used.

Pure mathematical approaches are mostly based on power series, trigonometric functions, on special functions, asymptotic integration, etc. (s., e.g., Kienzler, 1982; Preußer, 1984; Reissner, 1985; Vekua, 1985; Touratier, 1991). The mathematical approaches are very helpful if one wants to check the accuracy of the given approximation. A nice comparison of the different approximations in the series approach is given in Kienzler (2002) where first time was shown a new approach based on consistent formulations. An actual reference for the consistent approach and the comparison with other approaches is given in Kienzler and Schneider (2016); Schneider et al (2014).

The direct approach is based on the a priori introduction of a two-dimensional deformable surface. This approach was applied by Green et al (1965); Palmow and Altenbach (1982); Rothert (1973); Zhilin (1976), among others. The main advantage of these theories is that their derivation does not rely on assumptions or series expansions and is mathematically and physically as strong and exact as the three-dimensional continuum mechanics. This approach is still under discussion, since the application is not trivial, and a relationship between the constitutive laws of the deformable surface and the corresponding three-dimensional body has to be found.

The development of shell theories was similar. One has to distinguish

- theories based on hypotheses (s., for example, Aron, 1874; Novozhilov, 1970; Donnell, 1976; Love, 1906; Mushtari and Galimov, 1961),
- theories formulated with help of mathematical techniques (Vekua, 1985),
- theories introducing deformable surfaces (Naghdi, 1972, among others)

Details will be not discussed here.

1.2 Modeling of Composites

Development and applications of composite materials and structural elements composed of composite materials have been very rapid in the last decades. The motivation for this development is the significant progress in material science and technology of the composite constituents. In addition, the requirements for high performance materials are not only in aircraft and aerospace structures. The increasing performance of composites is also related to the development of very powerful experimental equipments and numerical methods. With the development of composite materials a new material design is possible that allows an optimal material composition in connection with the structural design. In addition, with the application of electrorheological, magnetorheological, etc. materials as layers in laminates one can suppress vibrations, prevent buckling, among others.

A useful and correct application of composite materials requires a close interaction of different engineering disciplines such as structural design and analysis, material science, mechanics of materials, process engineering, etc. The main topics of composite material research and technology are

- investigation of all characteristics of the constituents and the composite materials,
- material design and optimization for the given working conditions,
- development of analytical modeling and solution methods for determining material and structural behavior,
- development of experimental methods for material characteristics, stress and deformation states, failure,
- modeling and analysis of creep, damage, and life prediction,
- development of new and efficient fabrication and recycling procedures, among others.

1.2.1 Preliminary Remarks and Definitions

In material science the following classification of structural materials is given

- metals,
- ceramics, and
- polymers.

Sometimes there are more classes but we will limited us to these three classes. They are related to different application fields. It is difficult to give an assessment of the advantages and disadvantages of these basic material classes, because each of them covers whole groups of materials within which the range of properties is often as broad as the differences between the material classes. Some obvious characteristic properties can be identified (Altenbach et al, 2018):

- Mostly metals are of medium to high density. They have good thermal stability and can be made corrosion-resistant by alloying. Metals have useful mechanical characteristics and it is moderately easy to shape and join these materials. For this reason metals became the preferred structural engineering material, they posed less problems to the designer than either ceramic or polymer materials.
- Ceramic materials have great thermal stability and are resistant to corrosion, abrasion and other forms of attack. They are very rigid but mostly brittle and can only be shaped with difficulty.
- Polymer materials (plastics) are of low density, have good chemical resistance but lack thermal stability. They have poor mechanical properties, but are easily fabricated and joined. Their resistance to environmental degradation, e.g. the photomechanical effects of sunlight, is moderate.

Let us introduce some basic definitions with respect to the material behavior.

Definition 1.5 (Homogeneous material behavior).
A material is called homogeneous if its properties are the same at every point and therefore independent of the location.

Homogeneity is associated with the scale of modeling or the so-called representative volume and the definition describes the averaged material behavior on a macroscopic (phenomenological) level. On the microscopic level materials can be described as homogeneous, quasi-homogeneous, inhomogeneous or heterogeneous.

Definition 1.6 (Quasi-homogeneous material behavior).
A material is quasi-homogeneous if its effective (averaged) properties are the same at every point.

Definition 1.7 (Inhomogeneous material behavior).
A material is inhomogeneous if its properties depend on the location but there is only one phase.

Definition 1.8 (Heterogeneous material behavior).
A material is heterogeneous if its properties depend on the location but there are two or more phases.

In addition, the material behavior can be dependent on the loading direction.

Definition 1.9 (Isotropic material behavior).
A material is isotropic if its properties are independent of the orientation, they do not vary with direction.

Definition 1.10 (Anisotropic material behavior).
If the properties are changing with the loading direction the material behavior is called anisotropic.

A general anisotropic material has no planes or axes of material symmetry. Special cases of material symmetries are orthotropy (three orthogonal planes of symmetry), transverse isotropy (three orthogonal planes of symmetry and one axis of symmetry in one of the planes of symmetry), among others.

Definition 1.11 (Monolithic material).
If a material contains one constituent or one single phase only, the material is called monolithic.

The above mentioned classes of materials are in many cases on the macroscopic level more or less monolithic, homogeneous and isotropic.

1.2.2 Composite Materials

The group of materials which can be defined as composite materials is extremely large.

Definition 1.12 (Composite material).
A composite material (or shortened to composite) is any material that is a combination of two or more constituent materials and has material properties derived from the individual constituents. The constituents can be from the same material class or different classes.

In dependence of fabrication the properties may have the combined characteristics of the constituents or they are substantially different. Sometimes the material properties of a composite may exceed those of the constituents. The definition of composite materials include:

- reinforced concrete and masonry,
- composite wood such as plywood,
- reinforced plastics, such as fibre-reinforced polymer (long or short fibres) or fiberglass,
- ceramic matrix composites (composite ceramic and metal matrices),
- metal matrix composites and
- other advanced composite materials.

In many cases composites have some excellent properties like low weight in combination with high strength and stiffness which is necessary in modern structural design.

The simplest case of a composite is an assembly of two materials of same or different nature. The special class of reinforced plastics is related to one discontinuous material, called the reinforcement, and another material, mostly less stiff and weaker, continuous and called the matrix. In this case the properties of the composite depend on (Altenbach et al, 2018):

- the properties of the constituents,
- the geometry of the reinforcements, their distribution, orientation and concentration usually measured by the volume fraction or fiber volume ratio and
- the nature and quality of the matrix-reinforcement interface.

The prediction of the interface properties is up to now a problematic task. The properties of the fibres and the matrix can be measured separately, but the interface does not exist separately. As usual the properties of the interface are computed by inververse problems. Models of the interface behavior are presented in Hill (1963, 1964); Gurtin and Murdoch (1975); Murdoch (2005); Hashin (1991) among others. An overview on interface modeling is given, for example, in Nazarenko et al (2018a,b).

Summarizing the aspects defining a composite as a mixture of two or more distinct constituents or phases it must be considered that all constituents have to be present in reasonable proportions that the constituent phases have quite different properties from the properties of the composite material and that man-made composites are produced by combining the constituents by various means (Altenbach et al, 2018). Figure 1.1 shows typical examples of composites with different types of reinforcement. The reinforcement can be more or less regular or chaotic. Composites can be classified by their form and distribution of the constituents (Fig. 1.2). The

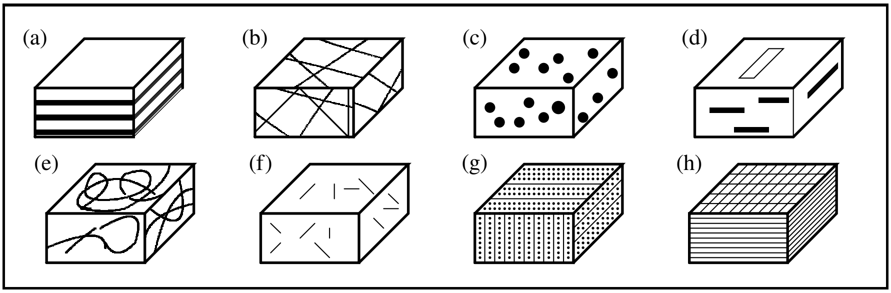

Fig. 1.1 Examples of composite materials with different forms of constituents and distributions of the reinforcements. (a) Laminate with uni- or bidirectional layers, (b) irregular reinforcement with long fibres, (c) reinforcement with particles, (d) reinforcement with plate strapped particles, (e) random arrangement of continuous fibres, (f) irregular reinforcement with short fibres, (g) spatial reinforcement, (h) reinforcement with surface tissues as mats, woven fabrics, etc. (Altenbach et al, 2018, with courtesy of Springer Publisher).

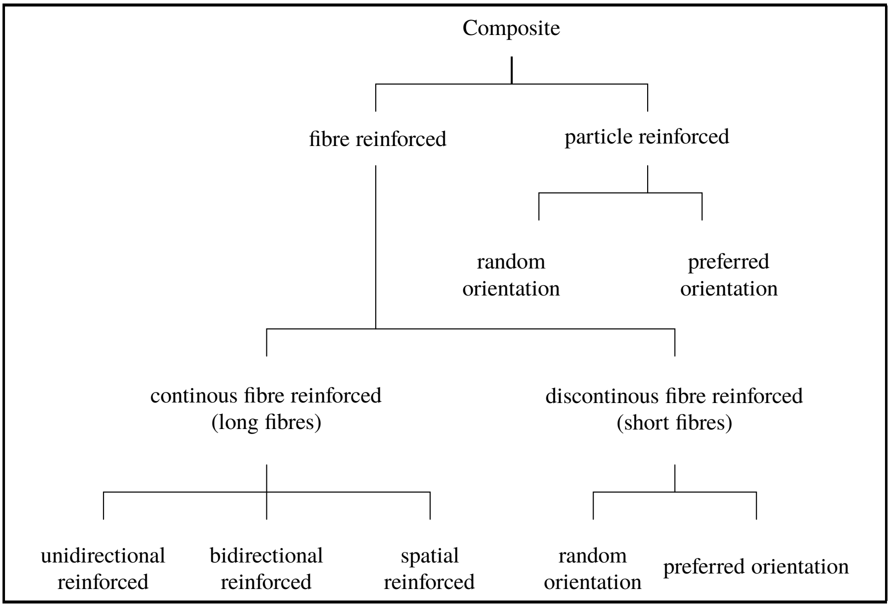

Fig. 1.2 Classification of composites (Altenbach et al, 2018, with courtesy of Springer Publisher).

reinforcement constituent can be described, for example, as fibrous or particulate. The fibres are assumed to be long (size of the structural element) or short (in comparison to the structural element's dimension). Long fibres are mostly arranged in uni- or bidirectional reinforcements, but also irregular reinforcements by long fibres are possible. The arrangement and the orientation of the fibres determine the mechanical properties of composites including the type of anisotropy. Particulate reinforcements can be spherical, platelet or of any regular or irregular geometry. Their arrangement may be random or regular with preferred orientations. In many practical applications particulate reinforced composites are considered to be randomly oriented and the mechanical properties are quasi-homogeneous and isotropic. In the case of mold injection manufacturing the particle orientation over the cross-section is partly in the flow direction, partly orthogonal to the flow direction, and partly chaotic (Gupta and Wang, 1993; Saito et al, 1998, 2000) and it was established that the structural elements can show anisotropic behavior (Altenbach et al, 2003, 2005). The preferred orientation in the case of long fibre composites is unidirectional for each layer or lamina. In this case, we have in each layer an transversely-isotropic material behavior. With the variation of the fibre angle in each layer one gets finally a laminate with anisotropic stiffness properties.

Composite materials can also be classified by the nature of their constituents. According to the nature of the matrix material we have organic, mineral or metallic matrix composites (Altenbach et al, 2018):

- Organic matrix composites are polymer resins with fillers. The fibres can be mineral (glass, etc.), organic (aramid, etc.) or metallic (aluminium, etc.).
- Mineral matrix composites are ceramics with metallic fibres or with metallic or mineral particles.
- Metallic matrix composites are metals with mineral or metallic fibres.

Fibre reinforced polymer resins can be used only in a low temperature range up to 200^0 to 300^0 C. The two basic classes of resins are thermosets and thermoplastics. Typical thermoset matrices include Epoxy, Polyester, Polyamide and Vinyl Ester, among popular thermoplastics are Polyethylene, Polystyrene and Polyether-ether-ketone (PEEK). Ceramic based composites can also be used in a high temperature range up to 1000^0 C and metallic matrix composites in a medium temperature range.

Polymer matrix composites are characterized by relatively low costs, simple manufacturing and high strength. Their main drawbacks are the low working temperature, high coefficients of thermal and moisture expansion and, in certain directions, low elastic properties. Polymer matrix composites are usually reinforced by fibres to improve such mechanical characteristics as stiffness, strength, etc. Fibres can be made of different materials (glass, carbon, aramid, etc.). Glass fibres are widely used because their advantages include high strength, low costs, high chemical resistance, etc., but their elastic modulus is very low and also their fatigue strength. Graphite or carbon fibres have a high modulus and a high strength and are very common in aircraft components. The functional requirements of fibres and matrices in a fibre reinforced polymer matrix composite can be summarized as follows:

- fibres should have a high modulus of elasticity and a high ultimate strength,
- fibres should be stable and retain their strength during handling and fabrication,
- the variation of the mechanical characteristics of the individual fibres should be low, their diameters uniform and their arrangement in the matrix is more or less regular,
- matrices have to bind together the fibres and protect their surfaces from damage,
- matrices have to transfer stress to the fibres by adhesion and/or friction and

- matrices have to be chemically compatible with fibres over the whole working period.

In some new applications more and more elastomers are used as a material of a sandwich or laminate layer. An elastomer is a polymer characterized by viscoelastic properties that means it shows viscose (time-dependent) and elastic (spontaneous) behavior. Sometimes, such behavior is named rubber-like behavior. An elastomer has very weak intermolecular forces, and the Young's modulus is low and the failure strain is high if we compare with other materials. Elastomers are amorphous polymers. At ambient temperatures, such rubbers are relatively soft and the Young's modulus $E \approx 3$ MPa. The deformability is high. In structures discussed later especially elastomeric layers are used as damping and insulating elements. In these cases electro- or magnetorheological elastomers consist of polymeric matrix with embedded micro- or nano-sized polarizable or ferromagnetic particles. In some application instead of elastomers are used electro- or magnetorheological fluids.

1.2.3 Volume Fibre Fraction

The fibre length, their orientation, their shape and their material are main factors which contribute to the mechanical performance of a composite. Their volume fraction usually lies between 0.3 and 0.7. The matrix materials generally have low mechanical properties as compared to fibres, but they influence many characteristics of the composite such as the transverse and shear moduli, the strength, the thermal resistance and expansion, etc.

The most important factor which determines the mechanical behavior of a composite material is the proportion of the matrix and the fibres expressed by their volume or weight fraction. These fractions can be established for a two phase composite in a simple way. The volume V of the composite is made from a matrix volume V_{m} and a fibre volume V_{f}

$$V = V_{\mathrm{f}} + V_{\mathrm{m}} \tag{1.1}$$

Then the following relations hold

$$v_{\mathrm{f}} = \frac{V_{\mathrm{f}}}{V}, \qquad v_{\mathrm{m}} = \frac{V_{\mathrm{m}}}{V} \tag{1.2}$$

with

$$v_{\mathrm{f}} + v_{\mathrm{m}} = 1, \qquad v_{\mathrm{m}} = 1 - v_{\mathrm{f}}$$

as the fibre and the matrix volume fractions, respectively. In a similar way the weight or mass fractions of fibres and matrix can be defined. The mass M of the composite is made from M_{f} and M_{m}

$$M = M_{\mathrm{f}} + M_{\mathrm{m}}$$

and

$$m_{\mathrm{f}} = \frac{M_{\mathrm{f}}}{M}, \qquad m_{\mathrm{m}} = \frac{M_{\mathrm{m}}}{M} \tag{1.3}$$

with

$$m_{\mathrm{f}} + m_{\mathrm{m}} = 1, \qquad m_{\mathrm{m}} = 1 - m_{\mathrm{f}}$$

m_{f} and m_{m} are the mass fractions of fibres and matrices, respectively. With the relation between volume, mass and density $\rho = M/V$, we can link the mass and the volume fractions

$$\begin{aligned}\rho = \frac{M}{V} = \frac{M_{\mathrm{f}} + M_{\mathrm{m}}}{V} &= \frac{\rho_{\mathrm{f}} V_{\mathrm{f}} + \rho_{\mathrm{m}} V_{\mathrm{m}}}{V} \\ = \rho_{\mathrm{f}} v_{\mathrm{f}} + \rho_{\mathrm{m}} v_{\mathrm{m}} &= \rho_{\mathrm{f}} v_{\mathrm{f}} + \rho_{\mathrm{m}}(1 - v_{\mathrm{f}})\end{aligned} \tag{1.4}$$

Starting from the total volume of the composite (1.1) we obtain

$$\frac{M}{\rho} = \frac{M_{\mathrm{f}}}{\rho_{\mathrm{f}}} + \frac{M_{\mathrm{m}}}{\rho_{\mathrm{m}}}$$

and

$$\rho = \frac{1}{\dfrac{m_{\mathrm{f}}}{\rho_{\mathrm{f}}} + \dfrac{m_{\mathrm{m}}}{\rho_{\mathrm{m}}}} \tag{1.5}$$

The equations of this subsection can be easily extended to multi-phase composites. Mass fractions are easier to measure in material manufacturing, but volume fractions appear in the theoretical equations for effective moduli. Therefore, it is helpful to have simple expressions for shifting from one fraction to the other. The volume fractions are the base of computing the material parameters of a reinforced composites. The averaged Young's modulus, shear modulus or Poisson's ratio can be expressed using rheological models combining the fibre and matrix properties with the help of parallel connection, connection in series or improved formulaes. The last one are based as usual on fitting experimental data. Some of these expressions are discussed in detail in Altenbach et al (2018).

The quality of a composite material decreases with increase in porosity. The volume of porosity should be less than 5 % for a medium quality and less than 1 % for a high quality composite. If the density is measured experimentally (ρ_{exp}) and calculated with (1.5) (ρ_{theor}), the volume fraction of porosity is given by

$$v_{\mathrm{por}} = \frac{\rho_{\mathrm{theor}} - \rho_{\mathrm{exp}}}{\rho_{\mathrm{theor}}} \tag{1.6}$$

1.2.4 Modeling of Structures Composed of Composites

Composite materials consist of two or more constituents and the modeling, analysis and design of structures composed of composites are different from conventional

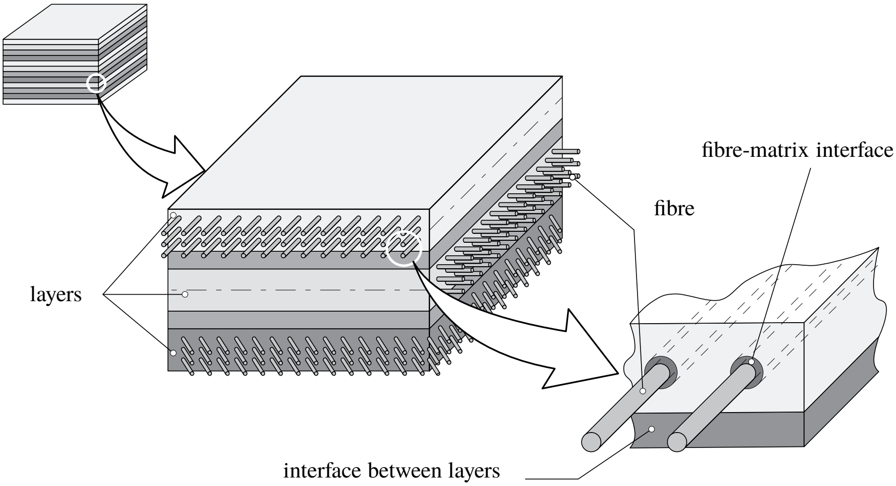

Fig. 1.3 Laminated plates - levels of modeling.

materials such as steel. For example, if we have a laminated structure there are two levels of modeling (Fig. 1.3).

At the micro-mechanical level the average properties of a single reinforced layer (a lamina or a ply) have to be determined from the individual properties of the constituents, the fibres and matrix, and may be the fibre-matrix interface. The average characteristics include the elastic moduli, the thermal and moisture expansion coefficients, etc. The micro-mechanics of a lamina does not consider the internal structure of the constituent elements, but recognizes the heterogeneity of the ply. The micro-mechanics is based on some simplifying approximations. These concern the fibre geometry and packing arrangement, so that the constituent characteristics together with the volume fractions of the constituents yield the average characteristics of the lamina. Note that the averaged properties are derived by considering the lamina to be quasi-homogeneous.

The calculated values of the averaged properties of a lamina provide the basis to predict the macrostructural properties. At the macro-mechanical level, only the averaged properties of a lamina are considered and the microstructure of the lamina is ignored. In some case the interfaces between the layers are taken into account. The properties along and perpendicular to the fibre direction, these are the principal directions of a lamina, are recognized and the so-called on-axis stress-strain relations for a unidirectional lamina can be developed. Loads may be applied not only on-axis but also off-axis and the relationships for stiffness and flexibility, for thermal and moisture expansion coefficients and the strength of an angle ply can be determined. A laminate is a stack of laminae. Each layer of fibre reinforcement can have various orientation and in principle each layer can be made of different materials. Knowing the macro-mechanics of a lamina, one develops the macro-mechanics of the laminate. Averaged stiffness, flexibility, strength, etc. can be determined for the whole laminate. The structure and orientation of the laminae in prescribed sequences to a laminate lead to significant advantages of composite materials when compared to a conventional monolithic material. In general, the mechanical response of laminates is anisotropic.

One very important group of laminated composites are sandwich structures. They as usual consist of two thin faces (the skins or sheets) sandwiching a core (Fig. 1.4). The faces are made of high strength materials having good properties under tension such as metals or fibre reinforced laminates while the core is made of lightweight materials such as foam, resins with special fillers, called syntactic foam, having good properties under compression. Sandwich composites combine lightness and flexural stiffness.

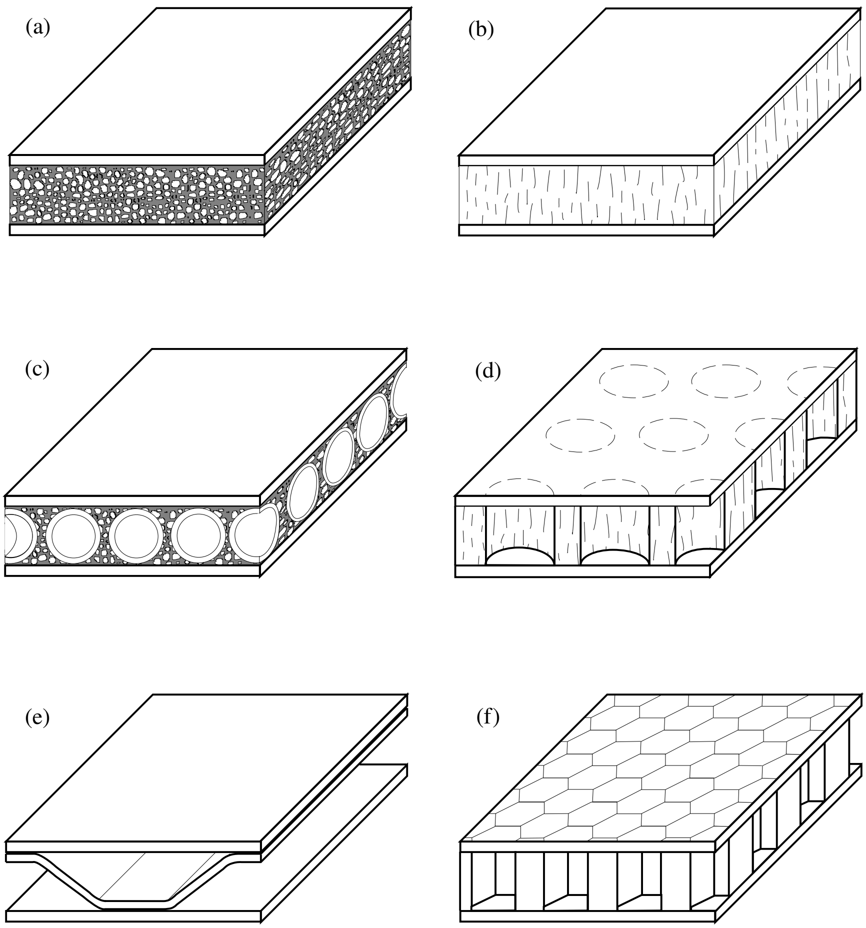

Fig. 1.4 Sandwich materials with solid and hollow cores. (a) foam core, (b) balsa wood core, (c) foam core with fillers, (d) balsa wood core with holes, (e) folded plates core and (f) honeycomb core (Altenbach et al, 2018, with courtesy of Springer Publisher).

In contrast to classical sandwiches in photovoltaic applications we have a opposite situation: thick stiff skin layers and a very thin and very weak core layer (Fig. 1.5). A detailed discussion of the specific properties and the mechanical analysis is given, for example, in Aßmus (2019).

When the micro- and macro-mechanical analysis for laminae and laminates or sandwiches are carried out, the global behavior of laminated composite materials is known. The last step is the modeling on the structure level and to analyze the global behavior of a structure made of composite material. By adapting the classical tools of structural analysis on anisotropic elastic structure elements the analysis of simple structures as beams or plates may be achieved by analytical methods, but for more general boundary conditions and/or loading and for complex structures, numerical methods are used.

Summarizing the different size scales of mechanical modeling structure elements composed of fibre reinforced composites it must be noted that, independent of the different possibilities to formulate beam, plate or shell theories, three modeling levels must be considered (Altenbach et al, 2018):

- *The microscopic level*, where the average mechanical characteristics of a lamina have to be estimated from the known characteristics of the fibres and the matrix material taking into account the fibre volume fracture and the fibre packing arrangement. The micro-mechanical modeling leads to a correlation between constituent properties and average composite properties. In general, simple mixture rules are used in engineering applications. If possible, the average material characteristics of a lamina should be verified experimentally. On the micro-mechanical level a lamina is considered as a quasi-homogeneous orthotropic material.
- The *macroscopic level*, where the effective (average) material characteristics of a laminate have to be estimated from the average characteristics of a set of laminae taking into account their stacking sequence. The macro-mechanical modeling leads to a correlation between the known average laminae properties and effective laminate properties. On the macro-mechanical level a laminate is considered generally as an equivalent single layer element with a quasi-homogeneous, anisotropic material behavior.

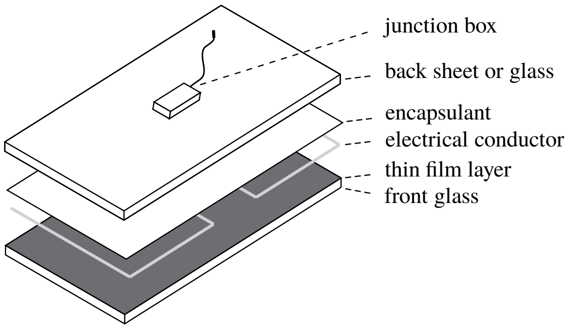

Fig. 1.5 Components of thin film solar module - *anti-sandwich* (Schulze et al, 2012; Weps et al, 2013).

- The *structural level*, where the mechanical response of structural members like beams, plates, shells etc. have to be analyzed taking into account possibilities to formulate structural theories of different order.

1.2.5 Material Characteristics of the Constituents

The optimal design and the analysis of structural elements requires a detailed knowledge of the material properties, which depend on the nature of the constituent materials but also on manufacturing. For structures made of composites as usual we have a more complicated situation. The list of composite materials is numerous but available standards and specifications are rare. The properties of each material used for both reinforcements and matrices of composites are extremely diversified. Structural design based on composite materials requires detailed knowledge about the material properties of the singular constituents of the composite and the fabrication of the composites for optimization of the material in the frame of structural applications and also detailed codes for modeling and analysis are necessary.

Let us focus on fibre reinforced composites with polymer resins. Material tests of the constituents of composites are in many cases a complicated task and so the material data in the literature are limited (Altenbach et al, 2018, and the references therein). In engineering applications the averaged data for a lamina are often tested to avoid this problem and in order to use correct material characteristics in structural analysis. The main properties for the estimation of the material behavior are

- density ρ,
- Young's modulus E, Poisson's ratio ν, shear modulus G,
- ultimate strength σ_{u} and
- thermal expansion coefficient α.

The material can be made in bulk form or in the form of fibres. To estimate properties of a material in the form of fibres, the fibre diameter d can be important.

The estimate of electro- and magneto-rheological properties is more complicated and will be not discussed here.

1.3 Modeling of Laminated Structures: Different Approaches

Many theories have been developed to model the mechanical behavior of laminated thin-walled structures. The most accurate models are based on the three-dimensional elasticity theory. However, this approach leads to complex problems of analysis the stress-strain state and rigid-body motions (s., among many others Shakeri et al, 2006; Saviz et al, 2007; Malekzadeh et al, 2009; Kulikov and Plotnikova, 2013) and since the computational effort is great this approach has found limited applications in the engineering practice. Taking into account thinness of the beams, plates and shell (in comparison to its other dimensions) researchers make simplifying assumptions, called hypotheses, which result in two- or one-dimensional representation of a shell with some predictable and reasonable accuracy.

Let us focus our attention at first to plates and shells. Theories for beams can be established in a similar manner. The 2D theories for thin laminated plates and shells may be divided into two basic models: the equivalent single layer (ESL) model and the layer-wise (LW) model. A short review of these models will be presented below. Later in this monograph the ESL model will be preferred. The ESL theories may be classified, for example, as in Qu et al (2013): classical shell theory (CST), the first-order shear deformation theory (FSDT), and the higher-order shear deformation theory (HSDT).

The CST is based on the Kirchhoff-Love hypotheses (Kirchhoff, 1850; Love, 1888). In the original paper of Kirchhoff the following two hypotheses are mentioned as the base of his theory

- straight line normal to the undeformed middle surface remains straight and normal to the deformed middle surface,
- the elements of the midplane during the deformation have no dilatation.

The first hypothesis results in neglecting the transverse shear strains. Considering the second hypothesis, in classical Kirchhoff theory one gets only an equation for the deflection. Love introduced also the in-plane displacements for the midplane of the shell.

Depending on different assumptions related to the strain-displacement, constitutive and equilibrium equations the CSTs may be conventionally subdivided into theories named by Ambartsumyan (1970), Donnell (1976), Flügge (1973), Mushtari and Galimov (1961), Love (1906), Mindlin (1951), Novozhilov (1970), Reissner (1944), Sanders (1959), Vlasov (1944), etc. All these approaches lead to three differential equations w.r.t. three unknowns. Surveys on the classical theories, initially derived for isotropic plates and shells, may be found in the monographs of Leissa (1973); Reddy (2004), and in a early work of Naghdi (1956). Obviously, the first studies on mechanical behavior of laminated plates and shells were performed in the framework of the CSTs (Reissner and Stavsky, 1961; Stavsky, 1961; Dong et al, 1962; Yang et al, 1966; Whitney and Leissa, 1969; Ambartsumyan, 1970; Bert, 1976, 1980). These approaches neglecting shear deformations have been shown to be adequate for the static analysis of thin laminates (Pagano, 1969, 1970). Considering dynamic problems for layered composite shells, such theories may be exploited in the low-frequency range (Qu et al, 2013), but they result in errors up to 30% in the prediction of large natural frequencies (Reddy, 2004). For thicker plates and shells pliable in shear as well as for thin layered structures consisting of a *soft* layer(s), the classical theories become inadequate even for predicting static deflections and stresses.

The first attempts to overcome the shortcomings of the CSTs were made by Reissner (1945, 1952); Lurie (1947); Hildebrand et al (1949) and Mindlin (1951). They proposed the so-called FSDTs in accordance to which the deflection w is independent of the normal coordinate z and the in-plane displacements u_1, u_2 of the middle surface are linear functions of z. These theories take into account the transverse shear strain components which are constant along the thickness. A detailed description of these theories may be found in Reissner (1975); Reissner and Wan (1982). In fact, these approaches may be considered as the development of the Timoshenko's beam theory (Timoshenko, 1921). Later, the extension of the FSDTs to laminated plates has been performed by Yang et al (1966); Whitney and Pagano (1970); Sun (1971), and a number of similar theories for thin and moderately thick laminated shells have been developed by Dong et al (1962); Dong and Tso (1972); Hsu and Wang (1970); Zukas and Vinson (1971); Reddy (1984a); Qatu (1999); Toorani and Lakis (2000); Auricchio and Sacco (2003). Aforementioned theories result, as a rule, in five coupled equations w.r.t. five unknowns. Recently Wang et al (2018) proposed a simple first-order shear deformation shell theory which contains only four unknowns and can be regarded as an enhanced CST with the consideration of the effects of transverse shear deformation and rotary inertia terms. The main defect of the FSDTs (as well as of classical shell theories) is that the traction conditions at the shell surfaces are violated and so, it requires shear correction factors (Reissner, 1944; Mindlin, 1951). The problem is that the shear correction factors are difficult to determine for arbitrary laminated plates and shells because they depend on the geometrical and lamination parameters, loading and boundary conditions as well (among many others, s. Srinivas et al, 1970; Chow, 1971; Whitney, 1973; Bert, 1973; Wittrick, 1987; Vlachoutsis, 1992).

In spite of the above mentioned drawbacks of the FSDTs, several improvements are suggested to study numerous applied problems on mechanical behavior of laminated shells. Qatu (1999) studied free vibrations of laminated simply supported cylindrical shells. Taking into account transverse shear deformation and rotary inertia effects as well, Toorani and Lakis (2001) considered the coupled problem on free vibrations of anisotropic laminated cylindrical shell partially or completely filled with liquids. Wang et al (2002) investigated the propagation of waves in orthotropic laminated spherical shells. Free vibrations of thick laminated anisotropic non-circular cylindrical shells were analyzed by Ganapathi and Haboussi (2003). The effect of transverse shear and rotary inertia on waves in laminated piezoelectric cylindrical shells in thermal environment was examined by Dong and Wang (2007). Ribeiro (2009) studied the effect of membrane inertia and shear deformation on geometrically nonlinear vibrations of open cylindrical laminated shells. Using a unified variational formulation based on the FSDT, Qu et al (2013) considered free, steady-state and transient vibrations of composite laminated shells of revolution subjected to various combinations of boundary conditions.

Further improvements of the shear deformable theories were based on quadratic, cubic and higher expansions at least of the in-plane displacements u_1, u_2 in terms of the transverse coordinate z. These theories are named higher-order shear deformation theories (HSDTs). First of all, we refer to Whitney and Sun (1973, 1974). They proposed a second-order theory in which the transverse displacement w is assumed as a linear function of the thickness coordinate z and the in-plane displacements u_1, u_2 of the reference surface are expanded as quadratic functions of z. This approach results in eight coupled equations w.r.t. eight unknowns. Due to the large number of dependent unknown magnitudes, this theory is results in more computational effort then the FSDTs. Furthermore, this second-order theory requires a correction to the transverse shear stiffness. In contrast to this theory, Reddy (1984a); Reddy and Liu (1985) developed a third-order but more simple shear deformation theory of laminated plates and shells. Although, this theory is based on a displacement field in which the in-plane displacements u_1, u_2 are expanded as cubic functions of z and the normal deflection w is constant through the thickness, it contains only five unknowns as in FSDTs but requires no shear correction factors. To date, there is a wide variety of higher-order theories (s. among many others Librescu et al, 1987; Librescu and Khdeir, 1988; Grigolyuk and Kulikov, 1988b; Mallikarjuna and Kant, 1993, 2002; Batra and Vidoli, 2002b; Ganapathi et al, 2002; Khare et al, 2003; Swaminathan and Ragounadin, 2004; Khare and Rode, 2005; Balah and Al-Ghemady, 2005; Tovstik and Tovstik, 2007; Amabili, 2015; Tovstik and Tovstik, 2017; Shi et al, 2018). In addition, we refer to the so-called *New HSDTs* proposed by Karama et al (2009); Aydogdu (2009); Mantari et al (2011a,b). In these theories, the transverse displacement is assumed to be independent of the thickness coordinate z, and the in-plane displacements of the reference surface are expanded as a combination of exponential and polynomial functions of z. Most of the well known shear deformable theories available in literature, including the aforementioned ones, were developed as particular cases. A common property of these theories is that they lead to a system of differential equations for five unknowns and comply with the traction-free boundary conditions on the top and bottom surfaces of the laminated plate/shell. Recently, Viola et al (2013) proposed a general variant of HSDTs which contains nine independent displacement parameters and unifies most of the known higher-order theories due to the incorporation of general shear functions.

In high accurate layer-wise theories (LWTs), accounting the zig-zag effects, each layer is considered as a shell with interface boundary conditions guaranteing the continuity of the displacement or/and stress fields. The early investigations in this direction, which were performed by Hsu and Wang (1970); Cheung and Wu (1972); Srinivas (1973); Sun and Whitney (1973); Bolotin and Novichkov (1980); Murakami (1986); Barbero et al (1990); Cho et al (1991); Gaudenzi et al (1995); Carrera (1998a,b), have shown the superiority of layer-wise models over ESL ones. Indeed, the LWTs provide more realistic kinematics of multi-layered plates and shells and turn out to be more accurate and effective to predict local effects (Reddy and Robbins, 1994; Carrera, 2001; Batra and Vidoli, 2002a; Khare et al, 2003; Demasi, 2009), high frequency response (Braga and Rivas, 2005; Oh, 2007) and formulate shell finite elements (Moreira et al, 2006; Yasin and Kapuria, 2013; Wu et al, 2018; Kordkheili and Soltani, 2018). To date, there are a lot of papers proposing improved and refined variants of layer-wise models (among many others, s. Sahoo and Singh, 2014; Naumenko and Eremeyev, 2014; Iurlaro et al, 2015; Naumenko and Eremeyev, 2017; Carrera et al, 2015; Akoussan et al, 2017; Shi et al, 2018; Flores et al, 2018) and studying topical problems on mechanical behavior of laminated plates and shells based on these models. Thus, Starovoitov and Leonenko (2010) analyzed free and resonant vibrations of circular sandwich plate using the zig-zag theory, Cetkovic (2015) studied thermo-mechanical bending of laminated composite and sandwich plates subjected to mechanical load and non-uniform temperature field, and in more recent papers (Nikbakht et al, 2017) employed the full layer-wise method to analyze the elastic bending of functionally graded plates up to yielding, Treviso et al (2017) used the refined zig-zag theory (RZT) in the framework of shell elements for vibration analysis of laminated and sandwich shells and shown that the RZT element can be effectively used to reduce the computational costs of dynamic simulations of laminated structures, and Moita et al (2018) developed a simple and efficient finite element model to examine damped vibrations of multilayered sandwich plates and shells with a viscoelastic core sandwiched between functionally graded material layers, and including piezoelectric layers.

Despite the variety of layer-wise shell theories, they have not gained wide popularity in modeling practical shell vibration problems because of extreme complexity of theoretical formulations and high computational costs. There are a few examples when only layer-wise theories yields in correct results as shown in Schulze et al (2012); Weps et al (2013); Aßmus (2019). It should be noted that each model of laminated plates and shells has its advantages as well as disadvantages (Reddy, 1993), and the correct choice of the theory depends on many factors, such as the shell geometry, the number of layers, the material of which each layer is made, as well as the loads. Another point affecting the choice of the shell model is the expected variability of the displacements, strains and stresses. So, if vibrations or buckling are accompanied by formation of a large number of short waves/dents, then the full system of governing equations is, as a rule, simplified and reduced to the shallow shell equations with a less number of unknowns (Grigolyuk and Kulikov, 1988b).

The above literature review does not pretend to be complete. We refer readers to the survey articles by Grigolyuk and Kulikov (1988a); Kapania (1989); Kapania and Raciti (1989a,b); Soldatos and Timarci (1993); Altenbach (1998); Toorani and Lakis (2000); Reddy (1993); Reddy and Wang (2000); Carrera (2002, 2003a); Qatu (2002); Qatu et al (2010); Atteshamuddin et al (2015); Caliri et al (2016), and books by Qatu (2004); Reddy (2004); Gorshkov et al (2005). One should also mention Carrera (2003b); Demasi et al (2017) where a unified formulation is proposed and models, types and classes of theories for laminated plates and shells are described.

Completing the short overview of existing theories for laminated shells, we draw attention to the approach developed by Grigolyuk and Kulikov (1988b) which will be used below. This ESL theory is based on the generalized kinematical hypotheses of Timoshenko for the in-plane displacements u_1, u_2 of the reference surface and the parabolic distribution of transverse shear stresses through both each layer thickness and the entire shell thickness. It complies with the traction-free boundary conditions on the top and bottom surfaces of a laminated shell and guaranties the continuity of transverse shear stresses in the direction of the thickness coordinate z. Recently, this model was adapted by Mikhasev et al (2011) to laminated cylindrical shells composed of smart materials (magnetorheological elastomers and electrorheological composites). The choice of this theory can be explained by the following items:

- if the stress and strain state of a shell has a large variability, even if by one coordinate, then the full system of differential equations w.r.t. five unknowns is readily

simplified and reduced to three equations written in terms of the displacement, stress and shear functions χ, Φ, ϕ;
- the governing equations written in terms of χ, Φ, ϕ completely coincide with similar equations derived by Tovstik and Tovstik (2007, 2017) from the 3D theory of elasticity, the assumed model unifying the simple equations of the Mushtary-Donnell-Vlasov technical theory and the HSDT equations;
- this theory is simple enough for prediction of the mechanical behavior of multi-layered shells, including smart structures;
- the accuracy of the governing equations has been verified by finite element simulations (s. Mikhasev et al, 2001; Korchevskaya et al, 2004; Mikhasaev et al, 2004).

References

Akoussan K, Hamdaoui M, Daya EM (2017) Improved layer-wise optimization algorithm for the design of viscoelastic composite structures. Composite Structures 176:342 – 358

Altenbach H (1998) Theories for laminated and sandwich plates. A review. Mechanics of Composite Materials 34(3):243–252

Altenbach H, Eremeyev VA (eds) (2011) Shell-like Structures: Non-classical Theories and Applications, Advanced Structured Materials, vol 15. Springer Science & Business Media, Berlin, Heidelberg

Altenbach H, Meenen J (2008) On the different possibilities to derive plate and shell theories. In: Jaiani G, Podio-Guidugli P (eds) IUTAM Symposium on Relations of Shell Plate Beam and 3D Models, Springer Netherlands, Dordrecht, pp 37–47

Altenbach H, Mikhasev GI (eds) (2014) Shell and Membrane Theories in Mechanics and Biology: From Macro- to Nanoscale Structures, Advanced Structured Materials, vol 45. Springer, Cham

Altenbach H, Naumenko K, L'vov GI, Pilipenko SN (2003) Numerical estimation of the elastic properties of thin-walled structures manufactured from short-fiber-reinforced thermoplastics. Mechanics of Composite Materials 39(3):221–234

Altenbach H, Naumenko K, Pylypenko S (2005) On the numerical prediction of the anisotropic elastic properties in thin-walled structures made from short-fiber reinforced plastics. Computer Assisted Mechanics and Engineering Sciences 12(4):329–339

Altenbach H, Altenbach J, Naumenko K (2016) Ebene Flächentragwerke, 2nd edn. Springer, Cham

Altenbach H, Altenbach J, Kissing W (2018) Mechanics of Composite Structural Elements, 2nd edn. Springer, Berlin, Heidelberg

Altenbach J, Kissing W, Altenbach H (1994) Dünnwandige Stab- und Stabschalentragwerke. Grundlagen und Fortschritte der Ingenieurwissenschaften, Vieweg, Braunschweig/Wiesbaden

Altenbach J, Altenbach H, Eremeyev VA (2010) On generalized Cosserat-type theories of plates and shells: a short review and bibliography. Archive of Applied Mechanics 80(1):73–92

Amabili M (2015) A new third-order shear deformation theory with non-linearities in shear for static and dynamic analysis of laminated doubly curved shells. Composite Structures 128:260–273

Ambartsumyan SA (1970) Theory of Anisotropic Plates. Technomic Publishing, Stamford

Aron H (1874) Das Gleichgewicht und die Bewegung einer unendlich dünnen, beliebig gekrümmten elastischen Schale. Journal für die reine und angewandte Mathematik 78:136–174

Aßmus M (2019) Structural Mechanics of Anti-Sandwiches - An Introduction. SpringerBriefs in Continuum Mechanics, Springer International Publishing

Atteshamuddin S, Sayyad, Ghugal YM (2015) On the free vibration analysis of laminated composite and sandwich plates: A review of recent literature with some numerical results. Composite Structures 129:177–201

Auricchio F, Sacco E (2003) Refined first-order shear deformation theory models for composite laminates. J Appl Mech 70(3):381–390

Aydogdu M (2009) A new shear deformation theory for laminated composite plates. Composite Structures 89:94–101

Balah M, Al-Ghemady H (2005) Energy-momentum conserving algorithm for nonlinear dynamics of laminated shells based on a third-order shear deformation theory. Journal of Engineering Mechanics 131(1):12–22

Barbero E, Reddy J, Teply J (1990) General two-dimensional theory of laminated cylindrical shells. AIAA J 28(3):544–553

Batra R, Vidoli S (2002a) Closed-form thermo-mechanical solutions of higher-order theories of cross-ply laminated shallow shells. Composite Structures 40(1):91–104

Batra RC, Vidoli S (2002b) Higher-order piezoelectric plate theory derived from a three-dimensional variational principle. AIAA J 40(1):91–104

Bert CW (1973) Simplified analysis of static shear correction factors for beams of nonhomogeneous cross section. Journal of Composite Materials 7:525–529

Bert CW (1976) Dynamics of composite and sandwich panels-Parts I and II (corrected title). Shock Vib Dig 8(11):15–24

Bert CW (1980) Analysis of shells. In: Broutman LJ (ed) Analysis and Performance of Composites, Wiley, New York, pp 207–258

Bolotin VV, Novichkov YN (1980) Mechanics of Multilayer Structures (in Russ.). Mashinostroenie, Moscow

Braga AMB, Rivas ACE (2005) High-frequency response of isotropic-laminated cylindrical shells modeled by a layer-wise theory. Int J Solids Struct 42(14):4278–4294

Caliri MF, Ferreira AJ, Tita V (2016) A review on plate and shell theories for laminated and sandwich structures highlighting the finite element method. Composite Structures 156:63 – 77

Carrera E (1998a) Evaluation of layerwise mixed theories for laminated plates analysis. AIAA J 36(5):830–839

Carrera E (1998b) Layer-wise mixed models for accurate vibration analysis of multilayered plates. J Appl Mech 65(4):820–828

Carrera E (2001) Developments, ideas, and evaluations based upon Reissner's mixed variational theorem in the modeling of multilayered plates and shells. Applied Mechanics Reviews 54(4):301–329

Carrera E (2002) Theories and finite elements for multilayered, anisotropic, composite plates and shells. Archives of Computational Methods in Engineering 9(2):87–140

Carrera E (2003a) Historical review of zig-zag theories for multilayered plates and shells. Appl Mech Rev 56(3):287–308

Carrera E (2003b) Theories and finite elements for multilayered plates and shells: A unified compact formulation with numerical assessment and benchmarking. Archives of Computational Methods in Engineering 10(3):215–296

Carrera E, Cinefra M, Lamberti A, Petrolo M (2015) Results on best theories for metallic and laminated shells including layer-wise models. Composite Structures 126:285 – 298

Cetkovic M (2015) Thermo-mechanical bending of laminated composite and sandwich plates using layerwise displacement model. Composite Structures 125:388 – 399

Cheung YK, Wu C (1972) Free vibrations of thick, layered cylinders having finite lengthwith various boundary conditions. J Sound Vib 24:189–200

Cho K, Bert C, Striz A (1991) Free vibrations of laminated rectangular plates analyzed by higher order individual-layer theory. J Sound Vib 145:429–442

Chow TS (1971) On the propagation of flexural waves in an orthotropic laminated plate and its response to an impulse load. Journal of Composite Materials 5:306–319

Demasi L (2009) ∞^6 mixed plate theories based on the generalized unified formulation. Part II: Layerwise theories. Composite Structures 87(1):12–22

Demasi L, Biagini G, Vannucci F, Santarpia E, Cavallaro R (2017) Equivalent single layer, zig-zag, and layer wise theories for variable angle tow composites based on the generalized unified formulation. Composite Structures 177:54 – 79

Dong K, Wang X (2007) The effect of transverse shear, rotary inertia on wave propagation in laminated piezoelectric cylindrical shells in thermal environment. J Reinforc Plast Compos 26:1523–1538

Dong SB, Tso FKW (1972) On a laminated orthotropic shell theory including transverse shear deformation. J Appl Mech 39:1091–1096

Dong SB, Pister K, Taylor RL (1962) On the theory of laminated anisotropic shells and plates. Journal of Aerospase Science 29(8):969–975

Donnell LH (1976) Beams, Plates and Shells. McGraw-Hill Inc, New York

Flores FG, Oller S, Nallim LG (2018) On the analysis of non-homogeneous laminates using the refined zigzag theory. Composite Structures 204:791 – 802

Flügge W (1973) Stresses in Shells, 2nd edn. Springer, Berlin, Heidelberg

Ganapathi M, Haboussi M (2003) Free vibrations of thick laminated anisotropic noncircular cylindrical shells. Composite Structures 60:125–133

Ganapathi M, Patel B, Pawargi D (2002) Dynamic analysis of laminated cross-ply composite non-circular thick cylindrical shells using higher-order theory. Int J Solids Struct 39:5945–5962

Gaudenzi P, Barboni R, Mannini A (1995) Free vibration analysis of laminated plates using a layer-wise theory. Composite Structures 30:427–440

Gorshkov AG, Starovoitov EI, Yarovaya AB (2005) Mechanics of Laminated Viscoelastoplastic Elements of Constructions (in Russ.). Fizmatlit, Moscow

Green AE, Naghdi PM, Wainwright WL (1965) A general theory of a Cosserat surface. Archive for Rational Mechanics and Analysis 20(4):287–308

Grigolyuk EI, Kulikov GM (1988a) General direction of development of the theory of multilayered shells. Mechanics of Composite Materials 24(2):231–241

Grigolyuk EI, Kulikov GM (1988b) Multilayered Reinforced Shells. Calculation of Pneumatic Tires (in Russ.). Mashinostroenie, Moscow

Grigolyuk EI, Seleznev IT (1973) Nonclassical Theories of Oscillations of Rods, Plates, and Shells (in Russ.), Itogi Nauki i Tekhniki. Ser. Mekh. Tverdogo Deformir. Tela, vol 5. VINITI, Moscow

Gupta M, Wang KK (1993) Fiber orientation and mechanical properties of short-fiber-reinforced injection-molded composites: Simulated and experimental results. Polymer Composites 14(5):367–382

Gurtin ME, Murdoch IA (1975) A continuum theory of elastic material surfaces. Archive for Rational Mechanics and Analysis 57(4):291–323

Hashin Z (1991) Thermoelastic properties of particulate composites with imperfect interface. Journal of the Mechanics and Physics of Solids 39(6):745–762

Hencky H (1947) Über die Berücksichtigung der Schubverzerrung in ebenen Platten. Ingenieur-Archiv 16(1):72–76

Hildebrand FB, Reissner E, Thomas GB (1949) Note on the foundations of the theory of small displacements of orthotropic shells. National Advisory Comm Aero Tech Notes, No 1833

Hill R (1963) Elastic properties of reinforced solids: Some theoretical principles. Journal of the Mechanics and Physics of Solids 11(5):357–372

Hill R (1964) Theory of mechanical properties of fibre-strengthened materials: I. elastic behaviour. Journal of the Mechanics and Physics of Solids 12(4):199–212

Hsu TM, Wang JTS (1970) A theory of laminated cylindrical shells consisting of layers of orthotropic laminae. AIAA J 8(12):2141–2046

Iurlaro L, Gherlone M, Sciuva MD, Tessler A (2015) Refined zigzag theory for laminated composite and sandwich plates derived from reissner's mixed variational theorem. Composite Structures 133:809 – 817

Jaiani G, Podio-Guidugli P (eds) (2008) IUTAM Symposium on Relations of Shell, Plate, Beam and 3D Models, IUTAM Bookseries, vol 9. Springer Science & Business Media, Dordrecht

Kapania RK (1989) A review on the analysis of laminated shells. J Press Vessel Technol 111(2):88–96

Kapania RK, Raciti S (1989a) Recent advances in analysis of laminated beams and plates. Part I - Shear effects and buckling. AIAA J 27(7):923–934

Kapania RK, Raciti S (1989b) Recent advances in analysis of laminated beams and plates. Part II: Vibrations and Wave Propagation. AIAA J 27(7):935–946

Karama M, Afaq K, Mistou S (2009) A new theory for laminated composite plates. Proceedings of the Institution of Mechanical Engineers, Part L: Journal of Materials: Design and Applications 223(2):53–62

Khare R, Rode V (2005) Higher-order closed-form solutions for thick laminated sandwich shells. Journal of Sandwich Structures & Materials 7(4):335–358

Khare RK, Kant T, Garg AK (2003) Closed-form thermo-mechanical solutions of higher-order theories of cross-ply laminated shallow shells. Composite Structures 59(3):313–340

Kienzler R (1982) Erweiterung der klassischen Schalentheorie; der Einfluß von Dickenverzerrung und Querschnittsverwölbungen. Ingenieur-Archiv 52:311–322

Kienzler R (2002) On consistent plate theories. Arch Appl Mech 72:229–247

Kienzler R, Schneider P (2016) Direct approach versus consistent theory. In: Naumenko K, Aßmus M (eds) Advances Methods of Continuum Mechanics for Materials and Structures, Advanced Structured Materials, vol 60, Springer, Singapore, pp 415–433

Kienzler R, Altenbach H, Ott I (eds) (2004) Critical Review of the Theories of Plates and Shells, New Applications, Lect. Notes Appl. Comp. Mech., vol 16, Springer, Berlin

Kirchhoff G (1883) Vorlesungen über Mathematische Physik, vol 1: Mechanik. B. G. Teubner, Leipzig

Kirchhoff GR (1850) Über das Gleichgewicht und die Bewegung einer elastischen Scheibe. Crelles Journal für die reine und angewandte Mathematik 40:51–88

Korchevskaya E, Mikhasaev G, Marinkovic D, Gabbert U (2004) Buckling and vibrations of composite laminated cylindrical shells under axial load. In: Proc. of "6th Magdeburg Days of Mechanical Engineering", Otto-von-Guericke-University Magdeburg, Logos, Berlin, pp 183–189

Kordkheili SAH, Soltani Z (2018) A layerwise finite element for geometrically nonlinear analysis of composite shells. Composite Structures 186:355 – 364

Kulikov GM, Plotnikova SV (2013) Advanced formulation for laminated composite shells: 3D stress analysis and rigid-body motions. Comp Struct 95:236–246

Leissa AW (1973) Vibration of Shells. US Government Printing Office, Washington

Levinson M (1980) An accurate, simple theory of the statics and dynamics of elastic plates. Mech Res Comm 7(6):343–350

Libai A, Simmonds JG (1998) The Nonlinear Theory of Elastic Shells, 2nd edn. Cambridge University Press, Cambridge

Librescu L, Khdeir AA (1988) Analysis of symmetric cross-ply laminated elastic plates using a higher-order theory. Part I: Stress and displacement. Composite Structures 9(3):189–213

Librescu L, Khdeir AA, Reddy JN (1987) A comprehensive analysis of state of stress of elastic anisotropic flat plates using refined theories. Acta Mechanica 70(1-4):57–81

Lo KH, Christensen RM, Wu EM (1977) A higher-order theory of plate deformation, Part 1: Homogeneous plates. Trans ASME J Appl Mech 44:663–668

Love AEH (1888) XVI. On the small free vibrations and deformations of the elastic shells. Phil Trans Roy Soc London, Ser A 179:491–546

Love AEH (1906) A Treatise on the Mathematical Theory of Elasticity, 2nd edn. University Press, Cambridge

Lurie AI (1947) Statics of Thin Elastic Shells (in Russ.). Gostekhizdat, Moscow

Malekzadeh P, Fiouz AR, Razi H (2009) Three-dimensional dynamic analysis of laminated composite plates subjected to moving load. Composite Structures 90(2):105–114

Mallikarjuna, Kant T (1993) A critical review and some results of recently developed refined theories of fiber-reinforced laminated composites and sandwiches. Composite Structures 23:293–312

Mallikarjuna, Kant T (2002) Analytical solutions for the static analysis of laminated composite and sandwich plates based on a higher order refined theory. Composite Structures 56:329–344

Mantari J, Oktem A, Guedes Soares C (2011a) A new higher order shear deformation theory for sandwich and composite laminated plates. Composites: Part B 43(3):1489–1499

Mantari J, Oktem A, Guedes Soares C (2011b) Static and dynamic analysis of laminated composite and sandwich plates and shells by using a new higher-order shear deformation theory. Composite Structures 94:37–49

Meenen J, Altenbach H (2001) A consistent deduction of von Kármán-type plate theories from threedimensional non-linear continuum mechanics. Acta Mechanica 147:1–17

Mikhasaev G, Korchevskaya E, Gabbert U, Marinkovic D (2004) Local buckling, stationary and non-stationary vibrations of the composite laminated shells having the weakest spots. In: Proc. of "Fourth International Conference on Thin-Walled Structures, ICTWS", London, pp 769–776

Mikhasev GI, Seeger F, Gabbert U (2001) Comparison of analytical and numerical methods for the analysis of buckling and vibrations of composite shell structures. In: Proc. of "5th Magdeburg Days of Mechanical Engineering", Otto-von-Guericke-University Magdeburg, Logos, Berlin, pp 175–183

Mikhasev GI, Botogova MG, Korobko EV (2011) Theory of thin adaptive laminated shells based on magnetorheological materials and its application in problems on vibration suppression. In: Altenbach H, Eremeyev V (eds) Shell-like Structures, Springer, Heidelberg, Advanced Structured Materials, vol 15, pp 727–750

Mindlin RD (1951) Influence of rotatory inertia and shear on flexural motions of isotropic elastic plates. Trans ASME J Appl Mech 18:31–38

Moita JS, Araújo AL, Correia VF, Soares CMM, Herskovits J (2018) Active-passive damping in functionally graded sandwich plate/shell structures. Composite Structures 202:324–332

Moreira R, Rodrigues J, Ferreira A (2006) A generalized layerwise finite element for multi-layer damping treatments. Comput Mech 37:426–444

Murakami H (1986) Laminated composite plate theory with improved in-plane responses. J Appl Mech 53:661–666

Murdoch AI (2005) Some fundamental aspects of surface modelling. Journal of Elasticity 80(1):33–52

Mushtari KM, Galimov KZ (1961) Nonlinear Theory of Thin Elastic Shells. NSF-NASA, Washington

Naghdi PM (1956) A survey of recent progress in the theory of elastic shells. Appl Mech Reviews 9(9):356–368

Naghdi PM (1972) The Theory of Shells and Plates. In: Flügge S (ed) Handbuch der Physik, vol VIa/2, Springer, New York, pp 425–640

Naumenko K, Eremeyev VA (2014) A layer-wise theory for laminated glass and photovoltaic panels. Composite Structures 112:283 – 291

Naumenko K, Eremeyev VA (2017) A layer-wise theory of shallow shells with thin soft core for laminated glass and photovoltaic applications. Composite Structures 178:434 – 446

Nazarenko L, Stolarski H, Altenbach H (2018a) Effective properties of particulate composites with surface-varying interphases. Composites Part B: Engineering 149:268–284

Nazarenko L, Stolarski H, Altenbach H (2018b) Thermo-elastic properties of random composites with unidirectional anisotropic short-fibers and interphases. European Journal of Mechanics - A/Solids 70:249–266

Nikbakht S, Salami SJ, Shakeri M (2017) Three dimensional analysis of functionally graded plates up to yielding, using full layer-wise finite element method. Composite Structures 182:99 – 115

Novozhilov V (1970) Theory of Thin Shells. Wolters-Noordhoff, Groningen

Oh I (2007) Dynamic characteristics of cylindrical hybrid panels containing viscoelastic layer based on layerwise mechanics. Composites Part B: Eng 38:159–171

Pagano NJ (1969) Exact solutions for composite laminates in cylindrical bending. Journal of Composite Materials 3:398–411

Pagano NJ (1970) Exact solutions for rectangular bidirectional composites and sandwich plates. Journal of Composite Materials 4:20–34

Palmow WA, Altenbach H (1982) Über eine Cosseratsche Theorie für elastische Platten. Technische Mechanik 3(3):5–9

Preußer G (1984) Eine systematische Herleitung verbesserter Plattentheorien. Ingenieur-Archiv 54:51–61

Qatu MS (1999) Accurate equations for laminated composite deep thick shells. Int J Solids Struct 36(19):2917–2941
Qatu MS (2002) Recent research advances in the dynamic behavior of shells: 1989-2000. Part 1: Laminated composite shells. Applied Mechanics Review 55(4):325–350
Qatu MS (2004) Vibration of laminated shells and plates. Elsevier, San Diego
Qatu MS, Sullivan RW, Wang W (2010) Recent research advances on the dynamic analysis of composite shells: 2000-2009. Composite Structures 93(1):14–31
Qu Y, Long X, Wu S, Meng G (2013) A unified formulation for vibration analysis of composite laminated shells of revolution including shear deformation and rotary inertia. Comp Struct 98:169–191
Reddy J, Robbins D (1994) Theories and computational models for composite laminates. Appl Mech Rev 47(6):147–165
Reddy JN (1984a) A refined nonlinear theory of plates with transverse shear deformation. Int J Solids Struct 20(9/10):881–896
Reddy JN (1984b) A simple higher-order theory for laminated composite plates. Trans ASME J Appl Mech 51(4):745–752
Reddy JN (1993) An evaluation of equivalent-single-layer and layerwise theories of composite laminates. Composite Structures 25:21–35
Reddy JN (2004) Mechanics of Laminated Composite Plates and Shells: Theory and Analysis, 2nd edn. CRC Press, Boca Raton
Reddy JN, Liu CF (1985) A higher-order shear deformation theory of laminated elastic shells. Int J Eng Sci 23(3):319–330
Reddy JN, Wang CM (2000) An overview of the relationships between of the classical and shear deformation plate theories. Compos Sci Technol 60:2327–2335
Reissner E (1944) On the theory of bending of elastic plates. J Math Phys 23:184–194
Reissner E (1945) The effect of transverse shear deformation on the bending of elastic plates. Trans ASME J Appl Mech 12(11):A69–A77
Reissner E (1952) Stress-strain relations in the theory of thin elastic shells. J Math Phys 31:109–119
Reissner E (1975) On transverse bending of plates, including the effect of transverse shear deformation. Int J Solids Struct 11:569–573
Reissner E (1985) Reflection on the theory of elastic plates. Applied Mechanics Review 38(11):1453–1464
Reissner E, Stavsky Y (1961) Bending and stretching of certain types of heterogeneous aeolotropic elastic plates. Trans ASME J Appl Mech 28(3):402–408
Reissner E, Wan FYM (1982) A note on the linear theory of shallow shear deformable shell. Zeitschrift für angewandte Mathematik und Physik ZAMP 33(3):425–427
Ribeiro P (2009) On the influence of membrane inertia and shear deformation on the geometrically nonlinear vibrations of open, cylindrical, laminated clamped shells. Compos Sci Technol 69:176–185
Rothert H (1973) Direkte Theorie von Linien- und Flächentragwerken bei viskoelastischen Werkstoffverhalten. Techn.-Wiss. Mitteilungen des Instituts für Konstruktiven Ingenieurbaus 73-2, Ruhr-Universität, Bochum
Sahoo R, Singh B (2014) A new trigonometric zigzag theory for buckling and free vibration analysis of laminated composite and sandwich plates. Composite Structures 117:316 – 332
Saito M, Kukula S, Kataoka Y (1998) Practical use of the statistically modified laminate model for injection moldings. Part 1: Method and verification. Polymer Composites 19(5):497–505
Saito M, Kukula S, Kataoka Y, Miyata T (2000) Practical use of statistically modified laminate model for injection moldings. Materials Science and Engineering: A 285(1):280–287
Sanders JL (1959) An improved first approximation theory for thin shells. NASA Report 24, NASA, Washington, DC
Saviz MR, Shakeri M, Yas MH (2007) Electrostatic fields in a layered piezoelectric cylindrical shell under dynamic load. Smart Mater Struct 16:1683–1695
Schneider P, Kienzler R, Böhm M (2014) Modeling of consistent second-order plate theories for anisotropic materials. ZAMM - Journal of Applied Mathematics and Mechanics 94(1-2):21–42

Schulze SH, Pander M, Naumenko K, Altenbach H (2012) Analysis of laminated glass beams for photovoltaic applications. International Journal of Solids and Structures 49(15):2027–2036
Shakeri M, Eslami MR, Daneshmehr A (2006) Dynamic analysis of thick laminated shell panel with piezoelectric layer based on three dimensional elasticity solution. Comput Struct 84:1519–1526
Shi P, Dong C, Sun F, Liu W, Hu Q (2018) A new higher order shear deformation theory for static, vibration and buckling responses of laminated plates with the isogeometric analysis. Composite Structures 204:342 – 358
Soldatos KP, Timarci T (1993) A unified formulation of laminated composites, shear deformable, five-degrees-of-freedom cylindrical shell theories. Composite Structures 25:165–171
Srinivas S (1973) A refined analysis of composite laminates. J Sound Vib 30(4):495–550
Srinivas SR, Joga Rao CV, Rao AK (1970) An exact analysis for vibration of simply-supported homogeneous and laminated thick rectangular plates. J Sound Vibr 12:187–199
Starovoitov EI, Leonenko DV (2010) Free and resonant vibrations of circular three-layer plate. Engineering&Automation Problems 1(1):98 – 103
Stavsky Y (1961) Bending and stretching of laminated aeolotropic plates. Proceedings of the American Society of Cicil Engineers, Journal of Engineering Mechanics Division 8:31–56
Sun CT (1971) Theory of laminated plates. Trans ASME J Appl Mech 38(1):231–238
Sun CT, Whitney JM (1973) On the theories for the dynamic response of laminated plates. AIAA J 11(2):372–398
Swaminathan R, Ragounadin D (2004) Analytical solutions using a higher-order refined theory for the static analysis of antisymmetric angle-ply composite and sandwich plates. Composite Structures 64:405–417
Timoshenko SP (1921) LXVI. On the correnction for shear of the differential equation for transverse vibrations of prismatic bar. The London, Edinburgh, and Dublin Philosophical Magazine and Journal of Science 41(245):744–746
Toorani MH, Lakis AA (2000) General equations of anisotropic plates and shells including transverse shear deformations, rotary inertia and initial curvature effects. J Sound Vibr 237(4):561–615
Toorani MH, Lakis AA (2001) Shear deformation in dynamic analysis of anisotropic laminated open cylindrical shells filled with or subjected to a flowing fluid. Comput Methods Appl Mech Eng 190:4929–4966
Touratier M (1991) An efficient standard plate theory. Int J Eng Sci 29(8):901–916
Tovstik PE, Tovstik TP (2007) On the 2D models of plates and shells including the transversal shear. ZAMM - Journal of Applied Mathematics and Mechanics 87(2):160–171
Tovstik PE, Tovstik TP (2017) Equations of equilibrium for a strongly heterogeneous shallow shell. Doklady Physics 62(11):522–526
Treviso A, Mundo D, Tournour M (2017) Dynamic response of laminated structures using a refined zigzag theory shell element. Composite Structures 159:197 – 205
Vekua I (1985) Shell Theory: General Methods of Construction. Pitman, Boston
Viola E, Tornabene F, Fantuzzi N (2013) General higher-order shear deformation theories for the free vibration analysis of completely doubly-curved laminated shells and panels. Composite Structures 95:639–666
Vlachoutsis S (1992) Shear correction factors for plates and shells. International Journal for Numerical Methods in Engineering 33:1537–1552
Vlasov VZ (1944) The principal differential equations of the general shells theory (in Russ.). Prikl Mat Mech 8(2):109–140
Wang Q, Shao D, Qin B (2018) A simple first-order shear deformation shell theory for vibration analysis of composite laminated open cylindrical shells with general boundary conditions. Composite Structures 184(15):211–232
Wang X, Lu G, Guillow SR (2002) Stress wave propagation in orthotropic laminated thick-walled spherical shells. Int J Solids Struct 39:4027–4037
Weps M, Naumenko K, Altenbach H (2013) Unsymmetric three-layer laminate with soft core for photovoltaic modules. Composite Structures 105:332–339

Whitney JM (1973) Shear correction factors for orthotropic laminates under static load. Trans ASME J Appl Mech 40(1):302–304
Whitney JM, Leissa AW (1969) Analysis of heteregeneous anisotropic plates. Trans ASME J Appl Mech 36(2):261–266
Whitney JM, Pagano NJ (1970) Shear deformation in heterogeneous anisotropic plates. Trans ASME J Appl Mech 37(4):1031–1036
Whitney JM, Sun CT (1973) A higher order theory for extensional motion of laminated anisotropic shells and plates. J Sound Vibr 30(1):85–97
Whitney JM, Sun CT (1974) A refined theory of laminated anisotropic cylindrical shells. Trans ASME J Appl Mech 41(2):471–476
Wittrick WH (1987) Analytical three-dimensional elasticity solutions to some plate problems and some observations on Mindlin's plate theory. International Journal of Solid and Structures 23(4):441–464
Wu Y, Xing Y, Liu B (2018) Analysis of isotropic and composite laminated plates and shells using a differential quadrature hierarchical finite element method. Composite Structures 205:11 – 25
Yang PC, Norris CH, Stavsky Y (1966) Elastic wave propagation in heterogeneous plates. International Journal of Solids and Structures 2:665–684
Yasin M, Kapuria S (2013) An efficient layerwise finite element for shalow composite and sandwich shells. Composite Structures 98:202–2014
Zhilin PA (1976) Mechanics of deformable directed surfaces. Int J Solids Struct 12:635–648
Zukas JA, Vinson JR (1971) Laminated transversely isotropic cylindrical shells. Trans ASME J Appl Mech 34:400–407

Chapter 2
Equivalent Single Layer Model for Thin Laminated Cylindrical Shells

Abstract In this chapter we consider the equivalent single layer model for thin multi-layered cylindrical shells. It is based on the generalized Timoshenko hypotheses and results in nonlinear governing equations for the whole stacked sequence of an elastic laminated shell. Considering variations of the nonlinear equations, we derive buckling equations of a thin elastic laminated shell loaded with static conservative loads. The derived dynamic equations are adapted for the case when a shell is assembled from elastic and viscoelastic layers with properties represented by a complex shear modulus. Viscoelastic layers or cores are assumed to be made of smart materials, such as magnetorheological elastomers and electrorheological composites. The reader can become acquainted with elastic and rheological properties of some smart viscoelastic materials which may be used as damping elements of smart thin-walled laminated shells.

2.1 Equations of Thin Elastic Laminated Cylindrical Shells

In this section we consider principle hypotheses for the two-dimensional theory taking into account transverse shear, the strain-displacement and constitutive relations. Applying a mixed variational principle, the nonlinear equations describing the motion of an elastic laminated cylindrical shell and the natural boundary conditions as well are deduced. For cases when vibrations occur with formation of short waves, the full system of equations is reduced to the simplified system of three differential equations for the stress, displacement and shear functions. The edge effect equations taking into account transverse shear are obtained. The asymptotic error of the derived equations is shortly discussed.

G. I. Mikhasev and H. Altenbach, *Thin-walled Laminated Structures*,
Advanced Structured Materials 106, https://doi.org/10.1007/978-3-030-12761-9_2

2.1.1 Laminated Cylindrical Shell

Consider a thin non-circular laminated cylindrical shell (s. Fig. 2.1) consisting of N transversely isotropic layers characterized by the following parameters: length L, thickness h_k, density ρ_k, Young's modulus E_k, shear modulus G_k, and Poisson's ratio ν_k, where $k = 1, 2, \ldots, N$ are the number of layers. It is assumed that each layer has a constant thickness.

The middle surface of any fixed layer is taken as the reference surface. We introduce a local orthogonal coordinate system by means of unit vectors $\boldsymbol{e}_1, \boldsymbol{e}_2$ and $\boldsymbol{n} = \boldsymbol{e}_1 \times \boldsymbol{e}_2$ with origin in the point O as shown in Fig. 2.1. Let α_1 and α_2 be the axial and circumferential coordinates, respectively, and $\alpha_3 = z$ is the normal coordinate. The radius of curvature of the reference surface is $R_2 = 1/k_{22}(\alpha_2)$. The shell is bounded by two not necessarily plane edges

$$\alpha_1^*(\alpha_2) \le \alpha_1 \le \alpha_1^{**}(\alpha_2) \tag{2.1}$$

and may be not closed in the direction of α_2 (the case of a non-circular cylindrical panel).

In this section, we assume that every layer is made of an elastic material which may be inhomogeneous. Then the Young's moduli E_k and Poisson's ratios ν_k are real numbers which may depend on the curvilinear coordinates α_1, α_2. Below, laminated shells and sandwiches with viscoelastic layers and cores will be also considered. In particular, we discuss the case when a sandwich is formed by embedding a magnetorheological elastomer or electrorheological composite between elastic layers. In this case parameters E_k and G_k corresponding to the viscoelastic laminas with adaptive elastic and viscous properties will be considered as complex functions of α_1, α_2 and time t.

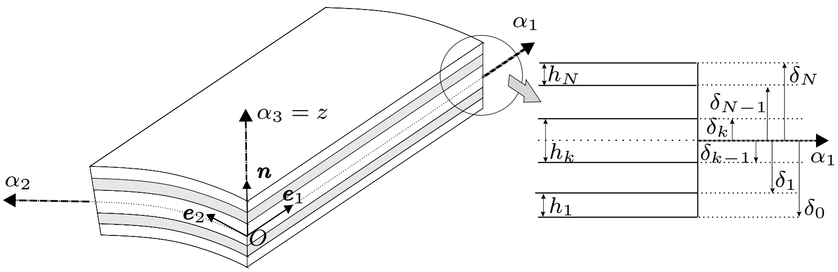

Fig. 2.1 Laminated cylindrical shell with a curvilinear coordinate system.

2.1.2 Principal Hypotheses

Now we introduce some additional notations. Let $z = \delta_k$ be the coordinate of the upper bound of the k^{th} layer, and $z = \delta_0$ is the coordinate of the inner surface of the shell, u_i and w are the tangential and normal displacements of points on the reference surface of the shell, respectively,

$$h = \sum_{k=1}^{N} h_k$$

is the total thickness of the laminate, $u_i^{(k)}$ are the tangential displacements of points of the k^{th} layer, σ_{i3} are the transverse shear stresses (s. Fig. 2.2), θ_i are the angles of rotation of the normal $\boldsymbol{n}$ about the vector $\boldsymbol{e}_i$ (s. Fig. 2.1). Here $i = 1, 2$; $k = 1, 2, \ldots, N$.

The following hypotheses of the laminated shell theory stated in Grigolyuk and Kulikov (1988) are assumed here:

1. The distribution law of the transverse tangent stresses across the thickness of the k^{th} layer is assumed to be of the form

$$\sigma_{i3} = f_0(z)\mu_i^{(0)}(\alpha_1, \alpha_2, t) + f_k(z)\mu_i^{(k)}(\alpha_1, \alpha_2, t)\ , \tag{2.2}$$

   where t is time, $f_0(z), f_k(z)$ are continuous functions introduced as follows

$$\begin{aligned} f_0(z) &= \frac{1}{h^2}(z-\delta_0)(\delta_N - z) && \text{for } z \in [\delta_0, \delta_N], \\ f_k(z) &= \frac{1}{h_k^2}(z-\delta_{k-1})(\delta_k - z) && \text{for } z \in [\delta_{k-1}, \delta_k], \\ f_k(z) &= 0 && \text{for } z \notin [\delta_{k-1}, \delta_k]. \end{aligned} \tag{2.3}$$

2. Normal stresses acting on the area elements parallel to the original one are negligible with respect to the other components of the stress tensor.

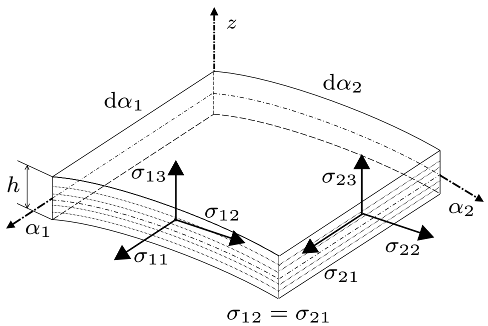

Fig. 2.2 Infinitesimal element of a laminated shell, reference surface and stresses (after Mikhasev and Botogova, 2017).

3. The deflection $w(\alpha_1, \alpha_2, t)$ does not depend on the coordinate z.
4. The tangential (in-plane) displacements are distributed across thickness of the layer package according to the generalized kinematic Timoshenko hypotheses

$$u_i^{(k)}(\alpha_1, \alpha_2, z, t) = u_i(\alpha_1, \alpha_2, t) + z\theta_i(\alpha_1, \alpha_2, t) + g(z)\psi_i(\alpha_1, \alpha_2, t), \quad (2.4)$$

where

$$g(z) = \int_0^z f_0(x)\mathrm{d}x.$$

In Eq. (2.4), ψ_i are required parameters characterizing the transverse shear in the shell. Hypothesis (2.4) permits to describe the non-linear dependence of the tangential displacements on z; at $g \equiv 0$ it turns into the linear Timoshenko hypotheses coinciding with the classical Kirchhoff-Love hypotheses if θ_i are functions of the tangential displacements and derivatives of the deflection.

In what follows, it will be shown that the functions $\mu_i^{(0)}(\alpha_1, \alpha_2), \mu_i^{(k)}(\alpha_1, \alpha_2)$ are coupled with the vector $\bar{\Psi} = (\psi_1, \psi_2)^{\mathrm{T}}$ and depend on elements of a matrix characterizing the shear deformability of the k^{th} layer. So, in the theory developed by Grigolyuk and Kulikov (1988) and based on the above hypothesis, the five components $w, u_i, \psi_i (i = 1, 2)$ are assumed to be independent functions, and θ_i are defined in the derivatives of the deflection w.

2.1.3 Strain-displacement Relations

We assume that the shell deformation under buckling or vibrations is accompanied by the formation of a large number of waves so that the shell may be considered as shallow one within the limits of one half-wave. Then, $\theta_i \approx -w_{,i}$, and taking into account the hypotheses accepted above, the strain-displacement relations will be as follows (Grigolyuk and Kulikov, 1988):

$$u_i^{(k)} = u_i - zw_{,i} + g(z)\psi_i, \qquad i, j = 2, \quad (2.5)$$

$$\epsilon_{ij} = e_{ij} + z\,\kappa_{ij} + g(z)\psi_{ij}, \;\; \epsilon_{i3} = f_0(z)\psi_i, \quad (2.6)$$

where

$$\begin{aligned} e_{ij} &= \frac{1}{2}(u_{i,j} + u_{j,i} + w_{,i}w_{,j}) + k_{ij}w, \\ \psi_{ij} &= \frac{1}{2}(\psi_{i,j} + \psi_{j,i}), \quad \kappa_{ij} = -w_{,ij}, \\ k_{11} &= k_{12} = 0, \quad k_{22} = \frac{1}{R_2(\alpha_2)}. \end{aligned} \quad (2.7)$$

Here, the differentiation with respect to the coordinate α_i is designated as $(\ldots)_{,i}$.

2.1.4 Constitutive Equations for Elastic Materials

Let us introduce the vectors

$$\bar{\sigma} = (\sigma_{11}, \sigma_{22}, \sigma_{12})^{\mathrm{T}}, \quad \bar{\epsilon} = (\epsilon_{11}, \epsilon_{22}, \epsilon_{12})^{\mathrm{T}} \tag{2.8}$$

of the tangential (with respect to the original surface) stresses and strains in the k^{th} elastic layer for the plane stress state. When taking the static hypothesis (2.2) into account, these stresses and strains are linked by Hooke's law

$$\bar{\epsilon} = \mathbf{A}^{(k)} \bar{\sigma}, \tag{2.9}$$

where

$$\mathbf{A}^{(k)} = \begin{pmatrix} a_{11}^{(k)} & a_{12}^{(k)} & a_{16}^{(k)} \\ a_{12}^{(k)} & a_{22}^{(k)} & a_{26}^{(k)} \\ a_{16}^{(k)} & a_{26}^{(k)} & a_{66}^{(k)} \end{pmatrix} \tag{2.10}$$

is the 3×3 matrix of the plane compliances for the k^{th} layer. If the layer is isotropic , then

$$a_{11}^{(k)} = a_{22}^{(k)} = \frac{1}{E_k}, \quad a_{12}^{(k)} = -\frac{\nu_k}{E_k}, \quad a_{66}^{(k)} = \frac{1+\nu_k}{E_k}, \quad a_{16}^{(k)} = a_{26}^{(k)} = 0 \tag{2.11}$$

and the constitutive equation (2.9) for the generalized plane stress state may be rewritten as it follows

$$\sigma_{ij} = \frac{E_k}{1-\nu_k^2} \Xi \epsilon_{ij}, \quad i, j = 1, 2, \tag{2.12}$$

where

$$\Xi \epsilon_{ij} = (1-\nu)\epsilon_{ij} + \nu \delta_{ij} (\epsilon_{11} + \epsilon_{22}), \tag{2.13}$$

δ_{ij} is the Kronecker symbol ($\delta_{ii} = 1$; $\delta_{ij} = 0, i \neq j$), and

$$\nu = \sum_{k=1}^{N} \frac{E_k h_k \nu_k}{1-\nu_k^2} \left(\sum_{k=1}^{N} \frac{E_k h_k}{1-\nu_k^2} \right)^{-1} \tag{2.14}$$

is the reduced Poisson's ratio for the whole stacked sequence (Grigolyuk and Kulikov, 1988).

The transverse shear stresses σ_{i3} have to satisfy the following matrix equation

$$\bar{\epsilon}_3 = \mathbf{A}_3^{(k)} \bar{\sigma}_3, \tag{2.15}$$

where

$$\bar{\sigma}_3 = (\sigma_{13}, \sigma_{23})^{\mathrm{T}}, \quad \bar{\epsilon}_3 = (\epsilon_{13}, \epsilon_{23})^{\mathrm{T}} \tag{2.16}$$

and

$$\mathbf{A}_3^{(k)} = \begin{pmatrix} a_{55}^{(k)} & a_{45}^{(k)} \\ a_{45}^{(k)} & a_{44}^{(k)} \end{pmatrix} \tag{2.17}$$

is the 2×2 matrix of the transverse shear compliances. For a isotropic layer, $a_{45}^{(k)} = 0, a_{55}^{(k)} = a_{44}^{(k)} = G_k^{-1}$. It is obvious that because of the accepted hypotheses (2.2), the constitutive equation (2.15) is not satisfied. However, it will be shown below that Eq. (2.15) may be satisfied integrally with some weight function for the thickness of the laminated package.

We also introduce the reduced Young's modulus

$$E = \frac{1-\nu^2}{h} \sum_{k=1}^{N} \frac{E_k h_k}{1-\nu_k^2}, \tag{2.18}$$

and the dimensionless stiffness characteristics

$$\gamma_k = \frac{E_k h_k}{1-\nu_k^2} \left(\sum_{k=1}^{N} \frac{E_k h_k}{1-\nu_k^2} \right)^{-1} \tag{2.19}$$

of the k^{th} layer. Then, from Eqs. (2.18) and (2.19) one obtains

$$\frac{E_k h_k}{1-\nu_k^2} = \frac{Eh}{1-\nu^2} \gamma_k \tag{2.20}$$

for any $k = 1, \ldots, N$. The parameters γ_k are important in the estimation of the error of governing equations derived below. In what follows, we assume that the stiffness characteristics γ_k for all layers are approximately the same. In the common case, when a material of some layer is inhomogeneous, the reduced modulus E and Poisson's ratio ν are functions of the curvilinear coordinates.

2.1.5 Stress Resultants

Let T_{ij}, Q_i and M_{ij} be the classical stress resultants (s. Fig. 2.3) which are introduced in the standard way as

$$T_{ij} = \sum_{k=1}^{N} \int_{\delta_{k-1}}^{\delta_k} \sigma_{ij} \, \mathrm{d}z, \quad Q_i = \sum_{k=1}^{N} \int_{\delta_{k-1}}^{\delta_k} \sigma_{i3} \, \mathrm{d}z, \quad M_{ij} = \sum_{k=1}^{N} \int_{\delta_{k-1}}^{\delta_k} z \, \sigma_{ij} \, \mathrm{d}z. \tag{2.21}$$

In addition to the classical resultants, we introduce the generalized stress resultants (Grigolyuk and Kulikov, 1988):

- the generalized transverse shear forces

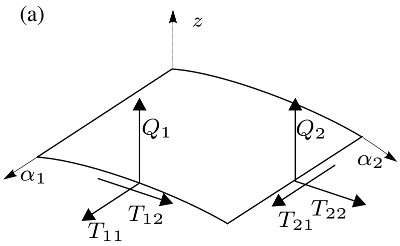

Fig. 2.3 Reference surface. Stress resultants: (a) in-plane forces T_{ij} and transverse shear forces Q_i, (b) moments M_{ij}.

$$Q_{0i} = \sum_{k=1}^{N} \int_{\delta_{k-1}}^{\delta_k} f_0(z)\sigma_{i3}\,\mathrm{d}z, \tag{2.22}$$

- and the generalized moments

$$L_{ij} = \sum_{k=1}^{N} \int_{\delta_{k-1}}^{\delta_k} g(z)\sigma_{ij}\,dz. \tag{2.23}$$

The introduction of the generalized forces and moments is caused by the presence of additional degrees of freedom corresponding to the transverse shear in the shell.

Taking into account Eqs. (2.12)-(2.14), (2.18), Eqs. (2.21), (2.23) can be rewritten

$$\begin{aligned} T_{ij} &= \frac{Eh}{1-\nu^2}\Xi e_{ij} + \frac{Eh^2}{2(1-\nu^2)}\left(c_{13}\Xi\kappa_{ij} + c_{12}\Xi\psi_{ij}\right), \\ M_{ij} &= \frac{1}{2}hc_{13}T_{ij} + \frac{Eh^2}{2(1-\nu^2)}\left(\eta_3\Xi\kappa_{ij} + \eta_2\Xi\psi_{ij}\right), \\ L_{ij} &= \frac{1}{2}hc_{12}T_{ij} + \frac{Eh^2}{2(1-\nu^2)}\left(\eta_2\Xi\kappa_{ij} + \eta_1\Xi\psi_{ij}\right), \end{aligned} \tag{2.24}$$

where

$$\begin{aligned} &c_{12} = \sum_{k=1}^{N}\xi_k^{-1}\pi_{3k}\gamma_k, \quad c_{13} = \sum_{k=1}^{N}(\zeta_{k-1}+\zeta_k)\gamma_k, \\ &\frac{1}{12}h^3\pi_{1k} = \int_{\delta_{k-1}}^{\delta_k} g^2(z)\mathrm{d}z,\ \frac{1}{12}h^3\pi_{2k} = \int_{\delta_{k-1}}^{\delta_k} z\,g(z)\mathrm{d}z,\ \frac{1}{2}h^2\pi_{3k} = \int_{\delta_{k-1}}^{\delta_k} g(z)\mathrm{d}z, \\ &\eta_1 = \sum_{k=1}^{N}\xi_k^{-1}\pi_{1k}\gamma_k - 3c_{12}^2,\ \eta_2 = \sum_{k=1}^{N}\xi_k^{-1}\pi_{2k}\gamma_k - 3c_{12}c_{13}, \\ &\eta_3 = 4\sum_{k=1}^{N}\left(\xi_k^2 + 3\zeta_{k-1}\zeta_k\right)\gamma_k - 3c_{13}^2,\ h\xi_k = h_k,\ h\zeta_n = \delta_n\ (n=0,\,k) \end{aligned} \tag{2.25}$$

Equations (2.24) differ from similar equations for homogeneous shells. They contain terms depending on torsion of the original surface and shear as well. The presence of these terms is not desirable. To eliminate them, we follow Grigolyuk and Kulikov (1988) and introduce the so-called generalized displacements and strains

$$\begin{aligned} u_i &= \hat{u}_i + \frac{1}{2}hc_{13}w_{,\,i} - \frac{1}{2}hc_{12}\psi_i, \\ e_{ij} &= \hat{e}_{ij} - \frac{1}{2}hc_{13}\kappa_{ij} - \frac{1}{2}hc_{12}\psi_{ij}. \end{aligned} \tag{2.26}$$

Then Eq. (2.24) for T_{ij} may be rewritten in terms of the generalized strains as follows

$$T_{ij} = \frac{Eh}{1-\nu^2}\varXi\hat{e}_{ij}. \tag{2.27}$$

Let us consider the following transformations (Grigolyuk and Kulikov, 1988)

$$\hat{M}_{ij} = M_{ij} - \frac{1}{2}hc_{13}T_{ij}, \quad \hat{L}_{ij} = L_{ij} - \frac{1}{2}hc_{12}T_{ij}. \tag{2.28}$$

They lead to equations for the so-called reduced moments and generalized moments

$$\begin{aligned} \hat{M}_{ij} &= \frac{Eh^3}{12(1-\nu^2)}\left(\eta_3\varXi\kappa_{ij} + \eta_2\varXi\psi_{ij}\right), \\ \hat{L}_{ij} &= \frac{Eh^3}{12(1-\nu^2)}\left(\eta_2\varXi\kappa_{ij} + \eta_1\varXi\psi_{ij}\right). \end{aligned} \tag{2.29}$$

The substitution of (2.2), (2.3) into (2.22) results in the following equations for the generalized shear stress resultants

$$Q_{0i} = \sum_{k=1}^{N}\left(\lambda_k\mu_i^{(0)} + \lambda_{k0}\mu_i^{(k)}\right), \quad i = 1, 2; \tag{2.30}$$

$$\lambda_k = \int\limits_{\delta_{k-1}}^{\delta_k} f_0^2(z)\mathrm{d}z, \qquad \lambda_{kn} = \int\limits_{\delta_{k-1}}^{\delta_k} f_k(z)f_n(z)\mathrm{d}z \qquad (n = 0, k).$$

It will be shown later that they may be expressed in terms of the functions ψ_i.

2.1.6 *Mixed Variational Principle*

To derive the equations of equilibrium we shall apply to the following mixed variational principle

$$\delta\varPi = \delta A_1^* + \delta A_2^*, \tag{2.31}$$

where A_1^* and A_2^* are the work of both external surface and boundary forces, respectively, and the functional Π is defined as (Grigolyuk and Kulikov, 1988)

$$\Pi = \iint_{\mathcal{D}} \left[\sum_{k=1}^{N} \int_{\delta_{k-1}}^{\delta_k} \left(\bar{\sigma}^{\mathrm{T}} \bar{\epsilon} + \bar{\sigma}_3^{\mathrm{T}} \bar{\epsilon}_3 - W_k \right) (1 + k_{22} z)\, \mathrm{d}z \right] \mathrm{d}\alpha_1 \mathrm{d}\alpha_2. \tag{2.32}$$

In (2.32),

$$W_k = \frac{1}{2} \left(\bar{\sigma}^{\mathrm{T}} \mathbf{A}^{(k)} \bar{\sigma} + \bar{\sigma}_3^{\mathrm{T}} \mathbf{A}_3^{(k)} \bar{\sigma}_3 \right) \tag{2.33}$$

is the strain-energy function of the k^{th} layer, and $\mathcal{D}$ is the domain of the reference surface bounded by a closed curve (s. Fig. 2.4)

$$\Gamma_{\mathcal{D}} = \Gamma_1 \cup \Gamma_2,$$

where

$$\begin{aligned}
&\Gamma_1 = \Gamma_1^* \cup \Gamma_1^{**}, \quad \Gamma_1^* = \{(\alpha_1, \alpha_2) : \alpha_1 = \alpha_1^*(\alpha_2)\}, \\
&\Gamma_1^{**} = \{(\alpha_1, \alpha_2) : \alpha_1 = \alpha_1^{**}(\alpha_2)\}, \quad \Gamma_2 = \Gamma_2^* \cup \Gamma_2^{**}, \\
&\Gamma_2^* = \{(\alpha_1, \alpha_2) : \alpha_2 = \alpha_2^*\}, \quad \Gamma_2^{**} = \{(\alpha_1, \alpha_2) : \alpha_2 = \alpha_2^{**}\}, \\
&0 \leq \alpha_2^* < \alpha_2^{**} \leq 2\pi.
\end{aligned}$$

If the shell is closed in the circumferential direction, then $\alpha_2^* = 0, \alpha_2^{**} = 2\pi$, otherwise, one has the cylindrical panel. In the mixed variational principle (2.31), displacements and stresses are varied independently.

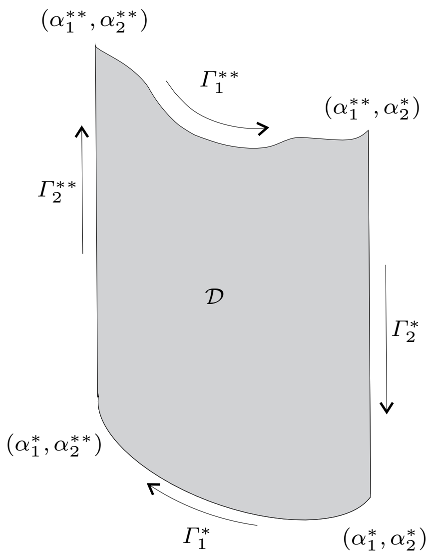

Fig. 2.4 Domain of the original surface and its bound. Path of integration.

The variation of the functional Π may be written in terms of the stress resultants, reduced moments and generalized strains $\hat{e}_{ij}$. Substituting Eqs. (2.5)-(2.9), (2.21)-(2.30) into (2.32) and introducing the generalized strains by (2.26), one obtains

$$\begin{aligned}\delta\Pi = \iint\limits_{\mathcal{D}} \Bigg\{ \sum_{i,j=1}^{2} \left(T_{ij}\delta\hat{e}_{ij} + \hat{M}_{ij}\delta\kappa_{ij} + \hat{L}_{ij}\delta\psi_{ij} \right) \\ + \sum_{i=1}^{2} Q_{0i}\delta\psi_i + \sum_{k=1}^{N} \int\limits_{\delta_{k-1}}^{\delta_k} \left(\bar{\epsilon}_3 - \mathbf{A}_3^{(k)}\bar{\sigma}_3 \right)^{\mathrm{T}} \delta\bar{\sigma}_3 \mathrm{d}z \Bigg\} \mathrm{d}\alpha_1 \mathrm{d}\alpha_2 .\end{aligned} \tag{2.34}$$

When deriving Eq. (2.34), we have neglected $k_{22}z$ $(k_{22}z \ll 1)$.

Let us apply the known generalized formula of partial integration

$$\iint\limits_{\mathcal{D}} F_1 \frac{\partial F_2}{\partial\alpha_1}\mathrm{d}\alpha_1\mathrm{d}\alpha_2 = \int\limits_{\Gamma_1} F_1F_2\mathrm{d}\alpha_2 - \iint\limits_{\mathcal{D}} F_2\frac{\partial F_1}{\partial\alpha_1}\mathrm{d}\alpha_1\mathrm{d}\alpha_2 . \tag{2.35}$$

The standard variational procedure in (2.34) results in the following equation for the variation of the functional Π

$$\begin{aligned}\delta\Pi = &-\iint\limits_{\mathcal{D}} \Bigg\{ \sum_{i=1}^{2} \left(T_{1i,i} + T_{2i,2}\right)\delta\hat{u}_i + \sum_{i=1}^{2}\left(\hat{L}_{1i,1} + \hat{L}_{2i,2} - Q_{0i}\right)\delta\psi_i \\ &+ \sum_{i,j=1}^{2}\left[\hat{M}_{ij,ij} + \left(T_{ij}w_{,i}\right)_{,j} - k_{22}T_{22}\right]\delta w \Bigg\} \mathrm{d}\alpha_1\mathrm{d}\alpha_2 \\ &+ \iint\limits_{\mathcal{D}} \Bigg\{ \sum_{k=1}^{N}\int\limits_{\delta_{k-1}}^{\delta_k} \left(\bar{\epsilon}_3 - \mathbf{A}_3^{(k)}\bar{\sigma}_3\right)^{\mathrm{T}} \left[f_0(z)\delta\bar{\mu}^{(0)} + + f_k(z)\delta\bar{\mu}^{(k)} \right] \mathrm{d}z \Bigg\} \mathrm{d}\alpha_1\mathrm{d}\alpha_2 \\ &+ \int\limits_{\Gamma_1} \Bigg[\sum_{i=1}^{2}\left(T_{i1}\delta\hat{u}_i + \hat{L}_{i1}\delta\psi_i\right) - \hat{M}_{11}\delta w_{,1} \\ &+ \left(\hat{M}_{11,\,1} + 2\hat{M}_{12,\,2} + T_{11}w_{,\,1} + T_{12}w_{,\,2}\right)\delta w \Bigg] \mathrm{d}\alpha_2 \\ &+ \int\limits_{\Gamma_2} \Bigg[\sum_{i=1}^{2}\left(T_{i2}\delta\hat{u}_i + \hat{L}_{i2}\delta\psi_i\right) - \hat{M}_{22}\delta w_{,2} \\ &+ \left(\hat{M}_{22,2} + 2\hat{M}_{12,2} + T_{12}w_{,1} + T_{22}w_{,2}\right)\delta w \Bigg] \mathrm{d}\alpha_1 ,\end{aligned} \tag{2.36}$$

where

$$\bar{\mu}^{(n)} = \left(\mu_1^{(n)},\, \mu_2^{(n)}\right)^{\mathrm{T}}, \quad n = 0, \ldots, k.$$

Let

$$\mathbf{q}_\mathrm{s} = \sum_{i=1}^{2} q_i \mathbf{e}_i + q_\mathrm{n} \mathbf{n} \tag{2.37}$$

be the vector of the external load acting on the unit area of the reference surface, where $q_i(\alpha_1, \alpha_2)$ are components of the tangential forces and $q_\mathrm{n}(\alpha_1, \alpha_2)$ is the normal load. Then the variation of the surface forces work will be

$$\delta A_1^* = \iint\limits_{\mathcal{D}} \left(\sum_{i=1}^{2} q_i \delta u_1 + q_\mathrm{n} \delta w \right) \mathrm{d}\alpha_1 \mathrm{d}\alpha_2. \tag{2.38}$$

When turning to the generalized tangential displacements $\hat{u}_i$ by (2.26) and applying Eq. (2.35), it is written as follows

$$\begin{aligned} \delta A_1^* = & \iint\limits_{\mathcal{D}} \left[\sum_{i=1}^{2} \left(q_i \delta \hat{u}_i + \hat{L}_{si} \delta \psi_i \right) + \hat{q}_{sn} \delta w \right] \mathrm{d}\alpha_1 \mathrm{d}\alpha_2 \\ & + \int\limits_{\Gamma_1} \hat{Q}_{b1} \delta w \mathrm{d}\alpha_2 + \int_{\Gamma_2} \hat{Q}_{b2} \delta w \mathrm{d}\alpha_1, \end{aligned} \tag{2.39}$$

where

$$\hat{q}_{sn} = q_\mathrm{n} - \frac{1}{2} h c_{13} \sum_{i=1}^{2} q_{i,\,i} \tag{2.40}$$

is the reduced normal load which contains additional forces acting on the surface located at the distance $hc_{13}/2$ from the reference surface of the laminated shell,

$$\hat{L}_{si} = -\frac{1}{2} h c_{12} q_i, \quad i = 1, 2 \tag{2.41}$$

are the reduced moments generated by the components q_i and acting on the surface which is located at the distance $hc_{12}/2$ from the reference one, and

$$\hat{Q}_{bi} = \frac{1}{2} h c_{13} q_i \tag{2.42}$$

are the reduced shear boundary forces applied to the shell edges Γ_i at the distance $hc_{13}/2$ from the original surface. In contrast to Grigolyuk and Kulikov (1988), where $\hat{L}_{si} = \hat{Q}_{bi} = 0$ and $\hat{q}_{sn} = q_\mathrm{n}$, Eq. (2.39) takes into account the work of the tangential surface forces q_i.

Let us consider the boundary stress resultants T_{ij}^*, Q_i^* and M_{ij}^* $(i, j = 1, 2)$ acting on the shell counter $\Gamma_{\mathcal{D}} = \Gamma_1 \cup \Gamma_2$. Here, notations are the same as shown in Fig. 2.3, and the asterisk means that an appropriate force or moment is considered at the shell edge. Taking into account the additional degrees of freedom corresponding to the magnitudes ψ_i, we introduce also the generalized moments L_{ij}^* at the shell edges. The variation of the work of the external boundary forces may be presented in the form

$$
\begin{aligned}
\delta A_2^* = & \int\limits_{\Gamma_1} \Bigg[T_{11}^* \delta u_1 + T_{12}^* \delta u_2 + M_{11}^* \delta \theta_1 \\
& + \left(\frac{\partial M_{12}^*}{\partial \alpha_2} + Q_1^* \right) \delta w + L_{11}^* \delta \psi_1 + L_{12}^* \delta \psi_2 \Bigg] \mathrm{d}\alpha_2 \\
& + \int\limits_{\Gamma_2} \Bigg[T_{22}^* \delta u_2 + T_{21}^* \delta u_1 + M_{22}^* \delta \theta_2 \\
& + \left(\frac{\partial M_{21}^*}{\partial \alpha_1} + Q_2^* \right) \delta w + L_{22}^* \delta \psi_2 + L_{21}^* \delta \psi_1 \Bigg] \mathrm{d}\alpha_1 .
\end{aligned}
\tag{2.43}
$$

Let us choose the path of integration in (2.43) as shown in Fig. 2.4. Then, introducing the generalized tangential displacements $\hat{u}_i$ by (2.26) and applying Eq. (2.35), one obtains the following equation

$$
\begin{aligned}
\delta A_2^* = & \int\limits_{\Gamma_1} \Big[T_{11}^* \delta \hat{u}_1 + T_{12}^* \delta \hat{u}_2 - \hat{M}_{11}^* \delta w_{,1} + \hat{L}_{11}^* \delta \psi_1 \\
& + \hat{L}_{12}^* \delta \psi_2 + \left(Q_1^* + \hat{M}_{12,2}^* \right) \delta w \Big] \mathrm{d}\alpha_2 \\
& + \int\limits_{\Gamma_2} \Big[T_{21}^* \delta \hat{u}_1 + T_{22}^* \delta \hat{u}_2 - \hat{M}_{22}^* \delta w_{,1} + \hat{L}_{22}^* \delta \psi_2 \\
& + \hat{L}_{21}^* \delta \psi_1 + \left(Q_2^* + \hat{M}_{21,1}^* \right) \delta w \Big] \mathrm{d}\alpha_1 + \frac{1}{2} h c_{13} \left[T_{12}^* \delta w \right]_{\Gamma} ,
\end{aligned}
\tag{2.44}
$$

where

$$
\hat{L}_{ij}^* = L_{ij}^* - \frac{1}{2} h c_{12} T_{ij}^*, \quad \hat{M}_{ij}^* = M_{ij}^* - \frac{1}{2} h c_{13} T_{ij}^*,
\tag{2.45}
$$

and

$$
\begin{aligned}
\left[T_{12}^* \delta w \right]_{\Gamma} = & \; T_{12}^* \delta w |_{(\alpha_1^*, \alpha_2^{**})} - T_{12}^* \delta w |_{(\alpha_1^*, \alpha_2^*)} \\
& + T_{21}^* \delta w |_{(\alpha_1^{**}, \alpha_2^{**})} - T_{21}^* \delta w |_{(\alpha_1^*, \alpha_2^{**})} \\
& + T_{12}^* \delta w |_{(\alpha_1^{**}, \alpha_2^*)} - T_{12}^* \delta w |_{(\alpha_1^{**}, \alpha_2^{**})} \\
& + T_{21}^* \delta w |_{(\alpha_1^*, \alpha_2^*)} - T_{21}^* \delta w |_{(\alpha_1^{**}, \alpha_2^*)} .
\end{aligned}
\tag{2.46}
$$

From Eqs. (2.6), (2.7), (2.24) it follows that $T_{12} = T_{21}$. Hence, one obtains that $T_{12}^* = T_{21}^*$. Then

$$
\left[T_{12}^* \delta w \right]_{\Gamma} = 0.
\tag{2.47}
$$

2.1.7 Equilibrium Equations and Natural Boundary Conditions

Let us substitute Eqs. (2.36), (2.39), (2.44), (2.47) into the mixed variational principle (2.31). Taking into account the first hypothesis (2.2) coupling the transverse shear stresses σ_{i3} with the introduced additional functions $\mu_i^{(0)}(\alpha_1, \alpha_2)$, $\mu_i^{(k)}(\alpha_1, \alpha_2)$, we assume the displacements u_i, w, ψ_i and the functions $\mu_i^{(0)}, \mu_i^{(k)}$ to be independent. Equating coefficients of the variations of independent magnitudes u_i, w, ψ_i, $\mu_i^{(0)}, \mu_i^{(k)}$, we obtain:

- the desired five differential equations of equilibrium in terms of the reduced stress resultants

$$\begin{aligned} T_{1i,\,1} + T_{2i,\,2} &= -q_i, \\ \hat{L}_{1i,\,1} + \hat{L}_{2i,\,2} &= Q_{0i} - \hat{L}_{si}, \\ \hat{M}_{11,\,11} + 2\hat{M}_{12,\,12} + \hat{M}_{22,\,22} & \\ +w_{,\,11}T_{11} + 2w_{,\,12}T_{12} + w_{,\,22}T_{22} - k_{22}T_{22} &= -\hat{q}_{sn}, \end{aligned} \tag{2.48}$$

  with $i = 1, 2$,
- the equations coupling the transverse shear stresses with the shear strains

$$\sum_{k=1}^{N} \int_{\delta_{k-1}}^{\delta_k} \left(\bar{\epsilon}_3 - \mathbf{A}_3^{(k)}\bar{\sigma}_3\right) f_0(z)\mathrm{d}z = 0, \tag{2.49}$$

$$\int_{\delta_{k-1}}^{\delta_k} \left(\bar{\epsilon}_3 - \mathbf{A}_3^{(k)}\bar{\sigma}_3\right) f_k(z)\mathrm{d}z = 0 \tag{2.50}$$

  with $k = 1, 2, \ldots, N$, and
- the natural boundary conditions

$$\begin{aligned} & T_{i1} = T_{i1}^* \quad \text{or} \quad \hat{u}_i = 0, \\ & \hat{L}_{i1} = \hat{L}_{i1}^* \quad \text{or} \quad \psi_i = 0, \\ & \hat{M}_{11} = \hat{M}_{11}^* \quad \text{or} \quad w_{,\,1} = 0, \\ & \hat{M}_{11,1} + 2\hat{M}_{12,2} + T_{11}w_{,1} + T_{12}w_{,2} = Q_1^* + \hat{M}_{12,\,2}^* + \hat{Q}_{b1} \quad \text{or} \quad w = 0 \end{aligned} \tag{2.51}$$

  for the not necessary plane contours $\Gamma_1^*[\alpha_1 = \alpha_1^*(\alpha_2)], \Gamma_1^{**}[\alpha_1 = \alpha_1^{**}(\alpha_2)]$, and

$$\begin{aligned} & T_{i2} = T_{i2}^* \quad \text{or} \quad \hat{u}_i = 0, \\ & \hat{L}_{i2} = \hat{L}_{i2}^* \quad \text{or} \quad \psi_i = 0, \\ & \hat{M}_{22} = \hat{M}_{22}^* \quad \text{or} \quad w_{,\,2} = 0, \\ & \hat{M}_{22,2} + 2\hat{M}_{12,1} + T_{12}w_{,1} + T_{22}w_{,2} = Q_2^* + \hat{M}_{21,\,1}^* + \hat{Q}_{b2} \quad \text{or} \quad w = 0 \end{aligned} \tag{2.52}$$

  for the straight contours Γ_2^* $(\alpha_2 = \alpha_2^*)$ and Γ_2^{**} $(\alpha_2 = \alpha_2^{**})$.

The equilibrium equations (2.48) as well as the boundary conditions (2.51), (2.52) take into consideration the shear forces q_i applied to the reference surface and they are different from similar equations and boundary conditions derived by Grigolyuk and Kulikov (1988).

2.1.8 Transverse Shear Stresses and Their Resultants

We remind that because of the accepted hypothesis (2.2), the constitutive equations (2.15) are not satisfied. However, as seen from Eqs. (2.49) and (2.50), the constitutive equations for the transverse tangent stresses hold *integrally* for both the thickness of all laminated package with the weighting function $f_0(z)$ and the thickness of the k^{th} layer with the weighting function $f_k(z)$.

Equations (2.49), (2.50) allow us to couple the vector $\bar{\Psi}$ to the additional vectors $\bar{\mu}^{(0)}, \bar{\mu}^{(k)}$ (Grigolyuk and Kulikov, 1988). Indeed, the substitution of Eq. (2.2) for σ_{i3} and Eq. (2.6) for ϵ_{i3} into Eqs. (2.49), (2.50) results in the following system of $N+1$ algebraic equations for the vectors $\bar{\mu}^{(0)}, \bar{\mu}^{(k)}$

$$\begin{gathered}\sum_{k=1}^{N} \mathbf{A}_3^{(k)} \left(\lambda_k \bar{\mu}^{(0)} + \lambda_{k0} \bar{\mu}^{(k)}\right) = \sum_{k=1}^{N} \bar{\Psi}, \\ \mathbf{A}_3^{(k)} \left(\lambda_{k0} \bar{\mu}^{(0)} + \lambda_{kk} \bar{\mu}^{(k)}\right) = \lambda_{k0} \bar{\Psi},\end{gathered} \tag{2.53}$$

where

$$\lambda_k = \int\limits_{\delta_{k-1}}^{\delta_k} f_0^2(z) \mathrm{d}z, \qquad \lambda_{kn} = \int\limits_{\delta_{k-1}}^{\delta_k} f_k(z) f_n(z) \mathrm{d}z, \qquad n = 0, k, \tag{2.54}$$

and

$$\mathbf{A}_3^{(k)} = \begin{pmatrix} G_k^{-1} & 0 \\ 0 & G_k^{-1} \end{pmatrix} \tag{2.55}$$

for the isotropic layers.

The solution of Eqs. (2.53) may be presented in the form

$$\mu_i^{(0)} = q_{44}^* \psi_i, \quad \mu_i^{(k)} = \frac{\lambda_{k0}}{\lambda_{kk}} \left(G_k \psi_i - \mu_i^{(0)}\right), \quad i = 1, 2; \; k = 1, 2, \ldots, N, \tag{2.56}$$

where

$$q_{44}^* = \frac{\sum\limits_{k=1}^{N} \left(\lambda_k - \lambda_{k0}^2 \lambda_{kk}^{-1}\right)}{\sum\limits_{k=1}^{N} \left(\lambda_k - \lambda_{k0}^2 \lambda_{kk}^{-1}\right) G_k^{-1}}. \tag{2.57}$$

Now, we can derive an equation for the generalized transverse stress resultants Q_{0i}. Substituting Eqs.(2.57) into (2.30), one obtains

$$Q_{0i} = q_{44} \, \psi_i, \tag{2.58}$$

where

$$q_{44} = \frac{\left[\sum\limits_{k=1}^{N} \left(\lambda_k - \frac{\lambda_{k0}^2}{\lambda_{kk}}\right)\right]^2}{\sum\limits_{k=1}^{N} \left(\lambda_k - \frac{\lambda_{k0}^2}{\lambda_{kk}}\right) G_k^{-1}} + \sum_{k=1}^{N} \frac{\lambda_{k0}^2}{\lambda_{kk}} G_k. \tag{2.59}$$

We shall call the magnitude $G = q_{44}/h$ as the reduced shear modulus for all package of the laminated shell.

2.1.9 Equations of Motion in Terms of Displacements

The system of five differential equations (2.48) together with Eqs. (2.27)-(2.29), (2.57) and Eqs. (2.6), (2.7), (2.26) for the stress resultants and strains, respectively, form the full system of equations for the five unknown generalized displacements $\hat{u}_i, w, \psi_i$. To derive these equations, it is convenient to write the stress resultants in terms of displacements.

The substitution of Eqs. (2.7), (2.26) into (2.27) and (2.29) results in the formulae for the in-plane stress resultants and reduced moments written in terms of the generalized displacements

$$\begin{aligned}
T_{ii} &= \frac{Eh}{1-\nu^2}\left[\hat{u}_{i,\,i} + \frac{1}{2}w_{,\,i}^2 + \nu\left(\hat{u}_{j,\,j} + \frac{1}{2}w_{,\,j}^2 + k_{ii}w\right) + k_{jj}w\right], \\
T_{ij} &= \frac{Eh}{2(1+\nu)}\left(\hat{u}_{i,\,j} + \hat{u}_{j,\,i} + w_{,\,i}w_{,\,j}\right), \\
\hat{M}_{ii} &= -\frac{Eh^3}{12(1-\nu^2)}\left[\eta_3(w_{,\,ii} + \nu w_{,\,jj}) - \eta_2(\psi_{i,\,i} + \nu\psi_{j,\,j})\right], \\
\hat{M}_{ij} &= -\frac{Eh^3}{12(1+\nu)}\left[\eta_3 w_{,\,ij} - \frac{1}{2}\eta_2(\psi_{i,\,j} + \psi_{j,\,i})\right], \\
\hat{L}_{ii} &= -\frac{Eh^3}{12(1-\nu^2)}\left[\eta_2(w_{,\,ii} + \nu w_{,\,jj}) - \eta_1(\psi_{i,\,i} + \nu\psi_{j,\,j})\right], \\
\hat{L}_{ij} &= -\frac{Eh^3}{12(1+\nu)}\left[\eta_2 w_{,\,ij} - \frac{1}{2}\eta_1(\psi_{i,\,j} + \psi_{j,\,i})\right],
\end{aligned} \tag{2.60}$$

where $i, j = 1, 2;\ i \neq j$. The generalized transverse stress resultants Q_{0i} are defined by (2.58), (2.59).

Introducing (2.60), (2.58), into Eqs. (2.48) yields the system of nonlinear differential equations in terms of the generalized displacements

$$
\begin{aligned}
&\hat{u}_{1,\,11} + \frac{1-\nu}{2}\hat{u}_{1,\,22} + \frac{1+\nu}{2}\hat{u}_{2,\,12} + \nu k_{22} w_{,\,1} \\
&+ w_{,\,1} w_{,\,11} + \nu w_{,\,2} w_{,\,21} + \frac{1-\nu}{2}(w_{,\,1} w_{,\,22} + w_{,\,2} w_{,\,12}) = -\tilde{q}_1, \\
&\frac{1+\nu}{2}\hat{u}_{1,\,12} + \frac{1-\nu}{2}\hat{u}_{2,\,11} + \hat{u}_{2,\,22} + (k_{22} w)_{,\,2} \\
&+ \frac{1-\nu}{2}(w_{,\,2} w_{,\,11} + w_{,\,1} w_{,\,12}) + w_{,\,2} w_{,\,22} + \nu w_{,\,1} w_{,\,12} = -\tilde{q}_2, \\
&\eta_2 \triangle w_{,\,1} - \eta_1 \left(\psi_{1,\,11} + \frac{1+\nu}{2}\psi_{2,\,12} + \frac{1-\nu}{2}\psi_{1,\,22} \right) \\
&\qquad + \frac{12(1-\nu^2)}{Eh^3} \left(q_{44}\psi_1 + \frac{1}{2} h c_{12} q_1 \right) = 0,
\end{aligned}
\tag{2.61}
$$

$$
\begin{aligned}
&\eta_2 \triangle w_{,\,2} - \eta_1 \left(\psi_{2,\,22} + \frac{1+\nu}{2}\psi_{1,\,12} + \frac{1-\nu}{2}\psi_{2,\,11} \right) \\
&\qquad + \frac{12(1-\nu^2)}{Eh^3} \left(q_{44}\psi_2 + \frac{1}{2} h c_{12} q_2 \right) = 0,
\end{aligned}
\tag{2.62}
$$

$$
\begin{aligned}
&\frac{h^2}{12(1-\nu^2)} \triangle \left[\eta_3 \triangle w - \eta_2 \left(\psi_{1,\,1} + \psi_{2,\,2} \right) \right] + \frac{k_{22}}{1-\nu^2} \left(\nu \hat{u}_{1,\,1} + \hat{u}_{2,\,2} + k_{22} w \right) \\
&- \frac{1}{1-\nu^2} \left\{ w_{,\,11} \left[\hat{u}_{1,\,1} + \nu(\hat{u}_{2,\,2} + k_{22} w) + \frac{1}{2}\left(w_{,\,1}^2 + \nu w_{,\,2}^2 \right) \right] \right. \\
&+ w_{,\,22} \left[\nu \hat{u}_{1,\,1} + \hat{u}_{2,\,2} + k_{22} w + \frac{1}{2}\left(w_{,\,2}^2 + \nu w_{,\,1}^2 \right) \right] \\
&\left. + (1-\nu) w_{1,\,12} (\hat{u}_{1,\,2} + \hat{u}_{2,\,1} + w_{,\,1} w_{,\,2}) - \frac{1}{2} k_{22} \left(w_{,\,2}^2 + \nu w_{,\,1}^2 \right) \right\} = \tilde{q}_{\mathrm{n}},
\end{aligned}
\tag{2.63}
$$

where

$$
\triangle = \frac{\partial^2}{\partial \alpha_1^2} + \frac{\partial^2}{\partial \alpha_2^2}
$$

is the Laplace operator, and

$$
\tilde{q}_i = \frac{(1-\nu^2) q_i}{Eh}, \quad \tilde{q}_{\mathrm{n}} = \frac{1}{Eh} \left(q_{\mathrm{n}} - \frac{1}{2} h c_{13} \sum_{i=1}^{2} q_{i,\,i} \right). \tag{2.64}
$$

The static balance equations (2.61)-(2.64) are in the usual way transformed into equations describing the shell motion. When neglecting the rotary inertia effects, in accordance with d'Alembert principle one assumes

$$
\begin{aligned}
\tilde{q}_i &= \frac{(1-\nu^2)}{Eh} \left(q_i - \sum_{k=1}^{N} \rho_k h_k \frac{\partial^2 \hat{u}_i}{\partial t^2} \right), \\
\tilde{q}_{\mathrm{n}} &= \frac{1}{Eh} \left(q_{\mathrm{n}} - \frac{1}{2} h c_{13} \sum_{i=1}^{2} q_{i,\,i} - \sum_{k=1}^{N} \rho_k h_k \frac{\partial^2 w}{\partial t^2} \right),
\end{aligned}
\tag{2.65}
$$

where ρ_k is the specific density of a material of the k^{th} layer, and t is time. If $q_i = q_{\rm n} = 0$, and $T^*_{ij}, L^*_{ij}, M^*_{ij}$ are specified static stress resultants on the shell edges, then Eqs. (2.61)-(2.64), together with (2.65), describe free vibrations.

2.1.10 In-plane Stress State Equations

Let us introduce the index of variation ι of the stress-strain state as

$$\max\{|Z_{,1}|,\ |Z_{,2}|\} \sim h_*^{-\iota} Z, \tag{2.66}$$

where $h_* = h/R$ is the dimensional thickness which is assumed as a small parameter, R is the characteristic dimension of the shell, and Z is any unknown function which determines this state. Here and below, the symbol $\sim$ means that two quantities have the same asymptotic orders at $h_* \to 0$ (s. the definition in Chapt. 6).

Depending on a value of ι and orders of all unknown functions in Eqs. (2.48) or (2.61)-(2.63), one can deduce simplified equations corresponding to different stress-strain state of a shell. The classification of the characteristic stress-strain states of a thin single layer isotropic shell has been proposed by Gol'denveizer (1961) and Novozhilov (1970).

In this subsection, we consider the simplest state called *the membrane* (*momentless*) stress-strain state[1]. This state is characterized by slow variation of all unknown functions ($\iota = 0$) and displacements $\hat{u}_i, w, R\psi_i$ being small quantities of the order Rh_*. The governing equations for this state can be derived from Eqs. (2.48) or (2.61)-(2.63). When omitting nonlinear terms in (2.48) and introducing the inertial terms, then the dynamic in-plane stress resultants satisfy the following system of equations

$$\begin{aligned}
\frac{\partial T_{11}}{\partial \alpha_1} + \frac{\partial T_{21}}{\partial \alpha_2} &= -q_1(\alpha_1, \alpha_2, t) + \rho_0 h \frac{\partial^2 \hat{u}_1}{\partial t^2},\\
\frac{\partial T_{12}}{\partial \alpha_1} + \frac{\partial T_{22}}{\partial \alpha_2} &= -q_2(\alpha_1, \alpha_2, t) + \rho_0 h \frac{\partial^2 \hat{u}_2}{\partial t^2},\\
k_{22} T_{22} &= \hat{q}_{sn}(\alpha_1, \alpha_2, t) - \rho_0 h \frac{\partial^2 w}{\partial t^2},
\end{aligned} \tag{2.67}$$

where

$$\rho_0 = \sum_{k=1}^{N} \rho_k \xi_k, \tag{2.68}$$

and ξ_k is computed by (2.25).

Equations (2.67) may be used to specify the dynamic stress-strain state if q_i and $\hat{q}_{sn}$ are slowly varying functions of time t and coordinates α_i. They may be rewritten in terms of the generalized displacements

[1] The term *membrane stress-strain state* is established in the literature. Since membranes cannot be affected by compression forces it is better to use *in-plane stress-strain state*.

$$
\begin{aligned}
\hat{u}_{1,11} + \frac{1-\nu}{2}\hat{u}_{1,22} + \frac{1+\nu}{2}\hat{u}_{2,12} + \nu k_{22} w_{,1} &= -\tilde{q}_1,\\
\frac{1+\nu}{2}\hat{u}_{1,12} + \frac{1-\nu}{2}\hat{u}_{2,11} + \hat{u}_{2,22} + (k_{22}w)_{,2} &= -\tilde{q}_2, \\
\frac{k_{22}}{1-\nu^2}\left(\nu\hat{u}_{1,1} + \hat{u}_{2,2} + k_{22}w\right) &= \tilde{q}_{\mathrm{n}}.
\end{aligned} \tag{2.69}
$$

The corresponding boundary conditions are defined for the in-plane stress resultants T_{ij} or displacements $\hat{u}_i$.

2.1.11 Technical Theory Equations

Equations (2.61)-(2.63), together with an appropriate variant of the boundary conditions (2.51) or (2.52), turn out to be complicated for the analysis of both static and dynamic stress-strain state. However, they may be significantly simplified under some additional assumptions.

We will consider here the stress state which is characterized by the index of variation $\iota = 1/2$ and the following estimates:

$$
w \sim h_* R, \quad k_{22} \sim R^{-1}, \quad u_i \ll w. \tag{2.70}
$$

It is obvious that $\hat{u}_i \ll w$ also. Let

$$
\max\{\hat{u}_i\} \sim h_*^{\zeta_u} R, \quad \max\{\psi_i\} \sim h_*^{\zeta_\psi}, \quad G \sim h_*^{\zeta_G} E, \tag{2.71}
$$

where ζ_u, ζ_ψ are the indexes of intensity of the quantities $\hat{u}_i, \psi_i$, respectively, and $h_*^{\zeta_G}$ is the order of the reduced shear modulus G with regard to the reduced Young's modulus E. If any layer is viscoelastic, then the last estimate in (2.71) is replaced by $G_{\mathrm{r}} \sim h_*^{\zeta_G} E_{\mathrm{r}}$, where $E_{\mathrm{r}} = \Re E, G_{\mathrm{r}} = \Re G$ are the real parts of moduli E, G. Then, analyzing the orders of all terms in Eqs. (2.61)-(2.63), we find

$$
\zeta_u = 3/2, \quad \zeta_\psi = 1/2, \quad \zeta_G = 1. \tag{2.72}
$$

The stress-strain state characterized by the above indexes of variation and intensity is called the nonlinear *combined* stress state (Tovstik and Smirnov, 2001). For this state all terms in Eqs. (2.61)-(2.63), including non-linear ones, has the same order. If $w \ll h_* R$, then non-linear summands in the governing equations may be omitted.

Let $q_i = 0$ and the inertia forces in the tangential directions are very small. Then Eqs. (2.61) or (2.48) become homogeneous

$$
T_{1i,1} + T_{2i,2} = 0. \tag{2.73}
$$

They are identically satisfied by the following functions

$$T_{ij} = \delta_{ij} \triangle F - F_{,\,ij}, \tag{2.74}$$

where δ_{ij} is the Kronecker delta, and F is the unknown stress function.

To couple the introduced stress function with the unknown displacements, we apply the strain compatibility condition. With this purpose in mind, we will write down the correlations, following from Eqs. (2.26) and (2.7), and linking the generalized strains and displacements

$$\begin{aligned} \hat{e}_{11} &= \hat{u}_{1,\,1} + \frac{1}{2}\left(w_{,\,1}\right)^2, \\ \hat{e}_{22} &= \hat{u}_{2,\,22} + k_{22} w + \frac{1}{2}\left(w_{,\,2}\right)^2, \\ \hat{e}_{12} &= \frac{1}{2}\left(\hat{u}_{1,\,2} + \hat{u}_{2,\,1} + w_{,\,1} w_{,\,2}\right). \end{aligned} \tag{2.75}$$

Eliminating $\hat{u}_i$, one obtains the strain compatibility equation

$$\hat{e}_{11,\,22} - 2\hat{e}_{12,\,12} + \hat{e}_{22,\,11} = k_{22} w_{,\,11} + \left(w_{,\,12}\right)^2 - w_{,\,11} w_{,\,22}. \tag{2.76}$$

Expressing the generalized strains $\hat{e}_{ij}$ by the stress function F by Eq. (2.27) and introducing them into (2.76) yield the following equation

$$\triangle^2 F - Eh\left[k_{22} w_{,\,11} + \left(w_{,\,12}\right)^2 - w_{,\,11} w_{,\,22}\right] = 0. \tag{2.77}$$

Considering Eqs. (2.62) and following Grigolyuk and Kulikov (1988), we introduce new functions a and ϕ so that

$$\psi_1 = a_{,\,1} + \phi_{,\,2}, \quad \psi_2 = a_{,\,2} - \phi_{,\,1}. \tag{2.78}$$

The substitution of (2.78) into (2.62) gives

$$\begin{aligned} \frac{Eh^3}{12(1-\nu^2)} \triangle(\eta_1 a - \eta_2 w)_{,\,1} + \frac{Eh^3}{24(1+\nu^2)} \eta_1 \triangle \phi_{,\,2} = q_{44}(a_{,\,1} + \phi_{,\,2}), \\ \frac{Eh^3}{12(1-\nu^2)} \triangle(\eta_1 a - \eta_2 w)_{,\,2} - \frac{Eh^3}{24(1+\nu^2)} \eta_1 \triangle \phi_{,\,1} = q_{44}(a_{,\,2} - \phi_{,\,1}). \end{aligned} \tag{2.79}$$

It may be seen that these equations are identically satisfied if

$$\frac{Eh^3}{12(1-\nu^2)} \triangle(\eta_1 a - \eta_2 w) = q_{44} a, \tag{2.80}$$

$$\frac{Eh^3}{24(1+\nu)} \eta_1 \triangle \phi = q_{44} \phi \tag{2.81}$$

are assumed.

Let us introduce the displacement χ as (Grigolyuk and Kulikov, 1988)

$$w = \left(1 - \frac{h^2}{\beta}\triangle\right)\chi, \tag{2.82}$$

$$a = -\frac{\eta_2}{\eta_1}\frac{h^2}{\beta}\triangle\chi \tag{2.83}$$

and substitute them into Eq. (2.80). It can be seen that Eq. (2.80) is identically satisfied if and only if

$$\beta = \frac{12(1-\nu^2)q_{44}}{Eh\eta_1}. \tag{2.84}$$

Then Eq. (2.81) can be rewritten as

$$\frac{1-\nu}{2}\frac{h^2}{\beta}\triangle\phi = \phi. \tag{2.85}$$

Consider the last equation of equilibrium, Eq. (2.63) may be rewritten as

$$\begin{aligned} &\frac{Eh^3}{12(1-\nu^2)}\triangle\left[\eta_3\triangle w - \eta_2\left(\psi_{1,\,1} + \psi_{2,\,2}\right)\right] \\ &-w_{,\,11}T_{11} - 2w_{,\,12}T_{12} - w_{,\,22}T_{22} + k_{22}T_{22} = q_{\mathrm{n}} - \sum_{k=1}^{N}\rho_k h_k\frac{\partial^2 w}{\partial t^2}. \end{aligned} \tag{2.86}$$

The substitution of Eqs. (2.74), (2.78), (2.82) and (2.83) into (2.86) after some transforms results in the following equation

$$D\left(1 - \frac{\theta h^2}{\beta}\triangle\right)\triangle^2\chi - F_{,22}w_{,\,11} + 2F_{,12}w_{,\,12} + F_{,11}(k_{22} - w_{,\,22}) = q_{\mathrm{n}} - \rho_0 h\frac{\partial^2 w}{\partial t^2}, \tag{2.87}$$

where

$$D = \frac{Eh^3}{12(1-\nu^2)}\eta_3 \tag{2.88}$$

is the reduced bending stiffness of the laminated cylindrical shell, and

$$\theta = 1 - \frac{\eta_2^2}{\eta_1\eta_3}. \tag{2.89}$$

Calculations performed by Grigolyuk and Kulikov (1988) have shown that θ is a small parameter. So, for a single layer shell $\theta = 1/85$.

The simplified system of governing equations (2.77), (2.82), (2.85) and (2.87) was at first derived by Grigolyuk and Kulikov (1988). The limiting process at $G \to \infty$ (or $\beta^{-1} \to 0$) implies

$$\chi \to w, \quad a \to 0,$$

and this system degenerates into that of nonlinear equations of the technical theory of thin isotropic shells based on the Kirchhoff-Love hypotheses

$$D\triangle^2 w - F_{,22}w_{,11} + 2F_{,12}w_{,12} + F_{,11}(k_{22} - w_{,22}) = q_{\mathrm{n}} - \rho_0 h\frac{\partial^2 w}{\partial t^2},$$
$$\triangle^2 F - k_{22}Ehw_{,11} + (w_{,12})^2 - w_{,11}w_{,22} = 0.$$

The linearization of Eqs. (2.77) and (2.87), with Eq. (2.82) taken into account, results in the following coupled equations

$$\begin{aligned} D\left(1 - \frac{\theta h^2}{\beta}\triangle\right)\triangle^2\chi - k_{22}F_{,11} &= q_{\mathrm{n}} - \rho_0 h\frac{\partial^2}{\partial t^2}\left(1 - \frac{h^2}{\beta}\triangle\right)\chi, \\ \triangle^2 F - Eh\left[k_{22}\left(1 - \frac{h^2}{\beta}\triangle\right)\chi_{,11}\right] &= 0. \end{aligned} \tag{2.90}$$

which will be generally used below for studying small forced and free vibrations of laminated cylindrical shells. When omitting the terms proportional to β^{-1}, one arrives at the well-known Mushtari-Donnell-Vlasov type equations (Mushtari and Galimov, 1961; Donnell, 1976; Wlassow, 1958).

2.1.12 *Error of Governing Equations*

The determination of an exact error of the developed single layer model for a multi-layered shell is a complicated problem which is not considered here. Below, to estimate approximately its error, we shall compare eigenvalues of some boundary-value problems on buckling and vibrations with results obtained by using the 3D finite-element simulation. In this subsection, we aim only to give some *asymptotic* estimations of errors of the governing equations based on the generalized Timoshenko hypotheses.

It is known that the error δ_{e} of the Kirchhoff-Love hypotheses has the order $\delta_{\mathrm{e}} \sim h_*$. It may be expected that accepted here the generalized Timoshenko hypotheses improves an accuracy of the governing equations and results in the error $\delta_{\mathrm{e}} \sim h_*^q$, where $q \geq 1$. However, as has been shown by Gol'denveizer (1961) and Koiter (1966), the index of variation ι of an expected solution may give the conclusive contribution in the estimation of an error. If $\iota < 1$, then in the framework of the Kirchhoff-Love hypotheses, this estimation is defined as

$$\delta_{\mathrm{e}} \sim \max\left\{h_*, h_*^{2-2\iota}\right\}.$$

For the governing equations (2.61)-(2.63) based on the generalized Timoshenko hypotheses, one has

$$\delta_{\mathrm{e}} \sim \max\left\{h_*^q, h_*^{2-2\iota}\right\}, \tag{2.91}$$

where $q \geq 1$. The peculiarity of Eqs. (2.61)-(2.63) and Eqs. (2.90) is that due to shears they have solutions with very high index of variation. So, for an isotropic and homogeneous shell with Young's and shear moduli E, G having the same asymptotic order ($E \sim G$), additional integrals taking into account shear have the index of variation $\iota = 1$. Then $\delta_e \sim 1$ and Eqs. (2.61)-(2.63) as well as Eqs. (2.90) become asymptotically incorrect. But if $G \sim h_*^{\zeta_G} E$, where $\zeta_G > 0$, then $\iota = 1 - \zeta_G/2 < 1$.

Now, consider Eqs. (2.90) which are analogous to the well-known Mushtari-Donnell-Vlasov type equations (Mushtari and Galimov, 1961; Donnell, 1976; Wlassow, 1958). They were obtained after significant simplifications which introduced the error of order $h_*^{2\iota}$. It is seen that the error of this equations has the order

$$\delta_e \sim \max\left\{h_*^{2\iota}, h_*^{2-2\iota}\right\}. \tag{2.92}$$

We remind that Eqs. (2.90) were derived under assumptions that $\iota = 1/2, \zeta_G = 1$. Hence, for solutions with the index $\iota = 1/2$, one obtains the error $\delta_e \sim h_*$.

Equations (2.90) can be also used to describe the *semi-momentless* dynamic stress state characterized by the index of variation $\iota = 1/4$ for a shear pliable shell with $\zeta_G \geq 1$. However, for solutions having the index of variation $\iota = 1/4$ (at $\zeta_G = 3/2$), the error increases and reaches the order $\delta_e \sim h_*^{1/2}$.

2.1.13 Displacement and Stress Function Boundary Conditions

If a problem (on buckling or vibration) is solved on the bases of the technical shell theory, the boundary conditions (2.51), (2.52) should be rewritten in terms of the displacements, stress and shear functions, χ, F and ϕ. Consider possible variants of the boundary conditions (2.51) at $\alpha_1 = \alpha_1^*$

1. The generalized displacements are bounded in the tangential directions

$$\hat{u}_1 = 0, \quad \hat{u}_2 = 0. \tag{2.93}$$

This variant is more difficult because the generalized displacements $\hat{u}_i$ are not expressed in the explicit form of χ, F and ϕ. However, Eqs. (2.7), (2.26), (2.27), (2.74), (2.78), (2.82) and (2.83) lead to the following system of differential equations for $\hat{u}_i$

$$\begin{aligned}
\hat{u}_{1,1} &= \frac{1}{Eh}(F,_{22} - \nu F,_{11}) + \frac{1}{2}hc_{13}\left(1 - \frac{h^2}{\beta}\triangle\right)\chi,_{11} \\
&\quad + \frac{1}{2}hc_{12}\left(\frac{\eta_2}{\eta_1}\frac{h^2}{\beta}\triangle\chi,_{11} - \phi,_{12}\right), \\
\hat{u}_{2,2} &= \frac{1}{Eh}(F,_{11} - \nu F,_{22}) + \frac{1}{2}hc_{13}\left(1 - \frac{h^2}{\beta}\triangle\right)\chi,_{22} \\
&\quad + \frac{1}{2}hc_{12}\left(\frac{\eta_2}{\eta_1}\frac{h^2}{\beta}\triangle\chi,_{22} - \phi,_{12}\right) - k_{22}\left(1 - \frac{h^2}{\beta}\triangle\right)\chi, \\
\hat{u}_{1,2} + \hat{u}_{2,1} &= -\frac{2(1+\nu)}{Eh}F,_{12} + hc_{13}\left(1 - \frac{h^2}{\beta}\triangle\right)\chi,_{12} \\
&\quad + \frac{1}{2}hc_{12}\left(\frac{2\eta_2}{\eta_1}\frac{h^2}{\beta}\triangle\chi,_{12} + \phi,_{11} - \phi,_{22}\right).
\end{aligned} \tag{2.94}$$

When solving Eqs. (2.94), we can satisfy conditions (2.93).

2. The edge is prestressed in the tangential directions

$$T_{11} = T_{11}^*, \quad T_{21} = T_{21}^*. \tag{2.95}$$

These conditions are equivalent to the following ones

$$F_{,22} = T_{11}^*, \quad F_{,21} = -T_{21}^*. \tag{2.96}$$

3. The conditions

$$\psi_1 = \psi_2 = 0 \tag{2.97}$$

mean that the shear in the axial and circumferential directions, respectively, are absent. They result in the equations

$$-\frac{\theta_2}{\theta_1}\frac{h^2}{\beta}\triangle\chi_{,1} + \phi_{,2} = 0, \quad \frac{\theta_2}{\theta_1}\frac{h^2}{\beta}\triangle\chi_{,2} + \phi_{,1} = 0. \tag{2.98}$$

4. The generalized bending and twisting couples are specified at the edge

$$\hat{L}_{11} = \hat{L}_{11}^*, \quad \hat{L}_{21} = \hat{L}_{21}^*. \tag{2.99}$$

These conditions are rewritten as follows

$$\begin{aligned} \chi_{,11} + \nu\chi_{,22} - (1-\nu)\phi_{,12} &= -\frac{\hat{L}_{11}^*}{D\gamma}, \\ \chi_{,12} - \frac{1}{2}(\phi_{,22} - \phi_{,11}) &= -\frac{\hat{L}_{21}^*}{D\gamma(1-\nu)}. \end{aligned} \tag{2.100}$$

5. The condition

$$w_{,1} = 0 \tag{2.101}$$

means that the edge does not rotate about the vector $\boldsymbol{e}_2$. It is reduced to the equation

$$\left(1 - \frac{h^2}{\beta}\triangle\right)\chi_{,1} = 0. \tag{2.102}$$

6. The generalized bending moment is specified

$$\hat{M}_{11} = \hat{M}_{11}^*. \tag{2.103}$$

This condition may be rewritten as

$$-\left(1 - \frac{\theta h^2}{\beta}\triangle\right)(\chi_{,11} + \nu\chi_{,22}) + (1-\nu)(1-\theta)\phi_{,12} = \frac{\hat{M}_{11}^*}{D}. \tag{2.104}$$

7. The condition $w = 0$ is equivalent to

$$\left(1-\frac{h^2}{\beta}\triangle\right)\chi=0. \tag{2.105}$$

8. The shear force in the $\boldsymbol{n}$-direction is specified

$$\hat{M}_{11,1}+2\hat{M}_{12,2}+T_{11}w_{,1}+T_{12}w_{,2}=Q_1^*+\hat{M}_{12,2}^*. \tag{2.106}$$

The substitution of Eqs. (2.60) for $\hat{M}_{1i}$ into Eq. (2.123), with Eqs. (2.7), (2.74), (2.78), (2.82) and (2.83) taken into account, results in the following condition at $\alpha_1 = \alpha_1^*$

$$-\left(1-\frac{\theta h^2}{\beta}\triangle\right)[\chi_{,111}+(2-\nu)\chi_{,122}]+(1-\nu)(1-\theta)\phi_{,222}$$
$$+\frac{1}{D}\left[F_{,22}\left(1-\frac{h^2}{\beta}\triangle\right)\chi_{,1}-F_{,12}\left(1-\frac{h^2}{\beta}\triangle\right)\chi_{,2}\right]=\frac{1}{D}\left(Q_1^*+\hat{M}_{12,2}^*\right). \tag{2.107}$$

If

$$Q_1^*+\hat{M}_{12,2}^*=0, \tag{2.108}$$

then the edge is free for displacements in the $\boldsymbol{n}$-direction, that is $w\neq 0$.

The natural boundary conditions listed above may be classified into four groups:

a) (2.93) and (2.96);
b) (2.98) and (2.100);
c) (2.102) and (2.104);
d) (2.105) and (2.107).

Within the range of each group, different boundary conditions are simultaneously not satisfied. For instance, if the homogeneous conditions (2.96) hold, then the edge $\alpha_1 = \alpha_1^*$ is free for the in-plane displacements, hence, $\hat{u}_i\neq 0$. And if conditions (2.100) are valid, then the shell is free for the shear in the α_i-direction, i.e., $\psi_i\neq 0$.

The list of boundary conditions given above is not complete. It does not contain the superposition of conditions from a fixed group from a)-d). For example, the equation

$$F_{,22}=k_{sp}\hat{u}_1 \quad \text{at} \quad \alpha_1=\alpha_1^*, \tag{2.109}$$

where, k_{sp} is the spring constant of a surrounding medium in the axial direction, represents the condition of elastic support of the edge in the $\boldsymbol{e}_1$-direction.

Some of the boundary conditions listed above are expressed by too complicated equations. However, in some cases their combinations result in simple equations:

1. The edge $\alpha_1=\alpha_1^*$ is simply supported, but there is the infinite rigidity diaphragm inhibiting shear along the edge plane

$$w=\hat{M}_{11}=\hat{L}_{11}=\psi_2=0. \tag{2.110}$$

In terms of the displacement, stress and shear functions, these conditions are represented by Eqs. (2.105), (2.103), (2.100) and (2.99), respectively, and after calculations may be reduced to the following conditions

$$\chi = \varDelta\chi = \varDelta^2\chi = \frac{\partial \phi}{\partial \alpha_1} = 0. \tag{2.111}$$

2. The edge $\alpha_1 = \alpha_1^*$ is simply supported, and the diaphragm is absent

$$w = \hat{M}_{11} = \hat{L}_{11} = \hat{L}_{12} = 0. \tag{2.112}$$

This combination of the boundary conditions is rewritten as follows

$$\begin{aligned}
&\left(1 - \frac{h^2}{\beta}\varDelta\right)\chi = 0, \quad \frac{\partial^2}{\partial \alpha_1^2}\left(1 - \frac{h^2}{\beta}\varDelta\right)\chi = 0,\\
&\left(\frac{\partial^2}{\partial \alpha_1^2} + \nu\frac{\partial^2}{\partial \alpha_2^2}\right)\chi - (1-\nu)\frac{\partial^2 \phi}{\partial \alpha_1 \alpha_2} = 0,\\
&2\frac{\partial^2 \chi}{\partial \alpha_1 \partial \alpha_2} + \frac{\partial^2 \phi}{\partial \alpha_1^2} - \frac{\partial^2 \phi}{\partial \alpha_2^2} = 0.
\end{aligned} \tag{2.113}$$

3. The edge $\alpha_1 = \alpha_1^*$ is clamped, and there is the infinite rigidity diaphragm inhibiting shear along the edge plane

$$w = \frac{\partial w}{\partial \alpha_1} = \psi_1 = \psi_2 = 0 \tag{2.114}$$

or

$$\begin{aligned}
&\left(1 - \frac{h^2}{\beta}\varDelta\right)\chi = 0, \quad \frac{\partial}{\partial \alpha_1}\left(1 - \frac{h^2}{\beta}\varDelta\right)\chi = 0,\\
&\frac{\partial \chi}{\partial \alpha_1} - \frac{\partial \phi}{\partial \alpha_2} = 0, \quad \frac{\partial \chi}{\partial \alpha_2} + \frac{\partial \phi}{\partial \alpha_1} = 0.
\end{aligned} \tag{2.115}$$

4. The edge $\alpha_1 = \alpha_1^*$ is clamped, and the diaphragm is absent

$$w = \frac{\partial w}{\partial \alpha_1} = \psi_1 = \hat{L}_{12} = 0 \tag{2.116}$$

or

$$\left(1 - \frac{h^2}{\beta}\varDelta\right)\chi = 0, \quad \frac{\partial \chi}{\partial \alpha_1} = \frac{\partial}{\partial \alpha_1}(\varDelta\chi) = \phi = 0. \tag{2.117}$$

It is seen that each variant from (2.111), (2.113), (2.115) or (2.117) is incomplete because it does not contain conditions for the generalized in-plane displacements $\hat{u}_i$ or stress resultants T_{i1}. For example, the conditions of free support, $T_{11} = \hat{e}_{22} = 0$, results in the additional conditions for the stress function (Grigolyuk and Kulikov, 1988)

$$F = \triangle F = 0 \quad \text{at} \quad \alpha_1 = \alpha_1^*. \tag{2.118}$$

In what follows, the boundary conditions (2.111) and (2.113) supplemented by Eqs. (2.118) will be considered as the basic ones. To study the main stress state of a shell with clamped edges, it will be sufficient to satisfy conditions (2.115) or (2.117) without considering the additional conditions for the in-plane displacements and/or the in-plane stress resultants.

2.1.14 Edge Effect Equations

In many cases the shell stress-strain state may be considered as a superposition of the main stress-strain stateand edge effects (Gol'denveizer, 1961). For a thin isotropic cylindrical shell the edge effect has the index of variation $\iota_1 = 1/2$ in the neighbourhood of an edge (e.g., $\alpha_1 = \alpha_1^*$) in the direction orthogonal to the edge and a small index of variation ι_2 in the circumferential direction. All magnitudes corresponding to this stress state are quickly decreasing functions as $|\alpha_1 - \alpha_1^*| \to \infty$.

In the theory of laminated shells based on the generalized Timoshenko hypotheses (2.2)-(2.4), the edge effect equations are derived in the same way as in the Kirchhoff-Love hypotheses based theory (Mikhasev, 2016). Let us consider the linearized Eqs. (2.61)-(2.63) and assume the following asymptotic estimates

$$\begin{gathered} w \sim h_* R, \quad \hat{u}_1 \sim h_*^{3/2} R, \quad \hat{u}_2 \sim h_*^{7/4} R, \quad \psi_i \sim h_*^{1/2}, \\ \left|\frac{\partial Z}{\partial \alpha_1}\right| \sim h_*^{-\iota_1} Z, \quad \left|\frac{\partial Z}{\partial \alpha_2}\right| \sim h_*^{-\iota_2} Z, \quad G \sim h_* E, \quad \iota_1 = 1/2, \quad \iota_2 \leq 1/4, \\ |q_1| \sim \frac{E}{1-\nu^2} h_*^{3/2}, \quad |q_2| \sim \frac{E}{1-\nu^2} h_*^{7/4}, \quad |q_{\mathrm{n}}| \sim E h_*^2 \quad \text{as} \quad h_* \to 0 \end{gathered} \tag{2.119}$$

which satisfy the above mentioned assumptions (2.70)-(2.72) for the *combined* stress state. In Eqs. (2.119), Z denotes any from the functions $\hat{u}_i, w, \psi_i$.

In each equation of system (2.61)-(2.63), we consider the main terms having the same order as $h_* \to 0$. In the first and second equations (2.61), the main summands have the orders $h_*^{1/2} R^{-1}$ and $h_*^{3/4} R^{-1}$, respectively. When taking these terms into account and omitting remaining ones, then Eqs. (2.61) are reduced to the differential equations

$$\frac{\partial^2 \hat{u}_1}{\partial \alpha_1^2} + \nu k_{22}(\alpha_2) \frac{\partial w}{\partial \alpha_1} = -\tilde{q}_1, \tag{2.120}$$

$$\frac{1+\nu}{2} \frac{\partial^2 \hat{u}_1}{\partial \alpha_1 \partial \alpha_2} + \frac{1-\nu}{2} \frac{\partial^2 \hat{u}_2}{\partial \alpha_1^2} + \frac{\partial}{\alpha_2} \left[k_{22}(\alpha_2) w\right] = -\tilde{q}_2. \tag{2.121}$$

In both Eqs. (2.62), the main terms have the order $h_*^{-1/2} R^{-2}$ and generate the following equations

$$\frac{\partial^2 \psi_2}{\partial \alpha_1^2} = \frac{2\beta}{(1-\nu) h^2} \psi_2, \tag{2.122}$$

$$\eta_2 \frac{\partial^3 w}{\partial \alpha_1^3} - \eta_1 \frac{\partial^2 \psi_1}{\partial \alpha_1^2} + \frac{\beta \eta_1}{h^2} \psi_1 = 0. \tag{2.123}$$

Writing these equations down, we have taken into account Eqs. (2.54), (2.59) and assumed the following estimation

$$q_{44} \sim h_* RG \tag{2.124}$$

as well. Finally, in Eq. (2.63), the main terms of the order $h_* R^{-1}$ give

$$\frac{h^2}{12(1-\nu^2)}\left(\eta_3 \frac{\partial^4 w}{\partial \alpha_1^4} - \eta_2 \frac{\partial^3 \psi_1}{\partial \alpha_1^3}\right) + \frac{k_{22}(\alpha_2)\nu}{1-\nu^2}\frac{\partial \hat{u}_1}{\partial \alpha_1} + \frac{k_{22}^2(\alpha_2)}{1-\nu^2} w = \tilde{q}_{\rm n}. \tag{2.125}$$

As seen, Eq. (2.122) for ψ_2 is independent of the others and the same as Eq. (2.85) for ϕ.

Let the surface load intensity be not high and its components satisfy the following inequalities

$$|q_1| \ll \frac{E}{1-\nu^2} h_*^{3/2}, \quad |q_2| \ll \frac{E}{1-\nu^2} h_*^{7/4}, \quad |q_{\rm n}| \ll E h_*^2. \tag{2.126}$$

Then $\tilde{q}_i, q_{\rm n}$ may be omitted,

$$\tilde{q}_{\rm n} = -\frac{\rho_0}{E}\frac{\partial^2 w}{\partial t^2},$$

and Eqs. (2.120), (2.121) and (2.124) degenerate into homogeneous ones which describe the simple edge effect.

From all solutions of the homogeneous equations (2.120)-(2.124), one needs to choose such integrals which satisfy conditions

$$\hat{u}_i, \psi_i, w \to 0 \quad \text{at} \quad |\alpha_1 - \alpha_1^*| \to \infty. \tag{2.127}$$

Fulfilling some transforms with the homogeneous equations (2.120), (2.123), (2.124), with condition (2.127) in mind, one obtains the basic equation of the dynamic edge effect

$$\frac{h^2\eta_3}{12(1-\nu^2)}\left(1 - \frac{\theta h^2}{\beta}\frac{\partial^2}{\partial \alpha_1^2}\right)\frac{\partial^4 \psi_1}{\partial \alpha_1^4} + \left(1 - \frac{h^2}{\beta}\frac{\partial^2}{\partial \alpha_1^2}\right)\left[k_{22}^2(\alpha_2)\psi_1 + \frac{\rho_0}{E}\frac{\partial^2 \psi_1}{\partial t^2}\right] = 0. \tag{2.128}$$

It is of interest to note that the edge effect equation written in terms of the normal displacement w has the same form

$$\frac{h^2\eta_3}{12(1-\nu^2)}\left(1 - \frac{\theta h^2}{\beta}\frac{\partial^2}{\partial \alpha_1^2}\right)\frac{\partial^4 w}{\partial \alpha_1^4} + \left(1 - \frac{h^2}{\beta}\frac{\partial^2}{\partial \alpha_1^2}\right)\left[k_{22}^2(\alpha_2)w + \frac{\rho_0}{E}\frac{\partial^2 w}{\partial t^2}\right] = 0. \tag{2.129}$$

In Eqs. (2.128), (2.129), terms proportional to $h^2/(R^2\beta)$ account for shear. When $\beta \to \infty$ ($G \to \infty$), Eq. (2.129) degenerates into the classical equation of the dynamical edge effect for a thin isotropic single layer shell in the Kirchhoff-Love hypotheses based theory. The properties of integrals of this equation are described in detail in Gol'denveizer (1961); Gol'denveizer et al (1979).

Equation (2.122) is independent of Eqs. (2.128), (2.129) and has two the exponentially decaying partial solutions. Its general solution is

$$\psi_2 = C_1 \exp\left[-\frac{1}{h}\sqrt{\frac{2\beta}{1-\nu}}(\alpha_1 - \alpha_1^*)\right] + C_2 \exp\left[-\frac{1}{h}\sqrt{\frac{2\beta}{1-\nu}}(\alpha_1^{**} - \alpha_1)\right], \tag{2.130}$$

where C_i are arbitrary constants. Now consider Eq. (2.128) or (2.129). Let Z be any of unknown functions (w, ψ_1 or any other). In static problems (including buckling ones based on the static Euler criteria) the inertia term $\partial^2 Z/\partial t^2$ is absent. Then, if $k_{22} \neq 0$, then Eqs. (2.128), (2.129) degenerate into the governing equations for the simple edge effect in the static shell theory accounting for shear. At $k_{22} = 0$ and $\partial^2 Z/\partial t^2 \neq 0$, one obtains the dynamic equations for laminated plates.

The properties of partial solutions of Eq. (2.129) depends strongly on the order of the reduced shear modulus G with respect to the reduced Young's modulus E. The case when $G \sim E$ is not considered here, because in this case $\beta \sim 1$ and Eq. (2.129) has solutions with the index of variation $\iota_1 = 1$. Let $Z = \hat{Z}e^{\mathrm{i}\omega t}$ and ω is a natural frequency of free vibrations.

Case 1. Let $G \sim h_* E$. Then $\beta \sim h_*$ and $K_1 = \frac{h^2}{\beta R^2} \sim h_* \sim \mu^2$, where

$$\mu^4 = \frac{h^2 \eta_3}{12(1-\nu^2)R^2}. \tag{2.131}$$

Then Eq. (2.129) may be rewritten in the dimensionless form which is more convenient for the asymptotic analysis

$$-\mu^6 \kappa\theta \frac{\partial^6 X}{\partial x^6} + \mu^4 \frac{\partial^4 X}{\partial x^4} - \mu^2 \kappa \left[k_2(\varphi) - \Lambda\right] \frac{\partial^2 X}{\partial x^2} + \left[k_2(\varphi) - \Lambda\right] X = 0. \tag{2.132}$$

Here

$$\begin{aligned} &w = \hat{w}e^{\mathrm{i}\omega t}, \quad \hat{w} = RX(x), \quad \alpha_1 = Rx, \quad \alpha_2 = R\varphi, \\ &K_1 = \mu^2\kappa, \quad k_2(\varphi) = Rk_{22}[R(\varphi)] \sim 1, \quad \Lambda = \frac{R^2\rho_0\omega^2}{E}. \end{aligned} \tag{2.133}$$

As shown by Gol'denveizer et al (1979), in the theory of thin elastic isotropic shells based on the Kirchhoff-Love hypotheses, the frequency parameter Λ satisfies the following asymptotic estimates

$$\Lambda = O\left(h_*^{2-4\iota}\right) \quad \text{if} \quad 1/2 \le \iota < 1 \tag{2.134}$$

and

$$\Lambda \sim h_*^{2-4\iota} \quad \text{for} \quad 0 \le \iota < 1/2, \tag{2.135}$$

where $\iota = \max\{\iota_1, \iota_2\}$ is the general index of variation of the stress-strain state. The definition of the symbol O is given in Chapt. 6. We remind (Gol'denveizer et al, 1979) that estimate (2.134) corresponds to the quasi-transverse vibrations, and case (2.135) does to the Rayleigh type vibrations.

Equations of the technical theory of laminated shells, derived in subsection 2.1.11, are valid in particular for cases when $\iota = 1/2$ and $\iota = 1/4$. So, estimates (2.134), (2.135) may be applied for the analysis of Eq. (2.132). The type of the edge integrals and their properties depend on the sign of the expression $\delta = k_2 - \Lambda$ in Eq. (2.132). If $\iota = 1/4$, then $\delta(\varphi) > 0$ for any φ, and when $\iota = 1/2$, then the positive sign may be changed for the opposite one for all φ. The case when $\delta(\varphi)$ changes the sign under variation of φ is not considered here.

Omitting calculations, we will give the approximate (asymptotic) estimations for the partial solutions of (2.132). Regardless of the sign of δ, this equation has the following two integrals

$$X_1 = \mathrm{e}^{-\frac{1}{\mu}\sqrt{\frac{1}{\theta\kappa}}(x - x^*)}[1 + O(\mu)], \quad X_2 = \mathrm{e}^{-\frac{1}{\mu}\sqrt{\frac{1}{\theta\kappa}}(x^{**} - x)}[1 + O(\mu)] \tag{2.136}$$

where $x(\varphi)^* \leq x \leq x^{**}(\varphi)$, and $x^* = \alpha^*/R$, $x^{**} = \alpha^{**}/R$.

Now, we assume that the inequality

$$\delta = k_2 - \Lambda > 0 \tag{2.137}$$

holds for any φ. Here, there are three different cases:

1) Let $\kappa > 2/\delta$ for any φ. Then, with accuracy up to the values of order $O(\mu)$, Eq. (2.132) gives the following four additional integrals

$$\begin{aligned} X_3 &\approx \mathrm{e}^{-\frac{1}{\mu}\sqrt{\frac{\kappa\delta + \sqrt{\kappa^2\delta^2 - 4\delta}}{2}}(x - x^*)}, \\ X_4 &\approx \mathrm{e}^{-\frac{1}{\mu}\sqrt{\frac{\kappa\delta + \sqrt{\kappa^2\delta^2 - 4\delta}}{2}}(x^{**} - x)}, \\ X_5 &\approx \mathrm{e}^{-\frac{1}{\mu}\sqrt{\frac{\kappa\delta - \sqrt{\kappa^2\delta^2 - 4\delta}}{2}}(x - x^*)}, \\ X_6 &\approx \mathrm{e}^{-\frac{1}{\mu}\sqrt{\frac{\kappa\delta - \sqrt{\kappa^2\delta^2 - 4\delta}}{2}}(x^{**} - x)}. \end{aligned} \tag{2.138}$$

2) It is assumed that $\kappa < 2/\delta$ for any φ. Then

$$\begin{aligned} X_3 &\approx \mathrm{e}^{-\frac{\delta}{\mu}(r_1 + \mathrm{i}r_2)(x - x^*)}, \quad X_4 \approx \mathrm{e}^{-\frac{\delta}{\mu}(r_1 + \mathrm{i}r_2)(x^{**} - x)}, \\ X_5 &\approx \mathrm{e}^{-\frac{\delta}{\mu}(r_1 - \mathrm{i}r_2)(x - x^*)}, \quad X_4 \approx \mathrm{e}^{-\frac{\delta}{\mu}(r_1 - \mathrm{i}r_2)(x^{**} - x)}, \end{aligned} \tag{2.139}$$

where $\mathrm{i} = \sqrt{-1}$ is the imaginary unit, and

$$r_1 = \cos\left(\frac{1}{2}\arctan\frac{\sqrt{4\delta-\kappa^2\delta^2}}{\kappa\delta}\right), \quad r_2 = \sin\left(\frac{1}{2}\arctan\frac{\sqrt{4\delta-\kappa^2\delta^2}}{\kappa\delta}\right).$$

3) Let $\kappa = 2/\delta$, where $k_2 = 1$ (a circular cylindrical shell). Then, one has

$$X_3 \approx \mathrm{e}^{-\frac{1}{\mu}\delta^{1/4}(x-x^*)}, \quad X_4 \approx \mathrm{e}^{-\frac{1}{\mu}\delta^{1/4}(x^{**}-x)},$$
$$X_5 \approx x\,\mathrm{e}^{-\frac{1}{\mu}\delta^{1/4}(x-x^*)}, \quad X_6 \approx x\,\mathrm{e}^{-\frac{1}{\mu}\delta^{1/4}(x^{**}-x)}. \tag{2.140}$$

The variant when the expression $\kappa - 2/\delta$ changes the sign at some line $\varphi = \varphi_*$ for a non-circular shell is not considered here.

It is seen that for $\kappa > 2/\sqrt{\delta}$, all partial solutions of Eq. (2.132) are not oscillating functions but exponentially decaying far from the edges. If $\kappa < 2/\sqrt{\delta}$, then Eq. (2.132) has four the oscillating and decaying integrals (2.139) and two the exponentially decreasing solutions (2.136).

Now, let

$$\delta = k_2 - \Lambda < 0 \tag{2.141}$$

for any φ. Then, in addition to the partial solutions (2.136), Eq. (2.132) has only the two integrals

$$X_3 \approx \mathrm{e}^{-\frac{1}{\mu}\sqrt{\frac{\kappa\delta+\sqrt{\kappa^2\delta^2-4\delta}}{2}}\,(x-x^*)},$$
$$X_4 \approx \mathrm{e}^{-\frac{1}{\mu}\sqrt{\frac{\kappa\delta+\sqrt{\kappa^2\delta^2-4\delta}}{2}}\,(x^{**}-x)} \tag{2.142}$$

with the properties of the edges effect integrals, and the last two partial solutions are the oscillating functions which are not written down here. Thus, in case (2.141), the edge effect equation (2.132) has only four the exponentially decaying integrals. It should be noted that the decay rate of functions (2.136) is higher than that of the remaining integrals. Indeed, a parameter θ is small. If we assume that $\theta \sim h_*^{\sigma_\theta}$, where $\sigma_\theta > 0$, then the index of variation for integrals (2.136) will be equal to $\iota_1 = (1+\sigma_\theta)/2$. Then, for integrals (2.136) to be asymptotically correct and satisfy the accuracy of our model, it should be assumed the inequality $\sigma_\theta < 1$. Thus, if $G \sim h_* E$, then the index of variation of the both integrals (2.136) lies in the interval $1/2 < \iota < 1$, and the index of variation for the remaining four integrals equals $\iota = 1/2$ as in the Kirchhoff-Love model.

Case 2. Now, we consider the case when $G \sim h_*^{3/2} E$. This estimate holds if a shell is assembled, for instance, out of elastic layers and cores made of a magnitorheological elastomer (s. Sect. 2.3). Here, $K_1 \sim h_*^{1/2}$ and Eq. (2.129) is rewritten as follows

$$-\mu^5\kappa\theta\frac{\partial^6 X}{\partial x^6}+\mu^4\frac{\partial^4 X}{\partial x^4}-\mu\kappa\left[k_2(\varphi)-\Lambda\right]\frac{\partial^2 X}{\partial x^2}+\left[k_2(\varphi)-\Lambda\right]X=0, \quad (2.143)$$

where $K_1=\mu\kappa$, $\kappa\sim 1$, and the remaining magnitudes are introduced by (2.133). The asymptotic analysis of Eq. (2.143) gives two the exponentially decreasing functions

$$\begin{aligned} X_1 &= \mathrm{e}^{-\dfrac{1}{\mu^{1/2}}\sqrt{\dfrac{1}{\kappa}}(x-x^*)}[1+O(\mu)], \\ X_2 &= \mathrm{e}^{-\dfrac{1}{\mu^{1/2}}\sqrt{\dfrac{1}{\kappa}}(x^{**}-x)}[1+O(\mu)] \end{aligned} \quad (2.144)$$

If $\delta>0$, then one obtains the additional four oscillating and decaying integrals,

$$X_3\approx \mathrm{e}^{-\dfrac{1}{\mu}\sqrt[4]{\dfrac{\delta}{4\theta}}(1+\mathrm{i})(x-x^*)},\quad X_4\approx \mathrm{e}^{-\dfrac{1}{\mu}\sqrt[4]{\dfrac{\delta}{4\theta}}(1+\mathrm{i})(x^{**}-x)},$$

$$X_5\approx \mathrm{e}^{-\dfrac{1}{\mu}\sqrt[4]{\dfrac{\delta}{4\theta}}(1-\mathrm{i})(x-x^*)},\quad X_6\approx \mathrm{e}^{-\dfrac{1}{\mu}\sqrt[4]{\dfrac{\delta}{4\theta}}(1-\mathrm{i})(x^{**}-x)}. \quad (2.145)$$

When $\delta<0$, Eq. (2.143) has only two the exponentially decreasing solutions,

$$X_3\approx \mathrm{e}^{-\dfrac{1}{\mu}\sqrt[4]{\dfrac{-\delta}{\theta}}(x-x^*)},\quad X_4\approx \mathrm{e}^{-\dfrac{1}{\mu}\sqrt[4]{\dfrac{-\delta}{\theta}}(x^{**}-x)}, \quad (2.146)$$

and the remaining two partial solutions are oscillating functions and not written down here. Taking into account the smallness of a parameter θ, one can conclude that the index of variation of integrals (2.145), (2.146) is larger than $1/2$. Assuming the estimate $\theta\sim h_*^{\sigma_\theta}$, we should to require the inequality $\sigma_\theta<2$.

So, in Case 2 (at $G\sim h_*^{3/2}E$), the properties of the edge effect integrals drastically differ from the ones of similar integrals in the classical Kirchhoff-Love model: two integrals (2.144) have the index $\iota=1/4$ and they may be carefully applied for the correction of the main stress state having the same index of variation and can not be considered as a correction for the state with more high index of variation; the remaining four integrals (2.145) (if $\delta>0$) or two ones (2.146) (at $\delta<0$) possess the index of variation $\iota=1/2+\sigma_\theta/4<1$ which is larger than this index in the classical theory. Integrals (2.145) or (2.146) may be used to correct the main stress state with the index of variation $\iota\le 1/2$. The index of variation of the shear parameter ψ_2 (s. Eq. (2.130)) also depends on the order of the reduced shear parameter G. When $G\sim h_*E$, then $\iota_1=1/2$, and for $G\sim h_*^{3/2}E$, one has $\iota_1=1/4$.

2.1.15 Governing Equations for Laminated Plates and Beams

In this item we shall consider governing equations for laminated plates and beams. They are derived, as particular cases, form equations for cylindrical shells.

2.1.15.1 Laminated Plates

Let the curvature $k_{22} = 0$. Then Eqs. (2.77), (2.87) degenerate into the nonlinear differential equations for a laminated plate

$$D\left(1-\frac{\theta h^2}{\beta}\triangle\right)\triangle^2\chi - F_{,22}\left(1-\frac{h^2}{\beta}\triangle\right)\chi_{,11} + 2F_{,12}\left(1-\frac{h^2}{\beta}\triangle\right)\chi_{,12} - F_{,11}\left(1-\frac{h^2}{\beta}\triangle\right)\chi_{,22} = q_{\mathrm{n}} - \rho_0 h\frac{\partial^2}{\partial t^2}\left(1-\frac{h^2}{\beta}\triangle\right)\chi, \tag{2.147}$$

$$\triangle^2 F - Eh\left\{\left[\left(1-\frac{h^2}{\beta}\triangle\right)\chi_{,12}\right]^2 - \left(1-\frac{h^2}{\beta}\triangle\right)\chi_{,11}\left(1-\frac{h^2}{\beta}\triangle\right)\chi_{,22}\right\} = 0. \tag{2.148}$$

For $w \ll h_* R$, these equations may be linearized, they reducing to the two independent equations for the displacement and stress functions:

$$D\left(1-\frac{\theta h^2}{\beta}\triangle\right)\triangle^2\chi = q_{\mathrm{n}} - \rho_0 h\frac{\partial^2}{\partial t^2}\left(1-\frac{h^2}{\beta}\triangle\right)\chi, \tag{2.149}$$

$$\triangle^2 F = 0. \tag{2.150}$$

Let the plate rests on an elastic foundation with a modulus of subgrade reaction c_{f}. Then Eq. (2.149) should be supplemented by the reaction force acting from the foundation:

$$D\left(1-\frac{\theta h^2}{\beta}\triangle\right)\triangle^2\chi + \left(c_{\mathrm{f}} + \rho_0 h\frac{\partial^2}{\partial t^2}\right)\left(1-\frac{h^2}{\beta}\triangle\right)\chi = q_{\mathrm{n}}. \tag{2.151}$$

The simplest model simulating the subgrade reaction is the Winkler foundation model. According to this model the spring constant c_{f} depends only on elastic properties of the foundation and is independent of the wave formation pattern of a plate. The detailed analysis of the response of an elastic foundation appears in Morozov and Tovstik (2010); Tovstik (2005). This analysis shows that the spring constant c_{f} depends on a number of waves on the surface of a thin-walled structure. Let the plate deflection be a periodic function of the coordinate α_1, α_2: $\chi = \chi_0 \sin k_1\alpha_1 \sin k_2\alpha_2$. Then, when assuming the rigid contact between the plate and foundation, one has

$$c_{\mathrm{f}} = \alpha_{\mathrm{f}} k, \quad \alpha_{\mathrm{f}} = \frac{2E_{\mathrm{f}}(1-\nu_{\mathrm{f}})}{(1+\nu_{\mathrm{f}})(3-4\nu_{\mathrm{f}})}, \quad k = \sqrt{k_1^2 + k_2^2}, \tag{2.152}$$

where $E_{\rm f}$ and $\nu_{\rm f}$ are the Young's modulus and Poison's ratio for the foundation. Eq. (2.152) has been obtained for an infinite plate rested on an elastic half-space. Therefore, the range of applicability of Eq. (2.151) is restricted by the following conditions:

1. it is valid far from the plate edges;
2. a foundation has to be sufficiently deep;
3. forces of inertia of a foundation are not taking into account.

2.1.15.2 Laminated Beams

Equation (2.151) may be readily reduced to the governing equation for a beam. We shall consider a laminated beam with the rectangular cross section with sides $h \times b$, where b is the beam width, and h is the total thickness of the beam. Let $q_{\rm n}$ and all required functions be independent of α_2. To proceed to the beam model, one needs to assume that ν_k, all functions with index 2, and derivatives of these functions with respect to α_2 are equal to zero in all foregoing equations. Then, multiplying Eq. (2.151) by b, one obtains the following equation

$$EI\eta_3 \left(1 - \frac{\theta h^2}{\beta}\frac{\partial^2}{\partial \alpha_1^2}\right)\frac{\partial^4 \chi}{\partial \alpha_1^4} + \left(c_{\rm f}' + \rho_l \frac{\partial^2}{\partial t^2}\right)\left(1 - \frac{h^2}{\beta}\frac{\partial^2}{\partial \alpha_1^2}\right)\chi = q_{\rm l}(\alpha_1, t), \tag{2.153}$$

where

$$I = \frac{h^3 b}{12}, \quad \rho_{\rm l} = \rho_0 bh, \quad q_{\rm l} = q_{\rm n} b, \quad c_{\rm f}' = c_{\rm f} b.$$

Here, I is the area moment 2nd order of the beam cross section, $\rho_{\rm l}, q_{\rm l}$ are the linear mass and load, respectively. Note also that θ, β, η_3 are calculated at $\nu_k = \nu = 0$.

Equation (2.153) should be supplemented by the one-dimensional equation (2.85) for ϕ. However, as will be shown below, the trivial solution $\phi = 0$ is the unique solution satisfying the appropriate boundary conditions for a beam. When $G \to \infty$ that means $\beta^{-1} \to 0$, then Eq. (2.153) degenerate into the classical equation which does not take shears into account.

2.2 Governing Equations of Shell Buckling

In this section we consider the principle equations which will be used in Chapt. 3 for the buckling analysis of thin laminated elastic cylindrical shells. The governing equations are derived from the geometrically non-linear equations obtained in the previous chapter. The physically non-linear formulation of the buckling problem, assuming the non-linear coupling of stresses on strains, is not considered below. The derived equations describe the bifurcation (branching) of both the moment and in-plane equilibrium stress-strain states. They are valid for cases when the shell thickness is small and buckling occurs with minor sizes of deflections.

2.2.1 Bending Stress State

In common case, buckling equations for a thin laminated cylindrical shell may be derived by considering variations of the full system of the nonlinear differential Eqs. (2.61)-(2.63), in which the inertia terms should be omitted. In this section, we consider the case when buckling occurs with minor sizes of dents at least at one of the directions at the shell surface. Then the simplified nonlinear equations (2.77), (2.85) and (2.87) of the technical theory of laminated shells written in terms of the functions F, χ, ϕ may be used as the initial ones.

It is assumed here and in what follows that the shell is under action of only conservative surface and/or edge loads. The load is called conservative, if the work done by it depends only on the end states of the shell and does not depend on the way of deformation. Problems on dynamic stability of the shell experiencing dynamic and non-conservative loads are not considered here. Solutions of similar problems may be found, for instance, in Lavrent'ev and Ishlinsky (1949); Srubschik (1985, 1988); Vol'mir (1972, 1976); Bolotin (1956); Fung and Sechler (1974). It should be noted that only the dynamic criterion gives accurate results for shells subjected to both dynamic and static non-conservative loads (Ziegler, 1968; Bolotin, 1956).

Let

$$F^\circ, \quad \chi^\circ, \quad \phi^\circ \tag{2.154}$$

be functions describing the initial (pre-buckling) stress state of a laminated cylindrical shell. Then, as follows from subsection 2.1.11, all the kinematic characteristics (normal deflection w°, generalized displacements $\hat{u}_i^\circ$, and angles of rotation ψ_i°) as well as the stress characteristics (in-plane stresses T_{ij}° and generalized moments $\hat{M}_{ij}^\circ, \hat{L}_{ij}^\circ$) are identically determined through the functions $F^\circ, \chi^\circ, \phi^\circ$. The functions $F^\circ, \chi^\circ, \phi^\circ$ or $w^\circ, \hat{u}_i^\circ, \psi_i^\circ, T_{ij}^\circ, \hat{M}_{ij}^\circ, \hat{L}_{ij}^\circ$ may be found from the linearized Eqs. (2.61)-(2.63), or (2.77), (2.85) and (2.87).

Following Euler, we consider the adjacent stress state which is infinitesimally close to the pre-buckling one and characterized by unknown functions

$$F^\circ + F, \quad \chi^\circ + \chi, \quad \phi^\circ + \phi. \tag{2.155}$$

Let us substitute functions (2.155) into the non-linear Eqs. (2.77), (2.85) and (2.87). Then, taking into account the fact that functions (2.155) satisfy the nonhomogeneous Eqs. (2.77), (2.85) and (2.87) with appropriate boundary conditions (which are not uniform in the common case) and performing linearization in a neighbourhood of the stress state characterized by (2.154), one obtains the following homogeneous buckling equations

$$
\begin{aligned}
&D\left(1-\frac{\theta h^2}{\beta}\Delta\right)\Delta^2\chi-\frac{\partial^2 w^\circ}{\partial\alpha_1^2}\frac{\partial^2 F}{\partial\alpha_2^2}+2\frac{\partial^2 w^\circ}{\partial\alpha_1\partial\alpha_2}\frac{\partial^2 F}{\partial\alpha_1\alpha_2}\\
&+\left(\frac{1}{R_2}-\frac{\partial^2 w^\circ}{\partial\alpha_2^2}\right)\frac{\partial^2 F}{\partial\alpha_1^2}-T_{11}^\circ\frac{\partial^2 w}{\partial\alpha_1^2}-2T_{12}^\circ\frac{\partial^2 w}{\partial\alpha_1\partial\alpha_2}-T_{22}^\circ\frac{\partial^2 w}{\partial\alpha_2^2}=0,\\
&\Delta^2 F=Eh\left(\frac{1}{R_2}\frac{\partial^2 w}{\partial\alpha_1^2}+2\frac{\partial^2 w^\circ}{\partial\alpha_1\partial\alpha_2}\frac{\partial^2 w}{\partial\alpha_1\partial\alpha_2}-\frac{\partial^2 w^\circ}{\partial\alpha_2^2}\frac{\partial^2 w}{\partial\alpha_1^2}-\frac{\partial^2 w^\circ}{\partial\alpha_1^2}\frac{\partial^2 w}{\partial\alpha_2^2}\right),\\
&w=\left(1-\frac{h^2}{\beta}\Delta\right)\chi,\qquad \frac{1-\nu}{2}\frac{h^2}{\beta}\Delta\phi=\phi,
\end{aligned}
\tag{2.156}
$$

where

$$
w^\circ=\left(1-\frac{h^2}{\beta}\Delta\right)\chi^\circ. \tag{2.157}
$$

When deriving Eq. (2.156), we used the introduced above Eq. (2.74)

$$
T_{ij}^\circ=\delta_{ij}\Delta F^\circ-\frac{\partial^2 F^\circ}{\partial\alpha_i\partial\alpha_j},\quad i,j=1,2. \tag{2.158}
$$

Equations (2.156) with appropriate homogeneous boundary conditions describe buckling of the moment stress state. If components of the external load (for instance, the external pressure q_{n} or the axial force T_{11}^*) are weakly varying functions of α_1,α_2, then the initial moment stress state may be found as a sum of the membrane stress state and the edge effect (Tovstik and Smirnov, 2001). The in-plane (momentless) stress state are determined by the stress-resultants T_{ij}° which are found from equations of the membrane shell theory, s. Eqs. (2.67), in which the inertia terms are omitted. The edge effect described by the displacement w° may be determined from the edge effect equation (2.129)

$$
D\left(1-\frac{\theta h^2}{\beta}\frac{\mathrm{d}^2}{\mathrm{d}\alpha_1^2}\right)\frac{\mathrm{d}^4 w}{\mathrm{d}\alpha_1^4}+\frac{Eh}{R_2^2}\left(1-\frac{h^2}{\beta}\frac{\mathrm{d}^2}{\mathrm{d}\alpha_1^2}\right)w=0. \tag{2.159}
$$

2.2.2 In-plane Stress State

Let the external load be such that the initial (pre-buckling) displacements u_i°, w° and the in-plane stress resultants T_{ij}° characterizing this state, are weakly varying functions of the curvilinear coordinates α_1,α_2. Then, the neutral surface before and after deformation may be identified (Tovstik and Smirnov, 2001). In other words, we may assume that being in the pre-buckling state the shell is stressed but not deformed (Alfutov, 2000). For this state called the in-plane stress state, it is assumed that $w^\circ=0$. Then the buckling equations (2.156) are simplified

$$D\left(1-\frac{\theta h^2}{\beta}\Delta\right)\Delta^2\chi+\frac{1}{R_2}\frac{\partial^2 F}{\partial\alpha_1^2}-\Delta_T w=0,$$
$$\Delta^2 F=\frac{Eh}{R_2}\frac{\partial^2 w}{\partial\alpha_1^2},\quad w=\left(1-\frac{h^2}{\beta}\Delta\right)\chi, \tag{2.160}$$
$$\frac{1-\nu}{2}\frac{h^2}{\beta}\Delta\phi=\phi,$$

where

$$\Delta_T w=T_{11}^{\circ}\frac{\partial^2 w}{\partial\alpha_1^2}+2T_{12}^{\circ}\frac{\partial^2 w}{\partial\alpha_1\partial\alpha_2}+T_{22}^{\circ}\frac{\partial^2 w}{\partial\alpha_2^2}, \tag{2.161}$$

and the in-plane stress-resultants T_{ij}° are found from the stationary counterparts of Eqs. (2.67) of the moment-less shell theory.

The differential equations (2.160) with an appropriate variant of boundary conditions (2.109)-(2.117) describe buckling of the in-plane stress state of a thin laminated shell. If the initial state is presented by the full system of in-plane stress resultants T_{ij}° (for instant, at combined loading), it is convenient to assume that the in-plane forces vary proportionally to a loading parameter λ

$$T_{ij}^{\circ}=\lambda t_{ij}^{\circ}. \tag{2.162}$$

Then the buckling problem is reduced to an eigenvalue problem which is to find the least positive $\lambda=\lambda^*$ for which this problem has a nontrivial solution. Found in this way the parameter λ^* is called buckling or critical loading parameter.

Equations (2.160) will be used in the next chapter for studying a number problems on the local buckling of thin sandwich and multi-layered cylindrical shells under different variant of loading. Note that at $\beta^{-1}\to 0$ (implying $G\to\infty$) Eqs. (2.160) degenerate into the well-known buckling equations of the technical theory of thin isotropic single layer shells which are based on the original Kirchhoff-Love hypothesis and were widely utilized by many researchers for investigation of an enormous number of problems (Donnell, 1976; Grigolyuk and Kabanov, 1978; Tovstik and Smirnov, 2001).

2.3 Laminated Cylindrical Shells with Viscoelastic Smart Layers

This section deals with laminated shells assembled from elastic and viscoelastic damping layers. In case of the harmonic response, elastic and viscous properties of damping layers are represented by the complex forms for Young's and shear moduli. It is discussed that smart materials, such as magnetorheological elastomers and electrorheological composites, may be used as damping elements of sandwich or multi-layered thin-walled structures. The mechanical and rheological properties of some smart viscoelastic magneto- and electrorheological materials affected by applied magnetic or electric field are given. The applicability of the equivalent single layer model for laminated shells with soft viscoelastic layers or cores is also discussed.

2.3.1 Viscoelastic Materials in Thin-walled Laminated Structures

Viscoelastic damping materials (VDMs) are used widely in thin-walled laminated structures. The traditional roles of their application usually are:

a) free layer damping (FLD);
b) constrained layer damping (CLD) (Zhou et al, 2015);
c) core damping (CD).

In the first case a), VDM is attached to the surface of an elastic layer, its outer surface being free. Earliest researches on application of VDMs in the capacity of FLD began in the early 1950s, by Oberst and Frankenfeld (1952) and Mead and Ae (1960).

In case b), VDM attached to the basic elastic lamina is in turn constrained by a backing very thin elastic layer or foil. A common example of CLD is the damping tape currently used in aircrafts. Kervin Jr. (1959); Ross et al (1959); Ungar and Kerwin Jr. (1962) may be the first studies where a quantitative analysis on the damping effectiveness of CLD was performed. After these research works, there were many other papers (e.g, s. DiTaranto, 1965; Mead and Markus, 1970; Yan and Dowell, 1972; Kumar and Singh, 2010; Wang and Chen, 2004; Raamesh and Ganesan, 1994) on vibrations of thin plates, beams, curved panels, cylindrical shells, and sandwiched structures tackled by CLD. The application of constrained viscoelastic treatments for improving damping capabilities became a very popular method in the case of thin-walled structures made of materials (e.g., steel, aluminium) which possess a little material damping. As a rule, a backing layer constraining VDM does not influence essentially the total stiffness of a thin-walled structure.

In the third variant c), VDM is embedded between two elastic layers, so that an assembled structure looks like a sandwich. In this case, both elastic layers are, as a rule, considerably stiffer than a soft VDM and serve as the bearing elements which define the total stiffness of a structure, whereas the embedded viscoelastic core ensures the damping mechanism. In the same way, multi-layered beams, plates or shells with alternating elastic and viscoelastic layers may be assembled. Pan (1969); Mead and Markus (1969), and DiTaranto (1965) must be the first who considered problems on damped vibrations of three-layered or multi-layered beams and shells with viscoelastic cores. By now, there are many papers which deal with different aspects of the influence of VDM as of damping core on suppression of vibrations of both sandwich and laminated thin-walled structures (s., among many others, Khatri, 1996; Zhou and Rao, 1996; Yu and Huang, 2001; Matter et al, 2011; Schwaar et al, 2011) and the survey article of Qatu et al (2010).

The damping capability of VDMs in a laminated structure depends not only on their viscous properties, but on densities of materials composing a structure, a number of layers (Saravanan et al, 2000) and correlations between thicknesses of elastic and viscolelastic laminas as well (Yan and Dowell, 1972; Hu and Huang, 2000; Jin et al, 2015).

2.3.2 Complex Moduli of Viscoelastic Materials

There are different theories on viscoelasticity and various models describing the dynamic response of the VDM (e.g., the simplest well known models of Maxwell and Kelvin-Voigt, their generalization to the Kelvin chain model (Parke, 1966) and Biot's one (Biot, 1958), numerous non-linear models listed in Bert (1947), the hereditary theory of material damping (Boltzmann, 1878; Gross, 1947; Volterra, 1950) and their subsequent generalizations, very popular fractional models as specific cases of the so-called hereditary continuous media (Koeller, 1984; Cosson and Michon, 1996, and many others).

The application of one or another model of a viscoelastic material depends on both its type and the character of the dynamic response of a structure. For instance, if a viscoelastic body or structure is subjected to the long-term exposure of external forces, or the force load is suddenly withdrawn and the non-stationary strain-stress state is characterized by the relaxation of stresses, then the hereditary theory of viscoelastic materials is usually applied. The fractional models are frequently used to study the dynamic response of elastomers (Cosson and Michon, 1996).

In the case of the harmonic (sinusoidal) response of polymers and elastomers, frequently utilized models are ones which are based on the assumption of the complex form for Young's and shear moduli (Kervin Jr., 1959; Ross et al, 1959)

$$E_{\mathrm{v}} = E'_{\mathrm{v}}(1 + \mathrm{i}\eta_1), \quad G_{\mathrm{v}} = G'_{\mathrm{v}}(1 + \mathrm{i}\eta_2), \tag{2.163}$$

where $E'_{\mathrm{v}}, G'_{\mathrm{v}}$ are storage moduli, and η_1, η_2 are loss factors. A storage modulus is a measure of VDM's elasticity and the loss factor determines how much energy will be dissipated in motion.

It is of interest to note that the first representation of stiffness in the complex form was given by Soroka (1949). According to Bert (1947), utilizing observations of Kimball and Lovell (1927) for many engineering VDMs, Soroka has proposed to replace the stiffness k in the undamped elastic system by the Kimball-Lovell *complex stiffness*

$$k = k' + \mathrm{i}k''. \tag{2.164}$$

Later, the viscoelastic models assuming the complex representation of the structural stiffness were used extensively in aircraft structural dynamic and flutter analyses (e.g., s. Scanlan and Rosenbaum, 1951).

In general case, for the VDM model represented by (2.163), the moduli $E_{\mathrm{v}}, G_{\mathrm{v}}$ are considered as independent magnitudes. If the VDM is assumed to be isotropic, then $E_{\mathrm{v}}, G_{\mathrm{v}}$ are coupled

$$G_{\mathrm{v}} = \frac{E_{\mathrm{v}}}{2(1 + \nu)}, \tag{2.165}$$

where ν is Poison's ratio of the VDM. As a rule, ν is taken as a real parameter for a viscoelastic material.

Regardless of the role of the VDM (FLD, CLD or CD) in a thin-walled structure, the shear phenomenon is the original source with which the VDM dissipates energy and damps vibrations. An analysis of the effect of this shear damping mechanism was first given by Kervin Jr. (1959) when studying vibrations of a constrained viscoelastic plate. Recently, Jin et al (2015) confirmed that the high damping capacity of the viscoelastic layer is mainly due to the shear deformations of the VDM. Furthermore, it has been shown that there exists an optimal shear modulus of the viscoelastic core which results in the best damping performance for a sandwich cylindrical shell.

Thus, the complex shear modulus $G_{\mathrm{v}} = G'_{\mathrm{v}} + \mathrm{i}G''_{\mathrm{v}}$ turns out to be basic in the damping mechanism, and its real and imaginary parts $G'_{\mathrm{v}}, G''_{\mathrm{v}}$ may be influenced by many factors. So, in accordance with Kerwin-Douglas-Yang model (Kervin Jr., 1959; Douglas and Yang, 1978), the parameters $G'_{\mathrm{v}}, G''_{\mathrm{v}}$ depend on the frequency ω and temperature T. Later, performing the finite-element simulation and companion experiment on vibrations of a damped sandwich plates with the viscoelastic core made of a polymer material (which belongs to class A of thermorheologically simple materials), Lu et al (1979) justified this model. The empirical equations for $G'_{\mathrm{v}}(\omega, T)$ and $G''_{\mathrm{v}}(\omega, T)$ were obtained by Drake in 1990 for seven different VDMs (s. Rao and He, 1992; Zhou and Rao, 1996).

Due to the long-range molecular order associated with their giant molecules, polymers and elastomers exhibit rheological behavior intermediate between that of a crystalline solid and a simple liquid (Bert, 1947). Important physical properties of these VDMs are the marked dependence of both stiffness and damping on frequency and temperature. However, traditional viscoelastic material are not affected by the action of other physical fields (such as electrical and magnetic ones). Because of the predetermined and limited range of variation of the complex shear modulus G_{v}, they are generally used for passive damping of vibrations.

2.3.3 Smart Electro- and Magnetorheological Materials [2]

Smart materials are designed materials having properties that can be significantly changed in a controlled manner by external stimulation of mechanical, electrical, magnetic, etc. fields. They have a lot of applications, for example as sensors or actuators. Thee modelling of their constitutive behavior is more complicated since mechanical responses with other physical fields should be considered. Finally, one gets a material for which a non-mechanical stimulus, for example changing of electrical or magnetic fields, can be transformed into changes of strains and stresses. Examples of similar materials are piezoelectric and magnetostrictive materials, shape memory alloys, electrorheological composites, magnetorheological fluids and elastomers.

---

[2] This subsection is written in cooperation with E.V. Korobko (A.V. Lykov Heat and Mass Transfer Institute of National Academy of Sciences of Belarus, Minsk, Belarus, e-mail: evkorobko@gmail.com).

The integration of viscoelastic smart materials (VSM) with traditional elastic ones or passive VDMs is a key idea in the modelling of smart structures and, particularly, smart thin-walled laminated structures. Indeed, a smart thin laminated shell (STLS) is able to develop stiffness and damping characteristics which can change in dependence of changes of the acting physical fields. Such an behavior is not related to a shell structure made of a traditional material. From all variety of VSMs we will study here magnetorheological fluids and elastomers and electrorheological composites. They will be considered as semi-active layers or cores in laminated beams, plates, panels and shells with viscoelastic properties.

Composite magnetorheological (MR) materials consist of magnetic micro - particles inserted into a diamagnetic or paramagnetic fluid, or into an elastic or viscoelastic medium (matrix). The magnetic interaction between these particles depend on many factors: magnetization direction of particles and their space distribution, the orientation of external magnetic field and the strain field in a composite material. Depending on the type of medium where magnetic particles are placed to, one differentiates magnetorheological elastomers (MRE), gels (MRG) and fluids (MRF).

MREs are magnetizable particles molded in non-magnetic elastomeric or rubber-like materials (Farshad and Benine, 2004; Li et al, 2009, 2010) including natural deformed polymer matrices (Farshad and Benine, 2004), natural rubbers (Yang et al, 2013) and synthetic ones (Sun et al, 2008; Bica et al, 2014; Wang et al, 2006; Sun et al, 2008), and MRFs are liquid dispersions of magnetic particles (Wiess et al, 1994; Zhurauski et al, 2008).

Composite electrorheological (ER) material, more often electrorheological fluid (ERF), is suspension of dielectric particles of different concentration in a viscous medium (Hao et al, 1998; Zhurauski et al, 2008). These materials can change their rheological properties under the action of electrical fields. Some ERFs with high concentration of dielectric particles under the action of electrical field show viscoelastic properties very close to properties of elastomer. Similar high-density smart liquid is often called electrorheological composite (ERC).

It should be noted that MR and ER fluids have some lacks. The first problem existing in MR/ER fluids is the particle sedimentation. Secondly, they do not keep their geometrical shape at a low electric or magnetic field level that leads to some technological problems at designing and running the solid-fluid structures. It is solid smart materials such as MREs that are mostly applicable in the vibration control of STLS (Ginder et al, 2001).

Viscoelastic properties of MR/ER materials strongly depend on both composition and ratio of all components. The optimum weight/density ratio of magnetic or dielectric particles, carrier viscous liquid and/or polymer matrix substantially determines shear modulus, viscosity and response time of VSMs. As far as MREs, their properties are also influenced by the technology of production. If a MRE is produced in the absence of a magnetic field, it possesses by isotropic properties (Venkateswara et al, 2010; Zajac et al, 2010). On the contrary, when the polymerization reaction is carried out in an external homogeneous magnetic field, then a MRE becomes highly polarized (Korobko et al, 2009) medium having anisotropic properties (Stepanov et al, 2007; Kallio et al, 2007; Bica et al, 2015). Furthermore, experimental works (Boczkowska et al, 2012) demonstrate that the maximum increase in the storage modulus G'_{v} of the polarized MRE placed in the homogeneous magnetic field strongly depends on the particles arrangement within the matrix with respect to the force lines of a magnetic field.

In the next two items, we will consider MRE and ERC elaborated in the Laboratory of Rheophysics and Macrokinetics (LRM) of A.V. Luikov Heat and Mass Transfer Institute (LHMTI) of the National Academy of Sciences of Belarus. For comparison, the elastic and rheological properties of other available smart composites will be considered as well.

2.3.3.1 Magnetorheological Elastomers

Let us consider here the anisotropic MRE consisting of deformed polymer matrix and magnetic particles embedded in this matrix (Korobko et al, 2012). The procedure of manufacturing this MRE was the following. A natural inorganic polymer (bentonite clay, size of laminar particles is 1 - 10 μm) in the synthetic oil *Mobil SAE* was used as a matrix for the MRE, and particles of carbonyl iron (particle size is about 20 μm) as a filler. The matrix for the MRE was prepared by thorough rubbing the polymer in surfactant-added oil. Then carbonyl iron particles were introduced (about 22 vol. %) into the prepared matrix. Densities of components and their volume concentrations for this MRE (called in what follows as MRE-1) are presented in Table 2.1.

The real and imaginary parts, G'_{v} and G''_{v}, of the complex shear modulus G_{v} for this MRE have been obtained by the method of rotational viscometry. The rheometer *Physica MCR 301* (Anton Paar) with the "plate-plate" measuring nest in the range of the magnetic field induction up to 1 Tesla (T) has been used for the experimental measurements. The viscoelastic properties were defined at different values of the magnetic induction B and for the amplitude of deformations varying from 0.01 to 2 %. The frequency of deformations was taken to be equal to $0.1,\ 10,\ 100$ Hz.

Figures 2.5 and 2.6 show the effect of the strain amplitude and the magnetic induction B on the storage and loss moduli G'_{v} and G''_{v} for the frequency $\omega = 10$ Hz. It is seen that the MRE-1 placed in a magnetic field keeps elastic properties only at small shear strains in the pre-yield regime; when the amplitude of shear deformations increases, the MRE structure reaches the yield point and begins to fail displaying the viscous flow features. For the MRE under consideration, the pre-yield regime

Table 2.1 Volume concentrations of the MRE-1 components and their densities.

MRE comonents	Density, g/sm^3	Weight, g	Volume concentration, %
Particles of carbonyl iron	7.50	54.8	22
Bentonite clay	1.65	21.5	39
Oil *Mobil SAE*	0.85	10.0	35
Surfactant oil	0.94	1.0	3
Total	2.63	87.3	100

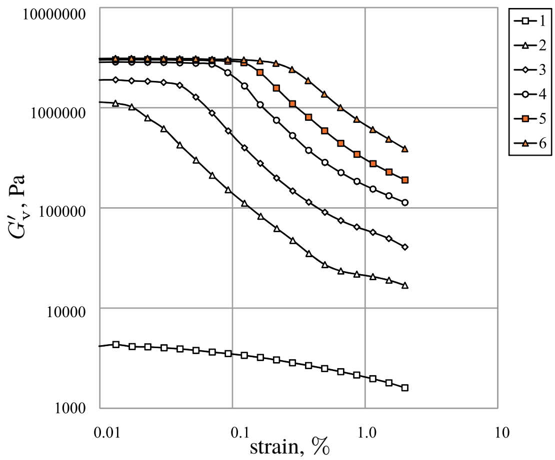

Fig. 2.5 Storage modulus G'_v of the MRE-1 vs. strain at the frequency $\omega = 10$ Hz for different values of the magnetic induction B:
1 - $B = 0$ mT,
2 - $B = 50$ mT,
3 - $B = 100$ mT,
4 - $B = 200$ mT,
5 - $B = 300$ mT,
6 - $B = 500$ mT.

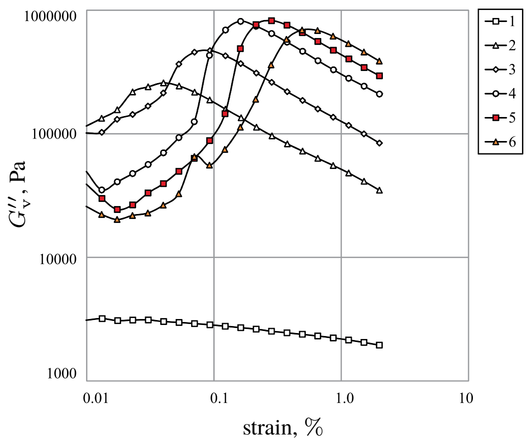

Fig. 2.6 Loss modulus G''_v of the MRE-1 vs. strain at the frequency $\omega = 10$ Hz for different values of the magnetic induction B:
1 - $B = 0$ mT,
2 - $B = 50$ mT,
3 - $B = 100$ mT,
4 - $B = 200$ mT,
5 - $B = 300$ mT,
6 - $B = 500$ mT.

strongly depends on the level of an applied magnetic field. In the absence of a magnetic field or for small values of B, the MRE pre-yield behavior is linearly viscoelastic only at very small shear deformations, but for $B = 300$ mT the pre-yield shear behavior is linearly viscoelastic for shear strains not exceeding $0.15\ \%$.

In Figs. 2.7 and 2.8, the dependence of the storage and loss moduli on the magnetic field induction are given for different frequencies of small shear deformations. As seen, under high frequency harmonic deformations of the MRE-1, the functions $G'_v(B), G''_v(B)$ display almost the same behavior. Thus, the storage and loss moduli of the MRE may be considered invariant with respect to the frequency of shear vibrations if this frequency exceeds about 10 Hz. These *invariants* (determined as average values in the frequency range from 10 to 100 Hz) versus the magnetic induction B are shown in Fig. 2.9 (Korobko et al, 2012). For the MRE-1, the maximum values of the storage and loss moduli, $\max G'_v \approx 3089$ kPa, $\max G''_v \approx 830$ kPa, are reached at $B \approx 500$ mT and $B \approx 250$ mT, respectively. The data presented in

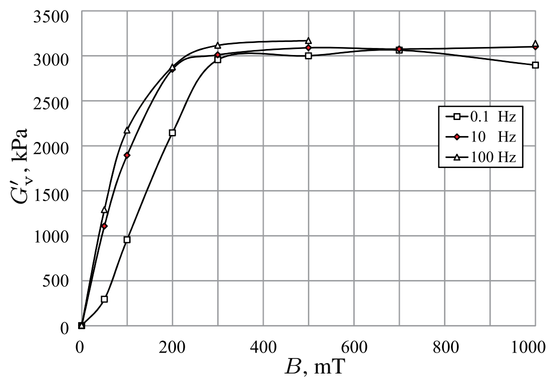

Fig. 2.7 Storage modulus G'_{v} of the MRE-1 vs. the magnetic induction B for different frequencies $\omega = 0.1; 10; 100$ Hz of excitation.

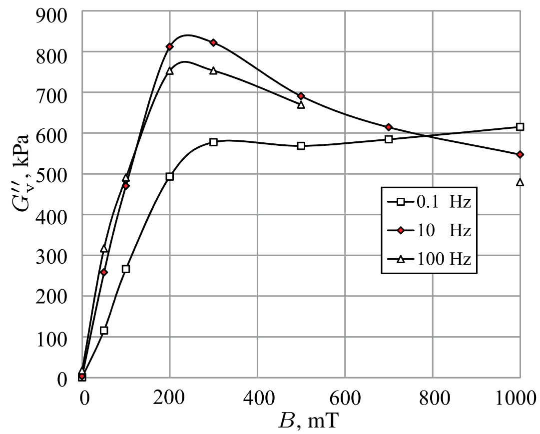

Fig. 2.8 Loss modulus G''_{v} of the MRE-1 vs. the magnetic induction B for different frequencies $\omega = 0.1; 10; 100$ Hz of excitation.

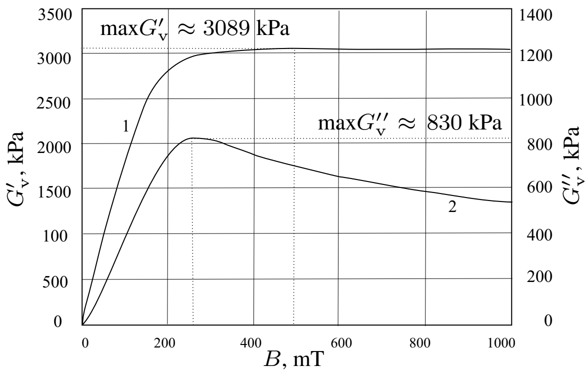

Fig. 2.9 Storage and loss moduli G'_{v} - line 1, G''_{v} - line 2 vs. the magnetic induction B for the MRE-1 (after Korobko et al, 2012).

Fig. 2.9 will be repeatedly used below for the analysis of damped vibrations of the MRE-based laminated beams, plates and shells. The major characteristic for a MRE is the loss factor which is determined by the ratio between the loss modulus G''_{v} and the storage modulus G'_{v} as

$$\eta_{\mathrm{v}} = \tan \delta_{\mathrm{v}} = \frac{G''_{\mathrm{v}}}{G'_{\mathrm{v}}}. \tag{2.166}$$

Figure 2.10 shows the effect of the applied magnetic field on the loss factor for the MRE-1 at different frequencies of shear deformations. One can see that at low-frequency oscillations of the sample, the loss factor η_{v} is the monotonically decreasing function of the magnetic induction B, but at frequencies exceeding 10 Hz there is a local maximum corresponding to the yield point of the MRE-1.

The analysis of actual researches reveals a large variety of MREs elaborated on the base of different polymeric materials. For comparison, we give here several examples of different MREs. The viscoelastic properties of the MRE-2 obtained by mixing the silicone oil and the RTV141A polymer with subsequent loading with 30% of ferromagnetic particles (Aguib et al, 2014) are presented in Table 2.2. According to Aguib et al (2014), the density of the MRE-2 equals 1.1 g/sm^3, Poisson's ratio is 0.44, and the Young' modulus is assumed to be the real constant magnitude, 1.7 MPa, independent of a magnetic field. So, the MRE-2 is treated as the transversally isotropic material.

Table 2.3 shows the compositions of different natural rubber based MREs elaborated by Chen et al (2008). For any of these elastomers, the matrix consists of the same components: 48.5% of natural rubber, 50% of plasticizers, and 1.5% of other additions. Properties of these MREs are presented in Tables 2.4-2.6.

When comparing properties of the MREs considered above, one can conclude that the MRE-1 possess the largest loss factor, and the MRE-5 with the highest content

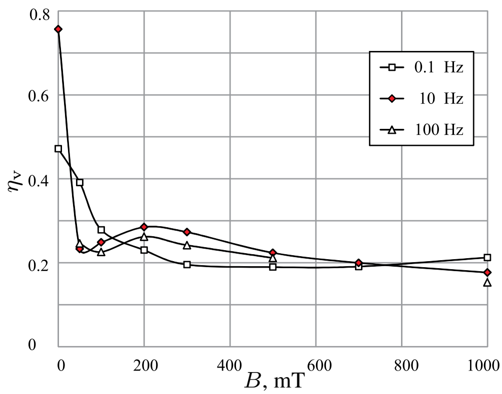

Fig. 2.10 Loss factor η_{v} for MRE-1 vs. the magnetic induction B at different frequencies of shear deformations.

Table 2.2 Storage and loss moduli G'_{v}, G''_{v} and loss factor η_{v} vs. the magnetic induction B for the MRE-2 (Aguib et al, 2014).

Magnetic induction B, mT	Storage modulus G'_{v}, kPa	Loss modulus G''_{v}, kPa	Loss factor η_{v}
0	1600	330	0.206
200	1760	500	0.284
350	1930	540	0.280
500	2070	350	0.170

Table 2.3 Composition of natural rubber based MREs elaborated by Chen et al (2008).

Sample	Magnetic particles, %	Carbon black, %	Matrix, %	Density, g/sm^3
MRE-3	33	0	67	1.895
MRE-4	33	4	63	1.872
MRE-5	33	7	60	1.855

Table 2.4 Storage and loss moduli $G'_{\rm v}$, $G''_{\rm v}$ and loss factor $\eta_{\rm v}$ vs. the magnetic induction B for the MRE-3 (Chen et al, 2007) containing 33% of iron particles and 0% of carbon black.

Magnetic induction B, MT	Storage modulus $G'_{\rm v}$, kPa	Loss modulus $G''_{\rm v}$, kPa	Loss factor $\eta_{\rm v}$
0	1000	220	0.22
200	1600	416	0.26
400	2100	504	0.24
600	2200	550	0.25
800	2300	1150	0.25

Table 2.5 Storage and loss moduli $G'_{\rm v}$, $G''_{\rm v}$ and loss factor $\eta_{\rm v}$ vs. the magnetic induction B for the MRE-4 (Chen et al, 2007) containing 33% of iron particles and 4% of carbon black.

Magnetic induction B, mT	Storage modulus $G'_{\rm v}$, kPa	Loss modulus $G''_{\rm v}$, kPa	Loss factor $\eta_{\rm v}$
0	2000	360	0.18
200	2200	440	0.20
400	2400	480	0.20
600	2500	500	0.20
800	2600	494	0.19

Table 2.6 Storage and loss moduli $G'_{\rm v}$, $G''_{\rm v}$ and loss factor $\eta_{\rm v}$ vs. the magnetic induction B for the MRE-5 (Chen et al, 2008) containing 33% of iron particles and 7% of carbon black.

Magnetic induction B, mT	Storage modulus $G'_{\rm v}$, kPa	Loss modulus $G''_{\rm v}$, kPa	Loss factor $\eta_{\rm v}$
0	4050	567	0.14
200	4250	723	0.17
400	6000	960	0.16
600	7900	1185	0.15
800	8000	1120	0.14

of carbon black has very large shear moduli. It is also interesting to note that adding carbon black results in the weak dependence of the loss factor on the magnetic field induction.

As mentioned above, viscoelastic properties of any MRE are very influenced by wether it is isotropic or anisotropic. Figure 2.11 illustrates the effect of a magnetic field on the storage modulus for the isotropic and anisotropic MREs with the matrix prepared from formoplast, which is a kind of silicon rubber (Demchuk and Kuzmin, 2002). The powder of iron with particles of the size about 23 μm was used as a filler for this MRE (called here as the MRE-6). It is seen that the orientation of magnetic

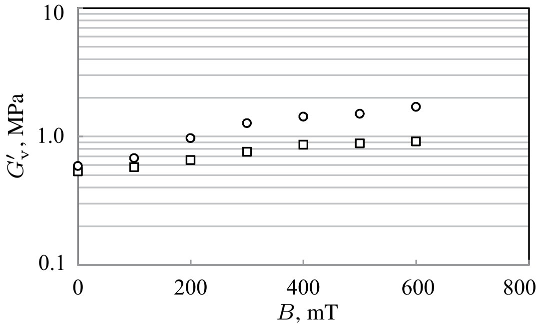

Fig. 2.11 Storage modulus G'_v (MPa) vs. the magnetic induction B (mT) for the isotropic and anisotropic MRE-6 (Demchuk and Kuzmin, 2002): □ - isotropic sample; ◯ - anisotropic sample.

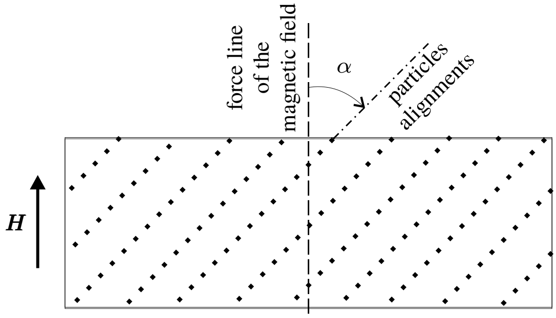

Fig. 2.12 Schematic representation of the particles alignment in the anisotropic MRE sample with reference to the force lines of the magnetic field.

particles influences the storage modulus: if a magnetic field is absent, this effect is weak, however in the magnetic field of a relatively high induction, the shear modulus of the anisotropic MRE-6 is about two times as much than for the isotropic sample.

The same effects were detected by other authors for the MREs made of natural rubber (Aguib et al, 2014) and polyurethane (Boczkowska et al, 2012). Furthermore, as follows from Boczkowska et al (2012); Kumar and Lee (2017), viscoelastic properties of a polarized MRE turn out to be very sensitive to the angle between the force lines of a magnetic field and the direction, in which the magnetic particles are aligned. In particular, samples of MREs with particles aligned perpendicular to the magnetic field (s. Fig. 2.12) and with isotropic distribution have exhibited relatively small rise in the storage modulus G'_v. But higher increase has been observed for the sample with parallel alignment ($\alpha = 0°$) and the highest for that with particle chains deflected at $\alpha = 45°$ and $\alpha = 30°$. So, at the frequency $\omega \approx 90$ Hz, the modulus G'_v for the sample with $\alpha = 30°$ was about 3.5 times as much than that for the sample with $\alpha = 0°$.

2.3.3.2 Electrorheological Composites

In this item, we shall consider a highly concentrated electrorheological liquid consisting of particles of goethite (wt. 45%), transformer oil (wt. 51%) and glycerol monooleate (wt. 4%). The viscoelastic properties of this ERC elaborated in the LRM of LHMTI strongly depend on the temperature. As seen from Figs. 2.13 and

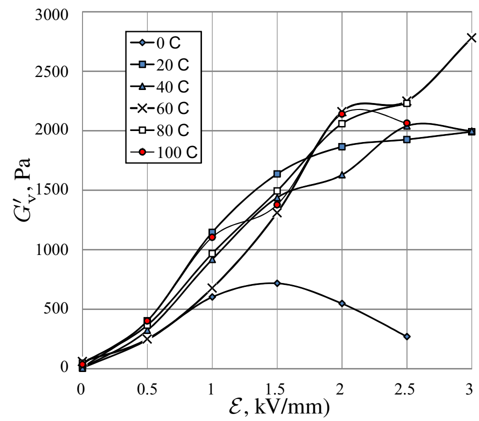

Fig. 2.13 Storage modulus G'_v vs. electric field strength $\mathcal{E}$ for the ERC with 45 % of the mass concentration of disperse phase.

2.14, the storage and loss moduli, G'_v and G''_v, increase together with the electric field strength $\mathcal{E}$ at all the interval from 0 to 2 kw/mm for any temperature from 20 to 80° C. At the zeroth temperature, the electrorheological activity of the dispersed phase is very low. At temperature 100° C, the effect of electric field drops. And the highest electrorheological activity is observed at 60° C: the moduli G'_v, G''_v are monotonically increasing functions of the electric field strength and reach large values (2779 and 504 kPa, respectively) for $\mathcal{E} = 3$ kw/mm.

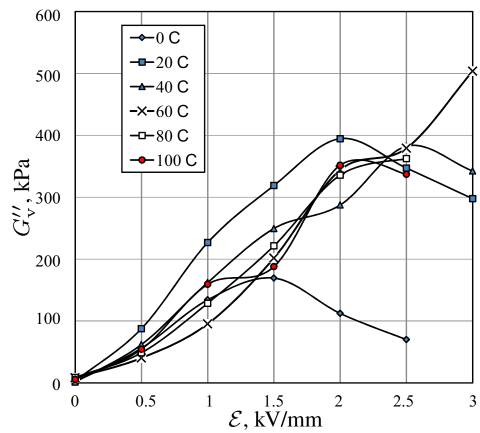

Fig. 2.14 Loss modulus G''_v vs. electric field strength $\mathcal{E}$ for the ERC with 45 % of the mass concentration of disperse phase.

2.3.3.3 Magnetorheological Fluids

We consider also three samples of magnetorheological fluids, MRF-1, MRF-2 and MRF-3, with the same percentage of iron particles in an oil (wt. 80%), but differing in particle size (s. Table 2.7). The elastic and rheological properties of these smart liquids elaborated in the LRM of LHMTI are presented in Tables 2.8-2.10.

The analysis of the loss factor η_v for all MRFs shows that in the absence of a magnetic field the MRF-1 with more large iron particles behaves as a less viscous liquid. When the value of the field induction exceeds 200 mT, there is the tendency of decreasing the value of η_v and the predominance of the elastic properties of the system as a whole.

When comparing all the smart magnetorheological materials presented above, one can see that for MRFs the increase in the magnetic field does not give a very large increment in the storage and loss moduli, which is characteristic of MREs. At the same time, MRFs posses the largest loss factor at the entire range of variation of a magnetic field induction.

The elastic and viscous properties of VSMs considered in this section will be used below for simulation of damping vibrations of the MRE/ERC/MRF-based laminated beams, plates and shells. It will be shown also that besides damping capabilities similar VSMs posses capacity to control the total stiffness of thin-walled structures and thus increase their load-carrying capability.

In what follows, all smart materials given in this section, except for MRE-2, will be treated as isotropic ones.

Table 2.7 Disperse phase of MRFs.

Sample	Graded of main component	Particle diameter, μm
MRF-1	S-1000	13
MRF-2	S-3700	3
MRF-3	S-3500	2

Table 2.8 The storage and loss moduli G'_v, G''_v and loss factor η_v vs. the magnetic induction B for the MRF-1.

Magnetic induction B, mT	Storage modulus G'_v, kPa	Loss modulus G''_v, kPa	Loss factor η_v
0	3.14	2.3	0.744
50	56.5	36.9	0.653
100	174.9	76.8	0.439
150	354.7	139.4	0.393
200	443.0	169.2	0.382
250	659.6	186.0	0.282
300	725.3	129.1	0.178
350	728.7	97.6	0.134

Table 2.9 The storage and loss moduli G'_{v}, G''_{v} and loss factor η_{v} vs. the magnetic induction B for the MRF-2.

Magnetic induction B, mT	Storage modulus G'_{v}, kPa	Loss modulus G''_{v}, kPa	Loss factor η_{v}
0	17.1	30.9	1.808
50	32.6	34.8	1.068
100	59.2	42.2	0.713
150	106.7	47.7	0.447
200	177.9	78.6	0.442
250	255.6	68.5	0.268
300	339.2	76.3	0.225
350	436.1	90.7	0.208

Table 2.10 The storage and loss moduli G'_{v}, G''_{v} and loss factor η_{v} vs. the magnetic induction B for the MRF-3.

Magnetic induction B, mT	Storage modulus G'_{v}, kPa	Loss modulus G''_{v}, kPa	Loss factor η_{v}
0	34.0	29.6	0.870
50	43.0	35.7	0.830
100	91.9	63.9	0.695
150	102.4	48.8	0.477
200	166.5	77.9	0.468
250	262.3	72.4	0.276
300	352.6	68.8	0.195
350	454.6	84.6	0.186
400	677.9	122.0	0.180
450	696.3	122.5	0.176

2.3.4 Governing Equations for Smart Cylindrical Shells

The differential equations derived in Sect. 2.2 may be adapted for the case when some of layers are made of viscoelastic material (Mikhasev et al, 2011). Let the k^{th} lamina be fabricated from a VSM described above. When assuming the harmonic (sinusoidal) dynamic response of a shell, the viscoelastic properties of this layer may be represented by the complex form (2.163) for Young's and shear moduli.

As mentioned above, many of VSMs possessing isotropy in absence of external magnetic or electric field, show anisotropic properties at high level of applied electromagnetic signal. For a thick layer this property has an essential effect on the modes for which the amplitudes of the tangential and normal displacements of a shell have the same order. But the thinner the VSM-based layer is, the less anisotropy affects the dynamic behaviour of a laminated shell. We assume everywhere that a thickness of each layer composing a laminated shell is sufficiently small with respect to the characteristic size R of a structure. In what follows, considering dynamic problems we will analyze only small flexural vibrations taking into account shear deformations. Then a viscoelastic layer may be assumed to be transversally isotropic. In this case, the complex moduli E_k and G_k for the k^{th} viscoelastic layer are coupled by

Eq. (2.165). For many elastomeric materials, Poison's ratio ν_{v} is about $0,4$ (White and Choi, 2005). Aguib et al (2014) consider a MRE (see above propereties for MRE-2) as a material closed to incompressible and assume $\nu_{\mathrm{v}} \approx 0.45$. We also consider Poisson's ratio ν_k for the k^{th} viscoelastic layer as a real parameter in the range from 0.4 to 0.45.

Because the moduli E_k and G_k are the complex magnitudes for the VSM-based layers, all coefficients appeared in the governing equations becomes complex functions of the magnetic induction B or electric field strength $\mathcal{E}$. In particular, the reduced Poisson's ratio ν, Young's modulus E, shear parameter β, bending stiffness D, and dimensionless stiffness γ_k defined by Eqs. (2.14), (2.18), (2.84), (2.88) and (2.19), respectively, will be complex. If a magnetic or electric field is not stationary, then they are complex function of time. In addition, due to different exposure of the external magnetic/electric field on different parts of the VSM-based layer, above complex magnitudes may depend on the curvilinear coordinates α_1, α_2.

The accuracy of the governing equations derived in Sect. 2.1 was formally discussed in Subsect. 2.1.13. However, the estimation of an error of the equivalent single layer (ESL) model for a multi-layered shell remains by an unsolved problem. One can states that the stiff characteristics of all layers composing a thin-walled multi-layered structure have to be approximately of the same order. One of the principle parameters affecting the error of the ESL model is the dimensionless stiffness γ_k. To minimize the total error, the geometrical and physical parameters of layers should be chosen in such away that parameters $|\gamma_k|$ were approximately the same for all $k = 1, 2, \ldots, N$, where N is a number of layers. As seen from (2.19), this requirement is equivalent to the estimate

$$\frac{|E_k|}{|E_{k+1}|} \sim \frac{h_{k+1}}{h_k} \quad \text{for any} \quad k = 1, 2, \ldots, N. \tag{2.167}$$

This condition becomes essential for shells assembled form elastic and more soft viscoelastic layers. As examples, we estimate here the parameters $|\gamma_k|$ for two three-layered plates having the same thicknesses of layers and made of different MREs. Let the top and bottom of both sandwiches be made of the ABS-plastic SD-0170 with parameters $E_1 = E_3 = 1.5 \cdot 10^3$ MPa, $\nu_1 = \nu_3 = 0.4$, and cores are fabricated from the MRE-1 and MRE-5, respectively. The viscoelastic properties of these materials were specified above (s. Fig. 2.9 and Table 2.4). Figures 2.15 and 2.16 show the parameters $|\gamma_1| = |\gamma_3|$, $|\gamma_2|$ for both samples versus the magnetic induction B at the fixed thickness $h_1 = h_3 = 0.5$ mm of the elastic top and bottom layers and different thicknesses $h_2 = 5, 8, 11, 15$ mm of the viscoelastic cores. It is seen that at a small level of a magnetic field, the parameters $|\gamma_k|$ differ appreciably for both cases, and with the increase of induction B (from 0 to 200 mT for MRE-1 and from 200 to 800 mT for MRE-5), plots for $|\gamma_1| = |\gamma_3|$ and $|\gamma_2|$ approach to each other, from above and below, respectively. The rise of the core thickness (under the fixed thicknesses of outer and innermost layers) also effects the stiff characteristics γ_k: the larger h_2 is, the faster values of $|\gamma_{1,3}|$ and $|\gamma_2|$ approach each other with increasing magnetic field. When comparing two types of MRE, one can conclude: for the MRE-5 based sandwich, condition (2.167) is satisfied better, whereas for the

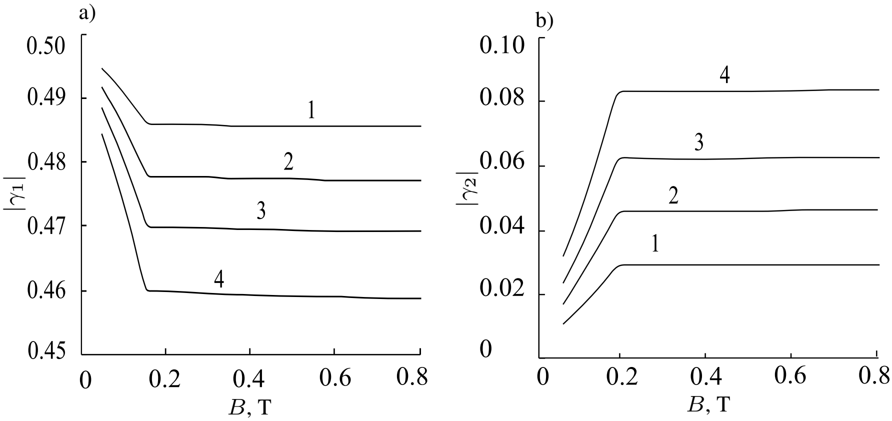

Fig. 2.15 Dimensionless stiffness parameters: a) $|\gamma_1| = |\gamma_3|$ and b) $|\gamma_2|$ vs. magnetic field induction B for MRE-1 at different thicknesses h_2 of the MRE-1 core: 1 - $h_2 = 5$ mm, 2 - $h_2 = 8$ mm, 3 - $h_2 = 11$ mm, 4 - $h_2 = 15$ mm.

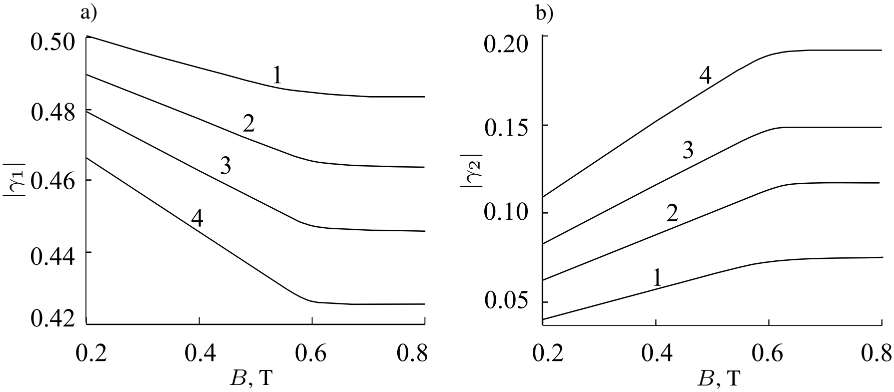

Fig. 2.16 Dimensionless stiffness parameters: a) $|\gamma_1| = |\gamma_3|$ and b) $|\gamma_2|$ vs. magnetic field induction B for MRE-5 at different thicknesses h_2 of the MRE-5 core:1 - $h_2 = 5$ mm, 2 - $h_2 = 8$ mm, 3 - $h_2 = 11$ mm, 4 - $h_2 = 15$ mm.

sample with the MRE-1 based core, this requirement can be reached by only further increment in the core thickness.

2.4 Finite Element Analysis

As mentioned above, the accurate estimate of an error of all equations derived in this chapter is still a subject for subsequent investigations. That is why it is a very important to have an alternative approach to compare solutions of problems found by different methods. The finite element method (FEM) is expected as the alternative and universal method permitting to evaluate the applicability of the governing equations and the ESL model in whole being developed in this book.

In the next chapters, to analyze buckling or vibrations of laminated cylindrical shell we will use the *SemiLoof* element family of the general purpose finite element package COSAR (Gabbert and Altenbach, 1990). The *SemiLoof* elements have been preferred due to their good overall accuracy in most shell applications and robustness compared with other possible finite shell elements. Originally, the *SemiLoof* element family was proposed by Irons (1976). The elements consists of 24 and 32 degrees of freedom (*dof*) for a curved six node triangular and an eight node quadrilateral element, respectively. These *dof* are the three displacements at each node, and additionally, the two tangential rotations at the two Gaussian integration points on each edge. The displacements and rotations are approximated by two families of shape functions, *Lagrange* polynomials are used for the displacements and *Legendre* polynomials are employed for the rotations. The element has $C^{(0)}$ continuity along the edges and a poitwise $C^{(1)}$continuity at the *Loof*-nodes (the two *Gaussian* integration points on the edges). The element fulfils the patch test.

In order to simulate different material layers the classical laminate theory (CLT) is used. For buckling analysis a second order theory is utilized (classical stability problem) to calculate the critical eigenvalues from the eigenvalue problem

$$(\mathbf{K}_{\mathrm{s}} - \lambda \mathbf{K}_{\sigma})\mathbf{u} = \mathbf{0} \tag{2.168}$$

with the stiffness matrix $\mathbf{K}_{\mathrm{s}}$, the geometric or initial stress matrix $\mathbf{K}_{\sigma}$ and the eigenvalue λ.

In stability problem (3.22), a single parameter load is considered where the critical stress state σ_{c} (first critical buckling point) is calculated from an initial stress state $\hat{\sigma}$ as

$$\sigma_{\mathrm{c}} = \lambda \hat{\sigma} \tag{2.169}$$

caused by the initial load state.

The initial stress state $\hat{\sigma}$ is calculated from a first linear solution of the cylindrical shell under the initial load state. In a second step the eigenvalue problem equation (3.22) is solved where the eigenvalue λ is the load parameter. The matrix $\mathbf{K}_{\sigma}$ is assembled from the following geometric element stiffness matrices (Zienkiewicz, 1977)

$$\mathbf{K}_{\sigma}^{(\mathrm{e})} = \int\limits_{V} \mathbf{G}_u^{\mathrm{T}} \hat{\sigma} \mathbf{G}_u \mathrm{d}V \tag{2.170}$$

where $\mathbf{G}_u$ contains the displacement gradient expressed by the shape function. The solution of the eigenvalue problem (2.168) results in the load factor λ, and the critical load level can be calculated by equation (2.169).

For a vibration analysis of elastic laminated shells the eigenvalue problem

$$(\mathbf{K}_{\mathrm{s}} - \omega^2 \mathbf{M}_{\sigma})\mathbf{u} = \mathbf{0} \tag{2.171}$$

has to be solved, where $\mathbf{M}$ is the mass matrix, and ω is the eigenfrequency.

References

Aguib S, Noura A, Zahloul H, Bossis G, Chevalier Y, Lançon P (2014) Dynamic behavior analysis of a magnetorheological elastomer sandwich plate. Int J Mech Sc 87:118–136

Alfutov NA (2000) Stability of Elastic Structures. Foundations of Engineering Mechanics, Springer, Berlin, Heidelberg

Bert CW (1947) Material damping: Introductory review of mathematic measures and experimental technique. J Sound Vibr 29(2):129–153

Bica I, Anitas EM, Bunoiu M, Vatzulik B, Juganaru I (2014) Hybrid magnetorheological elastomer: Influence of magnetic field and compression pressure on its electrical conductivity. J Indust Engng Chem 20(6):3994–3999

Bica I, Anitas EM, Averis LME, Bunoiu M (2015) Magnetodielectric effects in composite materials based on paraffin, carbonyl iron and graphene. J Indust Engng Chemist 21:1323–1327

Biot MA (1958) Linear thermodynamics and the mechanics of solids. In: Haythornthwaite RM (ed) Proc. of the Third U.S. National Congress on Applied Mechanics, ASME, New York, pp 1–18

Boczkowska A, Awietjan SF, Pietrzko S, Kurzydlowski KJ (2012) Mechanical properties of magnetorheological elastomers under shear deformation. Comp: Part B 43:636–640

Bolotin VV (1956) Dynamic Stability of Elastic Systems (in Russ.). Gostekhizdat, Moscow

Boltzmann L (1878) Zur Theorie der elastische Nachwirkung. Annalen der Physik lind Cbemie Suppl 241(11):430–432

Chen L, Gong XL, Jiang WQ, Yao JJ, Deng HX, Li WH (2007) Investigation on magnetorheological elastomers based on natural rubber. J Material Sc 42(14):5483–5489

Chen L, Gong XL, Li WH (2008) Effect of carbon black on the mechanical performances of magnetorheological elastomers. J Polymer Testing 27(3):340–345

Cosson P, Michon JC (1996) Identification by a non-integer order model of the mechanical behaviour of an elastomer. Chaos, Solutions and Fractals 7(11):1807–1824

Demchuk SA, Kuzmin VA (2002) Viscoelastic properties of magnetorheological elastomers in the regime of dynamic deformation. J Engng Phys Thermophys 75(2):396–400

DiTaranto RA (1965) Theory of vibratory bending for elastic and viscoelastic layered finite-length beams. Trans ASME J Appl Mech 32(4):881–886

Donnell LH (1976) Beams, Plates and Shells. McGraw-Hill Inc, New York

Douglas BE, Yang JCS (1978) Transverse compressional damping in the vibratory response of elastic-viscoelastic beams. AIAA J 16(9):925–930

Farshad M, Benine A (2004) Magnetoactive elastomer composites. Polymer Testing 23(3):347–353

Fung YC, Sechler EE (1974) Thin-Shell Structures: Theory, Experiments, and Design. Prentics-Hall, New Jersey

Gabbert U, Altenbach J (1990) COSAR - A reliable system for research and application (in Germ.). Technische Mechanik 11(3):125–137

Ginder GM, Schlotter WF, Nichhols ME (2001) Magnetorheological elastomers in tunable vibration absorbers. Proc SPIE 3985:103–110

Gol'denveizer AL (1961) Theory of Thin Elastic Shells. International Series of Monograph in Aeronautics and Astronautics, Pergamon Press, New York

Gol'denveizer AL, Lidsky VB, Tovstik PE (1979) Free Vibrations of Thin Elastic Shells (in Russ.). Nauka, Moscow

Grigolyuk EI, Kabanov VV (1978) Stability of Shells (in Russ.). Nauka, Moscow

Grigolyuk EI, Kulikov GM (1988) Multilayered Reinforced Shells. Calculation of Pneumatic Tires (in Russ.). Mashinostroenie, Moscow

Gross B (1947) On creep and relaxation. J Appl Phys 18(2):212–221

Hao T, Kawai A, Ikazaki F (1998) Mechanism of the electrorheological effect: evidence from the conductive, dielectric, and surface characteristics of water-fee electrorheological fluids. Langmuir 14(5):1256–1262

Hu YC, Huang SC (2000) The frequency response and damping effect of three-layer thin shell with viscoelastic core. Comp Struct 76(5):577–591

Irons BM (1976) The semiloof shell element. In: Ashwell DG, Gallagher R (eds) Finite Elements for Thin Shells and Curved Membranes, Wiley, New York, pp 197–222

Jin G, Yang C, Liu Z, Gao S, Zhang C (2015) A unified method for the vibration and damping analysis of constrained layer damping cylindrical shells with arbitrary boundary conditions. Comp Struct 130:124–142

Kallio M, Lindroos T, Aalto S, Karna T, Meinander T (2007) Dynamic compression testing of a tunable spring element consisting of a magnetorheological elastomer. Smart Mater Struct 16(2):506–514

Kervin Jr EM (1959) Damping of flexural waves by a constrained viscoelastic layer. The J Acoust Soc Am 31(7):952–962

Khatri KN (1996) Axisymmetric vibration of multilayered conical shells with core layers of viscoelastic material. Comp & Struct 58(2):389–406

Kimball AL, Lovell DE (1927) Internal friction in solids. Phys Rev Ser 2(30):948–959

Koeller RC (1984) Application of fractional calculus to the theory of viscoelasticity. Trans ASME J Appl Mech 51(2):299–307

Koiter WT (1966) On the nonlinear theory of thin elastic shells. Proc Koninkl Acad Westenschap B69:1–54

Korobko EV, Zhurauski MA, Novikova ZA, Kuzmin VA (2009) Rheological properties of magnetoelectrorheological fluids with complex disperse phase. J Phys: Conf Ser 149(1):012,065

Korobko EV, Mikhasev GI, Novikova ZA, Zurauski MA (2012) On damping vibrations of three-layered beam containing magnetorheological elastomer. Journal of Intelligent Material Systems and Structures 23(9):1019–1023

Kumar N, Singh SP (2010) Governing equations for vibrating constrained-layer damping sandwich plates and beams. Comp Struct 92(2):233–243

Kumar V, Lee DJ (2017) Iron particle and anisotropic effects on mechanical properties of magneto-sensitive elastomers. Journal of Magnetism and Magnetic Materials 441:105 – 112

Lavrent'ev MA, Ishlinsky AJ (1949) Dynamical modes of stability loss of elastic systems. Doklady Physics 64(6):776–782

Li WH, Zhou Y, Tian TF (2009) Sensing behavior of magnetorheological elastomers. J Mech Des 113(9):091,004–6

Li WH, Zhou Y, Tian TF (2010) Viscoelastic properties of mr elastomers under harmonic loading. Rheol Acta 49(7):733–740

Lu YP, Killian JW, Everstine GC (1979) Vibrations of three layered damped sandwich plate composites. J Sound Vibr 64(1):63–71

Matter M, Gmür T, Cugnoni J, Schorderet A (2011) Identification of the elastic and damping properties in sandwich structures with a low core-to-skin stiffness ratio. Comp Struct 93(2):331–341

Mead DJ, Ae DC (1960) The effect of a damping compound on jet-efflux excited vibrations: an article in two parts presenting theory and results of experimental investigation. Part I. The structural damping due to the compound. Aircraft Engineering and Aerospace Technology 32(3):64–72

Mead DJ, Markus S (1969) The forced vibration of a three-layer, damped sandwich beam with arbitrary boundary conditions. J Sound Vibr 10(2):163–175

Mead DJ, Markus S (1970) Loss factors and resonant frequencies of encastrè damped sandwich beams. J Sound Vibr 12(1):99–112

Mikhasev G, Botogova M, Korobko E (2011) Theory of thin adaptive laminated shells based on magnetorheological materials and its application in problems on vibration suppression. In: Altenbach H, Eremeyev V (eds) Shell-like Structures, Springer, Heidelberg, Advanced Structured Materials, vol 15, pp 727–750

Mikhasev GI (2016) Edge effect equations in the theory of thin laminated transversally-isotropic cylindrical shells with low shear stiffness (in Russ.). Vestnik BGU, Serie 1: Fiz Mat Inform 8(3):148–153

Mikhasev GI, Botogova GI (2017) Effect of edge shears and diaphragms on buckling of thin laminated medium-length cylindrical shells with low effective shear modulus under external pressure. Acta Mechanica 228(6):2119–2140

Morozov NF, Tovstik PE (2010) On modes of buckling for a plate on an elastic foundation. Mechanics of Solids 45(4):519–528

Mushtari K, Galimov K (1961) Nonlinear Theory of Thin Elastic Shells. NSF-NASA, Washington

Novozhilov V (1970) Theory of Thin Shells. Wolters-Noordhoff, Groningen

Oberst H, Frankenfeld K (1952) Über die Dämpfung der Biegeschwingungen dünner Bleche durch fest haftende Beläge. Acta Acustic united with Acustica 14(2, Suppl. 4):181–194

Pan HH (1969) Axisymmetrical vibrations of a circular sandwich shell with a viscoelastic core layer. J Sound Vibr 9(2):338–348

Parke S (1966) Logarithmic decrements at high damping. Brit J Appl Phys 17(2):271–273

Qatu MS, Sullivan RW, Wang W (2010) Recent research advances on the dynamic analysis of composite shells: 2000-2009. Comp Struct 93(1):14–31

Raamesh TC, Ganesan N (1994) Orthotropic cylindrical shells with a viscoelastic core: A vibration and damping analysis. J Sound Vibr 175(4):535–555

Rao MD, He S (1992) Analysis of natural frequencies and modal loss factors of simply supported beams with double-strap joints. J Acoust Soc Am 92(1):268–276

Ross D, Ungar EE, Kerwin EM (1959) Damping of flexural vibrations by means of viscoelastic laminae. In: Ruzicka JE (ed) Structural Damping, ASME, pp 49–87

Saravanan C, Ganesan N, Ramamurti V (2000) Vibration and damping analysis of multilayered fluid filled cylindrical shells with constrained viscoelastic damping using modal strain energy method. Comp Struct 75(4):395–417

Scanlan RH, Rosenbaum R (1951) Introduction to the Study of Aircraft Vibration and Flutter. Macmillan, New York

Schwaar M, Gmür T, Frieden J (2011) Modal numerical-experimental identification method for characterising the elastic and damping properties in sandwich structures with a relatively stiff core. Comp Struct 94(7):2227–2236

Soroka WW (1949) Note on the relations between viscous and structural damping coefficients. J Aeronautical Sc 16(7):409–410

Srubschik L (1988) Dynamical buckling of elastic shells under action of pulse loading. J Appl Math Mech 51(1)

Srubschik LS (1985) Energetic test of dynamical buckling of spherical shells. Soviet Phys Dokl 280(1)

Stepanov GV, Abramchuk SS, Grishin DA, Nikitin L, Kramarenko EY, Khokhlov AR (2007) Effect of a homogeneous magnetic field on the viscoelastic behavior of magnetic elastomers. Polymer 48(2):488–495

Sun TL, Gong XL, Jiang WQ, Li JF, Xu ZB, Li WH (2008) Study on the damping properties of magnetorheological elastomers based on cis-polybutadiene rubber. Polymer Testing 27(4):520–526

Tovstik PE (2005) Local buckling of plates and shallow shells on an elastic foundation. Mechanics of Solids 40(1):120–121

Tovstik PE, Smirnov AL (2001) Asymptotic Methods in the Buckling Theory of Elastic Shells. World Scientific, Singapore

Ungar EE, Kerwin Jr EM (1962) Loss factors of viscoelastic systems in terms of energy concepts. J Acoust Soc Am 34(7):954–957

Venkateswara RP, Maniprakash S, Srinivasan SM, Srinivasa AR (2010) Functional behavior of isotropic magnetorheological gels. Smart Mater Struct 19(8):085,019

Vol'mir AS (1972) Nonlinear Dynamics of Plates and Shells (in Russ.). Nauka, Moscow

Vol'mir AS (1976) Shells in a Liquid and Gas Flow. Problems of Aeroelasticity (in Russ.). Nauka, Moscow

Volterra E (1950) Vibrations of elastic systems having hereditary characteristics. Trans ASME J Appl Mech 17:363–371

Wang HJ, Chen LW (2004) Finite element dynamic analysis of orthotropic cylindrical shells with a constrained damping layer. Finite Elements in Analysis and Design 40(7):737–755

Wang YL, Hu Y, Deng HX, Gong XL, Zhang PQ, Jiang WQ, Chen Z (2006) Magnetorheological elastomers based on isobutylene-isoprene rubber. Polymer Engng & Sc 46(3):264–268

White J, Choi D (2005) Polyolefin. Processing, Structure, Development, and Properties. Carl Hanser, Munich

Wiess KD, Carlson JD, Nixon DA (1994) Viscoelastic properties of magneto- and electro-rheological fluids. J Intell Mater Syst Struct 5(6):772–775

Wlassow WS (1958) Allgemeine Schalentheorie und ihre Anwendung in der Technik. Akademie-Verlag, Berlin

Yan MJ, Dowell EH (1972) Governing equations for vibrating constrained-layer damping sandwich plates and beams. Trans ASME J Appl Mech 39(4):1041–1046

Yang IH, Yoon JH, Jeong JE, Jeong UC, Kim JS, Chung KH, Oh JE (2013) Magnetic-field-dependent shear modulus of a magnetorheological elastomer based on natural rubber. J Korean Phys Soc 62(2):220–228

Yu SC, Huang SC (2001) Vibration of a three-layered viscoelastic sandwich circular plate. Int J Mech Sc 43(10):2215–2236

Zajac P, Kaleta J, Lewandowski D, Gasperowicz A (2010) Isotropic magnetorheological elastomers with thermoplastic matrices: structure, damping properties and testing. Smart Mater Struct 19(4):045,014

Zhou H, Rao MD (1996) Damping of composite tubes with embedded viscoelastic layers. ASME J Vib Acoust 118(3):384–389

Zhou XQ, Yu DY, Shao X, Wang S, Zhang SQ (2015) Simplified-super-element-method for analyzing free flexural vibration characteristics of periodically stiffened-thin-plate filled with viscoelastic damping material. Thin-Walled Structures 94:234–252

Zhurauski MA, Dragašius E, Korobko EV, Novikova ZA (2008) Mechanical properties of smart fluids under combined electric and magnetic fields. Mechanika 6(74):21–24

Ziegler H (1968) Principles of Structural Statbility. Blaisdell Publ. Comp, Waltham, Massachusetts

Zienkiewicz OC (1977) The Finite Element Method. McGraw Hill Book Company Limited, New York

Chapter 3
Elastic Buckling of Laminated Beams, Plates, and Cylindrical Shells

Abstract In this chapter, we study the elastic buckling of thin-walled elastic laminated structures. As a preliminary, the simplest problems on stability of laminated beams and plates are considered in Sect. 3.1. Then, using the derived in Chapt. 2 governing equations based on the equivalent single-layer model, some classes of problem on the buckling of thin elastic laminated cylindrical shells under different loading (external pressure, axial compression and torsion) are considered. In Sect. 3.2, the buckling of a medium-length laminated cylindrical shell under external pressure is investigated. As the special case, using the asymptotic Tovstik's method, the localized buckling modes of a thin non-circular cylindrical shell with an oblique edge are studied. The problems on buckling of axially compressed laminated cylinders are considered in Sect. 3.3; a cylindrical shell under action of non-uniform axial forces is also examined. Finally, Sect. 3.4 is devoted to stability of laminated shells under axial torsion. In all cases, the influence of boundary conditions and transverse shears on the critical values of the buckling load parameter is analyzed. To verify the applied equivalent single-layer model, the finite-element analysis is performed for some of problems. We also show that the application of smart materials (i.e., magnetorheological elastomers) for assembling sandwiches or multi-layered thin cylinders allows to increase significantly the total stiffness of a structure and the critical buckling load as well.

3.1 Simple Problems on Buckling of Laminated Beams and Plates

In this section, we consider the simplest problems on buckling of laminated beam and plates with boundary conditions permitting to find a solution in an explicit form. In all cases, the geometrical and physical parameters are assumed to be constants so that coefficients in the governing equations do not depend on the coordinates α_1, α_2. The buckling loads and solutions found in such a way may be compared with well-known solutions for isotropic beams and plates.

G. I. Mikhasev and H. Altenbach, *Thin-walled Laminated Structures*,
Advanced Structured Materials 106, https://doi.org/10.1007/978-3-030-12761-9_3

3.1.1 Laminated Beams

At first, we consider a laminated beam of the total thickness h, width b and length L subjected to a uniform axial compression by the force N_1°. The differential equation describing buckling of the beam is easily obtained from the first equation of system (2.160)

$$EI\eta_3\left(1-\frac{\theta h^2}{\beta}\frac{\mathrm{d}^2}{\mathrm{d}x^2}\right)\frac{\mathrm{d}^4\chi}{\mathrm{d}x^4}+N_1^\circ\left(1-\frac{h^2}{\beta}\frac{\mathrm{d}^2}{\mathrm{d}x^2}\right)\frac{\mathrm{d}^2\chi}{\mathrm{d}x^2}=0. \tag{3.1}$$

where $x=\alpha_1$ is the axial coordinate. The bending stiffness D and the axial stress resultant T_{11}° are replaced by $EI=Eh^3b/12$ and $N_1^\circ=-T_{11}^\circ b$, respectively. We remind that for a beam the magnitudes β,θ are calculated at $\nu=\nu_k=0$. The third equation from system (2.160) describing the shear function becomes as follows

$$\frac{h^2}{2\beta}\frac{\mathrm{d}^2\phi}{\mathrm{d}x^2}-\phi=0. \tag{3.2}$$

Let us consider here only two basic sets of boundary conditions at $x=0,L$: the simple support and rigid clamping conditions. For a beam these conditions are substantially simplified

1. simple supported boundary conditions
   - edge with diaphragm
   $$\chi=\frac{\mathrm{d}^2\chi}{\mathrm{d}x^2}=\frac{\mathrm{d}^4\chi}{\mathrm{d}x^4}=0,\quad \frac{\mathrm{d}\phi}{\mathrm{d}x}=0, \tag{3.3}$$
   - edge without diaphragm
   $$\chi-\frac{h^2}{\beta}\frac{\mathrm{d}^2\chi}{\mathrm{d}x^2}=0,\quad \frac{\mathrm{d}^2\chi}{\mathrm{d}x^2}-\frac{h^2}{\beta}\frac{\mathrm{d}^4\chi}{\mathrm{d}x^4}=0,\quad \frac{\mathrm{d}^2\chi}{\mathrm{d}x^2}=0,\quad \frac{\mathrm{d}^2\phi}{\mathrm{d}x^2}=0, \tag{3.4}$$
2. rigid clamped boundary conditions
   - edge with diaphragm
   $$\chi-\frac{h^2}{\beta}\frac{\mathrm{d}^2\chi}{\mathrm{d}x^2}=0,\quad \frac{\mathrm{d}\chi}{\mathrm{d}x}-\frac{h^2}{\beta}\frac{\mathrm{d}^3\chi}{\mathrm{d}x^3}=0,\quad \frac{\mathrm{d}\chi}{\mathrm{d}x}=0,\quad \frac{\mathrm{d}\phi}{\mathrm{d}x}=0, \tag{3.5}$$
   - edge without diaphragm
   $$\chi-\frac{h^2}{\beta}\frac{\mathrm{d}^2\chi}{\mathrm{d}x^2}=0,\quad \frac{\mathrm{d}\chi}{\mathrm{d}x}=0,\quad \frac{\mathrm{d}^3\chi}{\mathrm{d}x^3}=0,\quad \phi=0. \tag{3.6}$$

It is obvious that $\phi=0$ is the unique solution of Eq. (3.2) for any variant of the boundary conditions listed above. It is also seen that within the scope of each set (simple support or rigid clamping) the boundary conditions become identical. In other words, a diaphragm does not effect on the buckling behavior of a laminated beam represented by our model.

The general solution of Eq. (3.1) has the form

$$\chi = c_1 \sin\left(\sqrt{r_1}\,\frac{x}{L}\right) + c_2 \cos\left(\sqrt{r_1}\,\frac{x}{L}\right) + c_3 \mathrm{e}^{\sqrt{r_2}\,\frac{x}{L}} + c_4 \mathrm{e}^{-\sqrt{r_2}\,\frac{x}{L}} + c_5 \frac{x}{L} + c_6, \tag{3.7}$$

where c_j are constants which should be determined using the boundary conditions, and

$$\begin{aligned}
&r_1\left(P^\circ\right) = b - a, \quad r_2\left(P^\circ\right) = a + b, \\
&a\left(P^\circ\right) = \frac{1 - K_1 P^\circ}{2\theta K_1}, \quad b\left(P^\circ\right) = \frac{\sqrt{1 - 2(1-2\theta)K_1 P^\circ + K_1^2 (P^\circ)^2}}{2\theta K_1}, \\
&P^\circ = \frac{L^2 N_1^\circ}{EI\eta_3}, \quad K_1 = \frac{h^2}{\beta L^2}.
\end{aligned} \tag{3.8}$$

3.1.1.1 Simply Supported Beams

Let us assume that both edges $x = 0, L$ are simply supported. The substitution of Eq. (3.7) into the boundary conditions (3.3) or (3.4) results in

$$c_1 \neq 0, \quad c_2 = c_3 = c_4 = c_5 = c_6, \quad \sin(\sqrt{r_1}) = 0. \tag{3.9}$$

From the last equation, one obtains

$$N_1^\circ = \frac{\pi^2 n^2 EI\eta_3 \left(1 + \dfrac{\pi^2 n^2 \theta h^2}{L^2 \beta}\right)}{L^2 \left(1 + \dfrac{\pi^2 n^2 h^2}{L^2 \beta}\right)}. \tag{3.10}$$

Then the critical buckling stress resultant

$$N_{\mathrm{cr}}^* = \max_n N_1^\circ = \frac{1 + \dfrac{\theta h^2}{\beta EI}\, N_{\mathrm{E}}^*}{1 + \dfrac{h^2}{\beta EI}\, N_E^*}\, N_{\mathrm{E}}^*\, \eta_3, \tag{3.11}$$

where

$$N_{\mathrm{E}}^* = \frac{\pi^2 EI}{L^2} \tag{3.12}$$

is the classical Euler's critical load of the buckling stress resultant (Euler, 1759). The corresponding buckling mode is

$$\chi(x) = c_1 \sin\left(\sqrt{r_1^*}\,\frac{x}{L}\right), \tag{3.13}$$

where

$$r_1^* = r_1\left(P_{\mathrm{cr}}^*\right), \qquad P_{\mathrm{cr}}^* = \frac{L^2 N_{\mathrm{cr}}^*}{EI\eta_3}.$$

Fulfilling the limit transition to the classical model, one has

$$\lim_{\beta \to +\infty} N_{\mathrm{cr}}^* = N_{\mathrm{E}}^*.$$

Example 3.1. Let us apply the derived Eq. (3.11) for a single-layer beam to compare the shear deformation induced correction based on our model with the correction presented in Timoshenko (1936). For the single-layer beam, the Eqs. (2.25), (2.54), (2.59), (2.84) and (2.89) yield

$$\theta = \frac{1}{85}, \quad \beta = \frac{9.09G}{E}, \quad \eta_3 = 1, \tag{3.14}$$

and Eq. (3.11) results in

$$N_{\mathrm{cr}}^* = \frac{1 + \dfrac{0.0155}{hbG}\,N_{\mathrm{E}}^*}{1 + \dfrac{1.32}{hbG}\,N_{\mathrm{E}}^*}\,N_{\mathrm{E}}^*, \tag{3.15}$$

where G is the shear modulus. We note that Eq. (3.15) for the critical stress resultant is based on the generalized (kinematical) hypothesis of Timoshenko stated in Chapt. 2, whereas the known Timoshenko's formula accounting shear has the following form (Timoshenko, 1936)

$$N_{\mathrm{cr}}^* = \frac{N_{\mathrm{E}}^*}{1 + (hbG)^{-1}\,N_{\mathrm{E}}^*}. \tag{3.16}$$

One can calculate the relative correction induced by (3.15) with respect to the classical Euler's force N_{E}^*. Assuming isotropic material with $G = E/2$, one obtains

$$\delta_N = \frac{N_{\mathrm{E}}^* - N_{\mathrm{cr}}^*}{N_{\mathrm{E}}^*} \approx 2.146\left(\frac{h}{L}\right)^2. \tag{3.17}$$

The similar correction from Timoshenko's formula is

$$\delta_N \approx 1.645\left(\frac{h}{L}\right)^2. \tag{3.18}$$

It is seen that our model based on the generalized hypothesis of Timoshenko (Grigolyuk and Kulikov, 1988b) gives slightly higher correction value in comparison with the known model by Timoshenko (1936).

3.1.1.2 Simply Supported and Clamped Beams

Let the edge $x = 0$ be simply supported, and $x = L$ be clamped. In this case, substituting (3.7) into the boundary conditions (3.3), (3.6) yields the coefficients

$$\begin{aligned} &c_2 = c_6 = 0, \quad c_4 = -c_3, \quad c_3 = \left(\frac{r_1}{r_2}\right)^{3/2} \frac{\cos(\sqrt{r_1})}{\mathrm{e}^{\sqrt{r_2}} + \mathrm{e}^{-\sqrt{r_2}}} c_1, \\ &c_5 = -\frac{r_1^{1/2}(r_1 + r_2)\cos(\sqrt{r_1})}{r_2} c_1 \end{aligned} \tag{3.19}$$

and the following transcendental equation for determining the critical dimensionless load parameter P^*_{cr} can be obtained

$$\tan\left(\sqrt{r_1 (P^\circ)}\right) = C (P^\circ), \tag{3.20}$$

where

$$C = \frac{r_1^{1/2}(r_1 + r_2)}{r_2(1 + K_1 r_1)} - \left(\frac{r_1}{r_2}\right)^{3/2} \frac{1 - K_1 r_2}{1 + K_1 r_1} \tanh\sqrt{r_2}, \tag{3.21}$$

and $r_1(P^\circ)$, $r_2(P^\circ)$ are determined by Eqs. (3.8). Equation (3.20) is invariant with respect to the geometrical and physical parameters of the laminated beam. Let P^*_{cr} be the least positive root of Eq. (3.20). Then

$$N^*_{\mathrm{cr}} = \frac{EI\eta_3}{L^2} P^*_{\mathrm{cr}} \tag{3.22}$$

is the critical buckling value of the axial stress resultant N_1°. In the limit case at $K_1 \to 0$, one obtains $r_1 \to P^\circ$, $r_2 \to +\infty$ and Eq. (3.20) degenerates into the known equation

$$\tan\left(\sqrt{P^\circ}\right) = \sqrt{P^\circ}$$

for a simply supported-clamped beam not taking into account transverse shear. The last equation gives $P^*_{\mathrm{cr}} \approx 20.2$ and we obtain the classical formula for the critical stress resultant (e.g., s. Alfutov, 2000)

$$N^*_{\mathrm{cr}} \approx \frac{20.2EI}{L^2}.$$

Example 3.2. Not specifying the number of layers and their geometrical and physical characteristics, we shall calculate the critical buckling force at different values of parameter θ. Table 3.1 displays the critical dimensionless load parameter P^*_{cr} versus the dimensionless shear parameter K_1 for $\theta = 0.01; 0.03; 0.05$. The increase of the shear parameter K_1 results in the increase of the critical buckling stress resultant P^*_{cr} for any θ. In addition, $P^*_{\mathrm{cr}} \to 20.2$ as $K_1 \to 0$ for any θ.

Table 3.1 Dimensionless load P_{cr}^* vs. dimensionless shear parameter K_1 at $\theta = 0.01;\ 0.03;\ 0.05.$

K_1	0	0.005	0.1	0.2	0.3	0.4	0.5	0.6	0.7	0.8	0.9	1.0
$\theta = 0.01$												
P_{cr}^*	20.20	18.20	8.913	7.817	7.416	6.605	6.117	5.791	5.557	4.196	4.060	2.961
$\theta = 0.03$												
P_{cr}^*	20.20	18.24	6.772	6.193	4.809	4.088	3.646	3.346	3.131	2.967	2.840	2.737
$\theta = 0.05$												
P_{cr}^*	20.20	18.28	7.055	4.639	3.614	3.043	2.680	2.427	2.241	2.099	1.986	1.894

3.1.2 Laminated Plates

Consider a rectangular plate with sides L_1, L_2 $(0 \le \alpha_1 \le L_1,\ 0 \le \alpha_2 \le L_2)$. The governing equation describing buckling of its in-plane stress state is deduced from Eqs. (2.160) assuming $1/R_2 = 0$

$$D\left(1 - \frac{\theta h^2}{\beta}\Delta\right)\Delta^2\chi - \left(T_{11}^\circ \frac{\partial^2}{\partial\alpha_1^2} + 2T_{12}^\circ \frac{\partial^2}{\partial\alpha_1\partial\alpha_2} + T_{22}^\circ \frac{\partial^2}{\partial\alpha_2^2}\right)\left(1 - \frac{h^2}{\beta}\Delta\right)\chi = 0, \tag{3.23}$$

$$\frac{1-\nu}{2}\frac{h^2}{\beta}\Delta\phi = \phi, \tag{3.24}$$

where D is the reduced bending stiffness defined by Eq. (2.88). The boundary conditions for the simply supported and clamped edges are given by Eqs. (2.110)-(2.117). We will consider here the simplest variant of boundary conditions (2.111), when all edges are simply supported and have diaphragm preventing shears along edges

$$\chi = \Delta\chi = \Delta^2\chi = \frac{\partial\phi}{\partial\alpha_1} = 0. \tag{3.25}$$

Then, one can assume $\phi = 0$.

Let the plate be loaded with only one or two forces acting in its plane along the α_1- or/and α_2-axes. The loading is assumed to be one-parametric and compressive so that

$$T_{11}^\circ = -T^\circ, \quad T_{22}^\circ = -\lambda T^\circ, \quad T_{12}^\circ = 0, \tag{3.26}$$

where $0 \le \lambda < +\infty$, and T° is a required positive stress resultant. The problem is to find the least value of T° for which the boundary-value problem (3.23)-(3.25) has a nontrivial solution. In the classical setting (when $\beta \to \infty$), this problem was considered by many researches (among them Alfutov, 2000; Donnell, 1976). With the chosen variant of boundary conditions, the solution of Eq. (3.23) can be found as follows

$$\chi = \chi_0 \sin\frac{\pi n \alpha_1}{L_1}\, \sin\frac{\pi m \alpha_2}{L_2}. \tag{3.27}$$

Introducing Eq. (3.27) into Eq. (3.23) results in

$$T^\circ = \frac{D\pi^2}{L_1^2} \frac{(n^2 + em^2)^2[1 + \theta K(n^2 + em^2)]}{(n^2 + \lambda em^2)[1 + K(n^2 + em^2)]}, \tag{3.28}$$

where

$$e = \left(\frac{L_1}{L_2}\right)^2, \quad K = \frac{h^2\pi^2}{\beta L_1^2}. \tag{3.29}$$

The critical value

$$T_{\mathrm{cr}}^* = \min_{n,m} T^\circ(n, m) = T(n^*, m^*) \tag{3.30}$$

depends on parameters λ, e, K and θ.

3.1.2.1 Uniformly Loaded Edges

Let $\lambda = 1$ that means all edges are uniformly loaded. This is probably the unique case when the critical buckling parameter T_{cr}^* and the wave numbers n^*, m^* for the rectangular laminated plate are found in the explicit form

$$n^* = m^* = 1, \quad T_{\mathrm{cr}}^* = T_{\mathrm{cl}}^* \frac{[1 + \theta K(1 + e)]}{1 + K(1 + e)}, \tag{3.31}$$

where

$$T_{\mathrm{cl}}^* = \frac{D\pi^2(1 + e)}{L_1^2} \tag{3.32}$$

is the classical value of the buckling stress resultant for a single-layer plate (Alfutov, 2000). For an isotropic plate with the Poisson's ratio ν, Eq. (3.31) gives the relative correction

$$\delta_T = \frac{T_{\mathrm{cl}}^* - T_{\mathrm{cr}}^*}{T_E^*} \approx 5.654(1 + \nu)(1 + e)\left(\frac{h}{L_1}\right)^2. \tag{3.33}$$

3.1.2.2 Non-uniformly Loaded Edges

Here we consider the case when the plate edges $\alpha_1 = 0, L_1$ and $\alpha_2 = 0, L_2$ are loaded by different forces $T_{11}^\circ, T_{22}^\circ$ and $\lambda \neq 1$. This case requires additional calculations for the specified parameters of the plate.

Example 3.3. Not defining the number of layers, we fix the parameters $e = 1$ and $\theta = 0.05$ and calculate the critical load parameter

$$P^* = \left.\frac{(n^2 + em^2)^2[1 + \theta K(n^2 + em^2)]}{(n^2 + \lambda em^2)[1 + K(n^2 + em^2)]}\right|_{n=n^*,\, m=m^*} \tag{3.34}$$

versus the shear parameter K for different values of the ratio $\lambda = 0; 0.2; 0.5; 1$. For all parameters specified above the buckling occurs at $n^* = m^* = 1$. Figure 3.1 shows that the increase of the shear parameter K results in the decrease of the critical

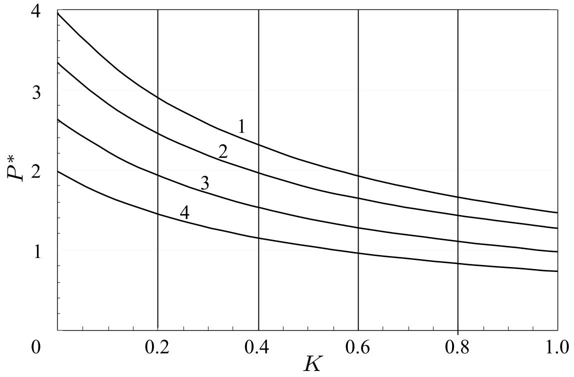

Fig. 3.1 Dimensionless load parameter P^* vs. shear parameter K at $\theta = 0.05$, $e = 1$ for different λ: 1 - $\lambda = 0$, 2 - $\lambda = 0.2$, 3 - $\lambda = 0.5$, 4 - $\lambda = 1$.

buckling load parameter P^*. Taking into account Eq. (3.29) for K and Eqs. (2.59), (2.84) showing the coupling with the reduced shear modulus G, one can conclude that introducing transverse shear into the equivalent single layer (ESL) model for laminated plates may considerably reduce the buckling resistance of the structure.

3.2 Laminated Medium-length Cylindrical Shell Under External Pressure

The problem on buckling of a thin single-layer isotropic circular cylindrical shell under external normal pressure is very well studied. Southwell (1913) was probably the first who obtained a very simple formula for the critical pressure

$$q_{\rm n}^* = -\frac{T_2^*}{R} = \frac{0.856E}{(1-\nu^2)^{3/4}} \left(\frac{h^5}{L^2R^3}\right)^{1/2}, \tag{3.35}$$

where T_2^* is the critical hoop stress resultant T_{22}°, R, L are the radius and length of the shell, and E, ν are the Young's modulus and Poisson's ratio, respectively. Considering a medium-length cylinder ($L \sim 2R$), it was shown that buckling occurs with formation of one semi-wave in the axial direction and an integer number m of dents/bulges in the circumferential direction, where m is the closest to

$$m^* = 2.77(1-\nu^2)^{1/8} \left(\frac{R^3}{L^2h}\right)^{1/4}. \tag{3.36}$$

Later, Papkovich (1929) has confirmed this formula and von Mises (1914); Timoshenko (1936) have derived similar equations using improved theories. It is generally accepted now that Eq. (3.35) is called the Southwell-Papkovich formula (Grigolyuk and Kabanov, 1978).

The problem of buckling of laminated cylindrical shells under external pressure is obviously more complicated than that for single-layer isotropic shells. Indeed, this problem can be reduced to the prediction of nonlinear behaviour of each layer with required satisfaction of boundary conditions on both edges and interfaces. Apparently, analytical solutions of this problem in an explicit form may be found only for sandwich shells, having three layers, with the simplest variant of boundary conditions, the simple support at both edges. For other boundary conditions, the buckling analysis of three-layer cylinders is performed usually by applying some numerical procedure, e.g., Galerkin's method (Lopatin and Morozov, 2015).

For multi-layered shells there are different approximate approaches to predict their buckling. Omitting papers where these problems are solved by some numerical method (e.g., FEM simulation) or by using new advanced theories based on 3D stress analysis and rigid-body motions or on the base of high-accuracy layer-wise theories (see the review in Chapt. 1), we refer to the buckling analysis based on the equivalent single layer (ESL) models which seems to be more simple for multi-layered shells.

The ESL theories may be subdivided into the classical laminate, the first-order shear deformation and higher-order shear deformation theories (the classification of these theories has been given in Chapt. 1). The accuracy of each of these models depends not only on the accepted kinematic hypotheses, but also on the correlations of thicknesses and elastic properties of all layers. Even though some layers are more soft than others, the ESL model gives an accurate result in the estimation of the critical buckling pressure if the total thickness of the shell is sufficiently small and stiffness of all layers is approximately of the same order (Grigolyuk and Kulikov, 1988b; Anastasiadis and Simitses, 1993; Mikhasev et al, 2001b; Han et al, 2004). So, studying the buckling of a thin sandwich cylinder with face sheets made of aluminum and an epoxy core, Mikhasev et al (2001b) showed that the divergence of eigenvalues obtained by using the ESL model (Grigolyuk and Kulikov, 1988b) and the FEM was varied from 1 to 4% for very thin and moderately thin shells, respectively. Han et al (2004) analyzed the buckling of cylindrical sandwiches of different total thicknesses with alloy-foam core and face sheets made of different materials (boron/epoxy, graphite/epoxy and kevlar/epoxy) in three ways:

a) considering the sandwich as a three-dimensional (3D) elastic body,
b) applying the ESL model accounting the transverse shear effects, and
c) performing the finite-element simulation.

The comparative analysis of different approaches has revealed that the error of the ESL model vs. the 3D model can varied (depending on the material of the face layers) from 3.1 to 16.6% for moderately thin shells ($R/h = 30$) and between 0.13 and 3.3% for thin and very thin shells ($R/h = 60$ and $R/h = 120$).

Remark 3.1. In some recent papers (Weps et al, 2013; Eisenträger et al, 2015) it was shown that the use of ESL yields sometimes not to satisfying results if the thickness ratio for core and face sheets and the material parameters ratio have extremal values (e.g., the material parameters ratio for ordinary laminates and sandwiches is $\approx 10^{-2}$, in extremal situations this value is 10^{-4} up to 10^{-5}). If it is so layerwise theories must be applied.

The ESL models turned out very fruitful and promoted a further development of higher-order shear deformation theories as well as numerous studies on pressure-induced buckling of laminated and sandwich cylindrical shells in different statements and under various factors (s., among many others, Wu et al, 2008; Li and Lin, 2010; Grover et al, 2013; Nguyen et al, 2016). In particular, in Li and Lin (2010) the governing equations based on the higher-order shear deformation shell theory with von Kármán-Donnell-type of kinematic nonlinearity have been used to study nonlinear buckling and postbuckling of a moderately thick anisotropic laminated cylindrical shell of finite length subjected to lateral pressure, hydrostatic pressure, and external liquid pressure. Grover et al (2013) proposed a new inverse hyperbolic shear deformation theory satisfying traction-free boundary conditions for the buckling response of laminated shells.

In this section, based on the ESL model (Grigolyuk and Kulikov, 1988b) and using the governing equations (2.160) derived in Chapt. 2, we shall study buckling of thin medium-length multi-layered and sandwich cylindrical shells under external pressure. Each layer of the shell is assumed to be elastic and transversally isotropic. At first, we shall consider the simplest problem when all geometrical and physical parameters as well as the pressure are constant. For simply supported edges with diaphragm this problem has an explicit solution. In the case of other variants of boundary conditions the asymptotic approach will be applied (Mikhasev and Botogova, 2017). The critical pressure values found by two methods will be compared with data of FEM simulation (Mikhasev et al, 2001b). As an example we shall analyze buckling of a sandwich (three-layer) shell with core made of a magnetorheological elastomer (MRE) under different levels of an applied magnetic field (Mikhasev and Mlechka, 2014). Another example will illustrate the buckling of a five-layered shell with very soft core made of an alloy-foam. We shall consider the common case when the shell is non-circular and its edges are not plane curves or lie in planes not perpendicular to the cylinder axis (Mikhasev et al, 2001a). Using the asymptotic method established by Tovstik and Smirnov (2001), the buckling modes will be constructed in the form of functions localized in the neighbourhood of some generatrix called the *weakest* one. In all examples, the influence of shear and various types of boundary conditions on the buckling pressure is analyzed.

3.2.1 Shell with Constant Parameters Under Uniform Pressure

Let a circular cylindrical shell of radius R be under action of an external constant hydrostatic pressure q_n. Then the pre-buckling hoop stress resultant is $T_{22}^\circ = Rq_\mathrm{n}$ and the remaining in-plane stress resultants are $T_{11}^\circ = T_{12}^\circ = 0$. In this case operator (2.147) takes the form

$$\varDelta_T w = T_{22}^\circ \frac{\partial^2 w}{\partial \alpha_2^2}. \tag{3.37}$$

Then the governing equations describing the pressure induced buckling may be rewritten as follows

$$
\begin{aligned}
&D\left(1-\frac{\theta h^2}{\beta}\Delta\right)\Delta^2\chi+\frac{1}{R_2}\frac{\partial^2 F}{\partial\alpha_1^2}-T_{22}^{\circ}\frac{\partial^2}{\partial\alpha_2^2}\left(1-\frac{h^2}{\beta}\Delta\right)\chi=0,\\
&\Delta^2 F=\frac{Eh}{R_2}\frac{\partial^2}{\partial\alpha_1^2}\left(1-\frac{h^2}{\beta}\Delta\right)\chi,
\end{aligned}
\tag{3.38}
$$

$$
\frac{1-\nu}{2}\frac{h^2}{\beta}\triangle\phi=\phi. \tag{3.39}
$$

We shall consider here only the boundary conditions for simple support

1. The edge $\alpha_1 = \alpha_1^*$ is simply supported and there is a diaphragm preventing transverse shears along the edge

$$
\chi=\Delta\chi=\Delta^2\chi=\frac{\partial\phi}{\partial\alpha_1}=0. \tag{3.40}
$$

2. The edge $\alpha_1 = \alpha_1^*$ is simply supported, and a diaphragm is absent

$$
\begin{aligned}
\left(1-\frac{h^2}{\beta}\Delta\right)\chi=0,\quad &\frac{\partial^2}{\partial\alpha_1^2}\left(1-\frac{h^2}{\beta}\Delta\right)\chi=0,\\
\left(\frac{\partial^2}{\partial\alpha_1^2}+\nu\frac{\partial^2}{\partial\alpha_2^2}\right)\chi-(1-\nu)&\frac{\partial^2\phi}{\partial\alpha_1\alpha_2}=0,\\
2\frac{\partial^2\chi}{\partial\alpha_1\partial\alpha_2}+\frac{\partial^2\phi}{\partial\alpha_1^2}&-\frac{\partial^2\phi}{\partial\alpha_2^2}=0.
\end{aligned}
\tag{3.41}
$$

These conditions should be supplemented by conditions for the tangential displacements or stress resultants. Let us assume that the edge is free in the axial direction and $\hat{e}_{22} = 0$, then one has the additional conditions for the stress function

$$
\frac{\partial^2 F}{\partial\alpha_2^2}=0 \quad\text{and}\quad \frac{\partial^2 F}{\partial\alpha_1^2}=0 \quad\text{at}\quad \alpha_1=\alpha_1^*. \tag{3.42}
$$

If the edge is free in the circumferential direction, then the second condition from Eqs. (3.42) should be substituted by

$$
\frac{\partial^2 F}{\partial\alpha_1\alpha_2}=0.
$$

In what follows, conditions (3.40) and (3.41), with appropriate conditions for F, will be called as the SSD (1.) and SSF (2.) boundary conditions, respectively.

The problem is to find the minimum value of stress resultant $|T_{22}^{\circ}|$ for which Eqs. (3.38) and (3.39) with appropriate boundary conditions have a nontrivial solution. Let all the geometrical and physical parameters be independent of coordinates α_1, α_2. Here, $\alpha_1^* = 0$ and $\alpha_1^{**} = L$ is the shell length. In this case all coefficients appearing in both Eqs. (3.38), (3.39) and boundary conditions are constants. Nevertheless, finding the buckling modes turns out to be not easy because the characteristic equation corresponding to Eqs. (3.38) is a tenth degree polynomial. Its roots may be found in the explicit form only for the boundary conditions (3.40) when both edges have diaphragm.

3.2.1.1 Simply Supported Shell with Diaphragm on Edges

Let the edges be simply supported and have a diaphragm of infinite rigidity (SSD conditions). In this case, Eq. (3.39) is not coupled with Eqs. (3.38) for χ and F, and the boundary condition (3.40) for a function ϕ is independent of residual conditions. As mentioned above, Eq. (3.39) has two nontrivial integrals describing the edge effects near both edges. It is easy to show that these integrals do not satisfy the residual boundary conditions (3.40) for ϕ. Hence, we can set $\phi = 0$.

The residual functions χ, F satisfying the boundary conditions (3.40), (3.42) are readily found as

$$\chi = \chi_0 \sin\frac{\pi n \alpha_1}{L} \sin\frac{m\alpha_2}{R}, \quad F = F_0 \sin\frac{\pi n \alpha_1}{L} \sin\frac{m\alpha_2}{R}, \tag{3.43}$$

where n, m are positive integers (n is a number of semi-waves along the shell generatrix and m is a number of waves in the circumferential direction). Substituting Eqs. (3.43) into Eqs. (3.38) yields the following equation for the hoop stress resultant

$$\begin{aligned}
T_{22}^{\circ} &= -\frac{\varepsilon^8 \pi^4 h E \Delta_{nm}}{m^2}, \quad \varepsilon^8 = \frac{h^2 \eta_3}{12(1-\nu^2)R^2}, \\
\Delta_{nm} &= \frac{1+\theta K \delta_{nm}}{1+K\delta_{nm}} \delta_{nm}^2 + \frac{n^4}{l^4 \pi^4 \varepsilon^8 \delta_{nm}^2}, \quad K = \frac{\pi^2 h^2}{\beta R^2}, \\
\delta_{nm} &= \frac{n^2}{l^2} + \frac{m^2}{\pi^2}, \quad l = \frac{L}{R}.
\end{aligned} \tag{3.44}$$

The minimization of T_{22}° over integer n and m results in the critical value for pressure

$$q_{\mathrm{n}}^* = T_2^*/R, \quad T_2^* = \min_{n,m} |T_{22}^{\circ}(n,m)| = |T_{22}^{\circ}(n^*, m^*)|. \tag{3.45}$$

For a single-layer thin isotropic cylinder, one has the following relations and estimates (Grigolyuk and Kulikov, 1988b; Tovstik and Smirnov, 2001)

$$\eta_3 = 1, \quad \theta = 1/85, \quad n^* = 1, \quad m^* \sim (R/h)^{1/4}, \quad n^*/l \ll m^*/\pi. \tag{3.46}$$

Omitting transverse shear ($K = 0$) and assuming that π^2/l^2 and 1 can be neglected compared to $(m^*)^2$, then Eq. (3.45) degenerates into the Southwell-Papkovich formula (3.35).

In Eq. (3.44), the principal mechanical characteristics influencing the buckling pressure are the reduced modulus of elasticity E and the reduced shear parameter K. However, the effect of these parameters on the critical pressure is also different and depends strongly upon the correlation of geometrical and physical parameters of layers composing a shell as well as on number of waves. For instance, if $n, m \sim 1$, and $R/L \sim 1$, then the effect of K is negligibly small, but on the other hand, the reduced modulus E will be the main parameter. But if we study buckling of a very thin medium-length cylinder ($n \sim 1$, $m \sim h_*^{-1/4}$, s. Tovstik and Smirnov, 2001), then the parameter K becomes main, and the influence of the reduced parameter E decreases. The detailed analysis of the impact of shear parameter K on the buckling pressure will be done below. But at first, we will perform the test calculations by using Eqs. (3.44), (3.45) and FEM simulation.

Example 3.4. Consider a thin sandwich cylinder with the geometrical parameters $R = 80$ mm, $L = 200$ mm. The top and bottom layers of the same thicknesses ($h_1 = h_3$) are made of aluminum with the Young's modulus $E_1 = E_3 = 70,3$ GPa, Poisson's ratio $\nu_1 = \nu_3 = 0.345$ and density $\rho_1 = \rho_3 = 2.7 \cdot 10^{-6}$ kg/mm^3. The core have a thickness h_2 and is made of epoxy for which $E_2 = 3,45$ GPa, $\nu_2 = 0.3$, $\rho_2 = 1.2 \cdot 10^{-6}$ kg/mm^3 are established. Both materials, aluminum and epoxy, are treated as the elastic and isotropic ones with the shear moduli defined as

$$G_i = \frac{E_i}{2(1+\nu_i)}.$$

We assume the following condition

$$h_1 = h_3 = h_1^\circ - \frac{1}{2}\frac{\rho_2}{\rho_1}\, h_2 \tag{3.47}$$

with $h_1^\circ = 0.5$ mm, which means that for all thicknesses h_i under consideration the shell weight remains constant.

One of the problems stated here is the problem of optimal design: it is required to find a core thickness h_2 for which the critical pressure $q_{\rm n}^*$ becomes the maximum value. The second and main objective is to verify our results obtained on the base of the ESL model represented by Eqs. (3.38). This problem was solved (Mikhasev et al, 2001b) by using the derived Eqs. (3.44), (3.45) and the finite element method based on package COSAR (Gabbert and Altenbach, 1990) described in Chapt. 2.

The dependence of $q_{\rm n}^*$ and m^* on the thickness h_2 is shown in Table 3.2. It may be seen that the optimal value of core thickness is $h_2 \approx 1.0$ mm. Here $n^* = 1$, $m^* = 5$ for all values of h_2. Table 3.2 shows that the divergence of results obtained by solving

Table 3.2 Buckling pressure $q_{\rm n}^*$ vs. thickness h_2.

h_2, mm	m^*	$q_{\rm n}^*$ found by Eqs. (3.44), (3.45), MPa	$q_{\rm n}^*$ found by using FEM, MPa
0	6	0.0867	0.0877
0.5	5	0.1320	0.1371
1.0	5	0.1701	0.1746
1.4	4	0.1614	0.1695
1.6	4	0.1459	0.1526
1.8	4	0.1224	0.1276
2.0	4	0.0894	0.0931

the governing equations (3.44), (3.45) and applying the FEM increases with the shell thickness. So, for $h_2 = 0$; 1.0; 2.0 mm the divergence between the exact solution (3.44), (3.45) and the numerical approach is equal to 1.0; 2.6; 4.0%, respectively. This fact is explained by the strong dependence of the error of Eqs. (3.38) on the number m of dents in the circumferential direction. When the thickness increases, the number m decreases, while the governing equations (3.38) have being derived at the assumption of minor sizes of dents/bulges.

3.2.1.2 Effect of Shear on the Critical Buckling Pressure

Equation (3.44) derived above for a simply supported shell with diaphragm allows us to analyse the influence of shear on the critical buckling pressure. Specifying neither a number of layers nor materials, we shall calculate the dimensionless critical load parameter

$$P^* = \frac{T_2^*}{\pi^4 E h} \tag{3.48}$$

for different values of the shear parameter K. Figure 3.2 shows the load parameter P^* vs. K at fixed $\theta = 0.05$, $l = 2$ and different values of the parameter ε characterizing the shell thickness. It is seen that taking into account shear results in decreasing the critical buckling pressure. The drop in the critical buckling pressure turns out to be more noticeable for very thin shells. Figure 3.3 demonstrates the effect of K on the buckling parameter P^* at fixed $\theta = 0.05$, $\varepsilon = 0.1$ and different values of the dimensionless length $l = L/R$. As accepted, the increase of the shell length reduces the effect of shear on the buckling pressure. Indeed, a lengthy cylindrical shell under the lateral pressure buckles with formation of the one semi-wave in the axial direction and a small number of waves in the circumferential direction. But as follows from Eq. (3.44), the influence of the shear parameter K on the buckling pressure becomes negligibly small at $n^*, m^* \sim 1$. We note that the reducing effect of shear illustrated in Figs. 3.2 and 3.3 is not associated with the boundary conditions, it reflects introducing shear (additional degrees of freedom) into the shell model.

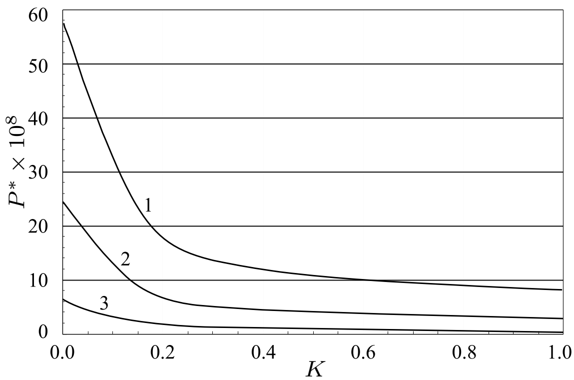

Fig. 3.2 Load parameter P^* vs. shear parameter K at fixed $\theta = 0.05$, $l = 2$ and different values of a parameter ε characterizing the shell thickness: $1 - \varepsilon = 0.1$; $2 - \varepsilon = 0.13$; $3 - \varepsilon = 0.15$ (after Mikhasev and Botogova, 2017).

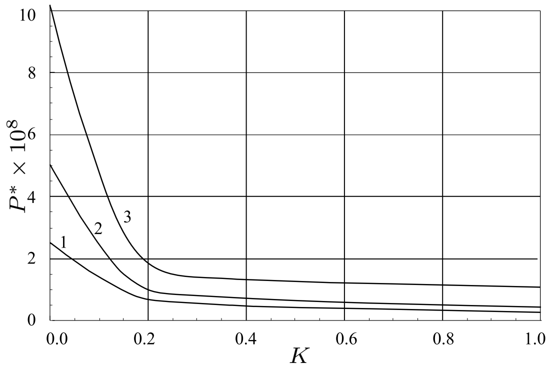

Fig. 3.3 Load parameter P^* vs. shear parameter K at fixed $\theta = 0.05$, $\varepsilon = 0.1$ and different values of a dimensionless length l: $1 - l = 4$; $2 - l = 2$; $3 - l = 1$ (after Mikhasev and Botogova, 2017).

In the following example we aim to show that the application of smart materials (e.g., magnetorheological elastomers) for assembling a laminated shell structure allows varying the reduced shear modulus and, in such a way, increasing the critical buckling pressure.

Example 3.5. Let us consider a sandwich (three-layer) thin cylinder with a core made of the magnetorheological elastomer MRE-1. The elastic properties of this material were specified in Chapt. 2 (s. Fig. 2.9). It is evident that its viscous and rheological properties are not taken here into consideration. The face skins having the same thickness $h_1 = h_3 = 0.5$ mm are fabricated of the ABS-plastic SD-0170 with parameters $E_1 = E_3 = 1.5 \cdot 10^9$ Pa, $\nu_1 = \nu_3 = 0.4$. The thickness of the MRE-core is $h_2 = 8$ mm. Table 3.3 shows the effect of applied magnetic field on the critical buckling pressure q_{n}^* for a sandwich shell of the length $L = 1$ m and radius $R = 0.5$ m. As seen from Fig. 2.9, the application of the magnetic field $B = 100$ mT results in the increase of the storage modulus G_{v} of the MRE-core from 31 to 1893 kPa. Table 3.3 shows that this rise of the elastic properties implies the decrease of the dimensionless shear parameter

$$\kappa = \frac{K}{\pi^2 \varepsilon^4} \tag{3.49}$$

for the sandwich and, as a consequence, leads to the considerable growth of the critical buckling pressure, from $q_{\mathrm{n}}^* = 7.937$ kPa at $B = 0$ mT to $q_{\mathrm{n}}^* = 12.162$ kPa at $B = 100$ mT.

Table 3.3 Dimensionless shear parameters κ and critical buckling pressure q_{n}^* vs. magnetic field induction B.

B, mT	0	20	40	60	80	100
κ	4.298	2.628	1.898	1.489	1.227	1.045
q_{n}^*, kPa	7.937	9.697	10.789	11.538	11.906	12.162

3.2.1.3 Simply Supported Shell Without Diaphragm on Edges

Let us consider the variant of boundary conditions (3.41), (3.42) corresponding to the simply supported edges without diaphragm (SSF conditions). In this case the boundary-value problem (3.38), (3.41), (3.42) does not admit the explicit form of a solution.

To estimate the effect of the SSF boundary conditions on the critical buckling pressure we will apply the asymptotic approach. This effect depends on the correlation between the reduced Young's and shear moduli. As mentioned above, Eqs. (3.38) are asymptotically correct if $G \ll E$ (not that E, G are the parameters for the laminated shell, s. Subsect. 2.1.12). Let us assume $G \sim h_*^{3/2}E$. This case takes place for the wide range of smart materials (MREs and ERCs introduced in Chapt. 2) and for the layer thicknesses to be considered below. Then, the following estimation for the shear dimensionless parameter K holds

$$\frac{K}{\pi^2} = \varepsilon^2\kappa, \quad \kappa \sim 1, \tag{3.50}$$

where ε is a small parameter introduced by (3.44).

Let us introduce dimensionless coordinates x, φ and a load parameter Λ

$$\alpha_1 = Rx, \quad \alpha_2 = R\varphi, \quad T_{22}^{\circ} = -\varepsilon^6 Eh\Lambda, \tag{3.51}$$

where $0 \leq x \leq l = L/R$. As seen from Eq. (3.44) and Example 3.4, buckling of a medium-length thin cylindrical shell under external pressure occurs with formation of one semi-wave in the axial direction and a large number m of dents/bulges in the circumferential direction so that $m \sim h_*^{-1/4} \sim \varepsilon^{-1}$. Then functions χ, F, ϕ may be sought in the form

$$\begin{aligned} \chi &= RX(x)\sin\left(\varepsilon^{-1}p\varphi\right), \\ F &= \varepsilon^4 EhR^2\Phi(x)\sin\left(\varepsilon^{-1}p\varphi\right), \\ \phi &= RS(x)\cos\left(\varepsilon^{-1}p\varphi\right), \end{aligned} \tag{3.52}$$

where $p \sim 1$.

The substitution of Eqs. (3.50)-(3.52) into Eqs. (3.38), (3.39) results in differential equations written in the dimensionless form

$$\begin{aligned} \varepsilon^4(1-\varepsilon^2\kappa\theta\Delta_\varepsilon)\Delta_\varepsilon^2 X + \frac{\mathrm{d}^2\Phi}{\mathrm{d}x^2} - \Lambda p^2(1-\varepsilon^2\kappa\Delta_\varepsilon)X = 0, \\ \varepsilon^4\Delta_\varepsilon^2\Phi - \frac{\mathrm{d}^2}{\mathrm{d}x^2}(1-\varepsilon^2\kappa\Delta_\varepsilon)X = 0, \end{aligned} \tag{3.53}$$

$$\frac{1-\nu}{2}\kappa_1\varepsilon^2\Delta_\varepsilon S = S, \tag{3.54}$$

where

$$\Delta_\varepsilon = \frac{\mathrm{d}^2}{\mathrm{d}x^2} - \varepsilon^{-2}p^2 \tag{3.55}$$

is a differential operator, and $\kappa_1 \equiv \kappa$ is introduced to analyze the effect of shear in the neighborhood of the edges.

The SSF boundary conditions (3.41), (3.42) for the edges $x = 0, l$ without diaphragm are rewritten as

$$(1-\varepsilon^2\kappa_1 \Delta_\varepsilon)X = 0, \quad \frac{\mathrm{d}^2}{\mathrm{d}x^2}(1-\varepsilon^2\kappa_1\Delta_\varepsilon)X = 0, \tag{3.56}$$

$$\left(\varepsilon^2\frac{\mathrm{d}^2}{\mathrm{d}x^2} - \nu p^2\right)X + \varepsilon(1-\nu)p\frac{\mathrm{d}S}{\mathrm{d}x} = 0, \tag{3.57}$$

$$2\varepsilon p\frac{\mathrm{d}X}{\mathrm{d}x} + \varepsilon^2\frac{\mathrm{d}^2 S}{\mathrm{d}x^2} + p^2 S = 0, \tag{3.58}$$

$$\Phi = 0, \quad \varepsilon^2\frac{\mathrm{d}^2\Phi}{\mathrm{d}x^2} - p^2\Phi = 0. \tag{3.59}$$

If the edges are free in both the axial and circumferential directions, then conditions (3.59) are substituted for the conditions

$$\Phi = 0, \qquad \frac{\mathrm{d}\Phi}{\mathrm{d}x} = 0. \tag{3.60}$$

The boundary-value problem (3.53)-(3.60) is singularly perturbed one. Its solution may be presented in the form of superposition of the main stress-strain state and the integrals of the edge effects (Gol'denveizer, 1961)

$$X = X^{(\mathrm{m})} + X^{(\mathrm{e})}, \quad \Phi = \Phi^{(\mathrm{m})} + \Phi^{(\mathrm{e})}, \tag{3.61}$$

where the superscript (m) denotes functions corresponding to the main stress-strain state with the zeroth index of variation, $\iota_1 = 0$, in the axial direction, and functions with the superscript (e) are the integrals of edge effects having a large index of variation. Contrary to the classical Kirchhoff-Love theory, our problem stated in terms of the displacement and shear functions, $X^{(\mathrm{e})}$ and S, has six edge integrals for $X^{(\mathrm{e})}$ and two edge integrals for the shear function S.

At first, we consider Eq. (3.54). It has the following general solution

$$S = \varepsilon^{\gamma_0}\left\{a_1 \exp\left(-\frac{\vartheta_\mathrm{s} x}{\varepsilon}\right) + a_2\exp\left[-\frac{\vartheta_\mathrm{s}(l-x)}{\varepsilon}\right]\right\}, \tag{3.62}$$

where a_1, a_2 are unknown constants, γ_0 is the index of intensity for the shear function, and

$$\vartheta_\mathrm{s} = \sqrt{\frac{2}{(1-\nu)\kappa_1} + p^2}. \tag{3.63}$$

The edge effect integrals $X^{(\mathrm{e})}$ may be found from the edge effect equation (2.129) and Eq. (2.82) coupling χ and w. Another way is to obtain their asymptotic estimations directly from Eqs. (3.53). Let us introduce

$$X^{(\mathrm{e})}(x) = \hat{X}^{(\mathrm{e})}\mathrm{e}^{\lambda x}, \quad \varPhi^{(\mathrm{e})}(x) = \hat{\varPhi}^{(\mathrm{e})}\mathrm{e}^{\lambda x}. \tag{3.64}$$

The substitution of Eqs. (3.64) into Eqs. (3.53) results in the characteristic equation

$$\begin{aligned}[1-\kappa_1\theta(\varepsilon^2\lambda^2-p^2)](\varepsilon^2\lambda^2-p^2)^4+\lambda^4[1-\kappa_1(\varepsilon^2\lambda^2-p^2)]\\ -\Lambda p^2(\varepsilon^2\lambda^2-p^2)^2[1-\kappa_1(\varepsilon^2\lambda^2-p^2)]=0,\end{aligned} \tag{3.65}$$

which has only six roots

$$\lambda_{1,2} = \pm\frac{1}{\varepsilon}\sqrt{\frac{1}{\kappa_1}+p^2}+O(\varepsilon^3), \tag{3.66}$$

$$\lambda_{3,4,5,6} = \pm\frac{1}{\varepsilon^2}\sqrt[4]{\frac{1}{4\theta}}(1\pm\mathrm{i})+O(1) \tag{3.67}$$

with nonzero real parts. The remaining four roots with zero real parts are not written down here. The corresponding partial solutions of Eqs. (3.53) form two groups of functions

$$\begin{aligned}
X_1^{(\mathrm{e})}(x;\varepsilon) &= \mathrm{e}^{-\frac{r_1}{\varepsilon}\,x}[1+O(\varepsilon)],\\
X_2^{(\mathrm{e})}(x;\varepsilon) &= \mathrm{e}^{-\frac{r_1}{\varepsilon}\,(l-x)}[1+O(\varepsilon)],\\
\varPhi_{1,2}^{(\mathrm{e})} &= -\varepsilon^2\frac{1-\theta}{\kappa_1(1+\kappa_1p^2)}X_{1,2}^{(\mathrm{e})},
\end{aligned} \tag{3.68}$$

and

$$\begin{aligned}
X_3^{(\mathrm{e})}(x;\varepsilon) &= \mathrm{e}^{-\frac{r_2}{\varepsilon^2}\,x}\cos\left(\varepsilon^{-2}r_2\,x\right)[1+O(1)],\\
X_4^{(\mathrm{e})}(x;\varepsilon) &= \mathrm{e}^{-\frac{r_2}{\varepsilon^2}\,x}\sin\left(\varepsilon^{-2}r_2\,x\right)[1+O(1)],\\
X_5^{(\mathrm{e})}(x;\varepsilon) &= \mathrm{e}^{-\frac{r_2}{\varepsilon^2}\,(l-x)}\cos\left[\varepsilon^{-2}r_2\,(l-x)\right][1+O(1)],\\
X_6^{(\mathrm{e})}(x;\varepsilon) &= \mathrm{e}^{-\frac{r_2}{\varepsilon^2}\,(l-x)}\sin\left[\varepsilon^{-2}r_2\,(l-x)\right][1+O(1)],\\
\varPhi_j^{(\mathrm{e})} &= \frac{\kappa_1}{\varepsilon^2}X_j^{(\mathrm{e})}, \quad j=3,4,5,6,
\end{aligned} \tag{3.69}$$

with the properties of the edge effect integrals, where

$$r_1 = \sqrt{\frac{1}{\kappa_1}+p^2}, \quad r_2 = \sqrt[4]{\frac{1}{\theta}}. \tag{3.70}$$

It is obvious that functions (3.69) have the index of variation $\iota_1 = 1/2$, that is the same as in the classical simple edge effect integrals (Gol'denveizer, 1961), whereas functions (3.68) have the index $\iota_1 = 1/4$ and coincide with the similar integrals (2.144) at $p = 0$.

We compose the following superposition of the found integrals

$$X^{(\mathrm{e})} = \varepsilon^{\gamma_1} \sum_{i=1}^{2} b_i X_i^{(\mathrm{e})} + \varepsilon^{\gamma_2} \sum_{j=3}^{6} c_j X_j^{(\mathrm{e})}, \tag{3.71}$$

where b_i, c_j are constants and γ_1, γ_2 are the indexes of intensity of the edge effect integrals which remain unknown at this step.

Now, we consider the main stress state. Unknown functions $X^{(\mathrm{m})}, \Phi^{(\mathrm{m})}$ corresponding to this state and the eigenvalue Λ are sought in the form of formal asymptotic series (the definition of asymptotic series is given in Chapt. 6)

$$X^{(\mathrm{m})} = X_0 + \varepsilon X_1 + \dots, \quad \Phi^{(\mathrm{m})} = \Phi_0 + \varepsilon \Phi_1 + \dots, \tag{3.72}$$

$$\Lambda = \Lambda_0 + \varepsilon \Lambda_1 + \dots. \tag{3.73}$$

We substitute Eqs. (3.72), (3.73) into Eqs. (3.53) and consider the first two approximations. In the zeroth-order approximation, one has the following homogeneous differential equation

$$\mathbf{L} X_0 \equiv \frac{\mathrm{d}^4 X_0}{\mathrm{d}x^4} + \frac{p^6[p^2 + \theta\kappa p^4 - \Lambda_0(1 + \kappa p^2)]}{1 + \kappa p^2} X_0 = 0 \tag{3.74}$$

with respect to X_0. The next approximation produces the non-homogeneous equation

$$\mathbf{L} X_1 = \Lambda_1 p^6 X_0. \tag{3.75}$$

The stress and displacement functions are coupled by the formula

$$\Phi_j = \frac{1 + \kappa p^2}{p^4} \frac{\mathrm{d}^2 X_j}{\mathrm{d}x^2}, \quad j = 1, 2. \tag{3.76}$$

Equations (3.75), (3.76) are of fourth order. So, we have to split the boundary conditions (3.56)-(3.59) and assign the main two conditions for X_j at each edge and the additional ones which will serve to determine constants a_i, b_i, c_j and parameters $\gamma_0, \gamma_1, \gamma_2$ as well. To this purpose, we substitute Eqs. (3.61), (3.71), (3.72) into the boundary conditions (3.56)-(3.59) and, taking into account the indexes of variation of all functions (we remind that $\mathrm{d}X_0/\mathrm{d}x \sim X, \mathrm{d}\Phi_0/\mathrm{d}x \sim \Phi_0$), demand the fulfillment of the following conditions

- the boundary conditions for X_0, Φ_0 should be homogeneous,
- at each edge, there is an inhomogeneous condition coupling a_i and the value of X_0 or its derivatives,
- at each edge, there is an inhomogeneous equation for b_i,
- it is desirable to get even one inhomogeneous equation for constants c_j and
- the boundary conditions for X_1, Φ_1 should be inhomogeneous and expressed in terms of a_i, b_i, c_j.

When taking into account the above conditions, the first equations from (3.56), (3.59) in the zeroth-order approximation result in the main boundary conditions

$$X_0 = \Phi_0 = 0 \quad \text{at} \quad x = 0, l. \tag{3.77}$$

The next approximation allows to determine parameters $\gamma_0, \gamma_1, \gamma_2$ depending on the second condition for the stress function Φ and generates the main conditions for X_1, Φ_1 and the additional equations for a_i, b_i, c_j as well. If we assume conditions (3.59), then one obtains $\gamma_0 = \gamma_1 = 1, \gamma_2 = 4$, and for boundary conditions (3.60), one has $\gamma_0 = \gamma_1 = 1, \gamma_2 = 3$. However, the chose of the second condition for Φ does influence neither the main conditions

$$\begin{aligned} &(1 + \kappa_1 p^2) X_1(0) - \kappa_1 r_1^2 b_1 = 0, \qquad (1 + \kappa_1 p^2) X_1(l) - \kappa_1 r_1^2 b_2 = 0, \\ &\Phi_1(0) = 0, \quad \Phi_1(l) = 0, \end{aligned} \tag{3.78}$$

for X_1, Φ_1 nor the following additional conditions

$$\begin{aligned} &c_j = 0, \quad \text{for} \quad j = 3, 4, 5, 6, \\ &-\nu p^2 X_1(0) + r_1^2 b_1 - (1 - \nu) p \vartheta_{\mathrm{s}} a_1 = 0, \\ &-\nu p^2 X_1(l) + r_1^2 b_2 - (1 - \nu) p \vartheta_{\mathrm{s}} a_2 = 0, \\ &2p \frac{\mathrm{d}X_0(0)}{\mathrm{d}x} + (\vartheta_{\mathrm{s}}^2 + p^2) a_1 = 0, \quad 2p \frac{\mathrm{d}X_0(l)}{\mathrm{d}x} + (\vartheta_{\mathrm{s}}^2 + p^2) a_2 = 0. \end{aligned} \tag{3.79}$$

Consider the boundary-value problem (3.74), (3.77) arising in the zero-order approximation. It should be noted that it is the same within the group of the boundary conditions for simply supported edges and does not depend on whether an edge has a diaphragm (SSD conditions) or not (SSF conditions). This problem has the solution

$$X_0 = A \sin(\pi n x / l), \tag{3.80}$$

if

$$\Lambda_0(p; n) = \frac{\pi^4 n^4}{l^4 p^6} + \frac{p^2(1 + \theta \kappa p^2)}{1 + \kappa p^2}, \tag{3.81}$$

where n is a number of semi-waves in the axial direction of the shell. Minimizing the function $\Lambda_0(p)$ over p and n, one obtains the zeroth-order approximation of the critical buckling load parameter

$$\Lambda_0^\circ = \min_{p,n} \Lambda_0(p, n) = \min_{p} \Lambda_0(p, 1) = \Lambda_0(p^\circ, 1) \tag{3.82}$$

and the corresponding eigenfunction

$$X_0 = A \sin(\pi x / l). \tag{3.83}$$

For $\kappa = 0$, we get

$$p^\circ = \sqrt[8]{\frac{3\pi^4}{l^4}}, \quad \Lambda_0^\circ = \frac{4\pi}{3^{3/4} l} \tag{3.84}$$

and the last equation from (3.51) results in the known Southwell-Papkovich formula (3.35) for the critical buckling pressure.

Now we consider the non-homogeneous boundary-value problem arising in the first-order approximation. From Eqs. (3.79), (3.83) and (3.84), one obtains

$$
\begin{aligned}
a_1 &= -\frac{2\pi p^\circ A}{l\left[(p^\circ)^2 + (\vartheta_{\mathrm{s}}^\circ)^2\right]}, \quad a_2 = -a_1, \\
b_1 &= b_2 = -\frac{2\pi(1-\nu)\vartheta_{\mathrm{s}}^\circ (p^\circ)^2 \kappa_1 A}{l\left[1 + (1-\nu)(p^\circ)^2\kappa_1\right]\left[(p^\circ)^2 + (\vartheta_{\mathrm{s}}^\circ)^2\right]},
\end{aligned} \tag{3.85}
$$

and the boundary conditions for Eq. (3.75) read

$$
\begin{aligned}
&X_1(0) = X_1(l) = -\frac{2\pi(1-\nu)\kappa_1\vartheta_{\mathrm{s}}^\circ (p^\circ)^2 A}{l\left[1 + (1-\nu)(p^\circ)^2\kappa_1\right]\left[(p^\circ)^2 + (\vartheta_{\mathrm{s}}^\circ)^2\right]}, \\
&\varPhi_1(0) = 0, \quad \varPhi_1(l) = 0,
\end{aligned} \tag{3.86}
$$

where $\vartheta_{\mathrm{s}}^\circ = \vartheta_{\mathrm{s}}(p^\circ)$. We have the non-homogeneous boundary-value problem (3.75), (3.86) on *spectrum*. The existence condition of a solution of this problem is

$$
\varLambda_1 (p^\circ)^6 \int_0^l X_0^2 \mathrm{d}x = X_0'''(0)X_1(0) - X_0'''(l)X_1(l). \tag{3.87}
$$

Hence, one obtains the formula for correction of the critical buckling parameter

$$
\varLambda_1^\circ = \frac{8\pi^4(1-\nu)\kappa_1\vartheta_{\mathrm{s}}^\circ}{l^5 (p^\circ)^4\left[1 + (1-\nu)(p^\circ)^2\kappa_1\right]\left[(p^\circ)^2 + (\vartheta_{\mathrm{s}}^\circ)^2\right]}. \tag{3.88}
$$

Then one gets

$$
X_1 = -\frac{2\pi(1-\nu)\kappa_1\vartheta_{\mathrm{s}}^\circ (p^\circ)^2 A}{l\left[1 + (1-\nu)(p^\circ)^2\kappa_1\right]\left[(p^\circ)^2 + (\vartheta_{\mathrm{s}}^\circ)^2\right]}\left(1 - \frac{2x}{l}\right)\cos\frac{\pi x}{l}. \tag{3.89}
$$

If the edge $x = 0$ has a diaphragm and the edge $x = l$ not, then $c_j = 0$ for $j = 3, 4, 5, 6$. The parameters a_1, b_1 and $X_1(0)$ are defined by Eqs. (3.85), (3.86), but $a_2 = b_2 = X_1(l) = 0$. Then the correction of the critical buckling parameter becomes half of the value determined by (3.88):

$$
\varLambda_1^\circ = \frac{4\pi^4(1-\nu)\kappa_1\vartheta_{\mathrm{s}}^\circ}{l^5 (p^\circ)^4\left[1 + (1-\nu)(p^\circ)^2\kappa_1\right]\left[(p^\circ)^2 + (\vartheta_{\mathrm{s}}^\circ)^2\right]}.
$$

Finally, we obtain the following equations for the critical buckling pressure for the simply supported shells without diaphragm on the edges

$$
q_{\mathrm{n}}^* = -\frac{\varepsilon^6 E h}{R}\varLambda^*, \quad \varLambda^* = \varLambda_0^\circ\left[1 + \varepsilon k_{\mathrm{s}} + O(\varepsilon^2)\right], \quad k_{\mathrm{s}} = \frac{\varLambda_1^\circ}{\varLambda_0^\circ}, \tag{3.90}
$$

where k_{s} is the normalized correction depending on the shear parameter $\kappa_1 \equiv \kappa$ and taking into account shear in the vicinity of the shell edges. This edge shear appears as a result of the absence of the edge diaphragms. Indeed, assuming $\kappa_1 = 0$, we ignore the edge effect equation (3.54). Then $k_s = 0$ and Eqs. (3.90) give an approximate value of the critical buckling pressure for the simply supported shells with diaphragm on both edges. Note that parameter p°, Λ_0° are also influenced by the shear parameter κ, but this effect is generated by shear in the shell but not by boundary conditions.

The approximate formula for the buckling mode will be as follows

$$\chi \approx R\sin\left(\varepsilon^{-1}p^\circ\varphi\right)\left\{\sin\frac{\pi x}{l} - \varepsilon\left[a_0\left(1-\frac{2x}{l}\right)\cos\frac{\pi x}{l} + b_1\left(\exp\left(-\frac{r_1^\circ x}{\varepsilon}\right) - \mathrm{e}\left(-\frac{r_1^\circ(l-x)}{\varepsilon}\right)\right)\right]\right\}, \tag{3.91}$$

where

$$a_0 = \frac{2\pi(1-\nu)\kappa_1\vartheta_s^\circ(p^\circ)^2 A}{l\left[1+(1-\nu)(p^\circ)^2\kappa_1\right]\left[(p^\circ)^2+(\vartheta_s^\circ)^2\right]}, \quad r_1^\circ = \sqrt{\frac{1}{\kappa_1}+(p^\circ)^2}, \tag{3.92}$$

and b_1 is calculated by (3.85). As seen, the edge integrals (3.69) with the index of variation $\iota_1 = 1/2$ do not make a contribution in the first-order approximation. Their effect may be estimated by considering higher approximations. However, the accuracy of Eqs. (3.38) is not sufficient to determine the correction $\varepsilon^2\Lambda_2$. For this purpose, the full system of nonlinear differential equations (2.61)-(2.63) written in terms of the generalized displacements $\hat{u}_i, w, \psi_i$ should be used. It is interesting to note that the construction of the second-order approximation for a thin single-layer simply supported ylindrical shell considering the Kirchhoff-Love theory also results in the zeroth coefficients c_j in Eq. (3.71). Whereas for other variants of boundary conditions (particularly, for the case of clamped edges), the edge effect integrals like (3.69) give a non-zeroth correction $\varepsilon^2\Lambda_2$ (Filippov, 1999).

Figures 3.4, 3.5 and 3.6 show the effect of the shear parameter κ on the parameters p°, Λ_0° and k_s at $l = 2.5$ and different values of a parameter θ. It is seen that at small

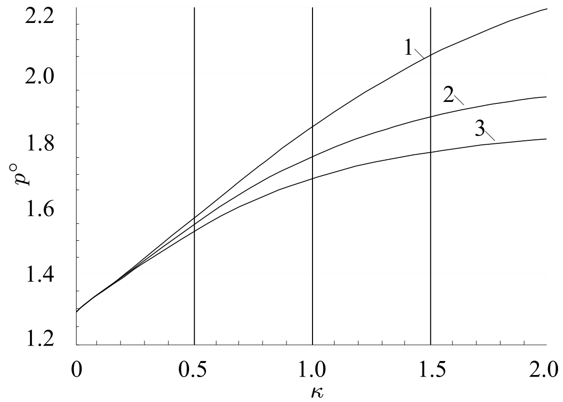

Fig. 3.4 Wave parameter p° vs. shear parameter κ at $l = 2.5$ and different θ: 1 - $\theta = 0.005$; 2 - $\theta = 0.025$; 3 - $\theta = 0.05$ (after Mikhasev and Botogova, 2017).

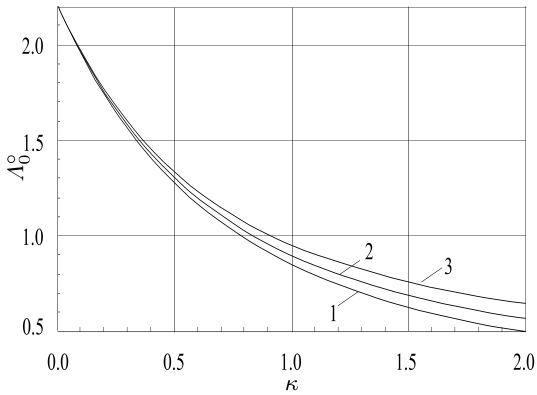

Fig. 3.5 Critical buckling parameter Λ_0° vs. shear parameter κ at $l = 2.5$ and different θ: 1 - $\theta = 0.005$; 2 - $\theta = 0.025$; 3 - $\theta = 0.05$ (after Mikhasev and Botogova, 2017).

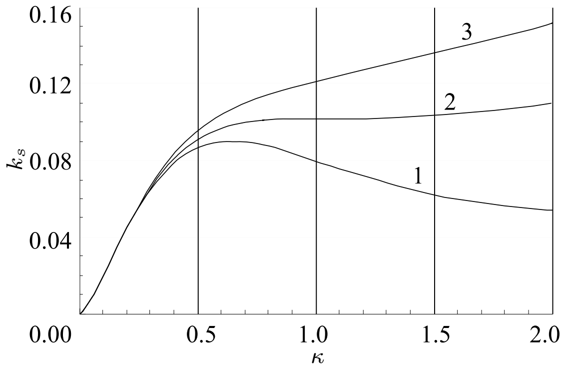

Fig. 3.6 Normalized correction k_s vs. shear parameter κ at $l = 2.5$ and different θ: 1 - $\theta = 0.005$; 2 - $\theta = 0.025$; 3 - $\theta = 0.05$ (after Mikhasev and Botogova, 2017).

values of κ (less than 0.25) the parameter θ does not affect on the dimensionless magnitudes p°, Λ_0° and k_s, and when increasing the shear parameter κ this influence becomes considerable. The increase of κ results in the increase of the wave parameter p° and the decrease of the critical buckling parameter Λ^* in the zero-order approximation. The effect of parameters κ and θ on the normalized correction k_s turns out to be more complicated: for small θ (here $\theta = 0.005$) the correction k_s growths together with κ and, approaching a maximum value at $\kappa \approx 0.52$, begins to fall, but at $\theta > 0.025$ it becomes a monotonically increasing function of κ.

Figure 3.7 displays the normalized correction k_s versus the shear parameter κ for different values of the dimensionless length l. As expected, the shorter the cylinder is, the larger the effect of the edge shear on the critical buckling pressure becomes. But the total impact of the edge shear on the critical pressure is not high. Calculations performed at $\varepsilon = 0.1, \kappa = 2, \theta = 0.05$ show that the edge effect integrals generated by the edge shear give positive buckling pressure increments of about 2.4 and 3.4 % for the lengths $l = 1.5$ and $l = 1$, respectively.

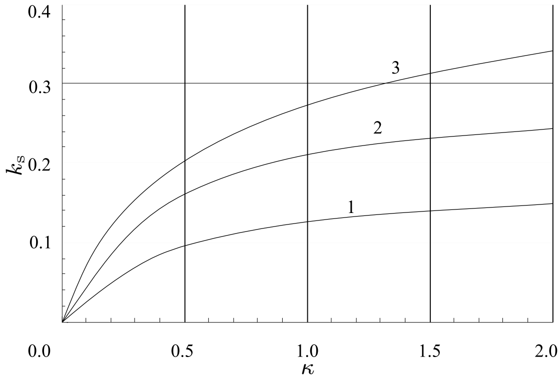

Fig. 3.7 Normalized correction k_s vs. shear parameter κ at $\theta = 0.05$ and different values of dimensionless length l: 1 - $l = 2.5$; 2 - $l = 1.5$; 3 - $l = 1$ (after Mikhasev and Botogova, 2017).

Now we shall consider two examples illustrating the effect of the edge shear on the buckling pressure.

Example 3.6. In this example, we shall study the buckling of a sandwich thin cylinder of the radius $R = 0.5$ m and length $L = 0.5$ m with a core made of MRE-1 and skins made of the ABS-plastic SD-0170. The skins have the same fixed thickness $h_1 = h_3 = 0.5$ mm, and a thickness h_2 of the soft MRE-core will be varied. The application of an external magnetic field leads to changing the mechanical properties of the core and the whole sandwich as well. It is evident that the viscous and rheological properties of the MRE are not taken here into consideration. Tables 3.4, 3.5 and 3.6 demonstrate the dependence of the wave numbers m^*, m°, parameter p° and the critical buckling pressures q_n^*, q_0°, q_n° on the magnetic induction B for the sandwiches with two variants of the boundary conditions (SSD and SSF conditions) and the MRE-core thicknesses $h_2 = 11, 12, 13$ mm, respectively. Here, parameters with the superscribes * and $^\circ$ correspond to the sandwiches with and without the edge diaphragm, respectively; the wave number m° is defined as the integer part of $\varepsilon^{-1}p^\circ$, and q_0° is the zeroth approximation of the critical buckling pressure for the SSF sandwich determined by Eq. (3.90) at $k_s = 0$. Tables 3.4, 3.5 and 3.6 also show the deviation

Table 3.4 Wave numbers m^*, m°, wave parameter p°, critical buckling pressures $q_n^*, q_0^\circ, q_n^\circ$ for the sandwich with the MRE-core of the thickness $h_2 = 11$ mm for two variants of boundary conditions (SSD, SSF) vs. magnetic induction B. The edge shears induced corrections δ, δ' (%) for the critical buckling pressure vs. magnetic induction B (after Mikhasev and Botogova, 2017).

B, mT	m^*	q_n^*, Pa	p°	m°	q_0°, Pa	q_n°, Pa	δ	δ'
0	9	11714	2.78	8	10246	10721	+4.64%	-8.48%
20	7	16883	2.45	7	13986	14652	+4.76%	-13.21%
40	7	19905	2.32	7	16789	17531	+4.40%	-14.00%
60	7	22102	2.25	7	17556	18121	+3.22%	-18.01%
80	6	23681	2.21	7	18551	19042	+2.65%	-19.59%
100	6	24705	2.18	7	19229	19727	+2.60%	-20.00%

Table 3.5 Wave numbers m^*, m°, wave parameter p°, critical buckling pressures $q_n^*, q_0^\circ, q_n^\circ$ for the sandwich with the MRE-core of the thickness $h_2 = 12$ mm for two variants of boundary conditions (SSD, SSF) vs. magnetic induction B. The edge shears induced corrections δ, δ' (%) for the critical buckling pressure vs. magnetic induction B (after Mikhasev and Botogova, 2017).

B, mT	m^*	q_n^*, Pa	p°	m°	q_0°, Pa	q_n°, Pa	δ	δ'
0	10	10872	3.00	9	9365	9549	+1.96%	-12.17%
20	8	17545	2.53	7	14561	14929	+2.53%	-14.91%
40	7	21593	2.37	7	16985	17360	+2.21%	-19.60%
60	7	24420	2.28	7	19333	19629	+1.53%	-19.62%
80	6	26355	2.23	7	20320	20620	+1.48%	-21.76%
100	6	27684	2.20	6	21344	21607	+1.23%	-21.95%

Table 3.6 Wave numbers m^*, m°, wave parameter p°, critical buckling pressures $q_n^*, q_0^\circ, q_n^\circ$ for the sandwich with the MRE-core of the thickness $h_2 = 13$ mm for two variants of boundary conditions (SSD, SSF) vs. magnetic induction B. The edge shears induced corrections δ, δ' (%) for the critical buckling pressure vs. magnetic induction B (after Mikhasev and Botogova, 2017).

B, mT	m^*	q_n^*, Pa	p°	m°	q_0°, Pa	q_n°, Pa	δ	δ'
0	12	9970	3.25	9	9070	9354	+3.13%	-6.18%
20	8	18196	2.60	7	15352	16145	+5.17%	-11.27%
40	7	23282	2.40	7	18905	19792	+4.69%	-14.99%
60	7	26782	2.30	7	21144	21970	+3.91%	-17.97%
80	6	29124	2.25	6	22691	23426	+3.24%	-19.56%
100	6	30790	2.21	6	23836	24483	+2.71%	-20.48%

$$\delta = \frac{q_n^\circ - q_0^\circ}{q_0^\circ} 100\%$$

induced by the edge shear with respect to the zeroth approximation of the critical buckling pressure q_0° for the shell with the SSF conditions and the deviation

$$\delta' = \frac{q_n^* - q_n^\circ}{q_n^*} 100\%$$

between the critical buckling pressures q_n^* and q_n° for the shells with the SSD and SSF conditions, respectively.

It is obvious that for any fixed values of the geometrical parameters, increasing the magnetic field induction B leads to decreasing the wave numbers m^*, m° and the wave parameter p° as well, increasing the total stiffness and, as result, the buckling pressures q_n^*, q_n° for the simply supported sandwiches with and without diaphragm. The dependence of the critical buckling pressure on the thickness h_2 of the soft MRE-core is more complicated: at low level of the applied magnetic field, or without it, the increase of B leads to the drop of the sandwich stiffness and the critical buckling pressure, but at $B \geq 20$ mT, the critical pressures q_n^*, q_n° grow together with h_2. It may be also concluded that the edge shear in simply supported sandwich shells without diaphragm have weak supporting effect, the deviation δ having maximum at about $B = 20$ mT. When comparing the critical values of pressure for the sandwich shells with the SSD and SSF boundary conditions, the critical buckling pressure $q_{\rm n}^{*}$ for the shell with the diaphragm is always more then the critical pressure $q_{\rm n}^{\circ}$ for the same shell but without diaphragm. It is also seen that the deviation δ' grows together with the induction B in a nonlinear manner as a function of the core thickness h_2.

Example 3.7. As the next example, we consider a five-layered cylindrical shell of the radius $R = 0.9$ m and length $L = 1.0$ m assembled from different laminas which are assumed to be isotropic:

- the first (innermost) layer of the thickness $h_1 = 0.5$ mm is the ABS-plastic SD-0170 with the elastic properties specified above;
- the fifth (outermost) layer of the thickness $h_5 = 0.5$ mm is made of silicon nitrate (ceramic, Si_3N_4) with the elastic moduli (Reddy, 2004) $E_5 = 3.484 \cdot 10^2$ GPa, $\nu_5 = 0.24$;
- the second and fourth layers with the same thicknesses $h_2 = h_4 = 3.0$ mm are made of epoxy for which $E_2 = E_4 = 3450$ Pa, $\nu_2 = \nu_4 = 0.3$;
- the third soft layer of the thickness h_3 is alloy-foam for which (Han et al, 2004) $E_3 = 4.59 \cdot 10$ MPa, $\nu_3 = 0.33$.

Table 3.7 shows the effect of different thicknesses of the soft alloy-foam core on the parameters m^*, m°, p° and the critical buckling pressures $q_{\rm n}^{*}$, q_0°, $q_{\rm n}^{\circ}$ for the SSD and SSF boundary conditions. As expected, increasing the thickness h_3 of the alloy-form core at fixed thicknesses of other layers increases the critical buckling pressures $q_{\rm n}^{*}$ and $q_{\rm n}^{\circ}$ for the both variants of boundary conditions. This effect is explained by increasing the reduced bending stiffness of the laminated shells. Clearly, this trends may be easily changed if one or more material or geometrical parameters are changed. For example, increasing the volume fraction of the alloy-form core will have another effect on the effective bending stiffness and buckling pressure. However, the basic results of this example concerns the influence of the soft core thickness on the edge shear induced correction. The increase of the thickness h_3 leads to the reduction of the effective shear modulus G and this results in growing the transverse shears near the simply supported edge without a diaphragm; in turn, rising edge shear with minor *supporting effect* give the growing positive correction δ for the zeroth approximation

Table 3.7 Wave numbers m^*, m°, wave parameter p°, critical buckling pressures $q_{\rm n}^{*}$, q_0°, $q_{\rm n}^{\circ}$ and the edge shear induced corrections δ, δ' for the 5-layered cylindrical shell for two variants of boundary conditions (SSD, SSF) vs. thickness h_3 of the alloy-foam core (after Mikhasev and Botogova, 2017).

h_3, mm	m^*	$q_{\rm n}^{*}$, kPa	p°	m°	q_0°, kPa	$q_{\rm n}^{\circ}$, kPa	δ	δ'
20	7	659.94	2.17	8	551394	565134	+2.49%	-14.37%
25	7	793.93	2.25	7	663738	689078	+3.82%	-13.21%
30	7	913.67	2.32	7	765320	802965	+4.92%	-12.12%
35	8	1010.00	2.39	7	861574	910589	+5.69%	-9.84%
38	8	1070.00	2.44	7	916356	971556	+6.02%	-9.02%

of the critical buckling pressure. As in the first example, the correction δ' is always negative, that is the edge diaphragm reinforces the laminated structure. However, in this example the value of the correction δ' decreases with the increase of the soft core thickness.

The outcomes of Subsect. 3.2.1 allow to make the following conclusions:

- taking into account the transverse shear in a thin laminated cylindrical shell results in decreasing the critical buckling pressure,
- if both edges of a cylindrical shell are simply-supported, then the simple edge effects with the index of variation $\iota_1 = 1/2$ are absent,
- if the simply-supported edges do not have any diaphragms, then the buckling mode consists of a slowly varying function and the shear edge effect integrals with the low index of variation equaled to $\iota_1 = 1/4$, the effect of these integrals on the buckling pressure being larger for short cylinders and
- the presence of a diaphragm in the plane of a simply-supported edge inhibits appearing any edge effects as of components of the buckling mode.

3.2.2 Localized Forms of Buckling

In this subsection we will consider the special case when a medium-length thin laminated cylindrical shell buckles in the neighbourhood of some generatrix called the *weakest* one (Mikhasev et al, 2001a,b). For the first time, similar problems on localized buckling of thin isotropic single-layer cylindrical and conical shells were studied by Tovstik (1983). Considering buckling and free vibrations of non-circular cylinders with slanted edges, he proposed the asymptotic method whereby the approximate solutions of the governing equations were constructed in the form of functions oscillating and quickly decreasing far away from the weakest generatrix. Later, this method was applied to study buckling of isotropic non-circular conical shells with slanted edges under nonuniform external pressure (Mikhasev and Tovstik, 1990). The concept of Tovstik's method as well as a great number of solved problems on buckling of isotropic single-layer shells may be found in Tovstik and Smirnov (2001).

The present subsection mainly aims to apply Tovstik's method (Tovstik, 1983) to study buckling of a thin non-circular multilayered cylindrical shell with oblique edges subjected to a normal external pressure. The specific goal defined herein is to consider the same problem utilizing the finite element method, and to compare the outcomes of different approaches. The effect of shear and different boundary conditions on the critical buckling pressure and localized buckling mode as well is studied.

3.2.2.1 Setting the Problem

Let a medium-length thin laminated cylindrical shell shell be non-circular with the radius of curvature $R_2(\alpha_2)$ and non-closed in the α_2- direction (cylindrical sandwich panel). The shell edges are not necessarily plane curves,

$$\alpha_1^*(\alpha_2) \leq \alpha_1 \leq \alpha_1^{**}(\alpha_2). \tag{3.93}$$

The shell is assumed to be sufficiently thin to facilitate application of asymptotic method. We introduce again a small parameter

$$\varepsilon^8 = \frac{h^2\eta_3}{12(1-\nu^2)R^2}, \tag{3.94}$$

where h is the total thickness of the sandwich, R is a characteristic dimension of the shell which will be introduced below, and a parameter η_3 is defined by (2.25). Other dimensionless parameters are introduced as follows

$$\begin{aligned} &\alpha_1 = Rs, \quad \alpha_2 = R\varphi, \quad R_2 = \frac{R}{k_2(\varphi)}, \quad T_{22}^\circ = -\varepsilon^6 EhΛ, \\ &\chi = R\chi_*, \quad w = Rw_*, \quad F = \varepsilon^4 EhR^2 F_*, \quad \phi = R\phi_*, \end{aligned} \tag{3.95}$$

where $Λ$ is an unknown positive parameter of loading, and all magnitudes with asterisk are dimensionless ones. It is also assumed here that $G \sim h_*^{3/2}E$ and the parameter θ is small so that the following asymptotic estimations are valid

$$\frac{K}{\pi^2} = \varepsilon^2\kappa, \quad \frac{K\theta}{\pi^2} = \varepsilon^3\tau, \tag{3.96}$$

where $\kappa, \tau \sim 1$ at $\varepsilon \to 0$. These assumptions hold for thin shells and those materials which are considered below as components of the layered package.

Taking into account (3.95), (3.96), the governing equations (3.38), (3.39) may be rewritten in the dimensionless form

$$\begin{aligned} \varepsilon^4(1-\varepsilon^3\tau\Delta)\Delta^2\chi_* + k_2(\varphi)\frac{\partial^2 F_*}{\partial s^2} + \varepsilon^2Λ\frac{\partial^2}{\partial\varphi^2}(1-\varepsilon^2\kappa\Delta)\chi_* = 0, \\ \varepsilon^4\Delta^2F_* - k_2(\varphi)\frac{\partial^2}{\partial s^2}(1-\varepsilon^2\kappa\Delta)\chi_* = 0, \end{aligned} \tag{3.97}$$

$$\frac{1-\nu}{2}\varepsilon^2\kappa\triangle\phi_* = \phi_*. \tag{3.98}$$

On edges (3.93), we consider one of two variants of boundary conditions (or their combination), i.e. the simple support (SS) boundary conditions with the infinite rigidity diaphragm (2.111), (2.118) or the rigid clamped (RC) ones without diaphragm (2.117), (2.118). In the dimensionless form these conditions read

$$\chi_* = \Delta\chi_* = \Delta^2\chi_* = \frac{\partial\phi_*}{\partial\alpha_1} = 0, \quad F_* = \triangle F_* = 0 \tag{3.99}$$

for the SS edges $s = s_1(\varphi), s = s_2(\varphi)$ and

$$\left(1 - \frac{h^2}{\beta}\Delta\right)\chi_* = 0, \quad \frac{\partial\chi_*}{\partial\alpha_1} = \frac{\partial}{\partial\alpha_1}(\Delta\chi_*) = \phi_* = 0, \quad F_* = \triangle F_* = 0 \tag{3.100}$$

for the RC edges, where $s_1(\varphi) = \alpha_1^*[R\varphi]/R$, and $s_2(\varphi) = \alpha_1^{**}[R\varphi]/R$.

The stress state of a shell comprises the basic stress state and the edge effects at the shell edges. As shown in Subsect. 3.2.1, for sandwich cylindrical shells governed by Eqs. (3.97), (3.98), the edges effects are described by integrals of two kinds. Without regard for the type of boundary conditions, one can conclude that the first one includes the integrals of the simple edge effect which, with an accuracy up to amplitudes depending on a coordinate φ, have the form (3.69) with the index of variation $\iota_1 \geq 1/2$; the edge effect integrals of the second type are generated by the transverse shears in a vicinity of the shell edges and governed by equations like Eqs. (3.62) and (3.68). For the boundary conditions (3.99), (3.100), the shear function ϕ is independent of the displacement function χ_* and so $\phi_* = 0$. As concerns integrals like (3.68), (3.69), then the asymptotic analysis of the boundary conditions (3.99), (3.100) shows that they may be determined in higher approximations; they give corrections of an order $O\left(\varepsilon^2\right)$ which coincide with an error of the governing equations (3.97), (3.98). So, to construct the main stress state, being semi-momentless one, one needs to satisfy only two boundary conditions at each edges. In our case, apart from the terms of order ε^2 these conditions are as follows

$$\chi_* = F_* = 0 \quad \text{at} \quad s = s_1(\varphi), s = s_2(\varphi) \tag{3.101}$$

and

$$\chi_* = \frac{\partial\chi_*}{\partial s} = 0 \quad \text{at} \quad s = s_1(\varphi), s = s_2(\varphi) \tag{3.102}$$

for the SS edges with diaphragm and the RC edges without diaphragm, respectively. The problem is to find the least eigenvalue Λ for the boundary-value problem (3.97), (3.101) or (3.97), (3.102).

3.2.2.2 Asymptotic Approach

It is assumed that the functions $k_2(\varphi), s_i(\varphi)$ are infinitely differentiable and orders of their derivatives do not exceed orders of original functions. Due to the variability of the curvature $k_2(\varphi)$ and the presence of the sloping edges $s_i(\varphi)$, buckling occurs such that the concavities do not spread over the entire surface of the shell.

Following the asymptotic approach stated in Tovstik (1983); Tovstik and Smirnov (2001), we assume that the buckling modes are localized near some generatrix $\varphi = \varphi_0$ called the weakest one. Then the periodic conditions in the circumferential direction φ may be changed for the following ones

$$|\chi_*|, \quad |F_*| \to 0 \quad \text{as} \quad |\varphi - \varphi_0| \to \infty. \tag{3.103}$$

When taking into account the presupposed localization of buckling modes, it is suitable to scale in the neighbourhood of the weakest generatrix and introduce a new local coordinate ξ

$$\varphi - \varphi_0 = \varepsilon^{1/2}\xi. \tag{3.104}$$

The formal asymptotic solution of the boundary-value problem is assumed to be in the form of

$$\begin{aligned}
\chi_* &= \sum_{j=0}^{\infty} \varepsilon^{j/2}\chi_j(\xi, s) \exp\left[\mathrm{i}\left(\varepsilon^{-1/2}p\xi + \frac{1}{2}b\xi^2\right)\right], \\
F_* &= \sum_{j=0}^{\infty} \varepsilon^{j/2}F_j(\xi, s) \exp\left[\mathrm{i}\left(\varepsilon^{-1/2}p\xi + \frac{1}{2}b\xi^2\right)\right],
\end{aligned} \tag{3.105}$$

$$\Im b > 0, \tag{3.106}$$

$$\Lambda = \Lambda_0 + \varepsilon\Lambda_1 + \varepsilon^2\Lambda_2 + \ldots, \tag{3.107}$$

where $\chi_j(\xi, s), F_j(\xi, s)$ are polynomials in ξ, p is a wave parameter, the symbol $\Im$ denotes the imaginary part, and a parameter b characterizes the rate of decay of the deflection amplitude when the distance from the weakest generatrix $\varphi = \varphi_0$ increases. Inequality (3.106) guarantees the attenuation of dents amplitudes far from the line $\varphi = \varphi_0$. The real and the imaginary parts of functions (3.105), with inequality (3.106) taking into account, give the two localized eigenmodes near the generatrix $\varphi = \varphi_0$.

To determine unknown functions χ_j, F_j and parameters $p, b, \varphi_0, \Lambda_j$, we substitute ansatz (3.105) into system (3.97) and the boundary conditions (3.101), (3.102) and equalize coefficients by the same powers of $\varepsilon^{1/2}$. All coefficients in Eqs. (3.97) as well as the functions s_j depending on φ are expended in a power series of $\varphi - \varphi_0 = \varepsilon^{1/2}\xi$. As a result, one obtains the following sequence of equations

$$\mathbf{L}_0\chi_0 = 0, \tag{3.108}$$

$$\mathbf{L}_0\chi_1 + \mathbf{L}_1\chi_0 = 0, \tag{3.109}$$

$$\mathbf{L}_0\chi_2 + \mathbf{L}_1\chi_1 + \mathbf{L}_2\chi_0 = 0, \quad \ldots \tag{3.110}$$

with

$$\begin{aligned}
\mathbf{L}_0 z &= \frac{\partial^4 z}{\partial s^4} + \frac{p^4[p^4 - \Lambda_0 p^2(1 + \kappa p^2)]}{k_2(\varphi_0)(1 + \kappa p^2)} z, \\
\mathbf{L}_1 z &= \left(b\frac{\partial \mathbf{L}_0}{\partial p} + \frac{\partial \mathbf{L}_0}{\partial \varphi_0}\right)\xi z - \mathrm{i}\frac{\partial \mathbf{L}_0}{\partial p}\frac{\partial z}{\partial \xi},
\end{aligned} \tag{3.111}$$

$$\mathbf{L}_2 z = \frac{1}{2}\left(b^2\frac{\partial^2 \mathbf{L}_0}{\partial p^2} + 2b\frac{\partial^2 \mathbf{L}_0}{\partial p \partial \varphi_0} + \frac{\partial^2 \mathbf{L}_0}{\partial \varphi_0^2}\right)\xi^2 z - \frac{1}{2}\frac{\partial^2 \mathbf{L}_0}{\partial p \partial \varphi_0} z$$
$$- \frac{1}{2}\frac{\partial^2 \mathbf{L}_0}{\partial p^2}\left(\mathrm{i}z + \frac{\partial^2 z}{\partial \xi^2}\right) - \mathrm{i}\left(b\frac{\partial^2 \mathbf{L}_0}{\partial p^2} + \frac{\partial^2 \mathbf{L}_0}{\partial p \partial \varphi_0}\right)\xi\frac{\partial z}{\partial \xi} + \mathbf{L}_* z + \mathbf{N}z,$$

where

$$\mathbf{L}_* z = \frac{p^{10}\tau}{k_2(\varphi)(1+\kappa p^2)} z, \qquad \mathbf{N}z = -\Lambda_1 p^6 z. \tag{3.112}$$

The sequence of boundary conditions for χ_j will be the following:

- for the simply supported edges $s = s_j(\varphi_0)$ with diaphragm

$$\chi_0 = 0, \qquad \frac{\partial^2 \chi_0}{\partial s^2} = 0,$$
$$\chi_1 + \xi s_i' \frac{\partial \chi_0}{\partial s} = 0, \quad \frac{\partial^2 \chi_1}{\partial s^2} + \xi s_i' \frac{\partial^3 \chi_0}{\partial s^3} = 0,$$
$$\chi_2 + \xi s_i' \frac{\partial \chi_1}{\partial s} + \frac{1}{2}\xi^2\left(s_i'' \frac{\partial \chi_0}{\partial s} + s_i'^2 \frac{\partial^2 \chi_0}{\partial s^2}\right) = 0, \tag{3.113}$$
$$\frac{\partial^2 \chi_2}{\partial s^2} + \xi s_i' \frac{\partial^3 \chi_1}{\partial s^3} + \frac{1}{2}\xi^2\left(s_i'' \frac{\partial^3 \chi_0}{\partial s^3} + s_i'^2 \frac{\partial^4 \chi_0}{\partial s^4}\right) - \frac{4\mathrm{i}s_i'}{p}\frac{\partial^3 \chi_0}{\partial s^3} = 0, \ldots,$$

- for the rigid clamped edges without diaphragm

$$\chi_0 = 0, \qquad \frac{\partial \chi_0}{\partial s} = 0,$$
$$\chi_1 + \xi s_i' \frac{\partial \chi_0}{\partial s} = 0, \quad \frac{\partial \chi_1}{\partial s} + \xi s_i' \frac{\partial^2 \chi_0}{\partial s^2} = 0,$$
$$\chi_2 + \xi s_i' \frac{\partial \chi_1}{\partial s} + \frac{1}{2}\xi^2\left(s_i'' \frac{\partial \chi_0}{\partial s} + s_i'^2 \frac{\partial^2 \chi_0}{\partial s^2}\right) = 0, \tag{3.114}$$
$$\frac{\partial \chi_2}{\partial s} + \xi s_i' \frac{\partial^2 \chi_1}{\partial s^2} + \frac{1}{2}\xi^2\left(s_i'' \frac{\partial^2 \chi_0}{\partial s^2} + s_i'^2 \frac{\partial^3 \chi_0}{\partial s^3}\right) - \frac{4\mathrm{i}s_i'}{p}\frac{\partial^2 \chi_0}{\partial s^2} = 0, \ldots$$

The prime $(\ldots)'$ means differentiation of $s_i(\varphi)$ with respect to φ. Note that Eqs. (3.113) and (3.114) guarantee a realization of the boundary conditions merely in the small vicinity of the weakest generatrix $s = s_i(\varphi_0)$. However, there is no sense to satisfy the boundary conditions on the entire surface of the shell.

The sequence of one-dimensional boundary-value problems (3.108)-(3.114) serves to determine unknown functions $\chi_j(s,\xi), F_j(s,\xi)$ and parameters Λ_j, p, b. The details of seeking these magnitudes are omitted here (s. Tovstik and Smirnov, 2001). We will outline only the principal equations. Let us consider the sequence of boundary-value problems step-by-step for $j = 0, 1, 2, \ldots$ We will call these problems as BVP0, BVP1, BVP2, ...

3.2.2.2.1 Zeroth-order Approximation

In the zeroth-order approximation, one has the homogeneous equation

$$\mathbf{L}_0\chi_0 \equiv \frac{\partial^4\chi_0}{\partial s^4} + \frac{p^4[p^4 - \Lambda_0 p^2(1+\kappa p^2)]}{k_2(\varphi_0)(1+\kappa^2)}\chi_0 = 0 \tag{3.115}$$

with the following homogeneous boundary conditions

$$\chi_0 = 0, \qquad \frac{\partial^2\chi_0}{\partial s^2} = 0 \quad \text{at} \quad s = s_i(\varphi_0) \tag{3.116}$$

for the simply supported (SS-SS) edges $s = s_i$;

$$\chi_0 = 0, \qquad \frac{\partial\chi_0}{\partial s} = 0 \quad \text{at} \quad s = s_i(\varphi_0) \tag{3.117}$$

for the rigidly clamped (RC-RC) edges $s = s_i$;

$$\begin{aligned} \chi_0 &= 0, \qquad \frac{\partial^2\chi_0}{\partial s^2} = 0 \quad \text{at} \quad s = s_1(\varphi_0), \\ \chi_0 &= 0, \qquad \frac{\partial\chi_0}{\partial s} = 0 \quad \text{at} \quad s = s_2(\varphi_0) \end{aligned} \tag{3.118}$$

for the simply supported and rigidly clamped (SS-RC) edges $s = s_1$ and $s = s_2$, respectively.

The stress and displacement functions χ_0 and F_0 are coupled by the relation

$$F_0 = \frac{k_2(\varphi_0)(1+\kappa p^2)}{p^4}\,\frac{\partial^2\chi_0}{\partial s^2}. \tag{3.119}$$

The solution of (3.115) may be presented as

$$\chi_0(\xi, s; \varphi_0) = P_0(\xi)z^\circ(s), \tag{3.120}$$

if

$$\Lambda_0(p, \varphi_0) = \frac{\alpha^4 k_2^2(\varphi_0)}{p^6 l^4(\varphi_0)} + \frac{p^2}{1+\kappa p^2}, \tag{3.121}$$

where $P(\xi)$ is an unknown polynomial in ξ, $l(\varphi_0) = s_2(\varphi_0) - s_1(\varphi_0)$, and α and z° are the least positive eigenvalue and the associated eigenfunction, respectively, of the equation $\mathrm{d}^4 z/\mathrm{d}x^4 - \alpha^4 z = 0$ with appropriate boundary conditions. If both edges are simply supported, then

$$z^\circ(s) = \sin(\alpha x), \quad \alpha = \pi, \quad x = \frac{s - s_1(\varphi_0)}{l(\varphi_0)}. \tag{3.122}$$

If the edge $s = s_2(\alpha)$ is clamped and the edge $s = s_1(\varphi_0)$ is simply supported, the results are

$$z^{\circ}(s) = \frac{\sin(\alpha x)}{\sin\alpha} - \frac{\sinh(\alpha x)}{\sinh\alpha}, \quad \alpha \approx 3.9266, \quad x = \frac{s - s_1(\varphi_0)}{l(\varphi_0)}. \tag{3.123}$$

When both edges are clamped, one has

$$z^{\circ}(s) = \frac{\cos(\alpha x)}{\cos\alpha/2} - \frac{\cosh(\alpha x)}{\cosh\alpha/2}, \quad \alpha \approx 4.73, \quad x = \frac{s - s_1(\varphi_0)}{l(\varphi_0)} - \frac{1}{2}. \tag{3.124}$$

Minimizing the function $\Lambda_0(p, \varphi_0)$ over p and φ_0 results in the following equations for the leading approximation of the buckling load parameter,

$$\begin{aligned} \Lambda_0^{\circ} &= \min_{p,\varphi_0} \Lambda_0(p, \varphi_0) = \Lambda_0(p^{\circ}, \varphi_0^{\circ}) \\ &= \frac{8}{3^{3/2}\alpha^2\kappa^3 g^{\circ}(\vartheta^{\circ})^3} + \frac{3^{1/2}\alpha^2\kappa g^{\circ}\vartheta^{\circ}}{2 + 3^{1/2}\alpha^2\kappa^2 g^{\circ}\vartheta^{\circ}}, \end{aligned} \tag{3.125}$$

where

$$\vartheta^{\circ} = 1 + \sqrt{1 + \frac{4}{3^{1/2}\alpha^2\kappa^2 g^{\circ}}}, \quad g(\varphi) = \frac{k_2(\varphi)}{l^2(\varphi)}, \quad g^{\circ} = g(\varphi_0^{\circ}). \tag{3.126}$$

The wave parameter

$$p^{\circ} = \alpha\sqrt{\frac{3^{1/2}\kappa g^{\circ}\vartheta^{\circ}}{2}} \tag{3.127}$$

and the weakest generatrix $\varphi = \varphi_o^{\circ}$ are found from the following equations:

$$\frac{\partial\Lambda_0}{\partial p} = 0, \quad \frac{\partial\Lambda_0}{\varphi_0} = 0. \tag{3.128}$$

The last equation in Eq. (3.128) is reduced to

$$\frac{\mathrm{d}g}{\mathrm{d}\varphi} = 0. \tag{3.129}$$

It is assumed here that

$$\frac{\mathrm{d}^2 g}{\mathrm{d}\varphi^2} > 0 \quad \text{at} \quad \varphi = \varphi_0^{\circ}. \tag{3.130}$$

It may be seen from (3.130) that in a circular cylindrical shell the longest generatrix is the weakest one, and in a shell with a constant generatrix length the asymptotic line with a minimum curvature will be the weakest one. The characteristic size of the shell may be introduced as

$$R = R_2(\varphi_0^{\circ}). \tag{3.131}$$

3.2.2.2.2 First-order Approximation

In the first-order approximation, one has the non-homogeneous differential equation (3.109). When taking into account the solution of boundary-value problem at the previous step, this equation can be rewritten as

$$\begin{aligned} &\mathbf{L}_0\chi_1 + G_1 = 0, \\ &G_1 = [b\xi P_0(\xi) - \mathrm{i}P_0'(\xi)]\frac{\partial \mathbf{L}_0}{\partial p}z^\circ(s) + \xi P_0(\xi)\frac{\partial \mathbf{L}_0}{\partial \varphi_0}z^\circ(s), \end{aligned} \tag{3.132}$$

where P_0' is the derivative of function $P_0(\xi)$. Without loss of generality, we will perform subsequent calculations for the case when both edges are simply supported. The appropriate boundary conditions for χ_1 at $s = s_i(\varphi_0)$ are given by

$$\chi_1 + \xi P_0(\xi)s_i'(\varphi_0^\circ)\frac{\mathrm{d}z^\circ}{\mathrm{d}s} = 0, \quad \frac{\mathrm{d}^2\chi_1}{\mathrm{d}s^2} + \xi P_0(\xi)s_i'(\varphi_0^\circ)\frac{\mathrm{d}^3\chi^\circ}{\mathrm{d}s^3} = 0. \tag{3.133}$$

We arrived at the non-homogeneous boundary-value problem BVP1 (3.132), (3.133) *on spectrum*. Taking into account the self-conjugacy of BVP0, the equality

$$\int_{s_1}^{s_2} z^\circ(\mathbf{L}_0\chi_1 + G_1)\mathrm{d}s = 0 \tag{3.134}$$

serves as the condition for existence of a solution of the BVP1.

The function G_1 is defined by the operators $\partial\mathbf{L}_0/\partial p, \partial\mathbf{L}_0/\partial\varphi_0$ (s. Eq. (3.111)). To define these operators, the BVP0 should be differentiated over p and φ_0

$$\begin{aligned} &\mathbf{L}_0\chi_p + \frac{\partial \mathbf{L}_0}{\partial p}\chi_0 - \frac{\partial \Lambda_0}{\partial p}\chi_0 = 0, \\ &\chi_p = \frac{\partial^2\chi_p}{\partial s^2} = 0 \quad \text{at} \quad s = s_j(\varphi_0). \end{aligned} \tag{3.135}$$

and

$$\begin{aligned} &\mathbf{L}_0\chi_\varphi + \frac{\partial \mathbf{L}_0}{\partial \varphi_0}\chi_0 - \frac{\partial \Lambda_0}{\partial \varphi_0}\chi_0 = 0, \\ &\chi_\varphi + s_i'\frac{\partial\chi_0}{\partial s} = 0, \quad \frac{\partial^2\chi_\varphi}{\partial s^2} + s_i'\frac{\partial^3\chi_0}{\partial s^3} = 0 \quad \text{at} \quad s = s_j(\varphi_0). \end{aligned} \tag{3.136}$$

Taking into account the self-conjugacy of the BVP0, one obtains

$$\begin{aligned} &\int_{s_1}^{s_2} \chi_0\mathbf{L}_0\chi_p\mathrm{d}s = \int_{s_1}^{s_2} \chi_p\mathbf{L}_0\chi_0\mathrm{d}s = 0, \\ &\int_{s_1}^{s_2} \chi_0\mathbf{L}_0\chi_\varphi\mathrm{d}s = \int_{s_1}^{s_2} \chi_\varphi\mathbf{L}_0\chi_0\mathrm{d}s = 0. \end{aligned} \tag{3.137}$$

Then, due to Eqs. (3.132), (3.135)-(3.137), condition (3.134) may be rewritten as

$$\left\{ \left[b\xi P_0(\xi) - \mathrm{i} P_0'(\xi) \right] \frac{\partial \Lambda_0}{\partial p} + \xi P_0(\xi) \frac{\partial \Lambda_0}{\partial \varphi_0} \right\} \int\limits_{s_1}^{s_2} (z^\circ)^2 \, \mathrm{d}s = 0. \tag{3.138}$$

Because

$$\int\limits_{s_1}^{s_2} (z^\circ)^2 \, \mathrm{d}s \neq 0$$

and $P_0(\xi)$ is a polynomial in ξ, Eq. (3.138) implies conditions (3.128) derived above. Now, the solution of BVP1 may be represented as

$$\chi_1 = P_1(\xi) z^\circ + \xi P_0(\xi)(b\chi_p + \chi_\varphi) - \mathrm{i} P_0'(\xi)\chi_p, \tag{3.139}$$

where χ_p, χ_φ are solutions of the boundary-value problems (3.135) and (3.136), respectively, at $\chi_0 = z^\circ$, and $P_1(\xi)$ is an unknown polynomial in ξ.

3.2.2.2.3 Second-order Approximation

In the second-order approximation, the non-homogeneous boundary-value problem (s. Eq. (3.110) with the corresponding boundary conditions (3.113) for χ_2 arises again. The compatibility conditions for this problem may be deduced from the equation

$$\int\limits_{s_1}^{s_2} z^\circ \left\{ \mathbf{L}_1 \left[P_1(\xi) z^\circ + \xi P_0(\xi)(b\chi_p + \chi_\varphi) - \mathrm{i} P_0'(\xi)\chi_p \right] + \mathbf{L}_2 P_0 z^\circ \right\} \mathrm{d}s = 0. \tag{3.140}$$

Omitting details for calculation of operators

$$\frac{\partial^2 \mathbf{L}_0}{\partial p^2}, \frac{\partial^2 \mathbf{L}_0}{\partial \varphi_0^2}, \frac{\partial^2 \mathbf{L}_0}{\partial p \partial \varphi_0}$$

appearing in $\mathbf{L}_2$, we reduce relation (3.140) to the following differential equation with respect to the polynomial $P_0(\xi)$

$$\begin{aligned} \mathcal{L} P_0 \equiv & -\frac{1}{2} \Lambda_{pp} P_0'' - \mathrm{i}(b\Lambda_{pp} + \Lambda_{p\varphi}) \left(\xi P_0' + \frac{1}{2} P_0 \right) \\ & + \left\{ \frac{\tau (p^\circ)^4}{k_2(\varphi_0^\circ)[1 + \kappa (p^\circ)^2]} - \Lambda_1 + c\xi^2 \right\} P_0 = 0, \end{aligned} \tag{3.141}$$

where

$$2c = b^2 \Lambda_{pp} + 2b\Lambda_{p\varphi} + \Lambda_{\varphi\varphi}. \tag{3.142}$$

Here, subscripts p, φ denote differentiation with respect to the corresponding variables p and φ_0, all derivatives being calculated at $p = p^\circ, \varphi_0 = \varphi_0^\circ$. Condition $c = 0$ is necessary for the existence of a polynomial form solution of Eq. (3.141). From the square equation $c = 0$ we find the unique value of b° such that $\Im b^\circ > 0$

$$b^\circ = (-\Lambda_{p\varphi} + \mathrm{i} r)/\Lambda_{pp}, \quad r = \sqrt{d}, \quad d = \Lambda_{pp}\Lambda_{\varphi\varphi} - (\Lambda_{p\varphi})^2. \tag{3.143}$$

It may be seen from Eqs. (3.142) that inequality $\Im b^\circ > 0$ is valid if inequalities $\Lambda_{pp} > 0$ and $d > 0$ hold simultaneously. For $c = 0$ and

$$\Lambda_1 = \Lambda_1^{(n)} = \left(n + \frac{1}{2}\right) r, \quad n = 0, 1, 2, \ldots \tag{3.144}$$

Eq. (3.141) has the solution

$$P_0(\xi) = \mathcal{H}_n(\zeta), \quad \zeta = \sqrt{\frac{r}{\Lambda_{pp}}}\xi, \tag{3.145}$$

where $\mathcal{H}_n$ are nth degree Hermite polynomials.

In our case, taking into account Eq. (3.120), one has

$$\begin{aligned}
\Lambda_{pp} &= \frac{42\alpha^4 (g^\circ)^2}{(p^\circ)^8} + \frac{2\left[1 - 2\kappa(p^\circ)^2 - 3\kappa^2(p^\circ)^4\right]}{[1 + \kappa(p^\circ)^2]^4}, \\
\Lambda_{\varphi\varphi} &= \frac{2\alpha^4 g^\circ g''(\varphi_0^\circ)}{(p^\circ)^6}, \qquad \Lambda_{p\varphi} = 0, \\
b^\circ &= \mathrm{i}\sqrt{\frac{\Lambda_{\varphi\varphi}}{\Lambda_{pp}}}
\end{aligned} \tag{3.146}$$

The eigenvalue Λ defined by (3.107), (3.125) and (3.144) has the least value at $n = 0$. Then

$$P_0 \equiv 1, \qquad \Lambda_1 = \frac{1}{2}\sqrt{\Lambda_{\varphi\varphi}\Lambda_{pp}} + \frac{\tau(p^\circ)^4}{1 + \kappa(p^\circ)^2}. \tag{3.147}$$

The polynomial $P_1(\xi)$ remains unknown in this approximation. To find it, one needs to consider the following two approximations.

3.2.2.2.4 Higher-order Approximations

The following approximations may be constructed in a similar way. We note that $\chi_j(s, \xi)$ are either even or odd polynomials in ξ. The existence conditions for χ_{2j+2} give

$$\mathcal{L}P_{2j} + \Lambda_j P_0 + \mathcal{F}_{2j}(\xi) = 0, \quad j > 0, \tag{3.148}$$

where $\mathcal{L}$ is the operator in the left side of equation (3.141) at $c = 0$, and $\mathcal{F}_{2j}(\xi)$ is expressed in terms of polynomials $P_{2j-1}, P_{2j-2}, \ldots$ found in the previous steps.

The value Λ_j is found from the existence conditions for polynomial form solution of (3.148). If the polynomials P_j are even, then the polynomials P_{j+1} and $\mathcal{F}_{j+1}$ are odd and vice-versa. In fact, the values of $\Lambda_j (j \geq 2)$ are not found here because they depend on the terms which were omitted in the governing equations for sandwich cylindrical shells. In addition, $\Lambda_j (j \geq 2)$ are influenced by the edge effect integrals which should be already taken into consideration in the fourth-order approximation. Finally, we obtain the following approximate formula for the buckling pressure

$$q_{\mathrm{n}}^{*} = \frac{\varepsilon^6 Eh\Lambda_0^{\circ}}{R}\left[1 + \varepsilon\Xi + O\left(\varepsilon^2\right)\right], \quad \Xi = \frac{\Lambda_1}{\Lambda_0^{\circ}}, \tag{3.149}$$

where Λ_0° and Λ_1 are evaluated by (3.125) and (3.147), respectively. When separating the real and imaginary parts in Eqs. (3.105) and taking into account Eq. (2.82) which couples the deflection w and the displacement function χ, one obtains the following two buckling modes

$$\begin{aligned} w_1 &= Z^{\circ}(s,\varphi)\cos\left[\varepsilon^{-1}p^{\circ}(\varphi - \varphi_0^{\circ}) + \Theta_0\right], \\ w_2 &= Z^{\circ}(s,\varphi)\sin\left[\varepsilon^{-1}p^{\circ}(\varphi - \varphi_0^{\circ}) + \Theta_0\right], \end{aligned} \tag{3.150}$$

where

$$Z^{\circ}(s,\varphi) = R\left\{\left[1 + \kappa\left(p^{\circ}\right)^2\right] z^{\circ}(s) + O\left(\varepsilon^{1/2}\right)\right\}\exp\left\{-\frac{1}{2}\varepsilon^{-1}b^{\circ}(\varphi - \varphi_0^{\circ})^2\right\}. \tag{3.151}$$

Θ_0 is an initial phase. Thus, the buckling pressure (3.149) is asymptotically double. The method used here does not allow determining a parameter $\Theta_0 = \text{const}$, nor does it allow one to distinguish the corresponding eigenvalues (s. details in Tovstik and Smirnov, 2001).

3.2.2.3 Effect of Shears on Buckling Pressure and Localized Modes

Equations (3.149) - (3.150) contain parameters κ, τ depending on transverse shear in the laminated shell. They generalize similar formulae derived by Tovstik (1983) for thin single-layer isotropic cylindrical shells based on the Kirchhoff–Love hypotheses. Figures 3.8-3.11 show the influence of the shear parameter κ on all magnitudes characterizing the buckling modes and pressure as well. The calculations were performed for three variants of boundary conditions: SS-SS, SS-RC, and RC-RC edges, respectively. Because the correction ratio Ξ depends on parameter θ (s. Eqs. (3.96) and (3.147)), its evaluation has been done for $\theta = 1/300$ and $\theta = 1/85$. The increase of the shear parameter κ results in the increase of the wave number p° and the parameter b° characterizing the rate of localization of eigenmodes in the neighbourhood of the weakest generatrix $\varphi = \varphi_0^{\circ}$. But the general conclusion is the following: neglecting the transverse shear leads to overstated evaluations of the load parameters Λ_0°, Ξ and as a result, the buckling pressure q_{n}^{*}. In the limit case, when $\kappa \to 0$, one obtains

$$
\begin{aligned}
&p^\circ \to \alpha^{1/2} 3^{1/8} (g^\circ)^{1/4}, \quad b^\circ \to \frac{\mathrm{i}}{2^{3/2} 3^{3/8}} \sqrt{\frac{\alpha g''(\varphi_0^\circ)}{(g^\circ)^{1/2}}}, \\
&\Lambda_0^\circ \to \frac{4\alpha (g^\circ)^{1/2}}{3^{3/4}}, \quad \Lambda_1 \to \frac{2^{3/2}}{3^{3/8}} \sqrt{\frac{\alpha g''(\varphi_0^\circ)}{g^{1/2}}}.
\end{aligned}
\tag{3.152}
$$

The limit values (3.152) are equal to the corresponding magnitudes for single-layer isotropic cylindrical shells without taking transverse shear into consideration (Tovstik, 1983).

Example 3.8. As an example, we consider a three-layer (sandwich) circular cylindrical shell with sloped edge as shown in Fig. 3.12. Here

$$
k_2 = 1, \quad s_1 = 0, \quad s_2\varphi = l_0 + \tan\alpha(\cos\varphi - 1). \tag{3.153}
$$

α is the inclination angle of the upper edge. The longest generatrix $\varphi = \varphi_0^\circ = 0$ is the weakest one, i.e. the shell buckling occurs in the vicinity of the longest generatrix.

Besides the asymptotic approach, we applied the finite element simulation (s. Sect. 2.4) to facilitate the estimation of a range to which the results obtained can be applied. Computations were performed for the cylinder with the maximum length $L = Rl_0 = 2000$ mm and the mid-surface radius $R = 800$ mm. The first and third layers having the thickness $h_1 = h_3 = 0.5$ mm are made of aluminum with the Young's modulus $E_1 = E_3 = 70,3$ GPa and Poisson's ratio $\nu_1 = \nu_3 = 0.345$, and the second one is an epoxy matrix with $E_2 = 3,45$ GPa and $\nu_2 = 0.3$.

For the analysis of the sandwich structure a finite element mesh with a sufficient number of elements in the longitudinal and circumferential directions has to be chosen to calculate the buckling load with sufficient accuracy. Especially if the buckling mode corresponds to a high wave number, a corresponding mesh density is required to ensure sufficient accuracy of the eigenvalues. The first tests revealed that the first buckling mode always corresponds to a higher wave number in circumferential direction, whereas in longitudinal direction only one semi-wave occurs. Several test calculations were performed to study the convergence behaviour of the solution

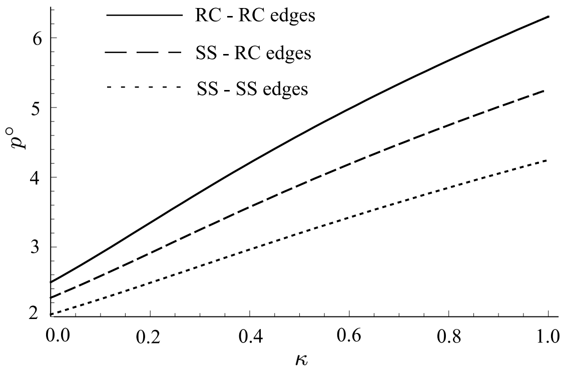

Fig. 3.8 Wave parameter p° vs. shear parameter κ for different variants of boundary conditions.

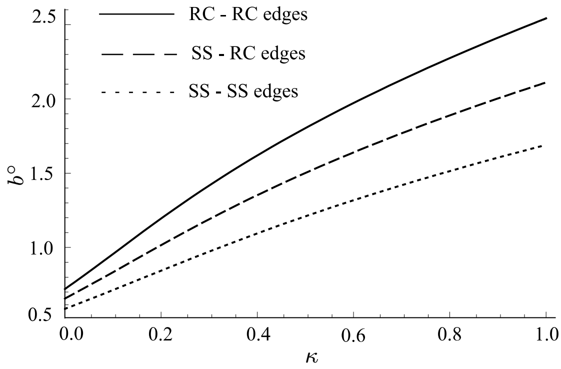

Fig. 3.9 Parameter b° vs. shear parameter κ for different variants of boundary conditions.

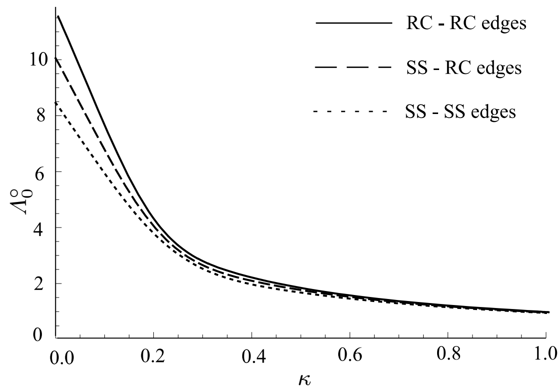

Fig. 3.10 Zero-order approximation of buckling load parameter Λ_0° vs. shear parameter κ for different variants of boundary conditions.

resulting in a high number of elements in circumferential direction and a lower number of elements in longitudinal direction. The convergence test was performed to find the minimum number of elements providing an acceptable accuracy. The cylinder type with $\alpha = 20^\circ$, clamped oblique and simply supported straight edges and $h_2 = 0.02$ mm was modeled to perform the convergence test. With a number of 300 elements in circumferential direction the eigenvalue converges to the final value. The number of elements over the height does not influence the accuracy of the outcomes. Figure 3.13 shows the first buckling (critical) mode of the cylinder with $\alpha = 30^\circ$, $h_2 = 0.02$ mm, clamped oblique edge and simply supported straight edge. This mode is localized in the neighbourhood of the longest generatrix.

The dependence of the buckling pressure q_{n}^* on the thickness h_2 of epoxy matrix and angle α for two variants of boundary conditions and their combination are shown in Tables 3.8 to 3.10. Acronyms AM and FEM correspond to results found by the asymptotic and finite element methods, respectively. It should be noted that assumptions (3.102) introduced above hold true for all geometrical and physical parameters taken into consideration. It can be seen that increasing the inclination angle α results in the increase of the critical pressure. The estimation of the influence of shear parameters κ, τ on the buckling pressure indicates that this influence is

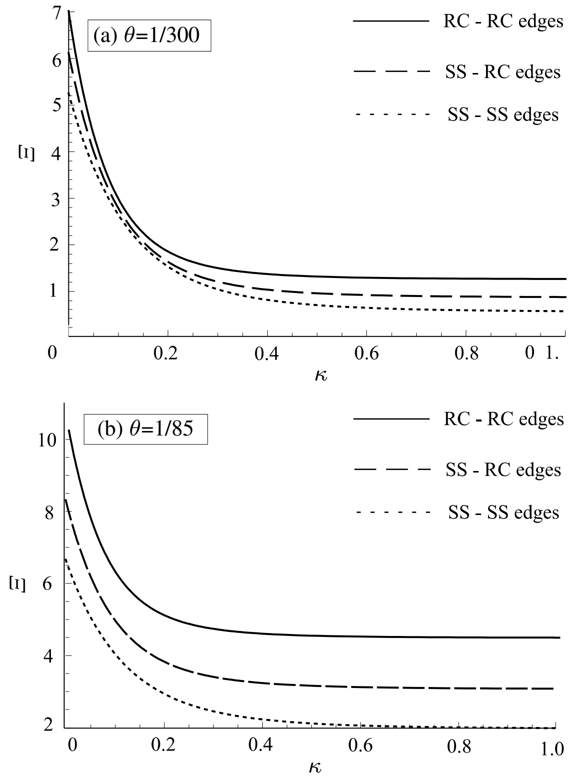

Fig. 3.11 Correction ratio for buckling load parameter, Ξ, vs. shear parameter κ for different variants of boundary conditions and parameter θ: (a) $\theta = 1/300$, (b) $\theta = 1/85$.

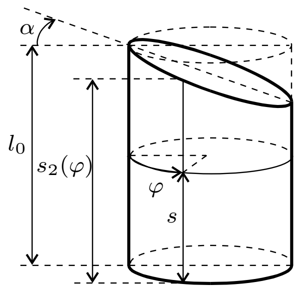

Fig. 3.12 Circular cylindrical shell with oblique edge.

insignificant for physical and geometrical parameters accepted in this example. In some cases it hardly reaches 1% (for the shell with $\alpha = 20°$, $h_2 = 0.1$ mm when both edges are simply supported). Calculations carried out by Grigolyuk and Kulikov (1988b) revealed that this influence grows with a higher number of layers having essentially different physical properties. In our example, the principal parameters are the reduced Young's modulus E and Poisson's ratio ν for the whole sandwich. The analysis of calculations revealed that the deviation of the results obtained by the asymptotic and numerical approaches increases with the core thickness h_2. This

Table 3.8 Dependence of the buckling pressure q_n^* on h_2 and angle α for RC-RC edges (after Mikhasev et al, 2001a).

h_2, mm	0	0.01	0.05	0.10	0.50	1.00	2.00
$\alpha = 20°$							
q_n^* (AM), kPa	2.33	2.38	2.60	2.89	5.73	10.30	22.50
q_n^* (FEM), kPa	2.30	2.35	2.56	2.84	5.61	10.10	21.96
$\alpha = 30°$							
q_n^* (AM), kPa	2.36	2.42	2.64	2.93	5.82	10.50	23.00
q_n^* (FEM), kPa	2.28	2.33	2.54	2.81	5.51	9.97	21.78

Table 3.9 Dependence of the buckling pressure q_n^* on h_2 and angle α when oblique edge is clamped and straight edge is simply supported (after Mikhasev et al, 2001a).

h_2, mm	0	0.01	0.05	0.10	0.50	1.00	2.00
$\alpha = 20°$							
q_n^* (AM), kPa	1.94	1.99	2.17	2.41	4.78	8.64	18.80
q_n^* (FEM), kPa	1.96	2.01	2.19	2.45	4.82	8.71	19.04
$\alpha = 30°$							
q_n^* (AM), kPa	1.97	2.02	2.21	2.45	4.87	8.81	19.20
q_n^* (FEM), kPa	1.971	2.015	2.198	2.44	4.77	8.68	18.88

Table 3.10 Dependence of the buckling pressure q_n^* on h_2 and angle α for SS-SS edges (after Mikhasev et al, 2001a).

h_2, mm	0	0.01	0.05	0.10	0.50	1.00	2.00
$\alpha = 20°$							
q_n^* (AM), kPa	1.57	1.60	1.75	1.94	3.86	6.98	15.20
q_n^* (FEM), kPa	1.62	1.65	1.81	2.01	3.98	7.25	15.95
$\alpha = 30°$							
q_n^* (AM), kPa	1.60	1.63	1.78	1.98	3.94	7.13	15.60
q_n^* (FEM), kPa	1.60	1.636	1.784	1.981	3.98	7.17	15.93

fact is attributable to a higher error rate of the asymptotic method when the shell thickness is increased.

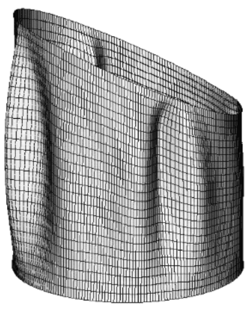

Fig. 3.13 Fist buckling mode of cylinder with $\alpha = 30°$, $h_2 = 0.02$ mm and RC-SS edges (after Mikhasev et al, 2001a).

3.3 Laminated Shell under Axial Compression

The first fundamental investigations on the buckling behaviour of axially compressed circular cylindrical shells were carried out at the beginning of the 20th century. Lorenz (1908) performed the linear analyses and derived an approximate formula for the axial compressive force resulting in the buckling of a medium-length simply supported single-layer cylindrical shell (s. also Lorenz, 1911)

$$T_1^* = -\frac{Eh^2}{R\sqrt{3(1-\nu^2)}}. \tag{3.154}$$

A few years later, Donnell (1934); von Kármán and Tsien (1941) considered this problem accounting large deflections and Koiter (1967); Donnel and Wan (1950) studied the influence of imperfections (sensitivity) on the shell stability behaviour of cylindrical single-layer shells and revealed that initial imperfections were responsible for the great inconsistency between analytical estimates and experimental data.

As regards the buckling of non-circular cylindrical shells under axial compression, the first studies have been done by Kempner and Chen (1964, 1967); Hutchinson (1968); Feinstein et al (1971a,b). They have showed that oval single-layer cylindrical shells are much less sensitive to imperfections than circular ones. Another important outcome of these and subsequent relevant papers (Tovstik, 1984; Sun, 1991; Meyers and Hyer, 1996; Soldatos, 1999) is that the buckling of an elliptical cylindrical shell occurs under the compressive axial force which is larger than the critical buckling force for a circular shell with the curvature being equal to the minimum curvature of the oval cylinder under consideration. Noticeable contribution to the study of buckling of thin non-circular cylindrical shells has been made by Tovstik (1984). He has showed that buckling modes of similar shells may be localized in the neighborhood of some generatrix called the weakest one. Following the asymptotic approach developed by Tovstik (1984) (s. also Tovstik and Smirnov, 2001), this generatrix is defined as the asymptotic line at which the radius of curvature has a local maximum, and the localized buckling mode is constructed in the form of exponentially decreasing function with a number of circumferential waves strongly depending on the shell length. In particular, a short thin cylinder buckles mostly without waves in the circumferential direction but with two bubbles located in the zone of maximum radius, whereas for a medium-length cylinder, buckling may occur with a large number of circumferential waves decaying far away from the weakest generatrix. In the same paper (Tovstik, 1984) and later in Li (1990), it has been shown that the critical load of a circular cylinder under axial compression is sensitive to imperfection of an applied load. In particular, the high rate of inhomogeneity of axial load may also result in localization of the buckling mode near the generatrix along which the axial stress resultant is maximum (Tovstik, 1984). In 2008, applying the generalized beam theory, Silvestre (2008) studied the local and global buckling behaviour of single-layer elliptical shells and thereby justified above mentioned results (Tovstik and Smirnov, 2001) as well as conclusions on the buckling force made by (Kempner and Chen, 1964, 1967; Feinstein et al, 1971a,b; Hutchinson, 1968).

In the past four decades, the wide application of composite materials in designing of thin-walled structures has excited numerous investigations on non-linear behaviour of laminated axially compressed, circular and non-circular, cylindrical shells. So, Soldatos and Tzivanidis (1982); Sheinman and Firer (1994); Firer and Sheinman (1995) have proposed the simplified models based on the Donnell-type theory. Later, Jaunky and Knight Jr (1999) has obtained the buckling loads of circular cylindrical laminated panels using different shell theories with a first-order shear deformation approach and showed that Donnell's theory could give error results for some lamination schemes. The higher order shear deformation theories (e.g., s. Reddy and Liu, 1985; Grigolyuk and Kulikov, 1988a) as well as the high-accuracy layer-wise ones (e.g., s. Reddy, 1993; Carrera, 1999, 2001; Reddy and Arciniega, 2004) promoted more accurate studies on buckling of axially compressed laminated plates, panels (Kim, 1996; Wu et al, 2008; Kheirikhah et al, 2012; Coburn and Weaver, 2016)) and circular cylindrical shells (s., among many others, Tennyson and Chan, 1990; Simitses, 1996; Soldatos, 1999). In addition, Sambandama et al (2003); Patel et al (2004) have studied the linear elastic stability behavior of laminated oval cylindrical shells through finite element approach taking into account transverse shear and deformations.

The basic conclusion of above-mentioned papers and other relevant studies is that the effect of the transverse shears on the buckling axial force may be significant for laminated shells and plates assembled from materials with different stiffness. So, the incorporation of transverse shear into the buckling model of sandwich plates (Kheirikhah et al, 2012) or cylindrical shells (Korchevskaya et al, 2003) with rigid face sheets but soft and shear pliable core may result in the noticeable reduction of the buckling axial load. Recently, preforming the buckling analysis of variable-stiffness sandwich panels, Coburn and Weaver (2016) have revealed that low transverse shear moduli of a core may be the cause of the local shear crimping instabilities. Mikhasev and Botogova (2017) have showed that the pressure induced buckling of a thin medium-length circular sandwich cylinder with a soft core is very affected by the edge shear for some variant of boundary conditions. If an edge is simply supported and free of a diaphragm preventing shear in the edge plane, then the external buckling pressure generates the edge shear deformations, being the part of buckling mode, which oscillate and exponentially decay far away from this edge, this edge integrals giving slight supporting effect for the shell.

In this section, we shall consider a thin medium-length laminated cylindrical shell under the action of axial in-plane stress resultant $T^\circ_{11} < 0 (T^\circ_{22} = T^\circ_{12} = 0)$. Here, the operator (2.161) is simplified

$$\varDelta_T w = T^\circ_{11} \frac{\partial^2 w}{\partial \alpha_1^2}.$$

Then the governing equations predicting buckling of axially compressed laminated cylindrical shell read

$$
\begin{aligned}
&D\left(1-\frac{\theta h^2}{\beta}\Delta\right)\Delta^2\chi+\frac{1}{R_2}\frac{\partial^2 F}{\partial\alpha_1^2}-T_{11}^{\circ}\frac{\partial^2}{\partial\alpha_1^2}\left(1-\frac{h^2}{\beta}\Delta\right)\chi=0,\\
&\Delta^2 F=\frac{Eh}{R_2}\frac{\partial^2}{\partial\alpha_1^2}\left(1-\frac{h^2}{\beta}\Delta\right)\chi.
\end{aligned}
\tag{3.155}
$$

It is assumed that both edges $\alpha_1 = L_i$ are simply supported and have the infinite rigidity diaphragm inhibiting shear in the edge planes. The appropriate boundary conditions are given by Eqs. (3.40) and (3.42).

As a preliminary, we will consider the simplest case when all geometrical and physical parameters are constant, and the axial load is uniform (Korchevskaya et al, 2003; Mikhasev et al, 2004). In this case buckling is accompanied by the formation of a regular pattern of small pits, and the governing equations allows us to write the explicit form of a solution. In particular, the problem on optimal design of multilayered cylindrical shell with fixed weight of elastic material and magnetorheological elastomer resulting in the maximum value of critical buckling axial force is considered (Mikhasev, 2018). Then we will study buckling of a non-circular sandwich cylinder subjected to non-uniform axial compression (Mikhasev and Zgirskaya, 2001). Using the asymptotic methods, the buckling modes will be constructed in the form of functions localized near the weakest generatrix on the shell surface (Mikhasev and Mlechka, 2018). The influence of physical properties of laminas as well as a number of layers composing the shell on the critical buckling force will be analyzed.

3.3.1 Circular Cylindrical Shell Under Uniform Axial Load

Let the geometrical characteristics R_2, L_i, h_k and the stress resultant T_{11}° be constants. Then a solution of Eqs. (3.155) with the boundary conditions (3.40), (3.42) can be found in the explicit form

$$
\chi=\chi_0\,\sin\frac{\pi m\alpha_1}{L}\cos\frac{n\alpha_2}{R},\quad F=F_0\,\sin\frac{\pi m\alpha_1}{L}\cos\frac{n\alpha_2}{R},
\tag{3.156}
$$

where m is a number of semi-waves along the shell generatrix, and n is a number of waves in the circumferential direction. The substitution of (3.156) into (3.155) results in the formula for the axial stress resultant

$$
T_{11}^{\circ}=-\pi^2 Eh\left(\frac{\mu^4 l^2\delta_{nm}^2}{m^2}\frac{1+\theta K\delta_{nm}}{1+K\delta_{nm}}+\frac{m^2}{\pi^4 l^2\delta_{nm}^2}\right),
\tag{3.157}
$$

where

$$
\mu^4=\frac{h^2\eta_3}{12(1-\nu^2)R^2},\quad K=\frac{\pi^2 h^2}{\beta R^2},\quad \delta_{nm}=\left(\frac{m^2}{l^2}+\frac{n^2}{\pi^2}\right),\quad l=\frac{L}{R}.
\tag{3.158}
$$

This simple formula was first time obtained by Grigolyuk and Kulikov (1988b). Minimizing T_{11}^{0} over integer n and m, one can find the critical buckling force

$$T_1^* = \min_{n,m} |T_{11}^{\circ}(n,m)| = |T_{11}^{\circ}(n^*,m^*)|. \tag{3.159}$$

In Eq. (3.157), E and K are the reduced Young's modulus and shear parameter which depend on a number of layers and their mechanical properties. For a thin laminated shell with the total thickness h, the new magnitude μ is a small parameter. The influence of E and K on the buckling axial force T_1^* is different and depends on the cylinder length. It is known that for a medium-length shell the buckling mode is characterized by a series of small dents so that, at least, a number n^* is large and has an order of $\mu^{-1} \sim \sqrt{R/h}$ (Tovstik and Smirnov, 2001). Whereas the buckling of a sufficiently long shell occurs in a manner similar to a rod of circular cross-section with $m^* = n^* = 1$. Thus, as seen from Eq. (3.157), the effect of the shear parameter K on the critical force T_1^* is more essential for thin cylinders having a moderate length. This conclusion is confirmed by numerical calculations performed by Grigolyuk and Kulikov (1988b). They have also showed that the decrease of a parameter K results in the increase of the buckling axial force.

The following Examples 3.9 and 3.10 illustrate the influence of a number of layers and thicknesses of interlayer cores as well on the critical buckling force. We will demonstrate also the manner in which formula (3.157) can be utilized for solving the optimal design problem for a thin laminated structure.

Example 3.9. Firstly we consider the problem of optimal design of a thin sandwich cylinder of the radius $R = 150$ mm and length $L = 450$ mm. Let the face sheets of the thickness $h_1 = h_3$ be made of aluminum, and the core of thickness h_2 is made of epoxy with properties specified in Example 3.4. It is assumed that the layer thicknesses h_i satisfy condition (3.47), where $h_1^{\circ} = 0.5$ mm. Then for all h_i the shell weight will be constant. It is required to find such value of h_2 for which the critical buckling stress resultant T_1^* is maximum. To verify our calculations based on Eqs. (3.157) and (3.159), we performed the FEM simulation as well. The outcomes of these calculations displayed in Table 3.11 show that the optimal thickness of the epoxy core is about $h_2 \approx 0.8$ mm. The performed calculations allow concluding that the deviation of results obtained by the analytical and finite element methods increases with the total thickness of the shell. This fact concurs with analogous conclusion made when considering Example 3.4. The computational effort in this

Table 3.11 Dependence of the buckling force T_1^* on the epoxy matrix thickness h_2 determined by using Eqs. (3.157), (3.159) and the FEM simulation (after Korchevskaya et al, 2003).

h_2, mm	0	0.2	0.5	0.7	0.8	1.0	1.1
Analytical calculations							
m^*	21	19	17	16	16	15	15
n^*	2	2	0	0	0	0	0
T_1^*, N/mm	288.18	322.10	358.11	370.08	372.58	367.27	361.62
FEM simulation							
m^*	22	20	17	16	16	15	15
n^*	0	0	0	0	0	0	0
T_1^*, N/mm	288.80	328.40	365.80	375.80	386.40	373.90	371.30

case was related to the mesh containing 3200 elements and 9760 nodes. The number of degrees freedom was 42880.

Example 3.10. This example concerns the buckling of laminated cylindrical shells containing core or layers made of MRE-1 under different intensity of an applied magnetic field. We will consider three-, five-, and seven-layer shells of the same length $L = 1$ m and radius $R = 0.5$ m. The layers with odd numbers are made of the ABS-plastic SD-0170, and the those having even numbers are the MRE-1 with properties specified in Chapt. 2. It is assumed that the following conditions for thicknesses hold:

- for the sandwich ($N = 3$),

$$h_1 = h_3 = \frac{h_{\rm pl}}{2}, \quad h_2 = h_{\rm el};$$

- for the five-layer cylinder ($N = 5$),

$$h_1 = h_3 = h_5 = \frac{h_{\rm pl}}{3}, \quad h_2 = h_4 = \frac{h_{\rm el}}{2};$$

- for the seven-layer shell ($N = 7$),

$$h_1 = h_3 = h_5 = h_7 = \frac{h_{\rm pl}}{4}, \quad h_2 = h_4 = h_6 = \frac{h_{\rm el}}{3},$$

where $h_{\rm pl} = 1$ mm is the total thickness of the plastic, and $h_{\rm el} = 8$ mm is the summarized thickness of the used elastomer. In each case the same quantity (weight) of both the plastic and MRE-1 are utilized to assemble the shells. Figure 3.14 shows the dependence of critical buckling force $F_{\rm cr} = 2\pi R T_1^*$ on the induction B of applied magnetic field for three samples of shells under consideration. As seen, the application of magnetic field increases the total stiffness of all shells and results in rising the critical buckling force. This influence is found to be very strong for the sandwich and weak for five-, and seven-layer structures. However, the effect

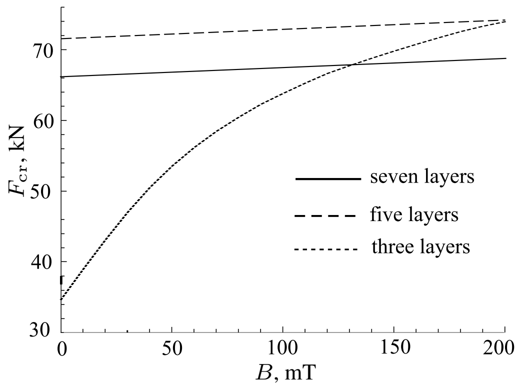

Fig. 3.14 Critical axial force $F_{\rm cr}$ for three- , five-, and seven-layered cylindrical shells containing MRE vs. induction B of magnetic field.

of elastomer distribution along the shell thickness on the buckling force is very complicated. At $B < 200$ mT, the five-layer cylinder possesses the highest buckling resistance, whereas for $B > 200$ mT the sandwich with the one MRE core becomes more stable than the shells with two, three and more MRE layers. Note that further increasing the number of layers (from seven and more) made of the MRE-1 leads to some lowering both the total stiffness and the bearing capacity.

3.3.2 Classification of Buckling Modes

Let all the geometrical parameters and the stress resultant T_{11}° be again constant. We shall perform the asymptotic analysis of relations Eqs. (3.157) and (3.159) under an additional assumption for the shear parameter K. This will enable us to make the classification of possible buckling modes and deduce the corresponding simple equations for the critical buckling forces. These equations will be used below for studying localized buckling modes of laminated cylindrical shells.

In what follows, we assume that the reduced shear modulus G is sufficiently small with regard to the reduced Young's modulus E so that

$$G \sim \mu^2 E, \tag{3.160}$$

where μ is a natural small parameter. Then

$$\frac{K}{\pi^2} = \mu^2 \kappa, \quad \kappa \sim 1. \tag{3.161}$$

We introduce new notations

$$r_m = \frac{\mu \pi m}{l} \sim 1, \quad p_n = \mu n \sim 1, \quad l = \frac{L}{R}, \quad \Delta_{nm} = r_m^2 + p_n^2. \tag{3.162}$$

Note that a parameter θ is independent of μ, but it is also small. So, for a single-layer isotropic shell $\theta = 1/85$ (Grigolyuk and Kulikov, 1988b). Then term $\theta K \delta_{nm}$ may be omitted and Eq. (3.157) can be rewritten as

$$T_{11}^{\circ} = \mu^2 E h \lambda, \quad \lambda = \frac{\Delta_{nm}^2}{r_m^2} \frac{1}{1 + \kappa \Delta_{nm}} + \frac{r_m^2}{\Delta_{nm}^2}, \tag{3.163}$$

where λ is an invariant with respect to the geometrical parameters l and μ.

The problem is to find such integer numbers m^*, n^* which would guarantee a minimum value λ^* for the function λ. First, we assume that m (and hence r_m) is fixed. Now we can rewrite Eq. (3.163) to the form

$$\lambda(p_n, m; \kappa) = \frac{z^2}{1 + \kappa r_m z} + \frac{1}{z^2}, \quad z = \frac{\Delta_{nm}}{r_m} = \frac{r_m^2 + p_n^2}{r_m} \tag{3.164}$$

and perform the minimization of $\lambda(p_n, m; \kappa)$. There are three different cases:

(A) $r_m < z_0$,
(B) $r_m > z_0$,
(C) $r_m = z_0 = r_c$,

were z_0 is a positive root of the algebraic equation

$$-2(1 + \kappa r_m z)^2 + z^4(2 + \kappa r_m z) = 0 \tag{3.165}$$

by z. In case (C), the root r_C is determined from the equation

$$\kappa z_0^6 + 2z_0^4 - 2(1 + \kappa z_0^2)^2 = 0. \tag{3.166}$$

Equations (3.165) and (3.166) contain a parameter κ accounting for shears in the laminated shell. If shears are disregarded ($\kappa = 0$), this root $z_0 = 1$. This case (for $\kappa = 0$) was in detail considered by Tovstik and Smirnov (2001) when studying buckling of single-layer isotropic shells. In particular, Eqs. (3.163) and (3.164) give the well-known formula $T_1^* = Eh^2/[R\sqrt{3(1-\nu^2)}]$ obtained by Lorenz (1911) for a medium-length shell.

Consider cases (A), (B) and (C) at $0 \leq \kappa < 1$. In Fig. 3.15 (a), $z_0(r_m)$ is plotted as a function of r_m at fixed $\kappa \in [0, 1)$, and Fig. 3.15 (b) shows roots r_C for different κ. In case (A), we obtain

$$\lambda_A = \min_{p_n} \lambda(p_n, r_m; \kappa) = \frac{z_0^4 + \kappa r_m z_0 + 1}{z_0^2(1 + \kappa r_m z_0)}, \quad p_n = \sqrt{r_m(z_0 - r_m)} \neq 0, \tag{3.167}$$

and in case (B), one has

$$\lambda_B = \min_{p_n} \lambda(p_n, r_m; \kappa) = \frac{r_m^4 + \kappa r_m^2 + 1}{r_m^2(1 + \kappa r_m^2)}, \quad p_n = 0. \tag{3.168}$$

Case (C) is the special one, here Eqs. (3.167) and (3.168) give the same formulae

$$\lambda_C = \min_{p_n} \lambda(p_n, r_m; \kappa) = \frac{r_c^4 + \kappa r_c^2 + 1}{r_c^2(1 + \kappa r_c^2)}, \quad p_n = 0. \tag{3.169}$$

Case (A) refers to the nonaxisymmetric buckling mode and occurs if $\lambda_A < \lambda_B$, and case B corresponds to the axially symmetric eigenmode with $n^* = 0$ and takes place when $\lambda_B < \lambda_A$. It is seen that the function $\lambda_B(r_m)$ has the minimum value $\lambda_\kappa = \lambda_B(r_\kappa)$ at $r_m = r_\kappa = (1 - \kappa)^{-1/2}$. However, the magnitude λ_κ is not necessarily the critical buckling load parameter, since the real argument r_m possesses discrete values. Consider the search procedure of parameters m^*, n^* and λ^*. At first, we note that the derived equations (3.167) and (3.169) are not valid for very long shells. Let the shell be sufficiently short so that

$$L < \mu\pi R\sqrt{1 - \kappa} = \pi \sqrt[4]{\frac{R^2h^2\eta_3(1 - \kappa)^2}{12(1 - \nu^2)}}. \tag{3.170}$$

Due to (3.162), $r_m > z_0$ for $m = 1$ (s. also 3.15) and case (B) takes place. Let inequality (3.170) be fulfilled, then one obtains the following relations for the critical buckling stress resultant

$$\lambda^* = \frac{r_1^4 + \kappa r_1^2 + 1}{r_1^2(1 + \kappa r_1^2)}, \quad T_1^* = \frac{Eh^2}{R}\sqrt{\frac{\eta_3}{12(1-\nu^2)}}\,\lambda^*. \tag{3.171}$$

We note that for $L^4/(\mu\pi R)^4 \ll 1$ and $\kappa = 0$, Eq. (3.171) degenerates into the well-known Euler formula $T_1^* = Eh^3\pi^2/(12(1-\nu^2)L^2)$ for the buckling of an isotropic beam-strip.

If inequality (3.170) does not hold, then the buckling modes may be both axially symmetric and nonaxisymmetric. To define the appropriate parameters m^*, n^*, λ^*, one needs to calculate two integers $m' = [lr_\kappa/(\mu\pi)] = [l/(\mu\pi\sqrt{1-\kappa})]$ and $m'' = 1 + m'$, where $[x]$ is the integer part of x, and then compare the real numbers $r_{m'} = \mu\pi m'/l$ and $r_{m''} = \mu\pi m''/l$. When $r_{m'} < r_c$, the criti-

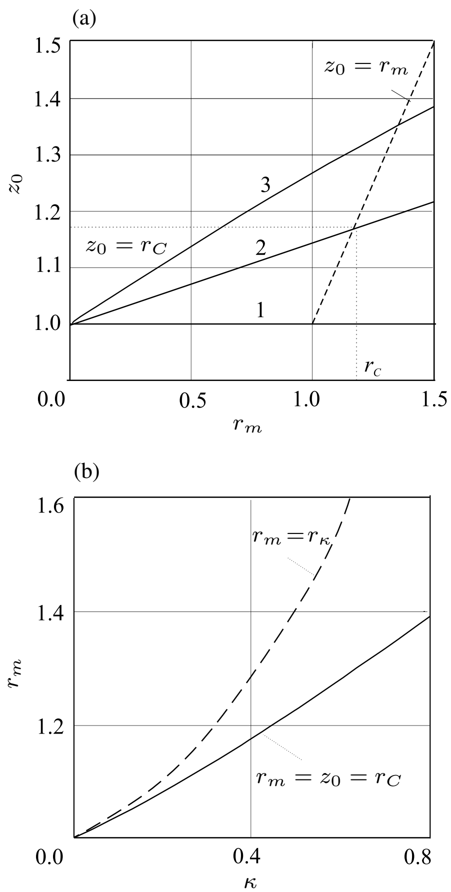

Fig. 3.15 (a) Roots z_0 of Eq. (3.165) vs. r_m for different κ: 1 – $\kappa = 0$, 2 – $\kappa = 0.4$, 3 – $\kappa = 0.75$. (b) Parameter $r_m = z_0 = r_C$ for different κ (after Mikhasev and Mlechka, 2018)

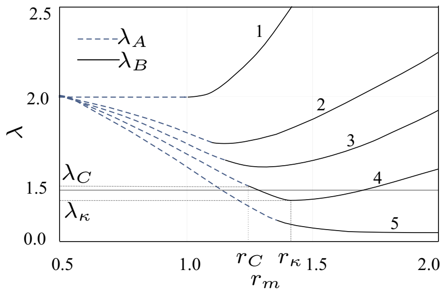

Fig. 3.16 Functions λ_A and λ_B vs. r_m for different κ: 1 – $\kappa = 0$, 2 – $\kappa = 0.25$, 3 – $\kappa = 0.5$, 4 – $\kappa = 0.75$ (after Mikhasev and Mlechka, 2018).

cal buckling eigenvalue is $\lambda^* = \min\{\lambda_A(r_{m'}), \lambda_B(r_{m''})\}$, and if $r_{m'} \geq r_c$, then $\lambda^* = \min\{\lambda_B(r_{m'}), \lambda_B(r_{m''})\}$. The number m^* of semi-waves in the axial direction is determined from integers m' and m'' as a number corresponding to the minimum value of a load parameter λ, and number n^* of waves in the circumferential direction (if case (A) takes place) is found to within one and equals either $[p_n^*]$ or $[p_n^*]+1$, where p_n^* is calculated by (3.167) with $r_m = r_{m^*} = \mu\pi m^*/l$. The qualitative analysis of Fig. 3.16 allows also concluding that the most preferable buckling mode of a medium-length laminated shell with a low reduced shear modulus (e.g., s. plots corresponding to $\kappa \geq 0.5$) is an axially symmetric mode.

3.3.3 Non-Circular Cylinder Under Non-uniform Axial Load

Now we consider a problem (Mikhasev and Botogova, 2017) on the buckling of a non-circular laminated cylindrical shell under inhomogeneous axial compression (s. Fig. 3.17). Let R_2, T_{11}° be functions of α_2. The addition assumptions for these functions will be introduced below. Let us introduce the following dimensionless magnitudes

$$s = \frac{\alpha_1}{R}, \quad \varphi = \frac{\alpha_2}{R}, \quad k_{22}(\varphi) = \frac{R}{R_2(\alpha_2)}, \quad \chi_*(s,\varphi) = \frac{\chi(\alpha_1,\alpha_2)}{R},$$
$$F_*(s,\varphi) = \frac{F(\alpha_1,\alpha_2)}{\mu^2 EhR}, \quad t_1(\varphi) = -\frac{T_1^\circ(\alpha_2)}{\lambda\mu^2 Eh}, \tag{3.172}$$

where λ is a positive load parameter, R is a characteristic dimension which will be specified below, and the shear and small parameters, K and μ, are calculated by Eqs. (3.158). Both edges $\alpha_1 = L_i$ are assumed to by simply supported and have an infinite rigidity diaphragm. The appropriate boundary conditions are given by Eqs. (3.40) or (3.42). Let estimations (3.160), (3.161) for the reduced shear modulus be valid. In addition, we assume that

$$\frac{K\theta}{\pi^2} = \mu^3\tau, \quad \tau \sim 1 \quad \text{as} \quad \mu \to 0. \tag{3.173}$$

Then the governing equations (3.155) may be rewritten in the dimensionless form

$$\begin{aligned}
&\mu^2(1-\mu^3\tau\triangle)\triangle^2\chi_* + k_{22}(\varphi)\frac{\partial^2 F_*}{\partial s^2} + \lambda t_1(\varphi)\frac{\partial^2}{\partial s^2}(1-\mu^2\kappa\triangle)\chi_* = 0,\\
&\mu^2\triangle^2 F_* - k_{22}(\varphi)\frac{\partial^2}{\partial s^2}(1-\mu^2\kappa\triangle)\chi_* = 0.
\end{aligned} \tag{3.174}$$

The appropriate boundary conditions at $s = 0, l$ for dimensionless magnitudes become

$$\chi_* = \triangle\chi_* = \triangle^2\chi_* = F_* = \triangle F_* = 0 \quad \text{at} \quad s = 0, l = L/R. \tag{3.175}$$

The problem is to find the lowest positive value of λ for which system (3.174) has a nontrivial solution satisfying the boundary conditions (3.175). Due to the presence of the functions $t_1(\varphi), k_{22}(\varphi)$, this boundary-value problem does not have a solution in the explicit form. However, with assumptions for the functions $t_1(\varphi), k_{22}(\varphi)$, there exist the buckling forms which will be localized in a neighborhood of some generatrix. To construct these forms, we apply the asymptotic method of Tovstik, s. Tovstik and Smirnov (2001).

3.3.3.1 Asymptotic Solution

A formal asymptotic solution of the boundary-value problem (3.174), (3.175) is constructed in the following form

$$\chi_* = \sin\frac{r_m s}{\mu}\chi_m(\xi,\mu), \quad F_* = \sin\frac{r_m s}{\mu}F_m(\xi,\mu), \tag{3.176}$$

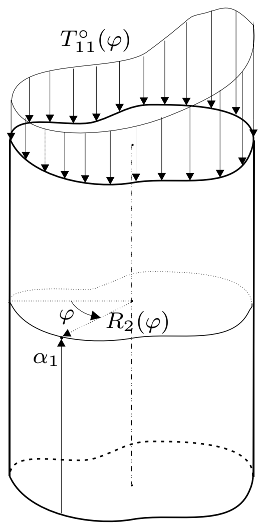

Fig. 3.17 Middle surface of non-circular laminated cylindrical shell under non-uniform axial load and curvilinear coordinates.

$$\begin{aligned} \chi_m &= \sum_{j=0}^{\infty} \mu^{j/2} \chi_{mj}(\xi) \exp\left[\mathrm{i}\left(\mu^{-1/2} p\xi + \frac{1}{2} b\xi^2\right)\right], \\ F_m &= \sum_{j=0}^{\infty} \mu^{j/2} f_{mj}(\xi) \exp\left[\mathrm{i}\left(\mu^{-1/2} p\xi + \frac{1}{2} b\xi^2\right)\right], \\ \lambda &= \lambda_0 + \mu\lambda_1 + \mu^2\lambda_2 + \dots, \end{aligned} \tag{3.177}$$

where

$$\begin{aligned} &\xi = \mu^{-1/2}(\varphi - \varphi_0), \quad \Im b > 0, \\ &|\chi_{mj}|,\, |f_{mj}|,\, \lambda_j,\, p,\, |b|,\, r_m = \frac{\mu\pi m}{l} \sim 1 \quad \text{as} \quad \mu \to 0, \end{aligned} \tag{3.178}$$

and $\chi_{mj}(\xi), f_{mj}(\xi)$ are polynomials in ξ. Here, $\varphi = \varphi_0$ is a weakest generatrix which is unknown. Functions (3.176) and (3.177) approximate the buckling mode localized in the vicinity of the line $\varphi = \varphi_0$.

Expending the functions $k_{22}(\varphi), t_1(\varphi)$ in power series of $\varphi - \varphi_0 = \mu^{1/2}\xi$ and substituting Eqs. (3.176) - (3.178) into Eqs. (3.174), one obtains the sequence of algebraic equations

$$\sum_{k=0}^{j} \mathbf{L}_k \mathbf{X}_{j-k} = 0, \quad j = 0, 1, 2, \dots \tag{3.179}$$

where $\mathbf{X}_j = (\chi_{mj}, f_{mj})^{\mathrm{T}}$ are vectors, $\mathbf{L}_0$ is the 2×2 matrix with the elements

$$\begin{aligned} &l_{11} = (r_m^2 + p^2)^2 - \lambda_0 r_m^2 t_1(\varphi_0)[1 + \kappa(r_m^2 + p^2)], \; l_{12} = -k_{22}(\varphi_0) r_m^2, \\ &l_{21} = k_{22}(\varphi_0) r_m^2 [1 + \kappa(r_m^2 + p^2)], \qquad\qquad l_{22} = (r_m^2 + p^2)^2, \end{aligned} \tag{3.180}$$

the matrix operators $\mathbf{L}_j$ for $j \geq 1$ are expressed by the matrix $\mathbf{L}_0$ as

$$\begin{aligned} \mathbf{L}_1 z &= \left(b\frac{\partial \mathbf{L}_0}{\partial p} + \frac{\partial \mathbf{L}_0}{\partial \varphi_0}\right)\xi z - \mathrm{i}\frac{\partial \mathbf{L}_0}{\partial p}\frac{\partial z}{\partial \xi}, \\ \mathbf{L}_2 z &= \frac{1}{2}\left(b^2 \frac{\partial^2 \mathbf{L}_0}{\partial p^2} + 2b\frac{\partial^2 \mathbf{L}_0}{\partial p \partial \varphi_0} + \frac{\partial^2 \mathbf{L}_0}{\partial \varphi_0^2}\right)\xi^2 z - \frac{1}{2}\frac{\partial^2 \mathbf{L}_0}{\partial p \partial \varphi_0} z \\ &\quad - \frac{1}{2}\frac{\partial^2 \mathbf{L}_0}{\partial p^2}\left(iz + \frac{\partial^2 z}{\partial \xi^2}\right) - \mathrm{i}\left(b\frac{\partial^2 \mathbf{L}_0}{\partial p^2} + \frac{\partial^2 \mathbf{L}_0}{\partial p \partial \varphi_0}\right)\xi\frac{\partial z}{\partial \xi} + \mathbf{L}_* z + \mathbf{N} z, \end{aligned} \tag{3.181}$$

and $\mathbf{N}$ is the 2×2 matrix with the unique nonzero element

$$n_{11} = \tau(r_m^2 + p^2)^3, \quad n_{12} = n_{21} = n_{22} = 0. \tag{3.182}$$

The sequence of equations (3.179) serves to determine all unknowns functions χ_{mj}, f_{mj} and parameters p, b, λ_j appearing in (3.176)-(3.178). Because the procedure for seeking these magnitudes is the same as in Tovstik and Smirnov (2001), we omit transitional calculations and give only the principle equations. Considering the homogeneous system of algebraic equations (3.179) for $j = 0$, one obtains the zeroth approximation for the load parameter,

$$\lambda_0 = f(p, r_m, \varphi_0; \kappa) = \frac{1}{t_1(\varphi_0)} \left\{ \frac{(r_m^2 + p^2)^2}{r_m^2[1 + \kappa(r_m^2 + p^2)]} + \frac{k_{22}^2(\varphi_0) r_m^2}{(r_m^2 + p^2)^2} \right\}. \tag{3.183}$$

Holding a number m (and thus, a parameter r_m) fixed, we minimize function (3.183) over p and φ. As a result, one obtains the following equations

$$\frac{\partial f}{\partial p} = 0, \quad \frac{\partial f}{\partial \varphi_0} = 0 \tag{3.184}$$

which serve to determine p° and φ_0°.

In what follows, we shall consider only two variants:

(i) k_{22} is constant (circular shell) and $t_1(\varphi_0)$ is a function (non-uniform compression), then the second equation from (3.184) results in

$$t_1'(\varphi_0) = 0; \tag{3.185}$$

(ii) t_1 is constant (uniform compression), but $k_{22}(\varphi_0)$ is a function (non-circular shell) so that Eq. (3.184) leads to

$$k_{22}'(\varphi_0) = 0. \tag{3.186}$$

In Eqs. (3.185) and (3.186) and hereinafter, the prime $(')$ means differentiation by φ_0. It is obvious that cases (i) and (ii) do not exclude the variant when φ_0° satisfies Eqs. (3.185) and (3.186) simultaneously. After the weakest generatrix $\varphi = \varphi_0^\circ$ is found, one can introduce the characteristic dimension $R = R_2(\varphi_0^\circ)$. Then $k_{22}(\varphi_0^\circ) = 1$. Without losing generality, it is also assumed that $t_1(\varphi_0^\circ) = 1$. It is seen that Eq. (3.183) coincides with (3.164). Consider the first equation from (3.184). Having solved it, we again come to three different cases (A), (B), (C) described above. Then, the zero-order approximation of the load parameter,

$$\lambda_0^\circ = \min_p f(r_m, p, \varphi_0^\circ; \kappa) = f(r_m, p^\circ, \varphi_0^\circ; \kappa), \tag{3.187}$$

will be defined by Eqs. (3.167), (3.168) and (3.169) for cases (A), (B) and (C), respectively. A solution of the homogeneous system of algebraic equations (3.179) at $j = 0$ may be written as

$$\mathbf{X}_0 = P_0(\xi)\mathbf{Y}_0, \tag{3.188}$$

where $P_0(\xi)$ is an unknown polynomial in ξ, and $\mathbf{Y}_0 = (1, -l_{11}/l_{12})$ is a vector.

In the first-order approximation ($j = 1$), one has the non-homogeneous system of algebraic equations (3.179). When taking both Eqs. (3.184) into account, this system turns into identities. Let us consider the non-homogeneous system of equations (3.179) in the second-order approximation ($j = 2$). The compatibility condition for this system results in the formula (Tovstik and Smirnov, 2001)

$$b = \mathrm{i}\sqrt{f_{\varphi\varphi}/f_{pp}} \tag{3.189}$$

and leads to the equation

$$\frac{\mathrm{d}^2 P_0}{\mathrm{d}\xi^2} + 2\mathrm{i}b\xi\frac{\mathrm{d}P_0}{\mathrm{d}x} + \frac{2}{f_{pp}}\left(\lambda_1 + \frac{1}{2}\mathrm{i}f_{pp}b + I_{A,B}\right)P_0 = 0 \tag{3.190}$$

with respect to P_0, where

$$\begin{aligned} I_A &= \frac{\tau r_m^6}{1+\kappa r_m^2} \qquad \text{at} \quad r_m > z_0, \\ I_B &= \frac{\tau r_m^3 z_0^3}{1+\kappa r_m z_0} \qquad \text{at} \quad r_m < z_0. \end{aligned} \tag{3.191}$$

It is seen that $I_A = I_B$ for $r_m = z_0 = r_C$, where r_C is the root of Eq. (3.166). For both cases, (A) and (B), Eq. (3.190) has the solution

$$P_0(\xi) = \mathcal{H}_n\left(\sqrt{f_{\varphi\varphi}/f_{pp}}\ \xi\right), \tag{3.192}$$

where $\mathcal{H}_n(x)$ is the n^{th} degree Hermite polynomials in x, if

$$\lambda_1 = \left(\frac{1}{2}+n\right)\sqrt{f_{pp}f_{\varphi\varphi}} + I_{A,B}. \tag{3.193}$$

Here, the subscripts p, φ denote the differentiation by variables p, φ_0 at $p = p^\circ$, $\varphi_0 = \varphi_0^\circ$. A parameter λ_1 has the least value at $n = 0$. Then $P_0(\xi) = \mathcal{H}_0 \equiv 1$.

Let us consider variant (i) when the weakest generatrix is determined from Eq. (3.185). Then Eqs. (3.189) and (3.193) result in the following formulae for parameters b and λ_1:

(A) $r_m < z_0$,

$$b = \mathrm{i}z_0(1+\kappa r_m z_0)\sqrt{\frac{-t_1''(\varphi_0^\circ)r_m(1+\kappa r_m z_0 + z_0^4)}{8(z_0 - r_m)[z_0^4 + 3(1+\kappa r_m z_0)^3]}}, \tag{3.194}$$

$$\begin{aligned} \lambda_1 = &\frac{\sqrt{-2t_1''(\varphi_0^\circ)(z_0 - r_m)(1+\kappa r_m z_0 + z_0^4)[z_0^4 + 3(1+\kappa r_m z_0)^3]}}{z_0^3 r_m^{1/2}(1+\kappa r_m z_0)^2} \\ &+ \frac{\tau r_m^3 z_0^3}{(1+\kappa r_m z_0)} \end{aligned} \tag{3.195}$$

(B) $r_m > z_0$,

$$b = \mathrm{i}r_m\sqrt{\frac{-t_1''(\varphi_0^\circ)(1+\kappa r_m^2)(1+\kappa r_m^2 + r_m^4)}{2[r_m^4(2+\kappa r_m^2) - 2(1+\kappa r_m^2)^2]}}, \tag{3.196}$$

$$\lambda_1 = \frac{1}{2r_m^3}\sqrt{\frac{-2t_1''(\varphi_0^\circ)(1+\kappa r_m^2+r_m^4)[r_m^4(2+\kappa r_m^2)-2(1+\kappa r_m^2)^2]}{(1+\kappa r_m^2)}} + \frac{\tau r_m^6}{1+\kappa r_m^2} \tag{3.197}$$

It is seen from (3.194) and (3.196) that the inequality $\Im b > 0$ holds if $t_1''(\varphi_0^\circ) < 0$. Thus, the weakest generatrix is the more compressed one.

Finally, for variant (ii) when the weakest generatrix is found from (3.186), one has:

(A) $r_m < z_0$,

$$b = \frac{\mathrm{i}z_0}{2}\sqrt{\frac{k_{22}''(\varphi_0^\circ)(1+\kappa r_m z_0)^3}{(z_0-r_m)[z_0^4+3(1+\kappa r_m z_0)^3]}}, \tag{3.198}$$

$$\lambda_1 = \frac{2}{z_0^3}\sqrt{\frac{k_{22}''(\varphi_0^\circ)(z_0-r_m)[z_0^4+3(1+\kappa r_m z_0)^3]}{r_m}(1+\kappa r_m z_0)^3} + \frac{\tau r_m^3 z_0^3}{1+\kappa r_m z_0} \tag{3.199}$$

(B) $r_m > z_0$,

$$b = \mathrm{i}r_m(1+\kappa r_m^2)\sqrt{\frac{k_{22}''(\varphi_0^\circ)}{r_m^4(2+\kappa r_m^2)-2(1+\kappa r_m^2)^2}}, \tag{3.200}$$

$$\lambda_1 = \frac{\sqrt{k_{22}''(\varphi_0^\circ)[r_m^4(2+\kappa r_m^2)-2(1+\kappa r_m^2)^2]}}{r_m^3(1+\kappa r_m^2)} + \frac{\tau r_m^6}{1+\kappa r_m^2}. \tag{3.201}$$

Here, Eqs. (3.199) and (3.201) show that the weakest generatrix is the line with the minimum curvature. We did not consider here higher order approximations because system (3.155) is not sufficiently accurate since it does not contain some terms which effect the third and subsequent approximations.

Now, let an integer m vary. Then due to (3.178), r_m takes on a sequence of discreet values. Following the procedure described above, we can find m^* and $\lambda_0^* = \lambda_0^\circ(r_{m^*})$, where $r_{m^*} = \mu\pi m^*/l$. If $r_{m^*} - r_C = O(1)$ at $\mu \to 0$, then the approximate value of the critical buckling load parameter is

$$\lambda^* = \lambda_{A,B}^* = \lambda_0^* + \mu\lambda_1(r_{m^*}) + O\left(\mu^2\right), \tag{3.202}$$

where $\lambda_1(r_{m^*})$ is determined by equations derived above depending on case (A) or (B) and variant (i) or (ii) as well. The corresponding eigenforms are the following

$$\chi^* = \sin\frac{r_{m^*}s}{\mu}\exp\left\{\frac{\mathrm{i}}{\mu}\left[\sqrt{r_{m^*}(z_0-r_{m^*})}(\varphi-\varphi_0^\circ)+\frac{1}{2}b(\varphi-\varphi_0^\circ)^2\right]\right\} \times \left[1+O(\mu^{1/2})\right] \tag{3.203}$$

for case (A) at $r_{m^*} < r_C$, and

$$\chi^* = \sin \frac{r_{m^*} s}{\mu} \exp\left\{\frac{\mathrm{i}b(\varphi - \varphi_0^\circ)^2}{2\mu}\right\}\left[1 + O(\mu^{1/2})\right], \tag{3.204}$$

for case (B) when $r_{m^*} > r_C$. In both cases a parameter b is calculated at $r_m = r_{m^*}$. It may be seen that the buckling modes (3.203) and (3.204) are different for cases (A) and (B). If $r_{m^*} > r_C$, the eigenfunctions decay exponentially without oscillations ($p^\circ = 0$), and for $r_{m^*} < r_C$ the localized buckling modes have waves in the circumferential direction. It is also seen that

$$\lim_{r_{m^*} \to z_C} |b| = +\infty \tag{3.205}$$

for both cases (A), (B) and variants (i), (ii). Thus, requirement $|b| \sim 1$ at $\mu \to 0$ does not hold if the root r_{m^*} is close to $z_0 = r_C$, and Eqs. (3.203) and (3.204) are not applicable for this case. Case (C) for $r_{m^*} \simeq r_C$ deserves the special consideration.

3.3.3.2 Reconstruction of Asymptotic Expansions

Let parameter $r_m = r_{m^*}$ be close to the root $z_0 = r_c$ of Eq. (3.166). As seen from Fig. 3.16, this case takes place when parameter κ is small. In what follows, for the sake of simplicity, the asterisk in m^* will be omitted. Without loss of generality, it is assumed that $k_{22} = 1$ and $t_1(\varphi)$ is a function. In this case, a solution of the boundary-value problem (3.174) and (3.175) is again found in the form of functions (3.176). The substitution of (3.176) into Eqs. (3.174) results in the following system of ordinary differential equations

$$\begin{aligned} (1 - \mu\tau\triangle_m)\triangle_m^2\chi_m - r_m^2\Phi_m - \lambda r_m^2 t_1(\varphi)(1 - \kappa\triangle_m)\chi_m &= 0, \\ \triangle_m^2\Phi_m + r_m^2(1 - \kappa\triangle_m)\chi_m &= 0, \end{aligned} \tag{3.206}$$

where

$$\triangle_m = \mu^2\frac{\mathrm{d}^2}{\mathrm{d}\varphi^2} - r_m^2 \tag{3.207}$$

is the differential operator.

We introduce the following estimates

$$\begin{aligned} &r_m = r_{m^*} = r_c + \tilde{\mu}r', \quad \lambda = \lambda_C + \tilde{\mu}^2\lambda', \quad \varphi - \varphi_0^\circ = \tilde{\mu}\eta, \\ &t_1(\varphi) = t_1(\varphi_0^\circ) + \frac{1}{2}\tilde{\mu}^2 t_1''(\varphi_0^\circ)\eta^2 + \ldots \end{aligned} \tag{3.208}$$

where $r', \lambda' \sim 1$ as $\tilde{\mu} \to 0$, and

$$\tilde{\mu} = \mu^{2/3} = \left[\frac{h^2\eta_3}{12R^2(1-\nu^2)}\right]^{1/6} \tag{3.209}$$

is a new small parameter, and we seek the solution of Eqs. (3.206) in the form of series

$$\chi_m = \sum_{k=0}^{\infty} \tilde{\mu}^k \chi_m^{(k)}(\eta), \qquad \Phi_m = \sum_{k=0}^{\infty} \tilde{\mu}^k \Phi_m^{(k)}(\eta), \tag{3.210}$$

where

$$\chi_m^{(k)}, \Phi_m^{(k)} \sim 1, \quad \text{and} \quad \chi_m^{(k)}, \Phi_m^{(k)} \to 0 \quad \text{as} \quad \eta \to \pm\infty. \tag{3.211}$$

In the zeroth- and first-order approximations, Eqs. (3.206) turn into identities if

$$\lambda_C = \frac{r_c^4 + \kappa r_c^2 + 1}{t_1(\varphi_0^\circ) r_c^2 (1 + \kappa r_c^2)}. \tag{3.212}$$

Note that Eq. (3.212) coincides with Eq. (3.169) at $r_m = z_0 = r_c$. Equation (3.212) gives the zeroth approximation for the eigenvalue λ. The eigenfunctions $\chi_m^{(0)}$ and $\Phi_m^{(0)}$ remain undefined at this step.

Let us consider the second-order approximation. When taking Eq. (3.212) into consideration, one gets the following equation with respect to $\chi_m^{(0)}$

$$a_4 \frac{\mathrm{d}^4 \chi_m^{(0)}}{\mathrm{d}\eta^4} + a_2(r') \frac{\mathrm{d}^2 \chi_m^{(0)}}{\mathrm{d}\eta^2} + [a_0(r') - a_\eta \eta^2 - \lambda' a_\lambda] \chi_m^{(0)} = 0, \tag{3.213}$$

where

$$\begin{aligned} a_4 &= 1 + \frac{\kappa}{r_c^2} + \frac{3}{r_c^4}, \qquad a_2(r') = -\frac{2(4 + 5\kappa r_c^2 + \kappa^2 r_c^4) r'}{r_c^3 (1 + \kappa r_c^2)}, \\ a_0(r') &= \frac{(5 r_c^4 - 6\kappa r_c^2 - 5\kappa^2 r_c^4 - 1) r'^2}{r_c^2 (1 + \kappa r_c^2)}, \\ a_\eta &= \frac{1}{2} \lambda_C r_c^2 (1 + \kappa r_c^2) t_1''(\varphi_0^\circ), \quad a_\lambda = r_c^2 (1 + \kappa r_c^2) t_1(\varphi_0^\circ). \end{aligned} \tag{3.214}$$

The problem is to find such values of $\lambda'(r')$, for which the nontrivial solutions of Eq. (3.213) satisfy the following condition

$$\chi_m^{(0)} \to 0 \quad \text{as} \quad \eta \to \pm\infty. \tag{3.215}$$

Applying the Fourier transform

$$\chi_m^{(0)}(\eta) = \frac{1}{\sqrt{2\pi}} \int_{-\infty}^{+\infty} \chi^F(\tilde{\omega}) \exp(\mathrm{i}\tilde{\omega}\eta) \mathrm{d}\tilde{\omega}, \tag{3.216}$$

we arrive at the second order differential equation for a function χ^F,

$$\frac{\mathrm{d}^2 \chi^F}{\mathrm{d}x^2} + \left\{ \tilde{\Lambda} - [x^4 + 2\gamma(\kappa) x^2 + \gamma^2(\kappa)(1 + \Theta(\kappa))] \right\} \chi^F = 0, \tag{3.217}$$

where

$$
\begin{aligned}
\Lambda &= \lambda' \frac{r_c^2(1+\kappa r_c^2)\alpha^2 t_1(\varphi_0^\circ)}{(r_c^4+\kappa r_c^2+1)\varsigma}, \quad \varsigma = -\frac{t_1''(\varphi_0^\circ)}{2t_1(\varphi_0^\circ)}, \quad x = \frac{\tilde{\omega}}{\alpha}, \\
\alpha(\kappa) &= \left[\frac{\varsigma r_c^4(1+\kappa r_c^2+r_c^4)}{r_c^4+\kappa r_c^2+3}\right]^{1/6}, \quad \gamma(\kappa) = r'\Gamma(\kappa), \\
\Gamma(\kappa) &= \frac{4r_c+5\kappa r_c^3+\kappa^2 r_c^5}{(1+\kappa r_c^2)(r_*^4+\kappa r_c^2+3)}\left[\frac{r_c^4+\kappa r_c^2+3}{r_c^4(r_c^4+\kappa r_c^2+1)\varsigma}\right]^{1/3}, \\
\Theta(\kappa) &= \frac{\Xi\alpha^2(r_c^4+\kappa r_c^2+3)}{\Gamma^2\varsigma r_c^4(r_c^4+\kappa r_c^2+1)}, \\
\Xi(\kappa) &= r_c^2\left\{\frac{5(1-\kappa^2)r_c^4-6\kappa r_c^2-1}{(1+\kappa r_c^2)(r_c^4+\kappa r_c^2+3)} - \left[\frac{\kappa^2 r_c^4+5\kappa r_c^2+4}{(1+\kappa r_c^2)(r_c^4+\kappa r_c^2+3)}\right]^2\right\}.
\end{aligned}
\tag{3.218}
$$

For $\kappa = 0$, Eq. (3.217) is reduced to the equation derived in Tovstik and Smirnov (2001) for the classical model eliminating transverse shear.

For each γ, there is a countable set $\Lambda_j (j = 0, 1, \ldots)$ of values Λ, for which there exist non-trivial solutions of Eq. (3.217) such that $\chi^F \to 0 \quad \text{as} \quad x \to \pm\infty$. It may be seen from Eqs. (3.217) and (3.218) that the eigenvalues Λ_j depend on the fixed value of the shear parameter κ but are invariant with respect to parameter ς characterizing the rate of inhomogeneity of the axial load. The first eigenvalue $\Lambda = \Lambda_0$ versus parameter γ for different shear parameters $\kappa = 0; 0.25; 0.5; 0.75$ is plotted in Fig. 3.18. For $\kappa = 0$, the corresponding eigenvalues $\Lambda = \Lambda_0(\gamma)$ have been determined by Tovstik and Smirnov (2001). Figure 3.18 serves to calculate the correcting load parameter λ'. At first, one needs to find γ by Eqs. (3.208) and $(3.218)_5$. Then, using Fig. 3.18 and Eq. $(3.218)_1$, one can find the corresponding parameters Λ and λ'. To define the required buckling load parameter λ^*, one needs to compare $\lambda^*_{A,B}$ and $\lambda^*_C = \lambda_C + \tilde{\mu}^2\lambda'$ found by (3.202) and (3.218), respectively

$$
\lambda^* = \min\{\lambda_A^*, \lambda_B^*, \lambda_C^*\}. \tag{3.219}
$$

It is seen that the incorporation of transverse shear (the parameter κ) into the shell model results in more complex procedure for seeking the critical buckling axial load in comparison with a similar procedure at $\kappa = 0$ (Tovstik, 1984).

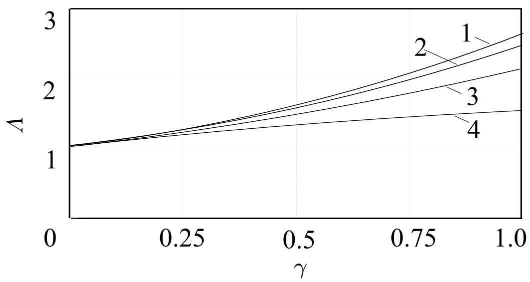

Fig. 3.18 First eigenvalue $\Lambda = \Lambda_0$ vs. γ for different κ $1 - \kappa = 0$; $2 - \kappa = 0.25$; $3 - \kappa = 0.5$; $4 - \kappa = 0.75$ (after Mikhasev and Mlechka, 2018) .

3.3.4 *Effect of Shear on Localized Buckling Modes and Critical Axial Force*

In this subsection, we will give several examples illustrating the effect of shear on localized buckling modes and corresponding critical force. However, as a preliminary we will perform the comparative calculations using the proposed above asymptotic technique and FEM simulation (Korchevskaya et al, 2003).

Example 3.11. Let us consider two sandwich-like cylinders (three-layered shells) of the radius $R = 150$ mm but having different length $L = 200$ mm and $L = 450$ mm. The first and third laminas with thicknesses $h_1 = h_3 = 0.3$ mm are made of aluminum, and the core of thickness $h_2 = 0.8$ mm is the epoxy matrix. The physical properties of both materials are the same as in Example 3.4. The shell is under the axial (dimensionless) force

$$t_1(\varphi) = 1 + \epsilon \cos \varphi, \tag{3.220}$$

where the parameter ϵ characterizes the rate of the load inhomogeneity in the circumferential direction. Here, the generatrix $\varphi = \varphi_0^\circ = 0$ is the weakest one.

The critical buckling forces T_1^* evaluated by using the asymptotic and finite element methods for two values of the length L and various ϵ are presented in Table 3.12. It may be seen that the deviation in results obtained by the asymptotic and numerical approaches are not large. So, for $L = 200$ mm and $\epsilon = 0, 0.5, 0.7, 1$ these deviation are about 1%, 3.8%, 3.9%, 4%, respectively. This fact is explained by both the applicability of the asymptotic formulas derived above and satisfactory convergence of the FEM solutions. Table 3.12 justifies indirectly the assumed ESL model and applicability of the buckling equations (3.155) for prediction of localized buckling of laminated cylindrical shells.

Now, special attention will be given to the case when the reduced shear modulus of a laminated shell is much less than the reduced Young's modulus. We will consider circular sandwiches containing cores made of MRE-1 with properties specified in Chapt. 2. The mechanical properties of MRE-1 are very influenced by an applied magnetic field. Without a magnetic field, it is a soft and shear pliable material, but under action of an external magnetic field it demonstrates properties of a pseudo-

Table 3.12 The critical axial force T_1^* vs. parameter ϵ found by the asymptotic method (AM) and finite-element method (FEM) (after Korchevskaya et al, 2003).

ϵ	0.0	0.5	0.6	0.7	0.8	0.9	1.0
$L = 200$ mm							
T_1^* (AM), N/mm	342.58	228.39	214.11	201.52	190.32	180.31	171.29
T_1^* (FEM), N/mm	347.90	237.60	222.80	209.70	198.20	187.80	178.50
$L = 450$ mm							
T_1^* (AM), N/mm	344.53	229.68	215.33	202.66	191.40	181.33	172.26
T_1^* (FEM), N/mm	355.00	239.92	224.90	211.60	199.90	189.50	179.30

rigid viscoelastic material with a high storage modulus. Changing the intensity of a magnetic field, we can vary the core rigidity and such a way, change the reduced shear modulus of the sandwich. It is obvious that viscose properties of MRE-1 are not taken here into consideration, so that the MRE is treated as the elastic and isotropic material. Table 3.13 gives the dependence of dimensionless shear parameter κ on the magnetic field induction B for the sandwich of radius $R = 1$ m with the face sheets made of the ABS-plastic SD-017. Thicknesses of layers composing the sandwich are $h_1 = h_3 = 0.5$ mm, $h_2 = 8$ mm. As seen, the increase of B results in the decrease of κ and as result, in the increase of the reduced (effective) shear modulus G, s. Eqs. (2.59), (2.84), (3.158) and (3.161).

Example 3.12. Let the circular sandwich assembled from the ABS-plastic and MRE-1 with parameters h_i and R specified above be under action of the inhomogeneous axial force T_1°. The dimensionless counterpart of this force is the function $t_1(\varphi) = A_t(1 + \epsilon \cos\varphi)$, where A_t and ϵ are constants. Here, $\varphi = \varphi_0^\circ = 0$ is the weakest generatrix. The type of buckling mode localized near this line (corresponding to one of cases (A), (B) or (C)) depends on the geometrical parameters, load parameters A_t, ϵ and induction B as well. The goal of this example is to demonstrate the sequence of necessary calculations to define a required buckling load. Table 3.14 shows the outcomes of this procedure for the shell of length $L = 4$ m at $A_t = 0.5, \epsilon = 1.25$, $B = 100$ mT. These calculations involve two stages. At the first step, we find parameters r_c, r_κ, $r_{m'}, r_{m''}$ and then calculate r_{m^*}, λ_0^*, λ_1 and $\lambda_B^* = 1.743$ by Eqs. (3.166), (3.197) and (3.202), respectively. At the second step, we compare r_m^* and r_c and calculate r', λ_C. Then, using data from Fig. 3.18, we estimate the correcting load parameter $\lambda' \approx 0.553$ and find $\lambda_C^* \approx 1.591$. As $\lambda_C^* < \lambda_B^*$, one declares $\lambda^* = \lambda_C^* \approx 1.591$.

Example 3.13. Now we shall study the effect of an applied magnetic field on the critical buckling force and other parameters characterizing buckling modes. Table 3.15 displays this effect for the sandwich of the length $L = 2$ m. The second column shows a possible case, (A), (B) or (C), which takes place for a fixed value of induction B. It is seen that at low level of the applied magnetic field (when the reduced shear

Table 3.13 Dimensionless shear parameter κ vs. magnetic field induction B.

B, mT	0	10	30	50	70	90	120	140	180	200
κ	0.662	0.590	0.469	0.389	0.333	0.292	0.247	0.222	0.188	0.176

Table 3.14 Parameters required to calculate buckling load parameter λ^* (after Mikhasev and Mlechka, 2018)

$\frac{r_c}{r_\kappa}$	$\frac{r_{m'}}{r_{m''}}$	r_{m^*}	λ_0^*	λ_1	λ_B^*	r'	λ_C	λ'	λ_C^*
$\frac{1.112}{1.173}$	$\frac{1.172}{1.225}$	1.119	1.732	0.188	1.743	-0.390	1.576	0.553	1.591

Table 3.15 Dimensionless parameters r_{m^*}, p_{n^*}, $\Im b^*$, λ^* and critical force T_1^* vs. induction B (after Mikhasev and Mlechka, 2018).

B, mT	Case	r_{m^*}	p_{n^*}	$\Im b^*$	λ^*	T_1^*, kN/m
0	(B)	1.712	0	1.22	1.398	9.728
30	(B)	1.282	0	1.59	1.573	10.99
60	(B)	1.147	0	2.45	1.668	11.71
90	(C)	1.172	0	-	1.717	12.21
150	(C)	1.064	0	-	1.791	12.90
180	(C)	1.062	0.900	-	1.815	13.13
210	(A)	1.060	0.770	2.71	2.621	13.28

modulus G is small) the critical buckling force T_1^* and parameters r_{m^*}, $\Im b^*$ are calculated by equations corresponding to case (B), for a medium intensity of the magnetic field, one has case (C), and for the induction $B \geq 200$ mT (when the sandwich stiffness becomes large), the required T_1^*, r_{m^*}, p_{n^*}, $\Im b^*$ are defined by formulae from case (A). One can conclude that growing magnetic field results in increasing the critical buckling force and rearrangement of the buckling modes as well: a number of waves in the circumferential direction decreases while the rate of localization of the buckling modes near the weakest generatrix increases.

It is obvious that the pattern of localized buckling mode is influenced by the rate of inhomogeneity of axial load. To study this effect we consider the following example.

Example 3.14. Let $t_1(\varphi) = A_t \exp\left\{-\epsilon\varphi^2\right\}$ with a positive parameter ϵ specifying the force variation in the circumferential direction. The geometrical dimensions of the circular sandwich are the following: $L = 2$ m, $R = 1$ m, $h_1 = h_3 = 0.5$ mm, $h_2 = 8$ mm. The skins and core are made of the same materials as in the previous examples. The calculations performed for the fixed induction $B = 20$ mT and different values of ϵ revealed that the buckling occurs without formation of dents in the circumferential direction ($n^* = 0$) and the critical force T_1^* is determined by equations corresponding to case (B). Table 3.16 displays that the wave number m^* and the zeroth approximation of load parameter, λ_0^*, are independent of ϵ, and the remaining parameters are increasing functions of ϵ. As expected, the influence of a parameter ϵ on the magnitude $\Im b$, specifying the rate of localization of buckling modes near the generatrix $\varphi = 0$, is very strong, whereas this effect on the resulting buckling force T_1^* is found to be weak.

The examples considered above have revealed that a laminated cylindrical shell subjected to non-uniform axial compression may buckle in three quite different modes. The first type of buckling modes (case A) may be approximated by a function which rapidly oscillates and exponentially decays far away from the *weakest* line, the second type of eigenmodes (case B) is given by an exponentially decaying

Table 3.16 Dimensionless parameters m^*, λ_0^*, λ_1, λ^*, $\Im b^*$ and critical buckling force T_1^* vs. parameter ϵ (after Mikhasev and Mlechka, 2018).

ϵ	Case	m^*	λ_0^*	λ_1	λ^*	$\Im b^*$	T_1^*, kN/m
0.4	(B)	14	1.487	0.742	1.538	1.651	10.739
0.9	(B)	14	1.487	1.101	1.562	2.477	10.909
1.5	(B)	14	1.487	1.414	1.584	3.198	11.058
2.5	(B)	14	1.487	1.819	1.611	4.128	11.250
4.5	(B)	14	1.487	2.432	1.653	5.538	11.542

function without oscillation, and the third one (case C) can not be represented by an exponentially decaying function and is found by applying Fourier transform. In the first two cases (A, B), the asymptotic formulae for the buckling modes and corresponding critical buckling force were readily written down in the explicit form, whereas for case (C), the second order differential equation with respect to Fourier transform and the required eigenvalue were reduced. It was discovered that the pattern of buckling modes depends not only on the geometrical dimensions of a shell, as has been previously shown by Tovstik (1984); Tovstik and Smirnov (2001), but on the shear compliance. In particular, the analysis of found solutions allowed us to conclude that the most preferable buckling mode for a medium-length laminated shell with a low reduced shear modulus (as compared with the reduced Young's modulus) corresponds to the second or third type of modes (case B or C).

The performed calculations have shown that the buckling formes for the MRE-sandwich and its buckling resistance are very affected by magnetic field. Under action of a weak magnetic field or without it, the MRE core turns out to be *soft* so that the applied axial force generates transverse shear which leads to buckling without formation of dents in the circumferential direction. However, increasing magnetic field results in the reduction of shears and as a consequence, in the rearrangement of buckling modes: the sandwich with large effective shear modulus *prefer* to buckle with formation of waves in the circumferential direction. The analysis of numerical calculations has also shown that the pattern of buckling mode is very influenced by imperfection of the axial force: the higher the variation of the applied axial force is, the larger the rate of localization of eigenforms becomes.

3.4 Laminated Cylinder Under Torsion[1]

The first analytical solution on buckling of a thin cylindrical shell under axial torsion was obtained by Schwerin (1925). Considering a very long single-layer isotropic

[1] This section is written in cooperation with I.R. Mlechka (Belarussian State University, e-mail: ignat.mlechka@gmail.com)

cylinder, a simple formula for the critical shear stress resultant was derived

$$T_{12}^* = \frac{Eh}{3\sqrt{2}(1-\nu^{3/4})}\left(\frac{h}{R}\right)^{3/2}, \tag{3.221}$$

where h, R, E, ν are the thickness, radius, Young's modulus and Poisson's ratio, respectively. The critical torque M_T^* and stress resultant T_{12}^* are linked by the equation

$$M_T^* = 2\pi R^2 T_{12}^*. \tag{3.222}$$

The buckling mode corresponding to M_T^* has the helical form with two waves in the circumferential direction

$$w = C\cos\left[\sqrt[4]{\frac{h}{(1-\nu^2)R}}\frac{\alpha_1}{R} - \frac{2\alpha_2}{R}\right]. \tag{3.223}$$

3.4.1 Short Review of the State of the Art

Equations (3.221) and (3.223) do not take into account the boundary conditions and can not be applied for medium-length and short shells. The problem on buckling of cylindrical shells of finite length under action of torsion torque is difficult because it does not allow to satisfy all boundary conditions. As a rule, it is assumed the buckling mode

$$w = C\cos\left(\frac{\pi\alpha_1}{L}\right)\cos\left[\frac{n}{R}\left(\alpha_2+\gamma\alpha_1\right)\right] \tag{3.224}$$

which satisfies only the one condition $w = 0$ at $\alpha_1 = \pm L/2$. It is seen that Eq. (3.209) satisfies neither simple support nor clamp support conditions. But it may be shown that

$$\int\limits_0^{2\pi R}\left(\frac{\partial w}{\partial\alpha_1}\right)\bigg|_{\alpha_1=\pm L/2}\mathrm{d}\alpha_2 = \int\limits_0^{2\pi R}\left(\frac{\partial^2 w}{\partial\alpha_1^2}\right)\bigg|_{\alpha_1=\pm L/2}\mathrm{d}\alpha_2 = 0.$$

The boundary conditions for clamped and simply supported edges are satisfied in the integral meaning.

The substitution of Eq. (3.224) into governing equations describing buckling of a medium-length cylindrical shell results in the following equation for the critical shear stress-resultant

$$T_{12}^* = k_{\mathrm{v}}\frac{Eh}{(1-\nu^2)^{5/8}}\left(\frac{h}{R}\right)^{5/4}\left(\frac{R}{L}\right)^{1/2}. \tag{3.225}$$

This equation with the factor $k_{\mathrm{v}} = 0.69$ was firstly derived by K. Mushtari in 1934. Afterwards, Batdorf (1947); Batdorf et al (1947) and Darevskiy (1957) obtained similar equation with factors $k_{\mathrm{v}} = 0.705$ and $k_{\mathrm{v}} = 0.740$, respectively.

The detailed investigations of the effect of different boundary conditions on the critical value of torsion torque were performed by Alumae (1954) and Yamaki and Kodama (1966) (s. also Yamaki, 1984). They have shown that the basic boundary conditions influencing essentially on the critical torque are conditions for the normal and axial displacements. Probably, the first study on the effect of initial imperfections on the buckling of thin isotropic cylinders under torsion has been done by Loo (1954) and Nash (1957) has additionally accounted large deflections.

As concerns buckling of anisotropic composite circular cylinders under torsion, the intensive investigations of these problems in various statements started in the beginning of the seventies (s. the review Tennyson, 1975). Based on the nonlinear Donnell-type kinematic relations, linearly elastic material behavior and usual lamination theory, Shaw et al (1983); Simitses et al (1985) analyzed buckling of both perfect and imperfect laminated circular cylindrical thin shells subjected to a uniform axial compression and torsion (individually applied and in combination). In Simitses (1996), problems on buckling of moderately thick laminated shells are analyzed; the analyzed papers were based on the first-order or higher-order shear deformation shell theories with or without a shear correction factor. Results obtained by these shell theories and by employing classical thin shell theory are compared to determine the range of applicability of different approaches. Using the first-order shear deformation theory with a shear correction factor of 5/6, Mao and Lu (1999) have performed the buckling analysis of a cross-ply laminated cylindrical shell under torsion subjected to mixed boundary conditions. They have shown that the mixed boundary conditions yield appreciably lower buckling torque and less circumferential wave number than the completely clamped boundary conditions. Later, Mao and Lu (2002) have analyzed the elastic-plastic buckling of cylindrical shells subjected to torsion under various boundary conditions. Based on the shell theory including anisotropy and transverse shear stiffness, Takano (2011) has investigated the effects of anisotropy and transverse shear stiffness on buckling under pure torsion and under combined axial compression. Comparing his own results with previous analyses, he has concluded that the Donnell-type theory is not appropriate for studying buckling of laminated shells and a more complex shell theory accounting transverse shear stiffness must be used.

3.4.2 Buckling Modes and Critical Torque

In this subsection, we study buckling of a laminated cylindrical shell under the torsional axial torque M_{T}. The pre-buckling in-plane stress resultants $T^{\circ}_{12} = M_{\mathrm{T}}/(2\pi R)$, $T^{\circ}_{11} = T^{\circ}_{22} = 0$, and the governing equations (3.14), (3.15) take the following form

$$
\begin{aligned}
&D\left(1-\frac{\theta h^2}{\beta}\Delta\right)\Delta^2\chi+\frac{1}{R_2}\frac{\partial^2 F}{\partial\alpha_1^2}-2T_{12}^{\circ}\frac{\partial^2}{\partial\alpha_1\alpha_2}\left(1-\frac{h^2}{\beta}\Delta\right)\chi=0,\\
&\Delta^2 F=\frac{Eh}{R_2}\frac{\partial^2}{\partial\alpha_1^2}\left(1-\frac{h^2}{\beta}\Delta\right)\chi.
\end{aligned}
\tag{3.226}
$$

Let both edges $\alpha_1 = L_i$ be simply supported and have a infinite rigidity diaphragm inhibiting relative shears of layers along the edges. The appropriate boundary conditions are specified by Eqs. (3.17) or (3.18). All geometrical parameters $L_1 = -L/2, L_2 = L/2, R_2$ and the shear stress-resultant T_{12}° are constants. Then a solution of Eqs. (3.226) may be found in the following explicit form

$$
\begin{aligned}
\chi &= \chi_0\cos\left(\frac{\pi\alpha_1}{L}\right)\cos\left(\frac{n}{R}[\alpha_2+\gamma\alpha_1]\right),\\
F &= F_0\cos\left(\frac{\pi\alpha_1}{L}\right)\cos\left(\frac{n}{R}[\alpha_2+\gamma\alpha_1]\right),
\end{aligned}
\tag{3.227}
$$

where γ is a slope ratio, and n is a number of waves in the circumferential direction. Functions (3.227) may be presented as

$$
\begin{aligned}
\chi &= \frac{1}{2}\chi_0\,[X_+(\alpha_1,\alpha_2)+X_-(\alpha_1,\alpha_2)],\\
F &= \frac{1}{2}F_0\,[X_+(\alpha_1,\alpha_2)+X_-(\alpha_1,\alpha_2)],
\end{aligned}
\tag{3.228}
$$

where

$$
\begin{aligned}
&X_+(\alpha_1,\alpha_2)=\cos\left(\frac{\alpha_1}{R_+}\right)\cos\left(\frac{n\alpha_2}{R}\right)-\sin\left(\frac{\alpha_1}{R_+}\right)\sin\left(\frac{n\alpha_2}{R}\right),\\
&X_-(\alpha_1,\alpha_2)=\cos\left(\frac{\alpha_1}{R_-}\right)\cos\left(\frac{n\alpha_2}{R}\right)-\sin\left(\frac{\alpha_1}{R_-}\right)\sin\left(\frac{n\alpha_2}{R}\right),\\
&\frac{1}{R_+}=\frac{n\gamma}{R}+\frac{\pi}{L},\qquad \frac{1}{R_-}=\frac{n\gamma}{R}-\frac{\pi}{L}.
\end{aligned}
\tag{3.229}
$$

The functions $X_+(\alpha_1,\alpha_2), X_-(\alpha_1,\alpha_2)$ are linearly independent in the domain $\Lambda = \{-L/2 \le \alpha_1 \le L/2, 0 \le \alpha_2 < 2\pi R\}$. Then, substituting (3.228) into Eqs. (3.226) and equating coefficients at these functions, one obtains two systems of algebraic equations with respect to χ_0 and F_0. The first system is as follows

$$
\begin{aligned}
&\left\{\left[\left(\frac{n^2}{R^2}+\frac{1}{R_+^2}\right)^2+\frac{h^2\theta}{\beta}\left(\frac{n^2}{R^2}+\frac{1}{R_+^2}\right)^3\right]\right.\\
&\qquad\left.+\frac{nT_{12}^{\circ}}{RR_+}\left[1-\frac{h^2}{\beta}\left(\frac{n^2}{R^2}+\frac{1}{R_+^2}\right)\right]\right\}\chi_0-\frac{1}{RR_+^2}F_0=0,\\
&\frac{Eh}{RR_+^2}\left[1+\frac{h^2}{\beta}\left(\frac{n^2}{R^2}+\frac{1}{R_+^2}\right)\right]\chi_0+\left(\frac{n^2}{R^2}+\frac{1}{R_+^2}\right)^2F_0=0.
\end{aligned}
\tag{3.230}
$$

The second one has the same form with R_+ replaced by R_-. The existence conditions of a nonzero solutions of these systems result in the following two equations for the shear stress-resultants

$$T_{12}^{(+)} = \frac{1}{2n}\left[\frac{EhL^4R^3}{R_+^3 g_+^2} + \frac{Dg_+^2 R_+(L^2R^2\beta + \theta h^2 g_+)}{L^4R^3(L^2R^2\beta + h^2 g_+)}\right], \tag{3.231}$$

$$T_{12}^{(-)} = \frac{1}{2n}\left[\frac{EhL^4R^3}{R_+^3 g_-^2} + \frac{Dg_-^2 R_+(L^2R^2\beta + \theta h^2 g_-)}{L^4R^3(L^2R^2\beta + h^2 g_-)}\right], \tag{3.232}$$

where

$$g_\pm = \pi^2 R^2 \pm 2\pi LnR\gamma + L^2n^2\left(1+\gamma^2\right), \tag{3.233}$$

D is the reduced bending stiffness of the sandwich, and β, θ are the shear parameters defined in Chapt. 2. It is obvious that Eqs. (3.231) and (3.232) give the same critical value of the shear stress-resultant. Hence, one has the equation coupling parameters n and γ,

$$T_{12}^{(+)}(n,\gamma) = T_{12}^{(-)}(n,\gamma). \tag{3.234}$$

Equations (3.231) and (3.232) serve to determine unknown parameters n^*, γ^* and the critical buckling stress-resultant

$$T_{12}^* = \min_n T_{12}^\circ[n,\gamma(n)] = T_{12}^\circ[n^*,\gamma(n^*)] = T_{12}^\circ(n^*,\gamma^*). \tag{3.235}$$

Equations (3.231)-(3.235) contain the parameters θ and β taking into account transverse shear in the shell. Because of these parameters, Eq. (3.235) is not reduced to the explicit form like (3.225).

Example 3.15. Consider a thin cylindrical sandwich shell with the outermost and innermost layers made of aluminium and the middle layer fabricated of epoxy. The geometrical and physical parameters are the same as in Example 3.4. Thicknesses h_i are assumed to satisfy condition (3.47) which means that for any thickness h_2 of the epoxy matrix the shell weight remains constant. Again, we set the problem to determine the optimal thickness of the internal matrix resulting in the maximum value of the buckling shear stress-resultant T_{12}^*. The results of calculations of T_{12}^* and parameters n^*, γ^* for different values of h_2 are presented in Table 3.17. As seen,

Table 3.17 Dependence of the buckling shear stress-resultant T_{12}^* and parameters n^*, γ^* on thickness h_2 of the epoxy matrix.

h_2, mm	0	0.1	0.2	0.5	0.7	0.8	1.0	1.1
n^*	21	21	19	17	16	16	15	15
γ^*	2	2	2	0	0	0	0	0
T_1^*, N/mm	288.18	2999	322.10	358.11	370.08	372.58	367.27	361.62

the sandwich with the thickness $h_2 = 0.8$ mm of the epoxy matrix withstands the greatest twisting load.

Example 3.16. Now we shall study the torsion induced buckling of three-, five-, and seven-layered cylinders of the same length $L = 1$ m and radius $R = 0.5$ m with MRE-layers. The layers with odd numbers are made of the ABS-plastic SD-0170, and the ones with even numbers are MRE-1 with properties specified in Chapt. 2. As well as in Example 3.10, the following conditions for thicknesses are assumed

- for a three-layered shell ($N = 3$),

$$h_1 = h_3 = \frac{h_{\mathrm{pl}}}{2}, \quad h_2 = h_{\mathrm{el}};$$

- for a five-layered cylinder ($N = 5$),

$$h_1 = h_3 = h_5 = \frac{h_{\mathrm{pl}}}{3}, \quad h_2 = h_4 = \frac{h_{\mathrm{el}}}{2};$$

- for a seven-layered sandwich ($N = 7$),

$$h_1 = h_3 = h_5 = h_7 = \frac{h_{\mathrm{pl}}}{4}, \quad h_2 = h_4 = h_6 = \frac{h_{\mathrm{el}}}{3},$$

where $h_{\mathrm{pl}} = 1$ mm and $h_{\mathrm{el}} = 8$ mm are the total thicknesses of the plastic and elastomer, respectively. Above conditions mean that the total weight of both the plastic and elastomer remains invariant for all cases.

The problem is to explore the effect of an applied magnetic field and a number of layers as well on the critical buckling stress-resultant T_{12}^*. The detailed analysis of this influence is presented in Tables 3.18 and 3.19 for the three-, five-, and seven-layered shells. It is seen that for all variants under consideration, the buckling stress-resultant T_{12}^* is a monotonically increasing function of the magnetic field induction B. However, the impact of B on T_{12}^* is more significant for the sandwich shell than for the five-, and seven-layered shells. So, for the three-layered shell, applying the magnetic field with the induction of about 200 mT results in increasing the buckling stress-resultant T_{12}^* up to 30%, whereas, for the shells with five and seven laminas, these increments are only 3 and 4%, respectively. The wave number n^* and slope ratio γ^* are less sensitive to magnetic field. For instance, $n^* = 6$ for the five-, and seven-layered shells, and $\gamma^* \approx 0.47$ and $\gamma^* \approx 0.46$ for the five-, and seven-layered shells, respectively, at any level of the applied magnetic field. The additional calculations shows that assembling multilayered shells with as much number of the MRE-layers as possible and fixed the total weight of plastic and elastomer does not give increasing the buckling shear stress-resultant. So, a seven-layered shell (with three MRE cores) turns out to be less stiffen then the three-, and five-layered ones (with one and two MRE cores, respectively) for any intensity of the magnetic field. But, when comparing the shells with three and five layers, the five-layered sandwich is more stable than the three-layered one at low level of the applied magnetic field ($B < 20$ mT). On the contrary, if a MRE-based shell is under action of very strong

Table 3.18 Critical buckling shear stress-resultant T^*_{12} and the corresponding wave parameter n^* and slope ratio γ^* vs. magnetic field induction B for the sandwich cylindrical shell.

B, mT	n^*	γ^*	T^*_{12}, N/m
0	7	0.522987	7942.30
10	7	0.525109	8296.41
20	6	0.488641	8539.79
30	6	0.489772	8735.90
40	6	0.490627	8908.54
50	6	0.491281	9061.97
60	6	0.491785	9199.46
70	6	0.492173	9323.58
80	6	0.492473	9436.38
90	6	0.492702	9539.51
100	6	0.492877	9634.30
110	6	0.493006	9721.87
120	6	0.493099	9803.12
130	6	0.493163	9878.82
140	6	0.493202	9949.62
150	6	0.493221	10016.1
160	6	0.493222	10078.7
170	6	0.493209	10137.8
180	6	0.493184	10193.7
190	6	0.493149	10246.9
200	6	0.493104	10297.5

Table 3.19 Critical buckling shear stress-resultants T^*_{12} vs. magnetic field induction B for five-, and seven-layered thin cylindrical shells.

B, mT	T^*_{12} for 5-layered shell	T^*_{12}, N/m, for 7-layered shell
0	8556.24	7677.34
20	8583.37	7704.66
40	8610.48	7731.97
60	8637.59	7759.28
80	8664.68	7786.59
100	8691.77	7813.89
120	8718.86	7841.2
140	8745.93	7868.49
160	8773.00	7895.79
180	8800.06	7923.08
200	8827.11	7950.37

magnetic field, then the variant of three-layered shell with one thick MRE core becomes more optimal.

The choice of the optimal number of the MRE-layers under modelling of adaptive thin-walled MRE-structures depends upon many factors: geometrical parameters of a structure, mechanical properties of materials utilized for assembling a shell, type of loading, boundary conditions, and an intensity of applied magnetic field. So, as opposed to the last example, the outcomes of the problem considered in Example 3.10 showed that for the MRE-sandwich under axial compression the total number of laminas equaled five (with two MRE-cores) turns out to be more optimal at all size of changing of the magnetic field induction.

Examples 3.10, 3.15 and 3.16 considered above have demonstrated that MREs embedded between elastic layers provide for a sandwich a wide range of mechanical properties (shear modulus, buckling force) when subjected to different magnetic field levels. The correct choice of a number of MRE-layers in a sandwich structure with a fixed total thickness and weight of an adaptive material (MRE) and basic components (here, a plastic) allows us to design a thin-walled structure with the bearing capacity being controlled by virtue of an applied magnetic field. In Chapt. 5, we will show that introducing the MRE-cores into a sandwich permits one solves another very important problem, an efficient suppression of vibrations in thin-walled structures with adaptive visco-elastic properties.

References

Alfutov NA (2000) Stability of Elastic Structures. Foundations of Engineering Mechanics, Springer, Berlin, Heidelberg

Alumae NA (1954) Critical load of a long cylindrical circular shell under torsion (in Russ.). Prikl Mat Mech 18(1):27–34

Anastasiadis JS, Simitses GJ (1993) Buckling of pressure-loaded, long, shear deformable, cylindrical laminated shells. Composite Structures 23(3):221–231

Batdorf SB (1947) A simplified method of elastic stability analysis for thin cylindrical shells. I. Donnell's equations. NACA Techn Note 1341, NACA

Batdorf SB, Stein M, Schildcrout M (1947) Critical stress of thin-walled cylinders in torsion. NACA Techn. Note 1344, NACA

Carrera E (1999) Multilayered shell theories accounting for layerwise mixed description. Part 1: Governing equations. AIAA J 37(9):1107–1116

Carrera E (2001) Developments, ideas, and evaluations based upon Reissners mixed variational theorem in the modeling of multilayered plates and shells. Applied Mechanics Review 54(9):301–329

Coburn BH, Weaver PM (2016) Buckling analysis, design and optimisation of variable-stiffness sandwich panel. International Journal of Solids and Structures 96(1):217–228

Darevskiy VM (1957) Stability of cylindrical shell under simultaneous action of torsion torques and normal pressure (in Russ.). Izvestia AN SSSR Otdel techn nauk (11):137–147

Donnel LH, Wan CC (1950) Effect of imperfections on the buckling of thin cylinders and columns under axial compression. Trans ASME Journal of Applied Mechanics 17(1):73–83

Donnell LH (1934) A new theory for the buckling of thin cylinders under axial compression and bending. Trans of ASME Aeronautical Engineering 56(7):795–806

Donnell LH (1976) Beams, Plates and Shells. McGraw-Hill Inc, New York

Eisenträger J, Naumenko K, Altenbach H, Meenen J (2015) A user-defined finite element for laminated glass panels and photovoltaic modules based on a layer-wise theory. Composite Structures 133:265–277

Euler L (1759) Sur la force des colonnes. Mémoires de l'Acadèmie de Berlin 13:252–282

Feinstein G, Chen YN, Kempner J (1971a) Buckling of clamped oval cylindrical shells under axial loads. AIAA Journal 9(9):1733–1738

Feinstein G, Erickson B, Kempner J (1971b) Stability of oval cylindrical shells. AIAA Journal 11(11):514–520
Filippov SB (1999) Theory of Joined and Stiffened Shells (in Russ.). St. Petersburg Univ. Press, St. Petersburg
Firer M, Sheinman I (1995) Nonlinear analysis of laminated non-circular cylindrical shells. International Journal of Solids and Structures 32(10):1405–1416
Gabbert U, Altenbach J (1990) COSAR - A reliable system for research and application (in Germ.). Technische Mechanik 11(3):125–137
Gol'denveizer AL (1961) Theory of Thin Elastic Shells. International Series of Monograph in Aeronautics and Astronautics, Pergamon Press, New York
Grigolyuk EI, Kabanov VV (1978) Stability of Shells (in Russ.). Nauka, Moscow
Grigolyuk EI, Kulikov GM (1988a) General direction of development of the theory of multilayered shells. Mech Compos Mater 24:231–241
Grigolyuk EI, Kulikov GM (1988b) Multilayered Reinforced Shells. Calculation of Pneumatic Tires (in Russ.). Mashinostroenie, Moscow
Grover N, Maiti DK, Singh BN (2013) A new inverse hyperbolic shear deformation theory for static and buckling analysis of laminated composite and sandwich plates. Compos Struct 95:667–675
Han JH, Kardomateas GA, Simitses GJ (2004) Elasticity, shell theory and finite element results for the buckling of long sandwich cylindrical shells under external pressure. Composites: Part B 35:591–598
Hutchinson JW (1968) Buckling and initial postbuckling behaviour of oval cylindrical shells under axial compression. Trans ASME Journal of Applied Mechanics 35(1):66–72
Jaunky N, Knight Jr N (1999) An assessment of shell theories for buckling ofcircular cylindrical laminated composite panels loaded inaxial compression. International Journal of Solids and Structures 36(25):3799–20
von Kármán T, Tsien HS (1941) The buckling of thin cylindrical shells under axial compression. Journal of Aeronautical Science 8(6):303–312
Kempner J, Chen Y (1964) Large deflections of an axially compressed oval cylindrical shell. In: In: Proceedings of the 11th International Congress on Applied Mechanics, Springer-Verlag, Berlin, pp 299–306
Kempner J, Chen YN (1967) Buckling and postbuckling of an axially compressed oval cylindrical shell. In: In: Symposium on the Theory of Shells to Honor Lloyd H. Donnell, McCuthan Publishers Co., pp 141–183
Kheirikhah MM, Khalili SMR, Fard KM (2012) Biaxial buckling analysis of soft-core composite sandwich plates using improved high-order theory. European Journal of Mechanics - A/Solids 31(1):54–66
Kim KD (1996) Buckling behaviour of composite panels using the finite element method. Composite Structures 36(1–2):33–43
Koiter WT (1967) On the Stability of Elastic Equilibrium. Report TT F 10-833, NASA
Korchevskaya E, Mikhasev G, Marinkovic D, Gabbert U (2003) Buckling and vibrations of composite laminated cylindrical shells under axial load. In: Proc. of "6th Magdeburg Days of Mechanical Engineering", Otto-von-Guericke-University Magdeburg, Logos, Berlin, pp 183–189
Li LY (1990) Influence of loading imperfections on the stability of an axially compressed cylindrical shell. Thin-Walled Structures 10(3):215–220
Li ZM, Lin ZQ (2010) Non-linear buckling and postbuckling of shear deformable anisotropic laminated cylindrical shell subjected to varying external pressure loads. Comp Struct 92(2):553–567
Loo TT (1954) Effects of large deflections and imperfections on the elastic buckling of cylinders under torsion and axial compression. In: Proc. of the 2nd US national congress on applied mechanics, pp 345–357
Lopatin A, Morozov E (2015) Buckling of the composite sandwich cylindrical shell with clamped ends under uniform external pressure. Composite Structures 122:209–216
Lorenz R (1908) Achsensymmetrische Verzerrungen in dünnwandingen Hohlzzylindern (in Germ.). Zeitschrift des Vereines Deutscher Ingenieure 52(43):1706–1713

Lorenz R (1911) Die nicht achsensymmetische Knickung dünnwandiger Hohlzylinder (in Germ.). Physical Zeitschrift 12(7):241–260

Mao R, Lu CH (1999) Buckling analysis of a laminated cylindrical shellunder torsion subjected to mixed boundary conditions. International Journal of Solids and Structures 36(25):3821–3835

Mao R, Lu G (2002) A study of elastic-plastic buckling of cylindrical shells under torsion. Thin-Walled Structures 40(12):1051–1071

Meyers CA, Hyer MW (1996) Response of elliptical composite cylinders to axial compression loading. Mechanics of Advanced Materials and Structures 6(2):169–194

Mikhasev G (2018) Thin laminated cylindrical shells containing magnetorheological elastomers: Buckling and vibrations. In: Pietraszkevich W, Witkowski W (eds) Shell Structures: Theory and Applications, CRC Press. Taylor & Francis Group, London, vol 4, pp 259–262

Mikhasev G, Mlechka I (2014) On influence of boundary conditions and transverse shear on buckling of thin laminated cylindrical shells under external pressure. Facta Univesitatis Series: Mechanical Engineering 12(2):95–106

Mikhasev G, Mlechka I (2018) Localized buckling of laminated cylindrical shells with low reduced shear modulus under non-uniform axial compression. ZAMM - Journal of Applied Mathematics and Mechanics / Zeitschrift für Angewandte Mathematik und Mechanik 98(3):491–508

Mikhasev G, Seeger F, Gabbert U (2001a) Local buckling of composite laminated cylindrical shells with oblique edges under external pressure: asymptotic and finite element simulation. Technische Mechanik 21(1):1–12

Mikhasev G, Korchevskaya E, Gabbert U, Marinkovic D (2004) Local buckling, stationary and non-stationary vibrations of the composite laminated shells having the weakest spots. In: Proc. of "Fourth International Conference on Thin-Walled Structures, ICTWS", London, pp 769–776

Mikhasev GI, Botogova GI (2017) Effect of edge shears and diaphragms on buckling of thin laminated medium-length cylindrical shells with low effective shear modulus under external pressure. Acta Mechanica 228(6):2119–2140

Mikhasev GI, Tovstik PE (1990) Stability of conical shells under external pressure. Mech Solids 25(4):106–119

Mikhasev GI, Zgirskaya OM (2001) Local buckling of thin laminated cylindrical shell under non-uniform axial load (in Russ.). Vestnik Vitebsk Univ 4(22):90–93

Mikhasev GI, Seeger F, Gabbert U (2001b) Comparison of analytical and numerical methods for the analysis of buckling and vibrations of composite shell structures. In: Proc. of "5th Magdeburg Days of Mechanical Engineering", Otto-von-Guericke-University Magdeburg, Logos, Berlin, pp 175–183

von Mises R (1914) Der kritische Aussendruck zylindrischer Rohre (in Germ.). VDI Zeitschrift 58(19):750–755

Nash WA (1957) Buckling of initially imperfect cylindrical shells subjected to torsion. Trans ASME J Appl Mech 24:125–130

Nguyen TN, Thai CH, Nguyen-Xuan H (2016) On the general framework of high order shear deformation theories for laminated composite plate structures: A novel unified approach. Int J Mech Sci 110:242–255

Papkovich PF (1929) Design formulas for a stability test of a cylindricaal shell of a submarine strength body (in Russ.). Bul nauchno-tekh kom UMVS RKKA 6(2):113–123

Patel BP, Munot CS, Gupta SS, Sambandam CT, Ganapathi M (2004) Application of higher-order finite element for elastic stability analysis of laminated cross-ply oval cylindrical shells. Finite Elements in Analysis and Design 40(9-10):1083–1104

Reddy JN (1993) An evaluation of equivalent-single-layer and layerwise theories of composite laminates. Composite Structures 25:21–35

Reddy JN (2004) Mechanics of Laminated Composite Plates and Shells: Theory and Analysis. CRC Press, New York

Reddy JN, Arciniega R (2004) Shear deformation plate and shell theories: from stavsky to present. Mech Adv Mater Struct 11:535–582

Reddy JN, Liu CF (1985) A higher-order shear deformation theory of laminated elastic shells. International Journal of Engineering Sciences 23(3):319–330

Sambandama CT, Patel BP, Gupta CS S Sand Munot, Ganapathi M (2003) Buckling characteristics of cross-ply elliptical cylinders under axial compression. Composite Structures 62(1):7–17
Schwerin E (1925) Die Torsionsstabilität des dünnwandigen Rohres (in Germ.). ZAMM 5(3):235–243
Shaw D, Simitses GJ, Sheinman I (1983) Imperfect, laminated, cylindrical shells in torsion and axial compression. Acta Astronautica 10(5–6):395–400
Sheinman I, Firer M (1994) Buckling analysis of laminated cylindrical shells with arbitrary non-circular cross-section. AIAA Journal 32(5):648–654
Silvestre N (2008) Buckling behaviour of elliptical cylindrical shells and tubes under compression. International Journal of Solids and Structures 45:4427–4447
Simitses GJ (1996) Buckling of moderately thick laminated cylindrical shells: a review. Composites Part B: Engineering 27(6):581–587
Simitses GJ, Shaw D, Sheinman I (1985) Inperfection sensitivity of laminated cylindrical shells in torsion and axial compression. Composite Structures 4(4):335–360
Soldatos KP (1999) Mechanics of cylindrical shells with non-circular cross-section: a survey. Applied Mechanics Reviews 52:237–274
Soldatos KP, Tzivanidis GJ (1982) Buckling and vibration of cross-ply laminated non-circular cylindrical shells. Journal of Sound and Vibration 82(3):425–434
Southwell R (1913) On the collapse of tubes by external pressure. Parts 1, 2, 3. Philos Mag 25(149):687–697
Sun G (1991) Buckling and initial post-buckling behaviour of laminated oval cylindrical shells under axial compression. Trans ASME Journal of Applied Mechanics 58:848–851
Takano A (2011) Buckling of thin and moderately thick anisotropic cylinders under combined torsion and axial compression. Thin-Walled Structures 49(2):304–316
Tennyson RC (1975) Buckling of laminated composite cylinders: a review. Composites 6(1):17–24
Tennyson RC, Chan KC (1990) Buckling of imperfect sandwich cylinders under axial compression. International Journal of Solids and Structures 26(9–10):1017–1036
Timoshenko SP (1936) Theory of Elastic Stability. McGraw-Hill Inc, New York
Tovstik PE (1983) Two-dimensional problems of buckling and vibrations of the shells of zero Gaussian curvature. Soviet Physics Doklady 28(7):593–594
Tovstik PE (1984) Local loss of stability by cylindrical shells under axial compression. Leningrad University Mechanics Bul 1:46–54
Tovstik PE, Smirnov AL (2001) Asymptotic Methods in the Buckling Theory of Elastic Shells. World Scientific, Singapore
Weps M, Naumenko K, Altenbach H (2013) Unsymmetric three-layer laminate with soft core for photovoltaic modules. Composite Structures 105:332–339
Wu Z, Cheung YK, Lo SH, Chen W (2008) Effects of higher-order global-local shear deformations on bending, vibration and buckling of multilayered plates. Compos Struct 82(2):277–289
Yamaki N (1984) Elastic Stability of Circular Cylindrical Shells. Elsevier Science Publishers B.V., Amsterdam-New York-Oxford
Yamaki N, Kodama S (1966) Buckling of circular cylindrical shells under torsion. Rept 1: 1965–1966 168, Rept lnst. High Speed Mech.

Chapter 4
Free Vibrations of Elastic Laminated Beams, Plates and Cylindrical Shells

Abstract In this chapter, based on the equivalent single layer model for thin laminated members, natural modes and corresponding eigenfrequencies for laminated elastic beams plates and cylindrical shells are studied taking into account shears. At first, elastic vibrations of laminated beams are analyzed in Sect. 4.1, the emphasis being made on non-uniformly stressed beams contacting with an elastic inhomogeneous medium. Then, in Sect. 4.2, the eigenmodes and frequencies of elastic rectangular plates are analyzed for two variants of boundary conditions: if all edges are simply supported and have diaphragms preventing shears, the boundary-value problem is solved in the explicit form; and if one of edges is free of a diaphragm, the solution of a corresponding boundary-value problem is constructed in the form of the superposition of the main stress-strain state and the edge effect integrals accounting for the edge shears. Section 4.3 is devoted to vibrations of a circular cylindrical shell of an arbitrary length with constant geometrical and physical parameters. In Sect. 4.4, the localized natural modes for a medium-length laminated cylinder is investigated. And finally, Sect. 4.5 contains the problem on free localized vibrations of a laminated cylindrical shell under axial forces no-uniformly distributed in the circumferential direction. In the last two sections, natural modes are constructed by using the asymptotic method. In all problems, the effect of shears on the natural frequencies is analyzed. Examples on free vibrations of laminated cylinders and panels assembled from different materials are considered.

4.1 Laminated Beams

In this section, we study free elastic vibrations of laminated beams. Particular attention will be paid to the problem on free vibrations of non-homogeneous beams with low reduced shear modulus. We will call a beam non-homogeneous if it has geometrical and/or physical parameters dependent of an axial coordinate, or if it is non-uniformly pre-stressed by compressive or tensile forces. Geometrically inhomogeneous beams are beams with the cross-sectional sizes (width, high, radius)

G. I. Mikhasev and H. Altenbach, *Thin-walled Laminated Structures*,
Advanced Structured Materials 106, https://doi.org/10.1007/978-3-030-12761-9_4

varying along the axis. Physically non-uniform beams are beams in which the material properties (elastic moduli, material density) depend on the axial coordinate. This heterogeneity can be induced by the action of external physical fields (temperature, magnetic field, etc.). Beams with functionally graded materials (FGM) along the beam axis are often considered as well. If the beam is in contact with an inhomogeneous elastic medium, then the dynamic reaction of the beam is also nonuniform along its axis. Within the framework of any deformation model for a non-uniform beam and regardless of the nature of inhomogeneity, the differential equations governing vibrations of similar beams contain variable coefficients, which significantly complicates the problem.

It should be noted that despite the complexity of the problems, vibrations of inhomogeneous beams were studied by many researchers. But for all that, a majority from numerous studies refer to isotropic single layer beams. Cranch and Adler (1956) and Suppiger and Taleb (1956) were probably the first who in 1956 investigated free bending vibrations of isotropic beams with variable section. Assuming the linear (Cranch and Adler, 1956) or exponential (Suppiger and Taleb, 1956) law of variation of the cross-section along the beam axis, they constructed exact solutions for beams with different boundary conditions. Later, applying different approximate analytical or numerical methods, a numerous investigations on free vibrations of isotropic beams with variable section, including tapered ones and beams with steppered sections, were carried out (s., among others, Conway and Dubil, 1965; Carnegie and Thomas, 1967; Sanger, 1968; Goel, 1976; Roy and Ganesan, 1994; Zhou and Cheung, 2000, 2001; Naguleswaran, 2002; Ece et al, 2007; Firouz-Abadi et al, 2007; Jaworski and Dowell, 2008). Free vibration analysis of geometrically no-uniform beams subjected to the axial compression or tension were made by Sato (1980); Naguleswaran (2003); Kukla and Zamojska (2007). The effect of uniform and non-uniform elastic foundations on natural frequencies and modes was examined by Lee and Ke (1990); Wang (1991). Bending vibrations of FGM beams with variation of material properties were studied in (Murin et al, 2010; Huang and Li, 2010; Alshorbagy et al, 2011; Mohanty and Rout, 2012).

As for laminated beams, there are only a few papers considering vibrations taking into account initial axial stresses or response of a surrounding medium or foundation. Li et al (2008, 2016) investigated free vibration and buckling behaviors of axially loaded laminated composite beams having arbitrary lay-up. Using the dynamic stiffness method (Li et al, 2008) and based on a unified higher-order shear deformation beam theory (Li et al, 2016), they analyzed the influences of axial forces, shear deformation and rotary inertia on the natural frequencies, buckling loads and mode shapes. Using a three-node shear flexible beam element, Patel et al (1999) studied nonlinear free flexural vibrations of laminated orthotropic beams resting on a two parameter elastic foundation. Similar problem was considered by Jafari-Talookolaei and Ahmadian (2007). Using FEM on the basis of Timoshenko beam theory, they investigated free vibrations of a cross-ply laminated composite beam on elastic Pasternak foundation. The effect of viscoelastic support on free vibrations of laminated fiberglass beam was examined by Koutsawa and Daya (2007). Large amplitude free vibration analysis of laminated composite thin beams on linear and nonlinear elastic foundations was presented by Malekzadeh and Vosoughi (2009); Baghani et al (2011).

In the aforementioned papers, composite laminated beams were assumed to be shear deformable. However, axial stresses (Li et al, 2008, 2016) and elastic/viscoelastic properties of foundations (Patel et al, 1999; Jafari-Talookolaei and Ahmadian, 2007; Koutsawa and Daya, 2007; Malekzadeh and Vosoughi, 2009; Baghani et al, 2011) were considered to be constant along the beam axis. Apparently, Farghaly and Gadelrab (1995); Dong et al (2005) are among the few available studies in which laminated beams are geometrically heterogeneous in the axial direction. Based on the first order shear deformation theory, they performed vibration analysis of stepped laminated composite Timoshenko beams. We also refer readers to the reviews (Hajianmaleki and Qatu, 2013; Sayyad and Ghugal, 2017), which give some insight of state of the art on dynamics of laminated elastic beams.

4.1.1 Governing Equation

Let us consider a laminated beam consisting of N elastic laminas. It is assumed that the beam is compressed by the axial force F° and/or rest on an elastic foundation with the modulus of substrate reaction c_f. The beam is characterized by the total thickness $h = \sum_{j=1}^{N} h_j$, bending stiffness EI and linear density ρ_l. If the beam cross section has a rectangular form with hight h and width b, then $I = bh^3/12$. In the common case, $F^\circ, \rho_\mathrm{l}, c_\mathrm{f}$ may be functions of the coordinate α_1 $(0 \le \alpha_1 \le L)$. We apply here again the ESL theory stated in Chapt. 2. Taking into account the response of elastic foundation and the dependence of the axial force on α_1, Eq. (2.153) governing dynamics of a multi-layered beam is rewritten as

$$
\begin{aligned}
EI\eta_3 \left(1 - \frac{\theta h^2}{\beta}\frac{\partial^2}{\partial\alpha_1^2}\right)\frac{\partial^4\chi}{\partial\alpha_1^4} - \frac{\partial}{\partial\alpha_1}\left[F^\circ\left(1 - \frac{h^2}{\beta}\frac{\partial^2}{\partial\alpha_1^2}\right)\right]\frac{\partial\chi}{\partial\alpha_1} \\
+ c_\mathrm{f}\left(1 - \frac{h^2}{\beta}\frac{\partial^2}{\partial\alpha_1^2}\right)\chi + \rho_\mathrm{l}\left(1 - \frac{h^2}{\beta}\frac{\partial^2}{\partial\alpha_1^2}\right)\frac{\partial^2\chi}{\partial t^2} = 0,
\end{aligned}
\tag{4.1}
$$

where the reduced Young's modulus E and shear parameters β, θ are calculated by equations derived in Chapt. 2 with $\nu = \nu_k = 0$.

For the Winkler foundation, the spring constant c_f is only influenced by the elastic properties of the foundation. Assuming the alternative model represented in Chapt. 2, s. Eq. (2.152), then

$$
c_\mathrm{f} = \alpha_\mathrm{f} b\pi n/L, \quad \alpha_\mathrm{f} = \frac{2E_\mathrm{f}(1-\nu_\mathrm{f})}{(1+\nu_\mathrm{f})(3-4\nu_\mathrm{f})}, \tag{4.2}
$$

where n is the wave number in the function $\chi = \chi_0 \sin \pi n\alpha_1/L$ describing the beam response and E_f, ν_f are the Young's modulus and Poison's ratio of the foundation.

Remark 4.1. Equation (4.1) may be used if E, I, β, θ and η_3 are functions of α_1. The error of the equation depends on the index of variation of these functions by α_1. The higher this index is, the larger the error of Eq. (4.1).

4.1.2 Simply Supported Beam with Constant Parameters

Let the beam edges be simply supported and all parameters, including $F^\circ, \rho_0, c_\mathrm{f}$, be constants. Then the solution of (4.1) satisfying the boundary conditions (3.3) or (3.4) has the simple form

$$\chi = \chi_0 \sin \frac{\pi n \alpha_1}{L} \, \mathrm{e}^{\mathrm{i}\omega t}, \tag{4.3}$$

where L is the beam length, n is the number of waves and ω is the natural frequency.

The substitution of (4.3) into (4.1) results in the natural frequency

$$\omega = \frac{1}{\sqrt{\rho_1}} \sqrt{\frac{E I \eta_3 \pi^4 n^4 (1 + \theta K n^2)}{L^4 (1 + K n^2)} + \frac{F^\circ \pi^2 n^2}{L^2} + c_\mathrm{f}}, \tag{4.4}$$

where

$$K = \frac{\pi^2 h^2}{\beta L^2}.$$

If the foundation spring constant is represented by (4.2), then

$$c_\mathrm{f} = \frac{\alpha_\mathrm{f} b \pi n}{L},$$

and for the Winkler foundation c_f is a constant independent of n.

If $F^\circ > 0$, then the beam is stretched, and for $F^\circ < 0$, it is compressed. In the last case, it is assumed that $|F^\circ| < F^*_\mathrm{cr}$, where

$$F^*_\mathrm{cr} = \max_n \left\{ \frac{\pi^2 n^2 E I \eta_3 (1 + \theta K n^2)}{L^2 (1 + K n^2)} + \frac{c_\mathrm{f} L^2}{\pi^2 n^2} \right\} \tag{4.5}$$

is the critical buckling force. For $c_\mathrm{f} = 0$, it coincides with Eq. (3.11) derived in Chapt. 3. The increase of the tensile force F° and/or the spring constant c_f leads to the growth of the natural frequencies for any number n. In contrast, increasing the compressive force F° results in decreasing the eigenfrequencies; herewith, $\omega \to 0$ as $|N^\circ| \to N^*_\mathrm{cr}$.

Other important conclusions are the following:

a) the incorporation of the shear parameter K into the ESL beam model leads to the reduction of the natural frequencies and
b) the effect of K on the natural frequencies is weak for low-frequency vibrations and, in particular, for very long beams, but it becomes noticeable for higher modes (for large n).

Below, it will be shown that the conclusion b) becomes not valid for a medium-length laminated cylindrical shell.

4.1.3 Vibrations of Pre-stressed Beams on Elastic Foundation

Let $F^\circ, c_\mathrm{f}, \rho_\mathrm{l}$ be functions of α_1. The parameter β depends on the correlation between the reduced Young's and shear moduli E, G and may vary in a wide range. We consider here the case when $G \sim h_* E$, then $\beta \sim h_*$, where $h_* = h/L$ is a small parameter (the beam is assumed to be long). The parameter θ is also small. So, for a single layer beam $\theta = 1/85$, and for a multi-layered one it may be much less. Here, it is assumed that $\theta \sim h_*^\varsigma$, $1/2 < \varsigma < 1$. We introduce some assumptions concerning the elastic foundation and axial stress resultant. Let the foundation be *soft* and the axial force be sufficiently weak so that the following relations hold

$$c_\mathrm{f}(\alpha_1) = h_* \frac{Eb\eta_3}{12L}\, k(x), \quad F^\circ = h_*^2 \frac{LEb\eta_3}{12}\, f_1(x), \tag{4.6}$$

where $x = \alpha_1/L$ is a dimensionless coordinate. If $f_1(x) > 0$ for any $x \in [0,1]$, then the force F° is extensional in any point of the beam; when $f_1(x) < 0$ in some points from the segment $[0,1]$, the force F° is compressive in this points, but in this case it is assumed that $\max_x |f_1(x)| < f_\mathrm{cr}$, where f_cr is the critical value resulting in buckling of the beam (s. Chapt. 3).

In the case of free vibrations, the displacement function χ may be found in the form of

$$\chi = LX(x)\mathrm{e}^{\mathrm{i}\omega t}, \tag{4.7}$$

where ω is the natural frequency. Let us introduce a dimensionless parameter λ and the characteristic time t_c

$$\lambda = t_\mathrm{c}^2\omega^2, \quad t_\mathrm{c} = \sqrt{\frac{12\rho_\mathrm{lm}L^2}{h_* Eb\eta_3}}, \tag{4.8}$$

where $\rho_\mathrm{lm} = \max \rho_\mathrm{l}(Rx)$ is a maximum value of the reduced linear density for a nonhomogeneous beam.

Then Eq. (4.1) is rewritten as follows

$$\begin{aligned} -h_*^{3+\varsigma}\,\tau \frac{\mathrm{d}^6 X}{\mathrm{d}x^6} + h_*^2 \frac{\mathrm{d}^4 X}{\mathrm{d}x^4} - h_* \frac{\mathrm{d}}{\mathrm{d}x}\left[f_1(x)\left(1 - h_*\kappa \frac{\mathrm{d}^2}{\mathrm{d}x^2}\right)\frac{\mathrm{d}X}{\mathrm{d}x}\right] \\ + k(x)\left(1 - h_*\kappa\frac{\mathrm{d}^2}{\mathrm{d}x^2}\right) X - \lambda r(x)\left(1 - h_*\kappa\frac{\mathrm{d}^2}{\mathrm{d}x^2}\right) X = 0, \end{aligned} \tag{4.9}$$

where

$$\tau = h_*^{1-\varsigma}\theta\beta^{-1}, \qquad \kappa = h_*\beta^{-1}, \qquad r(x) = \rho_\mathrm{l}(Lx)\rho_\mathrm{lm}^{-1}. \tag{4.10}$$

It is assumed that κ, τ, $f_1(x)$, $k(x)$, $r(x) \sim 1$ as $h_* \to 0$. Equation (4.9) is the singular perturbed differential equation with variable coefficients. In common case, it does not admit a solution in the explicit form. However, from all variety of eigenforms, one can construct an asymptotic solution of a high variability and satisfying the condition $\mathrm{d}X/\mathrm{d}x \sim h_*^{-1/2}$ at $h_* \to 0$.

We apply the Wentzel-Kramers-Brillouin method (WKB-method) and seek a solution in the form of series

$$\begin{aligned} X &= \sum_{j=0}^{\infty} h_*^{j/2} X_j(x) \exp\left\{ h_*^{-1/2} \int g(x)(d)x \right\}, \\ \lambda &= \lambda_0 + h_* \lambda_1 + \ldots, \end{aligned} \tag{4.11}$$

where X_j, $g(x)$ are infinitely differentiable functions of $x \in [0, 1]$. It should be noted that a similar asymptotic approach has been applied by Firouz-Abadi et al (2007) to study free vibrations of an isotropic single layer Euler-Bernoulli beam of variable-cross-section with and without axial forces. They gave a compact third-order WKB-approximation for the mode shapes and found the corresponding natural frequencies.

Let us substitute (4.11) into Eq. (4.9) and equate coefficients at the same powers of $h_*^{1/2}$. Then we arrive at the series of equations. In the zeroth-order approximation (at $j = 0$), one has

$$\mathcal{F}(g, x) X_0 = 0. \tag{4.12}$$

where

$$\mathcal{F}(g, x) \equiv g^4 - f_1(x) g^2 (1 - \kappa g^2) + k(x)(1 - \kappa g^2) - \lambda_0 r(x)(1 - \kappa g^2). \tag{4.13}$$

We will find the natural frequencies satisfying the inequality

$$\lambda_0 r(x) > k(x) \tag{4.14}$$

for any $x \in [0, 1]$. Then, resolving the equation $\mathcal{F}(g, x) = 0$ with respect to g, one obtains

$$g_{1,2} = \pm \mathrm{i} \varphi_1(x), \quad g_{3,4} = \pm \varphi_2(x), \tag{4.15}$$

$$\begin{aligned} \varphi_1(x) &= \sqrt{\frac{\kappa \lambda_0 r - \kappa k - f_1 + \sqrt{(\kappa k - f_1 - \kappa \lambda_0 r)^2 + 4(\lambda_0 r - k)}}{2(1 + \kappa f_1)}}, \\ \varphi_2(x) &= \sqrt{\frac{-(\kappa \lambda_0 r - \kappa k - f_1) + \sqrt{(\kappa k - f_1 - \kappa \lambda_0 r)^2 + 4(\lambda_0 r - k)}}{2(1 + \kappa f_1)}}, \end{aligned} \tag{4.16}$$

where $\varphi_1(x), \varphi_2(x) > 0$ for any $x \in [0, 1]$.

In the first-order approximation ($j = 1$), we get the following equation

$$\mathcal{F}(g, x) X_1 + \mathcal{G}[g(x), x] X_0' + \left[\frac{1}{2} \mathcal{G}' + \kappa k' g - \kappa \lambda_0 r' g \right] X_0 = 0, \tag{4.17}$$

where the prime means the differentiation by x, and

$$\mathcal{G}[g(x), x] = \frac{\partial \mathcal{F}(g, x)}{\partial g}. \tag{4.18}$$

Owing to (4.15) and (4.16), $\mathcal{F}[g_i(x), x)] \equiv 0$ and Eq. (4.17) results in the differential equation by X_0 which has the following general solution

$$X_0 = \frac{c}{\sqrt{|\mathcal{G}[g(x), (x)]|}} \exp\left[\kappa \int g(\lambda_0 r' - k')\mathrm{d}x\right] \tag{4.19}$$

with an arbitrary constant c.

Considering the higher-order approximations ($j \geq 2$), one can get a sequence of differential equations by X_{j-1} with parameters λ_{j-1}. Let us interrupt this process and consider only the first two approximations. Taking into account (4.15) and (4.16), the general solution of the differential equation (4.9) may be written as follows:

$$\begin{aligned} X_0 = {} & \frac{c_1}{\sqrt{|\mathcal{G}_1(x)|}} \left\{\cos\left[h_*^{-1/2}\int_0^x \varphi_1(x)\mathrm{d}x + I_1(x)\right] + O\left(h_*^{1/2}\right)\right\} \\ & + \frac{c_2}{\sqrt{|\mathcal{G}_1(x)|}} \left\{\sin\left[h_*^{-1/2}\int_0^x \varphi_1(x)\mathrm{d}x + I_1(x)\right] + O\left(h_*^{1/2}\right)\right\} \\ & + \frac{c_3}{\sqrt{|\mathcal{G}_2(x)|}} \left\{\exp\left[-h_*^{-1/2}\int_0^x \varphi_2(x)\mathrm{d}x - I_2(x)\right] + O\left(h_*^{1/2}\right)\right\} \\ & + \frac{c_4}{\sqrt{|\mathcal{G}_2(x)|}} \left\{\exp\left[h_*^{-1/2}\int_1^x \varphi_2(x)\mathrm{d}x + I_2(x)\right] + O\left(h_*^{1/2}\right)\right\}, \end{aligned} \tag{4.20}$$

where

$$\begin{aligned} I_1(x) &= \kappa \int \varphi_1(x)[\lambda_0 r'(x) - k'(x)]\mathrm{d}x, \\ I_2(x) &= \kappa \int \varphi_2(x)[\lambda_0 r'(x) - k'(x)]\mathrm{d}x, \\ \mathcal{G}_1(x) &= \mathcal{G}[\varphi_1(x), x], \quad \mathcal{G}_2(x) = \mathcal{G}[\varphi_2(x), x], \end{aligned} \tag{4.21}$$

and c_i are constants which are found from the boundary conditions.

We assume here the following restrictions

$$\mathcal{G}_1(x) \neq 0, \quad \mathcal{G}_2(x) \neq 0 \tag{4.22}$$

for any $x \in [0, 1]$. The point $x^* \in [0, 1]$, for which $\mathcal{G}_1(x^*) = 0$ or $\mathcal{G}_1(x^*) = 0$, is generally called the turning point. The general solution (4.20) is the superposition of the integrals describing the basic dynamical stress state of the beam. It is interesting to note that the index of variation (see the definition given by Eq. (2.66)) of these basic integrals is equal to $\iota_1 = 1/2$ which coincide with the index of variation for the simple edge effect introduced above in Subsect. 2.1.13 for a shell. However, the integrals composing (4.20) do not depend on the parameter τ which appears at the highest derivative in Eq. (4.9). In other words, the general solution (4.20) defines the basic dynamic stress state of a high variability and does not take into account the special edge effects with the index of variation $\iota = (1+\varsigma)/2 > \iota_1 = 1/2$, where $1/2 < \varsigma < 1$. The omitted integrals define shears in a vicinity of the edges and may be incorporated in the general solution by considering the special edge effect equation

$$-h_*^{1+\varsigma}\,\tau\frac{\mathrm{d}^6 X}{\mathrm{d}x^6} + \frac{\mathrm{d}^4 X}{\mathrm{d}x^4} = 0 \tag{4.23}$$

and, afterwards, constructing the higher-order approximation at $j = 2$. The edge effect equation (4.23) gives two additional integrals,

$$X_5 = c_5 \exp\left[-h_*^{-\dfrac{1+\varsigma}{2}}\frac{x}{\sqrt{\tau}}\right], \quad X_6 = c_6 \exp\left[-h_*^{-\dfrac{1+\varsigma}{2}}\frac{1-x}{\sqrt{\tau}}\right]. \tag{4.24}$$

As seen from (4.10), the behavior of the shear edge effect integrals depends on the correlation between the shear parameters β, θ and the beam dimensions h, L.

In what follows, we disregard corrections due to the shear edge effect integrals and have to choose the basic boundary conditions corresponding to the basic stress state. As an example, we will consider the boundary conditions of the rigid clamping group (3.28) and (3.29). For this group, the basic boundary conditions are the following:

$$X_0' = 0, \quad X_0 - h_*\kappa X_0'' = 0 \quad \text{at} \quad x = 0,\, 1. \tag{4.25}$$

The substitution of the general solution (4.20) into (4.25) results in the homogeneous system of algebraic equations with respect to constants c_i $(i = 1, ..., 4)$:

$$\mathbf{A}\mathbf{C}^{\mathrm{T}} = 0, \tag{4.26}$$

where $\mathbf{C} = (c_1, c_2, c_3, c_4)$ is the three-dimensional vector, and $\mathbf{A}$ is the 4×4 - matrix with the elements

$$a_{11} = \frac{1+\kappa\varphi_1^2(0)}{\sqrt{|\mathcal{G}_1(0)|}}\cos[I_1(0)], \qquad a_{12} = \frac{1+\kappa\varphi_1^2(0)}{\sqrt{|\mathcal{G}_1(0)|}}\sin[I_1(0)],$$

$$a_{13} = \frac{1-\kappa\varphi_2^2(0)}{\sqrt{|\mathcal{G}_2(0)|}}\exp\left[-I_2(0)\right], \qquad a_{14} = 0,$$

$$a_{21} = -\frac{\varphi_1(0)}{\sqrt{|\mathcal{G}_1(0)|}}\sin[I_1(0)], \qquad a_{22} = \frac{\varphi_1(0)}{\sqrt{|\mathcal{G}_1(0)|}}\cos[I_1(0)],$$

$$a_{23} = -\frac{\varphi_2(0)}{\sqrt{|\mathcal{G}_2(0)|}}\exp\left[-I_2(0)\right], \qquad a_{24} = 0,$$

$$\begin{aligned}
a_{31} &= \frac{1+\kappa\varphi_1^2(1)}{\sqrt{|\mathcal{G}_1(1)|}}\cos[\Theta_1(1)], & a_{32} &= \frac{1+\kappa\varphi_1^2(0)}{\sqrt{|\mathcal{G}_1(0)|}}\sin[\Theta_1(0)],\\
a_{34} &= 0, & a_{34} &= \frac{1-\kappa\varphi_2^2(1)}{\sqrt{|\mathcal{G}_2(1)|}}\exp\left[\Theta_2(1)\right],\\
a_{41} &= -\frac{\varphi_1(1)}{\sqrt{|\mathcal{G}_1(1)|}}\sin[\Theta_1(1)], & a_{42} &= \frac{\varphi_1(1)}{\sqrt{|\mathcal{G}_1(1)|}}\cos[\Theta_1(0)],\\
a_{43} &= 0, & a_{44} &= \frac{\varphi_2(1)}{\sqrt{|\mathcal{G}_2(1)|}}\exp\left[I_2(1)\right],
\end{aligned} \tag{4.27}$$

depending on the eigenvalue λ_0. In Eqs. (4.27)

$$\Theta_1(x) = \frac{1}{h_*^{1/2}}\int\limits_0^x \varphi_1(x)\mathrm{d}x + I_1(x). \tag{4.28}$$

The transcendental equation $\det \mathbf{A} = 0$ serves for determining the series of unknown eigenvalues $\lambda_0 = \lambda_0^{(n)}$, $n = 1, 2, \ldots$.

Consider the particular case when the beam and foundation are uniform, and the axial stress resultant is a function of α_1. Then $r = 1, k$ are constants, $f_1 = f_1(x)$, and $I_1 = I_2 = 0$ for any $x \in [0, 1]$. For this case the equation $\det \mathbf{A} = 0$ is reduced to the following

$$\tan\left\{h_*^{-1/2}\int\limits_0^1 \varphi_1(x)\mathrm{d}x\right\} = \frac{\delta_{20}\delta_{11}\varphi_{10}\varphi_{21} + \delta_{10}\delta_{21}\varphi_{20}\varphi_{11}}{\delta_{10}\delta_{11}\varphi_{20}\varphi_{21} - \delta_{20}\delta_{21}\varphi_{10}\varphi_{11}}, \tag{4.29}$$

where

$$\begin{aligned}
&\delta_{10} = 1+\kappa\varphi_1^2(0), \quad \delta_{11} = 1+\kappa\varphi_1^2(1),\\
&\delta_{20} = 1-\kappa\varphi_2^2(0), \quad \delta_{21} = 1-\kappa\varphi_2^2(1),\\
&\varphi_{10} = \varphi_1(0), \quad \varphi_{11} = \varphi_1(1), \quad \varphi_{20} = \varphi_2(0), \quad \varphi_{21} = \varphi_2(1),
\end{aligned} \tag{4.30}$$

and the functions $\varphi_i(x)$ are specified by (4.16). When deriving Eq. (4.29), we have allowed for the following limiting correlations

$$\begin{aligned}
\lim_{h_*\to 0} h_*^{-j/2}\exp\left\{-h_*^{-1/2}\int\limits_0^1 \varphi_2(x)\mathrm{d}x\right\} &= 0,\\
\lim_{h_*\to 0} h_*^{-j/2}\exp\left\{h_*^{-1/2}\int\limits_1^0 \varphi_2(x)\mathrm{d}x\right\} &= 0
\end{aligned} \tag{4.31}$$

valid for any integer $j = 0, 1, \ldots$.

Constants c_i are defined as follows

$$
\begin{aligned}
c_2 &= -\frac{\delta_{10}\varphi_{20}}{\delta_{20}\varphi_{10}}\, c_1, \quad c_3 = -\sqrt{\left|\frac{\mathcal{G}_2(0)}{\mathcal{G}_1(0)}\right|}\, \frac{\delta_{10}}{\delta_{20}} c_1, \\
c_4 &= \sqrt{\left|\frac{\mathcal{G}_2(1)}{\mathcal{G}_1(1)}\right|}\, \frac{\varphi_{11}}{\varphi_{21}} \left\{ \sin\left[\frac{1}{h_*^{1/2}} \int_0^1 \varphi_1(x)\mathrm{d}x\right] \right. \\
&\quad \left. + \frac{\delta_{10}\varphi_{20}}{\delta_{20}\varphi_{10}} \cos\left[\frac{1}{h_*^{1/2}} \int_0^1 \varphi_1(x)\mathrm{d}x\right] \right\} c_1 .
\end{aligned}
\tag{4.32}
$$

To analyse the effect of the shear parameter κ and variable axial force on the natural frequencies we will present an example.

Example 4.1. Let $f_1 = 1 + \epsilon x$ be the linear function of x, where $\epsilon > -1$. It is seen from Eqs. (4.16) that $f_1 < \kappa(\lambda_0 - k)$. We remind that eigenvalues defined by Eq. (4.29) have to satisfy the inequality, s. Eq. (4.14),

$$
\lambda_0^{(n)} > k, \quad n = 1, 2, \dots \tag{4.33}
$$

Then the first natural frequency $\omega = \sqrt{\lambda_0^{(1)}}\, t_{\mathrm{c}}^{-1}$ with $\lambda_0^{(1)}$ satisfying (4.33) might be higher than one or several the lowest eigenfrequencies. Table 4.1 displays the first five eigenvalues $\lambda_0^{(n)}$ satisfying (4.33) versus the shear parameter κ for $k = 1$, $\epsilon = 1, h_* = 0.01$. One can see that the influence of the shear parameter κ on the first eigenvalue $\lambda_0^{(1)}$ is weak, but it increases together with the number n. The series of eigenvalues $\lambda_0^{(n)}$ for $n = 1, 2, \dots, 5$ and different values of a parameter ϵ is shown in Table 4.2. The calculations were performed at $\kappa = 1, k = 1, h_* = 0.01$. As seen that for any fixed number n each eigenfrequency $\lambda_0^{(n)}$ growths together with a parameter ε characterizing the rate of inhomogeneity of the axial force, this frequency increment being greater for a large number n.

It is well known that growing the compressive pre-buckling axial force leads to very quick decreasing the lowest eigenfrequency. Thus, one may conclude that the first

Table 4.1 Eigenvalues $\lambda_0^{(n)}$ vs. shear parameter κ.

κ	0.0	0.5	1.0	2.0
$\lambda_0^{(1)}$	1.225	1.198	1.186	1.173
$\lambda_0^{(2)}$	2.052	1.851	1.771	1.701
$\lambda_0^{(3)}$	3.928	3.085	2.825	2.621
$\lambda_0^{(4)}$	7.552	5.004	4.390	3.944
$\lambda_0^{(5)}$	13.858	7.662	6.477	5.668

Table 4.2 Series of eigenvalues $\lambda_0^{(n)}$ vs. parameter ϵ.

n	1	2	3	4	5
$\epsilon = 1$					
$\lambda_0^{(n)}$	1.186	1.771	2.825	4.390	6.477
$\epsilon = 2$					
$\lambda_0^{(n)}$	1.231	1.945	3.214	5.082	7.560
$\epsilon = 3$					
$\lambda_0^{(n)}$	1.275	2.110	3.582	5.739	8.587

eigenvalue $\lambda_0^{(1)}$ defined by our asymptotic procedure may do not equal the lowest natural frequency for the axially compressed laminated beam.

4.2 Laminated Plates

Consider a laminated rectangular plate with thickness h and sides $0 \leq \alpha_1 \leq L_1$ and $0 \leq \alpha_2 \leq L_2$. The plate is pre-stressed by the shear forces yielding in-plane stresses $T^\circ_{11}, T^\circ_{22}, T^\circ_{12}$. The governing equations for free vibrations of a pre-stressed plate resting on an elastic foundation may be easily obtained from Eqs. (3.23) by introducing additional terms accounting the inertia forces and response of an elastic foundation

$$D\left(1 - \frac{\theta h^2}{\beta}\Delta\right)\Delta^2\chi - \left(\Delta_T - c_\mathrm{f} - \rho_0 h\frac{\partial^2}{\partial t^2}\right)\left(1 - \frac{h^2}{\beta}\Delta\right)\chi = 0, \qquad (4.34)$$

were c_f is the spring constant for the elastic foundation and

$$\Delta_T = T^\circ_{11}\frac{\partial^2}{\partial\alpha_1^2} + 2T^\circ_{12}\frac{\partial^2}{\partial\alpha_1\partial\alpha_2} + T^\circ_{22}\frac{\partial^2}{\partial\alpha_2^2}. \qquad (4.35)$$

The above equations should be supplemented by the equation

$$\frac{1-\nu}{2}\frac{h^2}{\beta}\Delta\phi = \phi, \qquad (4.36)$$

for the shear function ϕ and the boundary conditions as well. We will consider here only the simple support group including the boundary conditions (2.111) or (2.113).

For the first variant of the boundary conditions (when all the edges have a diaphragm inhibiting relative shear)

$$\chi = \Delta\chi = \Delta^2\chi = \frac{\partial\phi}{\partial\alpha_i} = 0 \quad \text{at} \quad \alpha_i = 0, L_i, \quad i = 1, 2, \qquad (4.37)$$

one can set $\phi = 0$. For the second variant (diaphragm is absent at least on the one edge $\alpha_1 = 0$)

$$\left(1 - \frac{h^2}{\beta}\Delta\right)\chi = 0, \quad \frac{\partial^2}{\partial \alpha_1^2}\left(1 - \frac{h^2}{\beta}\Delta\right)\chi = 0,$$

$$\begin{aligned} \left(\frac{\partial^2}{\partial \alpha_1^2} + \nu\frac{\partial^2}{\partial \alpha_2^2}\right)\chi - (1-\nu)\frac{\partial^2 \phi}{\partial \alpha_1 \alpha_2} &= 0, \\ 2\frac{\partial^2 \chi}{\partial \alpha_1 \partial \alpha_2} + \frac{\partial^2 \phi}{\partial \alpha_1^2} - \frac{\partial^2 \phi}{\partial \alpha_2^2} = 0 \quad \text{at} \quad \alpha_1 &= 0 \end{aligned} \tag{4.38}$$

the function ϕ turns out to be coupled to the displacement function χ and should be taken into account when constructing the edge effects.

4.2.1 Simply Supported Plate with Diaphragm on Edges

At first, we will consider variant (4.37) of the boundary conditions. Let all coefficients in Eq. (4.34) be constants, and the shear stress resultant T_{12}° is equal to zero. Then the solution of the linear boundary-value problem (4.34), (4.37) is easily found as

$$\chi = \chi_0 \mathrm{e}^{\mathrm{i}\omega t} \sin\frac{\pi n \alpha_1}{L_1} \sin\frac{\pi m \alpha_2}{L_2}, \tag{4.39}$$

where n, m are numbers of semi-waves in the α_1- and α_2-directions, respectively, ω is the natural frequency, and χ_0 is a constant. The substitution of (4.39) into Eq. (4.34) leads to the following formula for the frequency

$$\omega^2 = \frac{\pi^4 D}{\rho_0 h L_2^4}\Lambda, \tag{4.40}$$

where

$$\begin{aligned} \Lambda &= \frac{\delta_{nm}^2(1 + \theta K \delta_{nm})}{1 + K\delta_{nm}} + t_1^{\circ} e^2 n^2 + t_2^{\circ} m^2 + k_{\mathrm{f}}, \\ K &= \frac{\pi^2 h^2}{\beta L_2^2}, \quad \delta_{nm} = e^2 n^2 + m^2, \quad e = \frac{L_2}{L_1}, \quad t_i^{\circ} = \frac{L_2^2}{\pi^2 D} T_{ii}^{\circ} \end{aligned} \tag{4.41}$$

The equation for k_{f} depends on the accepted model for the elastic foundation. For the Winkler foundation model can be assumed

$$k_{\mathrm{f}} = \frac{L_2^4}{\pi^4 D} c_{\mathrm{f}} \tag{4.42}$$

and for the model represented by Eq. (2.137) one has

$$k_{\mathrm{f}} = \frac{L_2^3 \alpha_{\mathrm{f}}}{\pi^3 D} \delta_{nm}^{1/2}, \tag{4.43}$$

where α_{f} is defined by (4.2).

It is obvious that for large numbers n, m, the Winkler model gives understated natural frequencies when comparing to the model represented by Eq. (2.152). It is also seen that the tensile initial stresses ($T_{ii}^{\circ} > 0$) raise eigenfrequencies and the compressive ones ($T_{ii}^{\circ} < 0$) reduce them. In the last case, the magnitudes $|T_{ii}^{\circ}|$ are to be less of the critical buckling values (s. Chapt. 3). Assuming the shear parameter K to be small, formula (4.41) may be rewritten in the following form

$$\Lambda = \delta_{nm}^2 \left[1 + \delta_{nm}^{-2}(t_1^{\circ} e^2 n^2 + t_2^{\circ} m^2 + k_{\mathrm{f}}) - K(1-\theta)\delta_{nm} + O\left(K^2\right)\right]. \tag{4.44}$$

It shows that ignoring shear results in overstating values for the natural frequencies.

4.2.2 Simply Supported Plate Without Diaphragm on Edges

Now, we consider the combination of the simple support conditions (4.37) and (4.38), herewith, the edges $\alpha_1 = 0, L_1$ (without diaphragm) satisfy conditions (4.38), and the edges $\alpha_2 = 0, L_2$ (with the diaphragm) to Eqs. (4.37). In this case, the boundary-value problem (4.34), (4.36)-(4.38) does not admit the explicit form of a solution. It may be found by using some numerical method. For instance, a solution may be represented by an infinite series of beam functions or by the sine- and cosine-series expansions in α_1 and α_2. But we, assuming the shear parameter K as a small one, will apply to the asymptotic approach and construct a solution for low-frequency vibrations in the form of the superposition of the main stress state and the edges effect integrals. This approach will permit us to obtain a simple asymptotic equation for eigenfrequencies and evaluate the effect of shear inside of the plate and in a neighbourhood of the edges as well.

Consider the case when $T_{ij}^{\circ} = c_{\mathrm{f}} = 0$. Let a parameter

$$\mu^2 = \frac{h^2}{\beta R^2}. \tag{4.45}$$

be small, where R is the characteristic size (one of the lengthes L_1, L_2 or $(L_1 L_2)^{1/2}$). The required functions satisfying (4.37) are south in the form:

$$\chi = R\,X(x_1)\,\sin\frac{\pi m x_2}{l_2}\,\mathrm{e}^{\mathrm{i}\omega t}, \qquad \phi = \mu^{v_1} RS(x_1)\,\cos\frac{\pi m x_2}{l_2}\,\mathrm{e}^{\mathrm{i}\omega t}, \tag{4.46}$$

where $x_i = \alpha_i/R$, $l_i = L_i/R$, $v_1 > 0$, $S, X \sim 1$ at $\mu \to 0$, and ω is the natural frequency.

The substitution of (4.46) into (4.34) and (4.36) yields

$$
\begin{gathered}
-\theta\mu^2\left(\frac{\mathrm{d}^6X}{\mathrm{d}x_1^6}-3\delta_m^2\frac{\mathrm{d}^4X}{\mathrm{d}x_1^4}+3\delta_m^4\frac{\mathrm{d}^2X}{\mathrm{d}x_1^2}-\delta_m^6X\right)\\
+\frac{\mathrm{d}^4X}{\mathrm{d}x_1^4}-2\delta_m^2\frac{\mathrm{d}^2X}{\mathrm{d}x_1^2}+\delta_m^4X-\lambda X+\mu^2\lambda\left(\frac{\mathrm{d}^2X}{\mathrm{d}x_1^2}-\delta_m^2X\right)=0
\end{gathered}
\tag{4.47}
$$

and

$$
\frac{\mathrm{d}^2S}{\mathrm{d}x_1^2}=\left(\frac{1}{\mu^2}\frac{2}{1-\nu}+\delta_m^2\right)S. \tag{4.48}
$$

Here

$$
\delta_m=\frac{\pi m}{l_2},\quad \lambda=\frac{\omega^2}{\omega_c^2},\quad \omega_\mathrm{c}^2=\frac{D}{\rho_0hR^4}, \tag{4.49}
$$

where ω_c is the characteristic frequency. The boundary conditions (4.38) for $X(x_1)$ and $S(x_1)$ on the edges $x_1=0,l_1$ become as follows

$$
X-\mu^2\left(\frac{\mathrm{d}^2X}{\mathrm{d}x_1^2}-\delta_m^2X\right)=0,\quad \frac{\mathrm{d}^2X}{\mathrm{d}x_1^2}-\mu^2\frac{\mathrm{d}^2}{\mathrm{d}x_1^2}\left(\frac{\mathrm{d}^2X}{\mathrm{d}x_1^2}-\delta_m^2X\right)=0 \tag{4.50}
$$

$$
\frac{\mathrm{d}^2X}{\mathrm{d}x_1^2}-\nu\delta_m^2X+\mu^2(1-\nu)\delta_m\frac{\mathrm{d}S}{\mathrm{d}x_1}=0, \tag{4.51}
$$

$$
2\delta_m\frac{\mathrm{d}X}{\mathrm{d}x_1}+\mu^2\left(\frac{\mathrm{d}^2S}{\mathrm{d}x_1^2}+\delta_m^2S\right)=0. \tag{4.52}
$$

Although a parameter θ is small, we assume here that $\theta\sim 1$. Consider Eq. (4.48). It has the following general solution

$$
S(x_1)=c_1\mathrm{e}^{-\frac{1}{\mu}\gamma x_1}+c_2\mathrm{e}^{-\frac{1}{\mu}\gamma(l_1-x_1)}, \tag{4.53}
$$

where c_1,c_2 are constants, and

$$
\gamma=\sqrt{\frac{2}{1-\nu}+\mu^2\delta_m^2}. \tag{4.54}
$$

Function (4.53) is the superposition of the two integrals which specify the shear edge effects near the ends $x_1=0$ and $x_1=l_1$. But apart from these integrals there are another pair of the edge effect integrals which embrace more narrow regions near the plate edges. These integrals are defined from an additional equation which is easily derived from Eq. (4.47). Let $\mathrm{d}z/\mathrm{d}x_1\sim\mu^{-\iota}$, where $\iota>0$. The asymptotic analysis of all summands in Eq. (4.47) gives $\iota=1$, the basic terms leading to the following additional equation

$$
\theta\mu^2\frac{\mathrm{d}^6X}{\mathrm{d}x_1^6}-\frac{\mathrm{d}^4X}{\mathrm{d}x_1^4}=0. \tag{4.55}
$$

It is obvious that only two integrals of this equation have the properties of the edge effect integrals. Their superposition gives the following general solution

$$X^{(e)} = c_3 \mathrm{e}^{-\dfrac{1}{\mu\sqrt{\theta}}x_1} + c_4 \mathrm{e}^{-\dfrac{1}{\mu\sqrt{\theta}}(l_1 - x_1)}, \tag{4.56}$$

where c_3, c_4 are arbitrary constants. It is seen that due to the smallness of θ, function (4.56) decreases faster than integral (4.53).

We seek a solution of the boundary-value problem (4.47), (4.50)-(4.52) in the following form

$$X = X^{(m)}(x_1) + \mu^{\upsilon_2} X^{(e)}(x_1), \quad X^{(m)},\, X^{(e)} \sim 1, \tag{4.57}$$

$$\lambda = \lambda_0 + \mu\lambda_1 + \ldots, \tag{4.58}$$

where $X^{(m)}$ is also expanded into the series

$$X^{(m)} = X_0(x_1) + \mu X_1(x_1) + \ldots \tag{4.59}$$

with functions X_i satisfying the condition $X_i' \sim X_i$. Here and below, the prime $\{'\}$ means the differentiation with respect to x_1.

Let us substitute (4.57) into the boundary conditions (4.51), (4.52) and compare the main terms. Taking into account the estimates $X_i' \sim X_i$, $\left(X^{(e)}\right)' \sim \mu^{-1}X^{(e)}$, $S' \sim \mu^{-1}S$, one gets the indexes of intensity for the functions describing edge effects: $\upsilon_1 = 2$ and $\upsilon_2 = 3$. The substitution of (4.57) - (4.59) into Eq. (4.47) and the boundary conditions (4.50)-(4.52) results in the sequence of the boundary-value problems. Let us consider them step by step.

In the zeroth-order approximation, one has the homogeneous boundary-value problem

$$\mathbf{L}_0 X_0 \equiv \frac{\mathrm{d}^4 X_0}{\mathrm{d}x_1^4} - 2\delta_m^2 \frac{\mathrm{d}^2 X_0}{\mathrm{d}x_1^2} + \delta_m^4 X_0 - \lambda_0 X_0 = 0 \tag{4.60}$$

$$X_0(0) = X_0(l_1) = X_0''(0) = X_0''(l_1) = 0, \tag{4.61}$$

which has the following nontrivial solution

$$X_0 = A\sin\frac{\pi n x_1}{l_1}, \quad \lambda_0 = (\delta_n^2 + \delta_m^2)^2, \quad \delta_n = \frac{\pi n}{l_1}. \tag{4.62}$$

Note that the boundary conditions (4.61) were derived from (4.50).

Keeping in mind the edge integrals (4.53) and solution (4.62), the boundary conditions (4.52) in the zeroth-order approximation results in the following equations

$$2\delta_m X_0' + \frac{2}{1-\nu}\left[c_1 \mathrm{e}^{-\frac{1}{\mu}\sqrt{\frac{2}{1-\nu}}x_1} + c_2 \mathrm{e}^{-\frac{1}{\mu}\sqrt{\frac{2}{1-\nu}}(l_1 - x_1)}\right] = 0 \quad \text{at} \quad x_1 = 0,\, l_1 \tag{4.63}$$

which give the formulae for constants

$$c_1 = -(1-\nu)\delta_n\delta_m A, \quad c_2 = (-1)^{n+1}(1-\nu)\delta_n\delta_m A. \tag{4.64}$$

In the first-order approximation, one gets the nonhomogeneous differential equation

$$\mathbf{L}_0 X_1 = \lambda_1 X_0. \tag{4.65}$$

and the nonhomogeneous boundary conditions at $x_1 = 0,\ l_1$

$$X_1 = 0, \quad X_1'' - \frac{1}{\theta^2}\left[c_3 \mathrm{e}^{-\frac{1}{\mu\sqrt{\theta}}x_1} + c_4 \mathrm{e}^{-\frac{1}{\mu\sqrt{\theta}}(l_1 - x_1)}\right] = 0,$$

$$X_1'' - \nu\delta_m^2 X_1 + \frac{1}{\theta}\left[c_3 \mathrm{e}^{-\frac{1}{\mu\sqrt{\theta}}x_1} + c_4 \mathrm{e}^{-\frac{1}{\mu\sqrt{\theta}}(l_1 - x_1)}\right]$$

$$-(1-\nu)\delta_m \frac{2}{1-\nu}\left[c_1 \mathrm{e}^{-\frac{1}{\mu}\sqrt{\frac{2}{1-\nu}}x_1} + c_2 \mathrm{e}^{-\frac{1}{\mu}\sqrt{\frac{2}{1-\nu}}(l_1 - x_1)}\right] = 0. \tag{4.66}$$

Taking Eqs. (4.64) into account, the last two conditions (4.66) written at $x_1 = 0, l_1$ result in the equations for constants

$$c_3 = -\frac{\sqrt{2(1-\nu)^3}\theta^2\delta_n\delta_m^2 A}{1+\theta}, \quad c_4 = \frac{(-1)^n\sqrt{2(1-\nu)^3}\theta^2\delta_n\delta_m^2 A}{1+\theta}. \tag{4.67}$$

Then the first two equations from (4.66) give the nonhomogeneous boundary conditions for X_1

$$\begin{aligned} &X_1(0) = X_1(l_1) = 0, \\ &X_1''(0) = -\frac{\sqrt{2(1-\nu)^3}\,\delta_n\delta_m^2 A}{1+\theta}, \\ &X_1''(l_1) = \frac{(-1)^n\sqrt{2(1-\nu)^3}\,\delta_n\delta_m^2 A}{1+\theta}. \end{aligned} \tag{4.68}$$

Problem (4.65), (4.68) is the nonhomogeneous boundary-value problem *on spectrum*. The existence condition for a solution of this problem produces the following formula for the correction λ_1

$$\lambda_1 = -\frac{4\sqrt{2(1-\nu)^3}\,\delta_n^2\delta_m^2}{l_1(1+\theta)}. \tag{4.69}$$

Then the solution of the boundary-value problem (4.65), (4.68) will be the following

$$\begin{aligned} X_1(x_1) &= a_1\sin\delta_n x_1 + a_2\cos\delta_n x_1 + a_3\mathrm{e}^{r_{mn}x_1} + a_4\mathrm{e}^{-r_{mn}x_1} \\ &+\frac{\lambda_1 A}{4\delta_n(\delta_n^2+\delta_m^2)}x_1\,\cos\delta_1 x_1, \end{aligned} \tag{4.70}$$

where $r_{mn} = \sqrt{2\delta_m^2 + \delta_m^2}$, and constants a_i are determined from the boundary conditions (4.68).

Let the characteristic size R be equal L_2. Then, when breaking the procedure of seeking the functions X_i and parameters λ_i, the approximate equation for natural frequencies may be represented as

$$\omega^2 = \frac{D\pi^4}{\rho_0 h L_2^4}\Lambda, \quad \Lambda = \delta_{nm}^2 \left\{ 1 - \mu \frac{4\sqrt{2(1-\nu)^3}\delta_n^2\delta_m^2}{e(1+\theta)\pi^4\delta_{nm}^2} + O(\mu^2) \right\}, \tag{4.71}$$

where δ_{nm}, e are determined by Eqs. (4.41). We note that the small parameter is proportional to the shear one (s. Eqs. (4.41) and (4.45)): $\mu^2 = K/\pi^2$. Then the asymptotic formula for the dimensionless frequency parameter Λ may be rewritten as

$$\Lambda = \delta_{nm}^2 \left\{ 1 - K^{1/2} \frac{4\sqrt{2(1-\nu)^3}\ n^2 m^2}{\pi e^3 (1+\theta)\delta_{nm}^2} + O(K) \right\} \tag{4.72}$$

One can compare it with the analogous Eq. (4.44). In Eq. (4.72), the shear induced correction generated by the edge effects has the order $K^{1/2}$, whereas the similar correction for simply supported plates with diaphragm, s. Eq. (4.44), is a value of the order K. Thus, when comparing these two cases, one can conclude: if the plate edges are free of diaphragm, then the eigenmodes contain additional components accounting the edge shear and called the edge effect integrals, these integrals may give more lower eigenfrequencies than transverse shear within the plate.

4.3 Simplest Problems on Free Vibrations of Thin Cylindrical Shells

In this section we will consider the class of the simplest boundary-value problems describing free linear vibrations of elastic laminated cylindrical shells. In all problems, the geometrical and physical parameters of layers and a shell in whole are assumed to be constants so that any natural mode defines a system of waves distributed evenly over the shell surface. The objective is to study the influence of different boundary conditions and shear as well on the natural frequencies and corresponding eigenmodes.

Let us consider a thin laminated cylindrical shell composed of N transversally isotropic elastic layers. Studying free vibrations, we assume $q_i = q_{\mathrm{n}} = 0$ in the governing equations (2.61)-(2.63). For linear vibrations, the required functions may be represented in the form

$$\{\hat{u}_i, \psi_i, w\} = R\,\{U_i(\alpha_1,\alpha_2), \Psi_i(\alpha_1,\alpha_2), W(\alpha_1,\alpha_2)\} \exp{(\mathrm{i}\omega t)}, \tag{4.73}$$

where $i = 1, 2$, ω is the natural frequency, and R is the characteristic dimension of the shell. We substitute (4.73) into Eqs. (2.61)-(2.63) and omit nonlinear terms. As a result, one obtains the following linear differential equations

$$
\begin{aligned}
&\frac{\partial^2 U_1}{\partial \alpha_1^2} + \frac{1-\nu}{2}\frac{\partial^2 U_1}{\partial \alpha_2^2} + \frac{1+\nu}{2}\frac{\partial^2 U_2}{\partial \alpha_1 \partial \alpha_2} + \nu k_{22}\frac{\partial W}{\partial \alpha_1} + \frac{\rho_0 \omega^2}{\tilde{E}} U_1 = 0,\\
&\frac{1+\nu}{2}\frac{\partial^2 U_1}{\partial \alpha_1 \partial \alpha_2} + \frac{1-\nu}{2}\frac{\partial^2 U_2}{\partial \alpha_1^2} + \frac{\partial^2 U_2}{\partial \alpha_2^2} + \frac{\partial (k_{22} W)}{\partial \alpha_2} + \frac{\rho_0 \omega^2}{\tilde{E}} U_2 = 0,\\
&\eta_2 \frac{\partial (\triangle W)}{\partial \alpha_1} - \eta_1 \left(\frac{\partial^2 \Psi_1}{\partial \alpha_1^2} + \frac{1+\nu}{2}\frac{\partial^2 \Psi_2}{\partial \alpha_1 \partial \alpha_2} + \frac{1-\nu}{2}\frac{\partial^2 \Psi_1}{\partial \alpha_2^2} \right) + \frac{12 q_{44}}{\tilde{E} h^3} \Psi_1 = 0,\\
&\eta_2 \frac{\partial (\triangle W)}{\partial \alpha_2} - \eta_1 \left(\frac{\partial^2 \Psi_2}{\partial \alpha_2^2} + \frac{1+\nu}{2}\frac{\partial^2 \Psi_1}{\partial \alpha_1 \partial \alpha_2} + \frac{1-\nu}{2}\frac{\partial^2 \Psi_2}{\partial \alpha_1^2} \right) + \frac{12 q_{44}}{\tilde{E} h^3} \Psi_2 = 0,\\
&\frac{h^2}{12} \triangle \left[\eta_3 \triangle W - \eta_2 \left(\frac{\partial \Psi_1}{\partial \alpha_1} + \frac{\partial \Psi_2}{\partial \alpha_2} \right) \right]\\
&+ k_{22} \left(\nu \frac{\partial U_1}{\partial \alpha_1} + \frac{\partial U_2}{\partial \alpha_2} + k_{22} W \right) - \frac{\rho_0 \omega^2}{\tilde{E}} W = 0
\end{aligned}
\tag{4.74}
$$

with $\tilde{E} = E/(1-\nu^2)$. The system of differential equations (4.74) may be used to study free vibrations of a shell of any length for any number of waves in the axial and circumferential directions. However, they turn out to be too inconvenient and cumbersome in the common case. The selection of governing equations depends on the class of problems under consideration. So, the above equations (4.74) may be used for studying free vibrations of a very long cylindrical shell with formation of long waves. However, to analyze vibrations with a large number of minor waves although in the one direction, it is more convenient to apply to the simplified equations of the technical shell theory (2.77), (2.85), (2.87).

Let us now apply to the variant of the technical shell theory. Assuming

$$
\chi = \tilde{\chi}(\alpha_1, \alpha_2) \mathrm{e}^{\mathrm{i}\omega t}, \quad F = \tilde{F}(\alpha_1, \alpha_2) \mathrm{e}^{\mathrm{i}\omega t}, \quad \phi = \tilde{\phi}(\alpha_1, \alpha_2) \mathrm{e}^{\mathrm{i}\omega t}, \tag{4.75}
$$

Eqs. (2.77), (2.85), (2.87) are reduced to the following ones

$$
\begin{aligned}
&D \left(1 - \frac{\theta h^2}{\beta} \triangle \right) \triangle^2 \tilde{\chi} + k_{22} \frac{\partial^2 \tilde{F}}{\partial \alpha_1^2} - \rho_0 h \omega^2 \left(1 - \frac{h^2}{\beta} \triangle \right) \tilde{\chi} = 0,\\
&\triangle^2 \tilde{F} - E h k_{22} \frac{\partial^2}{\partial \alpha_1^2} \left(1 - \frac{h^2}{\beta} \triangle \right) \tilde{\chi} = 0, \qquad \frac{1-\nu}{2} \frac{h^2}{\beta} \triangle \tilde{\phi} = \tilde{\phi}.
\end{aligned}
\tag{4.76}
$$

The systems of differential equations (4.74) and (4.76) should be supplemented by the boundary conditions (2.93)-(2.108) and (2.110)-(2.118), respectively. The classification of integrals for governing equations analogous to (4.74) as well as their detailed analysis for thin isotropic single-layer shells may be found in Gol'denveizer et al (1979); Mikhasev and Tovstik (2009).

4.3.1 Long Simply Supported Cylinder with Diaphragm on Edges

Let a lengthy cylindrical shell be circular, then $k_{22} = 1/R$ is a constant. From all variants of the boundary conditions, we consider here the simply supported edges with diaphragm. In terms of displacements and stress resultants these conditions are the following (s. Chapt. 2)

$$w = \hat{u}_2 = \psi_2 = \hat{M}_{11} = T_{11} = \hat{L}_{11} = 0 \quad \text{at} \quad \alpha_1 = 0, L. \tag{4.77}$$

Keeping in mind (4.73), we rewrite them in the terms of displacements

$$\begin{gathered}
W = U_2 = \Psi_2 = 0, \\
\eta_3 \left(\frac{\partial^2 W}{\partial \alpha_1^2} + \nu \frac{\partial^2 W}{\partial \alpha_2^2} \right) - \eta_2 \left(\frac{\partial \Psi_1}{\partial \alpha_1} + \nu \frac{\partial \Psi_2}{\partial \alpha_2} \right) = 0, \\
\frac{\partial U_1}{\partial \alpha_1} + \nu \frac{\partial U_2}{\partial \alpha_2} + \frac{\nu W}{R} = 0, \\
\eta_2 \left(\frac{\partial^2 W}{\partial \alpha_1^2} + \nu \frac{\partial^2 W}{\partial \alpha_2^2} \right) - \eta_1 \left(\frac{\partial \Psi_1}{\partial \alpha_1} + \nu \frac{\partial \Psi_2}{\partial \alpha_2} \right) = 0 \quad \text{at} \quad \alpha_1 = 0, L.
\end{gathered} \tag{4.78}$$

As seen, the above boundary conditions are satisfied by the following functions

$$\begin{aligned}
U_1 &= U_1^\circ \cos \frac{\pi n \alpha_1}{L} \cos \frac{m \alpha_2}{R}, \\
U_2 &= U_2^\circ \sin \frac{\pi n \alpha_1}{L} \sin \frac{m \alpha_2}{R}, \\
W &= W^\circ \sin \frac{\pi n \alpha_1}{L} \cos \frac{m \alpha_2}{R}, \\
\Psi_1 &= \Psi_1^\circ \cos \frac{\pi n \alpha_1}{L} \cos \frac{m \alpha_2}{R}, \\
\Psi_2 &= \Psi_2^\circ \sin \frac{\pi n \alpha_1}{L} \sin \frac{m \alpha_2}{R},
\end{aligned} \tag{4.79}$$

where n is a number of semi-waves in the axial direction, m is a number of waves in the circumferential direction, and $U_i^\circ, W^\circ, \Psi_i^\circ$ are constant values.

The substitution of (4.79) into Eqs. (4.74) yields the system of algebraic equations

$$\mathbf{A}\mathbf{X}^{\mathrm{T}} = 0, \tag{4.80}$$

where $\mathbf{X} = (U_1^\circ, U_2^\circ, W^\circ, \Psi_1^\circ, \Psi_2^\circ)$ is the vector, and $\mathbf{A}$ is the 5×5 matrix with the elements a_{ij}

$$\begin{aligned}
&a_{11} = -\delta_n^2 - \frac{1-\nu}{2} m^2 + (1-\nu^2) \frac{\omega^2}{\omega_0^2}, \qquad a_{12} = \frac{1+\nu}{2} \delta_n m, \\
&a_{13} = \nu \delta_n, \quad a_{14} = a_{15} = 0, \quad a_{21} = \frac{1+\nu}{2} \delta_n m,
\end{aligned}$$

$$
\begin{aligned}
&a_{22} = -\frac{1-\nu}{2}\delta_n^2 - m^2 + (1-\nu^2)\frac{\omega^2}{\omega_0^2}, \quad a_{23} = -m, \quad a_{24} = a_{25} = 0,\\
&a_{31} = a_{32} = 0, \quad a_{33} = -\eta_2\delta_n(\delta_n^2 + m^2),\\
&a_{34} = \eta_1\left(\delta_n^2 + \frac{1-\nu}{2}m^2\right) + \frac{q_{44}R^2\eta_3}{D},\\
&a_{35} = -\frac{\eta_1(1+\nu)}{2}\delta_n m, \quad a_{41} = a_{42} = 0, \quad a_{43} = -\eta_2 m(\delta_n^2 + m^2),
\end{aligned}
$$

$$
\begin{aligned}
&a_{44} = -\frac{\eta_1(1+\nu)}{2}\delta_n m, \quad a_{45} = \eta_1\left(m^2 + \frac{1-\nu}{2}\delta_n^2\right) + \frac{q_{44}R^2\eta_3}{D},\\
&a_{51} = -\frac{\nu}{1-\nu^2}\delta_n, \quad a_{52} = \frac{m}{1-\nu^2},\\
&a_{53} = \varepsilon^8(\delta_n^2 + m^2)^2 + \frac{1}{1-\nu^2} - \frac{\omega^2}{\omega_0^2},\\
&a_{54} = -\frac{\varepsilon^8\eta_2\delta_n}{\eta_3}(\delta_n^2 + m^2), \quad a_{55} = \frac{\varepsilon^8\eta_2 m}{\eta_3}(\delta_n^2 + m^2),
\end{aligned}
\tag{4.81}
$$

where

$$
\delta_n = \frac{\pi n}{l}, \quad l = \frac{L}{R}, \quad \varepsilon^8 = \frac{h^2\eta_3}{12(1-\nu^2)R^2}, \quad \omega_0^2 = \frac{E}{\rho_0 R^2}. \tag{4.82}
$$

Here, ε is a small parameter and ω_0 is the characteristic frequency.

The equation

$$
\det \mathbf{A} = 0 \tag{4.83}
$$

serves as the existence condition of a nontrivial solution of the homogeneous system (4.80). In the general case, it is the cubic equation with respect to the required frequency parameter $\Lambda = (1-\nu^2)\omega^2\omega_0^{-2}$. It will be used below in Chapt. 5 to study free vibrations of viscoelastic laminated shells containing MRE. As a particular case, we consider the axisymmetric vibrations for which $m = U_2^\circ = \Psi_2^\circ = 0$. Then, the cubic equation (4.83) degenerates into the quadratic one:

$$
\Lambda^2 - \left(1 + \delta_n^2 + \mu_1\delta_n^4 r_n\right)\Lambda + \delta_n^2\left(1 - \nu^2 + \mu_1\delta_n^4 r_n\right) = 0, \tag{4.84}
$$

where

$$
\mu_1 = (1-\nu^2)\varepsilon^8, \quad r_n = \frac{\pi^2 + \theta K\delta_n^2}{\pi^2 + K\delta_n^2}, \quad K = \frac{\pi^2 h^2}{\beta R^2}, \quad \theta = 1 - \frac{\eta_2^2}{\eta_1\eta_3}. \tag{4.85}
$$

For any fixed number n, there are two the positive roots

$$
\Lambda = \Lambda_j = \frac{1}{2}\left\{1 + \delta_n^2 + \mu_1\delta_n^4 r_n - (-1)^j\left[(1 - \delta_n^2 + \mu_1\delta_n^4 r_n)^2 + 4\nu^2\delta_n^2\right]^{1/2}\right\}, \tag{4.86}
$$

where $j = 1, 2$. Then the natural frequencies corresponding to the axially symmetric longitudinal and bending vibrations accounting transverse shear are defined as

$$\omega_j = \sqrt{\frac{E\Lambda_j}{\rho_0 R^2(1-\nu^2)}},$$

where ω_1 is the eigenfrequency of predominantly longitudinal vibrations, and ω_2 relates to bending vibrations. It is obviously, for the fixed n, $\omega_1 > \omega_2$.

The amplitudes of axial, normal and shear displacements are coupled by means of equations

$$U_1^\circ = -\frac{\nu\delta_n}{\Lambda - \delta_n^2}W^\circ, \quad \Psi_1^\circ = \frac{\eta_2 K\delta_n^3}{\eta_1(\pi^2 + K\delta_n^2)}W^\circ. \tag{4.87}$$

As seen from Eq. (4.86), $\Lambda_j - \delta_n^2 \neq 0$ for any n. When $K \to 0$, Eq. (4.86) gives the frequency parameter for an isotropic shell without taking into account shears. Because a parameter θ is small, it may be concluded that the incorporation of the shear parameter K into the shell model results in the reduction of the natural frequencies for any δ_n, the influence of the shear parameter K on eigenfrequencies being very weak for modes with small parameter δ_n and becoming essential at large δ_n and, particularly, for modes of bending vibrations with very large number of waves n in the axial direction (and/or for a very short cylindrical shell). This conclusion is confirmed by calculations performed at $m = 0, \nu = 0.4, \varepsilon = 0.2$. Figure 4.1 shows the parameters Λ_1 and Λ_2 corresponding to the axially symmetric longitudinal and bending vibrations, respectively, versus a wave parameter δ_n. Figure 4.2 demonstrates the behavior of the frequency parameter Λ_2 corresponding the bending modes as the function of δ_n for different values of K varying from 0 to 0.6. It is seen, the larger value of δ_n is, the higher effect of the shear parameter on eigenfrequencies of flexural vibrations becomes. Similar computations of the parameter Λ_1 corresponding to the longitudinal modes show that this effect is negligibly small. For instance, curves Λ_1 versus δ_n presented in Fig. 4.1 practically merge in the range of variation of δ_n form 0 to 40.

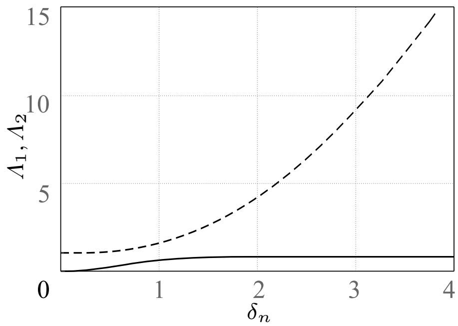

Fig. 4.1 Frequency parameters Λ_1 (dotted line) and Λ_2 (solid line) vs. parameter δ_n at $K = 0$.

Fig. 4.2 Frequency parameter Λ_2 vs. δ_n at different values of K: 1 - $K = 0, 2$ - $K = 0.02$, 3 - $K = 0.2$, 4 - $K = 0.4$, 5 - $K = 0.6$.

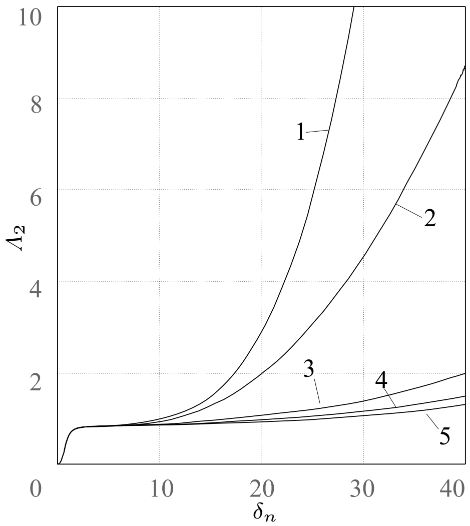

4.3.2 Medium-length Cylindrical Shells with Simply Supported Edges

In this subsection, we consider a medium-length cylindrical shell with simply-supported edges with and without diaphragm. The boundary conditions written in terms of the displacement and stress functions are the following:

- for the edges $\alpha_1 = 0, \alpha_1 = L$ with diaphragm (SSD boundary conditions)

$$\tilde{\chi} = \Delta\tilde{\chi} = \Delta^2\tilde{\chi} = \frac{\partial\tilde{\phi}}{\partial\alpha_1} = 0, \quad \frac{\partial^2\tilde{F}}{\partial\alpha_2^2} = 0, \quad \frac{\partial^2\tilde{F}}{\partial\alpha_1^2} = 0, \tag{4.88}$$

- for the edges without diaphragm (SSF boundary conditions)

$$\begin{gathered}\left(1 - \frac{h^2}{\beta}\Delta\right)\tilde{\chi} = 0, \quad \frac{\partial^2}{\partial\alpha_1^2}\left(1 - \frac{h^2}{\beta}\Delta\right)\tilde{\chi} = 0,\\ \left(\frac{\partial^2}{\partial\alpha_1^2} + \nu\frac{\partial^2}{\partial\alpha_2^2}\right)\tilde{\chi} - (1-\nu)\frac{\partial^2\tilde{\phi}}{\partial\alpha_1\alpha_2} = 0,\\ 2\frac{\partial^2\tilde{\chi}}{\partial\alpha_1\partial\alpha_2} + \frac{\partial^2\tilde{\phi}}{\partial\alpha_1^2} - \frac{\partial^2\tilde{\phi}}{\partial\alpha_2^2} = 0,\end{gathered} \tag{4.89}$$

$$\frac{\partial^2\tilde{F}}{\partial\alpha_2^2} = 0, \quad \frac{\partial^2\tilde{F}}{\partial\alpha_1\alpha_2} = 0. \tag{4.90}$$

4.3.2.1 Shell with Diaphragm on Edges: Solution in the Explicit Form

Variant (4.88) of the boundary conditions allows to write down a solution of Eqs. (4.76) in the explicit form

$$\tilde{\chi} = \chi_0\, sin\frac{\pi n \alpha_1}{L} sin\frac{m\alpha_2}{R}, \quad \tilde{F} = F_0\, sin\frac{\pi n \alpha_1}{L} sin\frac{m\alpha_2}{R}, \tag{4.91}$$

where n, m are positive integers. Inserting (4.92) into Eqs. (4.76) gives

$$\omega^2 = \frac{\varepsilon^8 \pi^4 E \varDelta_{nm}}{R^2 \rho_0}, \tag{4.92}$$

where

$$\begin{aligned} \varDelta_{nm} &= \left(\frac{1+\theta K \delta_{nm}}{1+K\delta_{nm}}\right)\delta_{nm}^2 + \frac{n^4}{l^4\pi^4\varepsilon^8\delta_{nm}^2}, \qquad K = \frac{\pi^2 h^2}{\beta R^2}, \\ \delta_{nm} &= \left(\frac{n^2}{l^2} + \frac{m^2}{\pi^2}\right), \qquad l = \frac{L}{R}. \end{aligned} \tag{4.93}$$

As seen from Eqs. (4.92), (4.93), the effect of the shear parameter K on the natural frequencies remains the same as for the laminated plates (s. Subsect. 4.1.2): the transverse shears leads to some reduction of all natural frequencies when compare them with eigenfrequencies at $K = 0$.

4.3.2.2 Shell without Diaphragm on Edges: Asymptotic Solution

Consider the boundary conditions (4.89), (4.90) corresponding to the case when diaphragm at both edges are absent. The boundary-value problem (4.76), (4.89), (4.90) does not admit the explicit form of a solution, but this problem on low-frequency vibrations is identical to the boundary-value problem on buckling of a medium-length cylindrical shell under external pressure considered in Subsubsect. 3.2.1.3 (s. Chapt. 3) and may be solved by the same asymptotic approach.

As in Subsubsect. 3.2.1.3, we assume that $G \sim h_*^{3/2} E$. Then $K/\pi^2 = \varepsilon^2 \kappa$, where $\kappa \sim 1$. Intending to study low-frequency vibrations, we seek the required functions $\tilde{\chi}, \tilde{F}, \tilde{\phi}$ in the form of

$$\begin{aligned} \tilde{\chi} &= RX(x)\sin\left(\varepsilon^{-1}p\varphi\right), \\ \tilde{F} &= \varepsilon^4 EhR^2 \varPhi(x)\sin\left(\varepsilon^{-1}p\varphi\right), \\ \tilde{\phi} &= RS(x)\cos\left(\varepsilon^{-1}p\varphi\right), \end{aligned} \tag{4.94}$$

where $p \sim 1$, $x = \alpha_1/R, \varphi = \alpha_2/R$. Then the governing equations (4.76) are rewritten as follows

$$\begin{aligned} \varepsilon^4(1-\varepsilon^2\kappa\theta\varDelta_\varepsilon)\varDelta_\varepsilon^2 X + \frac{\mathrm{d}^2\varPhi}{\mathrm{d}x^2} - \varLambda(1-\varepsilon^2\kappa\varDelta_\varepsilon)X &= 0, \\ \varepsilon^4\varDelta_\varepsilon^2\varPhi - \frac{\mathrm{d}^2}{\mathrm{d}x^2}(1-\varepsilon^2\kappa\varDelta_\varepsilon)X &= 0, \end{aligned} \tag{4.95}$$

$$\frac{1-\nu}{2}\kappa_1\varepsilon^2\varDelta_\varepsilon S = S, \tag{4.96}$$

where

$$\varLambda = \frac{\rho_0 R^2\omega^2}{\varepsilon^4 E}, \quad \varDelta_\varepsilon = \frac{\mathrm{d}^2}{\mathrm{d}x^2} - \varepsilon^{-2}p^2,$$

and the boundary conditions (4.89), (4.90) at $x = 0, l$ take the form

$$\begin{aligned} (1-\varepsilon^2\kappa_1\varDelta_\varepsilon)X = 0, \quad \frac{\mathrm{d}^2}{\mathrm{d}x^2}(1-\varepsilon^2\kappa_1\varDelta_\varepsilon)X &= 0, \\ \left(\varepsilon^2\frac{\mathrm{d}^2}{\mathrm{d}x^2} - \nu p^2\right)X + \varepsilon(1-\nu)p\frac{\mathrm{d}S}{\mathrm{d}x} &= 0, \\ 2\varepsilon p\frac{\mathrm{d}X}{\mathrm{d}x} + \varepsilon^2\frac{\mathrm{d}^2 S}{\mathrm{d}x^2} + p^2 S &= 0, \\ \varPhi = 0, \qquad \frac{\mathrm{d}\varPhi}{\mathrm{d}x} &= 0. \end{aligned} \tag{4.97}$$

Omitting details for construction of the asymptotic solution of the boundary-value problem (4.95)-(4.97), we outline here only the resultant equations. The shear function S is defined as

$$S = \varepsilon\left\{a_1\exp\left(-\frac{\vartheta_\mathrm{s}x}{\varepsilon}\right) + a_2\exp\left[-\frac{\vartheta_\mathrm{s}(l-x)}{\varepsilon}\right]\right\}, \tag{4.98}$$

where

$$\vartheta_\mathrm{s} = \sqrt{\frac{2}{(1-\nu)\kappa_1} + p^2}, \quad a_1 = -\frac{2\pi npA}{l\left(p^2+\vartheta_\mathrm{s}^2\right)}, \quad a_2 = (-1)^n a_1. \tag{4.99}$$

The displacement and stress functions $X, \varPhi$ and eigenvalue $\varLambda$ as well are evaluated as

$$\begin{aligned} X = X^{(\mathrm{m})} + X^{(\mathrm{e})}, &\quad \varPhi = \varPhi^{(\mathrm{m})} + \varPhi^{(\mathrm{e})}, \\ X^{(\mathrm{m})} = X_0 + \varepsilon X_1 + O\left(\varepsilon^2\right), &\quad \varPhi^{(\mathrm{m})} = \varPhi_0 + \varepsilon\varPhi_1 + O\left(\varepsilon^2\right), \end{aligned} \tag{4.100}$$

$$\varLambda = \varLambda_0 + \varepsilon\varLambda_1 + O\left(\varepsilon^2\right), \tag{4.101}$$

where the superscript (m) denotes functions corresponding to the main stress-strain state with the zeroth index of variation $\iota_1 = 0$ in the axial direction, and functions with the superscript (e) are the integrals of edge effects. All the required functions are determined by the following equations

$$
\begin{aligned}
X_0 &= A\sin\frac{\pi n x}{l}, \quad X_1 = -\frac{\Lambda_1 p^6 l^3 A}{4\pi^3 n^3}\, x\, \cos\frac{\pi n x}{l}, \\
X^{(\mathrm{e})} &= \varepsilon\left[b_1 \mathrm{e}^{-\dfrac{r_1}{\varepsilon}\, x} + b_2 \mathrm{e}^{-\dfrac{r_1}{\varepsilon}\,(l-x)} + O(\varepsilon)\right], \\
\Phi_j &= \frac{1+\kappa p^2}{p^4}\frac{\mathrm{d}^2 X_j}{\mathrm{d}x^2}, \quad \Phi^{(\mathrm{e})} = \frac{\kappa_1}{\varepsilon^2} X^{(\mathrm{e})}, \\
b_1 &= -\frac{2\pi n(1-\nu)\vartheta_{\mathrm{s}} p^2 A}{l r_1^2\left[1+(1-\nu)p^2\kappa_1\right]\left[p^2+\vartheta_{\mathrm{s}}^2\right]}, \quad b_2 = (-1)^n b_1,
\end{aligned}
\tag{4.102}
$$

and the frequency parameters Λ_0, Λ_1 are the following:

$$
\begin{aligned}
\Lambda_0(p;n) &= \frac{\pi^4 n^4}{l^4 p^4} + \frac{p^4(1+\theta\kappa p^2)}{1+\kappa p^2}, \\
\Lambda_1(p;n) &= \frac{8(-1)^{(n+1)}\pi^4 n^3 (1-\nu)\kappa_1 \vartheta_{\mathrm{s}}}{l^5 p^2\left[1+(1-\nu)p^2\kappa_1\right](p^2+\vartheta_{\mathrm{s}}^2)},
\end{aligned}
\tag{4.103}
$$

where n is a number of semi-waves in the axial direction of the shell, and $\kappa_1 \equiv \kappa$ is the shear parameter.

Contrary to the problem on buckling of a shell studied in Subsubsect. 3.2.1.3, there here is no need to minimize $\Lambda_0(p;n)$ over a parameter p and a number n. The only requirement for a parameter p is the following: it has to be of the order of the unit ($p \sim 1$) and chosen in such a way that $m = \varepsilon^{-1}p$ is a natural number. When minimizing $\Lambda_0(p;n)$ over p at fixed n, we obtain the eigenvalue

$$
\Lambda_0^\circ = \min_p \Lambda_0(p;n) = \Lambda_0(p^\circ;n) \tag{4.104}
$$

and its correction $\Lambda_1^\circ = \Lambda_1(p^\circ;n)$ corresponding to eigenfrequencies from the lowest part of spectrum at $n \sim 1$.

Finally, one can write out the asymptotic formula for the natural frequencies

$$
\omega^\circ = \varepsilon^2\sqrt{\frac{E\Lambda_0^\circ}{R^2\rho_0}}\left[1+\varepsilon k_s + O\left(\varepsilon^2\right)\right], \quad k_s = \frac{\Lambda_1^\circ}{2\Lambda_0^\circ}. \tag{4.105}
$$

It is necessary to distinguish the effect of parameters κ and κ_1 on eigenfrequencies. A parameter κ shows the total influence of the transverse shears on the main stress-state of a shell and the zeroth approximation for natural frequencies as well; as seen from (4.103), it reduces all frequencies when comparing them with ones obtained on the base of the model ignoring shears. And a parameter κ_1 gives the impact of shears generated only by boundary conditions and the edge effect integrals; its influence has a local character and depend on a number of semi-waves in the axial direction. If n is an odd number, then $\varepsilon\Lambda_1$ gives the positive correction for Λ_0, and this correction becomes negative for even n. It should be noted that the natural modes constructed above do not contain the classical (simple) edge effect integrals with the index of variation $\iota_1 = 1/2$, but they comprise the edge effect integrals (see above the functions $S(x)$ and $X^{(e)}(x)$) with the smaller index of variation, $\iota_1 = 1/4$.

It is of interesting to compare formula (4.105) with Eqs. (4.92), (4.93) predicting eigenfrequencies for a medium-length cylinder with the simply supported edges supplied with diaphragms. We assume $n = 1, m = \varepsilon^{-1}p^\circ$, then Eqs. (4.92), (4.93) give the following asymptotic formulas

$$\omega^* = \varepsilon^2 \sqrt{\frac{E\Lambda_0^\circ}{R^2\rho_0}}[1 + \varepsilon^2 k_s^* + O(\varepsilon^4)], \quad k_s^* = \frac{\Lambda_2^*}{2\Lambda_0^\circ}, \tag{4.106}$$

where Λ_2^* is calculated by

$$\Lambda_2^* = \frac{2\pi^2 n^2 p^2 + 3\pi^2\theta\kappa n^2 p^4}{l^2(1+\kappa p^2)} - \frac{\pi^2 n^2 p^4}{l^2(1+\kappa p^2)^2} - \frac{2\pi^6 n^6}{l^6 p^6}$$

at $p = p^\circ$. It is seen that (4.105) and (4.106) coincide only in the zeroth approximation, and the next approximations give corrections of different orders. In (4.105), the first correction of an order $O(\varepsilon)$ is generated by the non-classical edge effects, whereas the first correction in (4.106) is more less and not related to any edge effects.

Example 4.2. As an example, we consider the five-layered cylindrical shell of the radius and length $R = L = 0.9$ m assembled from laminas which are made of different materials:

- the first (innermost) layer (thickness $h_1 = 0.5$ mm) is the ABS-plastic SD-0170,
- the fifth (outermost) layer (thickness $h_5 = 0.5$ mm) is made of silicon nitrate (ceramic),
- the second and fourth layers are of the same thicknesses $h_2 = h_4 = 3.0$ mm and made of epoxy,
- the third soft layer of the thickness h_3 is alloy-foam.

All materials are assumed as elastic ones with properties given in Example 3.7 (s. Chapt. 3). Table 4.3 shows the influence of the soft alloy-foam core on the parameters m^*, m°, p° and the lowest frequencies ω^*, ω° for the SSD and SSF boundary conditions. Here, ω^* is calculated by (4.92), (4.93) which may be rewritten as

Table 4.3 Wave numbers m^*, m°, parameters p°, $\Lambda_0^\circ, \Lambda_1^\circ$ and the lowest frequencies ω^*, ω° for the 5-layered cylindrical shell for the two variants of boundary conditions (SSD, SSF) vs. thickness h_3 of the alloy-foam core.

h_3, mm	m^*	ω^*, Hz	p°	m°	Λ_0°	Λ_1°	ω°, Hz
20	6	634	1.84	6	17.82	0.42	628
25	5	614	1.87	6	16.99	0.63	611
30	5	593	1.90	6	16.19	0.80	596
35	5	577	1.94	6	15.46	0.92	582
38	5	569	1.96	6	15.07	0.97	576

$$\omega^* = \frac{\varepsilon^4\pi^2}{K}\sqrt{\frac{E}{\rho_0}\,\varDelta^*_{nm}}, \quad \varDelta^*_{nm} = \min_{n,m}\varDelta_{nm}(n,m) = \varDelta_{nm}(1,m^*).$$

The increase of the soft core thickness h_3 (at fixed thicknesses of other layers) results in the decrease of the first natural frequency for both variants of boundary conditions. This effect is explained by some reduction of the reduced Young's modulus with increasing h_3. Also, the correction $\varepsilon\varLambda_1^\circ$ generated by the edge shears turns out to be small, although it increases together with h_3. When comparing results for different boundary conditions, one can conclude: overlapping diaphragm on the edges increases the lowest eigenfrequency.

4.4 Free Low-frequency Localized Vibrations of Medium-length Cylindrical Shells

In this section, we will study free vibrations of elastic, medium-length, non-circular cylindrical shells or panels. It is assumed that the Young's and shear moduli are also functions of the circumferential coordinate. As follows from study (Mikhasev et al, 2014), similar inhomogeneity of physical properties takes place if a laminated shell is assembled from highly polarized MREs and/or placed in magnetic field. It has been also shown (Mikhasev et al, 2014), that the eigenmodes of MRE-based sandwich shells are very affected by applied magnetic field and may be characterized by strong localization in some area on the shell surface. Here, using the asymptotic Tovstik's method (Tovstik, 1983) stated in Subsect. 3.2.2, we will give the formal construction of these modes and find the corresponding natural frequencies. We note that the problem will be considered in the elastic statement, and viscoelastic properties of layers composing the shell will not be taken into account. The effect of viscoelastic properties of MREs on both free and forced vibrations will be studied in detail in the next chapter.

Let us introduce the dimensionless magnitudes by the following equations

$$\begin{aligned} &\alpha_1 = Rs, \quad \alpha_2 = R\varphi, \quad R_2 = \frac{R}{k_2(\varphi)}, \\ &\tilde{\chi} = R\chi_*, \quad \tilde{F} = \varepsilon^4 E^\circ h R^2 \varPhi_*, \quad \varLambda = \frac{\rho R^2\omega^2}{\varepsilon^4 E^\circ}, \end{aligned} \tag{4.107}$$

where E° is the characteristic value of the Young's modulus. We make also the following assumptions for the elastic modulus and shear parameter as well

$$E = E^\circ d(\varphi) = E^\circ[1+\varepsilon d_1(\varphi)], \quad \frac{K}{\pi^2} = \varepsilon^2\kappa_0(\varphi), \tag{4.108}$$

where $d_1, \kappa_0 \sim 1$ as $\varepsilon \to 0$. We note that the last estimate (4.108) for K holds if $G \sim h_*^{3/2}E$. The reduced Poisson's ratio ν and a parameter η_3 are assumed to be weakly dependent on coordinates and considered here as constants and parameter θ is taken as a very small one.

Taking into account (4.107), (4.108) and above assumptions as well, the first two equations from (4.76) are rewritten as

$$\begin{aligned}\varepsilon^4 d(\varphi)\Delta^2\chi^* + k_2(\varphi)\frac{\partial^2\Phi^*}{\partial s^2} - \Lambda[1-\varepsilon^2\kappa(\varphi)\Delta]\chi^* = 0,\\ \varepsilon^4\Delta^2\Phi^* - k_2(\varphi)\frac{\partial^2}{\partial s^2}[1-\varepsilon^2\kappa(\varphi)\Delta]\chi^* = 0,\end{aligned} \tag{4.109}$$

where $d(\varphi), \kappa_0(\varphi)$ are real functions of an angle φ.

Remark 4.2. Equations (4.76) have been derived on the supposition that the Young's and shear moduli as well as Poisson's ratio are constant for all layers. If they are functions of the curvilinear coordinates α_1, α_2, the governing equations like (4.76) and (4.109) will contain additional terms which however do not give the contribution into the asymptotic solution to be constructed below. Also, when deriving Eqs. (4.109) from Eqs. (4.76), we have omitted the operator $\Delta^3\tilde{\chi}$ because of the smallness of the shear parameter $K\theta$.

Consider here the simplest variant of boundary conditions

$$\chi^* = \Delta\chi^* = \Delta^2\chi^* = \Phi^* = \Delta\Phi^* = 0 \quad \text{at} \quad s = 0, l \tag{4.110}$$

corresponding to the simply supported edges with diaphragm. Let $\varphi = \varphi_0$ be the weakest generatrix in the neighbourhood of which one occurs localization of eigenmodes. The required eigenmodes and eigenvalues are approximated by the following series (Tovstik, 1983; Mikhasev and Tovstik, 2009)

$$\begin{aligned}\chi^* &= \sin\frac{\pi n s}{l}\sum_{j=0}^{\infty}\varepsilon^{j/2}\chi_j(\zeta)\exp\left\{\imath\left(\varepsilon^{-1/2}p\zeta + 1/2b\zeta^2\right)\right\},\\ \Phi^* &= \sin\frac{\pi n s}{l}\sum_{j=0}^{\infty}\varepsilon^{j/2}\Phi_j(\zeta)\exp\left\{\imath\left(\varepsilon^{-1/2}p\zeta + 1/2b\zeta^2\right)\right\},\end{aligned} \tag{4.111}$$

$$\Lambda = \Lambda_0 + \varepsilon\Lambda_1 + \dots. \tag{4.112}$$

where $\zeta = \varepsilon^{-1/2}(\varphi - \varphi_0)$, p is a real wave parameter, b is an imaginary parameter so that $\Im\, b > 0$ and χ_j, Φ_j are polynomials in ζ.

The functions $\kappa_0(\varphi), k_2(\varphi), d_1(\varphi)$ are expanded into series in the neighborhood of the generatrix $\varphi = \varphi_0$. In particular,

$$\kappa_0(\varphi) = \kappa_0(\varphi_0) + \varepsilon^{1/2}\kappa_0'(\varphi_0)\zeta + \frac{1}{2}\varepsilon\kappa_0''(\varphi_0)\zeta^2 + \dots \tag{4.113}$$

All unknown parameters and functions appeared in (4.111), (4.112) are found in such a way as in Subsect. 3.2.2. We outline here only the principal equations. The substitution of (4.111), (4.112) into Eqs. (4.109) produces the sequence of algebraic equations

$$\sum_{j=0}^{\varsigma} \mathbf{L}_j \boldsymbol{X}^{\mathrm{T}}_{\varsigma-j}, \quad \varsigma = 0, 1, 2, \ldots, \tag{4.114}$$

where $\mathbf{X}_j = (\chi_j, \Phi_j)$ are two-dimensional vectors, the superscript T denotes transposition and $\mathbf{L}_0$ is the 2×2 matrix with the elements

$$\begin{aligned} l_{11} &= p^4 - \Lambda_0[1 + \kappa_0(\varphi_0)p^2], & l_{12} &= -k_2(\varphi_0)\pi^2 n^2 l^{-2}, \\ l_{21} &= k_2(\varphi_0)[1 + \kappa_0(\varphi_0)p^2]\pi^2 n^2 l^{-2}, & l_{22} &= p^4 \end{aligned} \tag{4.115}$$

and the matrix operators $\mathbf{L}_j$ for $j \geq 1$ are expressed in terms of the matrix $\mathbf{L}_0$ by Eqs. (3.111), where $\mathbf{L}_* \equiv 0$ and

$$\mathbf{N} = -\Lambda_1 + d_1(\varphi_0)p^4. \tag{4.116}$$

Considering the homogeneous system of algebraic equations (4.114) at $\varsigma = 0$, one obtains

$$\Phi_0 = -\frac{g_n^{1/2}(\varphi_0)}{p^4}[1 + p^2\kappa_0(\varphi_0)], \tag{4.117}$$

$$\Lambda_0 = f(p, \varphi_0) = \frac{g_n(\varphi_0)}{p^4} + \frac{p^4}{1 + \kappa_0(\varphi_0)p^2}, \tag{4.118}$$

where

$$g_n(\varphi_0) = \pi^4 n^4 l^{-4} k_2^2(\varphi_0). \tag{4.119}$$

As seen from (4.117), $p \neq 0$. The compatibility condition for system (4.114) at $\varsigma = 1$ implies the equations

$$f_p = 0, \quad f_\varphi = 0, \tag{4.120}$$

which may be rewritten as follows

$$\kappa_0(\varphi_0)p^{10} + 2p^8 - 2g_n(\varphi_0)\kappa_0^2 p^4 - 4g_n(\varphi_0)\kappa_0 p^2 - 2g_n(\varphi_0) = 0, \tag{4.121}$$

$$g_n'(\varphi_0)[1 + \kappa_0(\varphi_0)p^2] - p^{10}\kappa_0'(\varphi_0) = 0, \tag{4.122}$$

where the subscript p, φ denote the partial derivatives of a function with respect to the corresponding variables p, φ_0, and the prime $(')$ means differentiation with respect to φ_0. These equations allow to find the wave number p° and the weakest generatrix $\varphi_0 = \varphi_0^\circ$. Finally, the compatibility condition for system (4.114) at $\varsigma = 2$ yields the following equations

$$f_{pp}b^2 + 2f_{p\varphi}b + f_{\varphi\varphi} = 0, \tag{4.123}$$

$$\lambda_1 = -\mathrm{i}(m + 1/2)(f_{pp}b + f_{p\varphi}) + p^4 d_1(\varphi_0), \tag{4.124}$$

$$\chi_0 = \mathcal{H}_m(z), \quad z = [f_{\varphi\varphi}f_{pp}^{-1} - f_{p\varphi}f_{pp}^{-1}]^{1/4}\zeta, \tag{4.125}$$

where $\mathcal{H}_m(z)$ is the Hermite polynomial of the mth degree. In Eqs. (4.123)-(4.125), the second derivatives of f with respect to p and φ_0 are calculated at $p = p^\circ$, and $\varphi_0 = \varphi_0^\circ$.

Equation (4.123) is used for definition of b. It may be seen that the inequality $\Im b > 0$ holds if the second differential of the function f at point $p = p^\circ$, $\varphi_0 = \varphi_0^\circ$ is a positive definite quadratic form, i.e.

$$\mathrm{d}^2 f = f^\circ_{pp}\mathrm{d}p^2 + 2f^\circ_{p\varphi}\mathrm{d}p\mathrm{d}\varphi_0 + f^\circ_{\varphi\varphi}\mathrm{d}\varphi_0^2 > 0. \tag{4.126}$$

The superscribe $^\circ$ denotes that the function f and its partial derivatives are calculated at $p = p^\circ, \varphi_0 = \varphi_0^\circ$. The conditions (4.120), (4.126) indicate that only eigenmodes corresponding to the lowest spectrum are considered here. For the inequality (4.126) to be hold, a solution of Eq. (4.120) should be chosen in such a way that $f^\circ_{pp} = f_{pp}(p^\circ, \varphi_0^\circ) > 0$. To determine the parameter Λ_ς and functions $\chi_\varsigma(\zeta)$, $\Phi_\varsigma(\zeta)$ appearing in (4.111), (4.112) for $\varsigma \geq 1$, one must consider responding system of nonhomogeneous equations (4.114) in the $(\varsigma + 2)$nd approximation. However, the formal procedure for constructing these functions is no longer for $\varsigma \geq 4$ because the correction introduced by appropriate approximations into solution (4.111) at the sixth step is of the order ε^2, which is the same as the error of the governing equations (4.76).

Consider two particular cases.

A) Let $k_2 = k_2(\varphi)$ (noncircular shell or panel) and κ_0, $d_1 = 0$ are constants. Here the weakest line $\varphi = \varphi_0^\circ$ is the generatrix with the minimum curvature and found from the conditions

$$k_2'(\varphi_0^\circ) = 0, \quad k_2''(\varphi_0^\circ) > 0, \tag{4.127}$$

and the natural frequency and parameter b are determined by equations

$$\begin{aligned} \omega &= \omega_\mathrm{c}\omega^*, \quad \omega^* = (f^\circ)^{1/2}\left[1 + \varepsilon\Xi + O(\varepsilon^2)\right] \\ \Xi &= \frac{(1+2m)\pi^2 n^2\sqrt{f^\circ_{pp}k_2''(\varphi_0^\circ)}}{4l^2 f^\circ(p^\circ)^2}, \\ b^\circ &= \frac{\mathrm{i}\,\pi^2 n^2}{l^2(p^\circ)^2}\sqrt{\frac{k_2''(\varphi_0^\circ)}{f^\circ_{pp}}}, \end{aligned} \tag{4.128}$$

where $\omega_\mathrm{c} = \varepsilon^2 R^{-1}(E^\circ/\rho)^{1/2}$ is the characteristic frequency and ω^* is the dimensionless frequency parameter.

B) If k_2 is constant (circular shell or panel), and the shear parameter $\kappa(\varphi)$ is a function, then the weakest line is the one at which the reduced shear parameter K approaches the local maximum:

$$\kappa_0'(\varphi_0^\circ) = 0, \quad \kappa_0''(\varphi_0^\circ) < 0. \tag{4.129}$$

As follows from Eqs. (2.59), (4.93), conditions (4.129) are equivalent to the ones of the local minimum for the reduced shear modulus G. Here, one obtains the following equations for the dimensionless parameters Ξ and b°

$$\begin{aligned}\Xi &= \frac{1}{2f^\circ}\left[\frac{(1+2m)(p^\circ)^3\sqrt{-f^\circ_{pp}\kappa_0''(\varphi_0^\circ)}}{2[1+(p^\circ)^2\kappa_0(\varphi_0^\circ)]} + d_1(\varphi_0^\circ)(p^\circ)^4\right],\\ b^\circ &= \frac{\mathrm{i}\,(p^\circ)^3}{1+(p^\circ)^2\kappa_0(\varphi_0^\circ)}\sqrt{-\frac{\kappa_0''(\varphi_0^\circ)}{f^\circ_{pp}}}\end{aligned} \tag{4.130}$$

If we ignore the shear deformations (assuming $\kappa_0 = 0$), then Eqs. (4.128), (4.130) are reduced to analogues equations obtained before for the Kirchhoff-Love theory-based thin elastic isotropic shell (Mikhasev and Tovstik, 2009).

Equations (4.128) and (4.130) show that increasing the parameter $k_2''(\varphi_0^\circ)$ or $\kappa''(\varphi_0^\circ)$ results in increasing the correction $\omega^* - \omega_0^*$ for the natural frequency, where $\omega_0^* = (f^\circ)^{1/2}$, and leads to growing the power of localization of eigenmodes.

4.5 Localized Vibrations of a Cylindrical Shell Pre-stressed by Distributed Axial Forces

In this section, we will study free localized vibrations of a thin, axially prestressed, multi-layered circular cylindrical shell consisting of N transversely isotropic layers (Mikhasev and Zgirskaya, 2001; Korchevskaya et al, 2004; Korchevskaya and Mikhasev, 2006; Mikhasev, 2017). It is assumed that simply supported edges are under action of a nonuniform axial forces $T^\circ_{11}(\alpha_2)$ as shown in Fig. 3.11. The governing equations describing free vibrations of the pre-stressed laminated cylindrical shell is readily obtained from Eqs. (2.160) by introducing the inertia term into the first equation

$$\begin{aligned}&\frac{Eh^3\eta_3}{12(1-\nu^2)}\left(1-\frac{\theta h^2}{\beta}\Delta\right)\Delta^2\chi + \frac{1}{R}\frac{\partial^2 F}{\partial\alpha_1^2} + T^\circ_{11}(\alpha_2)\frac{\partial^2}{\partial\alpha_1^2}\left(1-\frac{h^2}{\beta}\Delta\right)\chi\\ &\qquad + \rho h\frac{\partial^2}{\partial t^2}\left(1-\frac{h^2}{\beta}\Delta\right)\chi = 0,\\ &\Delta^2 F - \frac{Eh}{R}\frac{\partial^2}{\partial\alpha_1^2}\left(1-\frac{h^2}{\beta}\Delta\right)\chi = 0, \quad w = \left(1-\frac{h^2}{\beta}\Delta\right)\chi.\end{aligned} \tag{4.131}$$

Here, R is the radius of the reference surface of the laminated shell, and other notations are as above. In terms of the displacement and stress functions, the boundary conditions for simply supported edges are as follows

$$\chi = \triangle\chi = \triangle^2\chi = F = \triangle F = 0. \tag{4.132}$$

Inhomogeneity of the axial force T°_{11} results in the appearance of an area at the shell surface with large compressive axial stresses. If the axial stress resultant turns out to be sufficiently large and reaches the critical buckling value T_{11}^*, then, as shown in Chapt. 3, the shell buckles in the neighbourhood of the weakest generatrix $\alpha_2 = \alpha_2^\circ$, where $\max_{\alpha_2} T_{11}^\circ(\alpha_2) = T_{11}^*$. But if $T_{11}^\circ(\alpha_2) < T_{11}^*$ for any α_2, then the pre-buckling compressive forces distorts the natural modes and may result in strong localization of some ones. To study these modes, we use the same asymptotic approach as in Subsect. 3.3.3.

To take into account the influence of the shear parameter in the zeroth order approximation, we assume the following relations

$$\frac{K}{\pi^2} = \mu^2 \kappa, \quad \frac{K\theta}{\pi^2} = \mu^3 \tau, \quad \kappa, \tau \sim 1 \text{ as } \quad \mu \to 0, \tag{4.133}$$

which are valid for a sufficiently thin shell with the reduced shear modulus $G \sim h_* E$. Here

$$K = \frac{\pi^2 h^2}{R^2 \beta}, \quad \mu^4 = \frac{h^2 \eta_3}{12 R^2 (1 - \nu^2)} \tag{4.134}$$

The required functions χ and $\varPhi$ are sought in the form

$$\chi = R\hat{\chi}(s, \varphi) \sin \omega t, \qquad F = \mu^2 EhR\hat{\varPhi}(s, \varphi) \sin \omega t. \tag{4.135}$$

Then, Eqs. (4.131) can be rewritten as follows

$$\begin{aligned} \mu^4(1 - \mu^3 \tau \triangle)\triangle^2 \hat{\chi} + \mu^2 \frac{\partial^2 \hat{\varPhi}}{\partial s^2} + \mu^2 t_1(\varphi) \frac{\partial^2}{\partial s^2}(1 - \mu^2 \kappa \triangle)\hat{\chi} \\ -\varLambda(1 - \mu^2 \kappa \triangle)\hat{\chi} = 0, \\ \mu^2 \triangle^2 \hat{\varPhi} - \frac{\partial^2}{\partial s^2}(1 - \mu^2 \kappa \triangle)\hat{\chi} = 0, \end{aligned} \tag{4.136}$$

where

$$s = \frac{\alpha_1}{R}, \quad \varphi = \frac{\alpha_2}{R}, \quad l = \frac{L}{R}, \quad t_1(\varphi) = \frac{T_{11}^\circ(R\varphi)}{\mu^2 Eh}, \quad \varLambda = \frac{R^2 \rho}{E}\omega^2, \tag{4.137}$$

and the boundary conditions for functions $\hat{\chi}, \hat{\varPhi}$ will be

$$\hat{\chi} = \triangle \hat{\chi} = \triangle^2 \hat{\chi} = \hat{\varPhi} = \triangle \hat{\varPhi} = 0. \tag{4.138}$$

The problem is to find a positive value of $\varLambda$ for which the system of equations (4.136) has a nontrivial solution satisfying the boundary conditions (4.138).

4.5.1 Asymptotic Solution

A formal asymptotic solution of the boundary-value problem (4.136), (4.138) is constructed in the following form, s. Eqs. (3.164) and (3.165),

$$\hat{\chi} = \sin \frac{r_m s}{\mu} \chi_m(\xi, \mu), \tag{4.139}$$

$$\begin{aligned} \chi_m &= \sum_{j=0}^{\infty} \mu^{j/2} \chi_{mj}(\xi) \exp\left[\mathrm{i}\left(\mu^{-1/2} p\xi + \frac{1}{2} b\xi^2\right)\right], \\ \Lambda &= \Lambda_0 + \mu\Lambda_1 + \mu^2\Lambda_2 + \ldots. \end{aligned} \tag{4.140}$$

where ($\hat{\chi} \Rightarrow \hat{\Phi}, \chi_m \Rightarrow \Phi_m, \chi_{mj} \Rightarrow \Phi_{mj}$)

$$\begin{aligned} &\xi = \mu^{-1/2}(\varphi - \varphi_0), \quad \Im b > 0, \\ &|\chi_{mj}|, \, |\Phi_{mj}|, \, \Lambda_j, \, p, \, |b|, \, r_m = \frac{\mu\pi m}{l} \sim 1 \quad \text{as} \quad \mu \to 0, \end{aligned} \tag{4.141}$$

and $\chi_{mj}(\xi), \Phi_{mj}(\xi)$ are polynomials in ξ. Here, $\varphi = \varphi_0$ is a weakest generatrix which is unknown. Functions (4.139), (4.140) approximate the eigenmodes localized in a vicinity of the line $\varphi = \varphi_0$.

The substitution of Eqs. (4.139)-(4.141) into Eqs. (4.136) produces the sequence of algebraic equations

$$\sum_{k=0}^{j} \mathbf{L}_k \mathbf{X}_{j-k} = 0, \quad j = 0, 1, 2, \ldots \tag{4.142}$$

where $\mathbf{X}_j = (\xi_{mj}, \Phi_{mj})^{\mathrm{T}}$, and $\mathbf{L}_0$ is the 2×2 matrix with the elements

$$\begin{aligned} &l_{11} = (r_m^2 + p^2)^2 - [1 + \kappa(r_m^2 + p^2)][r_m^2 t_1(\varphi_0) + \Lambda_0], \\ &l_{12} = -r_m^2, \quad l_{21} = r_m^2[1 + \kappa(r_m^2 + p^2)], \quad l_{22} = (r_m^2 + p^2)^2, \end{aligned} \tag{4.143}$$

and the matrix operators $\mathbf{L}_j$ for $j \geq 1$ are expressed by the matrix $\mathbf{L}_0$ in the same way as in Sect. 3.2, s. Eqs. (3.111), but now the operator $\mathbf{N}$ is the 2×2 matrix with the unique nonzero element ($n_{12} = n_{21} = n_{22} = 0$)

$$n_{11} = \tau(r_m^2 + p^2)^3 - \Lambda_1[1 + \kappa(r_m^2 + p^2)]. \tag{4.144}$$

The sequence of Eqs. (4.142) serves to determine all unknown functions and parameters in (4.139) and (4.140). Because the procedure for seeking these magnitudes is the same as in Subsect. 3.3.2, we omit transitional calculations here and give only the principle equations. Considering the homogeneous system of algebraic equations (4.142) for $j = 0$, one obtains the zeroth-order approximation for the frequency parameter

$$\Lambda_0 = f(p, r_m, \varphi_0) = \frac{(r_m^2 + p^2)^2}{[1 + \kappa(r_m^2 + p^2)]} + \frac{r_m^4}{(r_m^2 + p^2)^2} - t_1(\varphi_0) r_m^2. \tag{4.145}$$

Holding a number m (and thus, a parameter r_m) fixed, we minimize the function (4.145) over p and φ. The necessary conditions of this minimum are the following equations

$$\frac{\partial f}{\partial p} = 0, \qquad \frac{\partial f}{\partial \varphi_0} = 0 \tag{4.146}$$

which serve for a determination of p° and φ_0°. When solving Eqs. (4.146), three different cases appear

- $r_m > z_0$ (case A),
- $r_m < z_0$ (case B),
- $r_m \approx z_0$, (case C),

were z_0 is a root of the algebraic equation

$$-2(1 + \kappa r_m z)^2 + z^4(2 + \kappa r_m z) = 0 \tag{4.147}$$

with respect to z. Equation (4.147) contains a parameter κ accounting for shears in the sandwich. If shears are disregarded ($\kappa = 0$), its root is $z_0 = 1$.

At first, we consider the cases A) and B). For $r_m > z_0$ (case A), we derive

$$\Lambda_0^\circ = \min_{p,\varphi_0} f(p, r_m, \varphi_0) = 1 - t_1(\varphi_0^\circ) r_m^2 + \frac{r_m^4}{1 + \kappa r_m^2}, \quad p^\circ = 0, \tag{4.148}$$

and for $r_m < z_0$ (case B), one has

$$\begin{aligned} \Lambda_0^\circ &= \min_{p,\varphi_0} f(p, r_m, \varphi_0) = \frac{z_0^2 r_m^2}{1 + \kappa r_m z_0} + \frac{r_m^2}{z_0^2} - t_1(\varphi_0^\circ) r_m^2, \\ p^\circ &= \sqrt{r_m(z_0 - r_m)}. \end{aligned} \tag{4.149}$$

Note that Eqs . (4.148), (4.149) are identical at $r_m = z_0$. For both cases, the weakest generatrix $\varphi = \varphi_0^\circ$ is determined from the following conditions

$$t_1'(\varphi_0^\circ) = 0, \quad t_1''(\varphi_0^\circ) < 0. \tag{4.150}$$

Now, a solution of the homogeneous system of equations (4.142) at $j = 0$ may be written as

$$\mathbf{X}_0 = P_0(\xi)\mathbf{Y}_0, \tag{4.151}$$

where $P_0(\xi)$ is an unknown polynomial in ξ, and $\mathbf{Y}_0 = (1, -l_{11}/l_{12})$ is the vector.

In the first-order approximation ($j = 1$), one has the non-homogeneous system of equations (4.142). When taking Eqs. (4.146) into account, this system turns into identities. Consider the non-homogeneous system (4.142) in the second order approximation ($j = 2$). The compatibility condition for this system generates the formula

$$b = \mathrm{i}\sqrt{f_{\varphi\varphi}/f_{pp}} \tag{4.152}$$

and the equation for P_0 is

$$\frac{\mathrm{d}^2 P_0}{\mathrm{d}\xi^2} + \mathrm{i}b\left(2\xi\frac{\mathrm{d}P_0}{\mathrm{d}xi}\right) + \frac{2\Lambda_1}{f_{pp}}P_0 + I_{A(B)} = 0, \tag{4.153}$$

where

$$I_A = \frac{2\tau r_m^6}{f_{pp}(1+\kappa r_m^2)}P_0 \quad \text{at} \quad r_m > z_0 \,(\text{case A}) \tag{4.154}$$

$$I_B = \frac{2\tau r_m^3 z_0^3}{f_{pp}(1+\kappa r_m z_))}P_0 \quad \text{at} \quad r_m < z_0 \,(\text{case B}) \tag{4.155}$$

If $r_m = z_0$, then $I_A = I_B$. For both cases

$$P_0(\xi) = \mathcal{H}_n\left(\sqrt{f_{\varphi\varphi}/f_{pp}}\xi\right). \tag{4.156}$$

Now we can calculate the complex parameter b characterizing the rate of the amplitude decrement far from the generatrix $\varphi = \varphi_0^\circ$. If $r_m > z_0$ (case A), then

$$b = \mathrm{i}\sqrt{\frac{r_m^4(1+\kappa r_m^2)^2[-t_1''(\varphi_0^\circ)]}{2r_m^4(2+\kappa r_m^2) - 4(1+\kappa r_m^2)^2}}, \tag{4.157}$$

and for $r_m > z_0$ (case B), one obtains

$$b = \mathrm{i}\sqrt{\frac{r_m(1+\kappa r_m^2)^3[-t_1''(\varphi_0^\circ)]}{4(z_0 - r_m)[8 + 9\kappa r_m z_0 + 3(\kappa r_m z_0)^2]}}. \tag{4.158}$$

It can be seen that

$$\lim_{r_m \to z_0} |b| = +\infty$$

for both cases (A) and (B). Thus, requirement (4.141) for b does not hold if a root r_m is close to z_0. We will not consider the higher-order approximations because system (4.131) does not contain some terms which affect the third and subsequent approximations.

Now we can write equations for the set of eigenvalues. If $r_m > z_0$, we derive

$$\begin{aligned}\Lambda^{(n,m)} &= 1 - t_1(\varphi_0^\circ)r_m^2 + \frac{r_m^4}{1+\kappa r_m^2} \\ &+ \mu\left\{\frac{(1+2n)\sqrt{-2t''(\varphi_0^\circ)[r_m^4(2+\kappa r_m^2) - 2(1+\kappa r_m^2)^2]}}{2(1+\kappa r_m^2)}\right. \\ &+ \left.\frac{\tau r_m^6}{1+\kappa r_m^2}\right\} + O(\mu^2),\end{aligned}$$

and for $r_m < z_0$ one has

$$
\begin{aligned}
\Lambda^{(n,m)} &= \frac{z_0^2 r_m^2}{1+\kappa r_m z_0} + \frac{r_m^2}{z_0^2} - t_1(\varphi_0^\circ) r_m^2 \\
&+ \mu \left\{ \frac{(1+2n)\sqrt{-t''(\varphi_0^\circ) r_m^3 (z_0 - r_m)[8 + 9\kappa r_m z_0 + 3(\kappa r_m z_0)^2]}}{(1+\kappa r_m^2)^3} \right. \\
&+ \left. \frac{\tau r_m^3 z_0^3}{1+\kappa r_m^2} \right\} + O(\mu^2).
\end{aligned}
$$

The corresponding eigenmodes will be the following: if $r_m > z_0$, then

$$
\chi^{(n,m)} = \sin\frac{r_m s}{\mu} \exp\left\{ \frac{ib(\varphi - \varphi_0^\circ)^2}{2\mu} \right\} \left\{ \mathcal{H}_n \left[\sqrt{\frac{ib}{\mu}} (\varphi - \varphi_0^\circ) \right] + O(\mu^{1/2}) \right\}, \tag{4.159}
$$

and for $r_m < z_0$, one obtains

$$
\begin{aligned}
\chi^{(n,m)} &= \sin\frac{r_m s}{\mu} \exp\left\{ \frac{\mathrm{i}}{\mu} \left[\sqrt{r_m (z_0 - r_m)} (\varphi - \varphi_0^\circ) \right] \right\} \\
&\times \exp\left\{ \frac{ib(\varphi - \varphi_0^\circ)^2}{2\mu} \right\} \left\{ \mathcal{H}_n \left[\sqrt{\frac{ib}{\mu}} (\varphi - \varphi_0^\circ) \right] + O(\mu^{1/2}) \right\}.
\end{aligned} \tag{4.160}
$$

It may be seen that the eigenmodes (4.159) and (4.160) are different for the cases (A) and (B). If $r_m > z_0$ (case A), the eigenfunctions decay exponentially without oscillations ($p^\circ = 0$), and for $r_m < z_0$ (case B) the localized eigenmodes have a large number (of the order μ^{-1}) of waves. If r_m is close to z_0, then Eqs. (4.159) and (4.160) are not applicable. The case (C), when $r_m \simeq z_0$, deserves the special consideration.

4.5.2 Reconstruction of Asymptotic Solution

Let parameter r_m be close to a root z_0 of Eq. (4.147). In this case, a solution of the boundary-value problem (4.136) and (4.138) is found again in the form of (4.139). The substitution of (4.139) into Eqs. (4.136) results in the following system of ordinary differential equations

$$
\begin{aligned}
(1 - \mu\tau\triangle_m)\triangle_m^2 \chi_m - r_m \Phi_m - (t_1 r_m^2 + \Lambda)(1 - \kappa\triangle_m)\chi_m - \Lambda = 0,& \\
\triangle_m^2 \Phi_m + r_m^2 (1 - \kappa\triangle_m)\chi_m = 0,&
\end{aligned} \tag{4.161}
$$

where

$$
\triangle_m = \mu^2 \frac{\mathrm{d}^2}{\mathrm{d}\varphi^2} - r_m^2 \tag{4.162}
$$

is the differential operator.

Consider Eq. (4.147) again. At $r_m = z_0$, it is reduced to the following algebraic equation

$$\kappa r_m^6 + 2r_m^4 - 2(1+\kappa r_m^2)^2 = 0. \tag{4.163}$$

Let $r_m = r_*$ be its root. We introduce the following estimations

$$\begin{aligned} r_m &= r_* + \tilde{\mu} r', \quad \Lambda = \Lambda_* + \tilde{\mu}^2 \Lambda', \quad \varphi - \varphi_0^\circ = \tilde{\mu}\eta, \\ t_1(\varphi) &= t_1(\varphi_0^\circ) + \frac{1}{2}\tilde{\mu}^2 t_1''(\varphi_0^\circ)\eta^2 + \dots \end{aligned} \tag{4.164}$$

where $r', \Lambda' \sim 1$ as $\tilde{\mu} \to 0$, and

$$\tilde{\mu} = \mu^{2/3} = \left[\frac{h^2\eta_3}{12R^2(1-\nu^2)}\right]^{1/6} \tag{4.165}$$

is a new small parameter.

We will seek a solution of Eqs. (4.161) in the form of series

$$\chi_m = \sum_{k=0}^{\infty} \tilde{\mu}^k \chi_m^{(k)}(\eta), \quad \Phi_m = \sum_{k=0}^{\infty} \tilde{\mu}^k \Phi_m^{(k)}(\eta), \tag{4.166}$$

where

$$\chi_m^{(k)}, \Phi_m^{(k)} \sim 1, \quad \text{and} \quad \chi_m^{(k)}, \Phi_m^{(k)} \to 0 \quad \text{as} \quad \eta \to \pm\infty. \tag{4.167}$$

In the zeroth- and first-order approximations, Eqs. (4.161) turn into identities if the following condition holds

$$\Lambda_* = 1 - t_1(\varphi_0^\circ) r_*^2 + \frac{r_*^4}{1+\kappa r_*^2}. \tag{4.168}$$

Note that Eq. (4.168) coincides with Eqs. (4.148) and (4.149) at $r_m = r_* = z_0$. Equation (4.168) gives the zeroth-order approximation for the eigenvalue Λ. The eigenfunctions $\chi_m^{(0)}$ and $\Phi_m^{(0)}$ remain undefined at this step.

Let us consider the second-order approximation. When taking Eq. (4.168) into consideration, one gets the following equation with respect to $\chi_m^{(0)}$

$$a_4 \frac{\mathrm{d}^4 \chi_m^{(0)}}{\mathrm{d}\eta^4} + a_2(r') \frac{\mathrm{d}^2 \chi_m^{(0)}}{\mathrm{d}\eta^2} + [a_0(r') - a_\eta \eta^2 - \Lambda' a_\lambda]\chi_m^{(0)} = 0, \tag{4.169}$$

where

$$\begin{aligned} a_4 &= 1 + \frac{\kappa}{r_*^2} + \frac{3}{r_*^4}, \quad a_2(r') = -4r_* r' + 2\kappa r_* r' - \frac{4r'}{r_*}, \\ a_0(r') &= (r')^2 \left[6r_*^2 - 1 - \kappa r_*^2 \left(5 + \frac{r_*^2}{1+\kappa r_*^2}\right)\right], \\ a_\eta &= \frac{1}{2} r_*^2 (1+\kappa r_*^2) t_1''(\varphi_0^\circ), \quad a_\lambda = (1+\kappa r_*^2). \end{aligned}$$

The problem is to find such values of r', $\Lambda'(r')$ which satisfy the following condition

$$\chi_m^{(0)} \to 0 \quad \text{as} \quad \eta \to \pm\infty. \tag{4.170}$$

Applying Fourier transform

$$\chi_m^{(0)}(\eta) = \frac{1}{\sqrt{2\pi}} \int\limits_{-\infty}^{+\infty} \chi^{\mathrm{F}}(\tilde{\omega}) \mathrm{e}^{\mathrm{i}\tilde{\omega}\eta} \mathrm{d}\tilde{\omega}, \tag{4.171}$$

we come to the second order equation for function χ^{F}

$$\frac{\mathrm{d}^2\chi^{\mathrm{F}}}{\mathrm{d}x^2} + \left\{\tilde{\Lambda} - [x^4 + 2\gamma x^2 + \gamma^2 Q(\kappa)]\right\} \chi^{\mathrm{F}} = 0, \tag{4.172}$$

where

$$\begin{aligned}
x \quad &= \frac{\tilde{\omega}}{\alpha(\kappa)}, \quad \gamma = C(\kappa) r', \quad \tilde{\Lambda} = \Lambda' \left\{ \frac{1 + \kappa r_*^2}{(r_*^4 + \kappa r_*^2 + 3)[-t_1''(\varphi_0^\circ)]^{1/2}} \right\}^{1/3}, \\
\alpha(\kappa) &= \left[-\frac{t_1''(\varphi_0^\circ) r_*^6 (1 + \kappa r_*^2)}{2(r_*^4 + \kappa r_*^2 + 3)} \right]^{1/6}, \\
C(\kappa) &= \frac{2 + 2r_*^4 - \kappa r_*^4}{r_* \left[-\frac{1}{2} t_1''(\varphi_0^\circ)(1 + \kappa r_*^2)(r_*^4 + \kappa r_*^2 + 3)^2 \right]^{1/3}}, \\
Q(\kappa) &= 1 + \frac{2A(\kappa)\alpha^2(\kappa)}{C^2(\kappa) t_1''(\varphi_0^\circ) r_*^2 (1 + \kappa r_*^2)}, \\
A(\kappa) &= \frac{1 - (1 - \kappa) r_*^2 (6 + 5\kappa r_*^2)}{1 + \kappa r_*^2} + \frac{(2 + 2r_*^4 - \kappa r_*^4)^2}{r_*^2 (r_*^4 + \kappa r_*^2 + 3)}.
\end{aligned}$$

For each γ, there is a countable set of values $\tilde{\Lambda}_j (j = 0, 1, \ldots)$ of $\tilde{\Lambda}$ for which there exist non-trivial solutions of Eq. (4.172) such that

$$\chi^{\mathrm{F}} \to 0 \quad \text{as} \quad x \to \pm\infty. \tag{4.173}$$

It may be seen from Eq. (4.172) that the eigenvalues $\tilde{\Lambda}_j$ depend on both the fixed value of the shear parameter κ and the axial stress resultant t_1. In Fig. 4.3, the first two eigenvalues $\tilde{\Lambda}_0$ and $\tilde{\Lambda}_1$ versus a parameter γ are presented for $\kappa = 0.5$ and $t_1(\varphi) = 0.5(1 + \cos\varphi)$. As seen from Fig. 4.3, for parameters accepted above, the function $\tilde{\Lambda}$ has the minimum value $\tilde{\Lambda}_0 \approx 0.924$ at $\gamma \approx -0.380$. Here $r_* \approx 1.220$ and $\Lambda_* \approx 0.782$, and applying Eqs. (4.173) one gets $\Lambda'_{\mathrm{min}} \approx 0.553$, and $r' \approx -0.217$. Then, the wave parameter r_m from Eq. (4.164) and the minimum eigenvalue Λ will be as follows

$$r_m \approx 1.22 - 0.217\varepsilon^{2/3}, \quad \Lambda_{\mathrm{min}} \approx 0.782 + 0.553\varepsilon^{4/3}. \tag{4.174}$$

Table 4.4 shows parameters $r_m, z_0, \Lambda_*, \Lambda'$, and Λ_{min} versus κ for the case (C) when $r_m \approx z_0$. It may be seen that increasing the shear parameter κ leads to a decrease of the minimum natural frequency of the laminated cylindrical shell.

Table 4.4 Minimum eigenvalue Λ versus κ at $r_m \approx z_0$ (after Mikhasev, 2017).

κ	r_m	z_0	Λ_*	Λ'	$\Lambda_{\min}$
0.037	0.993	1.014	0.990	0.590	1.005
0.100	1.017	1.039	0.972	0.586	0.986
0.250	1.077	1.102	0.917	0.575	0.931
0.400	1.142	1.171	0.843	0.563	0.857
0.500	1.186	1.220	0.782	0.553	0.796
0.600	1.229	1.271	0.710	0.539	0.723

Example 4.3. We consider a three-layered cylindrical shell with radius $R = 150$ mm and length $L = 450$ mm. The first and third layers have the thickness $h_1 = h_3 = 0.3$ mm and are made of aluminium with the Young's modulus $E_1 = E_3 = 70,3$ GPa, Poisson's ratio $\nu_1 = \nu_3 = 0.345$, and density $\rho_1 = \rho_3 = 2.7 \cdot 10^{-6}$ kg/mm^3, and the second one is an epoxy matrix with $h_2 = 0.8$ mm, $E_2 = 3,45$ GPa, $\nu_2 = 0.3$ and $\rho_2 = 1.2 \cdot 10^{-6}$ kg/mm^3. The dimensionless axial membrane stress resultant is assumed as follows

$$t_1(\varphi) = \frac{1}{2}(1 + \delta \cos \varphi). \tag{4.175}$$

Then the generatrix $\varphi = \varphi_0^\circ = 0$ will be the weakest one.

Figure 4.4 shows the dependence of the zeroth-order approximation of the eigenvalue Λ_0 upon both the shear parameter κ and parameter δ at $m = 20$ $(r_m = 1.3)$. In this case $r_m > z_0$ and all calculations were performed by equations corresponding to the variant (A). It may be seen that the eigenvalue Λ_0 is the monotonically decreasing function of both the axial force (in a neighborhood of the weakest generatrix) and the shear parameter κ.

Figure 4.5 demonstrates the nonlinear behavior of the relative correction Λ_1/Λ_0 for the eigenvalue Λ at varying the shear parameter κ for different values of δ. As accepted, the increase in parameter ϱ characterizing inhomogeneity of loading

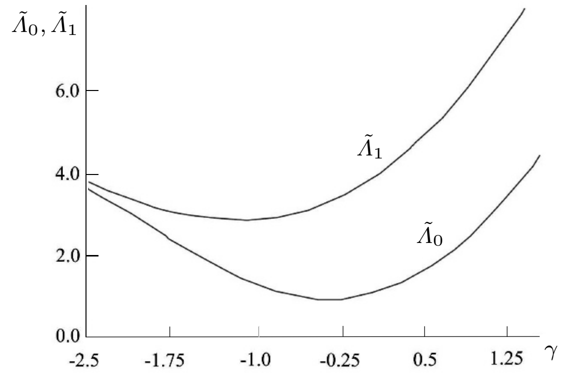

Fig. 4.3 First two eigenvalues $\tilde{\Lambda}_0, \tilde{\Lambda}_1$ vs. parameter γ (after Mikhasev, 2017).

involves the increase in the correction Λ_1/Λ_0 for any fixed κ. But for any fixed δ, there exists the maximum of Λ_1/Λ_0 being the function of κ. Approximately at $\kappa > 0.65$, the influence of inhomogeneity in loading on the natural frequencies becomes negligible.

Example 4.4. Let us consider again the three-layered cylindrical shell with the same geometrical and physical parameters as in the previous Example. In Table 4.5, the dependence of the parameters $\Im b$, Λ_0 (or Λ_* at $r_m \approx z_0$), and Λ_1/Λ_0 (or Λ'/Λ_* for $r_m \approx z_0$) on the wave parameter r_m found by two different asymptotic approaches is presented. The calculations have been performed at $\kappa = 0.5$ for the nonuniform dimensionless stress resultant $t_1(\varphi) = 0.5(1 + \cos\varphi)$. It may be seen that Λ_1/Λ_0 decreases and $\Im b$ increases as $r_m \to z_0 = 1.077$.

All the problems on free vibrations of laminated beams, plates and cylindrical shells considered in this chapter have revealed the general feature for the ESL model taking into account transverse shears: the incorporation of shears into the shell model reduces all natural frequencies, this effect being stronger for eigenmodes with a large number of waves and weaker for modes having a small number of waves. Since the eigenmodes for low-frequency vibrations of thin medium-length cylindrical shells are characterized by a large number of waves in the circumferential direction, than the shear induced lowering of natural frequencies may be too significant for these modes (corresponding to low-frequency vibrations). The outcomes obtained in this chapter, including the derived equations for natural frequencies, will be used below to study free and forced vibrations of laminated thin-walled structures assembled from the viscoelastic smart materials (MREs and ERCs).

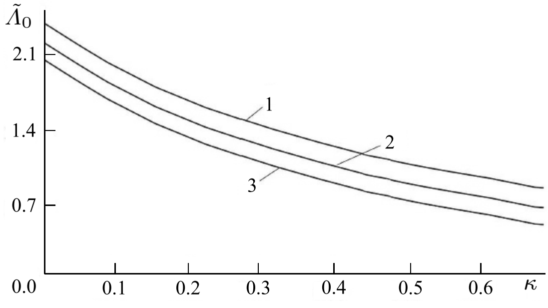

Fig. 4.4 Zero approximation Λ_0 of the eigenvalue Λ vs. the shear parameter κ.
$\delta = 0.8$ - curve 1,
$\delta = 1$ - curve 2,
$\delta = 1.2$ - curve 3
(after Mikhasev, 2017).

Table 4.5 Parameters $\Im b$, Λ_0 (or Λ_*), Λ_1/Λ_0 (or Λ'/Λ_*) vs. r_m (after Mikhasev, 2017).

Cases	r_m	$\Im b$	$\Lambda_0(\Lambda_*)$	$\Lambda_1/\Lambda_0(\Lambda'/\Lambda_*)$
B	0.844	0.285	0.575	1.117
B	0.909	0.347	0.656	0.942
B	0.974	0.448	0.741	0.752
C	1.077	-	0.917	0.627
A	1.360	1.588	1.490	0.552
A	1.490	1.026	1.949	0.564

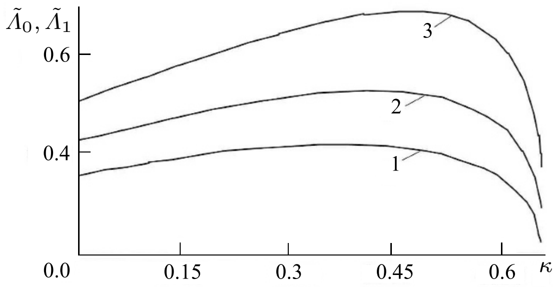

Fig. 4.5 Normalized correction Λ_1/Λ_0 vs. the shear parameter κ.
$\delta = 0.8$ - curve 1,
$\delta = 1$ - curve 2,
$\delta = 1.2$ - curve 3
(after Mikhasev, 2017).

References

Alshorbagy AE, Eltaher MA, Mahmoud FF (2011) Free vibration characteristics of a functionally graded beam by finite element method. Applied Mathematical Modelling 35(1):412–425

Baghani M, Jafari-Talookolaei RA, Salarieh H (2011) Large amplitudes free vibrations and post-buckling analysis of unsymmetrically laminated composite beams on nonlinear elastic foundation. Applied Mathematical Modelling 35:130–138

Carnegie W, Thomas J (1967) Natural frequencies of long tapered cantilevers. The Aeronautical Quarterly 18:309–320

Conway HD, Dubil JF (1965) Vibration frequencies of truncated wedge and cone beam. Journal of Applied Mechanics 32(4):932–935

Cranch ET, Adler A (1956) Bending vibrations of variable section beams. American Society of Mechanical Engineers 23(1):103–108

Dong XJ, Meng G, Li HG, Ye L (2005) Vibration analysis of a stepped laminated composite Timoshenko beam. Mechanics Research Communications 32(5):572–581

Ece MC, Aydogdu M, Taskin V (2007) Vibration of a variable cross-section beam. Mechanics Research Communications 34:78–84

Farghaly SH, Gadelrab RM (1995) Free vibration of a stepped composite Timoshenko cantilever beam. Journal of Sound and Vibration 187(5):886–896

Firouz-Abadi RD, Haddadpour H, Novinzadeh AB (2007) An asymptotic solution to transverse free vibrations of variable-section beams. Journal of Sound and Vibration 304:530–540

Goel RP (1976) Transverse vibration of tapered beams. Journal of Sound and Vibration 47(1):1–7

Gol'denveizer AL, Lidsky VB, Tovstik PE (1979) Free Vibrations of Thin Elastic Shells (in Russ.). Nauka, Moscow

Hajianmaleki M, Qatu MS (2013) Vibrations of straight and curved composite beams: A review. Composite Structures 100:218–232

Huang Y, Li XF (2010) A new approach for free vibration of axially functionally graded beams with non-uniform cross-section. Journal of Sound and Vibration 329(11):2291–2303

Jafari-Talookolaei RA, Ahmadian MT (2007) Free vibration analysis of a cross-ply laminated composite beam on Pasternak foundation. Journal of Computer Science 3(1):51–56

Jaworski JW, Dowell EH (2008) Free vibration of a cantilevered beam with multiple steps: comparison of several theoretical methods with experiment. J Sound Vibr 312(4-5):713–725

Korchevskaya E, Mikhasev G (2006) Free vibrations of laminated cylindrical shell under action of non-uniformly distributed axial forces. Mechanics of Solids 41(5):130–138

Korchevskaya E, Mikhasaev G, Marinkovic D, Gabbert U (2004) Buckling and vibrations of composite laminated cylindrical shells under axial load. In: Proc. of "6th Magdeburg Days of Mechanical Engineering", Otto-von-Guericke-University Magdeburg, Logos-Verl., Berlin, pp 183–189

Koutsawa Y, Daya EM (2007) Static and free vibration analysis of laminated glass beam on viscoelastic supports. International Journal of Solid and Structures 44(1):8735–8750

Kukla S, Zamojska I (2007) Frequency analysis of axially loaded stepped beams by Green's function method. Journal of Sound and Vibration 300(3-5):1034–1041

Lee SY, Ke HY (1990) Free vibrations of non-uniform beams resting on non-uniform elastic foundation with general elastic end restraints. Computers & Structures 34(3):421–429

Li J, Hua H, Shen R (2008) Dynamic stiffness analysis for free vibrations of axially loaded laminated composite beams. Composite Structures 84(1):87–98

Li J, Hu X, Li X (2016) Free vibration analyses of axially loaded laminated composite beams using a unified higher-order shear deformation theory and dynamic stiffness method. Composite Structures 158:308–322

Malekzadeh P, Vosoughi AR (2009) DQM large amplitude vibration of composite beams on nonlinear elastic foundations with restrained edges. Communications in Nonlinear Science and Numerical Simulation 14:906–915

Mikhasev G (2017) Some problems on localized vibrations and waves in thin shells. In: Altenbach H, Eremeyev V (eds) Shell-like Structures: Advanced Theories and Applications, CISM International Centre for Mechanical Sciences. Courses and Lectures, vol 572, Springer, Wien, pp 149–210

Mikhasev GI, Tovstik PE (2009) Localized Vibrations and Waves in Thin Shells. Asymptotic Methods (in Russ.). FIZMATLIT, Moscow

Mikhasev GI, Zgirskaya OM (2001) Local buckling of thin laminated cylindrical shell under non-uniform axial load (in Russ.). Vesnik Vitebsk Univ 4(22):90–93

Mikhasev GI, Altenbach H, Korchevskaya EA (2014) On the influence of the magnetic field on the eigenmodes of thin laminated cylindrical shells containing magnetorheological elastomer. Composite Structures 113:186 – 196

Mohanty SC, Rout T (2012) Vibration and dynamic stability analysis of a functionally graded Timoshenko beam on Pasternak elastic foundation. Int J Aerosp Lightw Struct 2(3):383–403

Murin J, Aminbaghai M, Kutis V (2010) Exact solution of the bending vibration problem of FGM beams with variation of material properties. Engineering Structures 32(6):1631–1640

Naguleswaran S (2002) Vibration of an Euler-Bernoulli beam on elastic end supports and with up to three step changes in cross-section. In J Mech Sc 44(12):2541–2555

Naguleswaran S (2003) Vibration and stability of an Euler-Bernoulli beam with up to three-step changes in cross-section and in axial force. Int J Mech Sc 45:1563–1579

Patel BP, Ganapathi M, Touratier M (1999) Nonlinear free flexural vibrations/postbuckling analysis of laminated orthotropic beams/columns on a two parameter elastic foundation. Composite Structures 46:189–196

Roy PK, Ganesan N (1994) Studies on the dynamic behavior of a cantilever beam with varying thickness. Journal of Sound and Vibration 177(1):1–13

Sanger DJ (1968) Transverse vibration of a class of non-uniform beams. Journal of Mechanical Engineering Science 16:111–120

Sato K (1980) Transverse vibrations of linearly tapered beams with ends restrained elastically against rotation subjected to axial force. International Journal of Mechanical Sciences 22:109–115

Sayyad AS, Ghugal YM (2017) Bending, buckling and free vibration of laminated composite and sandwich beams: A critical review of literature. Composite Structures 171:486–504

Suppiger E, Taleb N (1956) Free lateral vibration of beams of variable cross section. Journal of Applied Mathematics and Physics (ZAMP) 7(8):501–520

Tovstik PE (1983) Two-dimensional problems of buckling and vibrations of the shells of zero Gaussian curvature. Soviet Physics Doklady 28(7):593–594

Wang JI (1991) Vibration of stepped beams on elastic foundations. Journal of Sound and Vibration 149:315–322

Zhou D, Cheung YK (2000) The free vibration of a type of tapered beams. Computer Methods in Applied Mechanics and Engineering 188:203–216

Zhou D, Cheung YK (2001) Vibrations of tapered timoshenko beams in terms of static timoshenko beam functions. Journal of Applied Mechanics 68:596–602

Chapter 5
Vibrations of Laminated Structures Composed of Smart Materials

Abstract In this chapter, we consider thin-walled laminated beams, plates and shells containing layers made of viscoelastic smart materials (VSMs). Generally, from all variety of these materials, the magnetorheological elastomer MRE-1 with properties specified in Chapt. 2 will be used for damping layers or core. To compare the damping capabilities of this material with others, we will study also vibrations of thin-walled laminates assembled from other smart materials (MREs, MRFs and ERCs) described in Chapt. 2.

The basic purpose of this chapter is to analyze free and forced vibrations of thin-walled laminated structures with adaptive physical properties and to show that the application of VSMs embedded between elastic layers allows changing not only the total rigidity, as detected in Chapt. 3, but more the total damping capability of the structure when subjected to the action of an external magnetic or electric field. In particular, it will be shown that the application of a magnetic field may result in significant enhance of the damping capacity of a MRE-based laminated structure and as a consequence, in effective damping of both free and forced vibrations.

The chapter begins with a brief review of the state of the art of research on vibration of MR/ER-based laminated structures (Sect. 5.1). In Sect. 5.2, free and forced vibrations of sandwich beams with MRF or MRE cores are examined. In Sect. 5.3, free and forced vibrations of MRE-based rectangular plates are shortly discussed. Section 5.4 is the main one, it is devoted to free and forced vibrations of laminated and sandwich MRE/ERC-based panels and shells affected by stationary magnetic fields. The detailed analysis of damping capability of different VSMs materials (MREs and ERCs with properties specified in Chapt. 2) incorporated with sandwich panels is given. Finally, in Sects. 5.5 and 5.6, the impact of magnetic field on localized modes and non-stationary vibrations in medium-length MRE-based cylindrical shells is studied. In particular, the effect of soft suppression of travelling localized waves under slowly varying magnetic field is demonstrated.

G. I. Mikhasev and H. Altenbach, *Thin-walled Laminated Structures*,
Advanced Structured Materials 106, https://doi.org/10.1007/978-3-030-12761-9_5

5.1 Brief Review of the State of the Art

One of the main issues of any thin-walled structure are undesirable vibrations. The control of structural vibrations may be implemented by passive, semi-active or active manner. The passive damping of vibrations is provided by utilizing viscoelastic materials with fixed physical properties. A passive damped thin-walled structure is formed as a rule by placing viscoelastic damping material between elastic layers. The problems of free and forced vibrations of similar laminated structures assembled with traditional viscoelastic materials are well studied (we do not discuss here investigations arising to the earliest papers of DiTaranto (1965); Mead and Markus (1970) and refer only to the review article by Qatu et al, 2010).

The semi-active or active control of structural vibrations is attained as a rule by modifying the total stiffness and damping ratio (viscosity). A number of active materials such as piezoelectric, electromagnetotstrictive materials, electro- and magnetorheological fluids and elastomers, etc., may be used to vary the total viscoelastic characteristics of thin-walled smart structures (Gandhi et al, 1989; Gandhi and Thompson, 1992).

During the last two decades, electrorheological (ER) and magnetrheological (MR) fluids as well as magnetorheological elastomers (MREs) became to attract a heightened attention of researchers studying controllable damping vibrations of thin-walled laminated structures (Li et al, 2014). Gandhi et al (1989) reported on the first experimental investigation focussed on evaluating the electro-elastodynamic response of cantilevered multi-layered beams containing ER fluids. The results of this pioneering paper have clearly demonstrated for the first time the feasibility of actively controlling in real-time the dynamic characteristics (natural frequencies, amplitudes and damping ratio) of laminated structures fabricated upon ultra-advanced smart composite materials. Afterwards, numerous theoretical and experimental studies on the behavior of a sandwich beam with ER fluid were carried out (among many others, s. Choi et al, 1990; Lee, 1995; Berg et al, 1996; Oyadiji, 1996; Yalcintas and Coulter, 1995, 1998; Yalcintas and Dai, 1999; Shaw, 2000; Kang et al, 2001; Phani and Venkatraman, 2003; Allahverdizadeh et al, 2013). In particular, detailed investigations of the influence of ER materials on the composite structural vibration and damping have been carried out by Yalcintas and Coulter (1995, 1998); Yalcintas and Dai (1999). They and afterwards Kang et al (2001) have discussed variations of the modal loss factors with different designed parameters and showed that the possible damping capacity of ER based sandwich beams can be maximized by the proper choice of geometrical parameters and electric field. It has been also revealed that the adaptive nature of sandwich beams with ER liquid core was achieved by controlling the pre-yield rheology of ER smart materials in response to varying applied electric field levels. An important outcome of all aforementioned theoretical studies are analytical models of sandwich (three-layered) beams with a liquid ER core. The principle assumptions of these models are the following:

- ER liquid core exhibits linear shear behavior at small strain levels, corresponding to the pre-yield regime;

- the shear modulus of a viscoelastic core is a complex magnitude dependent of the electrical field level;
- no normal stresses in the ER layer;
- all three layers experience the same transverse displacement;
- no slipping between the elastic layers and ER layer.

All studies based on these models have reported that the definite increase in electric field across ER fluid, corresponding to the pre-yield regime, results in the increase of the loss factor of the ER layer and ultimately the equivalent damping ratio for a smart beam.

As for MR materials, they have demonstrated very quick time response, in the order of milliseconds, to an applied magnetic field (s. Chapt. 2), and thus become potentially applicable to smart tunable laminated structures (Sun et al, 2003). The available experimental studies (Yalcintas and Dai, 2004; Wei et al, 2008; Lara-Prieto et al, 2010; Chikh et al, 2016; Kozlowska et al, 2016; Irazu and Elejabarrieta, 2017) and numerous theoretical papers (Yalcintas and Dai, 1999; Sun et al, 2003; Zhou and Wang, 2005, 2006a,b,c; Hu et al, 2006; Mikhasev et al, 2010; Nayak et al, 2011, 2012; Korobko et al, 2012) have shown that the application of an external magnetic field results in very quick increasing of the stiffness and damping properties of sandwich beams containing MR fluids or elastomers. This effect may be efficiently used to tune the dynamic characteristics such as natural frequencies, vibration amplitudes, mode shapes and loss factors. As shown in Korobko et al (2012), for assumed and fixed geometrical and physical parameters of a MRE based beam, there is an optimal intensity of the magnetic field providing the maximum loss factor for a smart beam. In contrast to earlier papers on the ER fluid based sandwich beams, the theoretical investigations by Zhou and Wang (2006a,b,c); Choi et al (2010) containing mathematical models were based on the higher-order shear deformation theory for a soft MRE core, some of approaches (Zhou and Wang, 2006b,c) accounting the normal stresses in the MRE layer. The effect of non-homogeneous magnetic field on MRE sandwich beams fabricated from a MRE between two aluminum layers was examined by Hu et al (2011, 2012); Long et al (2013). Whereas the majority of investigations showed that the application of a uniform magnetic field results in increasing the total stiffness of a MRE based sandwich beam and leads to right shifting natural frequencies, the experimental tests performed by Hu et al (2011, 2012) have revealed unlooked-for result: the first natural frequency of the cantilever MRE beam decreased as the magnetic field applied to the beam was moved from the clamped edge to the free one. The left shift trend of the first natural frequency has been also confirmed by finite element simulations performed by Megha et al (2016). The nonlinear mechanical behavior of sandwich beams with a MRE core subjected to a permanent magnetic field was recently analyzed by Zeerouni et al (2018). They showed that MRE beams may exhibit a non-linear behavior even at small deformations due to the rheological properties of a MRE.

The vibration analysis becomes very important when the applied load is not constant and induces unstable modes or resonance. The advantages of using MR liquids or elastomers to active control the forced vibration of sandwich beams were illustrated in Dwivedy et al (2009); Rajamohan et al (2010); Nayak et al (2014);

Aguib et al (2016); Megha et al (2016); Yildirim et al (2016). Using finite element and Ritz' methods, Rajamohan et al (2010) have demonstrated the efficiency of utilizing MR fluid to suppress forced vibrations of a sandwich beam under harmonic force excitation. Dwivedy et al (2009) have examined parametric instability of a MRE based sandwich beam subjected to a periodic axial load. Aguib et al (2016) have experimentally and numerically studied the vibrational response of a MRE sandwich beam subjected to harmonic excitation by magnetic force applied at the free end. The nonlinear dynamic response of a clamped-clamped geometrically imperfect MRE sandwich beam with a concentrated mass at the centre under a point excitation has been investigated by Yildirim et al (2016). The numerical calculations and experimental tests on free and forced vibrations of sandwich beams and panels with carbon/epoxy composite skins and a honeycomb core filled with MRE were performed recently by de Souza Eloy et al (2018, 2019). Free and forced vibration tests conducted under several magnetic field intensities were performed to evaluate dynamic properties of the sandwich beams. The experiments showed the noticable reduction of mechanical vibrations, especially on the fundamental mode of the sandwich structure. It was also revealed shifting the natural frequencies to the right due to the increase of an induced magnetic field.

Contrary to laminated smart beams, the dynamics of sandwich plates and shells with embedded ER or MR cores remains less studied. The vibration analysis of isotropic and orthotropic sandwich rectangular plates with MRE core has been performed by Yeh (2013, 2014). In Aguib et al (2014) numerical and experimental studies of the dynamic behavior of sandwich plates consisting of two aluminum skins and a polarized MRE core (elaborated under the action of a magnetic field) have been performed. Eshaghi et al (2015) considered two sandwich plates consisting of polyethylene terephthalate face layers with two different magnetorheological fluids as core layers. At first, the dynamic responses of the cantilever sandwich plate were experimentally characterized; then, using a finite element model based on the classical plate theory, they showed enhanced vibration suppression properties of the magnetorheological sandwich plate over a wide frequency range. The dynamic performance of tapered laminated MRE sandwich plates has been analyzed in recent papers by Vemuluri and Rajamohan (2016); Vemuluri et al (2018). Applying FEM and carrying out experiments on the various prototypes of tapered composite silicon based MRE sandwich plates, they have investigated the effects of magnetic field, taper angle of the top and bottom layers and various end conditions on the dynamic properties of sandwich plates. Further, the transverse vibration responses of tapered sandwich plates under harmonic force excitation have been also analyzed at various levels of applied magnetic field. The nonlinear vibration analysis of a MRE sandwich plate was conducted experimentally by Zhang et al (2018). They have constructed the frequency-response curves in the vicinity of the fundamental natural frequency of a MRE sandwich plate in either the absence or presence of a localized external magnetic field at different geometrical locations. It was observed that all the MRE plates displayed strong hardening-type nonlinear behaviour, however, this behaviour transitioned to a weak hardening-type nonlinearity with increasing magnetic field.

As concerns shells, there are only a few investigations on the dynamic analysis of thin-walled structures containing ER or MR cores (Yeh, 2011; Mohammadi and Sedaghati, 2012; Mikhasev et al, 2011, 2014, 2016; Mikhasev, 2018). In Yeh (2011) vibrations of orthotropic cylindrical sandwich shells composed of ER core and constraining layers have been studied by utilizing the discrete layer FEM. The author has computed the natural frequencies and modal loss factors of an orthotropic cylindrical sandwich shell and concluded that by applying different electric fields, the natural frequencies and modal loss factors of the smart shell can be controlled and changed immediately. In Mohammadi and Sedaghati (2012) a nonlinear finite element model of a sandwich shell with an ER fluid in the core has been developed to perform nonlinear vibration analysis and examine the effect of small and large displacements, core thickness ratio and electric field intensity on the nonlinear damping behavior of the shell. The equivalent single-layer model for multi-layered cylindrical shells containing MRE cores has been proposed by Mikhasev et al (2011). Later, this model has been used to study the effect of an external magnetic field on the natural modes of a medium-length thin sandwich cylindrical shell containing a highly polarized MR core (Mikhasev et al, 2014). It has been revealed that applying a constant magnetic field may result in strong distortion of eigenmodes corresponding to the lowest eigenfrequencies. In Mikhasev et al (2016) the response of the MRE-based sandwich medium-length cylindrical shell to the initial localized perturbations and an applied time-dependent magnetic field has been studied. It has been shown that the time dependent magnetic field may result in soft suppression of running localized bending waves. Finally, the analysis of different problems considered in Mikhasev (2017, 2018) has clearly demonstrated that MREs may be successfully used in designing smart thin-walled laminated structures of variable and predictable mechanical properties. Some problems on free and forced vibrations of MRE based cylindrical shells studied in Mikhasev et al (2011, 2014); Mikhasev (2017, 2018) will be in detail considered in the subsequent sections of this chapter. Concluding the section, we refer readers to the review by Eshaghi et al (2016).

5.2 Sandwich and Multi-layered Beams with Magnetorheological Core

Consider a sandwich beam of the length L and the rectangular cross section with the sides h and b as shown in Fig. 5.1. The face sheets of the thickness h_1, h_3 are made of an elastic material, and the viscoelastic core of the thickness h_2 is fabricated from a magnetorheological composite (MRC). From all variations of smart composite materials, we consider here only the magnetorheological fluids (MRFs) and the magnetorheological elastomer (MRE-1) with properties given in Chapt. 2. Obviously, the choice of a mathematical model for the sandwich MR beam depends on whether the core is a liquid or an elastomer.

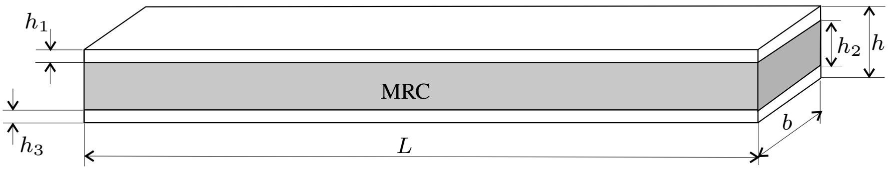

Fig. 5.1 Sandwich beam with MRC core.

5.2.1 Sandwich Beam with Magnetorheological Fluid Core

Let the core be a smart magnetorheological fluid, MRF. The ESL model for laminated beams presented in Chapt. 2 and based on the generalized hypotheses of Timoshenko can not be used here, because it presupposes the same order of stiffness for all layers composing a beam. We shall take here the simplest model proposed by Yalcintas and Dai (2004) and based on the assumptions stated in Sect. 5.1. According to this model for a sandwich beam with the same thicknesses for all layers ($h_1 = h_2 = h_3 = a$), the governing equations accounting tranverse shear in the liquid MR core are the following

$$\begin{aligned} \rho\frac{\partial^2 w}{\partial t^2} + 2EI\frac{\partial^4 w}{\partial x^4} - 4G_{\mathrm{v}}ab\left(\frac{\partial^2 w}{\partial x^2} - \frac{\partial \phi}{\partial x}\right) &= f, \\ J\frac{\partial^2 \phi}{\partial t^2} - 2Ea^2b\frac{\partial^2 \phi}{\partial x^2} - 4G_{\mathrm{v}}ab\left(\frac{\partial w}{\partial x} - \phi\right) &= 0, \end{aligned} \tag{5.1}$$

where w is the normal deflection of the beam (the medium line of the core), ϕ is the cross-sectional rotation, x is a coordinate at the core medium line, f is the external force per unit length, t is time, E is the Young's modulus of the surface layers, G_{v} is the complex shear modulus for the one of MRFs with properties given in Tables 2.8-2.10, ρ is the reduced density of the sandwich per unit length, I is the geometric moment of area 2nd order of the cross-section, and J is the moment of inertia per unit length. The magnitudes ρ, I, J are introduced as

$$\begin{aligned} \rho &= 2\rho_1 + \rho_2, \\ I &= \frac{9}{4}ba^3, \\ J &= a^2\left(\frac{13\rho_1}{6} + \frac{\rho_2}{12}\right), \end{aligned} \tag{5.2}$$

where ρ_1 and ρ_2 are densities per unit length of the face sheets and MRF, respectively. Let the edges be simply supported. The appropriate boundary conditions read

$$w = \frac{\partial^2 w}{\partial x^2} = \frac{\partial \phi}{\partial x} = 0 \quad \text{at} \quad x = 0, L. \tag{5.3}$$

5.2.1.1 Free Vibrations

Let $f = 0$. Then the natural modes corresponding to conditions (5.3) are given by functions

$$w = w_n(x,t) = \sin\lambda_n x\, \mathrm{e}^{\mathrm{i}\Omega t}, \quad \phi = \phi_n(x,t) = C_n \cos\lambda_n x\, \mathrm{e}^{\mathrm{i}\Omega t}, \quad n = 1, 2, \ldots \tag{5.4}$$

where

$$\lambda_n = \frac{\pi n}{L}, \quad C_n = \frac{2\lambda_n G_\mathrm{v}}{\lambda^2 a^2 E + 2G} \tag{5.5}$$

and

$$\Omega = \Omega_n = \lambda_n^2 \sqrt{\frac{E}{\rho}\left[2I + \frac{4G_\mathrm{v}ab}{E\lambda_n^2}\left(1 + \frac{2G_\mathrm{v}}{\lambda_n^2 a^2 E + 2G_\mathrm{v}}\right)\right]} \tag{5.6}$$

is the complex eigenvalue. Deriving Eq. (5.6), we neglected the rotation inertia of the cross-section. Separating in (5.6) the real and imaginary parts, one obtains the required natural frequency $\omega = \Re\Omega$ and the associated damping ratio $\alpha = \Im\Omega > 0$ of damped vibrations.

Remark 5.1. In addition to the complex eigenvalue $\Omega = \omega + \mathrm{i}\alpha$ defined by (5.6), the boundary-value problem (5.1), (5.3) has another eigenvalue $\Omega = -\omega - \mathrm{i}\alpha$. It is obvious that the second one does not satisfy the condition of damped vibrations, and so will not be taking into consideration in what follows.

To analyse the effect of magnetic field and the type of MRF chosen on damped vibrations, we consider the following example.

Example 5.1. Let the sandwich beam of the length $L = 390$ mm with the sides $a = 0.7$ mm, $b = 25$ mm in the cross-section be assembled from aluminum face sheets and MRF placed between these sheets. We consider three types of MRFs: MRF-1, MRF-2 and MRF-3, with properties given in Tables 2.8-2.10. Figures 5.2-5.4 demonstrate the effect of magnetic field on the natural frequencies $\omega = \Re\Omega$ corresponding to three modes with numbers of semi-waves $n = 1, 3, 5$ for the beams with different MRFs. As can be seen from the figures, the natural frequencies shift right as the applied magnetic field increases from 0 to 350 mT, these variations being observed more dominantly for the MRF-1, which contains iron particles of large size.

An important parameter characterizing the rate of vibration damping is the logarithmic decrement

$$D_\mathrm{l} = \frac{2\pi\alpha}{\sqrt{\omega^2 - \alpha^2}}. \tag{5.7}$$

Figures 5.5-5.7 show the behavior of scaled logarithmic decrement $d_\mathrm{l} = 50D_\mathrm{l}/\pi$ under varying the magnetic induction B for three types of MRFs. Calculations have been performed for $n = 1, 3, 5$. It is seen that the effect of magnetic field on the logarithmic decrement is very complicated due to complicated behavior of the loss factor η_v for all the MR liquids (s. Tables 2.8-2.10). The general conclusion related to all MRFs under consideration is that the logarithmic decrement decreases

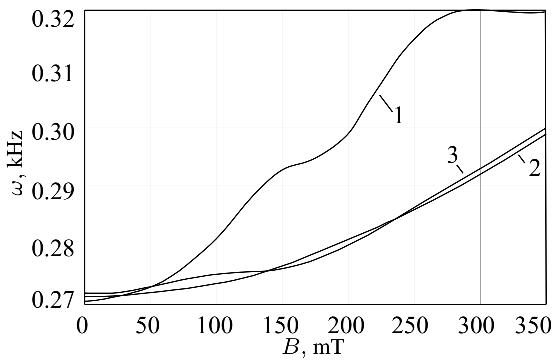

Fig. 5.2 First natural frequency $\omega_1 = \Re\Omega_1$ for sandwich beams with different MRF cores vs. induction B:
1 - MRF-1; 2 - MRF-2;
3 - MRF-3.

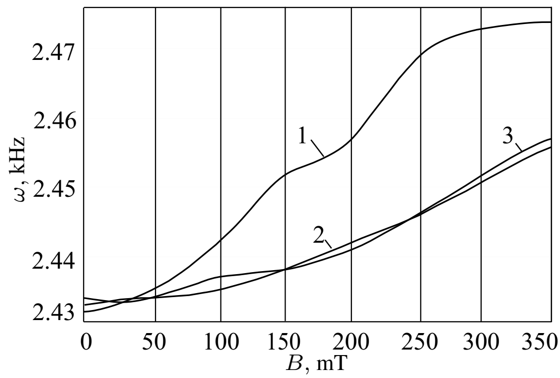

Fig. 5.3 Third natural frequency $\omega_3 = \Re\Omega_3$ for sandwich beams with different MRF cores vs. induction B:
1 - MRF-1; 2 - MRF-2;
3 - MRF-3.

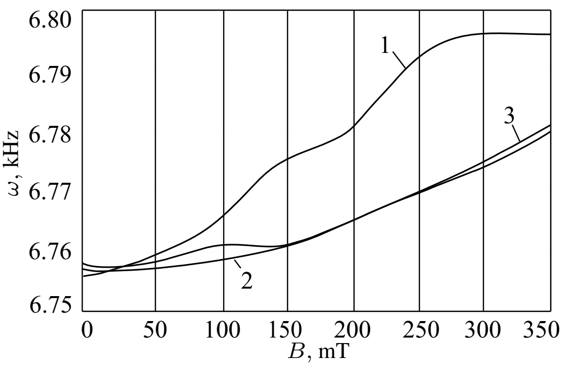

Fig. 5.4 Fifth natural frequency $\omega_5 = \Re\Omega_5$ for sandwich beams with different MRF cores vs. induction B:
1 - MRF-1; 2 - MRF-2;
3 - MRF-3.

with growing the mode number. Thus, the mathematical model for a sandwich used here shows that MRFs are most effective for damping low-frequency vibrations of three-layered beams with the MRF core.

Figures 5.8 and 5.9 allow us to compare the damping capabilities of different smart fluids on the first and third modes, respectively, at different levels of applied magnetic field. It is seen that the MRF-2 and MRF-3 possess the best damping

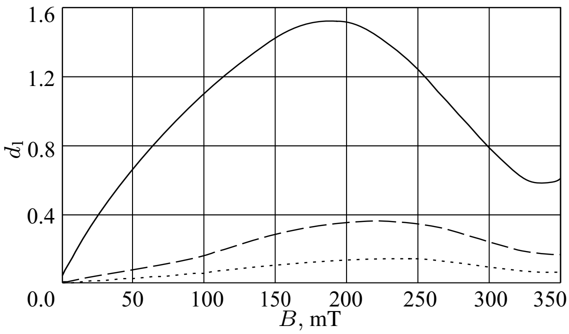

Fig. 5.5 Scaled logarithmic decrement d_1 for the sandwich beam with the MRF-1 core corresponding to different modes vs. induction B: solid line - $n = 1$, dashed line - $n = 3$, dotted line - $n = 5$.

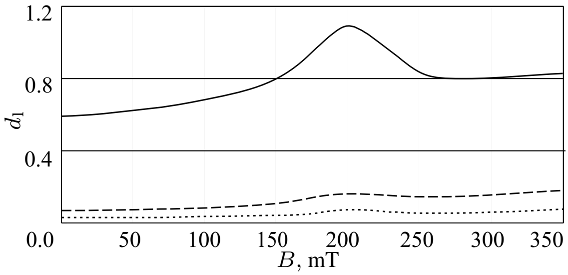

Fig. 5.6 Scaled logarithmic decrement d_1 for the sandwich beam with the MRF-2 core corresponding to different modes vs. induction B: solid line - $n = 1$, dashed line - $n = 3$, dotted line - $n = 5$.

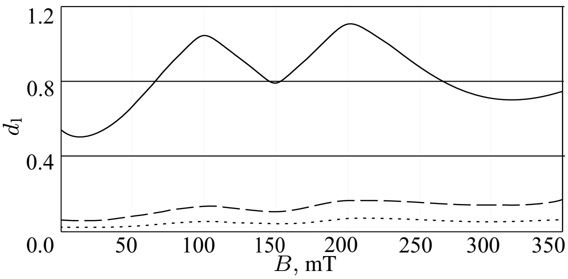

Fig. 5.7 Scaled logarithmic decrement d_1 for the sandwich beam with the MRF-3 core corresponding to different modes vs. induction B: solid line - $n = 1$, dashed line - $n = 3$, dotted line - $n = 5$.

capability at a weak magnetic field ($B < 50$ mT), while the MRF-1 demonstrates the highest damping effect for B varying from 50 to 300 mT.

5.2.1.2 Forced Stationary Vibrations

Now we consider forced vibrations under the external normal harmonic force

$$f = \rho F_0(x)\, \mathrm{e}^{\mathrm{i}\omega_\mathrm{e} t}, \tag{5.8}$$

where ω_e is the excitation frequency. The magnetic field, if applied, is constant and homogeneous (independent of time t and coordinate x).

A solution of Eqs. (5.1) with the boundary conditions (5.3) may be found in the form of series

Fig. 5.8 Scaled logarithmic decrement d_1 for the sandwich beam with different MRFs cores corresponding to the first mode ($n = 1$) vs. induction B: 1 - MRF-1; 2 - MRF-1; 3 - MRF-3.

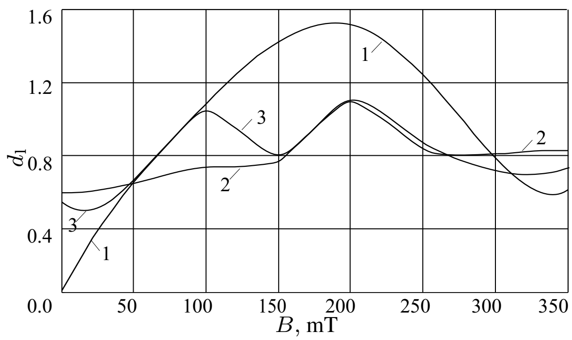

Fig. 5.9 Scaled logarithmic decrement d_1 for the sandwich beam with different MRFs cores corresponding to the third mode ($n = 3$) vs. induction B: 1 - MRF-1; 2 - MRF-1; 3 - MRF-3.

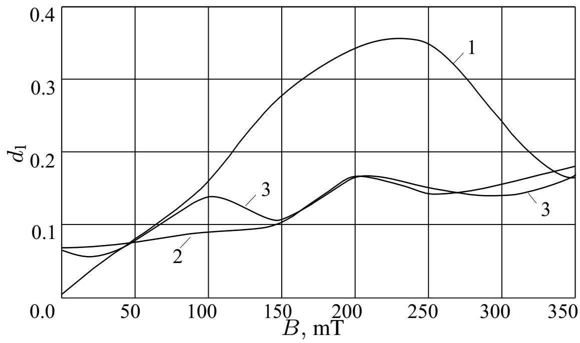

$$w(x,t) = \sum_{n=1}^{\infty} \sin(\lambda_n x)\, q_\mathrm{n}(t), \quad \phi(x,t) = \sum_{n=1}^{\infty} C_n \cos(\lambda_n x)\, q_\mathrm{n}(t), \tag{5.9}$$

where $q_\mathrm{n}(t)$ is the so-called generalized coordinates of the vibrating system. Substituting Eqs. (5.9) into (5.1), then multiplying them by $\sin(\lambda_n x)$ and integrating over the beam length, we obtain the following equation

$$\ddot{q}_n(t) + \Omega_n^2 q_\mathrm{n}(t) = F_n \mathrm{e}^{\mathrm{i}\omega_\mathrm{e} t}, \tag{5.10}$$

where

$$F_n = \int_0^L F_0(x) \sin(\lambda_n x) dx \tag{5.11}$$

is the generalized force corresponding to $q_\mathrm{n}(t)$. The partial solution of Eq. (5.10) is

$$q_\mathrm{n}(t) = F_n \frac{\mathrm{e}^{\mathrm{i}\omega_\mathrm{e} t}}{\Omega_n^2 - \omega_\mathrm{e}^2}. \tag{5.12}$$

Then the amplitude of forced stationary vibrations at any point of the beam will be defined by

$$w(x,t) = \sum_{n=1}^{\infty} \frac{F_n}{\Omega_n^2 - \omega_\mathrm{e}^2} \sin(\lambda_n x) \mathrm{e}^{\mathrm{i}\omega_\mathrm{e} t} = \sum_{n=1}^{\infty} \frac{F_n \sin(\lambda_n x) \mathrm{e}^{\mathrm{i}\omega_\mathrm{e} t}}{\omega_n^2 - \alpha_n^2 - \omega_\mathrm{e}^2 + 2\mathrm{i}\omega_n \alpha_n}. \quad (5.13)$$

Since the complex eigenfrequency Ω_n depend on the complex shear modulus G_v being the function of induction B, the amplitude of sustained forced vibrations becomes to some extent a controllable quantity.

5.2.1.3 Equivalent Model with External Friction for Prediction of Unsteady Vibrations

We note that the homogeneous equation corresponding to Eq. (5.10) has the two partial solutions, $\mathrm{e}^{-\alpha+\mathrm{i}\omega t}$ and $\mathrm{e}^{\alpha-\mathrm{i}\omega t}$, of which the second one does not satisfy the damping condition (s. Remark 5.1). Thus, the general solution of Eq. (5.10) based on the assumed above model for viscoelastic MRF with internal friction can not be used to describe unsteady forced vibrations of the MRF-based sandwich beam.

In order to give an approximate analysis of unsteady vibrations, we shall replace the initial model by an *equivalent model* with external friction. The idea of this substitution is the following. The dynamic unsteady response of the beam to the external harmonic excitation can be represented by the superposition of the damped eigenmodes and undamped forced modes (5.13). Each of the damped eigenmodes is characterized by the natural frequency $\omega_n = \Re\Omega_n$ and the associated damping ratio $\alpha_n = \Im\Omega_n$. We consider the series of viscoelastic n-oscillators

$$\ddot{y}_n + 2\alpha_n \dot{y}_n + (\omega_n^2 + \alpha_n^2) y_n = 0 \quad (5.14)$$

with the external friction and having the same natural frequencies ω_n and damping ratio α_n. Then Eq. (5.10) may be replaced by the following equation

$$\ddot{\tilde{q}}_n(t) + 2\alpha_n \dot{\tilde{q}}_n + (\omega_n^2 + \alpha_n^2)\tilde{q}_\mathrm{n} = F_n \mathrm{e}^{\mathrm{i}\omega_\mathrm{e} t}, \quad (5.15)$$

where $\tilde{q}_\mathrm{n}$ is the generalized coordinate of the *equivalent viscoelastic system* with damping ratio depending on the wave number n.

The general solution of Eq. (5.15) is

$$\tilde{q}_\mathrm{n} = \frac{F_n \mathrm{e}^{\mathrm{i}\omega_\mathrm{e} t}}{\omega_n^2 - \omega_\mathrm{e}^2 + \alpha_n^2 + 2\mathrm{i}\alpha_n \omega_\mathrm{e}}. \quad (5.16)$$

Then the amplitude of forced unsteady vibrations for the *equivalent smart beam* will be as follows

$$\begin{aligned} w(x,t) = \sum_{n=1}^{\infty} \Bigg[& \mathrm{e}^{-\alpha_n t} \left(c_n^{(s)} \sin \omega_n t + c_n^{(c)} \cos \omega_n t \right) \\ & + \frac{F_n \mathrm{e}^{\mathrm{i}\omega_\mathrm{e} t}}{\omega_n^2 - \omega_\mathrm{e}^2 + \alpha_n^2 + 2\mathrm{i}\alpha_n \omega_\mathrm{e}} \Bigg] \sin(\lambda_n x). \end{aligned} \quad (5.17)$$

We note that the component in Eq. (5.17) corresponding to the amplitude of forced unsteady vibrations does not coincide with the amplitude of forced stationary vibrations (5.13). However, the real parts of these components become the same for the resonance excitation, i.e. for $\omega_{\mathrm{e}} = \omega_n$. Equation (5.17) derived for the *equivalent beam* can be used only to estimate approximately unsteady vibrations of the smart beam under consideration. To make that, we shall consider the following example.

Example 5.2. Let the motionless sandwich MR beam with parameters specified in Example 5.1 be subjected to the periodic concentrated force

$$f = \rho\delta(x - x^*) \sin \omega_{\mathrm{e}} t$$

applied in the point $x = x^* \in (0, L)$ at $t \geq 0$, where $\delta(x)$ is the delta function. Then the generalized force

$$F_n = \frac{2}{L} \sin \lambda_n x^* .$$

We consider the case when the frequency of excitation is very close to the first natural frequency $\omega_{\mathrm{e}} \approx \omega_1 = \Re \varOmega_1$ of the beam when a magnetic field is absent. In Fig. 5.10, curve 1 shows the scaled amplitude $A = w_{\max} \times 10^5$ of the *resonance* vibrations of the *equivalent beam* without magnetic field, and the curve marked by 2 corresponds to vibrations of the same beam when the magnetic field of the constant induction $B = 250$ mT is applied. Here, $w_{\max}$ is the maximum amplitude. The calculations were performed for $x^* = L/7$ and $\omega_{\mathrm{e}} = 271$ Hz. It is clearly seen, that due to viscosity of the MRF-1 the small oscillations generated by the initial conditions quickly decay with and without magnetic field, while the amplitude of forced vibrations is the growing function which converges to some limited value at $t \to \infty$, if a magnetic field is absent. The application of magnetic field leads to slight shifting all natural frequencies, including the first one (s. again Fig. 5.2), to right and in that way prevents resonance vibrations.

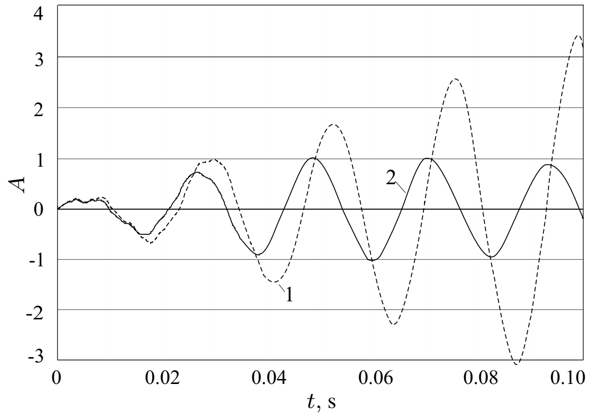

Fig. 5.10 Scaled maximum amplitude A of forced vibrations of the sandwich beam with the MRF-1 core vs. time t without magnetic field (curve 1) and under magnetic field of the induction $B = 250$ mT (curve 2).

5.2.1.4 Suppression of Forced Vibrations in Thin-walled Structures via Magnetic/Electric Fields

The basic principles of damping forced vibrations of MR/ER-based beams, plates and shells are to give a time signal of the magnetic/electric field and also to determine its optimal intensity. The criteria of selecting the signal time of an external physical field may be different. The simplest criterion is monitoring of the maximum amplitude of vibrations: the magnetic/electric field signal is fed, if the maximum amplitude (in some point) achieves a certain critical magnitude. Another criterion is based on the estimation of the total mechanical energy of the structure. For instance, for the sandwich beam considered in this section this energy is defined as

$$\mathbb{E}_{\mathrm{s}} = T + \Pi_1 + \Pi_2 + \Pi_3, \tag{5.18}$$

where

$$T = \frac{1}{2}\int_0^L \left(\frac{\partial w}{\partial t}^2\right) \rho\,\mathrm{d}x + \frac{1}{2}\int_0^L \left(\frac{\partial \phi}{\partial t}^2\right) J\,\mathrm{d}x,$$

$$\Pi_1 = ba^3 E \int_0^L \left(\frac{\partial \phi}{\partial t}^2\right) \mathrm{d}x, \quad \Pi_2 = EI \int_0^L \left(\frac{\partial w}{\partial t}^2\right) \mathrm{d}x,$$

$$\Pi_3 = \frac{1}{2} G'_{\mathrm{v}} ab \int_0^L \gamma^2 \rho \mathrm{d}x.$$

In Eq. (5.18), T is the kinetic energy of the beam, Π_1, Π_2 are the potential energy of tangential and bending deformations, and Π_3 is the potential energy of the transversal shears in the MR/ER core. We note that the energy (5.18) does not contain the work that goes to the heating the whole system, including the work on heating the MR/ER core, which depends on the loss modulus G''_{v} of the smart viscoelastic material.

The problem is to minimize the maximum amplitude of excited vibrations, the mechanical energy $\mathbb{E}_{\mathrm{s}}$ or the rate of its growth $\dot{\mathbb{E}}_{\mathrm{s}}$ (Lai and Wang, 1996). For instance, if at $t = t_{\mathrm{cr}}$ the energy achieves some critical value $\mathbb{E}_{\mathrm{s}}^{(\mathrm{cr})}$, a magnetic/electric field signal is applied, leading to a sudden or gradual change in the physical characteristics of a smart core.

Example 5.3. In this example, we study the response of the beam considered in the previous example when the magnetic field of the intensity $B = 270$ mT is suddenly applied at $t = t_{\mathrm{cr}} = 0.1$ s. Let $w^{(1)}(x,t)$ be the beam response to the resonance excitation at the interval $0 < t \le t_{\mathrm{cr}} = 0.1$ s (see the dotted line in Fig. 5.10). Consider the following initial conditions

$$w(x,t)|_{t_{\mathrm{cr}}} = w^{(1)}(x, t_{\mathrm{cr}}), \quad \dot{w}(x,t)|_{t=t_{\mathrm{cr}}} = \dot{w}^{(1)}(x, t_{\mathrm{cr}}) \tag{5.19}$$

for Eqs. (5.1). Let $w^{(2)}(x,t)$ be a solution of the initial boundary-value problem (5.1), (5.3), (5.19) for $t \ge t_{\mathrm{cr}}$ when the magnetic field signal is fed. We assume that after applying the magnetic field at $t = t_{\rm cr}$ the viscoelastic properties of the beam is changed in a moment. So, to use formulae (5.17) at $t \geq t_{\rm cr}$, one needs to recalculate at first all natural frequencies for the sandwich at $B = 270$ mT. Figure 5.11 shows the response of the equivalent MRF-1 sandwich at two time gaps, for $0 \leq t < t_{\rm cr}$ (the dotted line) and $t \geq t_{\rm cr}$ (the solid line). It is seen that the application of a magnetic field results in some high-frequency oscillations generated by the initial displacements and velocities (5.19), these oscillations being rapidly suppressed during the time. However, the basic effect of the applied magnetic field is a quick withdrawal of the beam from a regime of the resonance vibrations and stabilization of forced vibrations with more low amplitude.

Remark 5.2. It should be noted that the response of a smart material to a signal of magnetic/electric field depends on the ratio of timescales of controlling signal and the reaction of the very MR/ER medium (Korobko et al, 2012). So, at sudden application of a magnetic field, the time of reaction of MRF or MRE is about $10^{-3} - 10^{-2}$ s. An abrupt impact of an external physical field is the kind of a *parametric blow* for the adaptable mechanical system and can excite additional high-frequency modes.

Solution (5.17) found above for the *equivalent smart beam* as well as Examples 5.2, 5.3 relate to the case when the applied magnetic field is stationary. It is obvious that these solutions do not take into account the aforementioned parametric impact. In the next item, we shall construct high-frequency modes accounting for the real time response of a smart MR material to a signal of an external magnetic field.

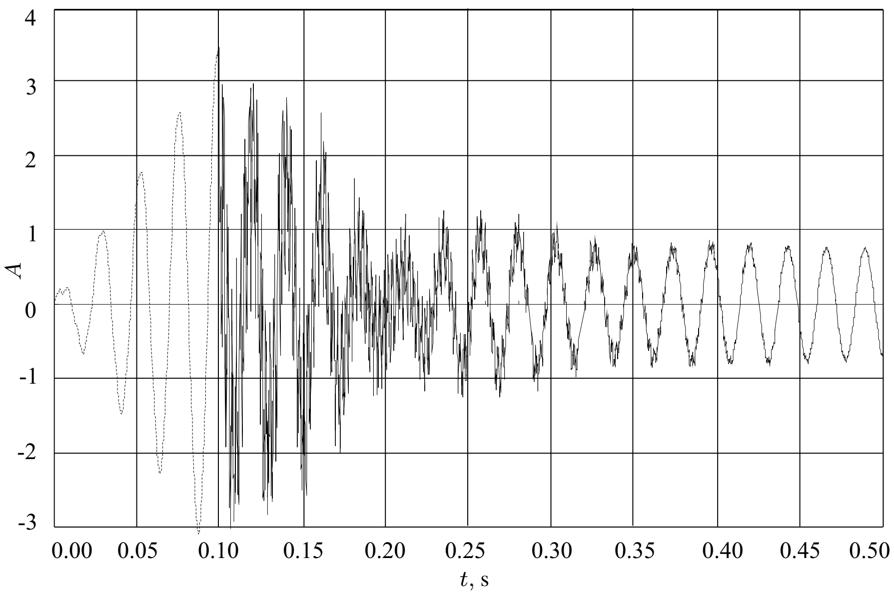

Fig. 5.11 Response of the MRF-1 based sandwich beam to the resonance harmonic force and magnetic field applied at $t = t_{\rm cr} = 0.1$ s.

5.2.1.5 High-frequency Response of Magnetorheological Beam on the Rapid Signal of a Magnetic Field

Let the complex shear modulus $G_\mathrm{v} = G_\mathrm{v}(v_r t)$ of the MRF be a function of time, where $v_\mathrm{r} = 1/t_\mathrm{r}$ is the speed of the liquid reaction on the signal of a magnetic field. For a majority of MRFs, v_r varies from 10^{-3} to 10^{-2} s^{-1}. Let $t_\mathrm{r} = 10^{-2}$ s be the characteristic time.

We introduce the dimensionless magnitudes

$$\begin{aligned} &w = LW^*, \quad t = t_\mathrm{r}\tau, \qquad g(\tau) = \frac{2G_\mathrm{v}(t_\mathrm{r}\tau)L^2}{\varepsilon^{1/2}Ea^2} \\ &\varepsilon = \frac{t_\mathrm{r}}{T_\mathrm{p}}, \qquad T_\mathrm{p} = \frac{1}{3}\sqrt{\frac{2\rho a}{Eb}}\,\frac{L^2}{a^2}, \end{aligned} \tag{5.20}$$

where T_p is the period of low-frequency vibrations of the beam without the MRF core. Furthermore, it is assumed that ε is a small parameter.

The dimensionless deflection and angle of rotation satisfying the boundary conditions (5.3) are sought in the form

$$W^* = W(\tau)\sin\frac{\pi n x}{L}, \quad \phi = \varPhi(\tau)\cos\frac{\pi n x}{L}, \quad n = \varepsilon^{-1/2}p,\ p \sim 1, \tag{5.21}$$

where n is an integer. Then Eqs. (5.1) can be rewritten as

$$\begin{aligned} \varepsilon\frac{\mathrm{d}^2 W}{\mathrm{d}\tau^2} + \delta^4 W + \frac{4}{9}\varepsilon^{1/2}\delta^2 g(\tau)W + \frac{4}{9}\varepsilon\delta g(\tau)\varPhi = 0, \\ \varepsilon\varsigma^2\frac{\mathrm{d}^2\varPhi}{\mathrm{d}\tau^2} + \delta^2\varPhi + \delta g(\tau)W - \varepsilon^{1/2}g(\tau)\varPhi = 0, \end{aligned} \tag{5.22}$$

where

$$\delta = \pi p, \quad \varsigma^2 = \frac{9\rho_J a^2}{2\rho L^2}, \quad \rho_J = \frac{13}{6}\rho_1 + \frac{1}{12}\rho_2, \quad g(\tau) = g_1(\tau) + \mathrm{i}g_2(\tau). \tag{5.23}$$

Here, g_1 and g_2 are the real and imaginary parts of the complex function $g(\tau)$, g_2 being positive.

To solve Eqs. (5.21), we apply to the multiple scale method. Let

$$\tau_0 = \varepsilon^{-1/2}\tau, \qquad \tau_1 = \tau, \qquad \tau_2 = \varepsilon^{1/2}\tau, \quad \ldots \tag{5.24}$$

be independent variables. The asymptotic solution of Eqs. (5.22) can be found in the form of series

$$W = W_0 + \varepsilon^{1/2}W_1 + \varepsilon W_2 + \ldots, \qquad \varPhi = \varPhi_0 + \varepsilon^{1/2}\varPhi_1 + \varepsilon\varPhi_2 + \ldots \tag{5.25}$$

where W_k and $\varPhi_k$ are functions of independent arguments τ_j defined by (5.24).

Substitution of (5.25) into Eqs. (5.22) results in the sequence of differential equations with respect to required W_k, Φ_k. Consider these equations step-by-step. In the zeroth-order approximation, one has the homogeneous equations

$$\frac{\partial^2 W_0}{\partial \tau_0^2} + \delta^4 W_0 = 0, \qquad \frac{\partial^2 \Phi_0}{\partial \tau_0^2} + \frac{\delta^2}{\varsigma^2}\Phi_0 + \frac{\delta}{\varsigma^2} g(\tau_1) W_0 = 0. \tag{5.26}$$

Their solution are

$$\begin{aligned} W_0 &= A_0(\tau_1,\ldots)\mathrm{e}^{\mathrm{i}\delta^2\tau_0} + \bar{A}_0(\tau_1,\ldots)\mathrm{e}^{-\mathrm{i}\delta^2\tau_0}, \\ \Phi_0 &= B_0(\tau_1,\ldots)\mathrm{e}^{\mathrm{i}\frac{\delta}{\varsigma}\tau_0} + \bar{B}_0(\tau_1,\ldots)\mathrm{e}^{-\mathrm{i}\frac{\delta}{\varsigma}\tau_0} \\ &\quad + \frac{g(\tau_1)}{\delta(1-\delta^2\varsigma^2)}\left[A_0\mathrm{e}^{\mathrm{i}\delta^2\tau_0} + \bar{A}_0\mathrm{e}^{-\mathrm{i}\delta^2\tau_0}\right], \end{aligned} \tag{5.27}$$

where $A_0(\tau_1, \tau_2, \ldots), B_0(\tau_1, \tau_2, \ldots)$ are required complex functions. In the first-order approximation, one obtains the nonhomogeneous system of differential equations

$$\begin{aligned} \frac{\partial^2 W_1}{\partial \tau_0^2} + \delta^4 W_1 &= -2\frac{\partial^2 W_0}{\partial \tau_0 \partial \tau_1} - \frac{4}{9}\delta^2 g(\tau_1) W_0, \\ \frac{\partial^2 \Phi_1}{\partial \tau_0^2} + \frac{\delta^2}{\varsigma^2}\Phi_1 + \frac{\delta}{\varsigma^2} g(\tau_1) W_1 &= -2\frac{\partial^2 \Phi_0}{\partial \tau_0 \partial \tau_1} - \frac{g(\tau_1)}{\varsigma^2}\Phi_0. \end{aligned} \tag{5.28}$$

In above equations, the right-hand members generate secular partial solutions. Eliminating these solutions, one arrives at the differential equations

$$\mathrm{i}\frac{\partial A_0}{\partial \tau_1} + \frac{2}{9} g(\tau_1) A_0 = 0, \quad 2\mathrm{i}\delta\varsigma\frac{\partial B_0}{\partial \tau_1} - g(\tau_1) B_0 = 0. \tag{5.29}$$

These equations have the solutions

$$\begin{aligned} A_0(\tau_1, \tau_2, \ldots) &= A_{01}(\tau_2, \ldots)\exp\left\{\frac{2\mathrm{i}}{9}\int\limits_0^{\tau_1} g(\tau)\mathrm{d}\tau\right\}, \\ B_0(\tau_1, \tau_2, \ldots) &= B_{01}(\tau_2, \ldots)\exp\left\{\frac{\mathrm{i}}{2\delta\varsigma}\int\limits_0^{\tau_1} g(\tau)\mathrm{d}\tau\right\}. \end{aligned} \tag{5.30}$$

When taking into account (5.30), the general solution of the system (5.28) becomes as follows

$$\begin{aligned} W_1 &= A_1(\tau_1,\ldots)\mathrm{e}^{\mathrm{i}\delta^2\tau_0} + \bar{A}_1(\tau_1,\ldots)\mathrm{e}^{-\mathrm{i}\delta^2\tau_0}, \\ \Phi_1 &= B_1(\tau_1,\ldots)\mathrm{e}^{\mathrm{i}\frac{\delta}{\varsigma}\tau_0} + \bar{B}_1(\tau_1,\ldots)\mathrm{e}^{-\mathrm{i}\frac{\delta}{\varsigma}\tau_0} \\ &\quad + C_1(\tau_1,\ldots)\mathrm{e}^{\mathrm{i}\delta^2\tau_0} + \tilde{C}_1(\tau_1,\ldots)\mathrm{e}^{-\mathrm{i}\delta^2\tau_0}, \end{aligned} \tag{5.31}$$

where

$$
\begin{aligned}
C_1 &= -\frac{g}{\delta(1-\delta^2\varsigma^2)}A_1 + \frac{4\varsigma^2\delta^2 g^2 - 9\mathrm{i}\delta^2 g' + 9g^2}{9\delta(1-\delta^2\varsigma^2)^2}A_0, \\
\tilde{C}_1 &= -\frac{g}{\delta(1-\delta^2\varsigma^2)}\bar{A}_1 + \frac{4\varsigma^2\delta^2 g^2 + 9\mathrm{i}\delta^2 g' + 9g^2}{9\delta(1-\delta^2\varsigma^2)^2}\bar{A}_0.
\end{aligned}
\tag{5.32}
$$

The unknown functions A_{01}, B_{01}, A_1, B_1 are found from the next approximation.

We limit ourselves to the first two approximations. Then the approximate formulae for the deflection and the angle of rotation become as follows

$$
\begin{aligned}
w = L\sin\left(\frac{\pi p s}{\varepsilon^{1/2}}\right)\exp\left[-\frac{2}{9}\int_0^\tau g_2(\tau)\mathrm{d}\tau\right]\Bigg\{A_{01}\exp\left[\mathrm{i}\left(\frac{\delta^2\tau}{\varepsilon^{1/2}} + \frac{2}{9}\int_0^\tau g_1(\tau)\mathrm{d}\tau\right)\right] \\
+ \bar{A}_{01}\exp\left[-\mathrm{i}\left(\frac{\delta^2\tau}{\varepsilon^{1/2}} + \frac{2}{9}\int_0^\tau g_1(\tau)\mathrm{d}\tau\right)\right]\Bigg\} + O\left(\varepsilon^{1/2}\right),
\end{aligned}
\tag{5.33}
$$

$$
\begin{aligned}
\phi = \cos\left(\frac{\pi p s}{\varepsilon^{1/2}}\right)\exp\left[-\frac{1}{2\delta\varsigma}\int_0^\tau g_2(\tau)\mathrm{d}\tau\right]\Bigg\{B_{01}\exp\left[\mathrm{i}\left(\frac{\delta\tau}{\varsigma\varepsilon^{1/2}} + \frac{1}{2\delta\varsigma}\int_0^\tau g_1(\tau)\mathrm{d}\tau\right)\right] \\
+ \bar{B}_{01}\exp\left[-\mathrm{i}\left(\frac{\delta\tau}{\varsigma\varepsilon^{1/2}} + \frac{1}{2\delta\varsigma}\int_0^\tau g_1(\tau)\mathrm{d}\tau\right)\right]\Bigg\} + O\left(\varepsilon^{1/2}\right),
\end{aligned}
\tag{5.34}
$$

where A_{01} and B_{01} are found from the initial conditions.

Equations (5.33) and (5.34) give the leading terms in the asymptotic series predicting high-frequency unsteady damping vibrations. It is seen that these terms are asymptotically independent. Equation (5.33) describes bending vibrations with the current frequency

$$\omega_\mathrm{b} = \frac{\delta^2\tau}{\varepsilon^{1/2}} + \frac{2}{9}\int_0^\tau g_1(\tau)\mathrm{d}\tau \tag{5.35}$$

and the damping ratio

$$\alpha_\mathrm{b} = \frac{2}{9}\int_0^\tau g_2(\tau)\mathrm{d}\tau, \tag{5.36}$$

and Eq. (5.34) predicts torsional vibrations with the frequency

$$\omega_\mathrm{r} = \frac{\delta\tau}{\varsigma\varepsilon^{1/2}} + \frac{1}{2\delta\varsigma}\int_0^\tau g_1(\tau)\mathrm{d}\tau \tag{5.37}$$

and the damping ratio

$$\alpha_{\mathrm{r}} = \frac{1}{2\delta\varsigma} \int_0^{\tau} g_2(\tau)\mathrm{d}\tau. \tag{5.38}$$

Thus, high-frequency vibrations are asymptotically decomposed into bending and torsional ones. The second terms in Eqs. (5.35) and (5.37) give nonstationary corrections for frequencies, these corrections are induced by the rapid variation of the storage modulus of the MRF under the impulse signal of the magnetic field. The time-dependent damping ratios (5.36) and (5.38) reflect the variation of the loss modulus of the smart viscoelastic core. If we take into account the next approximations, it would be detected that the bending vibrations defined by Eq. (5.33) generate torsional vibrations with amplitudes of order $O\left(\varepsilon^{1/2}\right)$ and vice versa, the high-frequency rotations of the beam cross-sections (5.34) cause small bending oscillations. Thus, the bending and torsional vibrations are coupled.

The above mentioned methods of vibration damping belong to semi-active methods. Obviously, they have both advantages and disadvantages. One of the advantages of these approaches, based on the application of MR/ER smart materials, is that without the use of any special damping devices it is possible to change reversibly the elastic and viscous properties of the entire mechanical system to withdraw it from the regime of resonance vibrations. In addition, these methods allow suppressing efficiently any free oscillations generated by the initial conditions. Their common drawback is that their implementation results in partial suppression of the forced vibrations only due to some increasing all natural frequencies.

5.2.2 Laminated Beams with Magnetorhelogical Elastomer Layers

In this subsection, we consider both sandwich and multi-layered beams with one ore several layers made of a MRE. To predict the dynamic response of the MRE-based laminated beams, we use the ESL theory stated in Chapt. 2. The differential equation governing forced vibrations of the beam represented in Fig. 5.1 is the following (2.153)

$$EI\eta_3 \left(1 - \frac{\theta h^2}{\beta}\frac{\partial^2}{\partial x^2}\right)\frac{\partial^4 \chi}{\partial x^4} + \rho_{\mathrm{l}}\left(1 - \frac{h^2}{\beta}\frac{\partial^2}{\partial x^2}\right)\frac{\partial^2 \chi}{\partial t^2} = q_{\mathrm{l}}, \tag{5.39}$$

where $q_{\mathrm{l}}(x,t)$ is the external normal force per unit length of the beam, ρ_{l} is the linear mass introduced in Sect. 2.1, χ is the displacement function coupled with the normal displacement w by

$$w = \left(1 - \frac{h^2}{\beta}\frac{\partial^2}{\partial x^2}\right)\chi. \tag{5.40}$$

In contrast to the cases considered in Chapt. 4, the reduced Young's modulus E and parameters η_3, θ, β are here complex magnitudes dependent on the induction B of the external magnetic field. The complex values of these parameters are calculated by Eqs. (2.18), (2.25), (2.84) and (2.89).

Consider here only one variant of boundary conditions

$$\chi = \frac{\mathrm{d}^2\chi}{\mathrm{d}x^2} = \frac{\mathrm{d}^4\chi}{\mathrm{d}x^4} = 0, \tag{5.41}$$

corresponding to the simply supported edges $\alpha_1 = 0, L$. We remind that for a laminated beam represented by the ESL model, boundary conditions for the simply supported edges with and without diaphragm are identical (s. Subsect. 3.1.1).

5.2.2.1 Free Vibrations

At first, we consider free vibrations ($q_l = 0$). The eigenmodes satisfying conditions (5.40) are written down

$$\chi = \chi_0 \sin \frac{\pi n x}{L} \, \mathrm{e}^{\mathrm{i}\Omega t}, \tag{5.42}$$

where n is the number of semi-waves, and Ω is the *complex natural frequency*. Then $\omega = \Re\Omega$ is the natural frequency and $\alpha = \Im\Omega$ is the damping ratio.

The substitution of Eq. (5.42) in Eq. (5.39) gives the formula for the complex eigenvalues

$$\Omega = \Omega_n = \frac{1}{\sqrt{\rho_l}} \sqrt{\frac{EI\eta_3 \pi^4 n^4 (1 + \theta K n^2)}{L^4 (1 + K n^2)}}, \tag{5.43}$$

where $K = \pi^2 h^2 / \beta L^2$ is the complex shear parameter. The variation of induction B allows changing the complex parameters η_3, θ, K and ultimately the natural frequencies $\omega = \Re\Omega$ and corresponding damping ratios $\alpha = \Im\Omega > 0$. To estimated this effect, we consider the following example.

Example 5.4. Let $L = 0.3$ m, $b = 15$ mm and $h_1 = h_3 = 1$ mm. The face sheets are made of aluminum. The smart core is the MRE-1 (see its properties in Chapt. 2). Figure 5.12 shows the influence of the magnetic field on the lowest frequency ω ($n = 1$) for different thicknesses h_2 of the smart material. Figure 5.13 gives the frequencies ω at $n = 9$ versus the induction B when the core thickness $h_2 = 12$ mm. It is clearly seen that the eigenfrequencies increase at the interval of varying of the induction B from 0 to 210 mT, however this influence is very weak for the first modes and thin core; it becomes noticeable with growing of the smart core layer thickness h_2 for a large number of mode (compare Figs. 5.12 and 5.13).

Figure 5.14 shows the scaled logarithmic decrement $d_l = 500\, D_l/\pi$, where D_l is calculated by (5.7), as a function of the increasing magnetic field. For the first and ninth modes and different thicknesses of the MRE core, the best damping takes place at about 280 mT, this effect becoming stronger with growing the MRE layer. Comparing outcomes presented on Fig. 5.14 with similar results for the sandwich beam with MRF core (s. Figs. from 5.5 to 5.9), one can conclude: MR liquids display the best damping capability at the lowest frequencies, while the MRE-1 does it for modes with large number n of semi-waves.

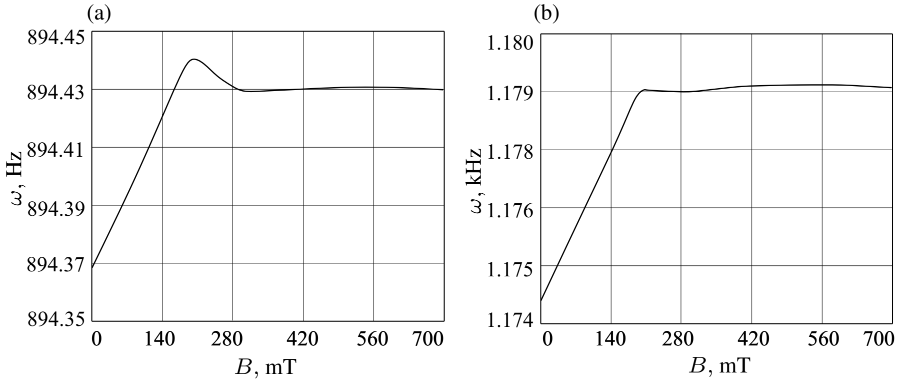

Fig. 5.12 Natural frequency ω at $n = 1$ vs. induction B for different values of thickness h_2. (a) $h_2 = 5$ mm; (b) $h_2 = 12$ mm.

Fig. 5.13 Natural frequency ω at $n = 9$ vs. induction B for $h_2 = 12$ mm.

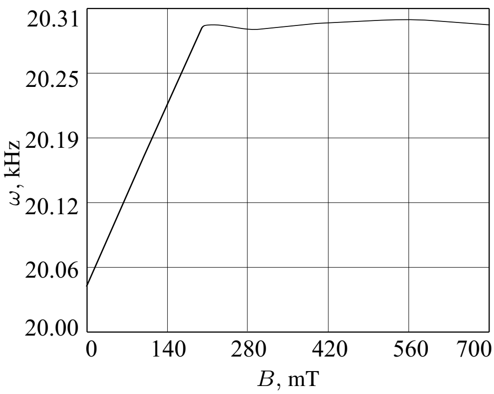

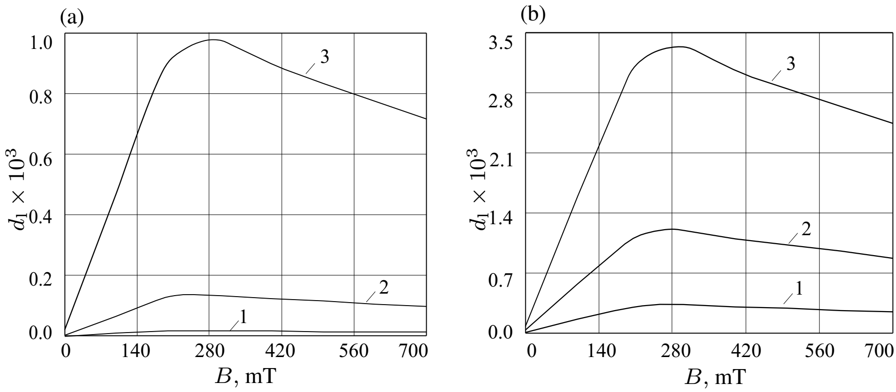

Fig. 5.14 Scaled logarithmic decrement d_1 vs. induction B at (a) $n = 1$ and (b) $n = 9$ for different values of thickness h_2: 1- $h_2 = 5$ mm; 2-$h_2 = 9$ mm; 3- $h_2 = 12$ mm.

It is of interesting to study the effect of a MRE uniformly distributed between different elastic layers on natural frequencies and decrement for multi-layered beams.

Example 5.5. We consider different beams of the same geometrical parameters as in Example 5.4, but consisting of three, five, seven and nine layers. The total thickness h_{Al} of sheets made of aluminum is equal to 2 mm, and the total thickness h_{MRE} of the MRE-1 laminaes is 12 mm. It is assumed that the elastic material (aluminum) and the MRE-1 are uniformly distributed between layers so that the thicknesses of laminas with odd and even numbers are as follows:

- for the sandwich ($N = 3$),

$$h_1 = h_3 = \frac{h_{\mathrm{Al}}}{2}, \quad h_2 = h_{\mathrm{MRE}};$$

- for the five-layer beam ($N = 5$),

$$h_1 = h_3 = h_5 = \frac{h_{\mathrm{Al}}}{3}, \quad h_2 = h_4 = \frac{h_{\mathrm{MRE}}}{2};$$

- for the seven-layer beam ($N = 7$),

$$h_1 = h_3 = h_5 = h_7 = \frac{h_{\mathrm{Al}}}{4}, \quad h_2 = h_4 = h_6 = \frac{h_{\mathrm{MRE}}}{3},$$

- for the nine-layer beam ($N = 9$)

$$h_1 = h_3 = h_5 = h_7 = h_9 = \frac{h_{\mathrm{Al}}}{5}, \quad h_2 = h_4 = h_6 = h_8 = \frac{h_{\mathrm{MRE}}}{4}.$$

Regardless of a number of layers, the quantity of elastic and smart viscoelastic materials is fixed. The outcomes for the sandwich beam ($N = 3$) are presented in Figs. 5.12 (b), 5.13 and 5.14.

The first and ninth frequencies and the corresponding logarithmic decrements for multi-layered beams are displayed in Figs. 5.15 and 5.16. As seen, the impact of magnetic field on eigenfrequencies and damping ratio becomes more weak with increasing number of layers. However, at the fixed induction B, the number of layers greatly influences on all the spectrum of natural frequencies and corresponding damping ratios. When comparing Figs. 5.12 (b) and 5.15 (a), then one concludes that increasing number of layers results in some decreasing the lowest natural frequency at all range of varying B. As for modes with a large number of semi-waves (for instance, compare Figs. 5.13 and 5.15 (b)), the corresponding natural frequencies unevenly increase when the beam is subjected to the partition into five, seven and more number of layers. So, for the ninth mode ($n = 9$) and $B \geq 200$ mT, the natural frequency jumps from 20.30 kHz (for the sandwich beam) up to about 63.60 kHz (for the five-ply beam) and then slightly decreases when the number of layers is increasing. The comparison of Figs. 5.14 and 5.16 shows that the increase of the number of layers leads to a dramatic decreasing of the logarithmic decrement for each mode at the fixed level of applied magnetic field, this reduction being more

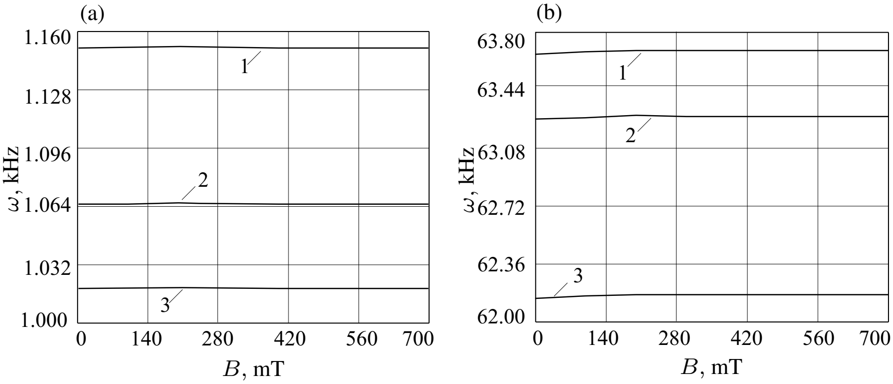

Fig. 5.15 First (a) and ninth (b) natural frequencies ω vs. induction B for different number of layers: 1 - $N = 5$; 2 - $N = 7$; 3 - $N = 9$.

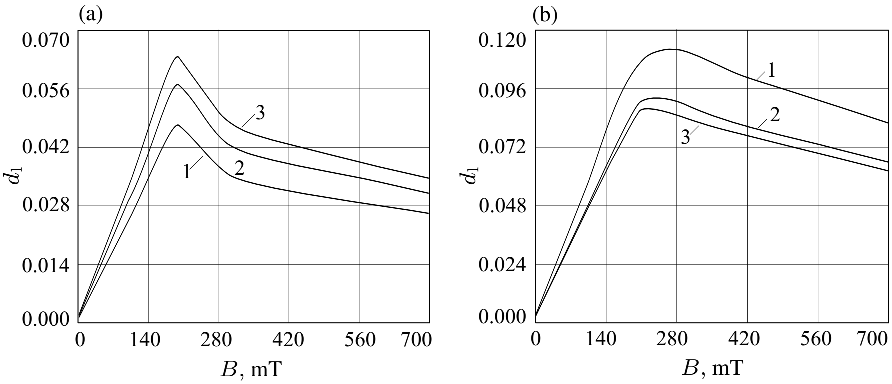

Fig. 5.16 Scaled logarithmic decrement for the first (a) and ninth (b) modes ω vs. induction B for different number of layers: 1 - $N = 5$; 2 - $N = 7$; 3 - $N = 9$.

noticeable for the highest modes. It is of interest to note the behavior of the scaled logarithmic decrement d_l corresponding to the first mode versus the number of layers: under increasing N from 3 to 5, the maximum value of d_l (at $B = 200$ mT) drops from about 1 to 0.046, and then it grows together with the number N of layers.

This example allows us to conclude: splitting the sandwich beam with the MRE core into a large number of layers under fixed quantity of elastic and viscoelastic smart materials results in the reduction of damping properties of the beam, however permits to change significantly the spectrum of natural frequencies (especially its part corresponding to highest modes) removing it to right. Obviously, this property may be used in designing smart laminated beam with adjustable elastic and damping properties.

5.2.2.2 Forced Stationary Vibrations and Their Suppression

Let the beam be under the external periodic force

$$q_{\mathrm{l}} = \rho_{\mathrm{l}} F_0(x)\, \mathrm{e}^{\mathrm{i}\omega_{\mathrm{e}} t}, \tag{5.44}$$

where ω_{e} is the excitation frequency. A solution of Eq. (5.39) with the boundary conditions (5.41) can be presented in the form of the series

$$\chi(x,t) = \sum_{n=1}^{\infty} \sin(\lambda_n x) q_{\mathrm{n}}(t). \tag{5.45}$$

Substituting (5.45) into Eq. (5.39), we obtain the series of equations

$$\ddot{q}_n + \mathit{\Omega}_n^2 q_{\mathrm{n}} = \frac{2F_n}{L(1+Kn^2)} \mathrm{e}^{\mathrm{i}\omega_{\mathrm{e}} t}, \quad n = 1, 2, \ldots, \tag{5.46}$$

where the generalized forces F_n are defined by Eq. (5.11). The partial solution of (5.46) is

$$q_{\mathrm{n}}(t) = \frac{2F_n}{L(1+Kn^2)(\mathit{\Omega}_n^2 - \omega_{\mathrm{e}}^2)}\, \mathrm{e}^{\mathrm{i}\omega_{\mathrm{e}} t}. \tag{5.47}$$

Then the amplitude of forced stationary vibrations will be given by

$$\chi = \sum_{n=1}^{\infty} \frac{2F_n\, \mathrm{e}^{\mathrm{i}\omega_{\mathrm{e}} t}}{L(1+Kn^2)(\mathit{\Omega}_n^2 - \omega_{\mathrm{e}}^2)} \sin(\lambda_n x). \tag{5.48}$$

Example 5.6. Consider the sandwich beam with parameters specified in Example 5.5. The thickness of the MRE core is equal to $h_2 = 12$ mm. We assume the following distribution of the normal periodic force

$$F_0(x) = 4\frac{x}{L}\left(1 - \frac{x}{L}\right). \tag{5.49}$$

Figures 5.17 and 5.18 demonstrate the amplitude-frequency characteristics for the sandwich beam subjected to the periodic force (5.44) with (5.49) in the frequency interval ω_{e} from 1.10 to 10.10 kHz, the dotted line showing the scaled amplitude A_{s} versus ω_{e} if the magnetic field is absent and the solid curve corresponds to the case, when the beam is in the magnetic field of the induction $B = 200$ mT. It is clearly seen that the applied magnetic field shifts the resonance regions to right, this shifting being slight for the lowest resonance frequencies and growing together with the mode number n. The relative reduction of the maximum amplitude $A_{\mathrm{s}}^B/A_{\mathrm{s}}^0$, where A_{s}^B and A_{s}^0 are the scaled amplitude calculated at $B = 200$ mT and $B = 0$ mT, respectively, depends also on n. So, it is equal to approximately 2, 16, 14 for $n = 1, 2, 3$, respectively. Thus, our conclusion made above on the basis of the modal analysis (see the previous example) is confirmed: MREs used as smart cores in sandwich beams reveal the best damping capability at the highest modes and so,

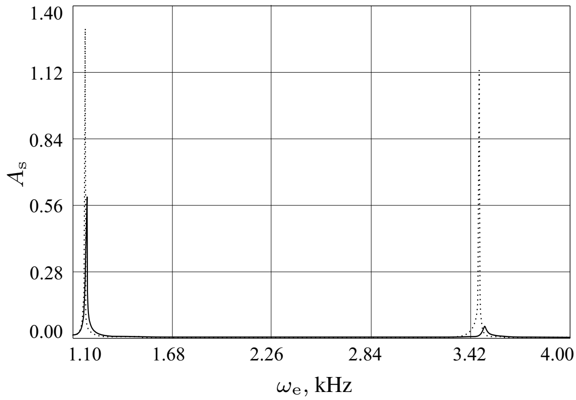

Fig. 5.17 Amplitude-frequency characteristics for the MRE-1 sandwich beam at the interval ω_e from 1.10 to 4.00 kHz for two different cases: dotted line - magnetic field is absent, solid line - magnetic field of the induction $B = 200$ mT is applied.

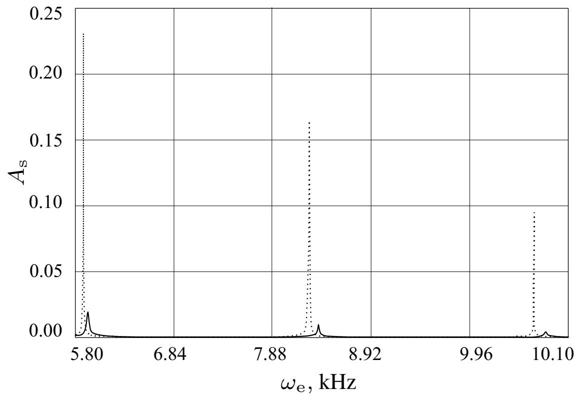

Fig. 5.18 Amplitude-frequency characteristics for the MRE-1 sandwich beam at the interval ω_e from 5.80 to 10.10 kHz for two different cases: dotted line - magnetic field is absent, solid line - magnetic field of the induction $B = 200$ mT is applied.

their application turns out to be more effective for suppression of high-frequency vibrations.

The next example illustrates the resonance response of the beam without magnetic field and after its application.

Example 5.7. Let the beam considered in the previous example be subjected to the resonance periodic force (5.44) applied in the point $x = x^* = L/7$, where the excitation frequency $\omega_e = 3.46$ kHz is close to the second natural frequency of the beam. In Fig. 5.19, the scaled maximum amplitude for the so-called *equivalent beam* with external friction is plotted at $0 \leq t < t_{cr}$, when the magnetic field is absent, and for $t \geq t_{cr}$ as well, where $t_{cr} = 0.2$ is the time of turning on the magnetic field of the induction $B = 300$ mT. In the initial moment the beam is motionless. Computations at $t \geq t_{cr}$ were performed by the approach applied in Example 5.2 in accordance to which the natural frequencies, damping ratio and modes were recalculated after applying the magnetic field. The high-frequency excited oscillations due to the impact action of magnetic field were disregarded. Figure 5.19 shows that the application of magnetic field *removed* the beam from the regime of resonance vibrations and resulted in about fourfold reduction of the amplitude of forced vibrations.

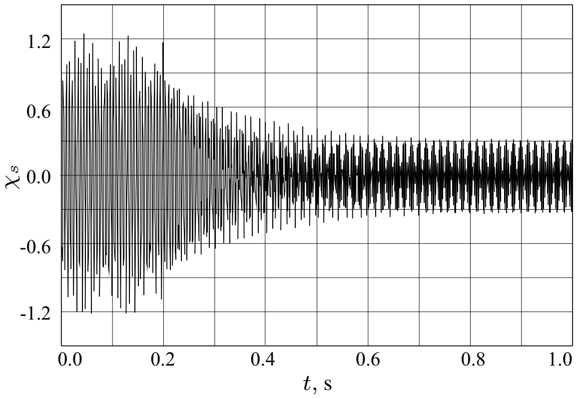

Fig. 5.19 Response of the *equivalent MRE-1 based sandwich beam* to resonance harmonic force and the magnetic field of induction $B = 300$ mT applied at $t = t_{\mathrm{cr}} = 0.2$ s.

5.3 Magnetorheological Sandwich and Multi-Layered Plates

In this section, we consider laminated plates consisting of N transversally isotropic laminas. The sides in the plate plane are equal to L_1 and L_2. Each layer with the number $k(k = 1, 2, \ldots, N)$ is characterized by the thickness h_k, Young's modulus E_k, shear modulus G_k and Poisson's ratio ν_k. If a plate is three-layered (sandwich), as shown in Fig. 5.1, then the face sheets are elastic and the core is a MRE. For multi-layered plate, elastic and smart viscoelastic laminas alternate, odd laminas being made of an elastic material, and even ones being MREs.

Assuming the ESL theory for laminated plate stated in Chapt. 2, we use here the following equations

$$\begin{aligned} & D\left(1 - \frac{\theta h^2}{\beta}\triangle\right)\triangle^2\chi + \rho_0 h\frac{\partial^2 w}{\partial t^2} = q_{\mathrm{ex}}, \quad w = \left(1 - \frac{h^2}{\beta}\triangle\right)\chi, \\ & \frac{(1-\nu)h^2}{2\beta}\triangle\phi = \phi, \end{aligned} \tag{5.50}$$

where $\triangle$ is the Laplace operator in a Cartesian coordinate system α_1, α_2, $(0 \le \alpha_1 \le L_1,\ 0 \le \alpha_2 \le L_2)$, w is the deflection of the plate, ϕ is the shear function, s. its introduction in Chapt. 2, Eq. (2.78), $q_{\mathrm{ex}}(\alpha_1, \alpha_2, t)$ is the normal load, t is time. All other notations appearing in Eq. (5.50) are the same as in Chapt. 2. We only note that the reduced bending stiffness D and the shear parameter β depend on the intensity of the applied magnetic field.

We consider here only one variant of boundary conditions. Let all the edges be simply supported and provided by diaphragm preventing edge shear

$$\chi = \triangle\chi = \frac{\partial\phi}{\partial\alpha_k} = 0 \quad \text{at} \quad \alpha_k = 0,\ L_k; \quad k = 1, 2. \tag{5.51}$$

Then, one can set $\phi = 0$.

5.3.1 Free Vibrations

At first, we analyse free vibrations ($q_{\rm ex} = 0$). The solution of the boundary-value problem (5.50), (5.51) can be found as

$$\chi = \chi_0 \sin \frac{\pi n \alpha_1}{L_1} \sin \frac{\pi m \alpha_2}{L_2} \mathrm{e}^{\mathrm{i}\Omega t}, \tag{5.52}$$

where n, m are numbers of semi-waves in the α_1- and α_2- directions, respectively, and Ω is the complex natural frequency.

Substituting Eq. (5.52) into Eqs. (5.50) gives a simple formula for the required complex eigenvalue

$$\Omega = \Omega_{nm} = \sqrt{\frac{\pi^2 D}{\rho_0 h L_1^4}}\, \Lambda^{1/2}, \tag{5.53}$$

where

$$\Lambda = \Lambda_{nm} = \frac{\delta_{nm}^2 (1 + \theta K \delta_{nm})}{1 + K\delta_{nm}}, \quad K = \frac{\pi^2 h^2}{\beta L_2^2}, \quad \delta_{nm} = n^2 + e^2 m^2, \quad e = \frac{L_1}{L_2}. \tag{5.54}$$

Equation (5.53) gives two complex eigenvalues. We need to chose only one value with the positive imaginary part.

If some of the edges is free of a diaphragm, then a solution of Eqs. (5.50) with corresponding boundary conditions (4.38) may be constructed by the asymptotic approach developed in Subsect. 4.2.2 for an elastic laminated plate. According to this approach, the solution is constructed in the form of superposition of functions corresponding to the main stress-strain state and edge effect integrals in the neighborhood of an edge which is free of diaphragm.

In Eqs. (5.53), (5.54), parameters D, K depend on the induction B, the shear parameter K being the principal one. Just as for a layered beam, a magnetic field and, as consequence, a parameter K have a weak effect on the lowest frequencies and the corresponding decrements. The effect of magnetic field and shears manifests itself on modes for which the number of waves is large in at least one direction. This conclusion is clearly confirmed by the following example.

Example 5.8. Let us consider a square sandwich plate with $L_1 = L_2 = 1$ m. The outer layers (thicknesses $h_1 = h_3 = 0.5$ mm) are made of ABS-plastic SD-0170 with parameters $E_1 = E_3 = 1.5 \cdot 10^3$ MPa, $\nu_1 = \nu_3 = 0.4$, $\rho_1 = \rho_3 = 1.4 \cdot 10^3$ kg/m^3. The core of thickness $h_2 = 10$ mm is MRE-1 with properties given in Chapt. 2 (s. Fig. 2.9). Figures 5.20 and 5.21 show the influence of the magnetic field induction on the natural frequencies $\omega = \Re\Omega$ and decrements $\alpha = \Im\Omega$ for modes with $n = 10$ waves in the α_1-direction and different number of waves in the other direction. It is seen, the larger the wave numbers m and/or n, the stronger the effect of the magnetic field on the characteristics of eigenmodes for the sandwich plate.

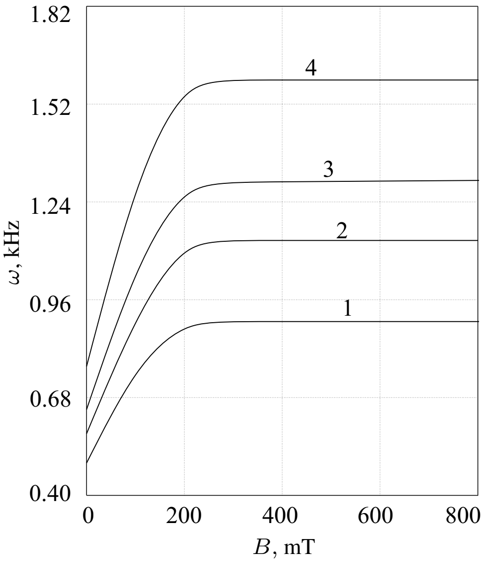

Fig. 5.20 Natural frequency ω vs. induction B for modes with $n = 10$ and different values of m: 1 - $m = 1$, 2 - $m = 5$, 3 - $m = 7$, 4 - $m = 10$.

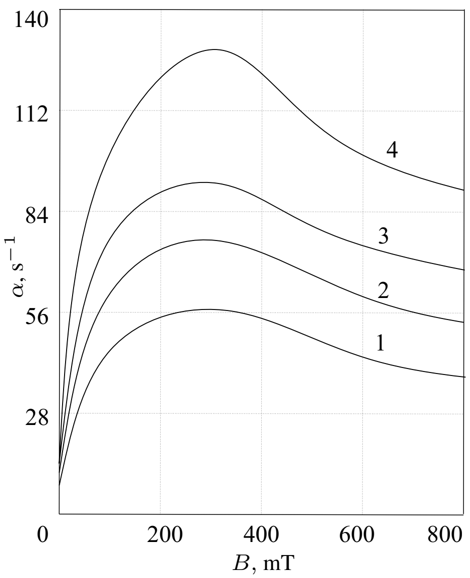

Fig. 5.21 Decrement α vs. induction B for modes with $n = 10$ and different values of m: 1 - $m = 1$, 2 - $m = 5$, 3 - $m = 7$, 4 - $m = 10$.

5.3.2 Forced Stationary Vibrations

Let the plate be under action of the periodic normal force

$$q_{\mathrm{ex}}(\alpha_1, \alpha_2, t) = F_0(\alpha_1, \alpha_2)\mathrm{e}^{\mathrm{i}\omega_{\mathrm{e}} t} \tag{5.55}$$

with the frequency ω_{e}. Here, a solution of Eq. (5.50) with boundary conditions (5.51) is found in the form of the double series

$$\chi(\alpha_1, \alpha_2, t) = \sum_{n=1}^{\infty} \sum_{m=1}^{\infty} \sin \frac{\pi n \alpha_1}{L_1} \sin \frac{\pi m n \alpha_1}{L_2} q_{nm}(t), \tag{5.56}$$

where $q_{nm}(t)$ is generalized coordinates of the system. We substitute (5.56) into Eq. (5.50) and expand function (5.56) into Fourier series. Then, we arrive at the series of differential equations

$$\ddot{q}_{nm} + \Omega_{nm}^2 \, q_{nm} = \frac{F_{nm}}{\rho h (1 + K \delta_{nm})}, \quad n, m = 1, 2, \ldots, \tag{5.57}$$

where

$$F_{nm} = \frac{4}{L_1 L_2} \int_0^{L_1} \int_0^{L_2} F_0(\alpha_1, \alpha_2) \sin \frac{\pi n \alpha_1}{L_1} \sin \frac{\pi n \alpha_2}{L_2} \tag{5.58}$$

are the generalized forces corresponding to the generalized coordinates $q_{nm}(t)$ and the Ω_{nm} are the complex eigenfrequencies defined by (5.54).

The partial solutions of Eqs. (5.58) are the functions

$$q_{nm}(t) = \frac{F_{nm} \mathrm{e}^{\mathrm{i}\omega_{\mathrm{e}} t}}{\rho h (1 + K \delta_{nm})(\Omega_{nm}^2 - \omega_{\mathrm{e}}^2)}, \quad n, m = 1, 2, \ldots \tag{5.59}$$

Then, the amplitude of forced steady-state vibrations will be as follows

$$\chi(\alpha_1, \alpha_2, t) = \sum_{n=1}^{\infty} \sum_{m=1}^{\infty} \frac{F_{nm} \mathrm{e}^{\mathrm{i}\omega_{\mathrm{e}} t}}{\rho h (1 + K \delta_{nm})(\Omega_{nm}^2 - \omega_e^2)} \sin \frac{\pi n \alpha_1}{L_1} \sin \frac{\pi n \alpha_2}{L_2}. \tag{5.60}$$

Equation (5.60) serves to predict the dynamic stationary response of the plate to the periodic force (5.55) arbitrary distributed along the surface. We note that $D, K, \theta, \Omega_{nm}$ are complex magnitudes depending on the magnetic field induction. Thus, applying a magnetic field one can affect the modes and the damping capability of a MRE embedded in the plate and reduce the response of the plate to external forces. We do not give here any examples because the mechanism of suppression of forced vibrations in MRE-based laminated plates is the same as for smart beams considered above.

5.4 Shells with Magneto- and Electrorhelogical Layers Affected by Magnetic/Electric Fields

In this section, we study free and steady-state forced vibrations of laminated MRE- and ERC-based cylindrical panels and shells affected by a constant magnetic or electric field. The main attention will be paid to sandwich panels with a core made of different smart materials whose elastic and rheological properties were given in Chapt. 2.

Let us consider a laminated cylindrical panel (cylinder not closed in the circumferential direction) of the radius R. The length of the straight side is equal to L_1 and the panel width is $L_2 = R\varphi_2$, where $[0, 2\pi) \ni \varphi_2$ is the apex angle of the panel. If $\varphi_2 = 2\pi$, one has a shell closed in the circumferential direction. The choice of the governing equations depends on the geometric dimensions of the panel as well as the expected vibration shape. So, to predict vibrations with formation of very long waves, one has to use the full system of differential equations (2.61)-(2.63) written in terms of displacements $\hat{u}_i, \psi_i, w$, while for studying vibrations accompanied by formation of a large number of short waves, equations of the technical shell theory (2.85) and (2.90) can be used.

5.4.1 Governing Equations and Boundary Conditions

At first, we apply to the full system of differential equations (2.61)-(2.63) which are universal and may be used to examine any type of vibrations for any geometrical dimensions. Omitting non-linear terms, one obtains the system of linear differential equations governing small vibrations of a laminated cylindrical shell

$$
\begin{aligned}
&\frac{\partial^2 \hat{u}_1}{\partial \alpha_1^2} + \frac{1-\nu}{2}\frac{\partial^2 \hat{u}_1}{\partial \alpha_2^2} + \frac{1+\nu}{2}\frac{\partial^2 \hat{u}_2}{\partial \alpha_1 \partial \alpha_2} + \frac{\nu}{R}\frac{\partial w}{\partial \alpha_1} + \frac{1-\nu^2}{Eh}\left(q_1 - \rho_0 \frac{\partial^2 \hat{u}_1}{\partial t^2}\right) = 0,\\
&\frac{1+\nu}{2}\frac{\partial^2 \hat{u}_1}{\partial \alpha_1 \partial \alpha_2} + \frac{1-\nu}{2}\frac{\partial^2 \hat{u}_2}{\partial \alpha_1^2} + \frac{\partial^2 \hat{u}_2}{\partial \alpha_2^2} + \frac{\partial}{\alpha_2}\left(\frac{w}{R}\right) + \frac{1-\nu^2}{Eh}\left(q_2 - \rho_0 \frac{\partial^2 \hat{u}_2}{\partial t^2}\right) = 0,\\
&\eta_2 \frac{\partial \triangle w}{\partial \alpha_1} - \eta_1 \left(\frac{\partial^2 \psi_1}{\partial \alpha_1^2} + \frac{1+\nu}{2}\frac{\partial^2 \psi_2}{\partial \alpha_1 \partial \alpha_2} + \frac{1-\nu}{2}\frac{\partial^2 \psi_1}{\partial \alpha_2^2}\right)\\
&\qquad + \frac{12(1-\nu^2)}{Eh^3}\left(q_{44}\psi_1 + \frac{1}{2}hc_{12}q_1\right) = 0,\\
&\eta_2 \frac{\partial \triangle w}{\partial \alpha_2} - \eta_1 \left(\frac{\partial^2 \psi_2}{\partial \alpha_2^2} + \frac{1+\nu}{2}\frac{\partial^2 \psi_1}{\partial \alpha_1 \partial \alpha_2} + \frac{1-\nu}{2}\frac{\partial^2 \psi_2}{\partial \alpha_1^2}\right)\\
&\qquad + \frac{12(1-\nu^2)}{Eh^3}\left(q_{44}\psi_2 + \frac{1}{2}hc_{12}q_2\right) = 0,\\
&\frac{h^2}{12(1-\nu^2)}\triangle\left[\eta_3 \triangle w - \eta_2\left(\frac{\partial \psi_1}{\partial \alpha_1} + \frac{\partial \psi_2}{\partial \alpha_2}\right)\right] + \frac{1}{R(1-\nu^2)}\left(\nu\frac{\partial \hat{u}_1}{\partial \alpha_1} + \frac{w}{R}\right)\\
&\qquad = \frac{1}{Eh}\left(q_{\mathrm{n}} - \frac{1}{2}hc_{13}\sum_{i=1}^{2}\frac{\partial q_i}{\partial \alpha_i} - \rho_0 \frac{\partial^2 w}{\partial t^2}\right),
\end{aligned}
\tag{5.61}
$$

where $\hat{u}_i$ are the generalized tangential displacements coupled with the corresponding tangential displacements u_i, deflection w and shear displacements ψ_i by Eq. (2.26), $q_i, q_{\mathrm{n}} (i = 1, 2)$ are components of the surface load, and parameters c_{12}, c_{13}, q_{44} and ρ_0 are calculated by Eqs. (2.25), (2.59) and (2.68), respectively.

Let the straight and curvilinear edges $\alpha_1 = 0, L_1$ and $\alpha_2 = 0, L_2$ be simply supported and provided by diaphragm. The appropriate boundary conditions are written as

$$w = \hat{u}_j = \psi_j = 0, \tag{5.62}$$

$$\hat{M}_{ii} = T_{ii} = \hat{L}_{ii} = 0 \tag{5.63}$$

for $\alpha_i = 0, L_i$, where $i, j = 1, 2$ and $i \neq j$. Taking into account Eqs. (2.60), the second set of boundary conditions (5.63) may be rewritten in terms of displacements

$$\begin{aligned} \eta_3 \left(\frac{\partial^2 w}{\partial \alpha_i^2} + \nu \frac{\partial^2 w}{\partial \alpha_j^2} \right) - \eta_2 \left(\frac{\partial \psi_i}{\partial \alpha_i} + \nu \frac{\partial \psi_j}{\partial \alpha_j} \right) &= 0, \\ \frac{\partial \hat{u}_i}{\partial \alpha_i} + \nu \frac{\partial \hat{u}_j}{\partial \alpha_j} + \frac{\nu w}{R} &= 0, \\ \eta_2 \left(\frac{\partial^2 w}{\partial \alpha_i^2} + \nu \frac{\partial^2 w}{\partial \alpha_j^2} \right) - \eta_1 \left(\frac{\partial \psi_i}{\partial \alpha_i} + \nu \frac{\partial \psi_j}{\partial \alpha_j} \right) &= 0. \end{aligned} \tag{5.64}$$

The linearized dynamic equations (2.85) and (2.90) of the technical shell theory are written as follows

$$\begin{aligned} D \left(1 - \frac{\theta h^2}{\beta} \triangle \right) \triangle^2 \chi + \frac{1}{R} \frac{\partial^2 F}{\partial \alpha_1^2} + \rho_0 h \frac{\partial^2 w}{\partial t^2} &= q_{\mathrm{n}}, \\ w = \left(1 - \frac{h^2}{\beta} \triangle \right) \chi, \qquad \triangle^2 F - \frac{Eh}{R} \frac{\partial^2 w}{\partial \alpha_1^2} &= 0, \\ \frac{1-\nu}{2} \frac{h^2}{\beta} \triangle \phi &= \phi. \end{aligned} \tag{5.65}$$

where χ, F are the displacement and the force functions, respectively, ϕ is the additional shear functions, s. Eqs. (2.78) and (2.83), β and D are the shear parameter and the reduced bending stiffness, respectively, introduced by Eqs. (2.84) and (2.88), respectively. The appropriate boundary conditions in terms of displacement, stress and shear functions for the straight and curvilinear edges are the following

$$\chi = \Delta \chi = \Delta^2 \chi = \frac{\partial \phi}{\partial \alpha_i} = 0, \quad \frac{\partial^2 F}{\partial \alpha_2^2} = 0, \quad \frac{\partial^2 F}{\partial \alpha_1^2} = 0 \quad \text{at} \quad \alpha_i = 0, L_i, \tag{5.66}$$

where $i = 1, 2$. We note that all coefficients $D, E, \nu, \beta, \eta_k, c_{12}, c_{13}, q_{44}$, appearing in the above equations and boundary conditions, are complex quantities depending on the magnitude of the magnetic or electric field depending on whether the shell contains MRE or ERE layers.

5.4.2 Free Vibrations

Let $q_i = q_{\mathrm{n}} = 0$. Then the natural modes for a shell governed by Eqs. (5.61) with the boundary conditions (5.66) can be represented by the following functions

$$
\begin{aligned}
\hat{u}_1 &= u_1^\circ \cos\frac{\pi n \alpha_1}{L_1}\sin\frac{\pi m \alpha_2}{L_2}\exp(\mathrm{i}\Omega t),\\
\hat{u}_2 &= u_2^\circ \sin\frac{\pi n \alpha_1}{L_1}\cos\frac{\pi m \alpha_2}{L_2}\exp(\mathrm{i}\Omega t),\\
w &= w^\circ \sin\frac{\pi n \alpha_1}{L_1}\sin\frac{\pi m \alpha_2}{L_2}\exp(\mathrm{i}\Omega t),\\
\psi_1 &= \psi_1^\circ \cos\frac{\pi n \alpha_1}{L_1}\sin\frac{\pi m \alpha_2}{L_2}\exp(\mathrm{i}\Omega t),\\
\psi_2 &= \psi_2^\circ \sin\frac{\pi n \alpha_1}{L_1}\cos\frac{\pi m \alpha_2}{L_2}\exp(\mathrm{i}\Omega t),
\end{aligned}
\tag{5.67}
$$

where $\Omega = \omega + \mathrm{i}\alpha$, $\omega = \Re\Omega$ is the required natural frequency, $\alpha = \Im\Omega > 0$ is the associated damping ratio, n, m are numbers of semi-waves in the axial and circumferential directions, respectively, and $u_i^\circ, w^\circ, \psi_i^\circ$ are constants. If the shell is closed in the circumferential direction, then m is an even number.

Substituting (5.67) into Eqs. (5.61), we arrive at the linear system of five algebraic equations

$$
\mathbf{A}\mathbf{X}^{\mathrm{T}} = 0, \tag{5.68}
$$

where $\mathbf{X} = (u_1^\circ, u_2^\circ, w^\circ, \psi_1^\circ, \psi_2^\circ)$ is the amplitude vector and $\mathbf{A}$ is the matrix with complex elements

$$
\begin{aligned}
a_{11} &= -\delta_n^2 - \frac{1-\nu}{2}\delta_m^2 + \frac{\rho_0 R^2(1-\nu^2)}{E}\Omega^2, \quad a_{12} = \frac{1+\nu}{2}\delta_n\delta_m,\\
a_{13} &= \nu\delta_n, \quad a_{14} = a_{15} = 0, \quad a_{21} = \frac{1+\nu}{2}\delta_n\delta_m,\\
a_{22} &= -\frac{1-\nu}{2}\delta_n^2 - \delta_m^2 + \frac{\rho_0 R^2(1-\nu^2)}{E}\Omega^2, \quad a_{23} = -\delta_m, \quad a_{24} = a_{25} = 0,\\
a_{31} &= a_{32} = 0,\ a_{33} = -\eta_2\delta_n(\delta_n^2 + \delta_m^2),\ a_{34} = \eta_1\left(\delta_n^2 + \frac{1-\nu}{2}\delta_m^2\right) + \frac{q_{44}R^2\eta_3}{D},\\
a_{35} &= -\frac{\eta_1(1+\nu)}{2}\delta_n\delta_m, \quad a_{41} = a_{42} = 0, \quad a_{43} = -\eta_2\delta_m(\delta_n^2 + \delta_m^2),\\
a_{44} &= -\frac{\eta_1(1+\nu)}{2}\delta_n\delta_m, \quad a_{45} = \eta_1\left(\delta_m^2 + \frac{1-\nu}{2}\delta_n^2\right) + \frac{q_{44}R^2\eta_3}{D},\\
a_{51} &= -\frac{\nu}{1-\nu^2}\delta_n, \quad a_{52} = \frac{1}{1-\nu^2}\delta_m,\\
a_{53} &= \frac{h^2\eta_3}{12(1-\nu^2)R^2}(\delta_n^2 + \delta_m^2)^2 + \frac{1}{1-\nu^2} - \frac{\rho_0 R^2}{E}\Omega^2,\\
a_{54} &= -\frac{h^2\eta_2}{12(1-\nu^2)R^2}\delta_n(\delta_n^2 + \delta_m^2), \quad a_{55} = \frac{h^2\eta_2}{12(1-\nu^2)R^2}\delta_m(\delta_n^2 + \delta_m^2),
\end{aligned}
\tag{5.69}
$$

where

$$\delta_n = \frac{\pi n R}{L_1}, \quad \delta_m = \frac{\pi m R}{L_2} = \frac{\pi m}{\varphi_2}. \tag{5.70}$$

Although, the structure of the matrix **A** with elements (4.81) and (5.71) is the same, but there are differences: all elements (4.81) are real, while the quantities η_k, ν, E, D in (5.71) are complex magnitudes; in (4.81), m is the number of waves in the circumferential direction for a cylinder closed in the circumferential direction and m appearing in Eqs. (5.71) denotes the number of semi-waves in this direction for a panel.

The condition for the existence of a nontrivial solution of Eqs. (5.70) leads to the equation

$$\det \mathbf{A} = 0 \tag{5.71}$$

which serves to find the complex eigenvalue Ω. For any fixed numbers n, m, this equation gives six complex roots

$$\begin{aligned} \Omega_{nm}^{(j)} &= \omega_{nm}^{(j)} + \mathrm{i}\alpha_{nm}^{(j)}, \quad \alpha_{nm}^{(j)} > 0, \\ \Omega_{nm}^{(j+3)} &= -(\omega_{nm}^{(j)} + \mathrm{i}\alpha_{nm}^{(j)}), \quad j = 1, 2, 3. \end{aligned} \tag{5.72}$$

It is obvious that the eigenvalues $\Omega_{nm}^{(4)}, \Omega_{nm}^{(5)}, \Omega_{nm}^{(6)}$ do not satisfy to the damping conditions and are not taken into consideration in what follows.

In the general case, the first three roots in (5.72) correspond to the coupled bending (out-of-plane) and tangential (in-plane) vibrations accounting for shears (we note that the inertia of shear deformations is here not taking into account). To study predominately bending vibrations, the terms containing Ω in the elements a_{11}, a_{22} of the matrix **A** might be omitted. Then Eq. (5.71) will give only the one root $\Omega_{nm}^{(1)}$ with the positive imaginary part $\alpha_{nm}^{(1)} > 0$.

Regardless of the mode type, the amplitudes of tangential and shear displacements are coupled with the normal displacement as follows

$$\begin{aligned} u_1^\circ &= b_1(n,m)w^\circ, \quad u_2^\circ = b_2(n,m)w^\circ, \\ \psi_1^\circ &= d_1(n,m)w^\circ, \quad \psi_2^\circ = d_2(n,m)w^\circ, \\ b_1(n,m) &= \frac{a_{13}a_{22} - a_{12}a_{23}}{a_{12}a_{21} - a_{22}a_{11}}, \quad b_2(n,m) = \frac{a_{23}a_{11} - a_{13}a_{21}}{a_{12}a_{21} - a_{22}a_{11}}, \\ d_1(n,m) &= \frac{a_{33}a_{45} - a_{35}a_{43}}{a_{44}a_{35} - a_{34}a_{45}}, \quad d_2(n,m) = \frac{a_{43}a_{34} - a_{44}a_{33}}{a_{44}a_{35} - a_{34}a_{45}}, \end{aligned} \tag{5.73}$$

where b_j, d_j are the functions of the number of semi-waves n and m in the axial and circumferential directions.

Consider a cylindrical shell closed in the circumferential direction. For axisymmetric modes ($m = 0$), Eq. (5.71) results in four complex roots calculated by the formula

$$\varOmega = \varOmega_{n0} = \pm\sqrt{\frac{E\varLambda_{n0}^{(j)}}{\rho_0 R^2(1-\nu^2)}}, \quad j = 1, 2, \tag{5.74}$$

where the complex $\varLambda_{n0}^{(j)}$ are found by (4.86)

$$\varLambda_{n0}^{(j)} = \frac{1}{2}\left[1 + \delta_n^2 + \mu_1\delta_n^4 r_n - (-1)^j\sqrt{(1-\delta_n^2+\mu_1\delta_n^4 r_n)^2 + 4\nu^2\delta_n^2}\right]. \tag{5.75}$$

Here,

$$\mu_1 = (1-\nu^2)\varepsilon^8, \quad r_n = \frac{\pi^2 + \theta K\delta_n^2}{\pi^2 + K\delta_n^2}, \quad K = \frac{\pi^2 h^2}{\beta R^2}, \quad \theta = 1 - \frac{\eta_2^2}{\eta_1\eta_3}. \tag{5.76}$$

Obviously, from four complex eigenmodes (5.74), one needs to choose only two ones, $\varOmega_{n0}^{(j)} = \omega_{n0}^{(j)} + \mathrm{i}\alpha_{n0}^{(j)}$, with $\alpha_{n0}^{(j)} > 0$ for $j = 1, 2$.

Now we consider Eqs. (5.65) corresponding to the technical shell theory. Their solution satisfying to the boundary conditions (5.68) at all edges is readily written down:

$$\begin{aligned} \chi &= \chi^\circ \sin\frac{\pi n\alpha_1}{L_1}\sin\frac{\pi m\alpha_2}{L_2}\exp(\mathrm{i}\varOmega t) \\ F &= F^\circ \sin\frac{\pi n\alpha_1}{L_1}\sin\frac{\pi m\alpha_2}{L_2}\exp(\mathrm{i}\varOmega t), \end{aligned} \tag{5.77}$$

where χ°, F° are constant amplitudes of flexural vibrations. The substitution of (5.77) into Eqs. (5.67) results in the required complex eigenfrequency

$$\varOmega = \varOmega_{nm} = \sqrt{\frac{E}{\rho_0 R^2}}\left[\frac{\eta h^2}{12R^2}\frac{\delta_{nm}^2(1+\theta K\delta_{nm})}{1+K\delta_{nm}} + \frac{n^4}{l_1^4\delta_{nm}^2}\right]^{1/2}, \tag{5.78}$$

where

$$\eta = \frac{\pi^4\eta_3}{1-\nu^2}, \quad \delta_{nm} = \frac{1}{\pi^2}(\delta_n^2 + \delta_m^2) = \frac{n^2}{l_1^2} + \frac{m^2}{\varphi_2^2}, \quad l_1 = \frac{L_1}{R},$$

and the magnitudes β, θ are calculated by Eqs. (2.84) and (2.89), respectively.

The frequency equation (5.71) with (5.69) may be used to predict the frequency and damping response of the smart viscoelastic laminated panel of arbitrary length L_1 and apex angle φ_2. If $L_2 \sim R$ and the angle φ_2 is large (close to 2π), then to predict low-frequency vibrations with a large number of semi-waves in the circumferential direction, one can apply to more simple formula (5.78).

5.4.2.1 Main Tunable Complex Parameters[1]

Coefficients of Eq. (5.71) depend on the following six complex parameters

[1] This subsection is written in cooperation with S.S. Maevskaya (Vitebsk State University, Belarus, Vitebsk, e-mail: svetlanamaevskaya@ya.ru).

$$\eta_1,\ \eta_2,\ \eta_3,\ E,\ q_{44}\,(\text{or } K),\ \nu, \tag{5.79}$$

which are functions of the magnitude of the applied magnetic/electric field. In the framework of the ESL theory, they can be considered as independent integral characteristics of variable viscoelastic properties regardless of the number of layers. It is of interest to note that their number is equal to the number of independent physical characteristics of the three-layer shell (sandwich) in the case when each layer is isotropic. As can be seen from Eqs. (5.74) for the axially symmetric modes, the quantity of these parameters may be reduced to five

$$\eta_3,\ \theta,\ E,\ K,\ \nu. \tag{5.80}$$

When assuming Eqs. (5.65) of the technical shell theory, the number of independent variable parameters is reduced to four, s. Eqs. (5.78),

$$\eta,\ \theta,\ E,\ K, \tag{5.81}$$

where η is expressed in terms of η_3 and ν.

Applying a magnetic or electric field (depending on whether a shell assembled form MR or ER smart material), one can vary the parameters (5.80) or (5.81) and, in such a way, to change the frequency characteristics and damping properties of a smart structure. It is obvious that the influence of the magnetic/electric field on the above tunable parameters is different. This effect depends on the correlation between layer thicknesses and their viscoelastic properties. To analyse this effect in detail, we consider several cylindrical sandwiches of the same radius $R = 0.5$ m with the face sheets of the thickness $h_1 = h_2 = 0.5$ mm made of ABS-plastic SD-0170 (see properties in Example 5.8). Other dimensions of the sandwiches are not specified here. The viscoelastic cores of these sandwiches are made of different smart materials (MRE-1, MRE-2, MRE-3, MRE-4, MRE-5, ERC) listed with their properties in Chapt. 2. The core thickness is also varied. Figures 5.22-5.25 show the behavior of the real and imaginary parts of parameters (5.81) versus the magnetic field induction B for different thicknesses h_2 of the viscoelastic smart core made of the MRE-1. Here $\eta_\mathrm{r} = \Re\eta, \eta_\mathrm{i} = \Im\eta$, $\theta_\mathrm{r} = \Re\theta, \theta_\mathrm{i} = \Im\theta$, $E_\mathrm{r} = \Re E, E_\mathrm{i} = \Im E$, $K_\mathrm{r} = \Re K$ and $K_\mathrm{i} = \Im K$.

As follows from equations given in Chapt. 2, parameters η, θ, E are expressed in terms of Young's moduli of all layers and independent of the shear moduli G_k, while the reduced shear parameter K is a function of G_k. However, if a smart viscoelastic material is treated as an isotropic one, then η, θ, E should be considered as functions of the variable shear modulus G_2 for the smart core. We remind that MRE-1 was assumed as the isotropic material (s. Chapt. 2). Therefore, η_r, η_i, $\theta_\mathrm{r}, \theta_\mathrm{i}$, E_r and E_i reveal some dependence on the magnetic field induction B, these dependencies being linear. It is seen from Fig. 5.23 that parameters θ_r and θ_i are very small and cannot be taken into account when calculating the eigenfrequencies. The real part of the reduced Young's modulus, E_r may be considered as a constant magnitude for the fixed value of h_2, while E_i is a monotonically increasing function of B. The shear parameters K_r and K_i are the main adaptive parameters affected by the applied magnetic field. Figure 5.25 demonstrates the nonlinear behavior of the principal dissipative parameter $K_{\rm i}$ when the magnetic field induction is varying, this nonlinearity is becoming more noticeable when increasing the thickness h_2 in comparison with the total thickness h. At a fixed value of h_2, the function $|K_{\rm i}(B)|$ has a maximum which increases together with h_2 but it is reached at more low level of the magnetic field.

The outcomes of calculations of parameters (5.81) for sandwich structures with a core made of other VSMs (MRE-3, MRE-4, MRE-5 and ERC) treated as isotropic materials are presented in Figs. 5.26-5.41. Their analysis allows concluding that the qualitative behavior of all tunable parameters versus the magnetic field induction (for the MRE-3, MRE-4 and MRE-5 based cores) or the electric field strength (for the ERC based core) is the same as for the MRE-1 based sandwich: the influence of the magnetic or electric field on $\eta_{\rm r}$, $\eta_{\rm i}$, $\theta_{\rm r}$, $\theta_{\rm i}$, $E_{\rm r}$ and $E_{\rm i}$ turns out to be minor or very small, while the shear parameters $K_{\rm r}$ and $K_{\rm i}$ reveal the nonlinear behavior and strong dependence on the intensity of applied magnetic or electric field.

Let us compare parameters (5.78) calculated for sandwiches containing isotropic smart cores with similar parameters for the MRE-2 based sandwich. MRE-2 is a

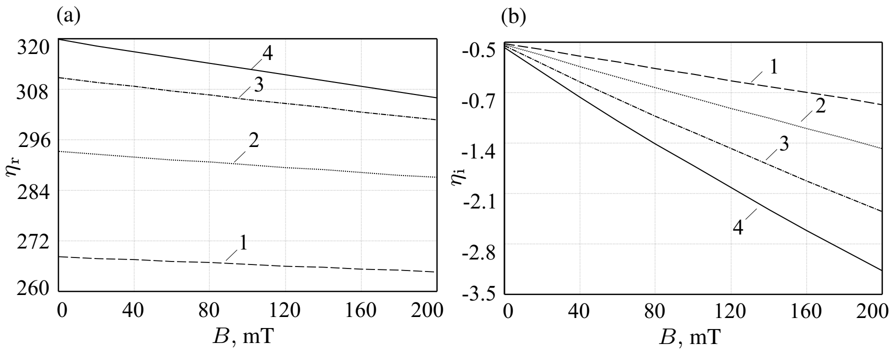

Fig. 5.22 Parameters $\eta_{\rm r}$ (a) and $\eta_{\rm i}$ (b) for sandwich with MRE-1 core vs. induction B at different values of thickness h_2: 1 - $h_2 = 3$ mm, 2 - $h_2 = 5$ mm, 3 - $h_2 = 8$ mm, 5 - $h_2 = 11$ mm.

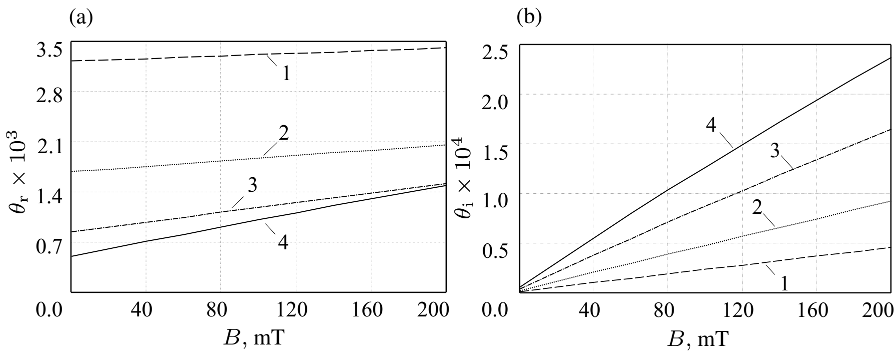

Fig. 5.23 Parameters $\theta_{\rm r}$ (a) and $\theta_{\rm i}$ (b) for sandwich with MRE-1 core vs. induction B at different values of thickness h_2: 1 - $h_2 = 3$ mm, 2 - $h_2 = 5$ mm, 3 - $h_2 = 8$ mm, 5 - $h_2 = 11$ mm.

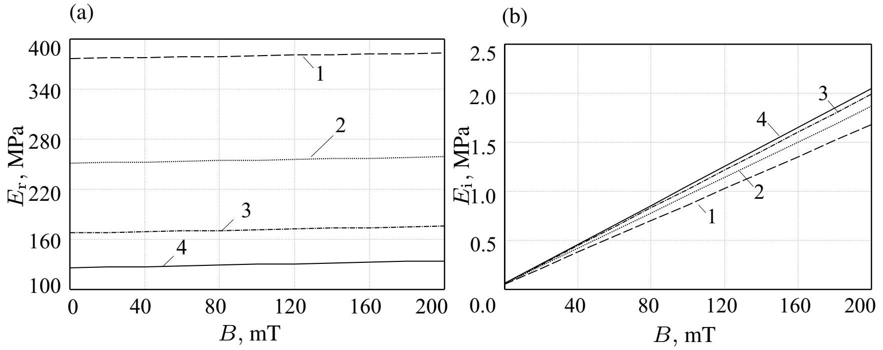

Fig. 5.24 Parameters E_r (a) and E_i (b) for sandwich with MRE-1 core vs. induction B at different values of thickness h_2: 1 - $h_2 = 3$ mm, 2 - $h_2 = 5$ mm, 3 - $h_2 = 8$ mm, 5 - $h_2 = 11$ mm.

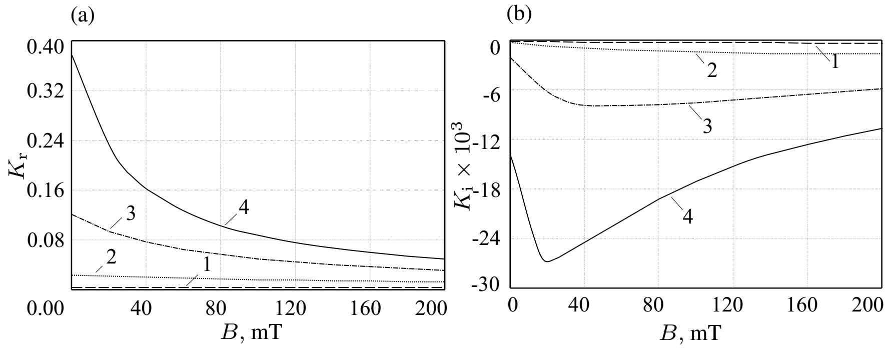

Fig. 5.25 Parameters K_r (a) and K_i (b) for sandwich with MRE-1 core vs. induction B at different values of thickness h_2: 1 - $h_2 = 3$ mm, 2 - $h_2 = 5$ mm, 3 - $h_2 = 8$ mm, 5 - $h_2 = 11$ mm.

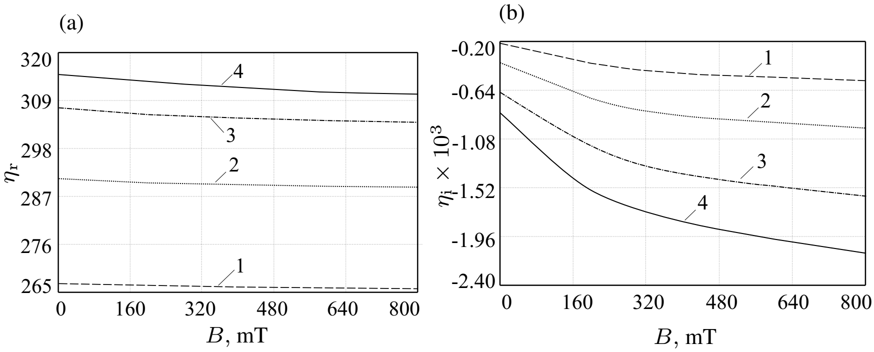

Fig. 5.26 Parameters η_r (a) and η_i (b) for sandwich with MRE-3 core vs. induction B at different values of thickness h_2: 1 - $h_2 = 3$ mm, 2 - $h_2 = 5$ mm, 3 - $h_2 = 8$ mm, 4 - $h_2 = 11$ mm.

isotropic material with the Young's modulus independent of the magnetic field induction B (Aguib et al, 2014). Table 5.1 shows that η, θ and the reduced Young's modulus E are real magnitudes depending only on the thickness h_2 of the transversally isotropic smart core made of MRE-2. Figure 5.42 demonstrates the strong

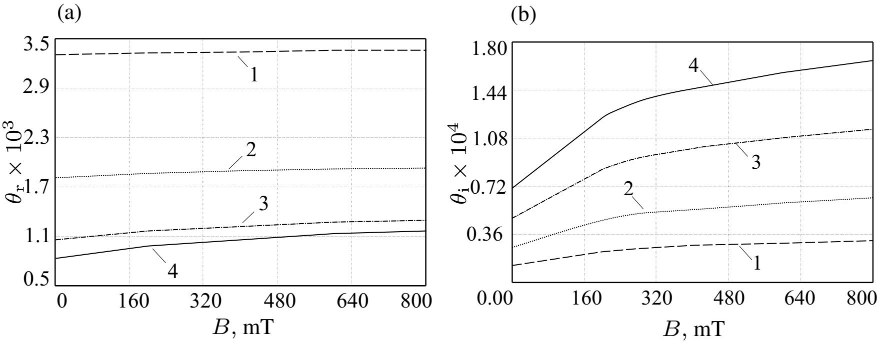

Fig. 5.27 Parameters $\theta_{\rm r}$ (a) and $\theta_{\rm i}$ (b) for sandwich with MRE-3 core vs. induction B at different values of thickness h_2: 1 - $h_2 = 3$ mm, 2 - $h_2 = 5$ mm, 3 - $h_2 = 8$ mm, 4 - $h_2 = 11$ mm.

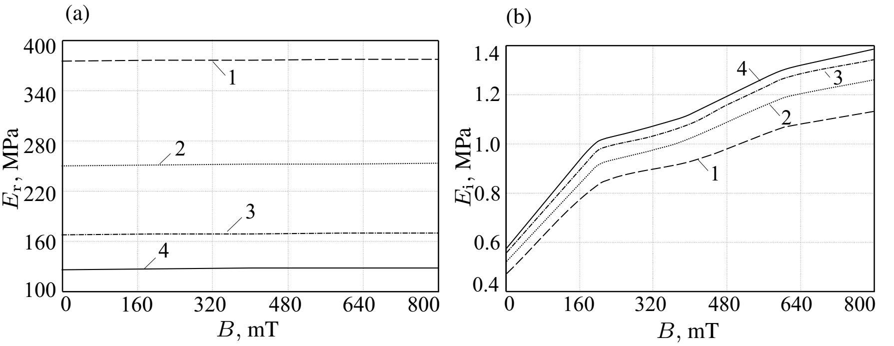

Fig. 5.28 Parameters $E_{\rm r}$ (a) and $E_{\rm i}$ (b) for sandwich with MRE-3 core vs. induction B at different values of thickness h_2: 1 - $h_2 = 3$ mm, 2 - $h_2 = 5$ mm, 3 - $h_2 = 8$ mm, 4 - $h_2 = 11$ mm.

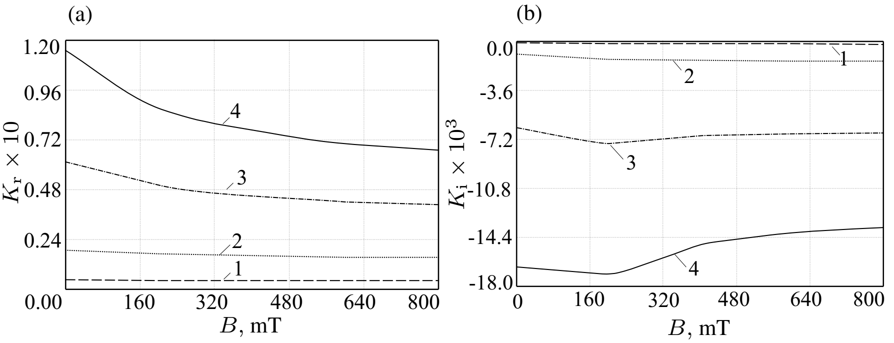

Fig. 5.29 Parameters $K_{\rm r}$ (a) and $K_{\rm i}$ (b) for sandwich with MRE-3 core vs. induction B at different values of thickness h_2: 1 - $h_2 = 3$ mm, 2 - $h_2 = 5$ mm, 3 - $h_2 = 8$ mm, 4 - $h_2 = 11$ mm.

influence of induction B on the shear parameters $K_{\rm r}$ and $K_{\rm i}$. When comparing the plots $K_{\rm r}(B)$ and $K_{\rm i}(B)$ for MRE-1 with the same curves for other smart materials listed in Chapt. 2, s. Figs. 5.26-5.41, one can conclude that MRE-1 reveals the highest sensitiveness to a signal of an external physical field.

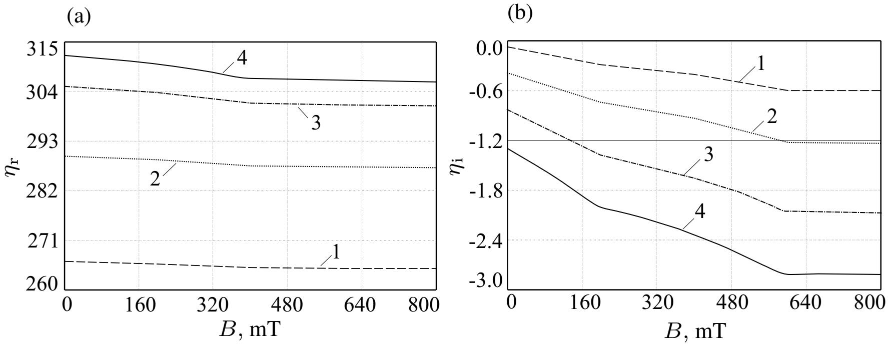

Fig. 5.30 Parameters η_r (a) and η_i (b) for sandwich with MRE-4 core vs. induction B at different values of thickness h_2: 1 - $h_2 = 3$ mm, 2 - $h_2 = 5$ mm, 3 - $h_2 = 8$ mm, 4 - $h_2 = 11$ mm.

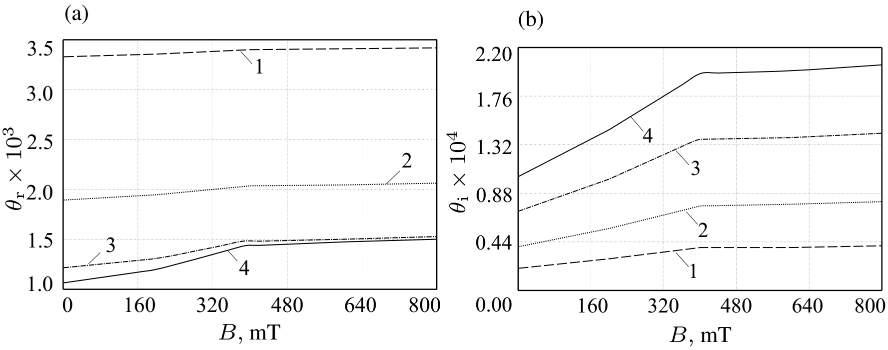

Fig. 5.31 Parameters θ_r (a) and θ_i (b) for sandwich with MRE-4 core vs. induction B at different values of thickness h_2: 1 - $h_2 = 3$ mm, 2 - $h_2 = 5$ mm, 3 - $h_2 = 8$ mm, 4 - $h_2 = 11$ mm.

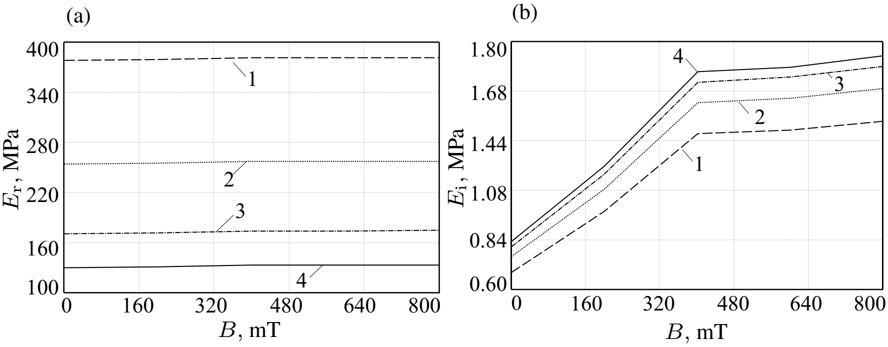

Fig. 5.32 Parameters E_r (a) and E_i (b) for sandwich with MRE-4 core vs. induction B at different values of thickness h_2: 1 - $h_2 = 3$ mm, 2 - $h_2 = 5$ mm, 3 - $h_2 = 8$ mm, 4 - $h_2 = 11$ mm.

5.4.2.2 Free Low-frequency Vibrations of Medium-length Cylindrical Sandwich Panels

To display the real damping capability of aforementioned VSMs, we study free low-frequency vibrations of thin cylindrical sandwiches with different viscoelastic cores.

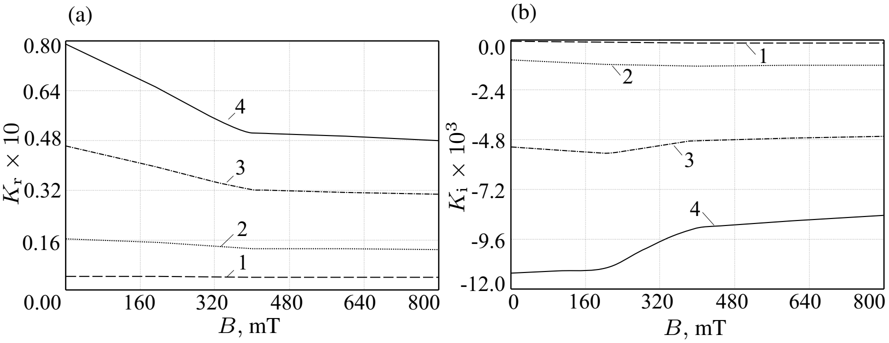

Fig. 5.33 Parameters K_{r} (a) and K_{i} (b) for sandwich with MRE-4 core vs. induction B at different values of thickness h_2: 1 - $h_2 = 3$ mm, 2 - $h_2 = 5$ mm, 3 - $h_2 = 8$ mm, 4 - $h_2 = 11$ mm.

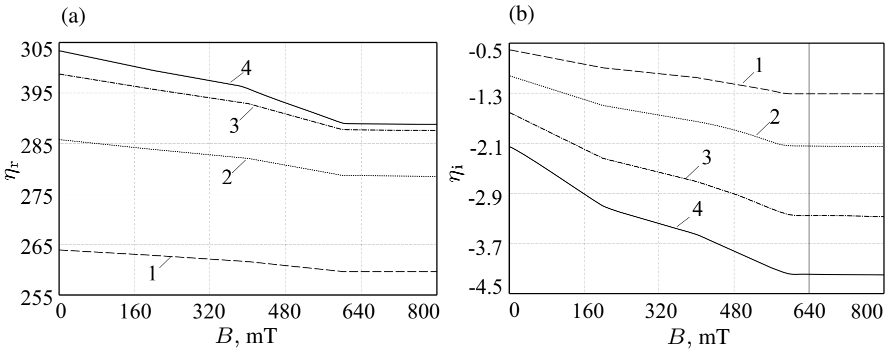

Fig. 5.34 Parameters η_{r} (a) and η_{i} (b) for sandwich with MRE-5 core vs. induction B at different values of thickness h_2: 1 - $h_2 = 3$ mm, 2 - $h_2 = 5$ mm, 3 - $h_2 = 8$ mm, 4 - $h_2 = 11$ mm.

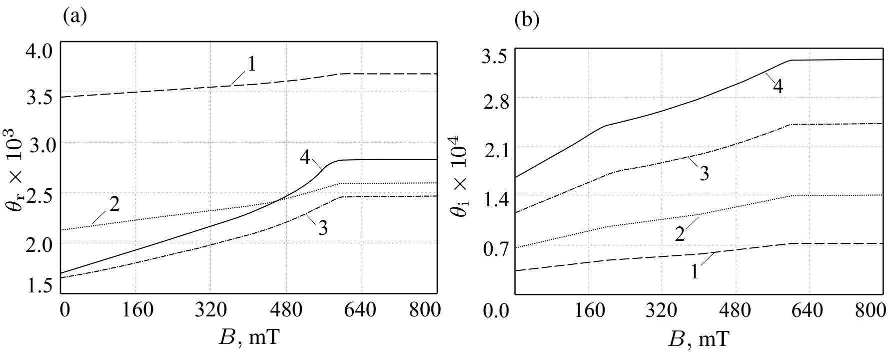

Fig. 5.35 Parameters θ_{r} (a) and θ_{i} (b) for sandwich with MRE-5 core vs. induction B at different values of thickness h_2: 1 - $h_2 = 3$ mm, 2 - $h_2 = 5$ mm, 3 - $h_2 = 8$ mm, 4 - $h_2 = 11$ mm.

Example 5.9. The sandwich has the length $L_2 = 1$ m, the radius of the reference surface $R = 0.5$ m and the apex angle $\varphi_2 = \pi$. The face sheets (thickness $h_1 = h_2 = 0.5$ mm) are made of ABS-plastic SD-0170. The smart core of the thickness $h_2 = 8$ mm is MRE-1. The natural modes of low-frequency vibrations of a thin

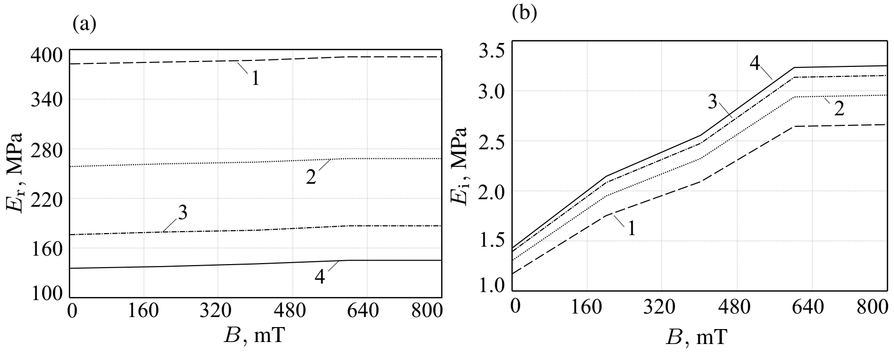

Fig. 5.36 Parameters E_{r} (a) and E_{i} (b) for sandwich with MRE-5 core vs. induction B at different values of thickness h_2: 1 - $h_2 = 3$ mm, 2 - $h_2 = 5$ mm, 3 - $h_2 = 8$ mm, 4 - $h_2 = 11$ mm.

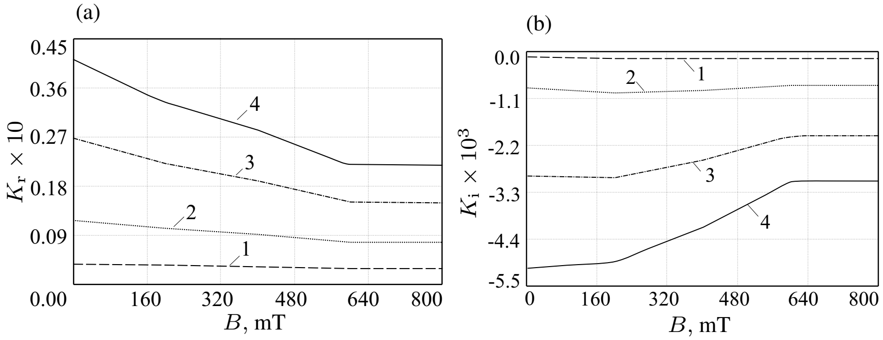

Fig. 5.37 Parameters K_{r} (a) and K_{i} (b) for sandwich with MRE-5 core vs. induction B at different values of thickness h_2: 1 - $h_2 = 3$ mm, 2 - $h_2 = 5$ mm, 3 - $h_2 = 8$ mm, 4 - $h_2 = 11$ mm.

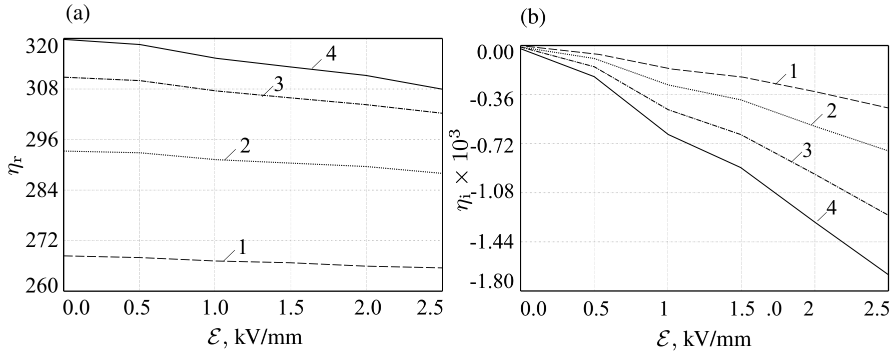

Fig. 5.38 Parameters η_{r} (a) and η_{i} (b) for sandwich with ERC core vs. electric field strength $\mathcal{E}$ at different values of thickness h_2: 1 - $h_2 = 3$ mm, 2 - $h_2 = 5$ mm, 3 - $h_2 = 8$ mm, 4 - $h_2 = 11$ mm.

medium-length cylindrical shell are characterized by one semi-wave in the axial direction and a large number of waves in the circumferential direction. To find the lowest eigenfrequencies $\omega = \Re\Omega$, we apply Eq. (5.78) for $n = 1$ and different numbers m of semi-waves in the circumferential direction. Figure 5.43 shows that

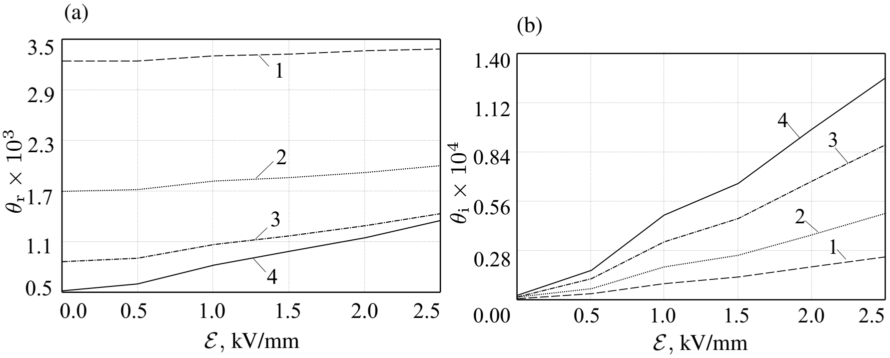

Fig. 5.39 Parameters θ_r (a) and θ_i (b) for sandwich with ERC core vs. electric field strength $\mathcal{E}$ at different values of thickness h_2: 1 - $h_2 = 3$ mm, 2 - $h_2 = 5$ mm, 3 - $h_2 = 8$ mm, 4 - $h_2 = 11$ mm.

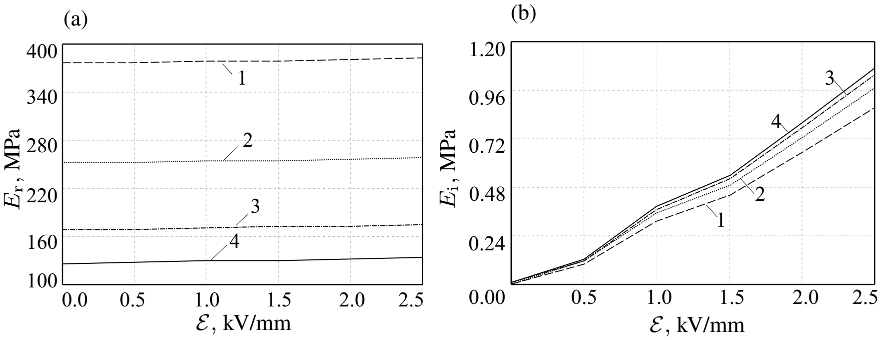

Fig. 5.40 Parameters E_r (a) and E_i (b) for sandwich with ERC core vs. electric field strength $\mathcal{E}$ at different values of thickness h_2: 1 - $h_2 = 3$ mm, 2 - $h_2 = 5$ mm, 3 - $h_2 = 8$ mm, 4 - $h_2 = 11$ mm.

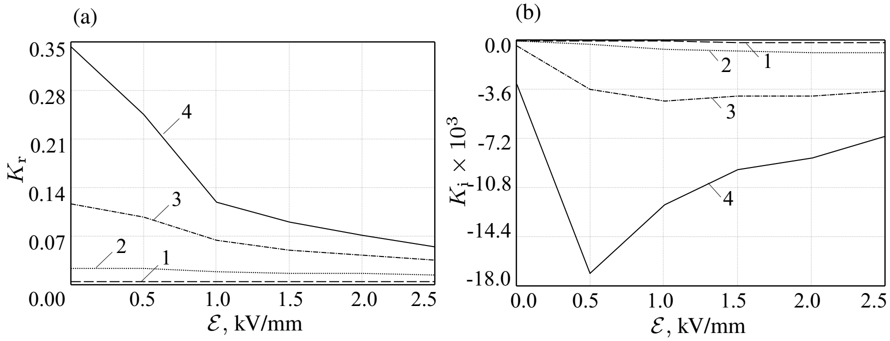

Fig. 5.41 Parameters K_r (a) and K_i (b) for sandwich with ERC core vs. electric field strength $\mathcal{E}$ at different values of thickness h_2: 1 - $h_2 = 3$ mm, 2 - $h_2 = 5$ mm, 3 - $h_2 = 8$ mm, 4 - $h_2 = 11$ mm.

for any B the lowest eigenfrequency refers to the mode with $m = 4$ semi-waves. The effect of magnetic field on natural frequencies turns out to be minor for modes with $m = 1, 2, 3$ semi-waves and becomes significant for a large number m beginning from $m = 5$. This effect depends on the core thickness and the type of VSM.

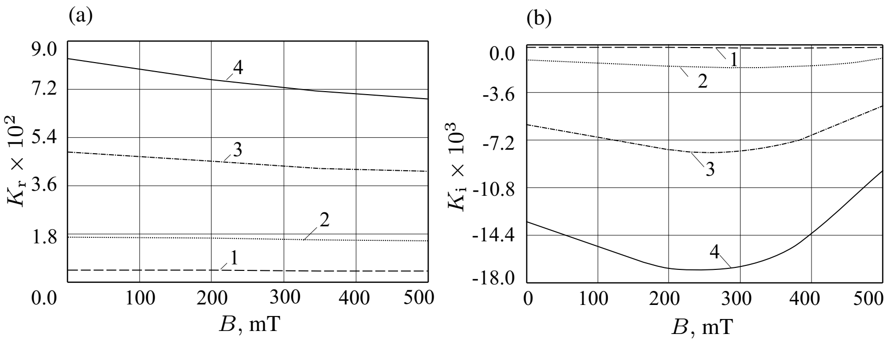

Fig. 5.42 Parameters K_r (a) and K_i (b) for sandwich with MRE-2 core vs. induction B at different values of thickness h_2: 1 - $h_2 = 3$ mm, 2 - $h_2 = 5$ mm, 3 - $h_2 = 8$ mm, 5 - $h_2 = 11$ mm.

Fig. 5.43 Natural frequencies of the MRE-1 based sandwich corresponding to $n = 1$ semi-waves in the axial direction and different number m of semi-waves in the circumferential direction vs. induction B. The plot number corresponds to a number m.

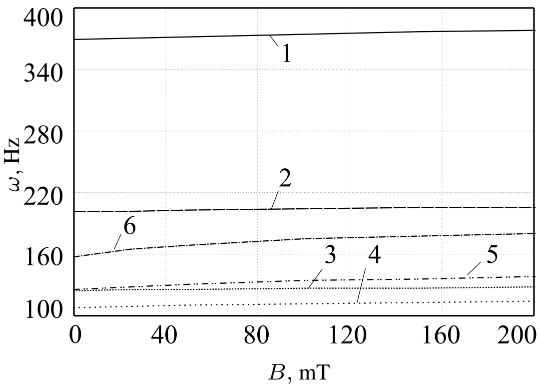

The next series of calculations is aimed to examine the effect of a thickness h_2 and available smart materials on the lowest natural frequencies and corresponding damping ratios at different levels of applied magnetic or electric field.

Example 5.10. We consider six different sandwiches, S-1, S-2, S-3, S-4, S-5 and S-6, with cores made of MRE-1, MRE-2, MRE-3, MRE-4, MRE-5 or ERC, respectively. The viscoelastic properties of these smart composite materials are given in Chapt. 2. The behavior of the principal complex parameters η, θ, E and K versus the magnetic induction (or electric strength) was shown above. The geometrical dimensions of all sandwiches are the same as in the previous example. In Figs. 5.44-5.49 the

Table 5.1 Parameters η, θ and reduced Young's modulus E vs. the core thickness h_2.

h_2, mm	η	$\theta \times 10^3$	E, MPa
3	267	3.265	376
5	292	1.751	251
8	308	0.963	168
11	317	0.693	127

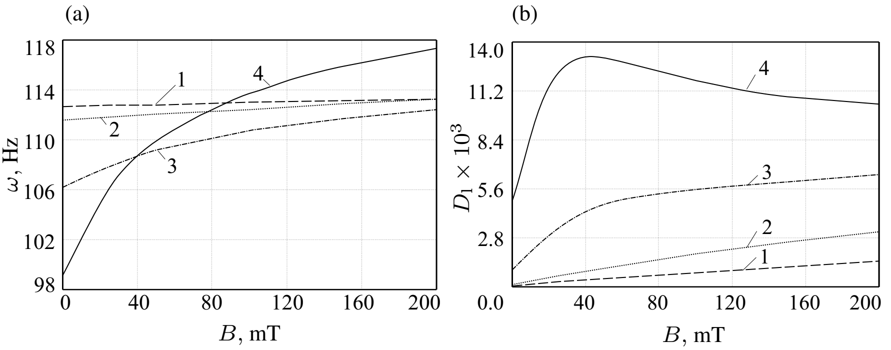

Fig. 5.44 Natural frequency ω (a) and logarithmic decrement D_1 (b) for sandwiches S-1 with MRE-1 core and different values of thickness h_2 vs. induction B: 1 - $h_2 = 3$ mm, 2 - $h_2 = 5$ mm, 3 - $h_2 = 8$ mm, 4 - $h_2 = 11$ mm.

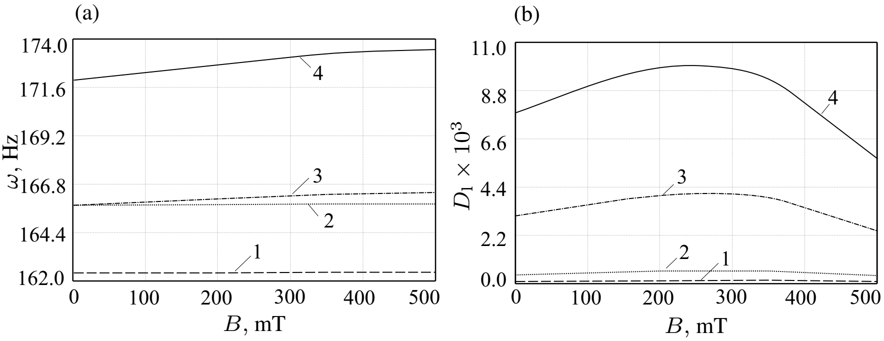

Fig. 5.45 Natural frequency ω (a) and logarithmic decrement D_1 (b) for sandwiches S-2 with MRE-2 core and different values of thickness h_2 vs. induction B: 1 - $h_2 = 3$ mm, 2 - $h_2 = 5$ mm, 3 - $h_2 = 8$ mm, 4 - $h_2 = 11$ mm.

lowest natural frequencies $\omega = \Re \Omega$ and corresponding logarithmic decrements D_1 calculated by Eq. (5.7) are plotted as functions of the magnetic field induction B (for sandwiches with MRE-core) or the electric field strength $\mathcal{E}$ (for S-6 sandwich with ERC-core) at different values of h_2. For any fixed h_2, the lowest eigenfrequencies are monotonically increasing functions of the intensity of the external physical field, the frequency gain being higher for sandwiches with more thick smart viscoelastic core. However, the behavior of ω vs. h_2 at a fixed B (or $\mathcal{E}$) is very complicated and strongly depends on the VSM embedded between elastic layers. For the sandwiches S-2 and S-5 assembled from MRE-2 and MRE-5 smart materials, respectively, the lowest eigenfrequencies increase together with the core thickness at any B, while for other sandwiches the monotonic growth of $\omega(h_2)$ is not detected. Note that MRE-2 is considered as a material with the Young's modulus independent of B, and MRE-5 with the highest content of carbon black and treated here as a material possesses a very large shear modulus. Interesting results are shown in Figs. 5.44 (a) and 5.49 (a) related to S-1 and S-6 sandwiches: if a magnetic (or electric) field is weak, then increasing the thickness of soft MRE-1 or ERC cores leads to some softening of

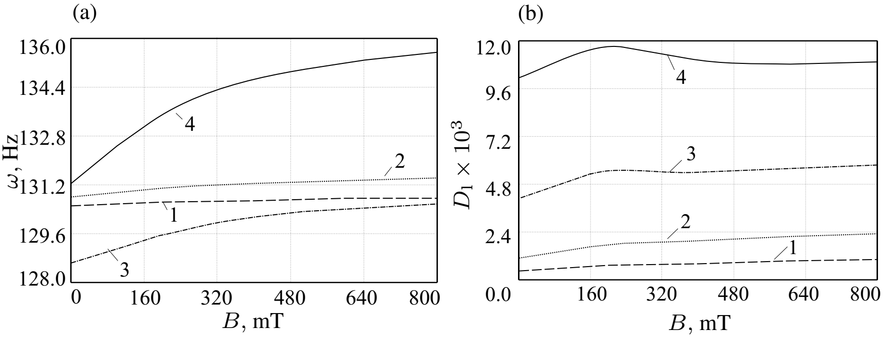

Fig. 5.46 Natural frequency ω (a) and logarithmic decrement D_l (b) for sandwiches S-3 with MRE-3 core and different values of thickness h_2 vs. induction B: 1 - $h_2 = 3$ mm, 2 - $h_2 = 5$ mm, 3 - $h_2 = 8$ mm, 4 - $h_2 = 11$ mm.

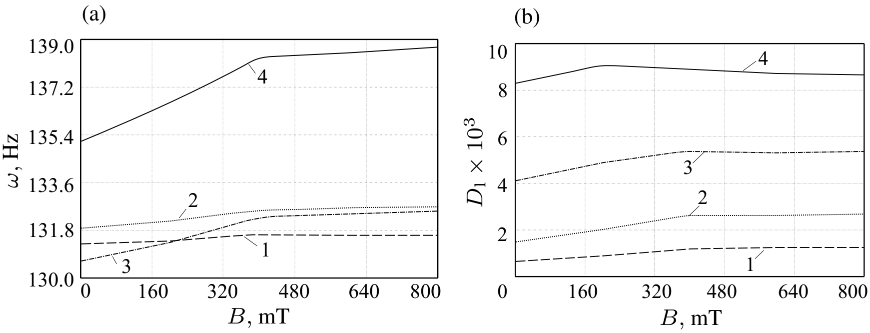

Fig. 5.47 Natural frequency ω (a) and logarithmic decrement D_l (b) for sandwiches S-4 with MRE-4 core and different values of thickness h_2 vs. induction B: 1 - $h_2 = 3$ mm, 2 - $h_2 = 5$ mm, 3 - $h_2 = 8$ mm, 4 - $h_2 = 11$ mm.

entire packet and, in such a way, to decreasing eigenfrequencies. The application of a strong physical field violent increases the core stiffness and, finally, results in growing natural frequencies.

As expected, the damping capabilities of all VSMs under consideration are different and strongly affected by the level of an applied physical field and thickness of a smart core as well. For the S-5 sandwich with the MRE-5 core possessing the highest shear modulus and lowest loss factor, the logarithmic decrement D_{L} monotonically increases at all range of varying the induction B, from 0 to 800 mT. The same behavior of D_{L} is observed for all other sandwiches (excluding S-2) with medium and very thin viscoelastic cores. For the S-2 sandwich with the transversally isotropic MRE-2 core as well as for other sandwiches but with thick viscoelastic cores (at about $h_2 = 11$ mm), there are value $B = B^*$ (or $\mathcal{E} = \mathcal{E}^*$) corresponding to the yielding point for a rheological material and resulting in the maximum value of the decrement D_{L}. Finally, when comparing damping capabilities of all VSMs at the same geometrical dimensions for sandwiches, the MRE-1 and MRE-3 reveal the best damping properties.

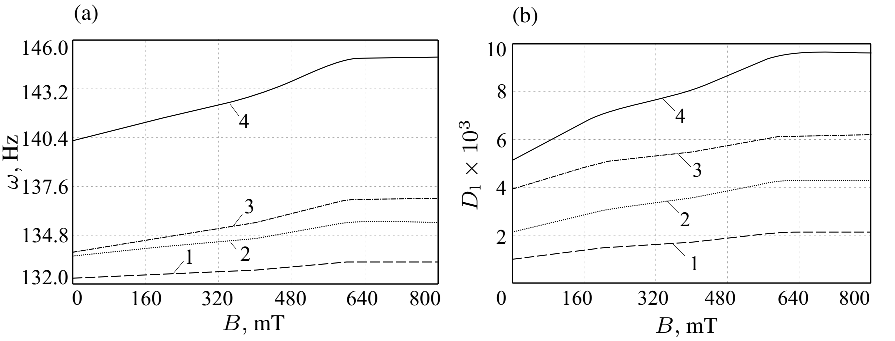

Fig. 5.48 Natural frequency ω (a) and logarithmic decrement D_1 (b) for sandwiches S-5 with MRE-5 core and different values of thickness h_2 vs. induction B: 1 - $h_2 = 3$ mm, 2 - $h_2 = 5$ mm, 3 - $h_2 = 8$ mm, 4 - $h_2 = 11$ mm.

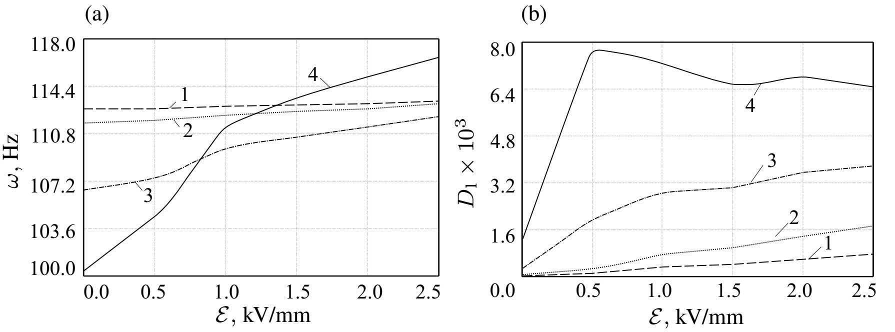

Fig. 5.49 Natural frequency ω (a) and logarithmic decrement D_1 (b) for sandwiches S-6 with ERC core and different values of thickness h_2 vs. the electric strength $\mathcal{E}$: 1 - $h_2 = 3$ mm, 2 - $h_2 = 5$ mm, 3 - $h_2 = 8$ mm, 4 - $h_2 = 11$ mm.

The example considered allows concluding:

- using VSMs and correctly choosing a thickness for smart core or layers, one can assemble a smart thin-walled medium-length cylindrical laminated (in particular, sandwich) panels with tunable viscoelastic properties;
- the application of an external physical field permits to shift right the spectrum of natural frequencies of a panel and greatly improve damping capacity of smart viscoelastic core or layers composing a laminated structure.

5.4.3 Steady-state Forced Vibrations and Their Suppression

Let us consider the nonhomogeneous coupled Eqs. (5.61) with the boundary conditions (5.64) for

$$q_{\mathrm{n}}(\alpha_1, \alpha_2, t) = q_3(\alpha_1, \alpha_2)\mathrm{e}^{\mathrm{i}\omega_{\mathrm{e}} t}, \tag{5.82}$$

where ω_e is the frequency of excitation and q_3 is some complex dimensionless amplitude function. Intending to study predominantly bending vibrations, we shall omit the inertia terms in the first two equations from (5.61). To satisfy the boundary conditions (5.64), we seek a solution of Eqs. (5.61) in the form of double series

$$\begin{aligned}
\hat{u}_1 &= R\sum_{n=1}^{\infty}\sum_{m=1}^{\infty} U_{nm}^{(1)}(t)\cos\frac{\pi n\alpha_1}{L_1}\sin\frac{\pi m\alpha_2}{L_2},\\
\hat{u}_2 &= R\sum_{n=1}^{\infty}\sum_{m=1}^{\infty} U_{nm}^{(2)}(t)\sin\frac{\pi n\alpha_1}{L_1}\cos\frac{\pi m\alpha_2}{L_2},\\
w &= R\sum_{n=1}^{\infty}\sum_{m=1}^{\infty} W_{nm}(t)\sin\frac{\pi n\alpha_1}{L_1}\sin\frac{\pi m\alpha_2}{L_2},\\
\psi_1 &= \sum_{n=1}^{\infty}\sum_{m=1}^{\infty} \Psi_{nm}^{(1)}(t)\cos\frac{\pi n\alpha_1}{L_1}\sin\frac{\pi m\alpha_2}{L_2},\\
\psi_2 &= \sum_{n=1}^{\infty}\sum_{m=1}^{\infty} \Psi_{nm}^{(2)}(t)\sin\frac{\pi n\alpha_1}{L_1}\cos\frac{\pi m\alpha_2}{L_2},
\end{aligned} \tag{5.83}$$

where $U_{nm}^{(j)}(t), W_{nm}(t), \Psi_{nm}^{(j)}(t)(j=1,2)$ are the required functions of t called the generalized co-ordinates of the mechanical system.

The function $q_3(\alpha_1,\alpha_2)$ is also expended into the series

$$q_3 = \sum_{n=1}^{\infty}\sum_{m=1}^{\infty} q_{nm}\sin\frac{\pi n\alpha_1}{L_1}\sin\frac{\pi m\alpha_1}{L_2}, \tag{5.84}$$

where

$$q_{nm} = \frac{4}{L_1L_2}\int_0^{L_1}\int_0^{L_2} q_3(\alpha_1,\alpha_2)\sin\frac{\pi n\alpha_1}{L_1}\sin\frac{\pi m\alpha_1}{L_2}\mathrm{d}\alpha_1\mathrm{d}\alpha_2. \tag{5.85}$$

We substitute Eqs. (5.83) and (5.84) into the governing equations (5.61), multiplying the equations by the following terms

$$\begin{aligned}
&\cos\frac{\pi i\alpha_1}{L_1}\sin\frac{\pi j\alpha_2}{L_2}, \quad \sin\frac{\pi i\alpha_1}{L_1}\cos\frac{\pi j\alpha_2}{L_2}, \quad \sin\frac{\pi i\alpha_1}{L_1}\sin\frac{\pi j\alpha_2}{L_2},\\
&\cos\frac{\pi i\alpha_1}{L_1}\sin\frac{\pi j\alpha_2}{L_2}, \quad \sin\frac{\pi i\alpha_1}{L_1}\cos\frac{\pi j\alpha_2}{L_2},
\end{aligned}$$

respectively, where i, j are fixed natural numbers, and integrate them over the panel surface. Then, eliminating $U_{nm}^{(\varsigma)}(t)$ and $\Psi_{nm}^{(\varsigma)}(t), \varsigma = 1,2$, from the first four equations, we arrive at the differential equation

$$\ddot{W}_{ij} + \Omega_{ij}^2 W_{ij} = \frac{q_{ij}}{\rho_0 hR}\mathrm{e}^{\mathrm{i}\omega_\mathrm{e} t}, \quad i,j = 1,2,\dots, \tag{5.86}$$

with respect to the functions $W_{ij}(t)$, where $\Omega_{ij} = \pm(\omega_{ij} + \mathrm{i}\alpha_{ij})$ are two complex eigenvalues determined from Eq. (5.71). Note that the in-plane inertia forces in (5.61) are neglected.

The partial solution of Eq. (5.86) is the function

$$W_{ij}(t) = \frac{q_{ij}}{\rho_0 h R(\Omega_{ij}^2 - \omega_{\mathrm{e}}^2)} \mathrm{e}^{\mathrm{i}\,\omega_{\mathrm{e}} t}. \tag{5.87}$$

Then the amplitude of forced steady-state vibrations at any point on the shell surface will be defined by the formula

$$w = R \sum_{n=1}^{\infty} \sum_{m=1}^{\infty} \frac{q_{nm} \mathrm{e}^{\mathrm{i}\,\omega_{\mathrm{e}} t}}{\rho_0 h R(\Omega_{nm}^2 - \omega_{\mathrm{e}}^2)} \sin \frac{\pi n \alpha_1}{R} \sin \frac{\pi m \alpha_2}{R}, \tag{5.88}$$

and the associated displacements $\hat{u}^{(1)}, \hat{u}^{(2)}, \psi^{(1)}, \psi^{(2)}$ are calculated by Eqs. (5.73), where

$$U_{nm}^{(\varsigma)}(t) = b_{\varsigma}(n,m)\tilde{W}_{nm}(t), \quad \Psi_{nm}^{(\varsigma)}(t) = d_{\varsigma}(n,m)\tilde{W}_{nm}(t), \quad \varsigma = 1, 2.$$

Equation (5.88) determines the amplitude-frequency response which depends on the distribution of harmonic force over the shell surface. Because the complex eigenvalue Ω_{nm} depends upon the effective complex shear modulus G being a function of the induction B, the amplitude of sustained forced vibration becomes to some extent a controlled quantity. To detect this effect, we consider the following example.

Example 5.11. Let two S-1 cylindrical sandwich panels (the notations of sandwiches are the same as in Example 5.10) with the opening angles $\varphi_2 = \pi/3$ and $\varphi_2 = \pi$ be subjected to the concentrated harmonic force

$$F = F_0 \sin \omega_{\mathrm{e}} t \tag{5.89}$$

applied in the point $\alpha_1 = \alpha_1^\circ = L_1/2$, $\alpha_2 = \alpha_2^\circ = L_2/2$, where F_0 is the amplitude of concentrated force which is not specified in view of the linearity of the problem. All other geometrical dimensions and physical characteristics are the same as in Example 5.10.

The normal pressure q_{n} per unit area can be expressed as follows

$$\begin{aligned} q_{\mathrm{n}} = \lim_{\substack{x_1 \to 0 \\ x_2 \to 0}} & \frac{F_0}{4x_1 x_2} [H_0(\alpha_1^\circ - x_1 - \alpha_1) - H_0(\alpha_1^\circ + x_1 - \alpha_1)] \\ & \times [H_0(\alpha_2^\circ - x_2 - \alpha_2) - H_0(\alpha_2^\circ + x_2 - \alpha_2)] \sin \omega_{\mathrm{e}} t, \end{aligned} \tag{5.90}$$

where $H_0(x)$ is the Heaviside function. Then

$$q_{ij} = -\frac{2\mathrm{i}F_0}{L_1 L_2} \sin \frac{\delta_i \alpha_1^\circ}{R} \sin \frac{\delta_j \alpha_2^\circ}{R}, \tag{5.91}$$

where δ_i, δ_j are determined by Eqs. (5.70).

We consider the real part of an amplitude of forced stationary vibrations calculated by Eq. (5.88) in the point of the force application

$$
\begin{aligned}
w_{\mathrm{r}}^{\circ} = {} & \frac{4F_0}{\rho_0 h L_1 L_2} \sum_{n=1}^{\infty} \sum_{m=1}^{\infty} \frac{\omega_{nm}^2 - \alpha_{nm}^2 - \omega_{\mathrm{e}}^2}{(\omega_{nm}^2 - \alpha_{nm}^2 - \omega_{\mathrm{e}}^2)^2 + 4\alpha_{nm}^2 \omega_{nm}^2} \\
& \times \sin^2 \frac{\delta_n L_1}{2R} \sin^2 \frac{\delta_m L_2}{2R}.
\end{aligned}
\tag{5.92}
$$

Figures 5.50 and 5.51 show the scaled amplitude w_{r}°, denoted by A_{m}, versus the frequency of excitation ω_{e} varying from 0 to 400 Hz. The amplitude-frequency plots for both sandwiches are displayed for three different cases, for $B = 0$ (magnetic field is absent), $B = 40$ and 200 mT. It may be seen that the application of a magnetic field results in significant reduction of the amplitude of resonance vibrations. So, for the first sandwich cylindrical panel with the opening angle $\varphi_2 = \pi/3$, one has about two- and three-fold reductions at $B = 40$ and $B = 200$ mT, respectively.

It is also seen that in all cases, with and without magnetic field, for the panel with the opening angle $\varphi_2 = \pi/3$, more intensive resonance vibrations occur on the lowest (first) eigenfrequency with one semi-wave in both the axial and circumferential

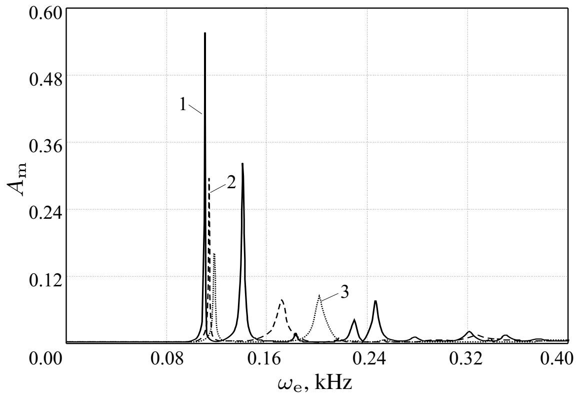

Fig. 5.50 Amplitude-frequency characteristic for the sandwich S-1 with the opening angle $\varphi_2 = \pi/3$ at different levels of applied magnetic field:
1 - $B = 0\,\mathrm{mT}$, 2 - $B = 40\,\mathrm{mT}$, 3 - $B = 200$ mT.

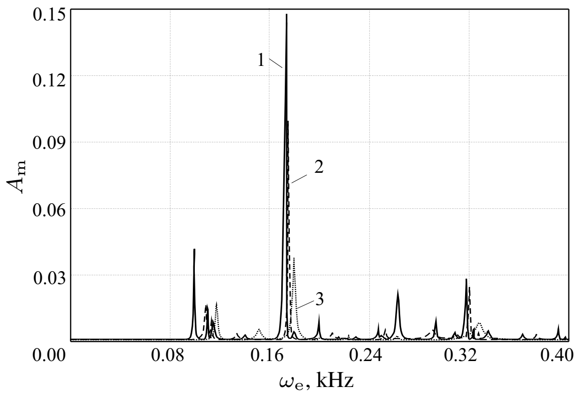

Fig. 5.51 Amplitude-frequency characteristic for the sandwich S-1 with the opening angle $\varphi_2 = \pi$ at different levels of applied magnetic field:
1 - $B = 0\,\mathrm{mT}$, 2 - $B = 40\,\mathrm{mT}$, 3 - $B = 200$ mT.

directions ($n = 1, m = 1$), while for the panel with $\varphi_2 = \pi$, the maximum amplitude of resonance vibrations is observed due to superposition of the fifth and sixth modes with the wave numbers $n = 2, m = 5$ and $n = 2, m = 6$, respectively, which have very close natural frequencies. Our additional accurate calculations (their outcomes are omitted here) detected that for cylindrical panels with a small opening angle as well as for plates, the amplitude of resonance vibrations is a monotonically decreasing function of the resonance frequency (at least at the low part of the spectrum), while for panels with a large φ_2 as well as for cylindrical shells closed in the circumferential direction, the peak of maximum amplitude shifts to the right (at the frequency axis) and corresponds to the superposition of two or more modes with very close associated eigenfrequencies.

It should be noticed that the *mechanisms* of suppression of resonance vibrations at the first eigenmode are different for sandwiches with small and large opening angles. So, Fig. 5.50 shows that applying magnetic field results in slight shifting of the first resonance frequency, and the suppression occurs mainly due to the increase the damping capability of the smart material (here, MRE-1). As for panels with large opening angle φ_2 (s. Fig. 5.51) and cylindrical shells closed in the circumferential direction, the action of magnetic field leads to very noticeable shifting the first resonance region to the right and about two-fold decreasing the resonance peak.

It is obvious that different VSMs incorporated with a sandwich panel possess different capability to suppress resonance vibrations. For instance, we choose here the MRE-3 because the logarithmic decrement corresponding to the lowest eigenfrequency for the sandwich S-3 (here, the sandwich notation is the same as in Subsect. 5.4.2) is larger (in the average for any induction B) than for other smart materials under consideration (compare Figs. (b) of 5.44-5.49). To estimate the damping power of MRE-3, we shall consider one more example.

Example 5.12. Let the sandwich cylindrical panel S-3 with MRE-3 based core (see the property of this smart material in Subsect. 2.3.3) has the opening angle $\varphi = \pi$ and all other geometrical and physical characteristics are the same as in Example 5.11. The panel experiences the same periodic load (5.89) and (5.90) applied at the point $\alpha_1 = \alpha_1^\circ = L_1/2, \alpha_2 = \alpha_2^\circ = L_2/2$. Figure 5.52 demonstrates the amplitude-frequency response of the panel without magnetic field and under its action with the induction $B = 800$ mT. The plots show that the application of very strong magnetic field leads to only shifting the first and second resonance regions to the right, while the reduction of amplitudes corresponding to these regions is very weak. The noticeable lowering of the amplitude (about twofold reduction) is observed for the resonance vibrations on the third natural frequency, however this reduction is reached by the application of very strong magnetic field in comparison with the sandwich S-2 (see the fifth resonance region in Fig. 5.51) subjected to more weak magnetic field. Similar calculations for other sandwiches (S-3, S-4 and S-5) and their comparison with outcomes for the S-1 sandwich revealed that the smart material MRE-1 possesses the best damping capability to suppress resonance vibrations. This suppression being provided by applying relatively weak magnetic field.

Fig. 5.52 Amplitude-frequency characteristic for the sandwich S-3 with the opening angle $\varphi_2 = \pi$ without and with magnetic field: 1 - $B = 0\,\text{mT}$, 2 - $B = 800\,\text{mT}$.

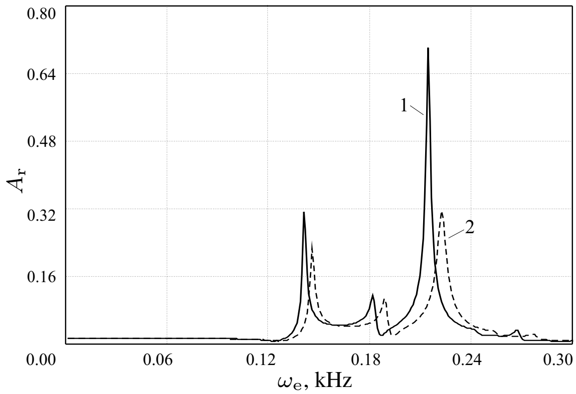

5.5 Influence of Stationary Magnetic Field on Localized Modes of Free Vibrations

In this section, we shall study localized modes of free vibrations of medium-length MRE-based laminated cylindrical shells. Using the asymptotic approach (Mikhasev and Tovstik, 2009) displayed in Chapt. 4, the effect of magnetic field on the natural frequencies, damping ratios and associated localized modes will be analyzed (Mikhasev et al, 2014). As an example, a sandwich cylinder with highly polarized MRE-1 embedded between two elastic face layers will be examined.

5.5.1 Setting the Problem

Let a medium-length laminated cylindrical shell with at least one layer made of a MRE be in a stationary magnetic field. The MRE is assumed to be inhomogeneous so that its complex shear and Young's moduli are functions of an angle φ. The reasons resulting in nonhomogeneity of viscoelastic properties of MRE layer may be different. The heterogeneous magnetic field may leads to not uniform distribution of magneto-sensitive particles in a MRE. But even if the magnetic field is uniform, their impact on various parts of a polarized MRE may be unequal because of different angles between the magnetic force lines and the alignment of magnetic particles (s. Fig. 5.53). This assumption is confirmed by experimental results presented in Boczkowska et al (2012). Studying the urethane MRE consisting of carbonyl-iron particles in a polyurethane matrix, it was found out that the maximum value of the modulus $G' = 0.5$ MPa was observed for samples with particles orientated at 30° with respect to the lines of magnetic field, whereas the minimum magnitude $G' = 0.1$ MPa corresponded to samples with angle 90° between the magnetic force lines and the particle alignment.

In what follows, not specifying the reason causing inhomogeneity of viscoelastic properties of a MRE, we assume that all magneto-sensitive complex magnitudes

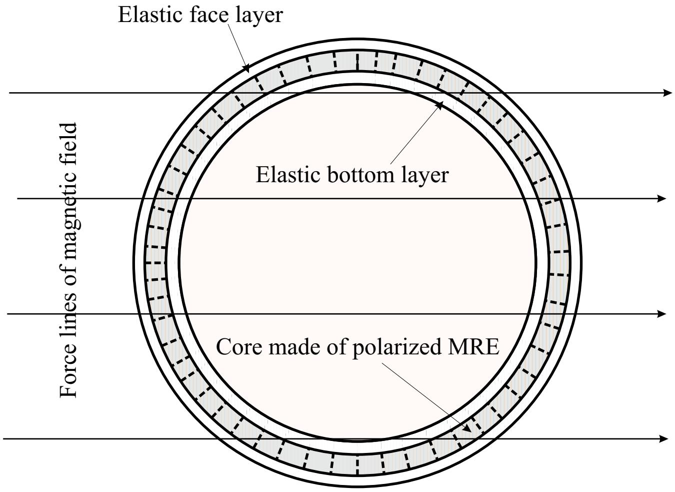

Fig. 5.53 Cross-section of sandwich cylindrical shell with the core made of polarized MRE in magnetic field with parallel force lines (after Mikhasev et al, 2014).

$\nu, \eta_3, E, \theta, \beta$ and K appearing in Eq. (5.65) are functions of the circumferential co-ordinate α_2. We introduce a small parameter

$$\varepsilon^8 = \frac{h_*^2 \eta_{3\mathrm{r}}^{(0)}}{12[1-(\nu_\mathrm{r}^{(0)})^2]}, \tag{5.93}$$

and consider sufficiently thin shells for which parameter h_* is a quantity of the order ~ 0.01 or less. In Eq. (5.93) and below, the superscript (0) means that an appropriate parameter is calculated at $B = 0$. Here, $\eta_{3\mathrm{r}} = \Re\,\eta_3$, $\nu_\mathrm{r} = \Re\,\nu$, $\nu_\mathrm{r}^{(0)} \approx 0.4$. We assume also the following asymptotic estimations for the basic tunable parameters

$$\begin{aligned}
\nu \quad &= \nu_\mathrm{r}^{(0)}[1+\varepsilon^4\delta\nu(\varphi)], \quad \theta_\mathrm{r} \sim \varepsilon^3, \quad \theta_\mathrm{i} \sim \varepsilon^4,\\
\eta_3 \quad &= \eta_{3\mathrm{r}}^{(0)}[1+\varepsilon^2\delta\eta_3(\varphi)], \quad \eta_{3\mathrm{r}}^{(0)} = \pi^{-4}\eta_\mathrm{r}^{(0)}[1-(\nu_\mathrm{r}^{(0)})^2],\\
E_\mathrm{r} \quad &= E_\mathrm{r}^{(0)} d(\varphi) = E_\mathrm{r}^{(0)}[1+\varepsilon d_1(\varphi)], \quad E_\mathrm{i}/E_\mathrm{r}^{(0)} \sim \varepsilon^4,\\
\pi^{-2}K &= \varepsilon^2\kappa(\varphi) = \varepsilon^2[\kappa_0(\varphi)+\mathrm{i}\varepsilon\kappa_1(\varphi)] \quad \text{for} \quad \varepsilon \to 0.
\end{aligned} \tag{5.94}$$

In Eqs. (5.94), $\delta\nu, \delta\eta_3$ and d_1, κ_0, κ_1 are complex and real functions of angle $\varphi = \alpha_2/R$, respectively, so that their absolute magnitudes are quantities of the order $O(1)$ at $\varepsilon \to 0$. Estimates (5.94) hold for laminated cylindrical panels and shells containing any MRE specified in Chapt. 2 with the summary thickness of a smart material not less then 70% from the total thickness h of a shell. In particular, these conditions are valid for the considered above S-1 sandwiches with the MRE-1 based core. In the general case, the shell is non-circular with the radius of curvature

$R_2 = Rk(\varphi)$. At the shell edges, the boundary conditions (5.66) are assumed. The solution of Eqs. (5.65) describing free vibrations (at $q_{\mathrm{n}} = 0$) are assumed to be of the form

$$\chi = \varepsilon^{-4} R\chi^*(s,\varphi)\exp(\mathrm{i}\Omega t), \quad F = E_{\mathrm{r}}^{(0)} hR^2 \Phi^*(s,\varphi)\exp(\mathrm{i}\Omega t), \quad \phi = 0, \tag{5.95}$$

where $s = \alpha_1/R$ is a dimensionless axial co-ordinate, Ω is a required complex eigenvalue, and χ^*, F^* are dimensionless displacement and stress functions.

The substitution of Eqs. (5.95) into Eqs. (5.65) results in the differential equations

$$\begin{aligned} \varepsilon^4 d(\varphi)\Delta^2\chi^* + k(\varphi)\frac{\partial^2\Phi^*}{\partial s^2} - \Lambda[1 - \varepsilon^2\kappa(\varphi)\Delta]\chi^* = 0, \\ \varepsilon^4\Delta^2\Phi^* - k(\varphi)\frac{\partial^2}{\partial s^2}[1 - \varepsilon^2\kappa(\varphi)\Delta]\chi^* = 0 \end{aligned} \tag{5.96}$$

written in the dimensionless form, where $\Lambda = \rho R^2\Omega^2/(\varepsilon^4 E_{\mathrm{r}}^{(0)})$ is the dimensionless frequency parameter. When deriving Eqs. (5.96) from Eqs. (5.65), we have omitted the operator $\Delta^3\chi$ because of smallness of the coefficient $K\theta$, s. Eqs. (5.76) for K and (5.94), and disregarded by very small dimensionless parameters $\varepsilon^4\delta\nu, \varepsilon^2\delta\eta_3, E_{\mathrm{i}}/E_{\mathrm{r}}^{(0)}$. It should be noticed that when studying low-frequency eigenmodes this simplification leads to the error of the order h_* which is comparable with the error of Eqs. (5.65). In Eqs. (5.96),

$$\kappa = \kappa_0(\varphi) + \varepsilon\mathrm{i}\kappa_1(\varphi) \tag{5.97}$$

is the principal complex shear parameter depending on both the co-ordinate φ and the magnetic field induction B. The appropriate boundary conditions are as follows

$$\chi^* = \Delta\chi^* = \Delta^2\chi^* = \frac{\partial^2\Phi^*}{\partial s^2} = \frac{\partial^2\Phi^*}{\partial\varphi^2} = 0 \quad \text{at} \quad s = 0,\, l, \tag{5.98}$$

where $l = L/R$.

5.5.2 Localized Natural Modes

The boundary-value problem (5.96), (5.98) is identical to the problem considered in Sect. 4.4. The difference lies in the fact that now the coefficients d, κ are complex functions those depend not only on the angle φ, but also on the induction of magnetic field. Varying the magnetic field, one can affect the localized natural modes. Furthermore, applying a nonuniform magnetic field, it is possible to disturb the uniform natural modes and result in localization of some modes corresponding to low-frequency vibrations.

Let y be any of the foregoing parameters depending on φ. It is assumed that $\mathrm{d}y/\mathrm{d}\varphi \sim y$ at $\varepsilon \to 0$. Then, under some additional conditions for the functions

$\kappa_0(\varphi), k(\varphi)$ (which will be specified below), the boundary value problem (5.96), (5.98) may have a solution localized in the neighborhood of some generator $\varphi = \varphi_0$ called the weakest one (Mikhasev and Tovstik, 2009). The required solution is seeking in the form identical to (4.111)

$$\begin{aligned}
\chi^* &= \sin\frac{\pi n s}{l}\sum_{j=0}^{\infty}\varepsilon^{j/2}\chi_j(\zeta)\exp\left\{\mathrm{i}\left(\varepsilon^{-1/2}p\zeta + 1/2b\zeta^2\right)\right\},\\
\Phi^* &= \sin\frac{\pi n s}{l}\sum_{j=0}^{\infty}\varepsilon^{j/2}\Phi_j(\zeta)\exp\left\{\mathrm{i}\left(\varepsilon^{-1/2}p\zeta + 1/2b\zeta^2\right)\right\},\\
\Lambda &= \Lambda_0 + \varepsilon\Lambda_1 + \ldots,
\end{aligned} \tag{5.99}$$

where $\zeta = \varepsilon^{-1/2}(\varphi - \varphi_0)$, p is a real wave parameter, b is a complex parameter so that $\Im\, b > 0$, and χ_j, Φ_j are polynomials in ζ.

The functions $\kappa_0(\varphi), \kappa_1(\varphi), k(\varphi), d_1(\varphi)$ are expanded into series in the neighborhood of the generatrix $\varphi = \varphi_0$. In particular,

$$\kappa_0(\varphi) = \kappa_0(\varphi_0) + \varepsilon^{1/2}\kappa_0'(\varphi_0)\zeta + \frac{1}{2}\varepsilon\kappa_0''(\varphi_0)\zeta^2 + \ldots \tag{5.100}$$

Because the procedure of seeking all required parameters and functions in series (5.99) are the same as in Sect. 4.4, we omit it and give only the resulting formulas and equations for two particular cases.

5.5.2.1 Non-circular Cylinder

Let only the dimensionless curvature $k(\varphi)$ be a function of the angle φ, and parameters $\kappa_0(B)$, $\kappa_1(B)$, $d_1(B)$ dependent only on the induction B. Here the weakest line is the generatrix with the minimum curvature which can found from the conditions

$$k'(\varphi_0^\circ) = 0, \quad k''(\varphi_0^\circ) > 0, \tag{5.101}$$

and the natural frequency and damping ratio are determined by equations

$$\begin{aligned}
\omega &= \Re\,\Omega = \omega_c\omega^*, \quad \alpha = \Im\,\Omega = \omega_c\alpha^*,\\
\omega^* &= (f^\circ)^{1/2} + \frac{\varepsilon}{2(f^\circ)^{1/2}}\left[\frac{(1+2m)\pi^2 n^2\sqrt{f_{pp}^\circ k''(\varphi_0^\circ)}}{2l^2(p^\circ)^2} + d_1(p^\circ)^4\right],\\
\alpha^* &= -\frac{\varepsilon(f^\circ)^{1/2}\kappa_1(p^\circ)^2}{2[1+\kappa_0(p^\circ)^2]},
\end{aligned} \tag{5.102}$$

where $\omega_c = \varepsilon^2 R^{-1}(E_{\mathrm{r}}^{(0)}/\rho)^{1/2}$ is the characteristic frequency, and ω^*, α^* are dimensionless parameters. The parameter b° is the same as for the elastic shell - to compare s. Eq. (4.128)

$$b^\circ = \frac{\mathrm{i}\pi^2 n^2}{l^2 (p^\circ)^2} \sqrt{\frac{k''(\varphi_0^\circ)}{f_{pp}^\circ}}. \tag{5.103}$$

Here, f_{pp}° is the second derivative of the function (s. Eq. (4.118))

$$f(p, \varphi_0) = \frac{\pi^4 n^4 k^2(\varphi_0)}{l^4 p^4} + \frac{p^4}{1 + \kappa_0(\varphi_0) p^2} \tag{5.104}$$

with respect to p calculated at constant κ_0 (not dependent of φ_0) and $p = p^\circ$, $\varphi_0 = \varphi_0^\circ$, and the parameter p° is found from Eq. (4.121)

$$\kappa_0 p^{10} + 2p^8 - 2\pi^4 n^4 k^2(\varphi_0^\circ) l^{-4} (\kappa_0^2 p^4 + 4\kappa_0 p^2 + 2) = 0. \tag{5.105}$$

Equations (5.102), (5.103) show that increasing the parameter $k''(\varphi_0^\circ)$ results in increasing the correction $\omega^* - \omega_0^*$ for the natural frequency, where $\omega_0^* = (f^\circ)^{1/2}$, and leads to growing power of localization of eigenmodes. To analysis the effect of a magnetic field on these modes we consider the following example.

Example 5.13. The sandwich cylindrical shell is assembled from the face sheets made of the ABS-plastic SD-0170 and MRE-1 core. The cross-section of the shell is an ellipse with semi-axes $e_1, e_2 (e_1 \le e_2)$. Here

$$k = \frac{r^2 + 2r'^2 - rr''}{(r^2 + r'^2)^{3/2}}, \tag{5.106}$$

where

$$r(\varphi) = \sqrt{\frac{e_1^2}{1 - \delta^2 \sin^2 \varphi}}, \quad -\pi < \varphi \le \pi, \quad \delta = \sqrt{1 - \frac{e_1^2}{e_2^2}}. \tag{5.107}$$

Then, one has two the weakest generatrix $\varphi = \varphi_0^\circ = 0$ and $\varphi = \varphi_0^\circ = \pi$. Table 5.2 shows the parameters p°, ω_0^*, $\omega^*, \alpha^*, \Im\, b^\circ$, $D_l = 2\pi\alpha^*/\omega^*$ versus the induction B for the shells with the following geometrical parameters: $R = 1$ m, $L = 1.5$ m, $e_1 = 1, e_2 = 2, h_1 = h_3 = 0.5$ mm, $h_2 = 11$ mm. The calculations were performed at $n = 1, m = 0$ in Eqs. (5.102), (5.103). The parameters $\kappa_0(\varphi_0^\circ), \kappa_1(\varphi_0^\circ), d_1(\varphi_0^\circ)$ were calculated by using Eqs. (5.94) and Figs. 5.24 and 5.25. To define the natural frequency ω and damping ratio α, the corresponding dimensionless parameters ω^*, α^* from Table 5.2 should be multiplied by the characteristic frequency ω_c dependent on the thickness h_2 for the MR layer. Table 5.2 reveals a weak dependence of the wave parameter p° on the induction B. As for the behavior of residual parameters, one can conclude that increasing the magnetic field induction results in some increase in the natural frequency (up to 7%) and minor decrease of the parameter $\Im\, b^\circ$ specifying the width of the area where intensive vibrations occur. The effect of a magnetic field on the damping capability of the MRE-1 is found to be more appreciable. In particular, in the presence of magnetic field with the induction from 25 to 75 mT, the damping ratio α^* is about three times than that at $B = 0$. Thus, the localized natural modes of the non-circular sandwich cylindrical shell with MRE-1 core are insignif-

Table 5.2 Parameters p°, ω^*, α^*, $\Im\, b^\circ$, D_l for a thin sandwich cylinder with ellipse-type cross-section vs. the magnetic induction B at $h_1 = h_3 = 0.5$ mm, $h_2 = 11$ mm, $\varepsilon = 0.248$ and $\omega_\mathrm{c} = 13.704$ Hz (after Mikhasev et al, 2014).

B, mT	p°	ω^*	α^*	$\Im\, b^\circ$	D_l
0	1.054	2.749	0.0040	0.2903	0.0136
25	1.040	2.846	0.0123	0.2678	0.0272
50	1.035	2.886	0.0110	0.2592	0.0240
75	1.032	2.907	0.0095	0.2546	0.0205
100	1.031	2.921	0.0082	0.2518	0.0176
125	1.029	2.930	0.0072	0.2499	0.0154
150	1.029	2.937	0.0064	0.2486	0.0136

icantly influenced by the magnetic field, but the associated decrement demonstrates the significant dependence on induction B for the MRE-1.

5.5.2.2 Circular Magnetorhelogical Elastomer-based Cylinder with Nonuniform Physical Properties

Let all geometrical parameters of a cylindrical shell be constant. The viscoelastic properties of a MRE composing layer(s) are nonuniform in the circumferential direction. Here $k \equiv 1$, and κ_0, κ_1, d_1 are functions of φ. Similar inhomogeneity of elastic and shear parameters may be observed if a magnetic field is spatially nonuniform or/and a MRE embedded between elastic layers is polarized and the angle between the magnetic force lines and the alignment of magnetic particles depends on a co-ordinate φ (Fig. 5.53).

Here, the weakest generatrix $\varphi = \varphi_0^\circ$ is the line at which the reduced shear parameter K_r introduced by (5.94) approaches the maximum:

$$\kappa_0'(\varphi_0^\circ) = 0, \quad \kappa_0''(\varphi_0^\circ) < 0. \tag{5.108}$$

In this case, the asymptotic approach stated in Sect. 4.4 results in the following new equations for the dimensionless frequency ω^*, damping ratio α^* and parameter b°

$$\omega^* = \frac{1}{(f^\circ)^{1/2}} \left\{ f^\circ + \frac{\varepsilon}{2} \left[\frac{(1+2m)(p^\circ)^3 \sqrt{-f_{pp}^\circ \kappa_0''(\varphi_0^\circ)}}{2[1+(p^\circ)^2 \kappa_0(\varphi_0^\circ)]} + d_1(\varphi_0^\circ)(p^\circ)^4 \right] \right\},$$

$$\alpha^* = -\frac{\varepsilon (f^\circ)^{1/2} \kappa_1(\varphi_0^\circ)(p^\circ)^2}{2[1+\kappa_0(\varphi_0^\circ)(p^\circ)^2]}, \qquad b^\circ = \frac{\mathrm{i}\,(p^\circ)^3}{1+(p^\circ)^2\kappa_0(\varphi_0^\circ)} \sqrt{-\frac{\kappa_0''(\varphi_0^\circ)}{f_{pp}^\circ}}.$$

Tables 5.3 and 5.4 reveal the effect of the applied magnetic field on parameters p°, $\omega^*, \alpha^*, \Im\, b^\circ$, D_l for two circular sandwich cylinders with nonuniform elastic and shear moduli of the same radius $R = 1$ m and length $L = 1.5$ m but having different thickness of the MRE-1 core ($h_2 = 8$ mm and $h_2 = 11$ mm, respectively). The face sheets are the same as in the previous example. The calculations were performed at $n = 1, m = 0$, $h_1 = h_3 = 0.5$ mm. The parameter $\kappa_0''(\varphi_0^\circ)$ characterizing the variability of the reduced shear modulus in the neighborhood of the weakest generator $\varphi = \varphi_0^\circ$ has been taken as $\kappa_0'' = -1.5$ for both cases. This is the approximate value estimated proceeding from the experimental data from Boczkowska et al (2012). The parameters $\kappa_0(\varphi_0^\circ), \kappa_1(\varphi_0^\circ), d_1(\varphi_0^\circ)$ were found from Eqs. (5.94) and Figs. 5.24, 5.25. Calculations shown that for both shells accounting inhomogeneity of the reduced shear parameter K results in increasing the natural frequency up to 20 %. For the second sandwich, increasing the level of magnetic field from $B = 0$ to $B = 150$ mT leads to increasing the natural frequency ω^* up to 8.4 % (from $3.304\omega_c$ at $B = 0$ mT to $3.582\omega_c$ at $B = 150$ mT) and minor decreasing the number of waves in the circumferential direction (the parameter p°). The effect of magnetic field on the damping ratio α^* and logarithmic decrement D_l is more complicated and appreciable. It is also influenced by the thickness h_2 of the MRE-1 core. For $h_2 = 8$ mm and $h_2 = 11$ mm, the best passive suppression of the eigenmodes takes place at $B = 75$ mT and $B = 25$ mT respectively. In particular, applying the magnetic field of the intensity $B = 75$ mT (at $h_2 = 8$ mm) gives three-fold increase in the damping ratio. Decreasing the parameter $\Im b^\circ$ under increasing the induction B indicates that applying strong magnetic field results in some spreading of localized modes over the shell surface.

Table 5.3 Parameters p°, ω^*, α^*, $\Im b^\circ$, D_l for a cylinder vs. induction B at $h_2 = 8$ mm, $\varepsilon = 0.231, \omega_c = 13.828$ Hz (after Mikhasev et al, 2014).

B, mT	p°	ω^*	α^*	$\Im b^\circ$	D_l
0	1.479	3.438	0.0025	0.498	0.0046
25	1.471	3.472	0.0091	0.487	0.0165
50	1.466	3.494	0.0107	0.480	0.0193
75	1.463	3.511	0.0108	0.475	0.0193
100	1.461	3.523	0.0104	0.472	0.0186
125	1.459	3.534	0.0098	0.470	0.0175
150	1.458	3.543	0.0093	0.468	0.0164

Table 5.4 Parameters p°, ω^*, α^*, $\Im b^\circ$, D_l for a cylinder vs. induction B at $h_2 = 11$ mm, $\varepsilon = 0.248, \omega_c = 13.704$ Hz (after Mikhasev et al, 2014).

B, mT	p°	ω^*	α^*	$\Im b^\circ$	D_l
0	1.532	3.304	0.0133	0.573	0.0253
25	1.494	3.436	0.0291	0.519	0.0532
50	1.480	3.493	0.0266	0.499	0.0479
75	1.472	3.527	0.0231	0.488	0.0411
100	1.467	3.550	0.0201	0.481	0.0355
125	1.464	3.568	0.0177	0.477	0.0311
150	1.462	3.582	0.0157	0.474	0.0276

5.6 Suppression of Travelling Vibrations in Magnetorhelogical Elastomer-based Shells

Below we consider the special class of vibrations, localized bending waves running in the circumferential direction in MRE-based cylindrical shells of medium length. Localized non-stationary vibrations may be generated in a shell by some static (Lukasiewicz, 1979) or transient forces (Skudrzyk, 1968) applied along a line or point on the shell surface. Similar vibrations may also appear as a result of parametric excitation of a shell with variable geometric parameters (e.g., curvature, thickness or generatrix length) and/or experiencing non-uniform loading (Mikhasev, 1997; Mikhasev and Kuntsevich, 1999) and/or situated in non-stationary temperature field (Botogova and Mikhasev, 1996; Mikhasev and Kuntsevich, 1997).

If some natural modes of a shell are localized in the neighbourhood of so-called weakest line or point, then dynamic loading may result in unsteady localized vibrations running over the shell surface. In particular, growing axial force (Avdoshka and Mikhasev, 2001) or external pressure (Mikhasev, 2002) leads to splitting natural modes localized near the weakest generatrix and, as a result, generate a family of bending waves (wave packets) travelling in the circumferential direction of an isotropic elastic cylindrical shell. A similar problem on packets of bending, tangential and torsional waves in an infinite thin elastic isotropic cylindrical pipe under non-uniform internal pressure was studied in Mikhasev (1998). The above-mentioned and other papers (e.g., s. Mikhasev, 1996a,b) have detected that unsteady localized vibrations may be accompanied by such complicated effects as multiple reflection of wave packets (WPs) from more stiffen regions, focusing WPs and growth of amplitudes, which are extremely undesirable and destructive because they are the cause of the noise radiation and results in concentration of dangerous stresses in a thin-walled structure.

The main purpose of this section is to show that the application of a magnetic field allows suppressing unsteady (running) localized vibrations in laminated shells containing layers or core made of a MRE (Mikhasev et al, 2016). Using the asymptotic approach (Mikhasev and Tovstik, 2009), a solution of equations governing motion of a medium-length cylindrical MRE-based laminated shell will be constructed in the form of travelling WPs with dynamic characteristics (current frequency, amplitude, width of WPs) being tunable by means of an applied magnetic field.

5.6.1 Setting of the Initial Boundary Value Problem

We consider a medium-length cylindrical laminated MRE-based shell as was stated in Sect. 5.5. The shell is sufficiently thin so that $h_* = h/R$ is a quantity of the order ~ 0.01 or less.

Let ε be a small parameter introduced by Eq. (5.93), where all notations are the same as were assumed in Sect. 5.5. Equations (5.65) are considered as the governing ones with the boundary conditions (5.66) at not plane edges $\alpha_j = L_2(\alpha_2)$ $(j = 1, 2)$. We assume also that the geometrical dimensions and viscoelastic properties of the layers composing the shell are such that the asymptotic estimations (5.94) hold. In our case, $\delta\nu(B), \delta\eta_3(B), d_1(B), \kappa_0(B), \kappa_1(B)$ are functions of induction B.

We introduce the dimensionless magnitudes χ^*, Φ^* and time τ as follows

$$\chi = \varepsilon^{-4} R\chi^*(s, \varphi, t), \quad F = E_{\mathrm{r}}^{(0)} hR^2 \Phi^*(s, \varphi, t), \quad t = \varepsilon^{-3} t_{\mathrm{c}} \tau, \tag{5.109}$$

where $t_{\mathrm{c}} = \sqrt{\rho R^2 / E_{\mathrm{r}}^{(0)}}$ is the characteristic time. Then Eqs. (5.65) may be rewritten in the dimensionless form

$$\begin{aligned} &\varepsilon^4 d(B) \Delta^2 \chi^* + k(\varphi) \frac{\partial^2 \Phi^*}{\partial s^2} + \varepsilon^2 \frac{\partial^2}{\partial \tau^2} [1 - \varepsilon^2 \kappa(B) \Delta] \chi^* = 0, \\ &\varepsilon^4 \Delta^2 \Phi^* - d(B) k(\varphi) \frac{\partial^2}{\partial s^2} [1 - \varepsilon^2 \kappa(B) \Delta] \chi^* = 0, \end{aligned} \tag{5.110}$$

and the corresponding boundary conditions are

$$\chi^* = \Delta \chi^* = \Delta^2 \chi^* = \Phi^* = \Delta \Phi^* = 0 \quad \text{at} \quad s = s_1(\varphi),\ s_2(\varphi), \tag{5.111}$$

where $s_j(\varphi) = L_j(R\varphi)/R$.

Let us consider the following initial conditions for the displacement function χ^*

$$\begin{aligned} &\chi^*|_{\tau=0} = \hat{\chi}_0 \exp\,[\mathrm{i}\varepsilon^{-1} S_0(\varepsilon)], \\ &\dot{\chi}^*|_{\tau=0} = \mathrm{i}\varepsilon^{-1} \hat{v}_0 \exp\,[\mathrm{i}\varepsilon^{-1} S_0(\varepsilon)], \\ &S_0(\varphi) = a^\circ \varphi + \frac{1}{2} b^\circ \varphi^2, \quad a^\circ > 0, \quad \Im b^\circ > 0, \end{aligned} \tag{5.112}$$

$$a^\circ,\ |b^\circ|,\ |\hat{\chi}_0|,\ |\hat{v}_0|,\ \left|\frac{\partial \hat{\chi}_0}{\partial s}\right|,\ \left|\frac{\partial \hat{v}_0}{\partial s}\right| = O(1) \quad \text{when} \quad \varepsilon \to 0, \tag{5.113}$$

where $\hat{\chi}_0(s, \varphi, \varepsilon), \hat{v}_0(s, \varphi, \varepsilon)$ are complex-valued functions satisfying (5.111).

The real and imaginary parts of functions (5.112) define the two initial wave packets localized near the generatrix $\varphi = 0$ on the shell surface. These functions may be considered as approximations of the initial perturbations being the result of some transient forces applied along the line $\varphi = 0$. It should be also noted that under some conditions for parameters a_0, b_0, functions (5.112) coincide with the eigenmodes (5.99) localized in a vicinity of the weakest generatrix. The problem is to construct a solution of the initial-boundary-value problem (5.110)-(5.112) and to analyze the effect of applied magnetic field on the dynamic characteristics of running WPs, including amplitudes.

5.6.2 Asymptotic Approach

Let

$$y_j(s,\varphi) = \sin\frac{\pi j[s - s_1(\varphi)]}{l(\varphi)} \quad \text{and} \quad \lambda_j = \frac{\pi^4 j^4}{l^4(\varphi)}, \quad j = 1, 2, 3, \ldots \tag{5.114}$$

be an infinite system of eigenfunctions and associated eigenvalues of the boundary-value problem

$$\frac{\mathrm{d}^4 y}{\mathrm{d}s^4} - \lambda y = 0, \tag{5.115}$$

$$y = y'' = 0 \quad \text{at} \quad s = s_1(\varphi),\ s = s_2(\varphi), \tag{5.116}$$

where $l(\varphi) = s_2(\varphi) - s_1(\varphi)$.

Because the functions $\chi_0(s,\varphi), v_0(s,\varphi)$ appearing in (5.112) satisfy the boundary conditions (5.111), they can be expanded in terms of the eigenfunctions $y_j(s,\varphi)$ into uniformly convergent series in some section $\varphi_1 \le \varphi \le \varphi_2$

$$\begin{aligned}
\hat{\chi}_0 &= \sum_{j=1}^{\infty} \chi_j^\circ(\varphi,\varepsilon) y_j(s,\varphi), \quad \chi_j^\circ = \int_{s_1(\varphi)}^{s_2(\varphi)} \hat{\chi}_0(s,\varphi,\varepsilon) y_j(s,\varphi)\mathrm{d}s,\\
\hat{v}_0 &= \sum_{j=1}^{\infty} v_j^\circ(\varphi,\varepsilon) y_j(s,\varphi), \quad v_j^\circ = \int_{s_1(\varphi)}^{s_2(\varphi)} \hat{v}_0(s,\varphi,\varepsilon) y_j(s,\varphi)\mathrm{d}s.
\end{aligned} \tag{5.117}$$

It is assumed that χ_j°, v_j° are polynomials of $\varepsilon^{-1/2}$ whose coefficients are regular functions of ε. Then they may be represented by the series

$$\chi_j^\circ = \sum_{i=0}^{\infty} \varepsilon^{i/2} \chi_{ji}^\circ(\zeta), \chi_{ji}^\circ(\zeta) = \sum_{\iota=0}^{M_{ji}} c_{ji\iota}^\circ \zeta^\iota, v_j^\circ = \sum_{i=0}^{\infty} \varepsilon^{i/2} v_{ji}^\circ(\zeta), v_{ji}^\circ(\zeta) = \sum_{\iota=0}^{M_{ji}} d_{ji\iota}^\circ \zeta^\iota \tag{5.118}$$

where $\zeta = \varepsilon^{-1/2}\varphi$, and $c_{j\,i\,\iota}^\circ, d_{j\,i\,\iota}^\circ = O(1)$.

Due to linearity of the initial-boundary-value problem (5.110)-(5.112), its solution may be presented in the form

$$\chi^* = \sum_{j=1}^{\infty} \chi_j^*(s,\varphi,\tau,\varepsilon), \quad \Phi^* = \sum_{j=1}^{\infty} \Phi_j^*(s,\varphi,\tau,\varepsilon), \tag{5.119}$$

where χ_j^*, Φ_j^* are the required functions localized in a neighborhood of moving generatrix $\varphi = q_j(\tau)$. Here $q_j(t)$ is a twice differentiable function such that $q_j(0) = 0$. The pair of functions χ_j^*, Φ_j^* is called the j^{th} wave packet (WP) with the center at $\varphi = q_j(\tau)$ (Mikhasev, 2002).

5.6.2.1 Initial Boundary Value Problem for the j^{th} Wave Packet

Let us hold any natural number j fixed and study the behavior of the j^{th} WP. It is convenient to go over to a local co-ordinate system $\varphi = q_j(\tau) + \varepsilon^{1/2}\xi_j$ associated with the moving center $\varphi = q_j(\tau)$. In the new co-ordinate system, equations (5.110) read

$$
\begin{aligned}
&d(B)\left(\varepsilon^2\frac{\partial^4\chi_j^*}{\partial\xi_j^4} + 2\varepsilon^3\frac{\partial^4\chi_j^*}{\partial\xi_j^2\partial s^2} + \varepsilon^4\frac{\partial^4\chi_j^*}{\partial s^4}\right) + k(\varphi)\frac{\partial^2\Phi_j^*}{\partial s^2} + \left(\varepsilon^2\frac{\partial^2}{\partial\tau^2}\right.\\
&\left.-2\varepsilon^{3/2}\dot{q}_j\frac{\partial^2}{\partial\xi_j\partial\tau} + \varepsilon\dot{q}_j^2\frac{\partial^2}{\partial\xi_j^2} - \varepsilon^{3/2}\ddot{q}_j\frac{\partial}{\partial\xi_j}\right)\left[\chi_j^* - \kappa(B)\left(\varepsilon\frac{\partial^2\chi_j^*}{\partial\xi_j^2} + \varepsilon^2\frac{\partial^2\chi_j^*}{\partial s_j^2}\right)\right] = 0,\\
&\varepsilon^2\frac{\partial^4\Phi_j^*}{\partial\xi_j^4} + 2\varepsilon^3\frac{\partial^4\Phi_j^*}{\partial\xi_j^2\partial s^2} + \varepsilon^4\frac{\partial^4\Phi_j^*}{\partial s^4}\\
&-d(B)k(\varphi)\frac{\partial^2}{\partial s^2}\left[\chi_j^* - \kappa(B)\left(\varepsilon\frac{\partial^2\chi_j^*}{\partial\xi_j^2} + \varepsilon^2\frac{\partial^2\chi_j^*}{\partial s_j^2}\right)\right] = 0,
\end{aligned}
\tag{5.120}
$$

where $\kappa = \kappa_0(B) + \mathrm{i}\kappa_1(B)$, and the function $k(\varphi)$, $s_1(\varphi)$, $s_2(\varphi)$ are expanded into a series in the neighborhood of the center $\varphi = q_j(\tau)$. For instance,

$$
k(\varphi) = k[q(t)] + \varepsilon^{1/2}k'[q(t)]\xi_j + \frac{1}{2}\varepsilon k''[q(\tau)]q_j^2 + \dots \tag{5.121}
$$

Here and in what follows, the dot $(\cdot)$ and prime $(\prime)$ denote differentiation with respect to dimensionless time τ and angle φ, respectively.

The initial conditions for j^{th} WP take the form

$$
\begin{aligned}
\chi_j^*|_{\tau=0} &= \chi_j^\circ(\varphi,\varepsilon)y_j(s,\varphi)\exp\left[\mathrm{i}\varepsilon^{-1}S_0(\varphi)\right],\\
\dot{\chi}_j^*|_{\tau=0} &= \mathrm{i}\varepsilon^{-1}v_j^\circ(\varphi,\varepsilon)y_j(s,\varphi)\exp\left[\mathrm{i}\varepsilon^{-1}S_0(\varphi)\right].
\end{aligned}
\tag{5.122}
$$

The dynamic stress state of the shell consists of the basic stress state and the dynamic edge-effect integrals describing the shell behavior in a small neighborhood of each edge. To study the basic state on each edge, we have to satisfy two basic conditions only. Apart from terms of the order ε^2, these conditions for the j^{th} WP have the form

$$
\chi_j^* = \Phi_j^* = 0 \quad \text{at} \quad s = s_1(\varphi), s_2(\varphi). \tag{5.123}
$$

We note that the functions $y_j(s,\varphi)$ should be also expended into series in a vicinity of the center $\varphi = q_j(\tau)$. In what follows, we omit the subscript j. For instance, the notations $\chi_j^*, \chi_j^\circ, y_j, \chi_{ji}^\circ, \xi_j, c_{ji\iota}^\circ$ are replaced by $\chi^*, \chi^\circ, y, \chi_i^\circ, \xi, c_{i\iota}^\circ$, respectively.

When following to the asymptotic approach developed in Mikhasev and Tovstik (2009), the solution of the initial-boundary-value problem (5.120), (5.122), (5.123) may be constructed in the form of complex WKB-approximations

$$
\begin{aligned}
&\chi^* = \sum_{\varsigma=0}^{\infty} \varepsilon^{\varsigma/2}\chi_\varsigma \exp\left(\mathrm{i}\varepsilon^{-1}S\right),\ \varPhi^* = \sum_{\varsigma=0}^{\infty} \varepsilon^{\varsigma/2}\varPhi_\varsigma \exp\left(\mathrm{i}\varepsilon^{-1}S\right),\\
&S(\xi,\tau) = \int_0^\tau \omega(\tilde{\tau})\mathrm{d}\tilde{\tau} + \varepsilon^{1/2}p(\tau)\xi + \frac{1}{2}\varepsilon b(\tau)\xi^2.
\end{aligned}
\tag{5.124}
$$

In anzatz (5.124), $\Im b(\tau) > 0$ for any time $\tau > 0$, $\chi_\varsigma(s,\xi,\tau), \varPhi_\varsigma(s,\xi,\tau)$ are polynomials in ξ with complex coefficients depending on τ and s, $|\omega(\tau)|$ is the current frequency of vibrations in the neighborhood of the moving center $\varphi = q(t)$, $p(\tau)$ is the variable wave parameter, and $b(\tau)$ defines the width of the j^{th} WP, the inequality $\Im b(\tau) > 0$ guaranteeing attenuation of wave amplitudes within the WP.

As seen, functions (5.124) approximate running unsteady localized vibrations in the shell. In the case when $q = 0$, and $\omega, p, b, \chi_\varsigma$ and $\varPhi_\varsigma$ are independent of time τ, expansions (5.124) are degenerated into the stationary WP, like (5.99), describing free localized vibrations in a vicinity of the fixed (weakest) generatrix.

5.6.2.2 Sequence of One-dimensional Boundary Value Problems on *Moving Generatrix*

To define all required functions appearing in ansatz (5.124), one needs to substitute them into governing equations and boundary conditions as well. The substitution of expansions (5.124) into Eqs. (5.120) results in a sequence of 1D differential equations

$$
\sum_{j=0}^{\varsigma} \mathbf{L}_j \chi_{\varsigma-j} = 0, \quad \varsigma = 0,1,2,\ldots \tag{5.125}
$$

where

$$
\mathbf{L}_0 z = \frac{k^2(q)d(B)[1+\kappa_0(B)p^2]}{p^4}\frac{\partial^4 z}{\partial s^4} + \left\{p^4 - [1+\kappa_0(B)p^2](\omega - \dot{q}p)^2\right\} z,
$$

$$
\begin{aligned}
\mathbf{L}_1 &= (b\mathbf{L}_p + \mathbf{L}_q + \dot{p}\mathbf{L}_\omega)\,\xi - \mathrm{i}\mathbf{L}_p\frac{\partial}{\partial \xi},\\
\mathbf{L}_2 &= \big(b^2\mathbf{L}_{pp} + 2b\mathbf{L}_{pq} + \mathbf{L}_{qq} + \dot{p}^2\mathbf{L}_{\omega\omega} + 2\dot{p}\mathbf{L}_{\omega q}\\
&\quad + 2\dot{p}b\mathbf{L}_{\omega p} + \dot{b}\mathbf{L}_\omega\big)\,\xi^2 - \frac{1}{2}\mathbf{L}_{pp}\frac{\partial^2}{\partial\xi^2} - \mathrm{i}\,(b\mathbf{L}_{pp} + \mathbf{L}_{pq} + \dot{p}\mathbf{L}_{\omega p})\,\xi\frac{\partial}{\partial\xi}\\
&\quad - \mathrm{i}\mathbf{L}_\omega\frac{\partial}{\partial t} - \mathrm{i}\left(\frac{1}{2}b\mathbf{L}_{pp} + \frac{1}{2}\dot{\omega}\mathbf{L}_{\omega\omega} + \dot{p}\mathbf{L}_{\omega p} + \frac{1}{2}\mathbf{L}_{pq} + \ddot{q}p + \mathbf{N}\right),\ldots,
\end{aligned}
\tag{5.126}
$$

$$
\mathbf{N} = \frac{\mathrm{i}\kappa_1(B)d(B)p^6(\tau)}{1+\kappa_0(B)p^2(\tau)}.
$$

In Eqs. (5.126), the subscripts p, q, ω denote the differentiation with respect to the corresponding variables p, q, ω. Operators L_ς for $\varsigma \geq 3$ are not written out here because of its awkwardness.

The functions Φ_ς may be found step by step from a sequence of inhomogeneous equations and expressed in terms of the functions χ_ς. The substitution of (5.124) into the basic boundary conditions lead to the sequence of boundary conditions at the moving center of the j^{th} WP

$$\chi_0 = 0, \qquad \frac{\mathrm{d}^2\chi_0}{\mathrm{d}s^2} = 0 \quad \text{at} \quad s = s_i[q(t)]; \tag{5.127}$$

$$\chi_1 + \xi s_i' \frac{\partial \chi_0}{\partial s} = 0, \quad \frac{\partial^2\chi_1}{\partial s^2} + \xi s_i' \frac{\partial^3\chi_0}{\partial s^3} = 0 \quad \text{at} \quad s = s_i[q(t)]; \quad \ldots \tag{5.128}$$

The sequence of the 1D boundary-value-problems (5.125)-(5.128) serves for determination of required functions appearing in (5.124). The procedure for their seeking is given in Mikhasev and Tovstik (2009); Mikhasev (2002). Omitting its details, we shall give here only the principal equations.

5.6.2.3 Zeroth-order Approximation

In the leading approximation ($\varsigma = 0$), one has the homogeneous ordinary differential equation (5.125) with the homogeneous boundary conditions (5.127). Its solution may be presented in the form

$$\chi_0(s, \xi) = P_0(\xi, \tau) y[s, q(\tau)], \tag{5.129}$$

where $P_0(\xi, \tau)$ is an unknown polynomial in ξ. Substituting Eq. (5.129) into Eq. (5.125) at $\varsigma = 0$ yields the relation

$$\omega = \dot{q}(\tau)p(\tau) \mp H[p(\tau), q(\tau), \tau] \tag{5.130}$$

coupling the current frequency $\omega(\tau)$ to the wave parameter $p(\tau)$ and the group velocity $v(\tau) = \dot{q}(\tau)$ of the j^{th} WP, where

$$H(p, q, \tau) = \sqrt{d[B(\tau)] \left\{ \frac{p^4}{1 + \kappa_0[B(\tau)]p^2} + \frac{\lambda(q)k^2(q)}{p^4} \right\}} \tag{5.131}$$

is the Hamilton function. In Eqs. (5.130), the signs $\pm$ indicate the availability of positive and negative branches of the required solution.

5.6.2.4 First-order Approximation

In the first-order approximation (at $\varsigma = 1$), we arrive at the non-homogeneous differential equation (5.125) with the non-homogeneous boundary conditions (5.128). The compatibility condition for this non-homogeneous boundary-value problem results in the two Hamiltonian systems

$$\dot{q} = \frac{\partial H}{\partial p}, \quad \dot{p} = -\frac{\partial H}{\partial q} \qquad \text{and} \qquad \dot{q} = -\frac{\partial H}{\partial p}, \quad \dot{p} = \frac{\partial H}{\partial q} \tag{5.132}$$

corresponding to the positive and negative branches of the solution, respectively. These solutions are associated with two WPs moving in the opposite directions. In what follows, all calculations are given for the positive j^{th} WP governed by Eqs. $(5.132)_1$. Comparing anzatz (5.124) with the initial condition (5.122) for the j^{th} WP, we readily obtain the initial conditions for the Hamiltonian system

$$p(0) = a^\circ, \quad q(0) = 0. \tag{5.133}$$

5.6.2.5 Second-order Approximation

The compatibility condition for the non-homogeneous boundary-value problem (5.125), (5.128) arising in the second-order approximation ($\varsigma = 2$) yields

$$(\xi^2 \mathbf{D}_b - 2\mathbf{D}_{\xi t}) P_0 = 0, \tag{5.134}$$

where

$$\mathbf{D}_b = \dot{b} + H_{pp} b^2 + 2H_{pq} b + H_{qq}, \quad \mathbf{D}_{\xi t} = \hat{h}_0 \frac{\partial^2}{\partial \xi^2} + \hat{h}_1 \xi \frac{\partial}{\partial \xi} + \hat{h}_2 \frac{\partial}{\partial t} + \hat{h}_3,$$
$$\hat{h}_0(t) = \frac{1}{2} H_{pp}, \quad \hat{h}_1(t) = \mathrm{i}(b H_{pp} + H_{pq}), \quad \hat{h}_2 = \mathrm{i},$$
$$\hat{h}_3(t) = \frac{\mathrm{i}}{2H} \left\{ b H H_{pp} - \dot{\omega} - 2H_q H_p + \ddot{q} p + \frac{1}{\eta} \int_{s_1}^{s_2} \mathbf{L}_\omega \dot{y} y \mathrm{d}s + \Gamma \right\},$$

$$\Gamma(t) = -\frac{2k(\tau)k'(\tau)d(B)[2 + \kappa_0(B)p^2(\tau)]\lambda[q(\tau)]}{p^5(\tau)} - \frac{d(B)\kappa_1(B)p^6(\tau)}{1 + \kappa_0(B)p^2(\tau)}.$$

Equation (5.134) has a solution of polynomial form if and only if the function $b(\tau)$ satisfies the Riccati equation

$$\dot{b} + H_{pp} b^2 + 2H_{pq} b + H_{qq} = 0. \tag{5.135}$$

The repeated comparison of Eqs. (5.124) and (5.122) gives the initial condition

$$b(0) = b^\circ \tag{5.136}$$

for the above equation.

Taking into account the Riccati equation, Eq. (5.134) is reduced to the following equation

$$\mathbf{D}_{\xi t} P_0 \equiv \hat{h}_0 \frac{\partial^2 P_0}{\partial \xi^2} + \hat{h}_1 \xi \frac{\partial P_0}{\partial \xi} + \hat{h}_2 \frac{\partial P_0}{\partial \tau} + \hat{h}_3 P_0 = 0 \tag{5.137}$$

called the amplitude one. Its solution in two different forms has been given in Mikhasev (2002). We adduce here the solution expressed in terms of the Hermite polynomials. Such presentation will be suitable in two special cases:

1. to compare expansion (5.124) with the localized natural mode (5.99);
2. to study the effect of non-stationary magnetic field on eigenmode (5.99).

The required polynomial $P_0(\xi, \tau)$ in ξ with coefficients depending on dimensionless time τ may be represented in the form:

$$P_0 = \Theta_m(\tau) \mathcal{H}_m(x), \tag{5.138}$$

where $\mathcal{H}_m(x)$ is the Hermite polynomials in x of the mth degree, and

$$x = \hat{\varrho}(\tau)\xi, \quad \hat{\varrho}(\tau) = \frac{\exp\left[-\int \frac{\hat{h}_1(\tau)\mathrm{d}\tau}{\hat{h}_2(\tau)}\right]}{\sqrt{4\int \frac{\hat{h}_0(\tau)}{\hat{h}_2(\tau)} \exp\left[-2\int \frac{\hat{h}_1(\tau)\mathrm{d}\tau}{\hat{h}_2(\tau)}\right] \mathrm{d}\tau}},$$
$$\Theta_m(\tau) = \frac{\left\{4\int (\hat{h}_0/\hat{h}_2) \exp\left[-2\int (\hat{h}_1/\hat{h}_2)\mathrm{d}\tau\right] \mathrm{d}\tau\right\}^{m/2}}{\exp\left[\int (\hat{h}_3/\hat{h}_2)\mathrm{d}\tau\right]}. \tag{5.139}$$

It is evident that the polynomial

$$P_0(\xi, \tau; c_m) = \sum_{m=0}^{M} c_m \Theta_m(\tau) \mathcal{H}_m[\hat{\varrho}(\tau)\xi] \tag{5.140}$$

of the Mth degree is also the solution of the amplitude equation (5.137), where c_m are arbitrary constants found from the initial conditions.

5.6.2.6 Higher-order Approximations

To find $\chi_\varsigma, \Phi_\varsigma$ for $\varsigma \geq 1$, one need to consider corresponding boundary-value problem (5.125), (5.128) in the $\varsigma + 2$nd approximation. The existence of a solution of this problem results in the non-homogeneous differential equation

$$\mathbf{D}_{\xi t} P_\varsigma = P_\varsigma^* \tag{5.141}$$

for a polynomial $P_\varsigma(\chi,\tau)$, where $P^*_\varsigma(\chi,\tau)$ is some polynomial expressed by means of polynomials $P_0,\ldots,, P_{\varsigma-1}$. However, we interrupt the formal procedure of seeking $\chi_1,\chi_2,\ldots$ because the accuracy of governing equations (5.110) is not sufficient.

5.6.3 Solution of the Initial Boundary Value Problem in the Leading Approximation

We note that there exist two branches of solutions of the initial boundary-value problem. Let $p^+(\tau), q^+(\tau)$ and $p^-(\tau), q^-(\tau)$ be solutions of the Hamiltonian systems $(5.132)_1$ and $(5.132)_2$, respectively. Here, $\varphi = q^+(\tau)$ and $\varphi = q^-(\tau)$ are centers of the positive and negative WPs moving in the opposite directions. We introduce also the local coordinates

$$\xi^{\pm} = \varepsilon^{-1/2}[\varphi - q^{\pm}(\tau)]. \tag{5.142}$$

in the scaled coordinate systems with centers at the moving generatrix $\varphi = q^{\pm}(\tau)$. Then

$$\omega^{\pm},\quad b^{\pm},\quad P_0^{\pm},\quad \chi_0^{\pm},\quad \Phi_0^{\pm} \tag{5.143}$$

are found above functions corresponding to the positive and negative WPs, respectively. Consider the following functions:

$$\chi = \chi^+ + \chi^-,\quad \Phi = \Phi^+ + \Phi^-, \tag{5.144}$$

where

$$\begin{aligned}
\chi^{\pm} &= \left[\chi_0^{\pm} + O\left(\varepsilon^{1/2}\right)\right]\exp\left(\mathrm{i}\varepsilon^{-1}S^{\pm}\right),\\
\Phi^{\pm} &= \left[\Phi_0^{\pm} + O\left(\varepsilon^{1/2}\right)\right]\exp\left(\mathrm{i}\varepsilon^{-1}S^{\pm}\right),\\
\chi_0^{\pm} &= P_0^{\pm}(\xi^{\pm},\tau;\, c_m^{\pm})y[s,q^{\pm}(\tau)],\quad P_0^{\pm} = \sum_{m=0}^{M} c_m^{\pm}\Theta_m(\tau)\mathcal{H}_m[\hat{\varrho}(\tau)\xi^{\pm}],\\
\Phi_0^{\pm} &= \frac{d(B)k[q^{\pm}(\tau)]P_0^{\pm}(\xi^{\pm}\!,\tau;\, c_m^{\pm})}{[p^{\pm}(\tau)]^4}\left[\frac{\partial^2 y(s,\varphi)}{\partial s^2} + \kappa(B)[p^{\pm}(\tau)]^2 y(s,\varphi)\right]_{\varphi=q^{\pm}(\tau)},\\
S^{\pm} &= \int_0^{\tau}\omega^{\pm}(\tilde{\tau})\mathrm{d}\tilde{\tau} + \varepsilon^{1/2}p^{\pm}(\tau)\xi^{\pm} + \frac{1}{2}\varepsilon b^{\pm}(\tau)(\xi^{\pm}).
\end{aligned} \tag{5.145}$$

The composed functions (5.144) are the leading approximation of the required solution of the initial-boundary-value problem (5.110)-(5.112) for the fixed j. They contain undefined constants $c_m^{\pm}$ which are found from the initial conditions for the WPs with the fixed number j (we remind that a number j is associated with the number of eigenvalue λ of the boundary-value problem (5.115), (5.116)). If the polynomials $P_0^{\pm}$ are expressed in terms of the Hermite polynomials, then as shown in Mikhasev (2002), these constants calculated by the equation

$$c_m^{\pm} = \frac{1}{2^{m+1} m! \sqrt{\pi} \Theta_m(0)} \int_{-\infty}^{+\infty} \mathrm{e}^{-\zeta^2} \mathcal{H}_m[\hat{\varrho}(0)\zeta] \left[\chi_0^{\circ}(\zeta) \mp \frac{v_0^{\circ}(\zeta)}{H^{\circ}} \right] \mathrm{d}\zeta, \tag{5.146}$$

where $\chi_0^{\circ} \equiv \chi_{j0}^{\circ}, v_0^{\circ} \equiv v_{j0}^{\circ}$ are polynomials evaluated by Eqs. (5.118), and $H^{\circ} = H(a^{\circ}, 0, 0)$ is the initial value of the Hamiltonian function.

Remark 5.3. Let the parameters $q = 0, p = a^{\circ}$ satisfy equations

$$H_p = 0, \quad H_q = 0, \tag{5.147}$$

and $b = b^{\circ}$ is the solution of the quadratic equation

$$H_{pp} b^2 + 2 H_{pq} b + H_{qq} = 0 \tag{5.148}$$

in the absence of magnetic field ($B = 0$). Then $p^{\pm}(\tau) \equiv a^{\circ}, q^{\pm}(\tau) \equiv 0$ and $b^{\pm}(\tau) \equiv b^{\circ}$ are the solutions of the Hamiltonian systems and Riccati equations, respectively, at $B = 0$. In this case, the constructed solution (5.144)-(5.146) gives the stationary WP with the center $\varphi = 0$, which coincide with the localized natural mode (5.99).

In what follows, we shall study the effect of growing magnetic field on the localized eigenmodes (5.99) being characteristics of a shell without magnetic field.

5.6.4 *Running Localized Vibrations in Magnetorhelogical Elastomer-based Cylindrical Shells vs. Magnetic Field*

The constructed asymptotic solution (5.144)-(5.146) may be used to predict the response of a laminated MRE-based shell to the initial localized perturbations at the shell surface taking into account an applied magnetic field. We note that the principal tunable parameters $d(B), \kappa(B)$ and $\kappa_1(B)$ appearing in the Hamiltonian function and amplitude equation depend on the magnetic field induction B. Varying the intensity of magnetic field, one can affect the behavior of running WPs and softly suppress vibrations as well.

5.6.4.1 Wave Packets in Shells with Constant Parameters

At first, we consider the simplest case when all geometrical parameters, including the curvature and the generatrix length, are constants, and the applied magnetic field is non-stationary. Here $k \equiv 1,\ s_1 = 0,\ s_2 = l$ and the induction $B(\tau)$ is a function of the dimensionless time τ. In this case, the Hamilton function for the j^{th} WP is simplified

$$H(p, \tau) = \sqrt{d[B(t)] \left\{ \frac{p^4}{1 + \kappa_0[B(t)] p^2} + \frac{\pi^4 j^4}{l^4 p^4} \right\}}, \tag{5.149}$$

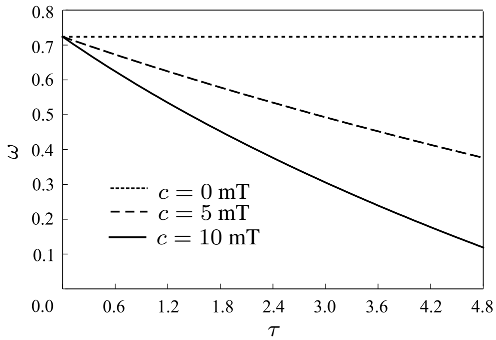

Fig. 5.54 Dimensionless current frequency $\omega = |\omega^{\pm}(\tau)|$ versus dimensionless time for different $c = 0, 5, 10$ mT (after Mikhasev et al, 2016).

and the Hamiltonian systems and Riccati equations admit solutions in the explicit form

$$p^{\pm} = a^{\circ}, \quad q^{\pm}(\tau) = \pm \int_0^{\tau} H_p \mathrm{d}\tau, \quad \omega^{\pm}(\tau) = \pm a^{\circ} H_p \mp H,$$
$$b^{\pm}(\tau) = \frac{b_0}{1 + b_0 \int_0^{\tau} H_{pp} \mathrm{d}\tau}. \tag{5.150}$$

If the magnetic field is constant, then the current frequencies $|\omega^{\pm}|$ for both WPs are constants; if not, then $|\omega^{\pm}(\tau)|$ are time-dependent. The functions $\Im b^{\pm}(\tau)$ characterize the size of the shell area spanned by vibrations and $\chi_0^{\pm}(\tau)$ define the amplitudes of these unsteady vibrations. To analyze the effect of magnetic field on travelling WPs in detail, we consider the following example.

Example 5.14. A sandwich cylindrical shell is assembled from two face sheets made of ABS-plastic SD-0170 and MRE-1 core. The geometrical parameters are the following: $R = 0.4$ m, $L = 1.5$ m, $h_1 = h_3 = 0.5$ mm, $h_2 = 11$ mm. The numerical computations of magnitudes $\omega = |\omega^{\pm}(\tau)|$, $\Im b = \Im b^{\pm}(\tau)$, $|\chi_0| = |\chi_0^{\pm}(\tau)|$ versus dimensionless time were performed for two different cases: (a) $B = 0$; (b) the magnetic induction $B(\tau) = c\tau$ is the linear function of dimensionless time at $c = 5, 10$ mT. The following parameters were considered as the initial ones: $a_0 = 2.5$, $b_0 = \mathrm{i}$, $\chi_1^{\circ} = 1$, $v_1^{\circ} = 0$ and $\chi_j^{\circ} = v_j^{\circ} = 0$ at $j > 1$. Figure 5.54 shows that for the accepted parameters and case (b) the current frequency $\omega(\tau)|$ is the decreasing function of time. As seen from Fig. 5.55, the width of the 1st running WP increases in time for both cases, (a) and (b), that means that the WP spreads in the circumferential direction. But the speed of this spreading depends weakly on whether the magnetic field is stationary or time-dependent. As concerns the wave amplitudes (s. Fig. 5.56), they demonstrate a very strong dependence on the visco-elastic properties of MREs which are affected by the applied magnetic field. The curve corresponding to $c = 0$ mT shows the capability of the MRE to damp travelling vibrations in the sandwich without magnetic field. The other two curves

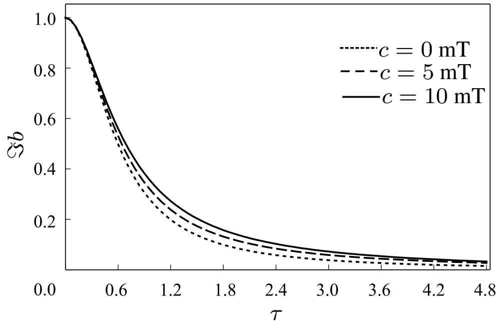

Fig. 5.55 Parameter $\Im b = \Im b^{\pm}(\tau)$ vs. dimensionless time for different $c = 0, 5, 10$ mT (after Mikhasev et al, 2016).

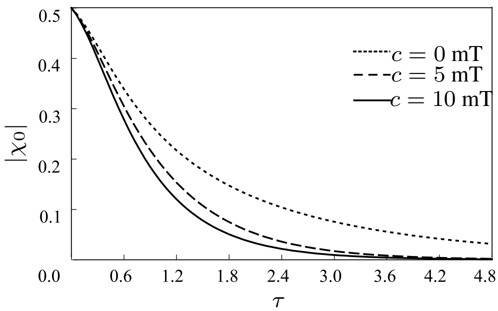

Fig. 5.56 Maximum amplitude $|\chi_0|$ versus dimensionless time for different $c = 0, 5, 10$ mT (after Mikhasev et al, 2016).

bring out clearly that this capability becomes stronger under the action of growing magnetic field. So, when comparing amplitudes at the fixed moment $\tau = 2.4$, one can see that the maximum amplitude $|\chi_0|$ for $c = 5$ mT and $c = 10$ mT are 3-and 6-times less, respectively, than that for $c = 0$ mT.

5.6.4.2 Wave Packets in Shells with Variable Geometrical Parameters

The numerical calculations performed by Mikhasev and Tovstik (1990) for single-layer isotropic shells revealed that behavior of excited WPs in shells with variable curvature or/and generatrix length may be very complicated and characterized by reflection of WPs possessing a small initial energy from some generatrix. As a rule, these reflections are accompanied by strong focusing of WPs and growing amplitudes. Additionally, if a shell is subjected to an external dynamic load (Avdoshka and Mikhasev, 2001; Mikhasev, 2002), then increasing amplitudes in running WPs may be dramatic and lead to possible dynamic instability of a structure. To study similar effects in MRE-based shell with variable geometrical parameters, we apply to the next example

Example 5.15. Consider a circular sandwich cylindrical shell with an oblique edge as shown in Fig. 5.57. Here

$$k = 1, \quad s_1 = 0, \quad s_2(\varphi) = l_0 + (\cos\varphi - 1)\tan\alpha, \tag{5.151}$$

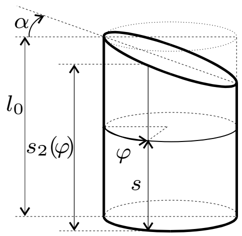

Fig. 5.57 Medium surface of a circular cylindrical shell with oblique edge. (after Mikhasev et al, 2016).

where Rl_0 is the longest generatrix length and α is the slope angle of the oblique edge. The viscoelastic properties of two elastic layers and MRE core are the same as in Example 5.14 and the geometrical parameters are the following: $h_1 = h_3 = 0.5$ mm, $h_2 = 11$ mm, $R = 0.4$ m, $l_0 = 2$.

For this shell, the longest generatrix $\varphi = \varphi_0^\circ = 0$ is the weakest one. The natural modes (5.99) localized in the neighbourhood of this line are characterized by parameters $p = a^\circ$, $b = b^\circ$ which jointly with $q = 0$ are determined as the solutions of Eqs. (5.138), (5.148) for $j = 1$ (s. Remark 5.3). As the initial conditions for Hamiltonian systems $(5.132)_1$, $(5.132)_2$ and Riccati equation (5.135), we assume the above parameters $p = a^\circ$, $q = 0$, $b = b^\circ$. In other words, up to amplitudes $\chi_j^\circ, \mathrm{i}\varepsilon^{-1}v_j^\circ$, one of the localized eigenmodes (5.99) with $j = 1$ semi-waves in the axial direction to be considered as the initial WP. It is of interest to study its behavior when apply non-stationary magnetic field with the induction $B = c\tau$.

Figures 5.58 to 5.62 show parameters $p^+, q^+, \omega^+, \Im b^+, |\Re\chi_0^+|, |\Im\chi_0^+|$ vs. dimensionless time τ for different $c = 0, 5$ and 10 mT. The calculations were performed for the 1^{st} positive WP (at $j = 1$) with the initial amplitudes $\chi_1^\circ = 1$, $v_1^\circ = 0$ in (5.122). Due to the symmetry of the shell and the initial WP with regard to the plane $\varphi = 0$, the curves for all functions corresponding to the negative WP are the same as in Figs. 5.58-5.62. In all figures the straight dotted lines correspond to the eigenform localized in the neighborhood of the longest generatrix $\varphi = 0$. Thus, if a magnetic field is absent ($c = 0$ mT), the initial WP coinciding with one of eigenmodes stays motionless, with the wave number p^+, eigenfrequency ω^+ and parameter b^+ being constants for any point of time. The maximum amplitude of free

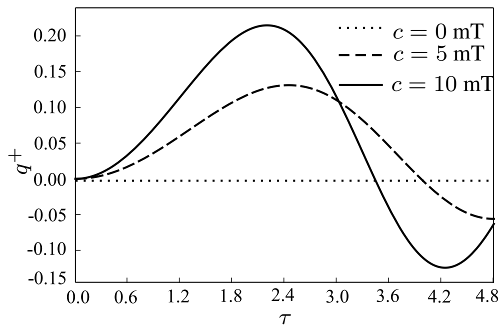

Fig. 5.58 Center $\varphi = q^+ = 0$ of the initial WP (at $c = 0$ mT) and the center $\varphi = q^+$ of the 1^{st} positive WP versus dimensionless time τ at different rates of growing of the magnetic field induction, $c = 5, 10$ mT (after Mikhasev et al, 2016).

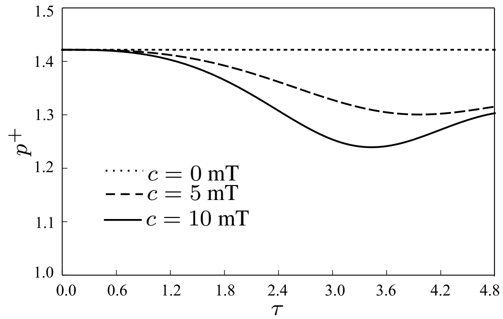

Fig. 5.59 Wave parameter $p^+ = a_0 \approx 1.41$ of the initial WP (at $c = 0$ mT) and parameter p^+ of the 1st positive WP versus dimensionless time τ at different rates of growing of the magnetic field induction, $c = 5, 10$ mT (after Mikhasev et al, 2016).

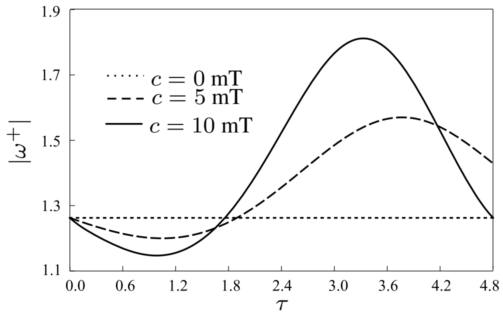

Fig. 5.60 Natural frequency $|\omega^+| = \omega_0 \approx 1.25$ of the initial WP (at $c = 0$ mT) and the current frequency $|\omega^+|$ of the 1st positive WP versus dimensionless time τ at different rates of growing of the magnetic field induction, $c = 5, 10$ mT (after Mikhasev et al, 2016).

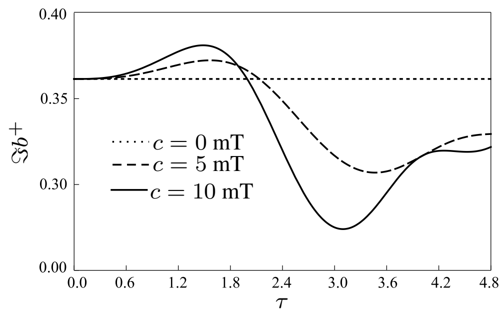

Fig. 5.61 Parameter $\Im b^+ = \Im b_0 \approx 0.36$ for the initial WP and parameter $\Im b^+$ for the 1st positive WP versus dimensionless time at different rates of growing of the magnetic field induction, $c = 5, 10$ mT (after Mikhasev et al, 2016).

vibrations (s. Fig. 5.62) is the decreasing function of the dimensionless time τ due to viscoelastic properties of the MRE core regardless of whether the magnetic field is applied or not.

Interesting effects are observed when the magnetic field is applied. After its turning on, the eigenmode (initial WP) is spitted into two WPs, positive and negative ones, travelling in the opposite directions (s. Fig. 5.58). Figure 5.58 shows also that the increase of the magnetic field results in the multiple refections of the WP from the certain generatrices $\varphi = \varphi_{\mathrm{r}} = q^+(\tau_{\mathrm{r}})$, these refections being accompanied by slight focusing (s. Fig. 5.61). Herewith, the larger the growth rate of the induction (parameter c, mT) is, the earlier the reflection occurs. So, for $c = 5$ mT the first reflection occurs from the generatrix $\varphi \approx 0.13$ at the point of time $\tau = \tau_{\mathrm{r}} \approx 2.45$, and for $c = 10$ mT, one has $\varphi \approx 0.21$, $\tau_{\mathrm{r}} \approx 2.1$. At $\tau = \tau_0$, the WP center goes back

Fig. 5.62 $|\chi_0^+|$ for the 1st positive WP versus dimensionless time at $c = 0$ and different rates of growing of the magnetic field induction, $c = 5, 10$ mT (after Mikhasev et al, 2016).

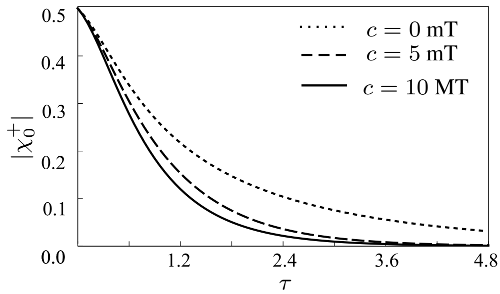

to the initial position at the longest generatrix ($\varphi = 0$). Here, $\tau_0 \approx 4.0$ and $\tau_0 \approx 3.58$ for $c = 5$ mT and $c = 10$ mT, respectively. Figures 5.59 and 5.60 demonstrate how the wave parameter p^+ and the dimensionless current frequency $|\omega^+|$ vary with time. In the beginning, the frequency $|\omega^+|$ drops slightly, but then it runs up together with the induction $B(\tau)$. The strong growth of the frequency is explained by increasing the total stiffness for the sandwich at high level of the applied magnetic field.

From the analysis of Fig. 5.62 follows that the increase of the magnetic field induction leads to a soft suppression of running vibrations. For instance, at $c = 10$ mT, the damping decrement is about two times than that without magnetic field (at $c = 0$ mT): the larger the growth rate of the magnetic field is, the faster the damping of running vibrations occurs.

References

Aguib S, Noura A, Zahloul H, Bossis G, Chevalier Y, Lançon P (2014) Dynamic behavior analysis of a magnetorheological elastomer sandwich plate. Int J Mech Sc 87:118–136

Aguib S, Nour A, Djedid T, Bossis G, Chikh N (2016) Forced transverse vibration of composite sandwich beam with magnetorheological elastomer core. J Mech Sc Techn 30(1):15–24

Allahverdizadeh A, Mahjoob M, Eshraghi I, Nasrollahzadeh N (2013) On the vibration behavior of functionally graded electrorheological sandwich beams. Int J Mech Sc 70:130–139

Avdoshka I, Mikhasev G (2001) Wave packets in a thin cylindrical shell under a non-uniform axial load. J Appl Maths Mechs 65(2):301–309

Berg CD, Evans LF, Kermode PR (1996) Composite structure analysis of a hollow cantilever beam filled with electro-rheological fluid. J Intell Mater Syst Struct 7(5):494–502

Boczkowska A, Awietjan SF, Pietrzko S, Kurzydlowski KJ (2012) Mechanical properties of magnetorheological elastomers under shear deformation. Comp: Part B 43:636–640

Botogova M, Mikhasev G (1996) Free vibrations of non-uniformly heated viscoelastic cylindrical shell. Technische Mechanik 16(3):251–256

Chikh N, Nour A, Aguib S, Tawfiq I (2016) Dynamic analysis of the non-linear behavior of a composite sandwich beam with a magnetorheological elastomer core. Acta Mechanica Solida Sinica 29(3):271–283

Choi W, Xiong Y, Shenoi R (2010) Vibration characteristics of sandwich beams with steel skins and magnetorheological elastomer cores. Advances in Structural Engineering 13(5):837–847

Choi Y, Sprecher AF, Conrad H (1990) Vibration characteristics of a composite beam containing an electrorheological fluid. J Intell Mater Syst Struct 1(1):91–104

DiTaranto RA (1965) Theory of vibratory bending for elastic and viscoelastic layered finite-length beams. Trans ASME J Appl Mech 32(4):881–886

Dwivedy SK, Mahendra N, Sahu KC (2009) Parametric instability regions of a soft and magnetorheological elastomer cored sandwich beam. J Sound Vibr 325(4–5):686–704

Eshaghi M, Sedaghati R, Rakheja S (2015) The effect of magneto-rheological fluid on vibration suppression capability of adaptive sandwich plates: experimental and finite element analysis. Journal of Intelligent Material Systems and Structures 26(14):1920–1935

Eshaghi M, Sedaghati R, Rakheja S (2016) Dynamic characteristics and control of magnetorheological/electrorheological sandwich structures: a state-of-the-art review. Journal of Intelligent Material Systems and Structures 27(15):2003–2037

Gandhi MV, Thompson BS (1992) Smart Materials and Structures. Chapman&Hall, London

Gandhi MV, Thompson BS, Choi SB (1989) A new generation of innovative ultraadvanced intelligent composite materials featuring electro-rheological fluids: an experimental investigation. J Comp Mater 23(12):1232–1255

Hu B, Wang D, Xia P, Shi Q (2006) Investigation on the vibration characteristics of a sandwich beam with smart composites - MRF. World Journal of Modelling and Simulation 2(3):201–206

Hu G, Guo M, Li W, Du H, Alici G (2011) Experimental investigation of the vibration characteristics of a magnetorheological elastomer sandwich beam under non-homogeneous small magnetic fields. Smart Materials and Structures 20(12):127,001–1–127,001–7

Hu G, Guo M, Li W (2012) Analysis of vibration characteristics of magnetorheological elastomer sandwich beam under non-homogeneous magnetic field. Appl Mech Mat 101–102:202–206

Irazu L, Elejabarrieta M (2017) Magneto-dynamic analysis of sandwiches composed of a thin viscoelastic-magnetorheological layer. J Intel Mat Syst Struct 28(20):3106–3114

Kang Y, Kim J, Choi S (2001) Passive and active damping characteristics of smart electrorheological composite beams. Smart Materials and Structures 10:724–729

Korobko EV, Mikhasev GI, Novikova ZA, Zurauski MA (2012) On damping vibrations of three-layered beam containing magnetorheological elastomer. J Intel Mat Syst Struct 23(9):1019–1023

Kozlowska J, Boczkowska A, Czulak A, Przybyszewski B, Holeczek K, Stanik R, Gude M (2016) Novel MRE/CFRP sandwich structures for adaptive vibration control. Smart Mater Struct 25(3):035,025

Lai J, Wang K (1996) Parametric contral of structural vibrations via adaptable stiffness dynamic absorbers. Journal of Vibration and Acoustics 118:41–47

Lara-Prieto V, Parkin R, Jackson M, Silberschmidt V, Kęsy Z (2010) Vibration characteristics of MR cantilever sandwich beams: experimental study. Smart Mater Struct 19(1):015,005

Lee CY (1995) Finite element formulation of a sandwich beam with embedded electrorheological fluids. J Intell Mater Syst Struct 6(5):718–728

Li Y, Li J, Li W (2014) A state-of-the-art review on magnetorheological elastomer devices. Smart Materials and Structures 23(12):123,001–1–123,001–24

Long M, Hu G, Wang S (2013) Vibration response analysis of MRE cantilever sandwich beam under non-homogeneous magnetic fields. Applied Mechanics and Materials 303–306:49–52

Lukasiewicz S (1979) Local loads in plates and shells. Springer Netherlands

Mead DJ, Markus S (1970) Loss factors and resonant frequencies of encastrè damped sandwich beams. J Sound Vibr 12(1):99–112

Megha S, Kumar N, D'Silva R (2016) Vibration analysis of magnetorheological elastomer sandwich beam under different magnetic fields. J Mech Engng Automat 6:75–80

Mikhasev G (1996a) Localized families of bending waves in a non-circular cylindrical shell with sloping edges. Journal of Applied Mathematics and Mechanics 60(4):629–637

Mikhasev G (1996b) Localized wave forms of motion of an infinite shell of revolution. Journal of Applied Mathematics and Mechanics 60(5):813–820

Mikhasev G (1997) Free and parametric vibrations of cylindrical shells under static and periodic axial loads. Technische Mechanik 17(3):209–216

Mikhasev G (1998) Travelling wave packets in an infinite thin cylindrical shell under internal pressure. Journal of Sound and Vibrations 209(4):543–559

Mikhasev G (2002) Localized families of bending waves in a thin medium-lenght cylindrical shell under pressure. Journal of Sound and Vibrations 253(4):833–857

Mikhasev G (2017) Some problems on localized vibrations and waves in thin shells. In: Altenbach H, Eremeev V (eds) Shell-like Structures. Advanced Theories and Applications, Courses and Lectures, vol 572, Springer, CISM International Center for Mechanical Sciences, pp 259–262

Mikhasev G (2018) Thin laminated cylindrical shells containing magnetorheological elastomers: Buckling and vibrations. In: Pietraszkiewicz W, Witkowski W (eds) Shell Structures: Theory and Applications, vol 4, Taylor&Francis Group, London, pp 259–262

Mikhasev G, Kuntsevich S (1997) Thermoparametric vibrations of noncircular cylindrical shell in nonstationary temperature field. Technische Mechanik 17(2):113–120

Mikhasev G, Kuntsevich S (1999) Parametric vibrations of viscoelastic cylindrical shell under static and periodic axial loads. Technische Mechanik 19(3):187–195

Mikhasev G, Botogova M, Korobko E (2011) Theory of thin adaptive laminated shells based on magnetorheological materials and its application in problems on vibration suppression. In: Altenbach H, Eremeyev V (eds) Shell-like Structures, Springer, Heidelberg, Advanced Structured Materials, vol 15, pp 727–750

Mikhasev G, Mlechka I, Altenbach H (2016) Soft suppression of travalling localized vibrations in medium-length thin sandwich-like cylindrical shells containing magnetorheological layers via nonstationary magnetic field. In: Awrejcewicz J (ed) Dynamical Systems: Theoretical and Experimental Ananlysis, Springer Proceedings in Mathematics&Statistics, vol 182, Springer, Singapore, pp 241–260

Mikhasev GI, Tovstik PE (1990) Stability of conical shells under external pressure. Mech Solids 25(4):106–119

Mikhasev GI, Tovstik PE (2009) Localized Vibrations and Waves in Thin Shells. Asymptotic Methods (in Russ.). FIZMATLIT, Moscow

Mikhasev GI, Korobko EV, Novikova ZA (2010) On suppression of vibrations of three-layered beam containing magnetorheological composite (in Russ.). Mechanics of Machines, Mechanisms and Materials 4:49–53

Mikhasev GI, Altenbach H, Korchevskaya EA (2014) On the influence of the magnetic field on the eigenmodes of thin laminated cylindrical shells containing magnetorheological elastomer. Composite Structures 113:186 – 196

Mohammadi F, Sedaghati R (2012) Nonlinear free vibration analysis of sandwich shell structures with a constrained electrorheological fluid layer. Smart Materials and Structures 21(7):075,035

Nayak B, Dwivedy SK, Murthy KSRK (2011) Dynamic analysis of magnetorheological elastomer-based sandwich beam with conductive skins under various boundary conditions. J Sound Vibr 325(9):1837–1859

Nayak B, Dwivedy SK, Murthy KSRK (2012) Multi-frequency excitation of magnetorheological elastomer-based sandwich beam with conductive skins. Int J Non-Linear Mech 47(5):448–460

Nayak B, Dwivedy SK, Murthy KSRK (2014) Dynamic stability of a rotating sandwich beam with magnetorheological elastomer core. Eur J Mech A/Solids 47:143–155

Oyadiji SO (1996) Applications of electro-rheological fluids for constrained layer damping treatment of structures. J Intell Mater Syst Struct 7(5):541–549

Phani AS, Venkatraman K (2003) Vibration control of sandwich beams using electrorheological fluids. Mech Syst and Signal Processing 17(5):1083–1095

Qatu MS, Sullivan RW, Wang W (2010) Recent research advances on the dynamic analysis of composite shells: 2000-2009. Composite Structures 93(1):14–31

Rajamohan V, Sedaghati R, Rakheja S (2010) Vibration analysis of a multi-layer beam containing magnetorheological fluid. Smart Materials and Structures 19(1):015,013–1–015,013–12

Shaw J (2000) Hybrid control of cantilevered er sandwich beam for vibration suppression. J Intell Material Systems and Struct, 11(1):26–31

Skudrzyk E (1968) Simple and Complex Vibratory Systems. Pennsylvania State Univ Pr (Trd), Pennsylvania de Souza Eloy F, Gomes G, Ancelotti A, da Cunha S, Bombard A, Junqueira D (2018) Experimental dynamic analysis of composite sandwich beams with magnetorheological honeycomb core. Engineering Structures 176(1):231–242

de Souza Eloy F, Gomes G, Ancelotti A, da Cunha S, Bombard A, Junqueira D (2019) A numerical-experimental dynamic analysis of composite sandwich beam with magnetorheological elastomer honeycomb core. Composite Structures 209(1):242–257

Sun Q, Zhou JX, Zhang L (2003) An adaptive beam model and dynamic characteristics of magnetorheological materials. J Sound Vibr 261(3):465–481

Vemuluri R, Rajamohan V (2016) Dynamic analysis of tapered laminated composite magnetorheological elastomer (MRE) sandwich plates. Smart Materials and Structures 25(3):035,006

Vemuluri R, Rajamohan V, Arumugam A (2018) Dynamic characterization of tapered laminated composite sandwich plates partially treated with magnetorheological elastomer. Journal of Sandwich Structures & Materials 20(3):308–350

Wei K, Meng G, Zhang W (2008) Experimental investigation on vibration characteristics of sandwich beams with magnetorheological elastomers cores. Journal of Central South University of Technology 15(1):239–242

Yalcintas M, Coulter J (1995) Electrorheological material based adaptive beams subjected to various boundary conditionss. Journal of Intelligent Material Systems and Structures 6:700–717

Yalcintas M, Coulter JP (1998) Electrorheological material based non-homogeneous adaptive beams. Smart Mater Struct 7(1):128–143

Yalcintas M, Dai H (1999) Magnetorheological and electrorheological materials in adaptive structures and their performance comparison. Smart Mater Struct 8(5):560–573

Yalcintas M, Dai H (2004) Vibration suppression capabilities of magnetorheological materials based adaptive structures. Smart Mater Struct 13(1):1–11

Yeh JY (2011) Vibration and damping analysis of orthotropic cylindrical shells with electrorheological core layer. Aerospace Sc Technology 15(4):293–303

Yeh JY (2013) Vibration analysis of sandwich rectangular plates with magnetorheological elastomer damping treatment. Smart Mater Struct 22:035,010–035,018

Yeh JY (2014) Vibration characteristics analysis of orthotropic rectangular sandwich plate with magnetorheological elastomer. Procedia Engng 79:378–385

Yildirim T, Ghayesh M, Li W, Alici G (2016) Experimental nonlinear dynamics of a geometrically imperfect magneto-rheological elastomer sandwich beam. Composite Structures 138:381–390

Zeerouni N, Aguib S, Nour A, Djedid T, Nedjar A (2018) Active control of the nonlinear bending behavior of magnetorheological elastomer sandwich beam with magnetic field. Vibroengineering Procedia 18:73–78

Zhang J, Yildirim T, Alici G, Zhang S, Li W (2018) Experimental nonlinear vibrations of an mre sandwich plate. Smart Structures and Systems 22(1):71–79

Zhou GY, Wang Q (2005) Magnetorheological elastomer-based smart sandwich beams with non-conductive skins. Smart Mater Struct 14(5):1001–1009

Zhou GY, Wang Q (2006a) Study on the adjustable rigidity of magnetorheological-elastomer-based sandwich beams. Smart Mater Struct 15(1):59–74

Zhou GY, Wang Q (2006b) Use of magnetorheological elastomer in an adaptive sandwich beam with conductive skins. Part I: magnetoelastic loads in conductive skins. Int J Solids Struct 43(17):5386–5402

Zhou GY, Wang Q (2006c) Use of magnetorheological elastomer in an adaptive sandwich beam with conductive skins. Part II: dynamic properties. Int J Solids Struct 43(17):5403–5420

Chapter 6
Appendix: Asymptotic Estimates and Series

Abstract In this appendix, the definitions of symbols O, o, $\sim$ and asymptotic expansions met in the book are shortly given.

6.1 Estimates of Functions

Let functions $f(z)$ and $g(z)$ be defined on a set $\mathbb{D}$ of the complex numbers, $\mathbb{C}$, or the real numbers, $\mathbb{R}$, and let a be a point of accumulation of $\mathbb{D}$.

Notation 1. We write

$$f(z) = O(g(z)) \quad \text{as} \quad z \to a \tag{6.1}$$

if there exists a neighborhood U of the point a and a constant C such that

$$|f(z)| \leq C|g(z)| \quad \text{for any} \quad z \in U \cap \mathbb{D}. \tag{6.2}$$

Notation 2. One writes

$$f(z) = O(g(z)) \tag{6.3}$$

if there exists a constant C such that the inequality

$$|f(z)| \leq C|g(z)| \tag{6.4}$$

holds for all $z \in \mathbb{D}$.

Notation 3. The notation

$$f(z) = o(g(z)) \quad \text{as} \quad z \to a \tag{6.5}$$

means that

$$\lim_{z \to a} \frac{f(z)}{g(z)} = 0. \tag{6.6}$$

G. I. Mikhasev and H. Altenbach, *Thin-walled Laminated Structures*,
Advanced Structured Materials 106, https://doi.org/10.1007/978-3-030-12761-9_6

Notation 4. If $f(z) = O(g(z))$ and $f(z) = o(g(z))$ hold simultaneously as $z \to a$, we write

$$f(z) \sim g(z) \quad \text{as} \quad z \to a. \tag{6.7}$$

The notations $O(g(z))$ and $o(g(z))$ define the class of functions which satisfy estimations (6.3) and (6.5), respectively. We list here some rules for operations with these symbols (classes of functions). As $z \to a$ and $z \in \mathbb{D}$, there are valid the following properties:

$$\begin{gathered} o(g(z)) + o(g(z)) = o(g(z)), \quad o(g(z)) + O(g(z)) = O(g(z)), \\ o(g(z)) \times o(f(z)) = o(g(z) \times f(z)), \quad o(g(z)) \times O(f(z)) = o(g(z) \times f(z)), \\ O(o(g(z))) = o(g(z)), \quad o(O(g(z))) = o(g(z)), \\ o(o(g(z))) = o(g(z)), \quad o(g(z)) = O(g(z)). \end{gathered} \tag{6.8}$$

The prove of some of the above relations as well as a large number of examples may be found in De Bruijn (1970); Nayfeh (1973); Olver (1974); Bauer et al (2015).

6.2 Asymptotic Series

Consider a sequence of functions $u_n(z)$, $n = 0, 1, 2, \ldots$, defined on $\mathbb{D}$ and let a be a point of accumulation of $\mathbb{D}$.

Definition 6.1. The sequence $u_n(z)$ is said to be *asymptotic* as $z \to a$, if for any integer $n \geq 0$,

$$u_{n+1}(z) = o(u_n(z)), \quad \text{as} \quad z \to a. \tag{6.9}$$

For example, the sequence $u_n(z) = F(z)(z-a)^m$ as $z \to a$, where $F(z)$ is an arbitrary function bounded on the set $\mathbb{D}$, is the asymptotic one. Similar sequence appear in Eqs. (3.105). Indeed, the sequence

$$u_n(\varepsilon; \xi, s) = \varepsilon^{n/2} \chi_n(\xi, s) \exp\left\{ \mathrm{i} \left(\varepsilon^{-1/2} p\xi + \frac{1}{2} b\xi^2 \right) \right\} \tag{6.10}$$

is the asymptotic as $\varepsilon \to 0$ for any fixed ξ, s.

Definition 6.2. Let the function $f(z)$ be defined on $\mathbb{D}$ and the sequence $u_n(z)$ is asymptotic as $z \to a$, then the series

$$f(z) \cong \sum_{n=0}^{\infty} a_n u_n(z) \quad \text{as} \quad z \to a \tag{6.11}$$

is called an asymptotic expansion of $f(z)$ in the Poincaré sense by means of the asymptotic sequence $u_n(z)$ if there are constants a_n such that for any integer $N \geq 0$

$$f(z) - \sum_{n=0}^{N} a_n u_n(z) = o(u_N(z)) \tag{6.12}$$

or

$$f(z) - \sum_{n=0}^{N} a_n u_n(z) = O(u_{N+1}(z)) \tag{6.13}$$

as $z \to a$.

If the function $f(z)$ is expanded into asymptotic series (6.11) by means of the asymptotic sequence $u_n(z)$, then the coefficients a_n in (6.11) are determined in a unique way; in other words, expansion (6.11) is unique.

We note that an asymptotic series may diverge. Asymptotic series may be summed, multiplied by functions, differentiated and integrated under special assumptions. Basic properties of asymptotic series and operations on them are given in Jahnke et al (1960); Evgrafov (1961); De Bruijn (1970); Nayfeh (1973); Olver (1974); Erdèlyi (2010); Bauer et al (2015).

References

Bauer SM, Filippov SB, Smirnov AL, Tovstik PE, Vaillancourt R (2015) Asymptotic Methods in Mechanics of Solids, International Series of Numerical Mathematics, vol 167. Springer, Basel

De Bruijn N (1970) Asymptotic Methods in Analysis, 3rd edn. North-Holland & Wolters Noordhoff, Groningen

Erdèlyi A (2010) Asymptotic Expansions. Dover Publication, New York

Evgrafov MA (1961) Asymptotic Estimates and Entire Functions. Gordon and Breach, New York

Jahnke E, Emde F, Lösch F (1960) Tables of Higher Functions, 6th edn. McGraw-Hill, New York

Nayfeh AH (1973) Perturbation Methods. Wiley, New York

Olver FWJ (1974) Asymptotic and Special Functions. Academic Press, New York, London

Index

G. I. Mikhasev and H. Altenbach, *Thin-walled Laminated Structures*, Advanced Structured Materials 106, https://doi.org/10.1007/978-3-030-12761-9